

INDIAN JOURNAL OF PHYSICS

VOL. XVIII

AND

PROCEEDINGS

OF THE

Indian Association for the Cultivation of Science, Vol. XXVII

(Published in Collaboration with the Indian Physical Society)

Indian Journal of Physics

(With Eight Plates)

PRINTED BY DINABANDHU GANGULEE, B.A., SUPERINTENDENT, CALCUTTA
UNIVERSITY PRESS, 48, HAZRA ROAD, BALLYGUNGE, CALCUTTA, AND
PUBLISHED BY THE SECRETARY, INDIAN ASSOCIATION FOR
THE CULTIVATION OF SCIENCE,
210, Bowbazar Street, Calcutta.

1946

Price Rs. 12 or £1-2-6

Volume 18—1944

CONTENTS

Part I

PAGE

1. The Dielectric properties of Lac ... G. N. Bhattacharya 1
2. On the Temperature of Solar Reversing Layer. K. Narahari Rao ... 23
3. Electrical properties of Indian Soils at Medium Broad-cast Frequencies. F. Rahaman and F. Muhi 31
4. Optically Catalytic action of Anthracene and Phenanthrene in giving Raman Shifts for some Organic Compounds. S. P. Sinha ... 38
5. Influence of Temperature on the Raman Bands of H_2O , D_2O and HDO . I. R. Rao and N. R. Rao 47
6. The λ -3338 Band of OD ... M. Ishaq 52
7. Mass Determination of Ionising particles recorded in photographic plates exposed to Cosmic Rays. Bibha Chaudhuri 57

Part II

8. Thermal Conductivity of Water ... M. F. Soonawala ... 71
9. On the Polarised Fluorescence of Dye-stuffs in Solution. Krishnadas Chaudhuri 74
10. Influence of the Intensity of Irradiation in the new Light-effect in Chlorine under Electrical Discharge. P. G. Deo ... 84
11. On the Experimental investigation of the Night-time E-Ion Densities and their determination by the application of Chapman's formula. M. M. Sen Gupta and S. K. Dutt. 88
12. The Dielectric properties of the constituents of Lac. G. N. Bhattacharya 97
13. The Dielectric properties of different mixtures of Hard and Soft Lac. G. N. Bhattacharya 116
14. The Dielectric properties of Modified Lacs. G. N. Bhattacharya 126

Part III

15.	Sound Absorption characteristics of Indian Materials, Part I.	S. Chatterjee and N. Dutt ...	135
16.	The Distortion of Plane χ -wave and its Effect on Elastic Scattering.	K. C. Kar ...	144
17.	The Crystal Structure of Metallic Fluoberyllates, Double Fluoberyllates and Sulphato-Fluoberyllates.	P. L. Mukherjee ...	148
18.	The Dielectric properties of Dammar and Mastic Resins.	G. N. Bhattacharya ...	159
19.	Non-Coulomb Central Field for Potassium Atoms.	Jatinder Nath Nanda ...	172
20.	Piezo-electric constants of Crystals Group-theoretical treatment.	Bishambhar Dayal Saksena ...	177
21.	The Band-spectrum of Bismuth Monoxide (BiO).	A. K. Sen Gupta ...	182
22.	Magnetic Studies of Potassium Permanganate.	A. Mookerjee ...	187
23.	The Dielectric Dispersion of a few Resins in Non-polar Solvents.	G. N. Bhattacharya ...	192

Part IV

24.	Faraday Rotations in Solution containing Ions of the First Transition Group.	A. K. Bose ...	199
25.	Energy in Liquid State	M. F. Soonawala ...	209
26.	Note on Cowling Model of a Convective-Radiative Star.	N. R. Sen and U. R. Burman...	212
27.	Humid Hysteresis of Mahajan's Optical Hygrometer.	L. D. Mahajan ...	216
28.	The Scattering of fast β -particles by Electron.	K. C. Kar and C. Basu ...	223
29.	Changes in the B-H Curves of Iron on sending Direct Electrical current through the specimen during Magnetisation.	H. R. Sarna and Om Parkash Sharma.	243
30.	Magnetic Studies on Molybdenite	Ajit Kumar Dutt ...	249

Part V

31.	On the Radium Content of a New mineral from Rajputana.	B. D. Nag Chaudhuri ...	257
32.	Rectification in Discharge Tubes	K. R. Chaudhuri ...	259

		PAGE
33.	On the Influence of Magnetic field on the Absorption spectra of Liquids.	A. K. Banerjee ... 264
34.	Disintegration of Boron by slow Neutrons.	S. D. Chatterjee ... 269
35.	A new Band System of HgBr Molecule.	K. R. Rao and G. V. S. R. Rao 281
36.	On the variation in the Experimentally determined values of the Meson Mass.	D. M. Bose and Bibha Chaudhuri. 285
37.	Time Lag and Humid Fatigue of Hygrometers.	L. D. Mahajan ... 293

Part VI

38.	Proton-Proton Scattering at Low Velocity.	K. C. Kar and S. N. Mitra ... 303
39.	Rupture of water drop over Liquid Surfaces.	B. K. Sahay ... 306
40.	Mobility of Atmospheric Vortices	S. N. Sen, H. R. Puri and S. Majumdar. 311
41.	Investigation on the Spectrum of Bromine, Part II—Structure of Br II.	R. Ramanadhan and K. R. Rao. 317.
42.	Ultra-violet Band Systems of the Mercury Iodide Molecule.	K. R. Rao, M. G. Sastry and V. G. Krishnamurti. 323
43.	On the Cathode Dark-space of a Glow Discharge in gases at low pressure.	R. M. Chaudhuri and S. H. Zubari. 333
44.	Acoustical Impedance of Fog	R. N. Ghosh ... 341
45.	On the study of Absorption and Fluorescent Spectra by some Aromatic Hydrocarbons in solution.	S. C. Ganguly ... 347

AUTHOR INDEX

AUTHOR	SUBJECT	PAGE
Banerjee, A. K. On the Influence of Magnetic field on the Absorption spectra of Liquids.	264
Bhattacharya, G. N.	... The Dielectric properties of Lac ...	1
„ „	... The Dielectric properties of constituents of Lac.	97
„ „	... The Dielectric properties of different mixtures of Hard and Soft Lac.	116
„ „	... The Dielectric properties of Modified Lac.	126
„ „	... Dielectric properties of Dammar and Mastic Resins.	159
„ „	... The Dielectric dispersion of a few Resins in Non-polar Solvents.	192
Bose, A. K. Faraday Rotations in Solutions containing Ions of the First Transition Group.	199
Bose, D. M. and Chaudhuri, Bibha.	On the variation in the Experimentally determined values of Meson Mass.	285
Chatterjee, S. D. Disintegration of Boron by slow Neutrons	269
Chatterjee, S. and Dutt, N. ...	Sound Absorption characteristic of Indian Materials, Part I.	135
Chaudhuri, Bibha	... Mass Determination of the Ionising particle recorded in photographic plates exposed to Cosmic Rays.	57
Chaudhuri, Krishnadas	... On the Polarised Fluorescence of Dye-stuffs in Solution.	74
Chaudhuri, K. R.	... Rectification in Discharge Tubes ...	259
Chaudhuri, R. M. and Zuberi, S. H.	On the Cathode Dark-space of glow discharge in gases at low pressure.	333
Deo, P. G. Influence of the Intensity of Irradiation in the new Light-effect in Chlorine under Electrical discharge.	84
Dutta, Ajit Kumar	Magnetic Studies on Molybdenite ...	249
Ganguly, S. C.	On the study of Absorption and Fluorescent spectra by some Aromatic Hydrocarbons in Solution.	347
Ghosh, R. N. ...	Acoustical Impedance of Fog ...	341
Ishaq, M. ...	The λ -3338 band of OD ...	52
Kar, K. C. ...	The Distortion of Plane χ -wave and its effect on Elastic Scattering.	144
Kar, K. C. and Basu, C.	The Scattering of fast β -particles by Electrons.	223
Kar, K. C. and Mitra, S. N.	Proton-Proton Scattering at Low Velocity	303
Mahajan, L. D. ...	Humid Hysteresis of Mahajan's Optical Hygrometer.	216

AUTHOR INDEX		vii
AUTHOR	SUBJECT	PAGE
Mahajan, L. D. ...	Time Lag and Humid Fatigue of Hygrometers.	293
Mookerjee, A. ...	Magnetic Studies on Potassium Permanganate.	187
Mukherjee, P. L. ...	The Crystal Structures of Metallic Fluoberyllates Double-Fluoberyllates and Sulphate Fluoberyllates.	148
Nag Chaudhuri, B. D. ...	On the Radium Content of a new Mineral from Rajputana.	257
Nanda, Jatinder Nath ...	Non-Coulomb central field of Potassium Atom.	172
Rahaman, F. and Muhi, F. ...	Electrical Properties of Indian Soils at Medium Broad-cast Frequencies.	31
Ramanadhan, R. and Rao, N. R.	Investigation on the Spectrum of Bromine, Pt. II—Structure of Br. II.	317
Rao, I. R. and Rao, N. R. ...	Influence of Temperature on Raman Bands of H ₂ O, D ₂ O and HDO.	47
Rao, K. Narahari ...	On the Temperature of Solar Reversing Layer.	23
Rao, K. R., Sastry, M. G. and Krishnamurti, V. G.	Ultra-violet Band System of the Mercury Iodide Molecule.	324
Rao, K. R. and Rao, G. V. S. R.	A new Band System of HgBr Molecule	281
Sahay, B. K. ...	Rupture of Water Drops over Liquid surface.	306
Saksena, B. D. ...	Piezo-electric Constants of Crystals Group-theoretical treatment.	177
Saina, H. R. and Sharma, Om Parkash.	Changes in the B-H curves of Iron on sending Direct Electrical current through the Specimen during Magnetisation.	243
Sen, N. R. and Burman, U. R.	Note on Cowling Model of a Convective Radiative Star.	212
Sen, S. N., Puri, H. R. and Mazumdar, S.	Mobility of Atmospheric Vortices	311
Sengupta, A. K. ...	Band Spectrum of Bismuth Monoxide (BiO).	182
Sengupta, M. M. and Dutt, S. K.	On the Experimental Investigation of the Night-time E-Ion Densities and their determination by the application of Chapman's formula.	88
Sinha, S. P. ...	Optically Catalytic action of Anthracene and Phenanthrene in given Raman Shifts for some organic compounds.	38
Soonawala, M. F. ...	Thermal Conductivity of Water	71
" "	Energy in the Liquid State	209

SUBJECT INDEX

SUBJECT	AUTHOR	PAGE
Absorption spectra of Liquids, On the influence of Magnetic field.	A. K. Banerjee 264
Absorption and Fluorescent spectra by some Aromatic Hydrocarbons in solution, On the study of.	S. C. Ganguly 347
Acoustical Impedance of Fog ...	R. N. Ghosh 341
Atmospheric Vortices, Mobility of ...	S. N. Sen, H. R. Puri and S. Mazumdar.	... 311
Band of OD, The λ -3338 ...	M. Ishaq 52
Band Spectrum of Bismuth Monoxide (BiO)	A. K. Sen Gupta 182
Band System of HgBr Molecule, A new	K. R. Rao and G. V. S. R. Rao	281
B-H curves of Iron on sending direct Electrical Current through the specimen during magnetisation, Changes in the.	H. R. Sarna and Om Parkash Sharma.	213
Bromine, Investigations on the spectrum of, Pt. II—Structure of Br II.	R. Ramanadhan and K. R. Rao	317
Cathode Dark-Space of a Glow Discharge in gases at low pressure, On the.	R. M. Chaudhuri and S. H. Zuberi.	333
Cowling model of a Convective Radiative star, Note on.	N. R. Sen and U. R. Burman	212
Crystal Structure of Metallic Fluoberyllates, Double Fluoberyllates and Sulphato-Fluoberyllates, The.	P. L. Mukherjee 148
Dielectric dispersion of a Few Resins in Non-polar solvents, The.	G. N. Bhattacharya	... 192
Dielectric properties of constituents of Lac	„	... 97
Dielectric properties of Dammar and Mastic resins.	„	... 159
Dielectric properties of different mixtures of Hard and Soft Lac.	„	... 116
Dielectric properties of Lac	„	... 1
Dielectric properties of Modified Lac	„	... 126
Disintegration of Boron by Slow Neutrons.	S. D. Chatterjee	... 269
Distortion of plane χ -wave and its effect on Elastic Scattering.	K. C. Kar 144
Energy in Liquid State ...	M. F. Soonawala 209
Faraday Rotation in Solutions containing Ions of the first transition Group.	A. K. Bose 199
Hygrometers, Time lag and Humidity fatigue of.	L. D. Mahajan 293

SUBJECT INDEX

SUBJECT	AUTHOR	PAGE
Hygrometers, Humid hysteresis of Mahajan's Optical.	L. D. Mahajan	216
Indian Soils, Electrical properties of, at medium Broadcast frequencies.	F. Rahaman and F. Muhi	31
Irradiation in the new Light-effect in chlorine under electrical discharge, Influence of intensity of.	P. C. Deo	84
Magnetic studies on Molybdenite	A. K. Dutta	249
Magnetic studies of Potassium per- manganate.	A. Mookerjee	187
Mass determination of Ionising particles recorded in Photographic plates ex- posed to Cosmic Rays.	Bibha Chaudhuri	57
Meson Mass, On the variation in the ex- perimentally determined values of.	D. M. Bose and Bibha Chau- dhuri	285
Night-time E-ion densities and their determination by Chapman's formula, On the experimental investigation of.	M. M. Sen Gupta and S. K. Dutt.	88
Non-Coulomb central fields of Potassium Atom	J. N. Nanda	172
Optically catalytic actions of Anthracene and Phenanthrene in giving Raman shifts for some Organic compounds.	S. P. Sinha	38
Piezo-electric constants of Crystals Group-theoretical treatment.	B. D. Saksena	177
Polarised Fluorescence of Dye-stuffs in solution, On the.	K. D. Chaudhuri	74
Proton-Proton scattering at low velocity	K. C. Kar and S. N. Mitra	303
Radium content of a new mineral from Rajputana, On the.	B. D. Nag Chaudhuri	257
Raman bands of H_2O , D_2O and HDO , Influence of temperature on the.	I. R. Rao and N. R. Rao	47
Rectification in Discharge tubes	K. R. Chaudhuri	259
Rupture of water drops over liquid surfaces.	B. K. Sahay	339
Scattering of fast β -particles by Elec- trons, The.	K. C. Kar and C. Basu	223
Solar reversing layer, On the tempera- ture of.	K. N. Rao	23
Sound-Absorption characteristic of Indian Materials, Part I.	S. Chatterjee and N. Dutt	135
Thermal Conductivity of Water	M. F. Soonawala	77
Ultra-Violet band system of the Mercury Iodide Molecule.	K. R. Rao, M. G. Sastry and V. G. Krishnamurti.	323

THE DIELECTRIC PROPERTIES OF LAC

By G. N. BHATTACHARYA

(Received for publication, January 3, 1944)

ABSTRACT. The dielectric properties of lac have been measured over a wide range of temperature and frequency. It has been observed that the total dielectric loss of lac is due to a d. c. component and an a. c. one. The pure a. c. loss of lac varies with temperature and frequency in a manner which is characteristic of a polar liquid. The variation of dielectric constant with temperature and frequency also behaves in a similar fashion. But it has been established from the diminished value of loss-maximum and wide dispersion band that there is a distributed range of relaxation times for the complex shellac molecule. The distribution coefficient has been calculated. Employing Stoke's law the average diameter of the rotator, which is responsible for the dielectric loss, has been obtained and this has yielded the interesting fact that only the hydroxyl groups rotate in the alternating field. The energy of activation of lac has been calculated from both d. c. conductance-temperature as well as viscosity-temperature relationship graphs and they agree fairly well. The indication of a 'brittleness point' of lac near about 35°C has again been obtained from a study of these dielectric properties.

INTRODUCTION

Broadly speaking resins may be classified under two heads according to their behaviour towards heat treatment, *viz.* (1) thermoplastic and (2) thermosetting. The two types of resins are believed to have different molecular structure, the thermoplastic resins consist of a long chain molecular structure whereas the thermosetting ones have a cross-linked or girder-like structure. Naturally therefore the molecules of a thermoplastic resin are in a position to respond more freely to impressed external forces such as heat or electrical field than those of a thermohardening resin.

According to their electrical properties however the resins can be divided into two other groups, *viz.* (1) polar and (2) non-polar. Their behaviour in an alternating electric field however is very different and important information regarding physical structure etc. may be obtained from a study of such behaviour and its dependence on temperature and frequency. All polar substances are expected to show anomalous dispersion and the accompanying dielectric loss somewhere in the frequency range determined by the size and shape of dipoles and the inner friction coefficient. Debye's simple dipole theory can very well account for such dispersion or absorption when the molecules are small. But as the molecular size increases it becomes more and more difficult to apply quantitatively Debye's equations meant for comparatively small molecules with a single relaxation time. For example, the bigger molecules may not have a single relaxation time but may have a distributed range of such

relaxation times depending upon the nature of different polar groups involved. For, it has been observed that giant molecules do not rotate as a whole when placed in an oscillating electric field, but only certain parts of these molecules respond to such disturbances.

If the material is a heterogeneous mixture, as most plastics are, the dispersion in the dielectric constant-frequency curve and the consequent absorption may also be explained as due to bound ions according to Maxwell-Wagner theory of polarisation (Maxwell, 1892; Wagner, 1914). The dipole absorption is usually considered to take place at or near radio frequencies, whereas the Maxwell-Wagner absorption at power or audio frequencies, provided the conductivities of the components are low. If one of the components however has high conductivity the absorption may take place at high frequencies too. Similarly dipole loss may also appear at low frequencies if only the inner viscosity of the material is very high. It is difficult therefore to distinguish between these two types of polarisation by observing the dispersion frequency range. It must be understood however that there is no essential difference between the two types of absorption. The loss depends upon the frequency and the relaxation time of the material. It is also known from the experiments of different investigators that the relaxation time of a substance may vary over a wide limit depending mostly upon temperature. The displacement of charge which results in the polarisation is essentially the same in both the cases whatever may be the nature of charge carriers. Morgan (1934) has in fact shown that Debye theory can very satisfactorily be applied to the case of dispersion and absorption in glycerine at temperatures from that of the room to -70°C over the frequency range of 30 cycles/sec. to 98 megacycles/sec. Jackson (1935) has also applied the theory to a chlorinated diphenyl with satisfactory results. The theory has even been applied to some crystalline solids (Sun and Williams, 1934) to explain their dielectric behaviour, *e.g.* Murphy (1934) has established the fact that ice at so low a temperature as -90°C still behaves like a very viscous polar liquid. Qualitatively Debye theory has been used to explain the dispersion and the accompanying absorption of many synthetic resins such as alkyd resins, vinyl resins, synthetic phenolic resins, etc. It is of interest therefore to study in detail the dielectric properties of lac resin and their dependence on temperature and frequency, especially since it has been observed (Bhattacharya, 1943) that lac and its chief constituents are polar in nature.

Lac is known to be a peculiar resin in so far as its thermal behaviour is concerned, *viz.*, it has got thermoplastic as well as thermohardening properties. On heating lac first melts and becomes viscous liquid but then slowly hardens passing through a rubbery stage, the time for hardening depending upon temperature. It has an average molecular weight of about 1000 and so the molecule is small compared to most high polymeric resins but may be sufficiently large for the quantitative application of Debye's equations of anomalous dispersion and loss. The object of the present paper, therefore, is to report the

results of an investigation into the dielectric properties of lac with a view to finding out an explanation for them.

THEORETICAL

The dielectric properties of a substance may be expressed in terms of a real and an imaginary part of the complex dielectric constant,

$$\epsilon = \epsilon' - i\epsilon''$$

where ϵ = the complex dielectric constant,

ϵ' = the real or the ordinary dielectric constant,

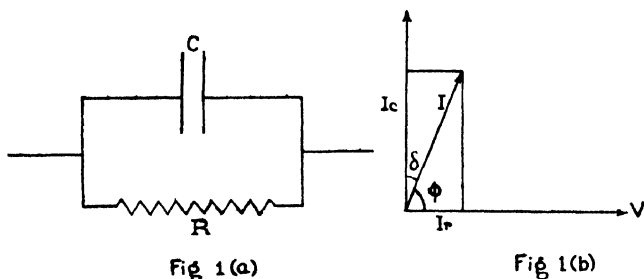
and ϵ'' = the imaginary part or the dielectric loss factor.

The relation between the dielectric loss factor ϵ'' and the dielectric constant ϵ' and the power factor which is generally expressed as $\cos \phi$ or $\tan \delta$ (where ϕ and δ are called the phase angle and the loss angle respectively) may be given by

$$\begin{aligned}\epsilon'' &= \epsilon' \cos \phi \\ &= \epsilon' \tan \delta\end{aligned}\quad \dots (1)$$

since δ is small and $\phi + \delta = 90^\circ$.

The dielectric constant ϵ' and the power factor $\tan \delta$ of a condenser may be determined over a Schering bridge or a capacity bridge. Hence the dielectric loss ϵ'' may be computed.



Now a condenser having dielectric loss may be looked upon as a perfect condenser C shunted by a resistance R (Fig. 1a). From the vector diagram (Fig. 1b) it may be easily seen that the current through the resistance,

$$I_r = I \sin \delta = I \tan \delta, \quad \dots (2)$$

since δ is usually very small.

Now the expression for current through a condenser C when a voltage V is impressed at its terminals is

$$\begin{aligned}I &= \omega CV \\ &= 2\pi f \cdot \frac{A\epsilon' \cdot V}{4\pi d \cdot 9 \times 10^{11}}\end{aligned}\quad \dots (3)$$

where f is the frequency, A and d are the area and the thickness of the

CALCULATION

The air capacitance of the test condenser formed by foil-electrodes was calculated from Kirchhoff's (1877) formula for parallel discs, viz.,

$$C = \frac{R^2}{4D} + \frac{R}{4\pi} \left[\log_e \frac{16\pi R(D+l)}{D^2} + \frac{l}{D} \log_e \frac{D+l}{l} - 3 \right]$$

where R = the radius of electrodes in cms.,

l = the thickness of electrodes in cms.,

D = the distance between the electrodes in cms.,

and C = capacity of the condenser in cms.

The correction for edge-capacitance was made according to the method given by Hartshorn (1941) and for connecting leads, etc., by finding out the capacity of these separately and deducting it from the measured capacitance.

For the cell type condenser the air-capacitance was obtained by filling it with pure and dry benzene from the relation

$$C_0 = \frac{\epsilon C_A - C_b}{\epsilon - 1}$$

where C_0 = 'zero-capacity', i.e., capacity of leads, etc.,

C_A = air capacity of the condenser,

C_b = capacity of the cell filled with benzene,

and ϵ = dielectric constant of benzene.

In the radio frequency bridge the plug plate in the jack board was placed in such a way that the standard capacitance and the standard resistance were in series. Hence the power factor in this case was calculated from the formula

$$\tan \delta = \cot \phi = \omega CR, \text{ since in a series circuit } \tan \phi = (1/\omega CR),$$

$$= 2\pi f \cdot CR \times 10^{-9}, \text{ if } f \text{ is expressed in Kilocycles and } C \text{ in micro-micro-farads,}$$

$$= f \cdot CR \times 6.28 \times 10^{-9}.$$

RESULTS

TABLE I

Dielectric constant—temperature data at different frequencies.

Frequency in Kilocycles per second.	Dielectric constant ϵ' at the temperature of									
	20°C	30°C	40°C	50°C	60°C	70°C	80°C	90°C	100°C	110°C
500	3.25	3.34	3.55	3.90	4.19	4.49	4.69	4.90	5.24	5.90
100	3.36	3.48	3.67	4.00	4.37	4.76	5.04	5.42	5.86	6.50
50	3.40	3.50	3.70	4.10	4.46	4.88	5.24	5.68	6.14	6.68
25	3.43	3.54	3.72	4.13	4.53	4.96	5.45	5.92	6.52	6.92
10	3.46	3.57	3.75	4.18	4.65	5.22	5.80	6.46	6.80	7.06
5	3.48	3.61	3.78	4.20	4.70	5.42	6.04	6.68	7.00	7.22
3	3.50	3.63	3.80	4.23	4.80	5.60	6.26	6.92	7.16	7.46
2	3.53	3.65	3.83	4.29	4.90	5.74	6.42	7.06	7.36	7.57
1	3.55	3.69	3.92	4.36	5.08	5.96	6.72	7.36	7.66	7.78
0.5	3.58	3.75	3.98	4.48	5.24	6.30	7.20	7.78	8.08	8.23
0.05	3.70	3.91	4.28	4.95	6.00	7.12	7.85

TABLE II

Measured power factor data at different temperatures and frequencies.

Frequency in Kilocycles per second.	Power factor (uncorrected for D.C. conductivity) at the temperature of									
	20°C	30°C	40°C	50°C	60°C	70°C	80°C	90°C	100°C	110°C
500	.0254	.0280	.0318	.0362	.0400	.0480	.0571	.0662	.0823	.0880
100	.0253	.0246	.0242	.0281	.0360	.0541	.0711	.0827	.0890	.0776
50	.0240	.0205	.0208	.0264	.0384	.0613	.0757	.0847	.0868	.0734
25	.0188	.0155	.0161	.0227	.0367	.0680	.0850	.0923	.0881	.0706
10	.0130	.0123	.0129	.0236	.0437	.0737	.0898	.0913	.0854	.0997
5	.0115	.0113	.0148	.0264	.0516	.0851	.0948	.0944	.0987	.1247
3	.0089	.0106	.0146	.0259	.0588	.0950	.1002	.0979	.1214	.2297
2	.0077	.0080	.0115	.0243	.0616	.1009	.1008	.1020	.1571	.3543
1	.0064	.0069	.0098	.0274	.0638	.1050	.1071	.1158	.1924	.5255
0.5	.0052	.0057	.0101	.0321	.0756	.1071	.1002	.1620	.4950	...
0.05	.0040	.0053	.0124	.0430	.0920	.1500	.2830

TABLE III

Total a.c. conductivity data at different temperatures and frequencies.

Frequency in Kilocycles per second.	Calculated ($K, \times 10^8$) values from measured power factor data at									
	20°C	30°C	40°C	50°C	60°C	70°C	80°C	90°C	100°C	110°C
500	2.29	2.59	3.13	3.92	4.66	5.98	7.43	8.98	11.98	14.4
100	.473	.477	.493	.623	.874	1.43	1.99	2.49	2.90	2.80
50	.2270	.199	.214	.301	.476	.831	1.10	1.34	1.48	1.36
25	.0898	.0765	.0830	.130	.231	.468	.643	.756	.797	.679
10	.0251	.0244	.0269	.0549	.113	.214	.289	.327	.323	.391
5	.0111	.0114	.0156	.0377	.0675	.128	.159	.175	.192	.250
3	.0052	.0064	.0093	.0183	.0470	.0886	.105	.113	.145	.286
2	.0030	.0033	.0049	.0116	.0335	.0644	.0719	.0800	.129	.298
1	.00127	.00143	.0021	.0066	.0180	.0348	.0399	.0473	.0819	.227
0.5	.000517	.000585	.00111	.0041	.0110	.0188	.0200	.0355
0.05	.000041	.000058	.00015	.00060	.00153	.00297	.00621

TABLE IV

Corrected Dielectric loss—temperature data at different frequencies.

Frequency in Kilocycles per second.	Dielectric loss ϵ'' (corrected for D.C. conductivity) at the temperature of									
	20°C	30°C	40°C	50°C	60°C	70°C	80°C	90°C	100°C	110°C
500	.083	.093	.113	.141	.167	.215	.267	.322	.427	.510
100	.085	.086	.089	.112	.157	.256	.357	.443	.502	.459
50	.082	.072	.077	.108	.171	.298	.395	.471	.493	.400
25	.065	.055	.060	.093	.166	.336	.459	.523	.494	.308
10	.046	.044	.049	.098	.203	.383	.512	.537	.383	.254
5	.040	.041	.056	.111	.243	.457	.555	.526	.295	...
3	.031	.038	.056	.109	.282	.525	.598	.503	.209	...
2	.027	.029	.044	.104	.301	.569	.602	.459	.166	...
1	.023	.026	.039	.119	.324	.606	.629	.329
0.5	.019	.021	.040	.143	.390	.640	.542	.233
0.05	.015	.020	.051	.200	.511	.710	.435

TABLE V

Corrected Power factor—temperature data at different frequencies

Frequency in Kilocycles per second	Power factor, $\tan \delta$, (corrected for D.C. conductivity) at the temperature of									
	20°C	30°C	40°C	50°C	60°C	70°C	80°C	90°C	100°C	110°C
500	.0254	.0280	.0318	.0361	.0398	.0479	.0570	.0657	.0815	.0854
100	.0253	.0246	.0242	.0280	.0360	.0538	.0708	.0817	.0856	.0706
50	.0240	.0205	.0208	.0264	.0382	.0610	.0753	.0829	.0802	.0700
25	.0188	.0155	.0161	.0227	.0365	.0676	.0839	.0883	.0757	.0445
10	.0130	.0123	.0129	.0236	.0435	.0733	.0883	.0831	.0563	.0359
5	.0115	.0113	.0148	.0264	.0515	.0843	.0919	.0787	.0421	...
3	.0089	.0106	.0146	.0258	.0586	.0937	.0955	.0727	.0292	...
2	.0077	.0080	.0115	.0242	.0615	.0991	.0937	.0650	.0225	..
1	.0064	.0069	.0098	.0271	.0636	.1016	.0936	.0447
0.5	.0052	.0056	.0100	.0320	.0748	.1042	.0752	.0300
0.05	.0040	.0051	.0120	.0410	.0851	.1000	.0554

DISCUSSION

The variation of power factor with temperature has been shown in figure 3. It may be seen that at ordinary room temperatures the power factor of Kusum lac is very low—less than .01 for about all frequencies below 10 kc/s, and less than .03 for frequencies below 500 kc/s and above 10 kc/s. The power factor begins to rise slowly from about 35°C and rapidly above 40°C. All these curves drawn for different frequencies reach a maximum and then fall again. The position of the peak of each curve is determined by the frequency, the higher frequency giving a shift towards the right, *i.e.*, towards higher temperature. The dielectric constant temperature and the dielectric loss temperature curves have been shown in figures 4 and 5 respectively. These data have been included in Tables I-V. The nature of all these curves suggests that they are due to polar molecules.

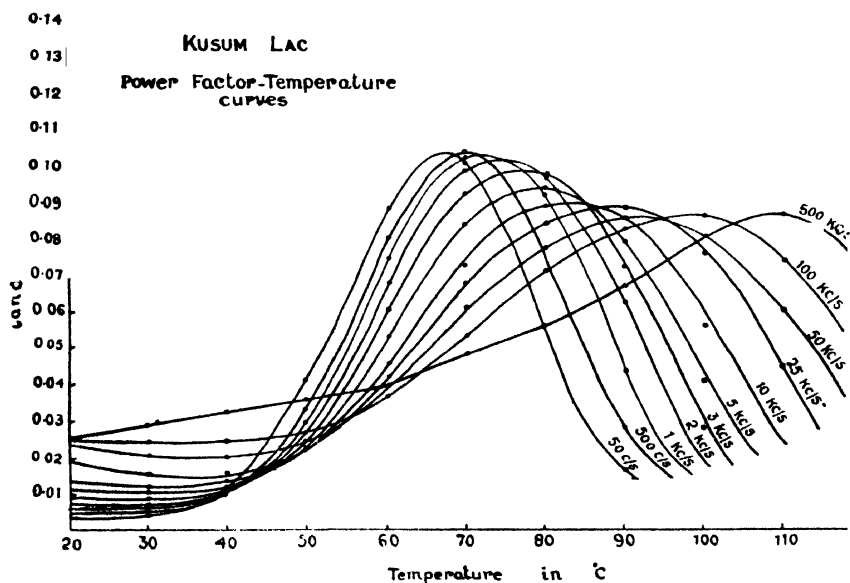
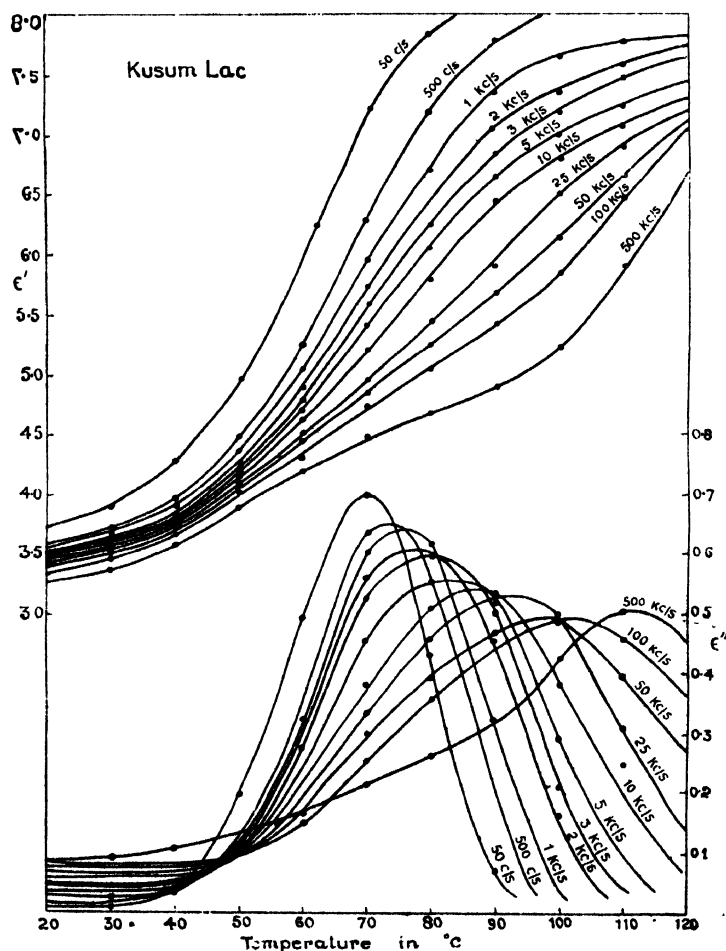


FIG. 3

According to Debye the dielectric loss is caused by the orientation of polar molecules when placed in an alternating current field against the inner frictional and other opposing forces. At lower temperatures when the substance is in a more or less solid state the inner binding forces of the molecules are very great and there is therefore very little chance for these polar molecules to orient themselves in response to the impressed alternating forces. The loss, therefore, is low. Again at very high temperatures the opposing forces due to thermal agitation are so great that it is difficult for the orientation of a good number of molecules to take place. The very few molecules which even then are oriented can however absorb little energy as the resistance to such orientation is small owing to the logarithmic

decrease of viscosity with temperature. As a result the loss at high temperatures is also low. Between these two extremes there will be states at which the molecules can respond more or less freely to the impressed vibrations against the opposing forces. The opposing forces of the molecules constitute the internal viscous forces of the substance as well as those due to thermal agitation. At higher and higher temperatures the thermal forces increase but the viscous forces decrease. At any temperature therefore the loss is determined by the frequency of the alternating field as well as the viscosity of the substance and the size and shape of the molecules giving the characteristic relaxation time.



FIGS. 4 & 5

It may be noted that the peak of any loss curve (Fig. 5) corresponds to a temperature at which the maximum variation of dielectric constant takes place in the corresponding curve in Fig. 4. This also is in accordance with Debye's theory. Each dielectric constant curve should reach a flat maximum after a sigmoid increase with temperature and then slowly head downward. For,

with the increase of temperature more polarisation takes place due to increased orientation of molecules resulting in the increase of dielectric constant. At low temperatures orientation is small owing to very high viscosity and therefore the dielectric constant is small. As the temperature reaches near about the softening point of lac the viscosity falls rapidly with the result that ϵ' rises steeply. Then it tends towards a flat maximum indicating a liquid state with the maximum number of oriented molecules. With a further rise of temperature the forces due to thermal agitation predominate and so the number of oriented molecules diminish resulting in a lower dielectric constant. This stooping portion of lac curves could not be obtained as it had been apprehended that appreciable polymerisation would take place in the lac before any reading could be taken at these high temperatures. Measurements were, therefore, carried up to a maximum of 110°C only since the rate of hardening of lac is known to be comparatively slow up to this temperature. Lac, as stated previously, is not a purely thermoplastic substance and at high temperatures it rapidly loses its 'life under heat' resulting in a hardened product which may have very different properties from ordinary lac. There is no doubt however that the curves resemble those of a polar liquid.

At the frequency of 50 c/s the maximum dielectric loss takes place at 69.5°C (Fig. 5), at 500 c/s this occurs at 74°C and at 1, 2, 3, 5, and 10 kc/s the peaks are at 76° , 77.5° , 80° , 83° and 87.5°C respectively. Thus within the audio frequency band the maximum loss point shifts about 18°C from the lowest to the highest one. For still higher frequencies the point moves further right and at 500 kc/s the maximum loss takes place at about 112°C . It may be seen from these curves that the maximum loss value ϵ''_{M} of each curve increases as we proceed towards lower temperature. Thus ϵ''_{M} of 50 c/s, which takes place at about 70°C , is 0.70 whereas ϵ''_{M} of 50 kc/s, appearing at 97.5°C , is only 0.50. The increase of ϵ''_{M} with decreasing temperature can be interpreted strictly according to dipolar theory. For, the maximum value of dielectric loss of a polar liquid can be represented as

$$\epsilon''_{\text{M}} = \frac{\epsilon_0' - \epsilon_{\infty}'}{2}$$

where ϵ''_{M} = the maximum value of loss,

ϵ_0' = the value of dielectric constant at zero frequency, i.e., the static dielectric constant,

and ϵ_{∞}' = the value of dielectric constant at very high frequencies,

and ϵ_0' the static dielectric constant should increase with decrease of temperature owing to less interference of thermal agitation with the orientation of dipoles.

Now for lac ϵ_0' at 80°C can be estimated from figure 6 as approximately 8.5 and $\epsilon_{\infty}' = 4.5$. Hence the maximum loss according to the above formula should have been about 2.0. But actually this is only 0.62, i.e., slightly less than $1/3$ of the theoretical value. Taking other values at different temperatures too, we find that ϵ''_{M} for lac falls far short of the theoretical value demanded by

In the case of a liquid Stokes's law is applicable and ξ can be written as equal to $8\pi\eta a^3$, so that

$$\tau = \frac{4\pi\eta a^3}{kT},$$

where η = coefficient of viscosity,

and a = radius of the rotator.

It has been found that proper values of molecular radii are obtained if the macroscopic value of viscosity of a liquid is taken for η . But for solids or solid solutions low values are generally obtained (Jackson, 1935; Sillars, 1938) for molecular radii if the macroscopic viscosity is used for η . Resins, however, are peculiar substances lying on the border line of solids and liquids. They are not crystalline solids nor do they behave as pure liquids. In a crystalline solid the molecules are bound together by means of three dimensional lattice forces whereas in a thermoplastic polymeric resin they are held together by some sort of loose mechanical binding. As a result they behave more like a liquid than a solid although they have certain physical properties like a solid, and outwardly they appear to be solids. That is why Fuoss (1938) has stated that these plastic materials occupy positions in the wide 'spectrum' of compounds lying between the viscous liquid and the elastic solid. It is not known therefore if it is proper to use for η the macroscopic viscosity of a molten resin, like lac, in order to get an idea of the dimensions of the rotating unit. Hartshorn and co-workers (1940), however used it for some synthetic phenolic resins and arrived at the interesting conclusion that only the hydroxyl groups in those molecules rotated when placed in an alternating field. If similarly we assume that Stoke's law is applicable to lac so that the macroscopic viscosity at any temperature may be put equal to η in that formula we may be in a position to obtain the radius of the rotating unit from the relation connecting ' τ ' and a . In order to do that τ was calculated from the relation $\omega\tau = \frac{\epsilon_0' + 2}{\epsilon_0' + 2}$ at the point where the dielectric loss is maximum for any frequency. The viscosity coefficient η of lac at these temperatures was obtained from Houwink's (1934) curve for fluidity of lac. Although Houwink's curve is for a sample of T.N. Shellac the deduced values from that curve have been used here in absence of any data for Kusmi lac on the consideration that η is related to the radius in the third power and that an approximate idea of the size of the rotator is only wanted here. Table VI shows the average radius of the rotating unit as well as the values of η and τ . As the average radius obtained in this way is only 1.5×10^{-8} cm, i.e., equal to the radius of a hydroxyl group it may be inferred that only the hydroxyl group of the lac molecule rotates in the a.c. field. It may be argued that the inner friction coefficient is quite different from the macroscopic viscosity and so the actual radius is very different from the radius obtained here. But the weight behind such an argument becomes extremely light if we consider that lac resin behaves as a liquid regarding its solubility, viscosity and other properties and

that for a liquid the macroscopic viscosity is the inner friction. Moreover the calculation gives the size of the most probable polar group in the molecule.

TABLE VI

Calculated relaxation time and radius of the rotator.

Temp. $t^{\circ}\text{C}$	Relaxation time τ	Frequency f	Viscosity η (from Houwink)	Radius of the rotator a
69.5°	.0019	50 c/s	2×10^6	$1.52 \times 10^{-8} \text{ cm.}$
74°	.00019	500 c/s	2×10^5	$1.52 \times 10^{-8} \text{ ,,}$
83°	.0000168	5 Kc/s	1.9×10^4	$1.50 \times 10^{-8} \text{ ,,}$

If even then instead of assuming the correctness of applying Stoke's law for lac it is only assumed that the frictional torque is at least proportional to viscosity we can write

$$\tau = \xi / 2kT = C \cdot \eta / T$$

$$\text{or } T\tau = C \cdot \eta$$

$$\text{or } \log T\tau = C' + \log \eta$$

Now Houwink (1934) has shown that for lac the logarithmic formula connecting viscosity and temperature holds good. Therefore, substituting for $\log \eta$ the above relation may be further written as

$$\log T\tau = C'' + \frac{Q}{RT}$$

where Q = molar activation energy,

and R = molar gas constant.

Now τ for a polar liquid and for some solids can be calculated from the relation

$$I = \frac{\epsilon_{\infty}' + 2}{\epsilon_0' + 2} \left\{ \epsilon_M'' \pm \sqrt{\epsilon_M''^2 - \epsilon_0''^2} \right\}$$

If therefore $\log T\tau$ is plotted against $1/T$ a straight line graph is expected.

Figure 9 shows this and it may be seen that the plot actually gives a straight line. The bottom three lines are for 50 c/s, 1 kc/s and 10 kc/s. Table VII shows these data. From this we may conclude that the assumption with which we started, viz., the frictional torque for dipoles at any temperature even in a resin, like lac, is at least proportional to macroscopic

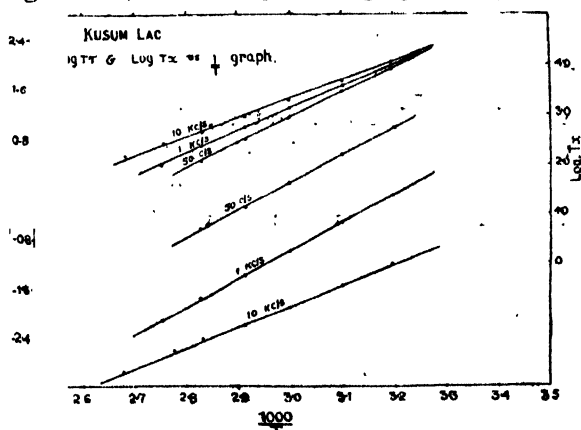


FIG. 9

TABLE VII

Log $T\tau$ and $\frac{1}{T}$ data

Frequency f	Temperature $t^\circ\text{C}$	Relaxation time τ	Temperature $T^\circ\text{K}$	$T\tau$	Log $T\tau$	$10^3 \times \frac{1}{T}$
10 Kc/s	40°	.000238	313	.0745	-1.128	3.195
	50°	.000130	323	.0420	-1.377	3.096
	60°	.000055	333	.0183	-1.738	3.003
	70°	.000024	343	.0082	-2.086	2.915
	80°	.000014	353	.0049	-2.310	2.833
	87°5	.000010	360.5	.0036	-2.444	2.774
	100°	.000004	373	.0015	-2.824	2.681
1 Kc/s	40°	.003530	313	1.105	0.043	3.195
	50°	.001260	323	0.407	-0.390	3.096
	60°	.000400	333	0.133	-0.876	3.003
	70°	.000142	343	0.049	-1.313	2.915
	80°	.000075	353	0.027	-1.580	2.833
	90°	.000027	363	0.010	-2.000	2.755
50 c/s	40°	.06000	313	18.78	1.27	3.195
	50°	.01620	323	5.23	0.72	3.096
	60°	.00500	333	1.67	0.22	3.003
	70°	.00190	343	0.65	-0.19	2.915
	80°	.00068	353	0.24	-0.62	2.833
	90°	.00034	363	0.12	-0.92	2.755

viscosity at that temperature, is fairly correct. If any doubt regarding the propriety of using the above formula for the calculation of τ is felt here, we can arrive at the same conclusions without making use of that relation also. Thus if we introduce a variable x such that

$$e''/e_0'' = \frac{2x}{1+x^2}$$

as Debye (1929) did, x will still be proportional to $\omega\tau$ even if it has any value other than the Debye value of $\omega\tau \frac{e_\infty' + 2}{e_0' + 2}$. In that case, therefore, for any particular

frequency

$$x = K \cdot \omega\tau = K'\tau$$

Substituting this in the above expression for $\log T\tau$, we get

$$\log T\tau = C''' + \frac{Q}{RT}$$

so that as obtained previously if $\log T\tau$ is plotted against $1/T$ a straight line graph is expected. The actual plot of this has been shown by the top lines of figure 9 and the data included in Table VIII.

TABLE VIII
Log $T\tau$ and $\frac{1}{T}$ data

Frequency f	Temperature		τ	$\log T\tau$	$\frac{1}{T} \times 10^3$
	$t^\circ\text{C}$	$T^\circ\text{K}$			
10 Kc/s	40	313	36.3	4.05	3.195
	50	323	13.3	3.63	3.096
	60	333	4.6	3.18	3.003
	70	343	2.4	2.92	2.915
	80	353	1.4	2.70	2.833
	90	363	0.82	2.47	2.755
	100	373	0.43	2.20	2.681
1 Kc/s	40	313	33.0	4.01	3.195
	50	323	12.5	3.61	3.096
	60	333	3.75	3.10	3.003
	70	343	1.50	2.71	2.915
	80	353	0.75	2.38	2.833
	90	363	0.26	1.97	2.755
50c/s	40	313	28.5	3.55	3.195
	50	323	6.5	3.35	3.096
	60	333	2.4	2.90	3.003
	70	343	1.0	2.53	2.915
	80	353	0.33	2.06	2.833
	90	363	0.10	1.56	2.755

This may be seen from another point of view. The d.c. conductance of an insulating material is believed to be due to the mobility of its free ions in the material. This mobility is evidently directly proportional to fluidity or inversely to viscosity at any temperature. From the temperature dependence of d.c. conductance therefore an idea can be had as to how the internal friction varies

with temperature. Table IX shows the values of d.c. conductance of lac at different temperatures. If

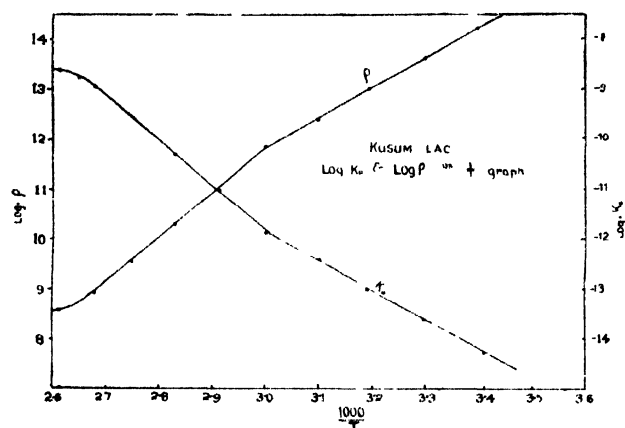


FIG. 10

now the logarithm of d.c. conductance K_0 is plotted against $1/T$, a straight line is obtained for the range 20° - 60°C . Above this temperature another straight line is obtained with less inclination to the x -axis. This linear relationship shows that the resistance to translational motion of ions to which conductivity is due varies similarly with temperature as the frictional torque for the rotation of dipoles does.

That is to say, the same value of inner friction is probably operative in both the cases and that value is proportional to the macroscopic viscosity.

TABLE IX

Resistivity or conductivity—Temperature data

Temperature		$\frac{1}{T} \times 10^3$	Resistivity ρ	D. C. conductivity K_0	Log K_0
$t^\circ\text{C}$	$T^\circ\text{K}$				
20°	293	3.413	1.8×10^{14}	0.56×10^{-14}	-14.25
30°	303	3.300	4.0×10^{13}	0.25×10^{-13}	-13.60
40°	313	3.195	1.0×10^{13}	1.00×10^{-13}	-13.00
50°	323	3.096	2.5×10^{12}	0.40×10^{-12}	-12.40
60°	333	3.003	7.8×10^{11}	0.13×10^{-11}	-11.89
70°	343	2.915	1.0×10^{11}	1.00×10^{-11}	-11.00
80°	353	2.833	2.0×10^{10}	0.50×10^{-10}	-10.30
90°	363	2.755	3.5×10^9	0.29×10^{-9}	-9.54
100°	373	2.681	9.0×10^8	0.11×10^{-8}	-8.95
110°	383	2.611	4.0×10^8	0.25×10^{-8}	-8.60

We shall try to explain now why two separate straight lines are obtained for logarithm of d.c. conductance— $1/T$ graph within the temperature range of 20°C and 100°C instead of having only one. It may be observed from the linearity of the $\log \tau$ and $1/T$ graphs that the molar activation energy Q for

dipole rotation remains fairly constant for a particular frequency over the range of temperature investigated. Q is easily determined from the slope of the straight line graph or by solving the equation taking two independent sets of readings. From the d.c. conductance $-1/T$ graph two values of Q are therefore obtained, *viz.*, 27.4 K-cal and 37.0 K-cal for the two temperature ranges, *viz.*, 20°-60°C and 60°C-100°C respectively. The values of Q calculated from a.c. data are 22.7 K-cal for 50 c/s, 20.5 K-cal for 1 kc/s and 15.0 K-cal for 10 kc/s. Q is thus found to increase with the decrease of frequency. If we then extrapolate these energy values to zero frequency, an activation energy of about 33 K-cal is obtained for d.c. This value is more or less in agreement with the value of 37.0 K-cal actually obtained from d.c. conductivity experiments above 60°C. Houwink's experiments (1934) on the plasticity of lac gave a value of about 35 K-cal for the activation energy, which is in fair agreement with the results obtained here. The lower energy value of 27.4 K-cal obtained here from d.c. conductivity experiments below 60°C should be explained on the basis of a sudden change of state taking place near about this temperature in lac. Glass and many other materials, such as asphalt, glucose, etc., have similarly shown two linear portions in their logarithm of viscosity $-1/T$ relation. For lac however Houwink (1937) could not observe this since he directed his experiments only above 55°C. He himself has explained this linear characteristic of lac by saying that "it is probably due to the fact that the measurements have not been made over a sufficiently wide range to make the observation of a deviation from the straight line possible." In fact, if he had carried his experiments only a few degrees further below he could have observed this deviation.

At very high temperatures, however, say at 110°C or above, the conductance begins to fall again. This deviation from the linear relationship is probably due to decreased mobility as a result of increased viscosity owing to hardening or condensation of lac. Any way, we find that in the temperature range 60°C-100°C the logarithm of viscosity of lac follows a linear law with $1/T$, which is generally applicable to liquids, and that below this range the same law is followed but with a change in the slope of the line. It may be concluded therefore that the resistance to the motion of dipoles of lac is due to the internal viscosity at different temperatures and so its dielectric losses at various frequencies and temperatures may be satisfactorily explained on the basis of dipole theory keeping in mind the fact that its molecules being comparatively large have a distributed range of relaxation times.

We shall now examine carefully the power factor-temperature curves (Fig. 3) or the dielectric-loss-temperature curves (Fig. 5) of lac and arrive at some interesting conclusions. It may be seen that most of these curves begin to rise abruptly between 35°C and 40°C and then they apparently follow the course of what may be called typical adsorption curves. Below 30°C the dielectric loss or the power factor is very low for all frequencies, but even then is not independent of frequency. At lower temperatures than 20°C these curves may show another absorption band as has recently been observed for

polyvinyl chloride (Fuoss, 1941). There is reason to expect such a behaviour from a study of its dielectric constant values at 20°C. They are still found to be high compared to the square of its refractive index at 20°C. ϵ' of lac at 20°C for different frequencies varies from 3.7 to 3.3 whereas the square of its refractive index is only 2.31 ($n_D = 1.525$). The investigation could not at present be pursued well below room temperature for want of necessary thermostatic equipment. However the heights of such low temperature absorption curves, if they appear at all, are sure to be very low owing to the very high internal viscosity existing at those low temperatures. 35°C may be called the 'transition temperature' or the 'brittleness point' of lac following the nomenclature used by others. Tammann (1933) also observed that shellac loses its brittleness at about 30.5°C and the softening range is between 30.5°C and 56.5°C. The specific heat experiments of lac reported previously (Bhattacharya, 1940) also pointed to the existence of such a transition temperature. Such characteristic temperatures have been observed for many other amorphous substances by other workers, too. Probably at such transition temperatures the molecules of a substance suddenly become somewhat free to slip past one another overcoming the peculiar type of binding forces existing among them. Many other physical properties have also been found to undergo a sudden change at the transition temperature of a substance.

There is another point worthy of consideration. The measurement of conductance of insulating materials, as is well known, presents some difficulties especially when their specific resistivities are very high. The current there decays exponentially with time assuming a more or less constant value after a considerable time. The values of d.c. conductance reported in this paper were obtained after about a minute of the application of voltage. In the alternating field however the actual value of K_0 may be quite larger than that recorded here depending upon the frequency. In such a case the right hand halves of the absorption curves (Figs. 3 and 5) will all be shifted slightly towards the left. The position of apex of each curve will also shift similarly towards left. But the nature of curves will not change appreciably and the left hand portion will be the least affected, since the d.c. conductance at lower temperatures is a negligible fraction of the total a.c. conductance. This may be understood better with reference to figure 11. Here the total dielectric loss without correction for d.c. conductance has been plotted against temperature. The effect of subtracting loss due to d.c. conductance has been shown in broken lines. If a larger value of K_0 is subtracted from total loss, the broken line curves will evidently shift towards left.

It may be understood from what has been stated above that the actual value of K_0 may not be constant for different frequencies but may give increasingly higher values at higher frequencies. The effect of this will be to diminish the maximum value of each curve more towards the right, i.e., towards the high

temperature end, giving a more pronounced effect of increased loss at decreased temperatures already present in the series of curves.

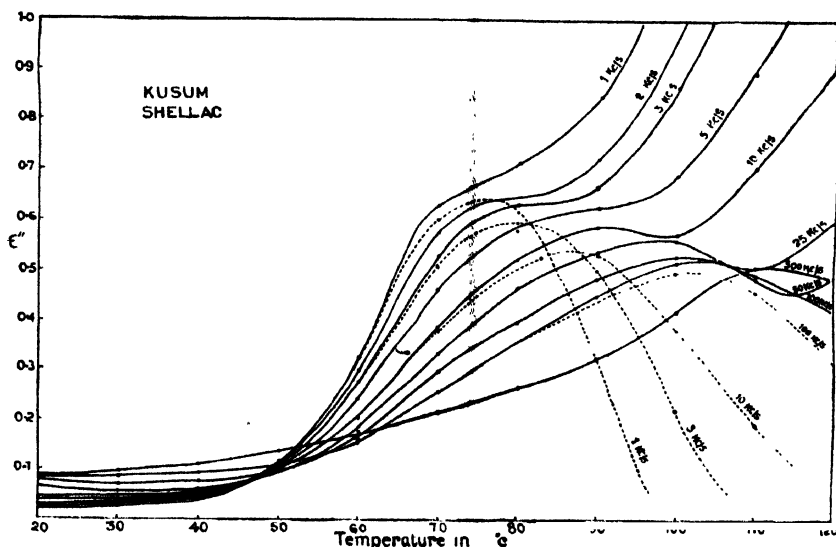


FIG. 11

Thus we see that the dipolar theory can be satisfactorily applied to resins like lac to explain their electrical behaviour provided all factors like the inner frictional forces, the distribution range of relaxation times of their molecules with regard to the size and shape of the rotator, etc., are properly taken into consideration.

ACKNOWLEDGMENT

It is a pleasure to acknowledge gratefulness to Dr. H. K. Sen, Director of this institute, for his kind interest in this work.

PHYSICAL & PHYSICO-CHEMICAL LABORATORIES,
INDIAN LAC RESEARCH INSTITUTE,
NAMKUM, RANCHI, BIHAR.

REFERENCES

- Bhattacharya, G. N., 1940, Specific heat of lac, *Ind. J. Phys.*, **14**, 415; 1942, The effect of surrounding medium on the dielectric strength of lac and lac-moulded materials, *Ind. J. Phys.*, **16**, 261; 1943, Dipole moment of the chief constituents of lac and rosin, *Ind. J. Phys.*, **17**, 153.
- Davies, J. M., Miller, R. F., and Busse, W. F. 1941, Dielectric properties of plasticised polyvinyl chloride, *J. Amer. Chem. Soc.*, **63**, 361.
- Debye, P., 1929, *Polar Molecules* (Chem. Cat. Co.) 92.

- Huoss, R. M., 1938, Discussions on Electrical Measurements of plastics, *Trans. Electrochem. Soc.*, **74**, 112; 1941, Electrical properties of solids, part VI, Dipole rotation in high-polymers, *J. Amer. Chem. Soc.*, **63**, 369.
- Huoss, R. M., and Kirkwood, J. G., 1941, Electrical properties of solids, part VIII, Dipole Moments in polyvinyl chloride—Diphenyl system, *J. Amer. Chem. Soc.*, **63**, 385.
- Hartshorn, L., 1941, *Radio Frequency Measurements* (Chapman and Hall), 193.
- Hartshorn, L., Megson, N. J., and Rushton, F., 1940, The electrical properties of thermoplastics, *Jour. Soc. Chem. Ind. (Trans.)* **59**, 129.
- Houwink, R., 1934, *Physikalische eigenschaften und feinebau von-Natur und Kunstharzen* (Akad. Verlags.), 63.
- Jackson, W., 1935, Mechanism of dielectric loss in paraffin wax solutions at high radio frequencies, *Proc. Roy. Soc.*, **A150**, 197; The dielectric loss characteristics of a chlorinated diphenyl, *Proc. Roy. Soc.*, **A153**, 158.
- Kirchhoff, G., 1877, *Berlin Akad. Monatsberichte*, 144 and *Condenser Dielect. Appl. Phys.* by Glazebrook (1922), **2**, 107.
- Maxwell, J. C., 1892, *Electricity and Magnetism* (Oxford) **1**, 328.
- Morgan, S. O., 1934, Two types of dielectric polarisation, *Trans. Electrochem. Soc.*, **65**, 109.
- Murphy, E. J., 1934, Temperature dependence of the relaxation time of polarisation in ice, *Trans. Electrochem. Soc.*, **65**, 133.
- Sillars, R. W., 1938, Behaviour of polar molecules in solid paraffin wax, *Proc. Roy. Soc.*, **A160**, 66.
- Sun, C. E., and Williams, J. W., 1934, Anomalous dispersion in crystalline solids. *Trans. Electrochem. Soc.*, **65**, 121.
- Taumann, G., 1933, *Der Glaszustand* (Verlag von Leopold voss).
- Wagner, K. W., 1913, Theory of dielectric lag, *Elektrotech. Zeit.*, **34**, 1279; 1914, The after-effect in dielectrics, *Arch. Elektrotech.*, **2**, 371.
- Yager, W. A., 1936, Distribution of relaxation times in typical dielectrics, *Physics*, **7**, 434.

ON THE TEMPERATURE OF THE SOLAR REVERSING LAYER

By K. NARAHARI RAO

(Received for publication, 10th January, 1944)

ABSTRACT. The Fraunhofer CN band $\lambda 3883$ was photographed with the high dispersion solar spectrograph, at the centre of the disc and at the limb of the sun. Points slightly within the limb are chosen for obtaining limb spectra. The methods of identifying the CN lines and measuring their intensities are described. By means of formulae deduced from the theory of band line intensities, temperatures of 5000°K and 4500°K are computed for the disc and limb respectively.

The proximity of the sun and its great brightness compared with other stars offer a unique opportunity for studying the physical state of the solar atmosphere. One can bring into operation the most powerful high dispersion spectrographs available without fear of inordinate exposure times. During the past two decades, on account of the large improvements in the observational technique, many interesting results regarding the solar atmosphere were brought to light. It is known for a long time that molecules exist in the reversing layer of the sun and that they give rise to band spectra. Determinations of the relative intensities of the lines in these bands furnish valuable information regarding the physical conditions in the reversing layer. In recent years, there have been several investigations in this direction. The relations that exist between the temperature of a diatomic gas in thermal equilibrium, the molecular constants and the relative intensities of the rotational lines have been applied for determining the temperature of the reversing layer.

TABLE I

Author	Method	Effective temperature for the integrated solar disc (in degrees absolute)
Milne	Stefan-Boltzmann law	5740
Bernheimer	Wien's law	6079
Fabry and Buisson	Planck's law 2932-3940Å	5830-6000
Lindbland	Planck's law	5950
Brill	Planck's law	5775-6075
Plaskett	Planck's law 4800-6700Å	6300-6600
Woolley	Ionisation of calcium	6310

Before applying the theory of band spectra to the molecular Fraunhofer lines, it is interesting to just review some of the results obtained by utilising other methods. The most often quoted result is that given by Abbot (1922) who, by the use of radiation laws, arrived at a value of 5740°K for the effective temperature of the sun. Milne(1921), Bernheimer, Fabry and Buisson(1922), Lindblad (1923), Brill, Plaskett(1923) and Woolley (1932) were among others who determined the effective temperature for sunlight integrated over the disc. The results obtained by them are summarised in Table I. In Table II are given the values of the excitation temperatures obtained by different authors from atomic line intensities and molecular band intensities. It will be seen that in general the excitation temperatures deduced from line intensities are lower than the effective temperatures.

TABLE II

Author	Lines used	Excitation temperature in degrees absolute
Atomic determinations :		
King (1938)	Ti I	4400
Menzel, Baker and Goldberg (1938)	Fe I	4150
	Ti I	4350
Molecular determinations :		
Birge (1922)	CN band at λ 3883	4000
Richardson (1931)	C ₂ band at λ 5165	5670 (Mean value)
Adam M.G. (1937-38)	C ₂ band at λ 5165	4550 (at the centre) 4790 (at the limb)
Roach (1939)	CN band at λ 3883	5630
Leon Blitzler (1940)	CN band at λ 3883	4490

Investigations on the determination of the temperature of the reversing layer from band line intensities are seriously hampered by the general faintness of the molecular lines and their blending with strong atomic lines. Perhaps due to this fact many of the investigations given above are only of a qualitative nature. As can be seen from Table II, the CN band at λ 3883 has been studied more than any other. The earliest determination of Birge was only from a visual comparison of the intensity distribution in the Fraunhofer CN lines with those in the arc and furnace spectra obtained in the laboratory. From a knowledge of the temperatures of these terrestrial sources of comparison he estimated the temperature of the reversing layer. Roach used Rowland intensities in his investigation. Blitzler made a quantitative study of the intensity distribution of the lines in the CN band from microphotometer tracings. He photographed the solar spectrum with the 75-foot tower telescope of Mt. Wilson having a linear dispersion of 3 mm per Angstrom. But his exposures for the solar spectrum were unusually long, ranging from 40 minutes to 4 hours. During such long intervals the sky conditions can never be constant and it is very necessary that plates, intended for photometric work, should be taken under constant sky conditions parti-

cularly to avoid the uncertain influence of the varying sky conditions. Since investigations of this nature provide valuable observational material for an analysis of the physical state of the solar atmosphere, spectrograms covering the region of the CN band at 3883 were secured by the author at the Kodaikanal Observatory during the past ten months. From the large number of plates available, only those of the finest quality were finally selected for photometry. The spectra were taken with a Glass Littrow spectrograph having a linear dispersion of 2.5 mm per Angstrom in the 3883 region. The instrument was particularly designed to minimise the systematic errors due to the scattered light in the spectrograph. A 12-inch Aluminised mirror, run by a siderostat, was used for reflecting the sun's image on to a lens which in turn gave a focussed image of about 6 inches in diameter on the slit of the spectrograph. Pictures at the centre of sun's disc were taken on days when the sky was very clear. Care was taken to see that photographs were obtained only when the centre of the sun's disc was undisturbed. Exposures of 1 to 2 minutes were found to be sufficient to give good pictures. Using a low dispersion spectrograph, standards were impressed on each plate by a step slit which was illuminated by diffuse reflection (by a paper) of the light from a 500-Watt lamp run on 110 volts D.C. The duration of exposure for these calibration spectra was just the same as that given for the solar spectrum. The spectrograms thus obtained were measured with a comparator estimating the intensity of each of the lines in the spectrum. These measurements were compared with the catalogue given in the Revised Rowland Table. The observed wavelength and strength of the lines gave a clue for identifying the lines due to the different elements. The intensities of the CN lines of the 3883 band identified in this manner were measured from microphotometer tracings using for this purpose the Cambridge Photo-electric Microphotometer. Only those lines of the above band which are free from blends and which have got well defined peaks in the microphotometer tracing were utilised for the evaluation of the temperature.

THEORY

The theory involved in these calculations is briefly discussed below :

It is known that the temperature of a diatomic gas in thermal equilibrium can be determined from a knowledge of the molecular constants and the relative intensities of the rotational lines in the band.

Intensity 'I' of the absorption line in the band is given by

$$I = C i e^{-E''/\kappa T} \quad \dots (1)$$

where 'C' is a constant for the band, 'i' the relative intensity factor for the rotational line, E'' the rotational energy in the lower molecular state, ' κ ' the Boltzmann constant and 'T' the temperature of the gas...

$$E'' = \frac{h^2 J''(J''+1)}{8\pi^2 I''} \quad \text{or} \quad = \frac{h^2 J''^2}{8\pi^2 I''} \quad \text{approximately}$$

Before applying the theory of band spectra to the molecular Fraunhofer lines, it is interesting to just review some of the results obtained by utilising other methods. The most often quoted result is that given by Abbot (1922) who, by the use of radiation laws, arrived at a value of 5740°K for the effective temperature of the sun. Milne(1921), Bernheimer, Fabry and Buisson(1922), Lindbland (1923), Brill, Plaskett(1923) and Woolley (1932) were among others who determined the effective temperature for sunlight integrated over the disc. The results obtained by them are summarised in Table I. In Table II are given the values of the excitation temperatures obtained by different authors from atomic line intensities and molecular band intensities. It will be seen that in general the excitation temperatures deduced from line intensities are lower than the effective temperatures.

TABLE II

Author	Lines used	Excitation temperature in degrees absolute
Atomic determinations :		
King (1938)	Ti I	4400
Menzel, Baker and Goldberg (1938)	Fe I	4150
	Ti I	4350
Molecular determinations :		
Birge (1922)	CN band at λ 3883	4000
Richardson (1931)	C ₂ band at λ 5165	5670 (Mean value)
Adam M.G. (1937-38)	C ₂ band at λ 5165	4550 (at the centre)
		4790 (at the limb)
Roach (1939)	CN band at λ 3883	5630
Leon Blitzer (1940)	CN band at λ 3883	4490

Investigations on the determination of the temperature of the reversing layer from band line intensities are seriously hampered by the general faintness of the molecular lines and their blending with strong atomic lines. Perhaps due to this fact many of the investigations given above are only of a qualitative nature. As can be seen from Table II, the CN band at λ 3883 has been studied more than any other. The earliest determination of Birge was only from a visual comparison of the intensity distribution in the Fraunhofer CN lines with those in the arc and furnace spectra obtained in the laboratory. From a knowledge of the temperatures of these terrestrial sources of comparison he estimated the temperature of the reversing layer. Roach used Rowland intensities in his investigation. Blitzer made a quantitative study of the intensity distribution of the lines in the CN band from microphotometer tracings. He photographed the solar spectrum with the 75-foot tower telescope of Mt. Wilson having a linear dispersion of 3 mm per Angstrom. But his exposures for the solar spectrum were unusually long, ranging from 40 minutes to 4 hours. During such long intervals the sky conditions can never be constant and it is very necessary that plates, intended for photometric work, should be taken under constant sky conditions parti-

cularly to avoid the uncertain influence of the varying sky conditions. Since investigations of this nature provide valuable observational material for an analysis of the physical state of the solar atmosphere, spectrograms covering the region of the CN band at 3883 were secured by the author at the Kodaikanal Observatory during the past ten months. From the large number of plates available, only those of the finest quality were finally selected for photometry. The spectra were taken with a Glass Littrow spectrograph having a linear dispersion of 2.5 mm per Angstrom in the 3883 region. The instrument was particularly designed to minimise the systematic errors due to the scattered light in the spectrograph. A 12-inch Aluminised mirror, run by a siderostat, was used for reflecting the sun's image on to a lens which in turn gave a focussed image of about 6 inches in diameter on the slit of the spectrograph. Pictures at the centre of sun's disc were taken on days when the sky was very clear. Care was taken to see that photographs were obtained only when the centre of the sun's disc was undisturbed. Exposures of 1 to 2 minutes were found to be sufficient to give good pictures. Using a low dispersion spectrograph, standards were impressed on each plate by a step slit which was illuminated by diffuse reflection (by a paper) of the light from a 500-Watt lamp run on 110 volts D.C. The duration of exposure for these calibration spectra was just the same as that given for the solar spectrum. The spectrograms thus obtained were measured with a comparator estimating the intensity of each of the lines in the spectrum. These measurements were compared with the catalogue given in the Revised Rowland Table. The observed wavelength and strength of the lines gave a clue for identifying the lines due to the different elements. The intensities of the CN lines of the 3883 band identified in this manner were measured from microphotometer tracings using for this purpose the Cambridge Photo-electric Microphotometer. Only those lines of the above band which are free from blends and which have got well defined peaks in the microphotometer tracing were utilised for the evaluation of the temperature.

THEORY

The theory involved in these calculations is briefly discussed below :

It is known that the temperature of a diatomic gas in thermal equilibrium can be determined from a knowledge of the molecular constants and the relative intensities of the rotational lines in the band.

Intensity 'I' of the absorption line in the band is given by

$$I = C i e^{-E''/\kappa T} \quad \dots (1)$$

where 'C' is a constant for the band, 'i' the relative intensity factor for the rotational line, E'' the rotational energy in the lower molecular state, ' κ ' the Boltzmann constant and 'T' the temperature of the gas...

$$E'' = \frac{h^2 J''(J'' + 1)}{8\pi^2 I''} \quad \text{or} \quad = \frac{h^2 J''^2}{8\pi^2 I''} \quad \text{approximately}$$

where $\frac{J''(J''+1)h}{2\pi}$ is the resultant angular momentum of the molecule in the lower energy state and I'' the moment of inertia of the molecule in the same state.

For the CN band (say for the R branch)

$$i = 2J'' \quad (\text{Jevon 1932}).$$

Therefore equation (1) becomes

$$\begin{aligned} I &= 2CJ'' \exp. \frac{-h^2 J''^2}{8\pi^2 I'' \kappa T} \\ &= C'J'' \exp. \frac{-h^2 J''^2}{8\pi^2 I'' \kappa T} \quad \dots (2) \end{aligned}$$

where C' is another constant.

We see from this equation that there will be a particular J'' for which the intensity is a maximum. By differentiating equation (2) with respect to J'' equating to zero and solving for T , we get

$$T = \frac{J''_{max}^2 h^2}{4\pi^2 I'' \kappa}$$

Further it can be easily shown that $h/4\pi^2 I''$ is the spacing between the consecutive lines at $J = +1$. Representing this by $\Delta\nu$ we get

$$T = \frac{h \cdot \Delta\nu \cdot J''_{max}^2}{\kappa}$$

For the CN band $\Delta\nu/C = 3.704$

$$\text{Hence} \quad J''_{max} = 0.434 \sqrt{T} \quad \dots (3)$$

This is one method of utilising equation (1). There is an alternative method of evaluating T . Taking logarithms of both sides of equation (1) and substituting for the known constants, we get

$$\log_{10} I/i = \log c - \frac{0.628B''}{T} J''(J''+1) \quad \dots (4)$$

$$\text{since } I/i = J''(J''+1)$$

Plotting $\log_{10} I/i$ against $J''(J''+1)$ we should get a straight line the gradient of which gives $\frac{0.628B''}{T}$ and hence ' T '. This was the method adopted by Roach and Blitzner.

It will be seen from these two methods that measurement of the position of the maximum intensity line in the band is a much better and more reliable method for determining stellar temperatures, as it involves the use of such quantities that are accurately measurable.

RESULTS

The results obtained in this investigation are given below in Table III. The wavelengths given in column 2 are taken from Uhler and Patterson (1915) and Heurlinger's notation is used for the quantum number.

TABLE III

Notation	λ	Relative intensity of the line	Rowland wavelengths in the vicinity of the $J=31$ line with their intensities and identifications
R_{12} (15)	3864.300	27	
R_{12} (24)	55.622	40	
R_{12} (28)	51.285	49	
R_{12} (31)	47.839	56	
R_1 (34)	44.250	46	3848.196 CN -1
R_2 (34)	.206		.116 CN -1
			.053 CN -1
			.17.967 CN -0
R_1 (41)	35.202	37	3847.873* CN 1
R_2 (41)	.147		.828 1
			47.694 -2
R_1 (50)	22.322	31	.521 -2
R_2 (50)	.259		.434 -1
R_1 (52)	19.278	28	
R_2 (52)	.213		

* Probably one line

It can be seen from the above table that the CN line with $J''=31$ has got the maximum intensity. Solar lines near this line are also given in the table for use in the following discussion. No doubt, it cannot be definitely ascertained that

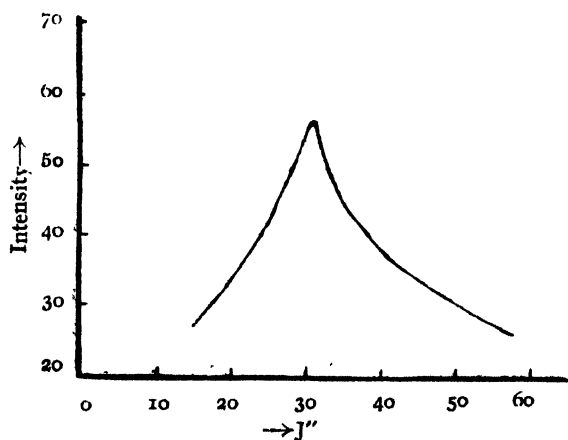


FIG. 1

J''_{max} falls at 31 as the CN line of wavelength 3847.967 which belongs to the singlet series from the second head is broad and diffuse and shades into the $J''=31$ line. But it can be seen from the graph (Fig. 1) drawn between J'' and intensity that with reasonable accuracy J''_{max} can be fixed in the vicinity of 31.

To confirm this by an alternative method Rowland intensities close to the $J''=31$ line are plotted against wavelengths and it is found that the resulting contour corresponds to that obtained on the microphotometer record at $J''=31$. In both

these the contours are asymmetrical the intense portion lying on the short wavelength side. The wavelength of this intense portion, as obtained from laboratory measurements, coincides with the $J''=31$ line. The temperature corresponding to this J''_{max} is, from equation (3), equal to 5100°K .

The other method of plotting $\log I/i$ against $J''(J''+1)$ was also utilised for evaluating ' T '. In Fig. 2 are plotted the

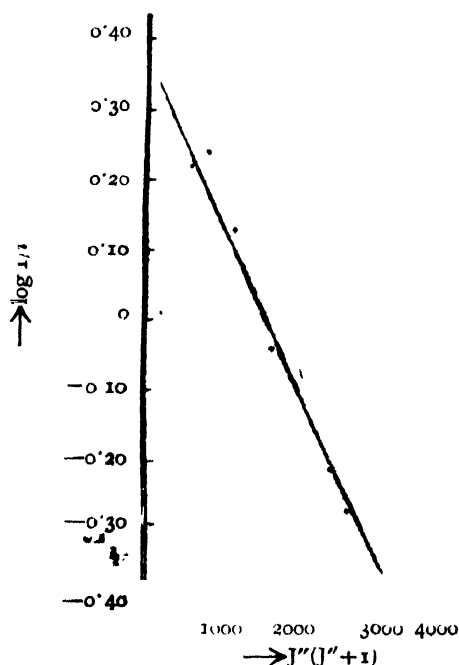


FIG. 2

values of $\log_{10} I/i$ against $J''(J''+1)$ and it will be seen that the points define a straight line with fair precision, showing that there is a thermal distribution of intensity along the band. A least squares solution was made to determine the line given by the points and a value of $T=4960 \pm 100^\circ\text{K}$ was obtained from the slope of the curve. The value given in Jevon's Band spectra of diatomic molecules p. 284 was taken for $B''_{v=1}$. Taking the mean of the two results obtained above, the excitation temperature of the solar reversing layer can be fixed at about 5000°K .

It is interesting to note that this value also, like all those obtained from a study of the intensities in the molecular Fraunhofer lines, is comparatively low.

This is probably due to the fact that intensity methods give a value of the excitation temperature while the others the kinetic temperature.

PART II

COMPARISON OF THE LIMB AND DISC SPECTRA

In a recent paper by Miss Adam (*loc. cit.*) it was reported for the first time that her investigations on the intensity distribution in the C_2 band at $\lambda 5165$ at the centre and the limb yielded a hitherto unsuspected higher temperature for the layers at the limb than those at the centre. This strengthening of faint lines towards the limb is attributed to an anomalous temperature distribution in the outer layers of the solar atmosphere. The assumption of reduced re-emission in a double layer atmosphere is shown to predict this strengthening. In order to examine this rather novel result of Adam and with a hope of clarifying the situation, it has been decided to study the intensity distribution in the CN band at $\lambda 3883$ photographed at the limb of the sun also.

The observational material consisted of spectrograms taken with the high dispersion instrument referred to in the previous section, on the west limb of

the sun on all clear days when the seeing was 5-7 on a scale of 1-10 (1 representing the poorest seeing and 10 the best). Standards were impressed on these plates and the intensities of the unblended cyanogen lines of the 3883 band were calculated from microphotometer tracings. The results are summed up in the following table :

Notation	$R_{12}(24)$	$R_{12}(28)$	$R_{12}(31)$	$R_1(34)$	$R_2(34)$	$R_1(41)$	$R_2(41)$	$R_1(50)$	$R_2(50)$
Relative intensity of the line	32	39	52	36			28		23

It has been pointed out previously that measurement of the position of the maximum intensity line in the band is the best method for determining stellar temperatures. But an unprejudiced result cannot be obtained by applying this method to the above values of intensities of the lines in the limb spectra, as there is not an appreciable change in temperature for the layers at the limb when compared with that for the disc. The second method is therefore adopted in this case.

A curve is drawn between $\log I/i$ and $J''(J'' + 1)$ and it will be seen from Fig. 3

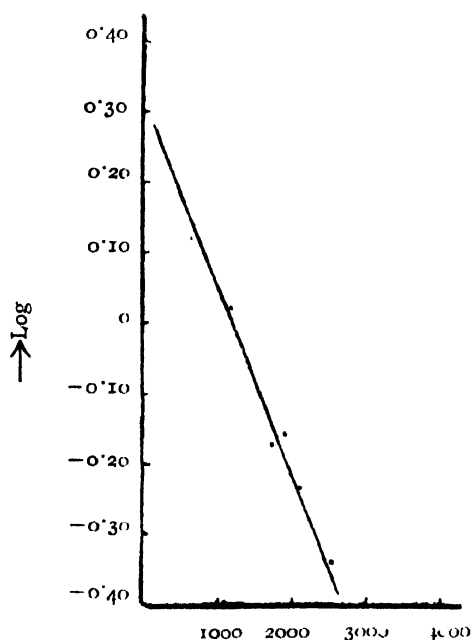


FIG. 3

that the points define a straight line with fair precision. A least squares solution was made to determine the straight line. As already discussed in the previous section, the slope of this straight line gives $0.628 B''_r/T$ where T is the temperature of the limb. T_{limb} was obtained to be $4500 \pm 100^\circ \text{K}$.

The intensities of the CN lines were in all cases found to be lower than those at the centre and T_{limb} evaluated from these intensity values less than T_{disc} .

It is interesting in this connection to recall the observation of Hale and Adams (1907) viz :

"..... Carbon and cyanogen are particularly interesting (for a comparison of the limb and disc spectra).

Many lines in the violet carbon band are of unchanged intensity or slightly strengthened at the limb. The cyanogen fluting, which begins at 3884 is, on the contrary, very decidedly weakened at the limb"

It is possible that the strengthening of the C_2 lines, observed by Miss Adam, is not due to the higher limb temperature but to some other cause. From these and other observations made by the author, it seems certain that there is a low excitation at the limb.

With a view to clarifying this point further, investigations are in progress, particularly as regards the intensity distribution in the CH and the C₂ bands in the laboratory and solar spectra.

The author is indebted to Dr. A. L. Narayau for his help and encouragement in the prosecution of this work.

SOLAR PHYSICS OBSRVATORY,
KODAIKANAL.

REFERENCES

- Abbot, C. G., 1922, *Smithsonian Ann.*, **4**.
 Adam, M. G., 1937-38, *M.N.R.A.S.*, **98**, 546
 Bernheimer, *Handbuch der Astrophysik*, **4**, 50.
 Birge, 1922, *A.P.J.*, **55**, 273.
 Blitzer, L., 1940, *A.P.J.*, **91**, 421.
 Brill, *Handbuch der Astrophysik*, **4**, 52
 Fabry and Buisson, 1922, *C.R.*, **175**, 156.
 Hale, G. E. and Adams W. S., 1907, *A.P.J.*, **25**, 310.
 Jevon, 1932—*Band spectra of diations molecules p.* 137.
 King, 1938, *A.P.J.*, **87**, 40.
 Lindbland, 1923, *Nova Acta Uppsala*, **4**.
 Menzel, Baker and Goldberg, 1938, *A.P.J.*, **87**, 81.
 Milne, 1921, *M.N.R.A.S.*, **81**, 361, 375 ;
 „ 1922, *Phil. Trans.*, **223**, 201.
 Plaskett, 1923, *Pub. D.A.O* , **2**, 213.
 Richardson, 1939, *A.P.J.*, **73**, 216.
 Roach, 1939, *A.P.J.*, **89**, 99.
 Uhler and Patterson, 1915, *A.P.J.*, **42**, 434.
 Woolley, 1932-33, *M.N.R.A.S.*, **93**, 691.

ELECTRICAL PROPERTIES OF INDIAN SOILS AT MEDIUM BROADCAST FREQUENCIES

By SHAH MD. FAZLUR RAHMAN

AND

FAIZUL MUHI

(Received for publication, the 28th January, 1944)

ABSTRACT. The electrical conductivity and the effective dielectric constant of soils from different places of India have been determined each for seven different frequencies within the medium broadcast frequency range and also with different moisture contents by the differential transformer method. Samples of soil were produced from Dacca, Calcutta, Lucknow, Delhi, Lahore, Peshawar, Bombay, Calicut (Madras Presidency), and Trichinopoly. The conductivity was observed to increase with both frequency and moisture content. But the rate of increase with moisture was very great while that with frequency was small. The effective dielectric constant was found to decrease with frequency and to increase with moisture contents.

From the observed values of the soil conductivity at 20% moisture the field strength attenuation curves for all the stations (except Delhi) of the All-India Radio have been drawn.

Suitable antenna-heights in relation to wave lengths have also been calculated for all the A.I.R. transmitting stations on the basis of the measured values of the soil conductivity.

INTRODUCTION

Owing to the rapid development of broadcasting service, the determination of the electrical constants of the soil is of considerable practical importance, especially in the case of medium radio frequencies. The methods generally employed for the purpose are:—(1) the field-method and (2) the laboratory method. The latter method found favour with recent-workers, since the soil can be studied under various controlled conditions.

Ratcliff and White (1930), made direct measurements of the electrical constants of some specimens of English soil by a laboratory method with medium radio-frequency fields. Previous to this work some measurements of the soil constants were made by Bairsto (1912). Similar investigations on medium frequencies were carried out by Smith-Rose (1933), in an elaborate manner with specimens of Cambridge soil for various values of moisture content and at different frequencies. Soils were also studied at medium frequencies in America by Dellinger (1933) and in Australia by Cheery (1930). In India Sengupta and Khastgir (1936), studied a few specimens of Dacca soil for medium frequencies. Ansari, Toshniwal and Toshniwal (1940), also studied on medium frequencies, the soil of Allahabad for various values of moisture content at three different frequencies. Some direct measurements were also carried out at Benares by Banerjee and Joshi (1937), on medium frequencies. The soil conductivity at medium broadcast frequency was determined by actual field measurements by

Roy (1936), in the case of Calcutta soil and by the Research department of the All-India Radio (Report...1940), in the case of Lahore, Lucknow and Delhi soils.

THE SCOPE OF THE INVESTIGATION

So far there has been no attempt at any systematic study of the electrical properties of soils from different parts of India. The rapid development of broadcasting in India during recent years, therefore, urged us to undertake a study of soil samples from Dacca to Peshawar and from Delhi to Trichinopoly. The samples were accordingly procured* from the places where there are broadcasting centres of the All-India Radio. The soils from the different places, *viz.*, Dacca, Calcutta, Lucknow, Delhi, Lahore, Peshawar, Bombay, Calicut (Madras Presidency) and Trichinopoly, can be taken to represent practically all types of Indian soils. A study of the electrical properties of these soils would, no doubt, be useful in determining service-areas, allocating suitable frequencies to transmitting stations, selecting suitable antenna heights and in various other ways. Measurements were, therefore, made of the effective dielectric constant and electrical conductivity of the different soils for various moisture contents and for various frequencies covering the medium broadcast frequency channels. The well-known differential transformer method was employed for the purpose. Calculations of service-areas and suitable antenna-heights in relation to wave lengths of the waves transmitted are also given.

EXPERIMENTAL DETAILS

To eliminate stray fields, the differential transformer was properly shielded. The oscillator was placed at some distance to avoid its direct effect of any part of the experimental arrangement. The connecting link between the coupling coil and the tuning condenser were also shielded.

The soil-condenser consisted of two rectangular parallel plates, each of area 3.1×4.3 sq. cm. and its capacity was $8 \mu\text{f.}$ when empty. The soil condenser plates were mounted on a rectangular framework made of ebonite. When filled up with soil it was bounded on all sides by thick ebonite sheets. The ramming of soil in the condenser was made such as it is generally found in the field.

EXPERIMENTAL RESULTS

The variations of the soil constants with moisture contents for the nine different Indian soils for 1 Mc/s field are illustrated in Figs. 1 and 2. The variations with frequency are illustrated in Figs. 3 and 4 for 15% moisture content.

(a) *Conductivity of the Soil*

For each sample, the electrical conductivity was determined for six frequencies within the range 600 Kc/s to 1500 Kc/s. In each case the value

*The only exception was Madras. The sample of soil profile was from Calicut in the Madras Presidency.

increased with increasing frequencies but the change was very small. On the other hand, the results obtained in the case of moisture variations showed a large increase with increasing moisture content. For smaller percentage

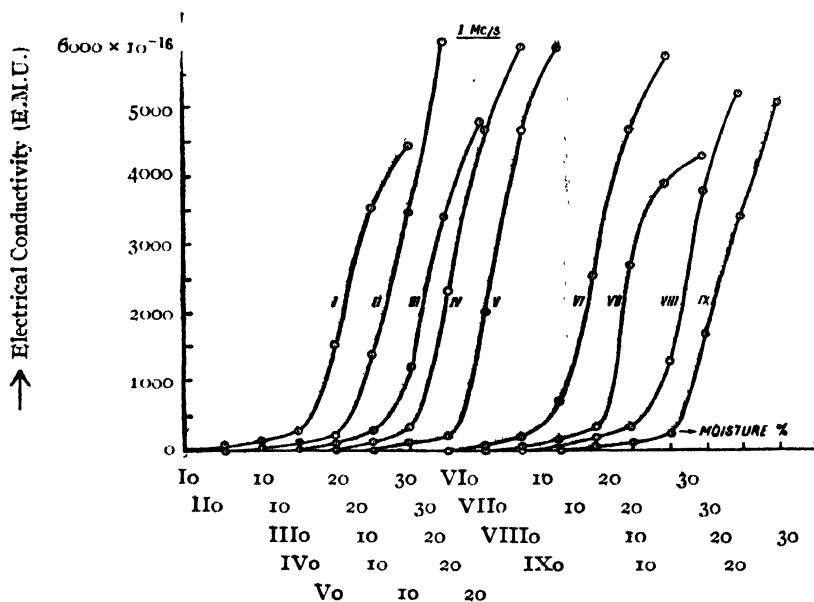


FIG. 1

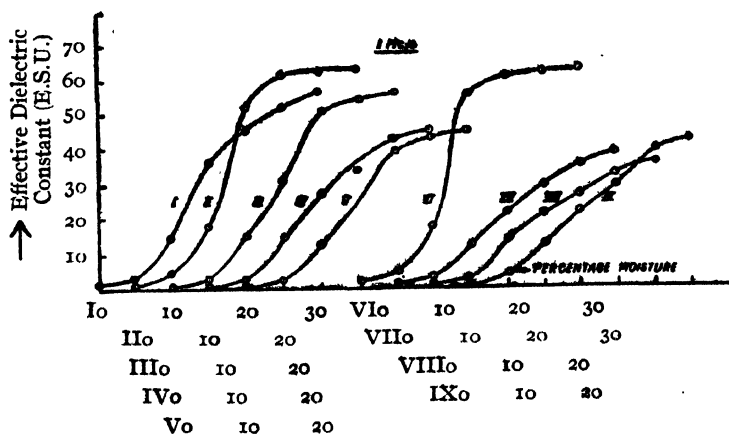


FIG. 2

of moisture, the variations was small while for larger percentages it was rapid. With further increase in the moisture content the results showed a tendency to become practically constant. The average value of σ was found to be about 2×10^{-16} e.m.u. when the sample was dry and about $.5 \times 10^{-15}$ e.m.u. at 30% moisture. At 20% moisture the average value was about 2×10^{-15} e.m.u.

The conductivity values, as obtained by Sengupta and Khastgir with two specimens of Dacca soil, are somewhat lower than the values obtained by us. Ansari, Toshniwal and Toshniwal's values for Allahabad soil and those for Benares soil, as obtained by Joshi, are of the same order as ours.

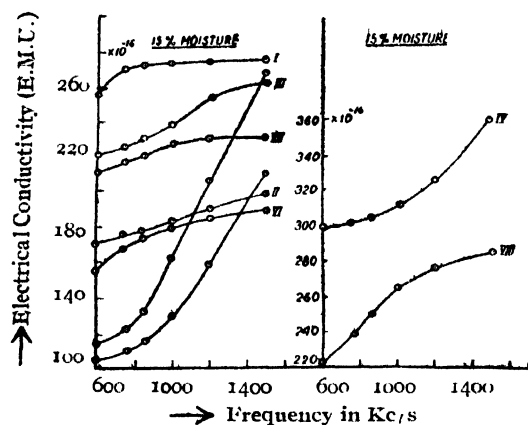


FIG. 3

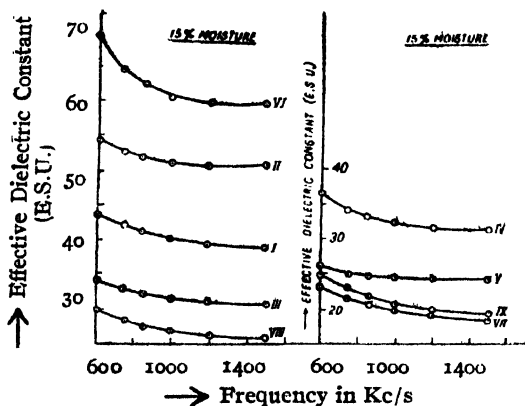


FIG. 4

According to K. Roy, the average value of the conductivity for Calcutta soil as determined by actual fieldstrength measurements, outside the city area could be taken as $2 \times 10^{-13} \text{ e.m.u.}$ The Research Department of A.I.R. found that for Lahore, Lucknow and Delhi soils, the conductivity values were $1.5 \times 10^{-13} \text{ e.m.u.}$, $1.75 \times 10^{-13} \text{ e.m.u.}$ and $1-1.5 \times 10^{-13} \text{ e.m.u.}$ respectively in the medium frequency range.

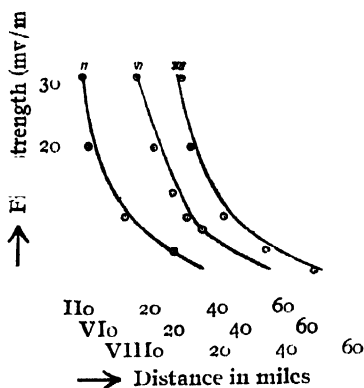
The measurements of the soil constants in Europe, America and Australia also give values which are of the same order as the values obtained with the Indian soils.

(b) Effective Dielectric Constant of the Soils

The rate of rise of the dielectric constant value was found to be very rapid for smaller percentage of moisture content. The rate varied appreciably in the different soils. For Dacca, Calcutta and Lucknow soils, the dielectric constant increased extremely rapidly when the moisture content was varied from 0 to 15%, whereas for the other soils, the rate of variation within that range of moisture content was much smaller. In the comparison of the dielectric constants of the different soils for 15% moisture content, the Dacca, Calcutta and Lucknow soils, therefore, showed comparatively large dielectric constant values at a frequency of 1000 Kc/s.

CALCULATION OF SERVICE AREAS

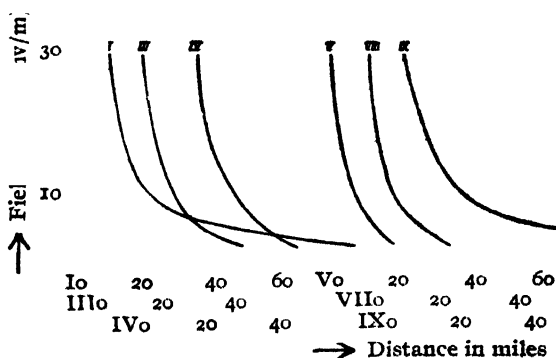
The fieldstrength attenuation curves for the different A.I.R. stations have been computed from the standard formula, the ground attenuation factor having been calculated from Van der Pol's expression. In the computation of the attenuation curves, the conductivity values of the different soils for 20% moisture content have been taken.



- II Calcutta (1.5 k.w.)
 $\lambda = 370.4$ m.
 $\sigma = 1.36 \times 10^{-13}$ e.m.u.
- VI Lucknow (5 k.w.)
 $\lambda = 293.5$ m.
 $\sigma = 2.49 \times 10^{-13}$ e.m.u.
- VII Lahore (5 k.w.)
 $\lambda = 266$ m.
 $\sigma = 2.60 \times 10^{-13}$ e.m.u.

Fieldstrength data

FIG. 5



- I Dacca (5 k.w.)
 $\lambda = 257.3$ m.
 $\sigma = 1.49 \times 10^{-13}$ e.m.u.
- III Delhi (20 k.w.)
 $\lambda = 338.6$ m.
 $\sigma = 1.18 \times 10^{-13}$ e.m.u.
- IV Bombay (1.5 k.w.)
 $\lambda = 244$ m.
 $\sigma = 2.3 \times 10^{-13}$
- V Madras (.25 k.w.)
 $\lambda = 211$ m.
 $\sigma = 2.0 \times 10^{-13}$ e.m.u.
- VIII Peshawar (.25 k.w.)
 $\lambda = 200$ m.
 $\sigma = 1.73 \times 10^{-13}$ e.m.u.
- IX Trichinopoly (5 k.w.)
 $\lambda = 295.8$ m.
 $\sigma = 1.62 \times 10^{-13}$ e.m.u.

FIG. 6

Figs. 5 and 6 show the computed fieldstrength attenuation curves for all the stations of A.I.R.* In the computed curves for Calcutta, Lahore and Lucknow shown in Fig. 5 the fieldstrength values actually obtained by K. Roy and the Research Department of A.I.R. are shown for comparison. The agreement is indeed very good. The fieldstrength values for the Delhi station are not shown in the graph, since the Delhi transmitter does not radiate energy uniformly in all directions.

In a tropical country like India, the atmospheric disturbances are considerable, so that a fieldstrength of 20 mv/m is generally regarded as good for radio reception in all seasons of the year. Following this standard, the service areas for all the A.I.R. medium wave stations as obtained from the computed attenuation curves are shown in Table I.

TABLE I
Service areas for a fieldstrength of 20 mv./m.

Serial number	A.I.R. stations	Power (Kw)	Wavelengths (metres)	Electrical conductivity of soils for 20% moisture (e.m.u.)	Service areas (miles)	h/λ for fading-free reception.
I	Dacca	5.0	257.1	1.49×10^{-13}	16	.563
II	Calcutta	1.5	370.4	1.36 „	9	.581
III	Delhi	20.0	338.6	1.18 „	—	.573
IV	Bombay	1.5	244.0	2.3 „	8	.573
V	Madras	0.25	211.0	2.0 „	4	.559
VI	Lucknow	5.0	293.5	2.49 „	16	.584
VII	Lahore	5.0	276.0	2.63 „	16	.584
VIII	Peshawar	0.25	200.0	1.73 „	4	.610
IX	Trichinopoly	5.0	295.8	1.62 „	17	.600

DETERMINATION OF SUITABLE ANTENNA-HEIGHTS

It has been shown by Ballantine (1943), that by a suitable choice of antenna-height the strength of the sky wave can be greatly reduced. This will obviously diminish fading. At great distances fading is a great disturbing factor in radio reception. So it was thought desirable to find out suitable antenna-heights in relation to the frequencies used by the broadcasting stations of All-India Radio.

A set of h/λ curves (not shown in the table) for medium broadcast frequencies corresponding to the conductivity values of the different soils were computed after the manner of Ballantine and the antenna-heights for the desired frequen-

*The attenuation curve for the Madras station was computed by supposing the electrical conductivity of the Madras soil essentially the same as that of Calicut (Madras Presidency). The soil conductivity of Calicut was taken.

cies, were determined from these curves. The results are shown in the last column of Table I.

Our sincere thanks are due to Dr. S. R. Khastgir for suggesting the problem and rendering valuable help during the progress of the work. Our thanks are also due to Prof. S. N. Bose for giving us all facilities for the work.

DEPARTMENT OF PHYSICS,
DACCA UNIVERSITY.

REFERENCES

- Ansari, Toshniwal and Toshniwal, (1940), *Proc. National Institute of Sciences of India*, **6**, 627.
- Ballantine, S. (1934), *Proc. I.R.E.*, **22**, 564.
- Banerjee and Joshi (1937), *Science and Culture*, **2**, 547.
- Baird (1912), *Proc. Roy. Soc.*, **96**, 363.
- Cheery, R. O. (1930), *Proc. Phys. Soc.*, **42**, 192.
- Dellinger, J. H. and others (1933), *Proc. I.R.E.*, **21**, 1419.
- Ratcliff and White (1930), *Phil. Mag.*, **10**, 607.
- Report on the Progress of Broadcasting in India (1940), 87.
- Roy, K. K. (1936), *Ind. Jour. Phys.*, **10**, 295.
- Sengupta and Khastgir (1936), *Phil. Mag.*, **22**, 265.
- Smith-Rose (1933), *Proc. Roy Soc. A*, **140**, 359.

OPTICALLY CATALYTIC ACTION OF ANTHRACENE AND PHENANTHRENE IN GIVING RAMAN SHIFTS OF SOME ORGANIC COMPOUNDS*

By S. P. SINHA

(Received for publication, January 20, 1944)

ABSTRACT. By taking the wavelengths of the absorption bands of anthracene in benzene, methyl alcohol, hexane, toluene and chlorobenzene and those of phenanthrene in benzene and methyl alcohol as giving the exciting frequencies the differences between these and the frequencies of the fluorescent bands have been calculated. These have been found to agree well with most of the Raman frequencies of the solvents. Some shifts observed in the present case which do not agree with any known Raman shift have been shown to be capable of being built up by the combinations of Raman shifts observed by the present or other authors.

INTRODUCTION

In a paper published Prosad and Bhattacharyya (1939) have described a new technique for the production of Raman effect. Compounds like $\text{Er}(\text{NO}_3)_3$ and KMnO_4 having sharp absorption bands are dissolved in small quantities in substances whose Raman spectra are to be obtained and the absorption and fluorescent spectra of the solutions are photographed. The latter are obtained in the usual way for getting Raman spectra. The differences between the frequencies of the absorption and fluorescent bands have been correlated with the Raman frequencies of the solvents with remarkable agreement. Some Raman shifts (*cf.* 3956cm^{-1} in case of water) by Collins (1939) obtained by the new method only have later on been discovered by the direct method and this stresses the importance of the technique.

The action of small quantities of salts like $\text{Er}(\text{NO}_3)_3$ and KMnO_4 which do not affect the Raman spectra of the solvents has been described as optically catalytic and the salts have been called optical catalysers by Prosad and Bhattacharyya (1936) and by Hartley (1937).

Earlier Prosad, Bhattacharyya and Chatterji (1935) had shown that by taking the wavelengths of the absorption bands of didymium glass as giving the exciting frequencies, the differences between these and the frequencies of the fluorescent bands observed with the same glass agreed well with most of the values of Raman shifts for different varieties of glass as measured by others. Working on the same lines, Banerji and Mishra (1937) had found the relation to hold good in case of a few organic liquids using anthracene as optical catalyser.

* (Communicated by K. Prosad).

This new technique for the production of Raman spectra has also been referred to by Hibben (1939) and by Glockler (1943).

Sambursky and Wolfsohn (1940) have studied the absorption and fluorescent spectra of anthracene and phenanthrene in different solvents but unaware of the work of Prosad and Bhattacharyya which was published later on, they did not make any attempt to verify the conclusions drawn by them.

In the present paper an attempt has been made to justify the optically catalytic action of anthracene and phenanthrene by calculating the Raman shifts from the absorption and fluorescent spectra of some organic compounds and comparing them with those found by others by the direct method. The data of the absorption and the fluorescent bands have been taken from the paper of Sambursky and Wolfsohn (*loc cit*).

CALCULATIONS AND DISCUSSIONS

Benzene.—Table I below gives the wavelengths and corresponding wave-numbers of the absorption and fluorescent bands obtained in the case of benzene with anthracene and phenanthrene as optical catalysers.

TABLE I

Benzene

Optical Catalyser	Absorption bands		Fluorescent bands	
	λ_{air} in Å.U.	ν_{vac} in cm.^{-1}	λ_{air} in Å.U.	ν_{vac} in cm.^{-1}
Phenanthrene	3095	32301 (a)	3405	29360 (A)
	3162	31636 (b)	3480	28727 (B)
	3237	30883 (c)	3573	27980 (C)
	3308	30221 (d)	3656	27344 (D)
	3392	29473 (e)	3758	26602 (E)
	3469	28818 (f)	3852	25953 (F)
	—	—	4068	24575 (G)
Anthracene	3790	26378 (g)	3828	26116 (H)
	3596	27801 (h)	4042	24733 (I)
	3420	29231 (i)	4280	23358 (J)
	3261	30657 (j)	4547	21986 (K)

Table II compares the Raman Shifts calculated with the help of Table I with those given by other authors. The agreement is fairly satisfactory.

TABLE II

Benzene

Some Raman shifts for Benzene calculated from the observed values of Table I.

$d\nu$ in cm.^{-1} by other authors Hibben (1939)	$d\nu$ in cm.^{-1} from Table I	$d\nu$ in cm.^{-1} by other authors	$d\nu$ in cm.^{-1} from Table I
	91 (f—B)	1693	1685 (h—H)
781	262 (g—H)	2128	2129 (e—D)
849	746 (e—B)	2925	2603 (c—C)
	838 (f—C)	—	—
	861 (d—A)	3047	3020 (g—J)
	mean 849.3	3062	3068 (h—I)
1473	1474 (f—D)	—	—
	1494 (d—B)	—	—
	1493 (e—C)	—	—
	mean 1487	—	—

TABLE III

Benzene

Some combination shifts built up by the Raman shifts compared with the observed shifts in the present case.

$d\nu$ by other authors Hibben (1939)	$d\nu$ by other ¹⁰	Shifts observed	Shifts by combination	Shifts observed	Shifts by combination
ν_1 606	ν_{11} 2358	2216 (f—E) 2241 (d—C)		4930 (c—F)	$\nu_8 + \nu_{10}$ 4916
ν_2 824	ν_{12} 2454	mean 2229	$\nu_2 + \nu_8$ 2228	5873 (i—J)	$\nu_{14} + \nu_{15}$ 5873
ν_3 979	ν_{13} 2618	2877 (d—D)		5924 (j—I)	$\nu_{12} + \nu_{18}$ 5924
ν_4 1030	ν_{14} 2925	2865 (f—F) 2871 (e—E)		6815 (h—K)	$\nu_{19} + \nu_{14}$ 6841
ν_5 1404	ν_{15} 2948	mean 2871	$\nu_5 + \nu_7$ 2882		
ν_6 1449	ν_{16} 3047	4268 (d—F)	$2\nu_{10}$ 4256		
ν_7 1478	ν_{17} 3116	4392 (g—K)	$\nu_9 + \nu_{11}$ 4388		
ν_8 1585	ν_{18} 3467	4443 (h—J)	$\nu_3 + \nu_{13}$ 4446		
ν_9 2030	ν_{19} 3916	4498 (i—I)	$\nu_6 + \nu_{16}$ 4496		
ν_{10} 2128	—	4541 (j—H)	$\nu_8 + \nu_{18}$ 4533		

TABLE IV

Methyl alcohol

Optical catalyser	Absorption bands		Fluorescent bands	
	λ_{air} in Å.U.	ν_{vac} in cm^{-1}	ν_{air} in Å.U.	ν_{vac} in cm^{-1}
Phenanthrene	3458	28910(a)	3464	28858(A)
	3381	29568(b)	3556	28113(B)
	3298	30313(c)	3637	27487(C)
	3228	30970(d)	3740	26730(D)
	3151	31727(e)	3829	26101(E)
Anthracene	3088	32374(f)	3778	—
	3753	26638(g)	3988	26461(F)
	3561	28074(h)	4220	25074(G)
	3388	29507(i)	4220	23690(H)
	3231	30941(j)	4480	22315(I)

TABLE V

Some Raman shifts for methyl alcohol calculated from Table V

$d\nu$ by other authors Hibben (1939)	$d\nu$ calculated from Table IV	$d\nu$ by other authors	$d\nu$ calculated from Table IV
2837	42 (a—A)	1458	1455 (b—B)
	177 (g—F)		1445 (c—A)
	700 (b—A)		1423 (a—C)
	797 (a—B)		mean 1441
	2809 (a—E)		2948 (g—H)
	2838 (b—D)	2942	3506 (f—A)
	2859 (c—A)		4240 (d—D)
	2857 (d—B)		4240 (e—C)
	mean 2838		

TABLE VI

Methyl alcohol

Some combination shifts built up by the Raman shifts compared with observed shifts in the present case.

ν by other authors Hibben (1939)		Shifts observed	Shifts by combination	Shifts observed	Shifts by combination
ν_1 1029	ν_{10} 2914	2081 (b-c)	$\nu_1 + \nu_2$ 2085	4887 (f-c)	$\nu_0 + \nu_{13}$ 4876
ν_2 1056	ν_{11} 2942	2102 (d-A)	$2\nu_2$ 2112	4997 (c-D)	$2\nu_1 + \nu_{11}$ 5000
ν_3 1111	ν_{12} 2987	2180 (a-D)	$\nu_1 + \nu_4$ 2182	5626 (c-E)	$\nu_0 + \nu_{14}$ 5610
ν_4 1153	ν_{13} 3506*	2200 (c-B)	$\nu_1 + \nu_5$ 2200	5759 (h-I)	$\nu_0 + \nu_{10}$ 5751
ν_5 1171	ν_{14} 4240*	3614 (c-B)	$\nu_1 + \nu_8$ 3617	5817 (i-II)	$2\nu_{10}$ 5828
ν_6 1370	—	4212 (c-E)	$\nu_6 + \nu_9$ 4207	7192 (i-I)	$\nu_{11} + \nu_{14}$ 7184
ν_7 1458	—	4323 (g-I)	$\nu_6 + \nu_{11}$ 4312	7251 (j-H)	$2\nu_{11} + \nu_0$ 7254
ν_8 2588	—	4384 (h-H)	$\nu_7 + \nu_{10}$ 4372	8626 (j-I)	$\nu_7 + \nu_{10} + \nu_{14}$ 8612
ν_9 2837	—	4433 (i-G)	$\nu_7 + \nu_{12}$ 4445	—	—

Two frequencies ν_{13} and ν_{14} , i.e., 3506 and 4240 which have not been noted by previous workers have been included in the above list on the basis of calculations shown in Table V. (One of these has occurred twice in Table V and three times in Table VI. It may further be noted that 2838 cm^{-1} which has been reported as one of the most intense Raman shift of the substance has occurred in four different combinations in Table V.

TABLE VII

Toluene

Optical catalyser	Absorption bands		Fluorescent bands	
	λ_{air} in Å.U.	ν_{vac} in cm^{-1} .	λ_{air} in Å.U.	ν_{vac} in cm^{-1} .
Anthracene	3787	26398(a)	3820	26170(A)
	3593	27824(b)	4032	24794(B)
	3417	29257(c)	4270	23412(C)
	3258	30685(d)	4536	22040(D)

TABLE VIII

Toluene

Some Raman shifts built up with the help of Table VII compared with those given by other authors.

$\delta\nu$ by others	$\delta\nu$ from Table VII	$\delta\nu$ by others	$\delta\nu$ from Table VII
218	228(a-A)	3070	3087(c-A)
1603	1604(a-B)	3026	3030(b-B)
1630	1654(b-A)	5848	5845(c-C)
2994	2986(a-C)	—	—

TABLE IX

Toluene

Some combination shifts built up by the Raman shifts compared with observed shifts in the present case.

$\delta\nu$ by other authors Ananthakrishnam (1936)		Shifts observed	Shifts by combination	Shifts observed	Shifts by combination
ν_1 519	ν_8 3002	4412 (b-C)	$\nu_4 + \nu_7$ 4414	4358 (a-D)	$\nu_3 + \nu_7$ 4356
ν_2 1377	ν_9 3205	4463 (c-B)	$\nu_6 + \nu_{10}$ 4468	7273 (d-C)	$\nu_3 + \nu_{12}$ 7282
ν_3 1434	ν_{10} 2865	4515 (d-A)	$\nu_6 + \nu_7$ 4510	5784 (b-D)	$\nu_7 + \nu_{10}$ 5787
ν_4 1492	ν_{11} 2941	5891 (d-B)	$2\nu_{11}$ 5882	7217 (c-D)	$\nu_2 + \nu_{12}$ 7225
ν_5 1588	ν_{12} 5848				
ν_6 1603	ν_{13} 4586				
ν_7 2922	—				

TABLE X

Chlorobenzene

Optical catalyser	Absorption bands		Fluorescent bands	
	λ_{air} in Å. U.	ν_{vac} in cm^{-1} .	λ_{air} in Å. U.	ν_{vac} in cm^{-1} .
Anthracene	3795	26343 (a)	3845	26068 (A)
	3600	27770 (b)	4050	24684 (B)
	3424	29197 (c)	4290	23303 (C)
	3265	30619 (d)	4561	21917 (D)

TABLE XI

Chlorobenzene

Some Raman shifts built up with the help of Table X compared with those due to other authors.

$d\nu$ by others	$d\nu$ from Table X	$d\nu$ by others	$d\nu$ from Table X
275	275 (a—A)	3068	3086 (b—B)
3028	3040 (a—C)	3129	3129 (c—A)

TABLE XII

Chlorobenzene

Some combination shifts built up by Raman shifts compared with those observed in the present case.

$d\nu$ by other Anantakrishnam		Shifts observed	Shifts by combination	Shifts observed	Shifts by combination.
ν_1 702	ν_8 1443	1659 (a—B)	$2\nu_2$ 1660	5853 (b—D)	$2\nu_7 + 2\nu_9$ 5874
ν_2 830	ν_9 1565	1702 (b—A)	$\nu_1 + \nu_8$ 1705	5894 (c—C)	$2\nu_8 + \nu_{10}$ 5894
ν_3 989	ν_{10} 3008	4426 (a—D)	$\nu_8 + \nu_{12}$ 4435	5935 (d—B)	$2\nu_8 + \nu_{11}$ 5954
ν_4 1003	ν_{11} 3068	4467 (b—C)	$\nu_9 + \nu_{13}$ 4461	7280 (c—D)	$\nu_8 + 2\nu_{12}$ 7283
ν_5 1295	ν_{12} 3140	4513 (c—B)	$\nu_8 + \nu_{11}$ 4511	7316 (d—C)	$\nu_3 + 2\nu_{13}$ 7319
ν_6 1321	ν_{13} 3165	4551 (d—A)	$\nu_7 + \nu_{13}$ 4537	8702 (d—D)	$\nu_8 + \nu_7 + 2\nu_{10}$ 8709
ν_7 1372	—	—	—	—	—

TABLE XIII

Hexane

Optical catalyser	Absorption bands		Fluorescent bands	
	λ_{air} in Å.U.	ν_{vac} in cm^{-1} .	λ_{air} in Å.U.	ν_{vac} in cm^{-1} .
Hexane	3748	26673 (a)	3770	26517 (A)
	3558	28097 (b)	3978	25131 (B)
	3386	29544 (c)	4210	23746 (C)
	3230	30950 (d)	4470	22365 (D)

It may be noted here that the Raman shift calculated in this case agrees only in one instance (2966 cm.^{-1} (b—B) and 2927 cm.^{-1} (a—C) with mean value 2946 cm.^{-1} agrees with 2940 cm.^{-1} as given in Table XIV) with the values of others. This may be either due to the particular substance not being an effective catalyser or else due to conditions more favourable for the production of large shifts only. The agreement between the values calculated and those built up by combinations as given in Table XIV is however quite satisfactory.

TABLE XIV

Hexane

Some combination shifts built up by the Raman shifts compared with those observed in the present case.

dν by other authors Andant etc. (1934)		Shifts observed	Shifts by combination	Shifts observed	Shifts by combination
ν ₁ 320	ν ₈ 1442	156 (a—A)	—	4432 (d—A)	ν ₁ +ν ₈ +ν ₁₀ 4445
ν ₂ 355	ν ₉ 2865	1542 (a—B)	ν ₄ +2ν ₁ 1540	5732 (b—D)	2ν ₉ 5730
ν ₃ 825	ν ₁₀ 2940	1580 (b—A)	ν ₄ +ν ₃ +ν ₁ 1575	5778 (c—C)	2ν ₈ +ν ₉ 5749
ν ₄ 900	—	3007 (c—A)	ν ₃ +ν ₈ +ν ₈ 3016	5819 (d—B)	ν ₉ +ν ₁₀ 5805
ν ₅ 1041	—	4308 (a—D)	ν ₁ +ν ₅ +ν ₁₀ 4301	7159 (c—D)	2ν ₈ +ν ₈ 7172
ν ₆ 1150	—	4351 (b—C)	ν ₂ +ν ₅ +ν ₁₀ 4336	7204 (d—C)	ν ₇ +2ν ₁₀ 7195
ν ₇ 1315	—	4393 (c—B)	ν ₈ +ν ₁₀ 4382	8585 (d—D)	3ν ₉ 8595

CONCLUSIONS

The results included in the above Tables indicate the fruitfulness of the new technique in obtaining Raman frequencies of the solvents in presence of some suitable substances which might act as optical catalysers. The agreement between the Raman frequencies obtained in the present case and those by direct method due to other authors is quite satisfactory. Prosad and Bhattacharyya have however obtained still better agreement which may be due to the fact that the optical catalyser used by them *viz.*, $\text{Er}(\text{NO}_3)_3$ and KMnO_4 have sharper absorption bands than anthracene and phenanthrene.

It may be worthwhile adding here that the existence of the phenomenon of optical catalysis has been supported by Hartley from the considerations of the classical theory of Raman effect. He has further predicted the effect of temperature and irradiating frequencies on the efficiency of the optically catalytic action of a particular substance. More work remains to be done in order to bring out the exact picture of the mechanism involved in the process and substantiate the predictions made by Hartley referred to above.

In the end, I would like to record my gratefulness to Principal K. Prosad, O.B.E., I.E.S., for his valuable suggestions.

PHYSICS DEPARTMENT,
SCIENCE COLLEGE, PATNA.

REFERENCES

- Anantakrishnam, 1936, *Indian Acad. Sci. Proc.*, **3**, 70.
Andant, Lambert and Lecomte, 1934, *Comptes Rendus*, **198**, 1316.
Banerji and Mishra, 1937, *Zeits. f. Phys.*, **106**, 669.
Collins, 1939, *Phys. Rev.*, **55**, 470.
Glockler, 1943, *Reviews of Modern Physics*, **15**, 160.
Hartley, 1937, *Nature*, **139**, 329.
Hibben, 1939, *The Raman effect and its chemical applications*.
Prosad and Bhattacharyya, 1939, *Zeits. f. Phys.*, **113**, 637.
Prosad and Bhattacharyya, 1936, *Nature*, **138**, 510.
Prosad, Bhattacharyya and Chatterji, 1935, *Zeits. f. Phys*, **98**, 324.
Sambursky and Wolfsohn, 1940, *Faraday Soc. Trans.*, **36**, 423.

INFLUENCE OF TEMPERATURE ON THE RAMAN BANDS OF H_2O , D_2O AND HDO

By I RAMAKRISHNA RAO

AND

N. RAJESWARA RAO

(Received for publication, September 17, 1943)

ABSTRACT. The experimental investigations on the structural variations with temperature, of the Raman bands of H_2O , D_2O and HDO reveal that (1) The HDO bands are narrower and sharper than the bands due to either H_2O or D_2O , (2) At the higher temperature, the maximum of the bands has a larger frequency in all cases than at the lower temperature except for D_2O , (3) The intensity of the band on the lower frequency side diminishes with temperature in all cases, (4) The intensity on the higher frequency side is greater at the higher temperature, than at the lower temperature for all the bands except for D_2O , (5) The total intensity of the HDO bands, taken as represented by the height of the maximum, or by the area of the intensity distribution curves is invariably less than that for the H_2O or D_2O bands.

These results are explained on the basis of the polymerisation of all the three types of liquids. The difference in the structure and intensity of the HDO on the one hand and the H_2O and D_2O bands on the other is attributed to the influence of the large proportion of H_2O and D_2O present in the former case and to the probable smallness of the specific intensity of the HDO band.

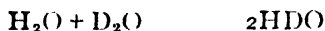
INTRODUCTION

It is well known that the Raman spectrum of water is unique in that it consists of a principal band which is very broad and diffuse, in contrast to most other liquids which give rise to sharp Raman lines. Its isotopic counterpart D_2O is exactly similar in this respect. In previous investigations by Rao (1934), on the structure of these Raman bands, the width and diffuseness were explained on the basis of the polymerisation of both water and heavy water. This explanation was supported by a study of the variation in the structure of these bands with temperature. The problem of the mutual influence of water and heavy water was later investigated by Rao and Rao (1940) and the following results were obtained. In a mixture containing equal proportions, by volume, of H_2O and D_2O , the Bands were found to be less broad and diffuse than those corresponding to the pure liquids. The shape of the D_2O band was very much altered in the mixture, the maximum of the component of the band with smaller frequency, so prominent in D_2O , being completely absent and replaced by an inflexion. In pure water, there was no corresponding maximum at shorter frequency, but the inflexion, in this position, which was distinct enough to

indicate the superposition of a second band over the central and more prominent component, disappeared in the mixture. This change, in the case of water, was similar to that obtained by Rao (1931) and by C. S. Rao (1934) with addition of dissolved substances.

On comparing the intensity of each band in the mixture with that for the pure liquid, it was found that, while for D_2O the intensity increased by 50% from the pure state to the mixture, there was no corresponding change for H_2O . These changes were explained as arising out of the formation of HDO , a compound intermediate between H_2O and D_2O .

A study of this intermediate compound was then taken up by Y. P. Rao (1942). But the mixture with equal proportions of the two components was not suitable for such a study. Assuming Urey and Rittenberg's (1933) value 3.28 for the equilibrium constant in the reaction



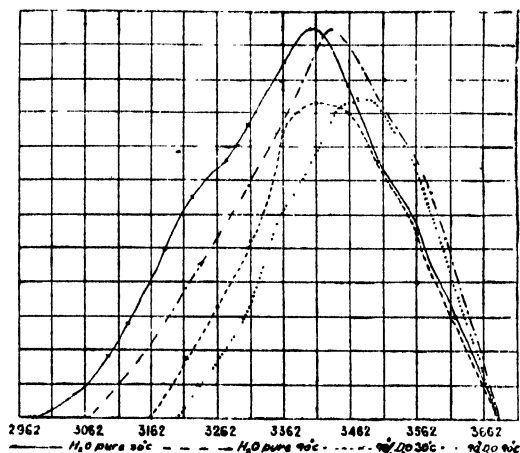
it was found that proportions of 1:9 and 9:1 are most suitable for such a study, since the relative amounts of HDO to H_2O on the one hand and of HDO to D_2O on the other were 17.8:1.1 in each case. In the Raman spectra of these mixtures, the band corresponding to HDO could thus be obtained without superposition of the H_2O or D_2O bands on it with any appreciable intensity. The two principal frequencies of the HDO band were found to be 2523 and 3363 cm^{-1} . These bands were however less broad than those of the pure substances independently.

An interesting point worth investigation is the temperature variation of the structure of the HDO bands. The present communication describes results on this aspect of the behaviour of these bands.

EXPERIMENTAL

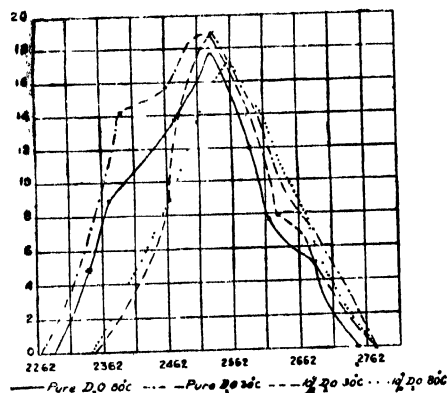
The same mixtures (1:9 and 9:1) of H_2O and D_2O are taken for this. On account of the longer exposures that are necessary to bring out the Raman bands of HDO with sufficient intensity, all traces of the superposed continuum are to be eliminated. For this purpose, the mixtures were distilled in vacuum directly into the Wood's tube, leaving only a small residue so that any possible differences in the relative proportions of H_2O and D_2O in the distillate and the residue will not bring about any alteration in the former from the required values of 1:9 and 9:1. With the usual experimental arrangement, the Raman spectra of these mixtures are obtained at temperatures of 30° and 80°C, for comparison of the changes in the HDO bands with those for H_2O and D_2O taken at these temperatures. For a quantitative study of these changes, the exposure with the mixture and each of the pure liquids were made inversely proportional to their relative concentrations, viz., 81.9:17.8 so that any differences in the relative intensities of these bands are due mainly to the inherent differences in the bands themselves and not to any differences in their molecular

concentrations. The Raman spectra are microphotometered and the intensity distribution of the bands is calculated, and the results are given in Figs. 1 and 2. These intensities are determined in the usual manner by taking on the same photographic plate along with the spectra, the density marks with a Zeiss step-filter, the intensity due to the continuum being eliminated in each case.



Intensity distribution curves of the Raman Bands of H_2O and HDO with intensity against Raman frequency.

FIG. 1



Intensity distribution curves of the Raman Bands of D_2O and HDO with intensity against Raman frequency.

FIG. 2

The following table containing the frequencies and intensities clearly illustrates the results :—

TABLE I

Raman bands of H_2O , D_2O and HDO

	Raman frequencies in cm^{-1} .					
	30°C			80°C		
	Position of maximum	Intensity	Extent of band	Position of maximum	Intensity	Extent of band
H_2O	3397	23.0	2987-3687	3442	23.0	3057-3687
HDO						
OH Oscillation	3412	18.8	3162-3687	3487	18.8	3202-3687
HDO						
OD Oscillation	2532	18.0	2342-2777	2562	17.6	2362-2777
D_2O	2532	19.0	2262-2777	2532	17.6	2262-2777

RESULTS

The following features are clearly evident from the intensity distribution curves :—

1. The HDO bands are narrower and sharper than the bands due to either H_2O or D_2O .
2. At the higher temperature the maximum of the bands has a larger frequency in all cases than at the lower temperature except for D_2O .
3. The intensity of the band on the lower frequency side diminishes with increasing temperature in all cases.
4. The intensity on the larger frequency side is greater at the higher than at the lower temperature for all the bands except for D_2O .
5. Total intensity of the HDO bands, taken as represented by the height of the maximum or by the area of the intensity distribution curves is invariably less than that for the H_2O or D_2O bands.

EXPLANATION OF THE RESULTS

The Raman bands of water and heavy water and their structural changes with temperature have been explained in the previous papers on assuming that both these liquids are highly polymerised, the relative proportions of the polymers changing with change of temperature. On account of the similarity in the valence forces between these two liquids and HDO, the latter should reveal similar changes in constitution with temperature. One important feature that is observed in this investigation is the narrowness of the HDO band compared to those of H_2O and D_2O .

In fact the HDO band here appears more like the H_2O bands obtained by Cross, Burnham and Leighton (1937) for temperatures much above the boiling point and in the neighbourhood of the critical temperature. It was reported by these authors that with increasing temperature approaching the critical temperature, the water band gets narrower. A similar effect, on the Raman band of water, was reported by one of us and later by C. S. Rao with increasing concentration of a dissolved substance. In the mixtures of H_2O and D_2O used in this work, HDO behaves, obviously, like the solvent water in the former work, the solute in this case being H_2O or D_2O . Since the concentration of the solute is much greater than the solvent itself, being in the ratio of 81.9 : 17.8, the effect in the case of HDO is greatest. It would have been interesting to compare the band for pure HDO with that for the two mixtures studied here, but till now there is no known process by which this compound can be obtained free from both H_2O and D_2O . Hence, such a comparison is not possible.

The increase in frequency of the maximum of the HDO band with temperature is similar to the effect obtained with H_2O . The latter was explained, in the previous investigation, as arising out of variation in the relative intensities of the three components comprising the H_2O band. With increasing temperature, the smaller frequency component, arising out of the higher polymer, diminishes

in intensity and the larger frequency component corresponding to the lower polymer increases. A similar explanation applies to the changes in the position and intensity of the HDO band, if this substance is also assumed to be highly polymerised. As in the case of H_2O , increasing temperature should bring about a diminution in the proportion of the higher polymers, resulting in a diminution in the intensity of the shorter frequency side of the HDO band arising out of this polymer. This result may therefore be responsible both for the shift in the maximum of the band and for its getting narrower on the shorter frequency side, the effects 2 and 3 summarised in a previous para.

The increase, with temperature, in the intensity of the larger frequency side of the HDO band may similarly arise out of increase in the relative proportion of the monomer giving rise to this component. This increase may also be partly responsible for the shift of the maximum of the band towards this side.

In both the mixtures, it is found that the HDO band is smaller in intensity than the H_2O or D_2O bands, though the times of exposure are made inversely proportional to the HDO, H_2O and D_2O contents. The HDO band in either case is superposed by the H_2O and D_2O bands arising out of the residual amounts of H_2O and D_2O in both the mixtures. The contribution to the intensity of the HDO band due to these residual amounts should be $1.1/17.8$ in each case. On this account, the HDO band ought to have been more intense than the bands due to H_2O and D_2O . But the effect observed is just the reverse of this. The above comparison is however, made on the assumption that the specific intensities (the intensity per molecule) of all these bands are the same. It is difficult to say how far this assumption is justified. In fact, the effect, in which the HDO bands are actually found to be smaller in intensity than the H_2O or D_2O bands, an effect which is contrary to what should be expected from the above argument, is probably due to the inapplicability of the above assumption. The specific intensity of the HDO bands may be smaller than for either H_2O or D_2O . If the bands were sharp and not diffuse and broad as is actually found, it would have been possible to evaluate the specific intensities. But, as it is, this is not possible, on account of various disturbing factors like the influence of the H_2O and D_2O present in the mixtures, in addition to that due to the polymers of HDO.

REFERENCES

- Cross, Burnham and Leighton (1937), *Journ. Amer. Chem. Soc.*, **59**, 1134.
Rao, C. S. (1934), *Current Science*, **3**, 154.
Rao, I. R. (1931), *Proc. Roy. Soc.*, **130**, 489.
Rao, I. R. and Rao, Y. P. (1940), *Ind. Journ. Phys.*, **14**, 135.
Rao, I. R. (1934), *Proc. Roy. Soc.*, **146**, 489.
Rao, Y. P. (1942), *Ind. Journ. Phys.*, **16**, 205.
Urey and Rittenburg (1933), *Journ. Chem. Phys.*, **1**, 137.

THE λ 3338 BAND OF OD*

By M. ISHAQ

(Received for publication, December 18, 1943)

ABSTRACT. The λ 3338 band of OD has been photographed in the 2nd order of a 10-foot concave grating. The band is similar to that of OH at λ 3428 which is attributed to a $^2\Sigma^+ \rightarrow ^2\Pi_{inv.}$ transition. An analysis of the rotational structure has been made and the values of the rotational constants determined and compared with those of the corresponding OH band

EXPERIMENTAL

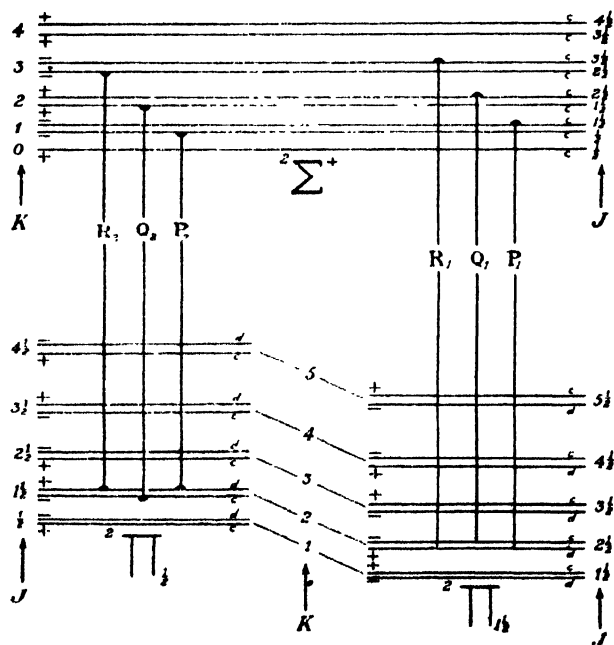
The discharge tube and the method of excitation have already been described (Ishaq, 1937). The heavy water was supplied by the Imperial Chemical Industries, Ltd., London, and was 99.2 per cent. pure.

The band was photographed in the 2nd order of a 10-foot concave grating at the Imperial College, London. The dispersion was about 2.5 Å. per mm. The time of exposure was about two hours.

Wave-lengths measurements were made by comparison with the iron arc. The iron standards were taken from the Transactions of the International Astronomical Union, 4, 1933, and from Kayser's Handbuch der Spectroscopie, Vol. VII.

THE STRUCTURE OF THE BAND

The structure is similar to that of OH band at λ 3428 which is attributed to a $^2\Sigma^+ \rightarrow ^2\Pi_{inv.}$ transition. The main branches are identified which are shown in the energy-level diagram given in the figure.



* Communicated by the Indian Physical Society.

Rotational term difference for the $^2\Sigma$ state

The main branches are observed. The satellites corresponding to the spin-doubling of levels are not resolved. Therefore the rotational levels of this state are treated as singlets.

The rotational term differences,

$$\Delta_2 F'(K) = F'(K+1) - F'(K-1),$$

are obtained from the combinations

$$\begin{aligned}\Delta_2 F'(K) &= R_1(K+1) - P_1(K+1) \\ &= R_2(K+1) - P_2(K+1).\end{aligned}$$

These intervals are given in Table I.

TABLE I

Rotational term differences for the $^2\Sigma$ state

K	$R_1(K+1) - P_1(K+1)$	$R_2(K+1) - P_2(K+1)$	K	$R_1(K+1) - P_1(K+1)$	$R_2(K+1) - P_2(K+1)$
1	90.51	89.80	9	374.65	374.31
2	126.32	126.16	10	409.01	409.05
3	162.73	162.02			
4	198.48	198.19	11	443.45	442.95
5	233.93	233.68	12	477.17	476.69
			13	510.69	510.48
6	269.58	269.16	14	543.43	543.36
7	304.89	304.34	15	575.39	576.17
8	339.80	339.53	16	608.01	608.43

Rotational term differences for the $^2\Pi$ state

The $^2\Pi$ state has two sub-states $^2\Pi_{1/2}$ and $^2\Pi_{3/2}$, which are split up into two close levels on account of Λ -doubling.

The rotational term differences

$$\Delta_1 F''(K + \frac{1}{2}) = F''(K+1) - F''(K)$$

are evaluated from the following combinations:—

$$\begin{aligned}^2\Pi_{1/2} \quad & \Delta_1 F''_{1cd}(K + \frac{1}{2}) = R_1(K) - Q_1(K+1) \\ & \Delta_1 F''_{1dc}(K + \frac{1}{2}) = Q_1(K) - P_1(K+1) \\ ^2\Pi_{3/2} \quad & \left\{ \begin{aligned} \Delta_1 F''_{2cd}(K + \frac{1}{2}) &= R_2(K) - Q_2(K+1) \\ \Delta_1 F''_{2dc}(K + \frac{1}{2}) &= Q_2(K) - P_2(K+1) \end{aligned} \right.\end{aligned}$$

The values of these differences are given in Table II.

TABLE II
Rotational term differences for the $^2\Pi$ state

$^2\Pi_{1/2}$ state.			$^2\Pi_{3/2}$ state	
K.	$R_1(K) - Q_1(K+1)$	$Q_1(K) - P_1(K+1)$	$R_2(K) - Q_2(K+1)$	$Q_2(K) - P_2(K+1)$
1	44.78	10.19	30.71	30.51
2	63.48	63.23	50.21	50.90
3	81.62	81.74	71.20	70.99
4	100.55	99.72	91.03	90.73
5	118.73	117.79	110.27	110.25
6	137.17	136.23	129.86	130.41
7	155.94	154.86	149.10	149.72
8	174.42	172.71	168.32	168.82
9	193.01	190.81	187.07	187.74
10	211.62	208.68	206.60	206.38
11	229.95	226.76	225.62	224.85
12	248.70	244.48	243.85	243.15
13	266.61	261.97	262.13	261.11
14	284.59	279.56	280.82	279.00
15	302.25	296.67	298.61	296.57
16	319.33	314.16	316.32	314.07
17	337.06	—	334.31	331.65
18	355.37	—	351.54	347.98
19	373.76	—	368.43	365.00
20	392.30	—	384.92	382.35
21	410.17	—	402.52	397.11
22	428.77	—	418.91	412.93
23	—	—	435.39	428.92
24	—	—	451.57	444.03
25	—	—	467.46	458.92
26	—	—	483.02	473.72
27	—	—	—	488.04

Λ -Doubling in $^2\Pi$ state.

As

$$\begin{aligned} & \Delta_1 F''_{d,c}(K + \tfrac{1}{2}) - \Delta_1 F''_{e,d}(K + \tfrac{1}{2}) \\ &= [F''_{d,c}(K+1) - F''_{e,c}(K+1)] + [F''_{d,c}(K) - F''_{e,c}(K)] \\ &= \Delta v_{d,c}(K+1) + \Delta v_{d,c}(K) = 2\delta_{d,c}(K + \tfrac{1}{2}). \end{aligned}$$

Therefore the differences between the values of $\Delta_1 F''_{d,c}(K + \tfrac{1}{2})$ and $\Delta_1 F''_{e,d}(K + \tfrac{1}{2})$ are a measure of Λ -doubling.

The quantity $\delta_{d,c}(K + \tfrac{1}{2})$ is the mean of the Λ -doubling in the levels $F''(K+1)$ and $F''(K)$. Their values are given in Table III.

TABLE III. Λ -Doubling

K	$^2\Pi_{1/2}$ state	$^2\Pi_{3/2}$ state	K	$^2\Pi_{1/2}$ state	$^2\Pi_{3/2}$ state
1	+0.21	-0.10	10	-1.47	-0.16
2	-0.16	+0.35	11	-1.60	-0.39
3	-0.08	-0.11	12	-2.11	-0.35
4	-0.42	-0.15	13	-2.82	-0.51
5	-0.47	-0.01	14	-2.52	-0.61
6	-0.42	+0.28	15	-2.79	-1.02
7	-0.54	+0.31	16	-2.59	-1.08
8	-0.54	+0.25	17	—	-1.33
9	-1.11	+0.06			

CALCULATION OF THE ROTATIONAL CONSTANTS

1. The term differences for the $^2\Sigma$ state are well represented by the energy function

$$F'(K) = B'_v K(K+1) + D'_v K^2(K+1)^2 + \dots$$

with values of B'_v and D'_v given in Table IV.

The differences are given by

$$\Delta_2 F'(K) = (4K+2) [B'_v + 2D'_v(K^2 + K+1) + \dots]$$

2. For the calculation of the rotational constants of the $^2\Pi$ state, the formula due to Hill and Van Vleck (1928) has been used :

$$F(J) = B[(J+\frac{1}{2})^2 - \Lambda^2 \pm \frac{1}{2}\{4(J+\frac{1}{2})^2 + \frac{A}{B}(\frac{A}{B} - 4)\Lambda^2\}^{\frac{1}{2}}] + \dots$$

For $^2\Pi$ state, $\Lambda = 1$

Splitting the formula into two parts, we have

$$F_1(J) = B[(J+\frac{1}{2})^2 - 1 + \frac{1}{2}\{4(J+\frac{1}{2})^2 + \frac{A}{B}(\frac{A}{B} - 4)\}^{\frac{1}{2}}] + \dots$$

$$F_2(J) = B[(J+\frac{1}{2})^2 - 1 - \frac{1}{2}\{4(J+\frac{1}{2})^2 + \frac{A}{B}(\frac{A}{B} - 4)\}^{\frac{1}{2}}] + \dots$$

On summation and adding a term containing D,

$$F_1(J) + F_2(J) = 2B[(J+\frac{1}{2})^2 - 1] + 2D[(J+\frac{1}{2})^2 - 1]^2 + \dots$$

The first differences

$$\Delta_1 F_1(J) + \Delta_1 F_2(J) = 4(J+1) [B + D(2J^2 + 4J + \frac{1}{2}) + \dots]$$

The rotational constants B'' and D'' given in Table IV are calculated by the help of the above equation.

TABLE IV.
Rotational constants

$V', V'' \Lambda$	B'_v	D'_v	B''_v	D''_v
OD (0, 1) 3338	9.038	-0.673×10^{-3}	9.594	-0.395×10^{-3}
OH (0, 1) 3428	6.924	-1.93×10^{-3}	17.824	-1.85×10^{-3}

The values for OH are taken from Tanaka and Koana (1933).

For the calculation of A, take the difference of $F_1(J)$ and $F_2(J)$:—

$$F_1(J) - F_2(J) = B \left\{ 4(J+\frac{1}{2})^2 + \frac{A}{B} \left(\frac{A}{B} - 4 \right) \right\}^{\frac{1}{2}}$$

Therefore

$$\left(\frac{A}{B} - 2 \right)^2 = \{F_1(J) - F_2(J)\}^2 / B^2 - 4\{(J+\frac{1}{2})^2 - 1\} + \dots$$

The small effects of Λ -doubling are neglected, and the intervals $F_1(J) - F_2(J)$ are given by the combinations

$$F_1(J) - F_2(J) = R_1(J) - Q_2(J) = Q_1(J) - P_2(J)$$

The values of A thus calculated are given in Table V.

TABLE V.
Values of A (cm^{-1})

J	cm^{-1}	J	cm^{-1}
$1\frac{1}{2}$	139.18	$6\frac{1}{2}$	140.22
$2\frac{1}{2}$	139.59	$7\frac{1}{2}$	140.11
$3\frac{1}{2}$	139.92	$8\frac{1}{2}$	141.11
$4\frac{1}{2}$	140.49	$9\frac{1}{2}$	139.27
$5\frac{1}{2}$	140.06	$10\frac{1}{2}$	138.72

TABLE VI(a)

TABLE VI(b)

K	R_1	Q_1	P_1	K	R_2	Q_2	P_2
	ν_{vac}	ν_{vac}	ν_{vac}		ν_{vac}	ν_{vac}	ν_{vac}
1	29951.06 (3)	29915.37 (3)	29897.21 (6)	1	29819.16 (4)	29783.86 (1)	29765.79 (1)
2	960.69 (3)	906.28 (4)	870.18 (2)	2	843.05 (4)	789.45 (3)	758.35 (3)
3	969.37 (3)	897.21 (6)	843.05 (4)	3	864.71 (2)	792.84 (3)	738.55 (2)
4	978.47 (3)	887.75 (6)	815.74 (3)	4	883.87 (3)	793.51 (3)	721.85 (2)
5	986.51 (3)	877.92 (5)	788.03 (3)	5	900.97 (2)	792.84 (3)	702.78 (3)
6	994.06 (3)	867.72 (4)	760.13 (3)	6	916.27 (3)	790.70 (2)	682.59 (2)
7	30000.93 (2)	856.89 (3)	731.55 (2)	7	929.45 (3)	786.41 (3)	660.29 (2)
8	006.92 (3)	844.99 (4)	702.03 (3)	8	941.03 (2)	780.35 (2)	636.60 (3)
9	012.08 (3)	832.50 (4)	672.28 (2)	9	951.06 (3)	772.71 (3)	611.53 (2)
10	016.34 (3)	819.07 (4)	641.69 (3)	10	959.28 (2)	763.39 (2)	584.97 (2)
11	019.40 (2)	804.72 (4)	610.69 (2)	11	966.06 (3)	752.59 (3)	557.01 (2)
12	021.41 (2)	789.45 (3)	577.96 (2)	12	970.69 (1)	740.44 (1)	527.74 (2)
13	022.14 (2)	772.71 (3)	544.97 (2)	13	973.98 (2)	726.84 (2)	497.29 (2)
14	021.41 (2)	755.53 (2)	510.74 (1)	14	976.21 (3)	711.85 (3)	465.73 (2)
15	019.40 (2)	736.82 (2)	475.97 (1)	15	976.21 (3)	695.39 (3)	432.85 (2)
16	015.34 (3)	717.15 (2)	440.15 (1)	16	974.99 (2)	677.60 (2)	398.82 (1)
17	011.00 (1)	696.21 (2)	402.99 (1)	17	972.06 (1)	658.57 (1)	363.53 (1)
18	005.86 (3)	673.94 (1)	—	18	967.32 (1)	637.76 (1)	326.92 (1)
19	29999.92 (1)	650.49 (1)	—	19	960.69 (3)	615.78 (3)	289.77 (1)
20	994.06 (2)	626.16 (1)	—	20	952.43 (1)	592.26 (1)	250.78 (1)
21	986.51 (3)	601.76 (1)	—	21	943.49 (2)	567.51 (2)	210.91 (1)
22	978.47 (3)	576.34 (1)	—	22	932.17 (2)	540.97 (2)	170.49 (1)
23	969.37 (3)	649.70 (1)	—	23	919.11 (1)	513.26 (3)	128.02 (1)
24	959.28 (2)	—	—	24	904.23 (2)	483.72 (2)	084.34 (1)
—	—	—	—	25	887.75 (6)	452.66 (2)	039.69 (1)
—	—	—	—	26	870.18 (2)	420.29 (2)	28993.74 (1)
—	—	—	—	27	—	386.23 (1)	946.57 (1)
—	—	—	—	28	—	350.48 (1)	898.19 (2)
—	—	—	—	29	—	312.45 (1)	—
—	—	—	—	30	—	274.14 (1)	—
—	—	—	—	31	—	233.23 (1)	—

I am glad to associate Mr. D. P. Varshney M.Sc., with this work for the measurement of the plate, analysis and calculations to some extent.

MUSLIM UNIVERSITY
ALIGARH

REFERENCES

- Hill, E. L. and Van Vleck, J. H., 1928, *Phys. Rev.*, **32**, 261.
 Ishaq, M. 1937, *Proc. Roy. Soc. A*, **180**, 110.
 Tanaka, T. and Koana, Z., 1933, *Proc. Phys. Math. Soc., Japan*, **15**, 272.

MASS DETERMINATION OF THE IONISING PARTICLES RECORDED IN PHOTOGRAPHIC PLATES EXPOSED TO COSMIC RAYS*

BY BIBHA CHOUDHURI

ABSTRACT. This paper contains an account of investigations on cosmic rays at high altitudes with photographic plates. A method for the estimation of the average mass of ionising particles producing single tracks in these plates is described. A discussion on the theoretical basis of the method and its limitations is also given.

INTRODUCTION

§1. Evidences have been obtained by a large number of investigators that some special types of photographic plates, when exposed to cosmic radiation at high altitudes can record tracks due to heavy ionising particles. Many of these are single tracks while others are multiples, consisting of two or more tracks radiating from a single point. The single tracks may be due to either charged primary particles or to charged secondaries produced in the emulsion by the action of some component of the primary rays. The multiple tracks are always due to charged secondaries produced in the material of the emulsion under the action of some component of the cosmic ray. The charged secondaries are usually assumed to be protons, produced by nuclear interactions (nuclear evaporation process) between photon and neutron components of the cosmic rays and atomic nuclei. In addition to these proton tracks, other dense ionisation tracks are found which are attributed to multiple charged particles, eg, α particles, etc.

Since 1939, we have been exposing Ilford halftone plates to cosmic radiation at different altitudes, *viz.*, Darjeeling (7000 ft.); Sandakphu (12,000 ft.) and Phari-jong (14,500 ft.). Some were exposed directly to the cosmic rays while others were exposed under different thicknesses of water paraffin and lead. As a result of such absorption experiments some definite information regarding the nature of primary cosmic radiation can be obtained. These primary penetrating particles are believed to be chiefly protons. These results are in course of publication.

During the examination of these plates, the first thing which struck us was, that some of the tracks were curved. These curvatures were evidently due to multiple scattering in the nuclear fields of different atomic particles in the emulsion.

According to our previous experience with proton, α particle and electron tracks in photographic emulsions, we were convinced that these tracks were

* Communicated by Dr. D. M. Bose.

due to some single charged ionising particle having a mass intermediate between proton and electron. In a communication to 'Nature' (Bose & Chowdhuri, 1941), it was shown that from a knowledge of the mean grain spacing along the track-length and their multiple scattering, the average mass of these particles, found in plates exposed under air, can be estimated; it was found to be of the same order of magnitude as that assumed for mesotron, *viz.*, about $200 m_0$.

The method used by us for the determination of the mass of the particle is a statistical one. The average mass of the ionising particles was found also to depend on the nature of the absorbing substance under which the plates were exposed.

In the present paper we propose to discuss in some detail the assumptions underlying the method used by us to determine the mass of the ionising particles and also the limitations of the method used.

In § 2 we have given a discussion of the theoretical basis of the method which has been used by us to estimate the average mass of the ionising particles.

In § 3 we have collected together all the experimental data regarding single ionisation tracks, which appear in plates exposed to cosmic rays under different conditions, and from which the average mass of these particles were determined.

In § 4 an interpretation of the experimental results is given, and in § 5 we have discussed the limitations of the method employed for the determination of the mass of the charged particles.

§ 2. It is known that the characteristics of the tracks of an ionising particle in a photographic emulsion are (i) its range R (ii) the mean grain spacing (m.g.s.) along its tracks length $R/n-1$, where n is the number of silver grains deposited along the track of length R , and (iii) the track curvature, which is measured by the angle between the tangents drawn at the end and the beginning of the track.

In a previous paper by Choudhury (1942-43) (we shall denote it as I), the relation which exists between the first two of these quantities, and the initial energy of the ionising particle has been discussed in detail.

Assuming that the energy loss of the charged particle is due to ionisation only, we have used the approximate integration of the ionisation loss equation given by Heitler and Ma (1940).

$$R = \frac{E^2}{2AMz^2 \log \frac{(\alpha E)}{M}} \quad \dots (1)$$

$$E = \frac{1}{2} M v^2;$$

where E = kinetic energy of charged particle, whose mass is M & nuclear charge ze .

$A = 2\pi\sigma Zr_0^2 mc^4$ $\alpha = 2\sqrt{2}/IZ$; σ = No. of atoms per c.c. of the medium.

Z = nuclear charge.

r_0 = classical electronic radius = e^2/mc^2 .

The mean grain spacing along a track, which is inverse to mean grain number, has been taken to vary inversely as the mean ionisation. Since E/R is the mean ionisation,

$$\text{m.g.s.} \sim v^2/4Az^2 \log \left(\frac{av^2}{2} \right) \quad \dots (2)$$

It follows from the above that if two different kinds of particles like proton and mesotron carrying the same unit charge e and of masses M and μ respectively, have the same m.g.s. along their tracks, then the ratio of their kinetic energies

$$\frac{W_M}{W_\mu} = \frac{M}{\mu} \quad (3)$$

The principle of the method used in estimating the mass of the ionising particles recorded in cosmic ray plates thus depends on the determination of the kinetic energies of protons and of the particles observed in cosmic ray plates having the same m.g.s. We have assumed that these particles are singly charged like protons.

(a) Determination of the energy of proton :

In paper I, a calibration curve connecting the kinetic energies of protons with the m.g.s. along their track lengths was given. It was shown there that for energies above 4 mV, the m.g.s. bears a linear relation to the energy of the protons.

Extrapolating this curve, energies of protons corresponding to different values of m.g.s. can be obtained. In doing so, we have assumed that this linear relation holds good also for higher proton energies. It has yet to be determined how far this linear relation holds good. To judge from the general trend of H & D curves, which Bose (1943), has shown to be roughly of the same nature for the action of photons and of ionising particles on photographic plates, this linearity relation cannot be expected to hold good for very high energy particles.

(b) Determination of the kinetic energy of the particles producing single tracks on the photographic plates exposed to cosmic radiation. As stated previously some of the tracks found in cosmic ray plates are curved due to multiple scattering suffered by the particles traversing the medium.

We have applied the theory of multiple scattering, modified to suit our experimental conditions, to determine the average energy of these particles. We have found it useful in this connection to develop an analogy between the mean displacement of a colloidal particle due to its Brownian motion and the mean deflection of the charged particle due to successive deflections by atomic nuclei traversed by it.

Consider the motion of a Brownian particle due to impacts suffered by it during an interval τ .

We fix our attention to the motion of one such particle and suppose that the motion takes place parallel to one direction only. During the interval τ , let

there be ' n ' number of collisions, which displaces the particle in equal steps of length ' l ', which may be at one instant positive and at another negative; n will be considered to be very large. Then the probability that the particle will be displaced $n/2 - b$ times in the negative and $n/2 + b$ times in the positive directions out of the total n steps will be $\frac{1}{2^n} \frac{n!}{(n/2 - b)!(n/2 + b)!}$, where b is taken to be small in comparison to $n/2$.

After such n collisions the resultant distance traversed by the particle will be $2 \times b l = a$

Now the probability that the particle describes a path between a and $a + da$ will be

$$p(a)da = \frac{1}{\pi s} e^{-\frac{a^2}{2s^2}} \pi s^2 da \quad (4)$$

$$\text{where } s^2 = \frac{2}{\pi} n l^2; n l^2 = \text{mean square of 'a'}; \bar{s} = \sqrt{\frac{2n}{\pi}} \cdot l \quad (4a)$$

Now consider a particle of charge ze traversing the coulomb fields of N nuclei present per c.c. of the material medium, the thickness of which is t . Let Ze be the charge on each nucleus. The particle experiences Nt deflections from its original trajectory. These deflections can take place in any direction. Then using Rutherford's scattering formula for small nuclear deflections, we find that the probability that a particle of charge ze and energy W travelling through a thickness t , is deflected through an angle between Θ and $\Theta + d\Theta$

$$\text{is } P(\Theta)d\Theta = 2\pi Nt \cdot \left(\frac{Zze^2}{W} \right)^2 \frac{d\Theta}{\Theta^3} \quad \text{Where } \Theta \ll 1.$$

Williams (1939) has shown, by considering the effect of shielding of the nuclear field by orbital electrons and of the finite size of the nucleus, that for a system of particles scattered according to the above formula, the average angle of scattering

$$= \left\{ 3 \cdot 69 + 2 \cdot 8 \log \frac{Z^4/3 \cdot \rho t}{A\beta^2} \right\} \left(\frac{Zze^2}{W} \right)^2 \sqrt{Nt} \quad (5)$$

$$\text{It can be written as } \alpha = \sqrt{Nt} \cdot \frac{2}{\pi} \frac{Zze^2}{W} \cdot C \quad \dots (5a)$$

Now according to Williams the distribution of the deflections of a charged particle due to scattering in the coulomb fields of different nuclei will follow the Gaussian law.

The probability that the particle will be deflected through an angle α as a result of Nt number of encounters suffered by it in traversing t thickness of medium consisting of N nuclei per c.c. is given by

$$P(a)da = \frac{2}{\pi a} \cdot e^{-\frac{a^2}{\pi a^2}} da. \quad \dots (6)$$

where \bar{a} is $\frac{2}{\pi}$ times mean square of a .

$$\bar{a} = \sqrt{\frac{2}{\pi} \cdot Nt} \cdot \Theta_0; \text{ (cf. 4a)} \quad \dots (7)$$

Θ_0 is considered to be the elementary angle through which the charged particle is deflected at each of its Nt encounters either in +ve or in -ve directions.

Comparing (5a) and (7) we find that

$$\Theta_0 = C \cdot \frac{Zze^2}{W}$$

Equation (5) has been deduced on the assumption that the forces between charged particle and the atomic nuclei are entirely of coulombian origin and it holds good for charged particles with different spin value, because the spin term effect can be neglected for small angles of deflection. The effect of shielding of nuclear field by the outer electrons and the finite size of the nucleus has also been considered.

The usual method of applying formula (5) is to select a homogeneous group of charged particles, by means of suitable electric or magnetic lens system, and to find out the average angle of scattering of the particles after passing through a thickness t of matter. Thus knowing \bar{a} and W the formula can be used to determine the charge carried by the scattered particle.

APPLICATION TO THE INVESTIGATION OF PENETRATING COSMIC RAY PARTICLES

Recently two investigators Wilson (1940), and Code (1941), have tried to verify the validity of the Gaussian distribution law for the case of fast cosmic ray particles which have suffered multiple scattering. They have applied Williams' formula to the Wilson chamber tracks of penetrating cosmic ray particles which are scattered by given thicknesses of lead, tungsten, etc. Owing to high energies of the particles, they had to use appreciably large thicknesses of scattering materials, leading to a loss of energy of the particles. To overcome this difficulty they have taken the average value W of the energies measured before and after passing through the scattering material. Further they had to deal with an energy spectrum of the incident particles as all of them were not of the same energy; owing to this difficulty of not getting a number of penetrating particles with the same energy W , they have determined the mean value $\overline{W}a$ rather than \bar{a} for a constant W . And they have used the following modified distribution formula

$$p(wa)d(wa) = \frac{2}{\pi(\overline{W}a)} \cdot e^{-\frac{(wa)^2}{\pi(\overline{W}a)^2}} d(wa) \quad (8)$$

In Wilson's investigation, particles of energy range between 2×10^8 to 10^9 eV traversing 1 cm. thick lead have been considered. F. Code used 3.8 cm. Tungsten scatterer for particles of average energy 10^9 eV. It is found that there are always a certain number of particles which show anomalous scattering. A detailed investigation of such cases is expected to furnish information regarding the non-coulombian interaction forces between the primary particles and atomic nuclei.

APPLICATION TO THE PRESENT INVESTIGATION

In our experiment with photographic plates, we have measured angles of deflections due to multiple scattering for different tracks with different m.g.s., (which is a measure of the energy of the particle) all of which are not of the same lengths.

So in applying Williams' formula to the case of ionising particles observed in photographic plates, we find that the particles considered neither traversed the same thickness t nor were they of the same energy W . It is not possible to select out of them a number of tracks all of the same length t with the same m.g.s. and to use such tracks for the determination of α the average angle to scattering. So we tried to apply the scattering formula in a modified form. Using such method we have determined the mass of ionising particles which are found to be of the order of the mass of mesotron.

Assuming that the angles of deflection due to multiple scattering follows Gaussian distribution law, it can be shown that if we suitably select the conditions of our experiment, so as to make α large, then it follows that under such conditions it is highly probable that the individual values of α will not deviate appreciably from the average value of $\bar{\alpha}$. Under such conditions, the deviation of an observed angle of scattering α from its mean value $\bar{\alpha}$ is

$$\delta = \frac{\alpha - \bar{\alpha}}{\bar{\alpha}} \ll 1 :$$

at the same time $\alpha - \bar{\alpha} = \delta \bar{\alpha} \gg 1$. The probability of occurrence of any angle α is given by ⁶

$$P(\alpha) d\alpha = P(\bar{\alpha}) e^{-\frac{\alpha^2 \delta^2}{2}} d\alpha \quad (9)$$

When the experimental conditions are so chosen as to satisfy the above relation any value of α obtained will be so near the mean value $\bar{\alpha}$ that we shall obtain satisfactory values for the mass of the scattered particles if in (5) we substitute

α for $\bar{\alpha}$. Putting $\bar{\alpha} = \beta \cdot \frac{\sqrt{Nt}}{W}$ we find the conditions required to be satisfied are,

large Nt and small W . Since particles with long tracks will start with large values of W , the two conditions are not mutually compatible. To overcome this difficulty we have used the following procedure.

We have proceeded first, to sort out particles with energies lying within certain specified limits. Since the m.g.s. along a track is a measure of the energy of the particle producing it, we have classified them according to their m.g.s. The tracks whose m.g.s. lie within a range of 1μ are put together in each group. Due to differences in the inclinations of the tracks to the surface of the film the tracks classified in a single group may not have the same length, *i.e.*, they do not traverse the same thickness of emulsion.

So our next procedure is to sum up the lengths of the tracks in each group and also the angles of deflection suffered by these tracks. Thus if m be the number of tracks included in a particular group then the combined length of all the tracks is $t_0 = \sum_{i=1}^m t_i$ and the total deflection suffered by the particle of track length t_0 is $\alpha_0 = \sum_{i=1}^m \alpha_i$ while the m.g.s. of the combined track will be

$\frac{\sum t_i}{\sum n_i - m}$ where n_i is the number of grains in a track. Now the energy of a particle having the track length t_0 and scattering angle α_0 can be found out by using the formula (5).

In applying the scattering formula we have made another assumption to suit our experimental conditions; since the photographic emulsion is heterogeneous in composition, it is assumed that the actual distribution of different kinds of atoms can be replaced by one kind of atom of mean charge Z and mean atomic weight A .

In equation (5) the atomic number occurs as $\sqrt{Z^2}$ so we have taken the value of Z as the root mean sq. of the atomic numbers of different atoms present in the emulsion, *i.e.*,

$$Z^2 = \frac{\sum Z_k^2 N_k^2}{\sum N_k} \quad (10)$$

where Z_k is the atomic number of the k th element and N_k is the number of atoms of the element per c.c. of the emulsion. The energies of the proton tracks, having m.g.s. equal to those found for the different groups of particles of unknown nature, can be obtained from the calibration curve given in (I). And the average mass of each group of particles is determined by applying eqn. (3).

§ 3. Experimental data :—

In this section we give in some detail the experimental arrangement used and the results obtained from different plates exposed under different conditions.

Our investigation consists of two parts : In the first part we have dealt with plates exposed under air only at Sandakphu (12,000 ft.) and in the second part of the experiment we have collected the data obtained from different plates kept under layers of different homogeneous materials at Sandakphu and at Pharijong.

(i) A number of untreated halftone plates ($70\ \mu$ thick) were exposed under air at Sandakphu on two different occasions. These plates were kept vertically on their long sides.

After development, when examined we observed a number of long single tracks and many multiple star-like tracks. In this paper we have considered only the single tracks in detail. We measured the lengths of these tracks in the emulsion their inclination θ to the surface of the film, the mean grain spacing along each track and the angles of the deflection due to multiple scattering. The actual lengths of these tracks $l/\cos \theta$ were calculated. The number of tracks per sq. cm. were also counted. All these data are given in Table I. From which the average mass of different groups of particles was calculated, following the method discussed in the previous section. In addition to the data given in Table I, the following data are also required for the calculation of the mass of the particles :—

Number of atoms per c.c. of the emulsion, $N = 1.4 \times 10^{22}$

Density of the emulsion $\rho = 2.89$.

Root mean sq. charge $\sqrt{Z^2} = 11.3$.

All these data are taken from paper I.

TABLE I

Plate	Place	No. of Tracks	Range of m.g.s.	m.g.s.	Σl	$\Sigma \theta$	Energy in Mev.		Mass	Average	No. of Tracks per Cm^2 per 100 days.
							Energy calculated	Energy of Proton.			
A	Sandakphu 12,000ft.	12	$6\mu \rightarrow 5\mu$	5.7 μ	0.15 Cm.	18°30'	2.7 Mv.	22.7 Mv.	221	214	55
		22	$5\mu \rightarrow 4\mu$	4.3 μ	0.24 Cm.	61°	1.05 Mv.	12.5 Mv.	160		
		33	$4\mu \rightarrow 3\mu$	3.2 μ	0.31 Cm.	120°	0.6 Mv.	4.2 Mv.	263		
B		10	$5\mu \rightarrow 4\mu$	4.1 μ	0.11 Cm.	39°30'	1.10 Mv.	11.2 Mv.	180	219	17
		25	$4\mu \rightarrow 3\mu$	3.3 μ	0.103 Cm.	60°	.68 Mv.	4.8 Mv.	257		

Time of exposure of Plate A—150 days.

Time of exposure of Plate B—163 days.

It is to be noted here that plates A and B were not equally sensitive to cosmic radiation; they belonged to two different batches of plates procured from England at different times.

ii (a). Effect of placing a layer of hydrogenous material above the plates:—

At Sandakphu a number of plates were kept under (i) 20 cm. water in a galvanized iron box, (ii) 20 cm. paraffin block. Both of these plates were placed vertically; on another occasion, a pair of plates was kept at Pharijong in a hut under a thick wooden roof. Data, similar to these collected for the plates exposed to air, were obtained for each of these plates. Average masses of the particles belonging to each group, which are responsible for single tracks on these plates, were calculated. All these data are given in Table II.

TABLE II

Place	Absorbing layer.	Range of m.g.s.	m.g.s.	ΣI	$\Sigma \theta$	Energy in Mev.		Mass	Average	No. of Tracks per Cm^2 per 100 days.	Ratio of proton Meson numbers.
						Energy calculated.	Energy of proton.				
Sandakphu 12,000 ft.	Water 20 Cm.	$5\mu \rightarrow 4\mu$	4.4 μ	.105 Cm.	$16^\circ 30'$	2.4 Mv.	13.8 Mv.	328	314	30	0.1
		$4\mu \rightarrow 3\mu$	3.4 μ	.23 Cm.	55°	1.06 Mv.	6.0 Mv.	355			
	Paraffin 20 Cm.	$5\mu \rightarrow 4\mu$	4.5 μ	.05 Cm.	9°	3.5 Mv.	14.5 Mv.	440	514	5	0.2
		$4\mu \rightarrow 3\mu$	3.45 μ	.041 Cm.	12°	2.0 Mv.	6.2 Mv.	588			
Pharijong 14,500 ft.	2½ ft. mud and wood	$6\mu \rightarrow 5\mu$	5.65 μ	.11 Cm.	$12^\circ 30'$	3.4 Mv.	22.5 Mv.	276	331	12	.09
		$5\mu \rightarrow 4\mu$	4.4 μ	.08 Cm.	12°	3.0 Mv.	13.8 Mv.	386			
		$4\mu \rightarrow 3\mu$	3.3 μ	.20 Cm.	66°	0.9 Mv.	5 Mv.	332			

Time of exposure of Sandakphu water plate—202 days.

Time of exposure of Sandakphu paraffin plate—163 days.

Time of exposure of Pharijong plate—209 days.

The plate exposed under water at Sandakphu and plate No. A of Table I were from the same batch. The plates exposed under paraffin and those kept of Pharijong were of the same batch as the plate No. B of Table I. The last column in the above table gives the ratio of proton to mestron which must be present in the ionising particles recorded in these plates, to give the average mass found.

ii (b). Effect of placing different thicknesses of lead :—

In their investigations Heitler (1939), and his co-workers noticed that there is an increase in the total number of tracks per unit area when plates were exposed at Jungfraujoch (13,800 ft.) under different thicknesses of lead. The maximum multiplication took place under 1.2 cm. Pb. In our experiment we have placed a number of halftone plates at Sandakphu under different thicknesses lead varying from 0.5 cm. to 5 cm. Pb. We have counted the number of tracks in equal areas of the different plates under each thickness of lead. It was observed that the frequency of tracks per unit area of plate initially increased with the lead thickness. The maximum transition effect was observed at 1.5 cm. Pb. almost coinciding with Rossi's first maximum. Then the frequency of tracks began to fall rapidly to a small value under 5 cm. Pb. Some of these results were discussed in a recent paper by Bose (1942-43). In Table III we have given all the data, from which the average mass of the ionising particles recorded in these plates was calculated. This investigation is being continued.

TABLE III

Time of exposure of lead plates—163 days.

Place	Absorbing layer.	Range of m.g.s.	m.g.s.	α_1	α_2	Energy in Mv.		Mass	Average	No. of Tracks per cm ² 100 days.	Ratio of proton Meson numbers.
						Energy calculated.	Energy of Proton.				
Sandakphu 12,000 ft.	0.5 Lead	6 μ →5 μ	5.46 μ	.03 cm.	7°30'	3.1 Mv.	21.5 Mv.	258	331	11.3	.09
		5 μ →4 μ	4.2 μ	.02 cm.	7°30'	2.15 Mv.	12.0 Mv.	331			
		4 μ →3 μ	3.4 μ	.06 cm.	25°	1.25 Mv.	6.0 Mv.	404			
	1 Cm. Lead.	5 μ →4 μ	4.6 μ	.11 cm.	8°	5.35 Mv.	15.3 Mv.	552	515	14	0.2
		4 μ →3 μ	3.24 μ	.071 cm.	27°	1.29 Mv.	4.6 Mv.	478			
	1.5 Cm. Lead.	5 μ →4 μ	4.3 μ	.077 cm.	12°30'	2.85 Mv.	12.3 Mv.	404	607	21.2	0.25
		4 μ →3 μ	3.52 μ	.09 cm.	14°	2.65 Mv.	6.5 Mv.	736			
	2 Cm. Lead.	5 μ →4 μ	4.4 μ	.13 cm.	17°	2.67 Mv.	13.8 Mv.	350	450	21.2	0.17
		4 μ →3 μ	3.6 μ	.09 cm.	27°	1.42 Mv.	4.7 Mv.	552			
	3 Cm. Lead.	5 μ →4 μ	4.4 μ	.06 cm.	11°	2.8 Mv.	13.8 Mv.	380	356	13.2	0.11
		4 μ →3 μ	3.67 μ	.08 cm.	31°	1.44 Mv.	7.9 Mv.	333			
	5 Cm. Lead.	5 μ →4 μ	4.3 μ	.02 cm.	7°30'	2.66 Mv.	12.3 Mv.	400	341	7	0.1
		4 μ →3 μ	3.4 μ	.043 cm.	30°	.92 Mv.	6.0 Mv.	282			

It is interesting to note here that we have also observed a number of very dense tracks in some of the multiple stars. The m.g.s. of these tracks were found to be less than 2.4 μ . According to the data given in paper I such tracks are due to α - and other multiple charged particles. Single dense tracks were also found. It is not possible to sort out from amongst such dense single tracks those due to α - particles from radio active contaminations from the others produced by the action of the radiations incident on the photographic plates from outside. These tracks have not been included in Table III.

§ 4. DISCUSSION OF THE EXPERIMENTAL RESULTS

Considering Table I, we find that the average masses of the particles are of the order of mesotron mass. We, therefore, conclude that a large number of slow mesotrons of energy 10⁶eV have been recorded in these plates exposed to air at Sandakphu. Further, our records show that in these plates the percentage of protons of energy 10⁷eV, which can produce tracks with the same m.g.s. as slow mesotrons, is very small. It is also found that the average mass of ionising particles observed in photographic plates kept under hydrogenous substances is much greater than mesotron mass. It varies from one and half to two times the mesotron mass.

The method, which we are following here for the determination of the mass of the ionising particles, can give only the average mass of the particles. So if in these plates protons are present in comparatively large numbers than those

found in the plates exposed to air, then there is a great probability that these also be included in different groups along with mesotrons. Thus the higher value of the mass of ionising particles gives a direct evidence that the plates exposed under this special condition have recorded a large number of protons of energy varying from 10^6eV to 10^7eV . We consider that this increase in the number of proton tracks is due to the fact that the penetrating part of the primary cosmic rays, consisting of fast neutrons and protons, traversing the hydrogenous matters produce many recoil protons of energy of the order of 10^7eV . These are recorded in the photographic plates and go to increase the average mass of the particles measured.

Further Table II shows that the frequency of tracks per unit area of these plates becomes smaller in comparison to that observed in the plates exposed to air at the same altitude (Table I). This also shows that a part of the primary component of cosmic ray is largely absorbed in hydrogenous substances; we consider this as a further indication that this part of the primary beam consists of neutrons and protons.

Another interesting information regarding the primary component of cosmic rays at high altitude has been obtained from the data given in Table III. It will be noticed there that the average mass increases gradually with lead thickness, reaching a maximum under 1.5 cm. pb. Then it shows a tendency to decrease with the increase of lead thickness placed above the plates and becomes 1.5 times the value of mesotron mass under 5 cm. pb. This also shows a transition effect under lead with a maximum at 1.5 cm. pb. Thus we see that there is a close relation between the average mass value of the secondary particles and the multiplication effect of the primary radiation in lead.

Such transition effect is now generally accepted to be due to the multiplication of the soft component of cosmic rays by cascade process. We suppose that this soft component which is produced due to multiplication in lead is responsible for the creation of protons and mesotrons, in the respective energy range for which the photographic plates are sensitive to these rays. These are produced in the lead absorbers placed above the plates or in the emulsion of the plates. It is probable that the protons, observed in these plates whose number shows a maximum under 1.5 cm. pb, are mainly produced by those soft secondaries which have energy of the order of critical energy in lead, i.e., $7 \times 10^6\text{eV}$.

By considering the ratio of proton/mesotron, we are convinced that in all of these plates mesotrons are also produced in large numbers.

A little consideration of the data given in Table III will show that the increase in the number of particles recorded per unit area of the plate under two different thicknesses of lead, e.g., under 0.5 and 1.5 cm. respectively, is not due entirely to protons produced by a photo-nuclear process, but a certain number of mesotrons are also produced. There has been a doubling of the number of tracks per unit area, on increasing the lead thickness from 0.5 to 1.5 cm. If all the new tracks were due to protons only, then the calculated

value of the average mass would come out to be of the order of 1000 m_0 , against the measured value of 607 m_0 .

§ 5. LIMITATION OF THE METHOD

We have seen in §3 that the average mass of the particles producing ionisation tracks in photographic plates exposed to air at Sandakphu, is very near that of the accepted value of mesotron mass. In this section we shall discuss some of the limitations of the method used here, which at present preclude its application as a precision method for mesotron mass determination. The principal theoretical drawbacks of the method are (i) the procedure of adding together of the individual track deflections α_i to a resultant α_0 and (ii) the substitution of this α_0 for $\bar{\alpha}_0$ in equ. (5), for the determination of the average energy of the ionising particle producing tracks with a certain value of m.g.s. We shall now discuss whether by adding together the characteristics of an increasing number of tracks, the accuracy of the mass determination is correspondingly increased.

We suppose $\nu_1, \nu_2, \nu_3, \dots, \nu_i$ be the number of atoms in the thicknesses $t_1, t_2, t_3, \dots, t_i$ of the scattering medium, and we put $t_0 = \sum t_i$; $\nu_0 = \sum \nu_i$ and $\alpha_0 = \sum \alpha_i$. Further we denote by $\bar{\alpha}_0$ the average angle of scattering of a large number of tracks each of length t_0 . In each of the strips the deflection $\alpha_i \sim \nu_i^+ - \nu_i^-$, where ν_i^+ and ν_i^- are the number of positive and negative deflections suffered by the particles, so that $\nu_i = \nu_i^+ + \nu_i^-$ and $\overline{\nu_i^+ - \nu_i^-} = \sqrt{\frac{2}{\pi} \cdot \frac{\nu_i}{\nu_i^+}}$

In a track of length t_0 which is broken up into m small strips t_1, \dots, t_m the total scattering produced is the algebraic sum of the deflections produced in the individual strips, i.e., in some the deflections will be in the positive and in others in the negative direction. But in the procedure followed by us, we add together the absolute values of the deflections produced in the strips t_1, \dots, t_m ; when the number of strips added together is small, the discrepancy between $\alpha_0 = \sum \alpha_i$ and $\bar{\alpha}_0$ will not be large; on the other hand when the deflection due to a large number of strips is added together, the value of α_0 increases monotonously with t_0 while $\bar{\alpha}_0$ will increase with $\sqrt{t_0}$. After a certain thickness t_0 has been reached, the value of α_0 will be always greater than $\bar{\alpha}_0$. Since the value of W and ultimately of the mass of ionising particle depends inversely on $\bar{\alpha}$, we expect that for larger values of t_0 , when α_0 becomes greater than $\bar{\alpha}_0$, the calculated values of the mass of ionising particle will diminish.

We illustrate the correctness of our deduction by the following example. We have already obtained estimates of the mass of the ionising particle from the data obtained from two plates A & B exposed to air at Sandakphu. In Table IV we have given the masses calculated from the two plates separately with tracks grouped together under defined limits and also the same have been calculated when the tracks belonging to the same m.g.s. groups in the two

plates have been combined together. It will be seen that mass determined from the combined data always comes out smaller than the masses estimated from the separate data.

TABLE IV

m.g.s.	No. of tracks in			Mass calculated from		
	Plate A	Plate B	Plates A + B	Plate A	Plate B	Plates A + B
6 μ →5 μ	12 (0.15 cm.)	2 (0.02 cm.)	14 (0.17 cm.)	221	not calculated	193
5 μ →4 μ	22 (0.24 cm.)	10 (0.11 cm.)	32 (0.35 cm.)	160	180	130
4 μ →3 μ	33 (0.31 cm.)	15 (0.10 cm.)	48 (0.41 cm.)	263	250	202

In the columns under tracks number in each row the upper figure represents the number of tracks and lower figure in brackets, their total length in cm.

We propose to send up a large number of plates to Sandakphu to be exposed under air, and we shall find out the value of the average mass of the ionising particles for each group of m.g.s. for each of the plates separately. We shall try to find out whether an empirical criterion can be obtained regarding the grouping up of the tracks within certain m.g.s. limits, which will lead to the most consistent values for the mass determination of the ionising particles. It is also necessary to draw fresh proton energy calibration curves for the plates, using a higher range of proton energy than is available to us at present; probably such plates will be calibrated in future by using higher energy protons and α -particles produced by large cyclotrons.

The author is greatly indebted to Dr. D. M. Bose, for many helpful discussions on the theoretical basis of the method of measuring the mass of the penetrating particles described in this paper.

SUMMARY

This paper contains an account of investigations on cosmic rays at high altitudes with photographic plates. A method for the estimation of the average mass of ionising particles producing single tracks in these plates is described. A discussion on the theoretical basis of the method and its limitations is also given.

The following results were obtained :

(1) The average mass of the ionising particles producing single tracks on the photographic plates kept exposed to air at Sandakphu approximate to the accepted value for the mass of mesotron. It is found to be 216 m_0 . The energy of these particles is of the order of 10^6 eV. Protons of energy 10^7 eV which produce the same m.g.s. as 10^6 eV mesotron are rare.

(2) In the plates exposed under layers of hydrogenous substances (20 cm. water, and paraffin and $2\frac{1}{2}$ ft. wood and mud) the average mass of the particles is found to be about one and half to two times the mesotron mass. It varies from 340 to 514, which indicates the presence of a comparatively larger number of proton tracks. The cause of this effect has been ascribed to the presence of fast primary cosmic ray penetrating particles like neutrons and protons which traversing the hydrogenous substances produce recoil protons of energy of the order of 10^6 eV to 10^7 eV. These protons have the same m.g.s. as those due to the mesotron recorded on the plates and thus increase the average mass of the recorded particles.

(3) Photographic plates were exposed at Sandakphu under different thicknesses of lead varying from 0.5 cm. to 5 cm. pb. It is found that the average mass of the particles increases to a maximum value under 1.5 cm. pb and then gradually it comes down to 1.5 times the value of mesotron mass under 5 cm. pb. It is concluded that the soft component of primary radiation undergoes multiplication in traversing the lead plates and the secondaries formed thereby cause the emission of heavy ionising particle either in the lead plates or in the emulsion of the photographic plates.

The secondaries having energy of the order of critical energy, i.e., 7×10^6 eV, are probably responsible for the production of protons by some photonuclear process. The ratio of proton-mesotron present in each plate has been calculated. The conclusion is drawn that in the transition layer of lead not only protons but also fresh mesotron are produced.

BOSE RESEARCH INSTITUTE,
CALCUTTA.

REFERENCE

- Bosè, D. M. and Choudhuri, Bibha (1941), *Nature*, **148**, 259.
 Bose, D. M. (1942-43), *Trans. Bose Inst.*, **18**, 55.
 Bose, D. M. (1943), *Ind. Jour. Phys.* **17**, 27.
 Choudhuri, Bibha, paper I (1942-43), *Trans. Bose Inst.*, **18**, 29.
 Code, F. L. (1941), *Phys. Rev.*, **69**, 229.
 Furt h, Reinhold, *Schwankungserseheinungen in der Physik*, 90.
 Heitler, Powell, Fertel (1939), *Nature*, **144**, 283.
 Heitler and Ma (1940), *Proc. Roy. Soc.*, **176**, 368.
 Willams, E. J. (1939), *Proc. Roy. Soc.*, **169**, 539.
 Wilson, J. G. (1940), *Proc. Roy. Soc.*, **174**, 73.

THERMAL CONDUCTIVITY OF WATER *

By M. F. SOONAWALA

(Received for publication, March 10, 1914)

ABSTRACT. Thermal conductivity of water is determined by the periodic flow method of Angstrom. A mean value of 0.00146 is obtained.

The determination of the thermal conductivities of liquids is attended with errors, the principal of which is that due to the convection currents set up. The film method surmounts this difficulty with success, the principal measurement being the quantity of heat passing through the film, for which a number of factors have to be taken into account.

The results of an experiment are reported below in which the periodic flow method is employed to obtain the conductivity of water. A heating coil, C, (Fig. 1) is made of resistance wire of about 3 ohms resistance wound as a flat spiral. This is held horizontal a few centimetres below the surface of water in a fair-sized beaker. One junction, T, of a copper-iron thermocouple was kept projecting out of a glass tube B, the other junction dipping in water in another beaker at room temperature. The glass tube B, was attached firmly to a stand with scale and vernier and could be moved vertically up and down. The thermocouple readings were taken on a sensitive galvanometer. A current of about 1 ampere was passed steadily through the heating coil, C, for about 10 minutes, and then switched off for the same time. This was kept on to produce a periodic heat wave, which travelled down the liquid and was registered by the thermocouple. The thermocouple readings settled down to fairly even periodicity after about half a dozen periods. This was recorded as the scale deflection of the galvanometer in mms.

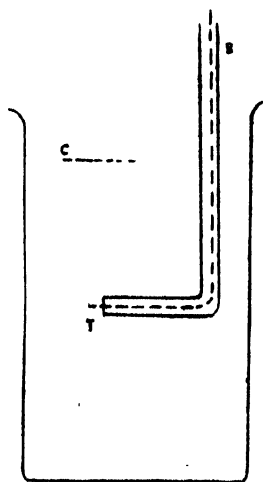


FIG. 1

The water was siphoned out of the beaker, the thermocouple junction, T, lowered a few mms., and the experiment repeated with the same period and heating current as before. The two periodic curves so obtained can be represented by the equations,

$$\theta = A_0 + A_1 \sin (pt + \delta_1) + A_2 \sin (2 pt + \delta_2) + \dots$$

$$\text{and} \quad \theta' = A_0' + A_1' \sin (pt + \delta_1') + A_2' \sin (2 pt + \delta_2') + \dots \quad (1)$$

θ and θ' being the temperatures at the two positions, x , and x' , of the junction, T; and $p = 2\pi/T$, where T is the period of the heat wave. Then,

$$A_1 = a_1 \cdot e^{-\alpha_1 x} \text{ and } A_1' = a_1 \cdot e^{-\alpha_1 x'}; \text{ etc.} \quad \dots (2)$$

giving

$$\alpha_1 l = \log \frac{A_1}{A_1'} \quad (3)$$

As is well known,

$$k = \frac{\pi l^2}{T(\delta n - \delta n') \log \frac{A_1}{A_1'}} \quad (4)$$

Here $l = x - x'$, and $k = K.D/c$, where K is the thermal conductivity, D the density and c the specific heat of the liquid. The variation of temperature with time at any level is approximately simple harmonic, the slow drift of the mean value of θ being also apparent. Fig. 2 shows curves of experiment 4 of Table III. The even harmonics are absent in a flat topped curve of the kind employed, and the influence of the third harmonic is shown as an irregular depression of the curves, A and B, near their maxima and minima. A and B are the experimental curves and C a simple harmonic curve of the same period and of the amplitude of B. The curves were subjected to harmonic analysis for the determination of the amplitudes and phases. The measurement of the phase angles, δ and δ' , requires a word of explanation. Readings of the galvanometer deflection in mms. recorded every minute in experiment 5 of Table III are reproduced here as Table I for the purpose. The first reading is taken the moment the current is stopped in the heating coil. The first set of readings shows that the maximum deflection is seen two minutes after the heating current is switched off; while, in the second set, the maximum follows 6 minutes after the stopping of the heating current.

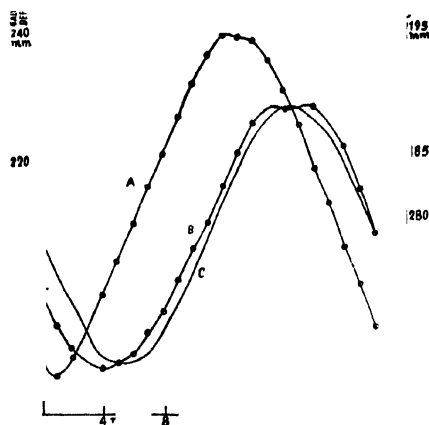


FIG.

TABLE I

210 mm. 214, 217, 216, 213.5, 208, 202, 194, 187, 180; 173, 169.5, 170, 175, 181, 187, 193, 200, 206, 213, 219.
182 mm., 184, 188, 190, 192, 192.5, 193, 192, 189, 185; 181, 177, 175, 173, 174, 174, 175, 177, 179.5, 183, 185.

This can be represented as follows:

In Fig. 3. A refers to the epoch of the first set, measured from the maximum, M. The angle $A' M'$ is $2/20 \times 360^\circ$, as the period is 20 min., and the angle OA' is 54° . B represents the initial point of the second curve, measured as preceding M by 6 min., or $6/20 \times 360^\circ = 108^\circ$. It is the angles OA' , OB' that are measured as phase angles $64^\circ 19'$ and $7^\circ 17'$ by harmonic analysis, the angles being measured with reference to O. Hence, the phase difference, $\delta - \delta'$, in this case is $A' B'$, or $71^\circ 36'$ Table II gives similar set of readings for experiment 4.

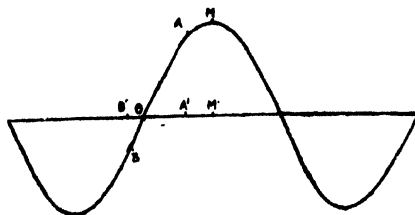


FIG. 3

TABLE II

191 mm., 186, 189, 193, 199, 204, 210 ; 216, 221, 227, 232, 237, 240, 239.5, 239, 236, 231, 225.5, 218.5, 213, 206, 200, 198.

175 mm., 172, 170, 169, 168.5, 169, 169.5, 171.5, 173, 175.5, 178 ; 180, 183, 186, 188, 189.3, 189, 190, 189.3, 188, 186, 182.5, 179.

Here, the phases are 1 min. and 4 min. preceding the maximum ; which correspond to angles 16° and 65° respectively. As calculated from the analysis of the curves, these are found to be $6^\circ 38'$ and $63^\circ 4'$. This gives a phase difference of $56^\circ 43'$. It is from such considerations that $\delta - \delta'$ is calculated. The amplitudes and phase differences obtained by analysis correspond approximately to those of the curves assumed to be simple harmonic. The value of $\delta - \delta'$ is very small in experiment 2, and its result is liable to a greater error. Table III shows the results of six such experiments. Room temperature is shown as t° .

TABLE III

Exp. No.	T (min).	l (cm.)	δ .	δ	$\delta - \delta'$.	$\log A_1/A_1'$.	t ($^\circ\text{C}$).	k .
1	20	0.90	$58^\circ 56'$	$9^\circ 19'$	$68^\circ 15'$	0.501	25.0	0.00154
2	24	0.50	$43^\circ 7'$	$16^\circ 47'$	$26^\circ 33'$	0.401	21.8	0.00129
3	18	0.80	$1^\circ 53'$	$40^\circ 27'$	$38^\circ 52'$	0.761	30.1	0.00157
4	22	0.80	$63^\circ 4'$	$6^\circ 38'$	$56^\circ 43'$	0.432	31.0	0.00156
5	20	0.80	$64^\circ 19'$	$7^\circ 17'$	$71^\circ 36'$	0.418	33.1	0.00140
6	24	0.80	$60^\circ 17'$	$11^\circ 25'$	$71^\circ 42'$	0.345	33.0	0.00141

The method is free of any errors due to measurements of temperatures, temperature gradients, or quantities of heat, or radiation effects. The principal errors would be the convection currents which would be set up above levels in the liquid undergoing periodic heating and cooling. The difference of levels at which the periodic variations of temperature are investigated has necessarily to be reduced to small distances due to this effect as well as due to the fact that the amplitudes of the temperature variation becomes insensibly small for distances greater than a few millimetres. The convection effect would tend to increase the temperatures uniformly, and more so at higher levels nearer the heating coil. This would raise the mean temperature of the levels. As the mean temperature is registered by the amplitude $a_1 e^{-\alpha_1 x}$ of equation (2), this is equivalent to lowering the value of α_1 for a wave of a certain period ; and, therefore, of lowering the value of $\log A'/A_1'$. This would yield higher values of k than the real one. Convection currents, if really strong, would mix up the liquid and destroy all tendency towards regularity. As found in the experiments, the periodicity remains very pronounced even for small temperature amplitudes. The method, though not one of precision, has the merit of simplicity and directness at all stages.

DEPARTMENT OF PHYSICS ;
MAHARAJA'S COLLEGE,
JAIPUR (RAJPUTANA).

REFERENCE

Preston's Theory of Heat (3rd edition), pp. 635-637.

ON THE POLARISED FLUORESCENCE—PART DYESTUFFS IN SOLUTION

By KRISHNADAS CHOUDHURI

(Received for publication, March 14, 1944)

ABSTRACT. The variation of the polarisation of fluorescence of the dyestuffs with the wavelengths of the exciting radiation has been investigated in detail. It is found that the polarisation decreases with the increase in wavelength of the exciting radiation, reaches a negative value and then increases again. The negative value occurs at wavelengths of the exciting radiation characteristic for the molecules of the dyestuff. A comparison of the polarisation curves and the absorption curves of the fluorescent dyestuffs has also been made.

The variation of the polarisation of fluorescence of the dyestuffs with the change of (1) the viscosity of the solution, (2) the temperature of the solution and (3) the concentration of the dyestuff has been investigated experimentally. It has been observed that the degree of polarisation tends to vanish asymptotically at low viscosities or at high temperatures or at high concentrations of the dyestuffs, while the polarisation tends to attain asymptotically a certain maximum value at very high viscosities or low temperatures or at very low concentration of the dyestuff. For a particular solvent this maximum value is dependent on (1) the nature of the dyestuff, (2) the wavelength of the exciting radiation. Besides the investigations mentioned above the average life of the dyestuff molecules in the excited state has also been calculated. The results have been discussed on the basis of Perrin's theory.

INTRODUCTION

The phenomenon of fluorescence of the dyestuffs in solution is quite well known and a lot of experimental investigations has been made during recent years. But the results obtained by the various workers are highly contradictory and the discrepancy is so much wild and wide that they can be considered only as giving the order of the magnitude. This is true of all the dominion of fluorescence, including the phenomena of polarisation of the fluorescent radiation emitted by the dyestuffs in solution.

In view of the contradictory nature of the results obtained by the various workers a systematic measurement was undertaken on the polarisation of fluorescence of a few dyestuffs in solution and its exact dependence on the wavelengths of the exciting radiations, on the temperatures, concentration of the dyestuff in solution and the viscosities of the solvent. For our measurements we have selected a set of dyestuffs which has not been systematically investigated as yet. The present report gives the results of our measurement. The results in the case of the inorganic compounds will be given in a subsequent report.

EXPERIMENTAL ARRANGEMENT

The experimental arrangement adopted in our present investigation is as follows :—Light from a mercury arc, automatic zinc or cadmium arcs, rendered monochromatic with the help of a monochromator or suitable colour filters was focused by a lens on a fused quartz cell containing the fluorescent solution. In order to eliminate the uncertain polarisation introduced by the monochromator a polarising prism of Glan type was introduced between the cell and the lens. Thus the fluorescent light was excited by plane polarised monochromatic radiation. The

partial polarisation of the transverse fluorescent light was measured in the usual way with a double image prism and a nicol (Cornu method). Measurements were also made with a Savart plate and an analyser coupled with a pile of glass plates.

As regards the notation adopted by us, the measurements refer to the fluorescent radiation normal to the plane containing the direction of vibration and the direction of propagation of the incident light. The fluorescent light, as already alluded to, is partially polarised, its vibration along with direction of propagation I_2 being usually less intense than that of vibration I_1 perpendicular to the above direction, the percentage of polarisation is given by the relation

$$P = \frac{I_1 - I_2}{I_1 + I_2} \cdot 100 = p_{100}; \text{ when } I_2 > I_1, P \text{ is negative.}$$

DEPENDENCE OF POLARISATION OF THE FLUORESCENCE ON THE EXCITING WAVELENGTHS.

The fact that the polarisation of the fluorescent radiations emitted by the dyestuffs in viscous solution depends markedly on the wavelength of the exciting radiation was first observed by Fröhlich (1925) and nearly a systematic study was first attempted by Wawilow (1929, 1931) who measured the polarisation of a few dyestuffs (Fluorescein, Eosin, Rhodamine) in glycerine solution, when excited by five different wavelengths. The experimental arrangement used by him was to use the light from the monochromator (which was illuminated by a mercury arc) to excite the fluorescence, and measure the polarisation by the Cornu method. Wawilow assumed that the light issuing out of the monochromator, which was used for the excitation of the fluorescence is perfectly unpolarised: but it can readily be seen (as was observed by Krishnan and Sirker, 1931) if a measurement be made that the light issuing out of the monochromator is in general considerably polarised,—the actual degree of polarisation differing for different wavelengths. This may be explained as arising out of the selective refraction of the two principal vibrations at the refracting faces of the prism, coupled with a rotation of the plane of polarisation on passing through the quartz parts of the monochromator. On the face of this, the results obtained by Wawilow cease to be of much significance. Later on, Mitra (1939), Jablonski (1934) and Griseback (1936) carried out a systematic investigation on the point.

The results of our measurements of the polarisation of fluorescence excited by different wavelengths are given in the following tables. These tables conclusively show that the polarisation generally decreases to a minimum value as the wavelengths of the exciting radiations decrease and then increases on the further decrease of the wavelengths. This minimum value is negative (*i.e.*, $I_2 > I_1$) and is reached when the exciting light is near about $\lambda_{3131} \text{ \AA}$.

Jablonski observed that in the cases of Rose Bengal and other colouring matters in glycerine solutions, the polarisation of the fluorescent radiation progressively decreased with the decrease in wavelengths of the exciting radiation—under the ultraviolet excitation, the polarisation practically vanishes. We are unable to agree with his observation even in the case of Rose Bengal. It seems that Jablonski measured the polarisation of the fluorescent light only for a very few exciting radiations of widely spaced wavelengths and was consequently misled to the wrong conclusions.

It may be mentioned in passing that Griseback observed in the case of eosin that the polarisation attains the maximum negative value at two wavelengths of the exciting radiation instead of at one ($312 \text{ m}\mu$), which was observed by Wawilow and Mitra. But in all the different dyestuffs that have been investigated, we did not observe any such thing.

TABLE I

Percentage of polarisation of fluorescence of a few dyestuffs in glycerine solution

Temperature :—28°C
Concentration :—c gm/c.c.

Wavelengths in $m\mu$	Succ. Fluorescein $c = 5 \cdot 10^{-5}$	Pinakriptol yellow $c = 25 \cdot 10^{-5}$	Acridflavin $c = 8 \cdot 10^{-5}$
546	..	36	..
535	..	40	..
517	..	42	..
509	..	43	..
436	45	41	45
405	45	..	44
365	41	38	40
320	0
313	-10	20	-7
298	-9	-8	..
278	6	0	..
265	20
254	31	12	36

TABLE I—contd.

Percentage of Polarisation of a few dyestuffs in glycerine solution

Wavelengths in $m\mu$	Pinaflavol $c = 05 \cdot 10^{-5}$	Rose Bengal $c = 5 \cdot 10^{-5}$	Succ. Eosin $c = 4 \cdot 10^{-5}$	Erythrosin $c = 4 \cdot 10^{-5}$
546	46	42	39	50
535	43	50
509	49
436	36	38	45	45
405	41
365	26	27	27	24
326	-8	8
313	14	-9	-9	-10
298	-8	..	-7	-5
278	-8
254	20	37	36	35

POLARISED FLUORESCENCE IN OTHER SOLVENTS

We have also measured the polarisation of the fluorescent radiation emitted by these dyestuffs in other solvents. The solvents used were castor oil, collodion-ether mixture, sugar solution, etc. The Tables and curves show beyond doubt that the value of "P" is different for different solvents, the general nature of the graphs practically remains the same as in glycerine.

TABLE II

Percentage of Polarisation of Fluorescence in Castor oil

Concentration :—c gm/c.c.
Temperature :—28°C

TABLE II

Percentage of Polarisation of Fluorescence in collodion-ether mixture

Concentration :—c gm/c.c.
Temperature :—28°C

TABLE III

Percentage of Polarisation of Fluorescence in sugar solution

Concentration of the compounds :—c gm/c.c.
Temperature :—28°C

Wavelength in $m\mu$	Succ. Fluorescein $c = 5 \cdot 10^{-5}$	Succ. Eosin $c = 4 \cdot 10^{-5}$	Acridflavin $c = 8 \cdot 10^{-5}$	Pinaflavol $c = 05 \cdot 10^{-5}$	Wavelength in $m\mu$	Succ. Fluorescein $c = 5 \cdot 10^{-5}$	Succ. Eosin $c = 4 \cdot 10^{-5}$	Acridflavin $c = 8 \cdot 10^{-5}$	Pinaflavol $c = 05 \cdot 10^{-5}$	Wavelength in $m\mu$	Succ. Fluorescein $c = 5 \cdot 10^{-5}$	Succ. Eosin $c = 4 \cdot 10^{-5}$	Acridflavin $c = 8 \cdot 10^{-5}$	Pinaflavol $c = 05 \cdot 10^{-5}$
546	..	35	..	42	546	..	40	..	45	546	..	42	..	41
436	42	40	42	32	436	45	43	42	38	436	43	40	41	36
365	38	25	35	24	365	40	29	40	25	405	41
326	0	-10	326	0	-5	365	35	25	36	26
313	-12	-8	10	-9	313	-12	-8	..	12	326	0	-8
278	5	-9	278	-6	313	-10	-10	-9	8
254	25	30	32	20	254	20	30	33	21	278	6	-7
										254	21	27	30	23

ULTRAVIOLET ABSORPTION OF THE DYESTUFF AND
THE NEGATIVE POLARISATION

The observations of Griseback and Mitra reveal the resemblance of the absorption and the polarisation curves of the fluorescent dyestuffs. Griseback found in the case of fluorescein, eosin and rhodamine B that the maximum negative value for the polarisation was obtained when the dyestuff is excited by radiation of wavelength which corresponds to the junction of the two absorption bands in the ultraviolet. On the other hand Mitra observed the same in the case of fluorescein alone but not in the case of eosin or rhodamine B.

However, as the ultraviolet absorption data are now at our disposal (Chowdhury and Bose, 1943) we can gauge how far contentions of the aforesaid workers are true. In the accompanying graphs are drawn the absorption coefficient curves as well as the polarisation curves superimposed on the same graph :—

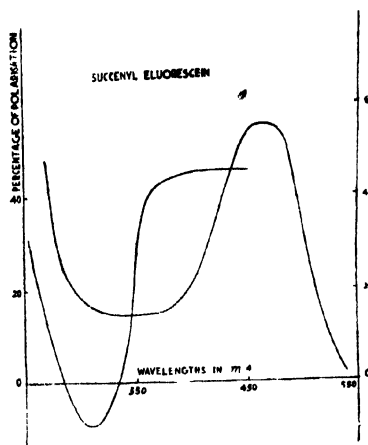


FIG 1

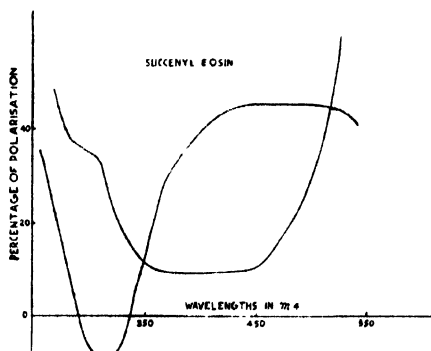


FIG 2

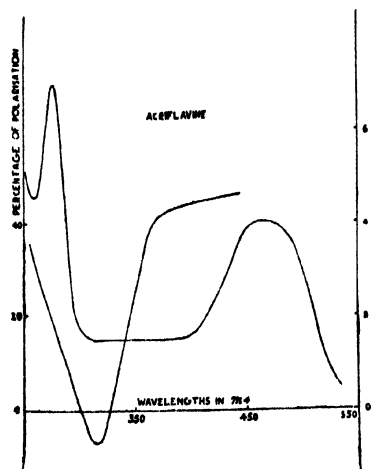


FIG. 3

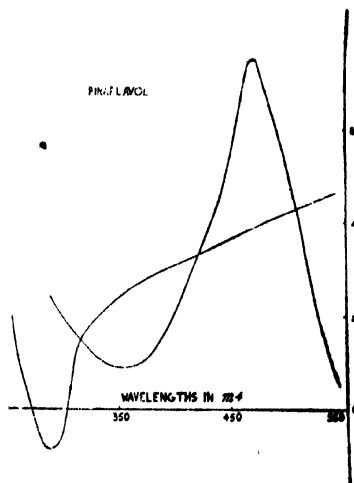


FIG. 4

Fig. 1, 2, 3, 4 show absorption and polarisation curves of Succ. Fluorescein, Succ. Eosin, Pinaflavol, and Acriflavin.

INFLUENCE OF THE VISCOSITY OF THE SOLUTION OF THE POLARISATION

We have already alluded to the fact that the polarisation of the fluorescence depends on the viscosity of the fluorescing solution. This has been experimentally demonstrated by the investigations of Pringsheim (1924), Perrin (1929), Wawilow (1922), Mitra (1938, 1939) and others.

It is first Perrin who gave a satisfactory theory of the dependence of the polarisation on the viscosity of the fluorescing solution, and deduced on the basis of the theory of Brownian rotation of the molecules an expression for the above dependence. The principle of his theory is as follows:—Assuming that the molecules are rigidly fixed in space, if an incident polarised light excites fluorescence in the medium, the polarisation of the fluorescent radiations will have a certain value p_0 which is characteristic of the substance. If, on the other hand, as in actual experiments, the molecules are rotating, the mean square of the angle of rotation per second can be calculated in terms of the viscosity of the solution and its temperature from Einstein's theory of Brownian motion; hence the "expectation" of rotation for a time τ can be calculated, where τ is the mean duration of the molecules in the excited state. The smaller this angle of rotation, the more closely would the actually observed value of the polarisation p approach the ideal value p_0 . Thus for very large viscosity p should reach asymptotically the limiting value p_0 , while at low viscosities the polarisation ought to reach again asymptotically zero value.

TABLE IV

Polarisation of Acriflavin in glycerine-water mixtures. Exciting wavelength:— λ 4358 Å.

Percentage by wt. of glycerine	Viscosity in poises	Percentage of Polarisation	
		$c = 3 \cdot 10^{-5}$ gm/c.c.	$c = 80 \cdot 10^{-5}$ gm/c.c.
98	4.56	44	45
90.9	1.65	38	42
83.3	.611	30	34
76.9	.367	23	28
71.4	.185	17	22
66.6	.127	12	17
62.5	.097	8	12
58.5	.070	5	9
51.2		almost zero	5

TABLE V

Percentage of Polarisation of Acriflavin in glycerine-water mixtures. Exciting wavelength:— λ 3650 Å

Percentage by wt. of glycerine	Viscosity in poises	Percentage of Polarisation	
		$c = 3 \cdot 10^{-5}$ gm/c.c.	$c = 80 \cdot 10^{-5}$ gm/c.c.
98	4.56	40	42
90.9	1.65	34	38
83.3	.611	25	30
76.9	.367	18	23
71.4	.187	11	15
66.6	.127	6	9
62.5	.097	—	5

We shall quote here only the final expression obtained by Perrin, viz.,

$$\frac{1}{p} = \frac{1}{p_0} + \frac{1}{p_0} \cdot \frac{R\theta}{V\eta} \tau.$$

where p is the degree of polarisation observed under the actual condition of the experiment and p_0 the value for the same molecules when they are not allowed to rotate from their initial

orientations. R is the gas constant, V , the gram-molecular volume, η the co-efficient of viscosity and θ the absolute temperature and τ is the mean duration of the fluorescing molecules in the excited state.

TABLE VI

Percentage of Polarisation of Erythrosine in glycerine-water mixtures.

Exciting wavelength:—
 λ 4358 Å

Concentration:—
 $2 \cdot 10^{-5}$ gm/c.c.

TABLE VII

Percentage of Polarisation of Rose Bengal in glycerine-water mixtures.

Exciting wavelength:—
 λ 4358 Å

Concentration:—
 $1 \cdot 2 \cdot 10^{-5}$ gm/c.c.

TABLE VIII

Percentage of Polarisation of Succ. Fluorescein in glycerine-water mixtures.

Exciting wavelength;—
 λ 4358 Å

Percentage by wt. of glycerine.	Viscosity in poises.	Percentage of Polarisation
98	4.56	35
90.9	1.65	27
83.3	.611	20
76.9	.367	14
71.4	.185	9
66.5	.127	5

Percentage by wt. of glycerine.	Viscosity in poises	Percentage of Polarisation.
98	4.56	35
90.9	1.65	26
83.3	.611	18
76.9	.367	13
71.4	.185	7
66.5	.127	3

Percentage by wt. of glycerine.	Viscosity in poises.	Percentage of Polarisation	
		$c = .05 \cdot 10^{-5}$ gm/c.c.	$c = .5 \cdot 10^{-5}$ gm/c.c.
98	4.56	48	45
90.9	1.65	44	40
83.3	.611	36	31
76.9	.367	29	25
71.4	.185	24	19
66.6	.127	17	11
62.5	.097	12	5

TABLE IX

Percentage of Polarisation of Succ. Fluorescein in glycerine-water mixtures.

Exciting wavelength:—
 λ 3650 Å.

TABLE X

Percentage of Polarisation of Pinaflavol in glycerine-water mixtures.

Exciting wavelength:— λ 4358 Å.
Concentration:— $.05 \cdot 10^{-5}$ gm/c.c.

TABLE XI

Percentage of Polarisation of Pinakriptol yellow in glycerine-water mixtures.

Exciting wavelength:—
 λ 4358 Å. Concentration:— $.25 \cdot 10^{-5}$ gm/c.c.

Percentage by wt. of glycerine.	Viscosity in poises.	Percentage of Polarisation	
		$c = .05 \cdot 10^{-5}$ gm/c.c.	$c = .5 \cdot 10^{-5}$ gm/c.c.
98	4.56	40	38
90.9	1.65	36	34
83.3	.611	30	26
76.9	.367	25	20
71.4	.185	19	13
66.6	.127	14	8
62.5	.097	9	3

Percentage by wt. of glycerine.	Viscosity in poises	Percentage of Polarisation.
98	4.56	38
90.9	1.65	32
83.3	.611	24
76.9	.367	18
71.4	.185	12
62.5	.097	4
58.3	.070	Zero

Percentage by wt. of glycerine.	Viscosity in poises	Percentage of Polarisation
98.	4.56	38
90.9	1.65	27
83.3	.611	17
76.9	.367	12
66.6	.127	5
58.8	.070	0

In order to be able to have some information regarding this duration of the molecules in the excited states or the average life of the fluorescing molecules, as they are sometimes called, measurements were made on the polarisation of the fluorescence of the dyestuffs under investigation in glycerine-water mixtures, whose relative proportions and hence the viscosity could be varied over a wide range. The concentration of the dyestuffs per c.c. of the solution was kept constant in all the cases, so also the temperature of the solution.

The values of the viscosity were calculated from the extensive measurements as given by Shelly (1932) on viscosity at different temperatures and various concentrations by graphical interpolation.

The results of our measurements are shown in the accompanying tables. It will be observed that in all cases the degree of polarisation tends at high viscosity to reach asymptotically the maximum limiting value p_0 , whereas at low viscosity the polarisation tends towards zero value. This limiting value does not only depends on the nature of the dyestuff but also on the wavelength of the exciting radiation.

The mean life of the fluorescing molecules in the excited states τ has also been calculated, the following gives the results of our calculation. It is evident from the nature of the expression for τ that for values of p very near p_0 , as also very near zero, the calculated value of τ cannot be reliable. Hence τ has been calculated only for the values of $p > .10 < .45$.

TABLE XII

Average life τ of Acriflavin in glycerine water mixture.

Viscosity in poises	Excitation by λ 4358		Excitation by λ 3650	
	$c = 3.10^{-5}$ gm/c.c.	$c = 8.10^{-5}$ gm/c.c.	$c = 3.10^{-5}$ gm/c.c.	$c = 8.10^{-5}$ gm/c.c.
1.65	$1.2.10^{-8}$ Sec.	$7.5.10^{-9}$ Sec.		
.611	$1.1.10^{-8}$ Sec.	$6.9.10^{-9}$ Sec.	$1.0.10^{-8}$ Sec.	$6.0.10^{-9}$ Sec.
.367	$1.3.10^{-8}$ Sec.	$7.1.10^{-9}$ Sec.	$1.1.10^{-8}$ Sec.	$7.0.10^{-9}$ Sec.
.185	$1.2.10^{-8}$ Sec.	$7.4.10^{-9}$ Sec.	$1.2.10^{-8}$ Sec.	$7.7.10^{-9}$ Sec.

TABLE XIII

Average life τ of Sacc. Fluorescein in glycerine water mixture.

Viscosity in poises	Excitation by λ 4358		Excitation by λ 3650	
	$c = 5.10^{-5}$ gm/c.c.	$c = .05.10^{-5}$ gm/c.c.	$c = 5.10^{-5}$ gm/c.c.	$c = .05.10^{-5}$ gm/c.c.
1.65	$10.6.10^{-9}$ Sec.	$6.0.10^{-9}$ Sec.	$9.7.10^{-9}$ Sec.	$6.8.10^{-9}$ Sec.
.611	$9.7.10^{-9}$ Sec.	$6.1.10^{-9}$ Sec.	$9.4.10^{-9}$ Sec.	$6.1.10^{-9}$ Sec.
.367	$9.7.10^{-9}$ Sec.	$6.8.10^{-9}$ Sec.	$10.1.10^{-9}$ Sec.	$6.2.10^{-9}$ Sec.
.185	10.10^{-9} Sec.	$5.2.10^{-9}$ Sec.	$10.3.10^{-9}$ Sec.	$5.6.10^{-9}$ Sec.

TABLE XIV

"Average life" of Pinaflavol in glycerine-water mixtures.

Exciting wavelengths = λ 4358 A.

Concentration = $.05.10^{-5}$ gm/c.c.

Viscosity in poises =

4.56

1.65

.116

.673

.518

$\frac{(3-p_0).R\theta}{V} \cdot \tau$

1.44

1.54

1.37

1.46

1.38

It is evident from the tables that within the limits of the experimental errors the values of τ is practically independent of the viscosity (provided it is low), though the values are widely different for the different concentrations of the dyestuffs. Moreover, the values of the average life are independent of the exciting wavelengths.

We have already reported the phenomena of quenching of fluorescence by foreign neutral salts. We can consider this act of quenching as something like a quantum mechanical resonance, if we look at it in the light of collision process of the second kind. If now on undergoing different excitations with different wavelengths, the excited molecules had different probabilities of quenching, some dependence of the quenching on the wavelength of exciting light should be observed. But experimentally it was shown by Wawilow (1929) Sveshnikow

(1935) and Mitra (1938), that there is no dependence of the quenching action on the exciting wavelengths. Their conclusions show that the excited molecules have all the same energy level during the excited state. Thus our conclusions arrived at from the polarisation measurements are in agreement with those of the aforesaid investigators.

INFLUENCE OF TEMPERATURE ON THE POLARISATION OF THE FLUORESCENT RADIATIONS

As regards the influence of temperature on the polarisation of fluorescence Pringsheim and Perrin observed that with increase of temperature, the polarisation gradually dwindles down, finally vanishing to zero. Mitra, over and above this observed that with the decrease of temperature, the polarisation asymptotically tends towards the maximum value " p ."

We have also measured the polarisation of the dye-stuffs under investigation in glycerine solution at various temperatures of the solvent. The results of our measurements are given below.

We can readily understand that the influence of temperature on the polarisation will be two-fold; directly owing to the greater thermal agitations at higher temperatures the "expectations" of rotation of the molecules after excitation from their initial positions will be greater and hence the value of the polarisation will correspondingly be smaller. It also affects indirectly by changing the viscosity of the solution. Both the effects work in the same direction; viz., to diminish the polarisation at higher temperatures. Both these effects have been taken into consideration in the already alluded Perrin's theory. If now these are the only effects of temperature, the average life calculated on the basis of the aforesaid theory ought to be independent of the temperatures. Such an independence was shown by Mitra to be experimentally true only in the case of dilute solution of the dyestuff; but in the case of concentrated solutions the life-time of the molecules gradually falls down with the increase of temperature, showing thereby that there are other effects of temperature besides the two already mentioned.

Experimentally the value of the polarisation was measured for the temperatures from 0° to about 90°C .

The results of our measurements are given in the following Tables:—

TABLE XV

Influence of temperature on the polarisation of fluorescence of Acriflavin in glycerine excited by λ 4358

Temperature in $^{\circ}\text{C}$	Percentage of Polarisation		
	$c = 3.10^{-5}$ gm/c.c.	$c = .8 \cdot 10^{-5}$ gm/c.c.	$c = .1 \cdot 10^{-5}$ gm/c.c.
10	50	50	50
20	48	50	50
30	44	46	50
40	38	41	44
50	33	36	39
60	27	31	34
70	21	25	29
80	16	20	23
90	10	15	18

TABLE XVI

Influence of temperature on the polarisation of fluorescence of Acriflavin in glycerine excited by λ 3650

Temperature in $^{\circ}\text{C}$	Percentage of Polarisation		
	$c = 3.10^{-5}$ gm/c.c.	$c = .8 \cdot 10^{-5}$ gm/c.c.	$c = .1 \cdot 10^{-5}$ gm/c.c.
0	42	42	42
10	42	42	42
20	41	42	42
30	37	38	40
40	32	34	36
50	27	29	31
60	22	24	26
70	16	18	20
80	10	12	15
90	4	7	10

TABLE XVII

Influence of temperature on the polarisation of fluorescence of Pinaflavol and Rose Bengal in glycerine excited by λ_{4358}

Concentration: 1×10^{-5} gm./c.c.

TABLE XVIII

Influence of temperature on the polarisation of fluorescence of Pinakriptal in glycerine

Concentration— 1.19×10^{-5} gm./c.c.

TABLE XIX

Influence of temperature on the polarisation of fluorescence of Succ. Eosin in glycerine

Concentration = 2.10×10^{-5} gm/cc.

Temperature in °C	Percentage of Polarisation		Temperature in °C	Percentage of Polarisation excited by λ		Temperature in °C	Percentage of Polarisation excited by λ	
	Pinaflavol	Rose Bengal		4358	3650		4358	3650
0	42	45	0	45	42	0	45	42
10	42	44	10	45	42	8	45	42
20	42	41	20	41	36	20	43	39
30	41	35	30	36	32	30	39	35
40	36	29	40	30	25	40	35	28
50	28	22	50	24	18	50	29	23
60	22	15	60	16	12	60	24	17
70	15	8	70	10	6	70	19	11
80	8	—	80	5	—	80	13	6
90	—	—						

The general nature of the curves is the same as that representing the variation of p with the viscosity. At low temperatures p tends to reach asymptotically the limiting value p_0 as for large viscosities, while at high temperatures p tends to vanish. (On calculating the value of τ on the basis of the Perrin's theory we get the following results:—

TABLE XX

Influence of temperature on the average life of the Acriflavin molecules in the excited state.

Exciting wavelength — λ_{4358}

Temperature in °C	Average life of the molecules		
	$c = 3.19 \times 10^{-5}$ gm./c.c.	$c = 8.10 \times 10^{-6}$ gm./c.c.	$c = 1.10 \times 10^{-5}$ gm./c.c.
30	13.10^{-9} sec.	8.10^{-9} sec.	—
40	13.10^{-9} „	9.10^{-9} „	6.10^{-9} sec.
50	11.10^{-9} „	8.10^{-9} „	6.10^{-9} „
60	13.10^{-9} „	9.10^{-9} „	7.10^{-9} „

TABLE XXI

Influence of temperature on the average life of the Acriflavin molecules in the excited state,

Exciting wavelength — λ_{3650}

Temperature in °C	Average life of the molecules		
	$c = 3.10 \times 10^{-5}$ gm./c.c.	$c = 8.16 \times 10^{-6}$ gm./c.c.	$c = 1.10 \times 10^{-5}$ gm./c.c.
30	13.10^{-9} sec.	10.10^{-9} sec.	—
40	13.10^{-9} „	10.10^{-9} „	7.10^{-9} sec.
50	11.10^{-9} „	9.10^{-9} „	7.10^{-9} „
60	13.10^{-9} „	10.10^{-9} „	7.10^{-9} „

These results reveal that though the value shows a very striking dependence on the concentration of the dyestuff, it is practically independent of the temperature within the ranges of concentrations we have studied. This shows conclusively that only effects of raising the temperature are through increased thermal agitation and the consequent larger value of expectation of the Brownian rotation of the dyestuff molecule per second and through diminished viscosity.

DEPENDENCE OF THE POLARISATION ON THE CONCENTRATION OF THE DYESTUFF IN SOLUTION

We have also seen from the foregoing tables that the polarisation of fluorescence exhibits a conspicuous change with the change of the concentration of the fluorescing dyestuffs.

The dependence was first experimentally shown by Pringsheim, who observed that as the concentration is increased the polarisation decreases. This observation was afterwards confirmed by Gaviola, Wawilow and others. Mitra carried out a detailed investigation and found that with the increase of concentration polarisation tends to vanish while at very small concentration it tends to reach asymptotically the same limiting value as is reached at large viscosities and low temperatures.

Our data also reveal that with the increase of concentration the values of the polarisation tend to vanish; while at very small dilutions, it tends to reach asymptotically the same limiting value as is reached at large viscosities or low temperatures.

ON THE MAXIMUM VALUE OF THE POLARISATION OF THE FLUORESCENCE OF THE DYESTUFFS

It has already been referred that the limiting value of the polarisation is its value when the molecules after excitation are not allowed to rotate from their initial orientations, which is evidently the value of the polarisation when the viscosity is very large or temperatures very low. The following table exhibits the values of this limiting polarisation for the various dyestuffs in glycerine solution when excited by radiation of various wavelengths as were obtained in our present investigation.

TABLE XXII

Dyestuffs in glycerine	Excitation wavelength in \AA	Maximum limiting value of polarisation
Acridflavin	4358	.50
	3650	.42
Pinakriptol	4358	.45
	3650	.42
Succ. Eosin	4358	.45
	3650	.42
Rose Bengal	4358	.45
Pinaflavol	4358	.42

In conclusion, it gives me great pleasure to thank Prof. S. N. Bose for his kind interest in the work. Thanks are also due to Dr. S. M. Mitra for his kind help and guidance.

PHYSICS LABORATORY,
Dacca University.

REFERENCES

- Choudhury and Bose, 1943, *Ind. J. Phys.*, **17**, 43.
 Griseback, 1936, *Zeit. f. Phys.*, **101**, 13.
 Krishnan and Sirkar, 1931, *Ind. J. Phys.*, **6**, 193.
 Mitra, 1939, *Ind. J. Phys.*, **13**, 349.
 Perrin, 1929, Thesis, Paris
 Sveshnikow, 1935, *Acta. Phys. Chem. U.R.S.S.*, **3**, 257.
 Weigart, 1922, *Verh. Phys. Phy. Gress.*, **2**, 531.
 Wawilow, 1931, *Zeit. f. Phys.*, **80**, 100.
 Frohlick, 1925, *Zeit. f. Phys.*, **36**, 193.
 Jablonski, 1934, *Acad. Pol. Sci. et letters Bul.*, **1-2A**, 14.
 Mitra, 1938, Thesis, Dacca.
 Pringsheim, 1924, *Phys. Zeit.*, **24**, 24.
 Shelly, 1932, *Indus. Eng. Chem.*, **24**, 1060.
 Wawilow, 1922, *Phys. Zeit.*, **23**, 173.
 Wawilow, 1929, *Zeit. f. Phys.*, **88**, 690.

INFLUENCE OF THE INTENSITY OF IRRADIATION ON THE NEW LIGHT-EFFECT IN CHLORINE UNDER ELECTRICAL DISCHARGE

By P. G. DEO

(Received for publication, March 16, 1944.)

(Plate I)

ABSTRACT. General conditions for the production of a new light-effect, *viz.*, a photo-diminution of the conductivity in chlorine subjected to electrical discharge, are indicated. The effect increases by increasing the frequency of irradiation, the violet being most active, which happens to be the region of absorption by chlorine. In agreement with Joshi's views, who regards this phenomenon as distinct from a negative photo-electric effect, the influence of the light-intensity on the effect is not linear.

INTRODUCTION

Occurrence of a photo-diminution of the conductivity due to electrical discharge in chlorine and other gases has been established by Joshi (1943) and co-workers (1939, 1941, 1943). The present communication reports results for the dependence of this new electro-optical phenomenon upon the applied potential, the nature, and the intensity of irradiation.

EXPERIMENTAL ARRANGEMENT

The experimental arrangement and electrical circuit are shown in Fig. 1. Single-phase alternating current of 50 cycles frequency was obtained from a 1 k.W. rotary converter worked off the D.C. mains. The potential was stepped up by means of a high tension transformer (2 KVA, 150/40,000 volts, 50-500 μ). With the help of a potentiometric arrangement it was possible to regulate the primary potential of the transformer within 1 per cent. The primary current and voltage were observed by an ammeter A and a volt-meter V (Fig. 1) respectively. V, the secondary potential was obtained from a knowledge of the transformer ratio.

Chlorine was prepared electrolytically from concentrated hydrochloric acid by passing a current of 0.25 amp. It was freed from the acid by bubbling through water, and dried by leading through concentrated sulphuric acid and finally over freshly prepared phosphorus pentoxide.

Further purification was effected by freezing the gas in a trap cooled by liquid air and pumping out with a Töpler any uncondensed gases. This process of drying and purification was repeated several times until the spectrum of a sample of the gas viewed through a direct vision spectroscope was found to be free from impurities.

The discharge was produced in the annular space of a Siemens' type glass ozonizer, of which two (A', A) were used; they were filled with chlorine at pressures of 5.6 and 11.0 cm. Hg. respectively. The discharge current i was measured by a Cambridge A.C. microammeter, shunted with a suitable non-inductive resistance, introduced in the secondary circuit. A 200 watt incandescent bulb run at 180 volts was the light source. The water-cell W (Fig. 1)

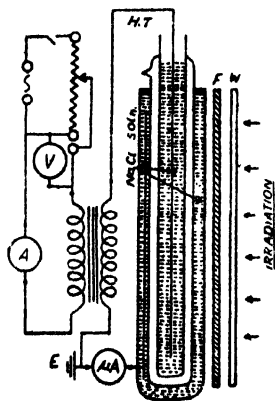


FIG. 1

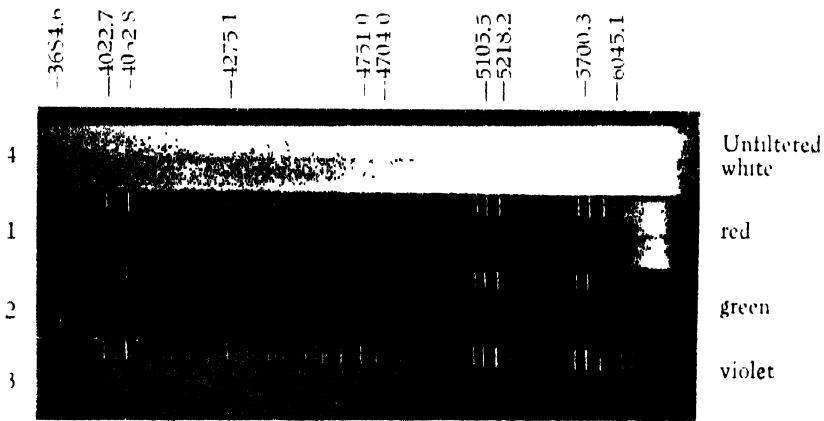


FIG. 4

served to minimise the heat radiations. The effective frequency of irradiation was varied by employing coloured glass strips F; the size of the ozonizer did not permit the use of Wratten or similar light filters.

RESULTS AND DISCUSSION

Using ozonizer A' data for the characteristic V-i curves were obtained with V, varied within the range 7.0 to 13.0 kV. (Fig. 2). These curves show the essence of the new phenomenon, namely that the discharge current produced due to various applied potentials diminishes as a result of irradiation. Table I shows that for a given wave-band, Δi the light-effect increases with V. At constant V, Δi varies in the order: white > violet violet (double) > red; the corresponding intensity of incident energy, observed with a Kipps 37 thermopile, expressed in relative units was 34.1 (white), 16.5 (violet), 8.7 (violet double) and 22.2 (red). This shows that *ceteris paribus*, frequency is the main determining factor in the production of this phenomenon. The influence of the light intensity at constant frequency is illustrated by the fact that for the whole series, Δi for double filtered violet is less than that when one violet filter is used (Fig 2, curves 3 & 4). It is instructive to recall at this stage a previous observation, viz., that the variation of Δi with I, the intensity is markedly influenced by the initial value of I; and that at higher intensity Δi tends to a limiting value probably as a consequence of saturation. This factor may be responsible for the fact that $\Sigma \Delta i$ expressed as the sum of Δi observed separately under each of the various bands

comprising the white light is greater than Δi for the white. It is to be anticipated that this effect will decrease at lower intensity (*vide infra*).

TABLE I

Variation with V the Applied Potential and different Irradiations, of i the Discharge Current in Cl_2

(Ozonizer A', $PCl_2 = 5.6$ cm. Hg.)

Primary volts (r.m.s.)	V, Secondary kilo- volts (r.m.s.)	Red				Violet (double)			Violet			White			2+4	
		2				3			4			5			2+4	
		i	i	Δi	% Δi	i	Δi	% Δi	i	Δi	% Δi	i	Δi	% Δi	$\Sigma \Delta i$	% $\Sigma \Delta i$
28.5	7.6	40.0	38.0	2.0	5.0	26.0	14.0	35.0	22.5	17.5	43.9	22.5	17.5	43.9	19.5	48.9
33.5	8.9	50.0	48.5	1.5	3.0	35.0	15.0	30.0	32.0	18.0	36.0	31.0	19.0	38.0	19.5	39.0
38.0	10.2	60.0	58.0	2.0	3.3	45.0	15.0	25.0	41.5	18.5	30.8	40.5	39.5	32.5	20.5	34.1
42.0	11.2	70.0	67.5	2.5	3.6	55.0	15.0	21.4	51.0	19.0	27.1	50.0	20.0	28.5	21.5	30.7
45.0	12.0	80.0	77.5	2.5	3.1	65.0	15.0	18.7	57.0	19.0	23.7	59.5	20.5	25.2	21.5	26.8
48.5	12.9	90.0	87.0	3.0	3.3	75.0	15.0	16.7	71.0	19.0	21.1	69.0	21.0	23.3	22.0	24.4

The above findings have been investigated in some detail on another system (ozonizer A), particularly in regard to the influence of I the intensity. In this series of experiments V the applied potential (9.3 kV. r.m.s.) was kept constant; i the corresponding discharge current in dark was 55 micro-amps. Δi , the diminution in i produced due to each of the various frequency-bands is shown in Table II. The relative total intensities of these bands were measured with a Kipps 37 thermopile and also with a RCA 918, caesium coated photo-cell, applying 50 volts as the accelerating potential (*cf.* Table II): the relative intensity is also indicated by the corresponding spectra (Fig. 4) taken with a Fuess spectrograph on Kodak P 1200 super-panchromatic plates with a 10 second exposure. I was varied by varying the ozonizer-distance from the light source over a range of 30 to 100 cms. Whilst Δi , due to the (unfiltered) white and violet was appreciable at even longer distances, that due to red and green had practically reached the limit of the sensitivity of the available microammeter at even less than 100 cms. Assuming the inverse square law to a first approximation the Δi -distance⁻² curves in Fig. 3 show the variation with intensity of Δi in different spectral regions, at a constant exciting potential.

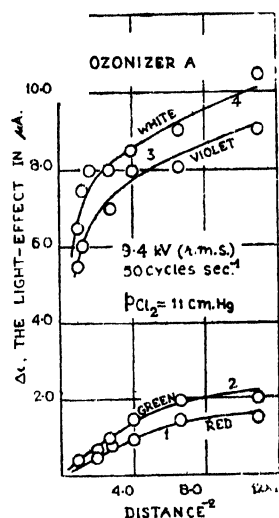


FIG. 3

TABLE II

Variation with I the Intensity of Irradiation in different Spectral Regions of Δi the Light-effect in Cl_2 at constant Potential

(Ozonizer A'; $PCl_2 = 11$ cm. Hg.; 9.4 kV)

Distance cms.	Red 1	Δi Light-effect in μA			$\Sigma \Delta i$ 1+2+3
		Green 2	Violet 3	White 4	
30	1.5	2.0	9.0	10.5	12.5
40	1.5	2.0	8.0	9.0	11.5
50	1.0	1.5	8.0	8.5	10.5
60	1.0	1.0	7.0	8.0	9.0
70	0.5	0.5	7.0	8.0	8.0
80	...	0.5	6.5	8.0	7.0
90	6.0	7.5	6.0
100	5.5	6.5	5.5
I , total intensitv (relative)	100 460	0.1 0.3-0.4	120 440	45.6 1050	with thermopile with photocell

As observed earlier by Joshi and others these results show that this light-effect under white and violet is much more pronounced than that due to green and red which may be associated with the fact that both the former include appreciably the absorption spectrum of chlorine. It

is known that the spectral sensitivities of a photo-electric cell and a thermo-pile are not the same. The results of both these methods (Table II) and the spectra in Fig. 4 show, however, the same order of variation in respect of the intensity of the light-band, viz., green < violet < red < white. A comparison of Δi due to these light-bands shows that intensity is not the primary determinant of the magnitude of this phenomenon. The greater Δi under green (Fig. 3, curve 2) despite its low intensity compared with red (curve 1) shows that the frequency is the more predominant factor. It is also instructive to observe that whilst the over-all intensity in the region beginning from about 4704 Å towards the ultra-violet is much greater in the unfiltered white (Plate I) (spectrogram 4) than the violet (spectrogram 3), and that the former contains a more intense short-wave region, viz., 4032 to 3684 Å than the latter, the magnitude of the light-effect is not correspondingly greater under white than violet (Table II). This may be due to saturation; it is also suggested by a comparison of the sum, $\Delta i_{\text{red}} + \Delta i_{\text{green}} + \Delta i_{\text{violet}} = \Sigma \Delta i$ (say), with the corresponding Δi under white (Table II). It is seen that $\Sigma \Delta i$ the additive effect exceeds the corresponding Δi due to white, and that the excess is the more pronounced, the greater the intensity of irradiation. At small I , when the saturation effect should be low, $\Sigma \Delta i$ is less than that for white, as is to be expected. It is also seen from Fig. 3 that comparatively, the increase of Δi with I is more steep in white > violet > green > red. That Δi tends generally to fall off subsequently, i.e., when I is large, is an additional indication of saturation.

Fig. 3 shows that Δi is not a linear function of the corresponding intensity of irradiation, a result which has been emphasized by Joshi as differentiating this phenomenon from the classical photo-electrical effect.

Grateful thanks of the author are due to the Indian Association for the Cultivation of Science, Calcutta, for the loan of the Fuess spectrograph, to Dr. M. W. Chiplonker, Physics Department, S. P. College, Poona, for the loan of an A. C. microammeter and to Dr. S. S. Joshi for kind interest and valuable suggestions.

COLLEGE OF SCIENCE,
BENARES HINDU UNIVERSITY,

REFERENCES

- Joshi (1943), *Proc. Indian Sci. Cong.* (Presidential Address, Chemistry Sec.).
 Joshi and others (1939), *Curr. Sci.*, **8**, 548.
 „ „ (1943), „ „ **9**, 536.
 „ „ „ „ „ **12**, 306.
 „ „ (1941), *Nature*, **147**, 806.
 „ „ (1943), „ **151**, 561.

ON THE EXPERIMENTAL INVESTIGATION OF NIGHT-TIME E ION-DENSITIES AND THEIR DETERMINATION BY THE APPLICATION OF CHAPMAN'S FORMULA

BY M. M. SENGUPTA

AND

S. K. DUTT

(Received for publication, March 22, 1944)

ABSTRACT. The present work embodies results of experiments to verify whether the observed night-time E ion-density values in different seasons vary in accordance with Chapman's formula. It appears that Chapman's formula does not account wholly for the results of observation. This is also corroborated by the data obtained at Watheroo which is situated near about the same latitude as Patna but in the opposite hemisphere; the ionospheric conditions of these places have been taken to be the same for the purpose of comparison. It is suggested that the value of σ_0 in the Chapman's formula which is taken to be constant throughout for calculations, does not hold good at least during night-time and the discrepancy may perhaps be due to this.

Chapman's (1931) formula from which ion-density values of different layers of the ionosphere can be calculated is given by

$$\sigma_0 \frac{dv}{d\phi} + v^2 = \exp. [1 - z - \exp. (-z) f(R, x)] = F(z, x) \dots (\text{day}) \quad (1)$$

$$= 0 \dots (\text{night}) \quad (2)$$

where z —a linear function of the height

$f(R, x)$ —a complicated function of a parameter R and angle x

h —height of the point of observation above the ground

θ —angular distance from the North pole (the Co-lat.)

δ —north declination of the sun

x —zenith distance of the sun at the point and time considered ($\cos x = \sin \delta \cos \theta + \cos \delta \sin \theta \cos \phi$)

t or ϕ —the local time reckoned from noon.

ϕ is in angular measure and t in seconds. Thus $t = 1.37 \times 10^{-4} \phi$.

n —ion-density at any time at height h

n_0 —the steady value which n would attain at the level $h_0 (z=0)$ at the equator at midday (when $z=0, x=0$).

$$v = n/n_0$$

$$1/\sigma_0 = 1.37 \times 10^4 (I_0 a)^{\frac{1}{2}}$$

where a is the coefficient of recombination and I_0 is the production value corresponding

to n_0 ; $n_0 = (I_0/a)^{\frac{1}{2}}$

Chapman shows that for a given angle x the height in terms of z at which the rate of ionization is greatest is given very nearly by $\log_e f(R, x)$, so that if z_0 is the height corres-

ponding to x_0 , the value of x at noon, z_0 will be given by $z_0 = \log_e f(R, x)$. The above equation can then be written in the form

$$\sigma_0 \frac{d\nu}{dx} + \nu^2 = \frac{f(R, x)}{f(R, x_0)} \exp. \left(1 - \frac{f(R, x)}{f(R, x_0)} \right) \quad (\text{day}) \quad (3)$$

$$= 0 \quad (\text{night}).$$

In Table I the values of ν obtained by solving the differential equation (3) following the numerical method for latitude 24°N * at winter and summer solstices are given.** It may be noted here that for the purpose of calculation the value of σ_0 has been taken to be $1/25$ as has been suggested by Champman (1931), and Best, Farmer and Ratcliffe (1938).

It will be seen from the graph (Fig. 1) that the ratio of $\frac{\nu_{\text{winter}}}{\nu_{\text{summer}}}$ at any hour of the day and night is less than unity and indeed this should be so, as the formula involves the zenith angle x whose value at any place at any hour is less in summer months than in winter months, the solar radiation being the main cause of ionization

TABLE I

ϕ reckoned from noon	Hr. min.	ν winter solstice	ν summer solstice	$\frac{\nu_{\text{winter solstice}}}{\nu_{\text{summer solstice}}}$
0	12.00	.823	1.000	.823
.2	12.46	.816	.994	.821
.4	13.31	.786	.968	.812
.6	14.17	.726	.923	.786
.8	15.02	.629	.852	.738
1.0	15.48	.472	.749	.630
1.1	16.11	.366	.679	.539
1.2	16.34	.254	.596	.426
1.3	16.57	.166	.498	.341
1.4	17.19	.116	.394	.294
1.6	18.05	.074	.182	.407
1.8	18.50	.054	.096	.563
2.0	19.36	.042	.065	.646
2.2	20.22	.035	.049	.714
2.4	21.07	.030	.039	.769
2.6	21.53	.026	.033	.788

As ν is proportional to the square of the critical frequency (f_c), $\frac{\nu_{\text{winter}}}{\nu_{\text{summer}}}$ is given by

$\frac{f_c^2(\text{winter})}{f_c^2(\text{summer})}$. Hence experimental values of $\frac{\nu_{\text{winter}}}{\nu_{\text{summer}}}$ can be obtained from the results of

systematic investigations of the ionosphere that have been carried out by the modern automatic multi-frequency equipment at Huancayo (Lat. $12^\circ 2'$ S. Long. $75^\circ 20'$ W.) and

Watheroo (Lat. $30^\circ 19'$ S. Long. $115^\circ 53'$ E.). The Table II gives the values of $\frac{\nu_{\text{winter}}}{\nu_{\text{summer}}}$

calculated from the observed values of critical frequencies at Watheroo by Parkinson and Prior (1939).

* The latitude 24°N has been chosen as this is the mean latitude between Patna and Calcutta

** The values of ν have been calculated in the same way as Millington (1932).

TABLE II

(All the critical frequencies (Mc/s) are for the E layer at Watheroo
(Lat. $30^{\circ}19'$ S, Long. $115^{\circ}53'$ E))

Hours	f_o winter June, 1939	f_o summer Dec., 1938	f_o^2 winter	f_o^2 summer	$\frac{v_w}{v_s} = \frac{f_o^2 \text{ winter}}{f_o^2 \text{ summer}}$
12	3.51 Mc/s	4.02 Mc/s	12.32	16.16	.76
13	3.44	3.96	12.83	15.68	.76
14	3.37	3.83	11.36	14.67	.78
15	3.05	3.80	9.30	14.44	.65
16	2.61	3.50	6.81	12.25	.56
17	1.91	3.10	3.65	9.61	.38
18	1.17	2.44	1.37	5.95	.23
19	1.00	1.46	1.00	2.13	.47
20	0.94	0.75	0.88	0.56	1.56
21	0.81	0.63	0.66	0.40	1.64
22	0.58	0.58	0.53	0.34	1.59
23	0.53	0.53	0.56	0.28	2.00

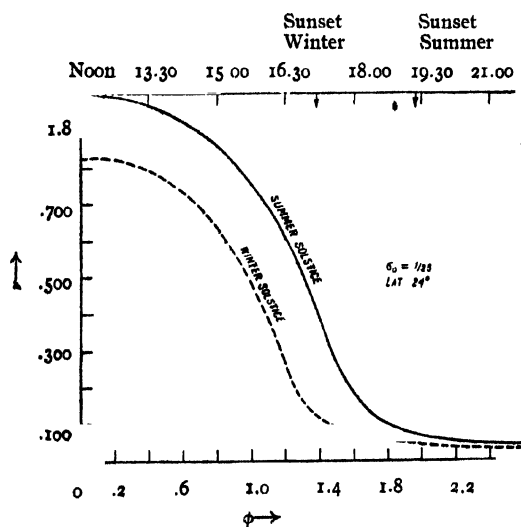


FIG. 1

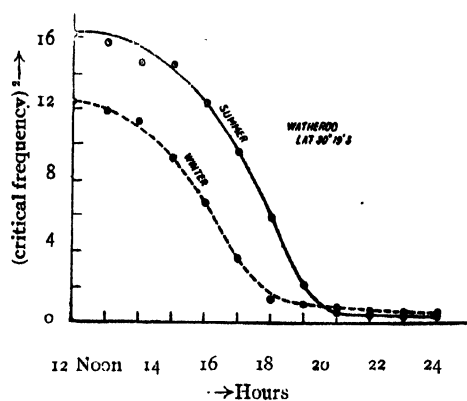


FIG. 2

It will be seen from the plot of f_o^2 against hour of the day (Fig. 2) that during daytime the ratio of v_{winter} to v_{summer} is less than unity, that is, quite in agreement with that indicated in theory; in night-time, however, the condition is reversed as shown by the intersection of the curves which is absent in the theoretical curves of Fig. 1.

The present work has been undertaken to verify whether the ion-density values vary with seasons in a similar way during night-time at a place having approximately the same latitude but in the opposite hemisphere. In his report Mitra (1935), has given data for such a place (Calcutta Lat. $22^{\circ}31'$ N, Long. $88^{\circ}21'$ E) and found fairly good agreement with theory of values of v in summer only; but as no data for winter months are given in his paper, no definite conclusion can be drawn regarding the disagreement of the experimental results of night-time Watheroo from theory. Owing to difficulties arising out of war conditions it was not found possible for us to set up the necessary multifrequency transmitter

required in the usual critical frequency method. We have, therefore, followed a different plan for our purpose.

EXPERIMENT.

In the method adopted by us the angles i of the downcoming waves of a particular frequency (810 kc/s) from a given station have been measured. Since the distance between the transmitting and receiving stations is known, the angle i_0 of the downcoming waves refracted back from the E layer (110 Km) for the given receiving station is also known. If the deflection is occurring in the E layer, the angle of the downcoming waves should be this particular value i_0 .* The value of ion-density corresponding to any angle of reflection can be obtained from the application of the Appleton-Hartree formula and hence the value of N_{0E} corresponding to i_0 can be found, thus giving the lower limit of the ion-density which the E layer can have for the particular frequency during the period of observation; the ion-density, however, may have any value higher than this, but not less. For all other values less than i_0 the wave must have penetrated the E layer as is shown in Fig. 3 and deflection is no longer taking place from this layer but from a layer at a higher level where

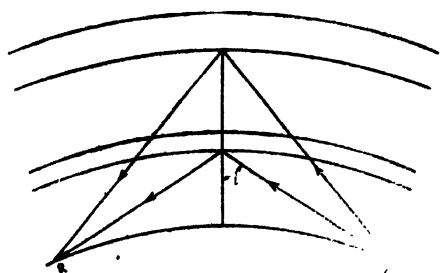


FIG. 3

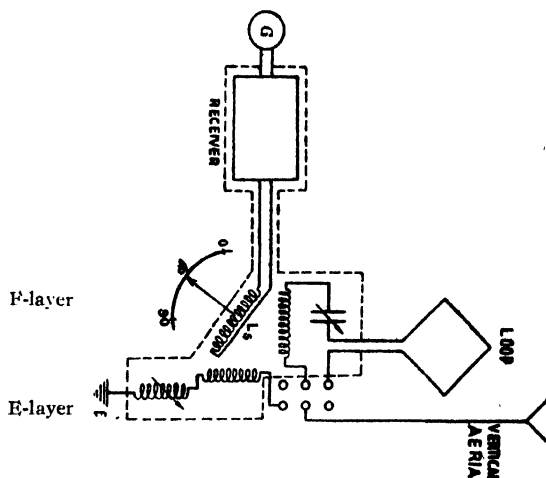


FIG. 4

the ion-density has a value corresponding to the observed i , in other words the value of the E ion-density must have fallen below the lower limiting value N_{0E} . Our method will, therefore, give whether the ion-density is greater or less than N_{0E} — the critical value of the E ion-density for the given stations and the frequency chosen; but since the variation in the ion-density can change the angle of the downcoming waves between two limiting values i_0 and i' (i' corresponding to next higher layer), a definite conclusion as to whether the ratio of the seasonal ion-densities is greater or less than unity is possible from a study of the variation of the angle of the downcoming waves.

The experimental arrangement is essentially the same as given by Smithrose and Barfield (1926). An outline of the arrangement is shown in Fig. 4.

* Slight variation of i_0 is possible, since there is variation in the height of the layer.

The angle (η) through which L_s is rotated is measured and from it the angle i of the down-coming waves is obtained from the relation $\sin i = \tan \eta$. The whole experiment was done in the most aperiodic conditions of the two aerials to minimise the effect of the coupled inductance due to the secondary circuit of the search coil L_s . It can be seen from an analysis that to attain this condition $\omega^2 M^2$ should be relatively small compared to the impedance of the aerial circuit for which the circuit must be as aperiodic as could be made without making the final galvanometer deflection small. In our case the deflections in the equality condition were never less than 6 cms. in spite of the fact that the aperiodicity was as great as 60 to 80% off the resonance. This ensured high accuracy of the whole experiment.

In our case the ground wave was found negligible after proper tests as done by Sengupta and Dutt (1941), and the formula $\frac{E_A}{E_L} = \sin i$

where

E_A = e.m.f. induced in the vertical aerial.

E_L = e.m.f. induced in the loop aerial.

i = angle of incidence with the vertical.

will hold good under all conditions as shown by Appleton (1927). The absence of the ground wave also simplified experimental arrangement and interpretation of results.

In order to minimise the antenna effect as much as possible, the dimensions of the loop were made purposely small. The loop was nearly 86 cms. square and the number of turns of wire was six. The effective height was about 100 cms. Proper tests were carried out to know definitely the amount of antenna effect and it was found negligible.

The receiver was properly shielded and was thoroughly tested for pick-up which was never more than a millimetre or two; as the readings were not usually less than 6 cms. the effect due to pick-up was negligible. The goniometer angle could be read accurately within half a degree and the individual readings varied by about $\pm 2^\circ$.

The possibility of laterally deviated indirect rays reaching Patna should not be excluded; but it is easily seen that lateral deviation will produce large values of i and not small values. To determine the degree of lateral deviation observations were taken with another loop aerial. The arrangement of this loop was such that the loop could be rotated both about the vertical and horizontal axes. From the observations taken it was found that the plane of the down-coming waves was practically vertical, the deviation being generally within 5° and occasionally going up to 11° . The experiments of Smithrose and Barfield have shown that such lateral deviation is not very appreciable for conditions similar to those of this experiment for λ lying between 300 and 500 metres.

RESULTS

The results of our experiment given in Fig. 5 show the average of the observed values of the angle i during the period of observation (generally from 7 P.M. to 10 P.M. local time). It will be observed that during the winter months it is the E layer which is generally taking part in reflection; this is, however, no longer true during the summer months, the layer being penetrated during this time.

In order to obtain the value of $\frac{v_{\text{winter}}}{v_{\text{summer}}} = \frac{n_w/n_0}{n_s/n_0} = \frac{n_w}{n_s}$ from our observations we have

obtained the lower limiting values of n , (summer ionic density) and n_w (winter ionic density) from the corresponding values of i averaged over each month by using the Appleton-Hartree formula as mentioned before. Taking into account the curvature of the earth and the great circle distance PC (Fig. 6) between the two stations Patna and Calcutta, the angle of incidence

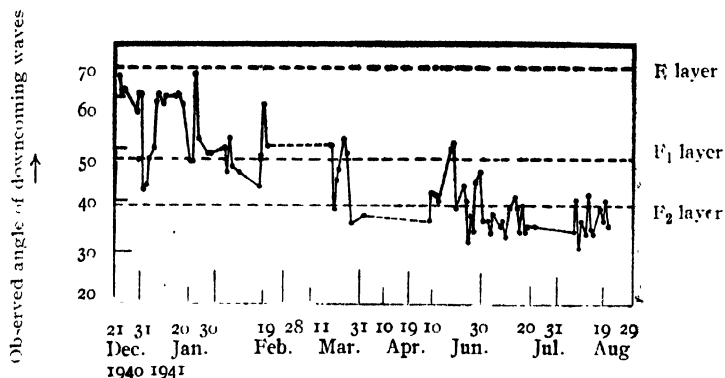


FIG. 5

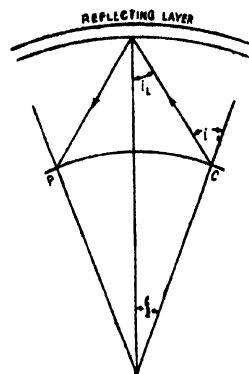


FIG. 6

at the reflecting layer is given by $i_L = i - b/2$

where b is obtained from the relation

$$\cos b = \cos \theta \cos \phi \cos \theta' \cos \phi' + \cos \theta \sin \phi \cos \theta' \sin \phi' + \sin \theta \sin \theta'$$

where θ , θ' and ϕ , ϕ' are the latitudes and longitudes of Patna and Calcutta respectively.

$$\text{Patna} \quad \theta = 25^\circ 30' \text{N} \quad \phi = 85^\circ 15' \text{E}$$

$$\text{Calcutta} \quad \theta' = 22^\circ 34' \text{N} \quad \phi' = 88^\circ 55' \text{E}$$

$b/2$ comes out to be $2^\circ 3' = 2.1$ approximately.

The value of N_{0E} has been calculated from the Appleton-Hartree formula, absorption and and friction having been neglected.

$$\sin^2 i_L = \mu^2 = 1 - \frac{2p_0^2}{2p^2 - \frac{p^2 p_\tau^2}{p^2 - p_0^2} \mp \left[\frac{p_4 p_\tau^4}{(p^2 - p_0^2)^2} + 4p^2 p^2 \right]^{1/2}}$$

where $p_0^2 = 4\pi Ne^2/m$

e , m = electronic charge and mass

N = number of equivalent electrons per c.c.

$p = 2\pi \times \text{frequency of the wave}$

$p_\tau = eH_\tau/mc$, $p_L = eH_L/mc$.

H_τ , H_L = Intensities of earth's magnetic field transverse and parallel to the direction of propagation of the waves

c = the velocity of light.

p_0^2 has been taken to be equal to $4\pi Ne^2/m$ and thus the Lorentz correction term has been eliminated in accordance with the reasons and arguments put forth by Darwin (1934), and supported by others like Mimm (1937).

Assuming symmetrical reflection taking place at the ionized layer at a point M (Fig. 7) midway between Patna and Calcutta on the great circle passing through the places.

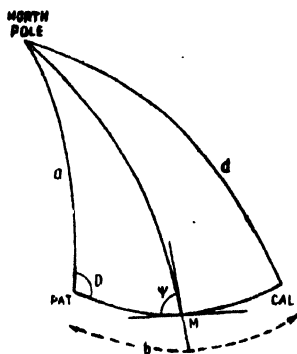
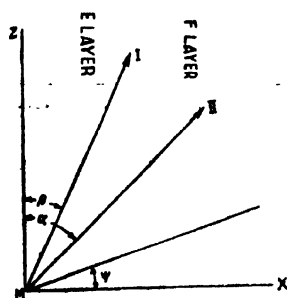


FIG. 7



MZ—is the vertical through M
I—Magnetic Field
II—Direction of propagation

FIG. 8

$$H_{\perp} = H(\sin \alpha \sin \beta \cos \psi + \cos \alpha \cos \beta)$$

and

$$H_{\parallel} = H [1 - (\sin \alpha \sin \beta \cos \psi + \cos \alpha \cos \beta)^2]^{\frac{1}{2}}$$

α and ψ being given by the equations

$$\tan \alpha = \frac{r \sin \frac{a}{2}}{r + h - r \cos \frac{b}{2}} \quad (\text{from Fig. 6})$$

$$\text{and } \cos \frac{b}{2} \cos D = \sin \frac{b}{2} \cot \alpha - \sin D \cot \psi \quad (\text{from Fig. 7})$$

D is known from

$$\cos d = \cos a \cos b + \sin a \sin b \cos D \quad \dots \quad (\text{from Fig. 8})$$

where

r = radius of the earth

h = height of M (E layer)

$b = 4.1^\circ$ (already found)

D = angle made by the meridian great circle at Patna, and the great circle passing through Patna and Calcutta (Fig. 7).

a = co-lat of Patna ($= 64^\circ 30'$)

d = co-lat of Calcutta ($= 67^\circ 26'$)

β = the complement of the dip at M

ψ = angle made by the great circles—one passing through Patna, M and Calcutta, and the other passing through M and the North Pole.

In all these calculations, the declination at M has been supposed to be zero, as those of Calcutta and Bombay being only $0^\circ 32'$ E and $0^\circ 41'$ E, any place lying between those two must have a small declination of this order. H and the dip for M have been taken to be the mean of the corresponding values for Patna and Calcutta. The values obtained are given in Table III.

TABLE III

α	β	ψ	D	H	H_L	H_T	N_{02}
$63^{\circ}32'$	54°	$44^{\circ}22'$	$134^{\circ}58'$.456	.356	.286	$.98 \times 10^4$

In the following Table IV the monthly averages of i and corresponding i_L obtained in our experiments during the period of observation are given.

TABLE IV

Season	Months	i average	i_L	E ion- density	n_o/n_s	Remarks
Winter	{ December, 1940	$61^{\circ}.5$	$59^{\circ}.4$	$> .98 \times 10^4$	> 1	Reflection from E Layer.
	{ January, 1941	$53^{\circ}.9$	$51^{\circ}.8$			
	{ February	$48^{\circ}.9$	$46^{\circ}.8$			
	{ March	$45^{\circ}.1$	$43^{\circ}.0$			
	{ April	$37^{\circ}.0$	$34^{\circ}.9$			
Summer	{ May	—	—	$> .98 \times 10^4$	> 1	Penetration of E Layer.
	{ June	$41^{\circ}.0$	$38^{\circ}.9$			
	{ July	$36^{\circ}.1$	$34^{\circ}.0$			
	{ August	$36^{\circ}.5$	$34^{\circ}.4$			

Assuming some variation in the height of the layer, i_L corresponding to E layer has been taken as lying between 63° and 51° ; values below this must be taken as penetration of the E layer. It will be thus clear from the above Table that during winter months reflection is taking place from E layer whose ionic density is at least $.98 \times 10^4$. During summer, however, the reflections are definitely not from the E layer whose ionic density must have fallen below $.98 \times 10^4$ according to the results obtained. It is, therefore, obvious from our experimental results that v_o/v_s must be greater than unity during night-time, thus corroborating the experimental results of Watheroo.

It may be observed from the above Table that the frequency 810 Kc/s used in our experiment is less than the critical frequency for E layer in winter and more than that in summer. Thus our experimental results are in full agreement with those obtained at Watheroo (given in Table II) by a different method using most modern equipment.

It is thus seen from our results and also corroborated by the data obtained at Watheroo that Chapman's formula does not account wholly for the conditions of the ionosphere. This discrepancy may perhaps be due to the fact that the value of σ_0 has been taken to be constant throughout. It seems to us that during winter night-time recombination is less than the summer nights. It may, therefore, be suggested that the value of σ_0 cannot be taken to be the same during all hours both in summer and winter for the calculation of night-time E ion-densities in accordance with Chapman's formula.

In conclusion we record our thanks to Prof. V. Rangacharya for his help in some of the mathematical calculations and Prof. K. Prosad, O.B.E., I.E.S., Principal, Science College, for the interest he has taken in our work.

REFERENCES

- Appleton, 1927, *P.R.S. A.*, **115**, 291.
Best, Farmer and Ratcliffe, 1938, *P.R.S.(A)*, **164**, 96.
Chapman, 1931, *Proc. Phy. Soc., Lond.*, **43**, 44.
Chapman, 1931, *Proc. Phy. Soc., Lond.*, **43**, 26 and 483.
Darwin, 1934, *P.R.S.*, **146**, 17.
Millington, 1932, *Proc. Phy. Soc., Lond.*, **44**, 580.
Mimno, 1937, *Rev. Mod. Phys.*, **9**, 1.
Mitra, S. K., 1935, *Proc. Nat. Inst. Sci. Ind.*, **1**, 131.
Parkinson and Prior, 1939, *Terr. Mag. and Atmos. Elec.*, **44**, 204 and 403.
Sengupta and Dutt, 1941, *Ind. Jour. Phys.*, **15**, 447.
Smithrose and Barfield, 1926, *P.R.S. (Lond.)*, **110A**, 580.

THE DIELECTRIC PROPERTIES OF THE CONSTITUENTS OF LAC

By G. N. BHATTACHARYA

ABSTRACT. The dielectric properties of the chief constituents of lac, *viz.*, pure lac, soft lac and lac-wax, have been measured separately over a wide range of temperature and frequency. The dielectric constant as well as pure a.c. loss-factor for all these components show typical dipolar characteristics regarding temperature and frequency variation. A distributed range of relaxation times for the first two components has been established and these distribution coefficients calculated. The calculation of the average diameter of soft lac resin rotator shows that as in whole lac, the hydroxyl group is the main polar group responsible for dielectric loss. Measurement of viscosity of soft lac over a range of temperature shows that the logarithmic law, meant for liquids, is strictly followed by it regarding the variation of temperature. The values of activation energy calculated from viscosity data as well as d.c. conductance data of soft lac agree quite well. They also agree with the activation energy obtained from a.c. data. No transition point could be observed for soft lac but hard lac exhibits such a point near about 50°C. The anomalous dispersion of lac-wax has been observed near its softening point although the extent of dielectric constant variation is small.

INTRODUCTION

It has been observed recently (Bhattacharya, 1944) that lac as such behaves as a typical polar resin. It shows anomalous dispersion at ordinary temperatures and the maximum dielectric loss for any frequency takes place at a definite temperature. The loss curve is a typical absorption curve which shifts towards high temperature side with the increase of frequency. But having a comparatively large molecule it has a distributed range of relaxation times due to which it has a wide dispersion range as well as a diminished value of maximum dielectric loss. The application of Stoke's law in order to calculate the radius of the 'lac molecule' has revealed the interesting fact that only the hydroxyl group of the molecule is responsible for the loss and probably the general rotation of the whole molecule does not take place. But lac, as we know now, is a mixture of a few constituents. It is of interest, therefore, to study the dielectric properties of these constituents in order to understand the dielectric behaviour of lac in a better way.

There are three constituents of lac—(i) pure lac resin, α -lac or simply hard lac, (ii) soft lac and (iii) lac-wax. Pure lac is insoluble in diethyl ether but soluble in alcohol, while soft lac is soluble in moist ether. Pure lac is the main fraction of lac comprising about 70% of the whole, soft lac comprises 25-30%, whilst lac-wax is only about 4% of the total. Lac-wax is again a mixture of two main fractions according to its solubility in alcohol. The alcohol-soluble fraction is the main constituent comprising more than 6/7 of the whole and the alcohol insoluble but benzene soluble part comprises only 1/7 of the total wax. These two main fractions are again mixtures of several components.

Pure lac softens at a higher temperature than whole lac, does not melt to a thin fluid and readily hardens at high temperatures. Soft lac, on the other hand, is a cooled glass-like substance at low temperatures, becoming a thin fluid at higher temperatures and is not easily hardened by heat.

From the results of the study of dielectric properties of individual components of lac it can easily be seen if of the two main components one is very different from the other regarding dielectric loss and if so whether the exclusion of one or the other constituent from lac results in a better product in this respect.

The electrical industry, in general, prefers to use de-waxed lac instead of whole lac. This has, in certain quarters, given rise to the notion that the dielectric properties of lac-wax are

undesirable (Rangaswami & Sen, 1942) although there seems to be no such record which can justify this view. An elaborate study of the dielectric properties of the constituents of lac may naturally throw light on many such practices which are being observed in many industries even today.

THEORETICAL

The complex dielectric constant ϵ of a substance is usually expressed as

$$\epsilon = \epsilon' - i\epsilon''$$

where

$\epsilon' =$ the real or the ordinary dielectric constant,

and

$\epsilon'' =$ the imaginary part of it or the dielectric loss factor.

The dielectric loss factor is related to the ordinary dielectric constant through a factor which is usually called the power factor and is generally expressed as $\cos \phi$ where ϕ is the phase angle, i.e., the angle between the applied voltage and the current vectors. This relation is $\epsilon'' = \epsilon' \cos \phi$. The complementary phase angle is called the loss angle and is generally expressed by δ . Hence

$$\epsilon'' = \epsilon' \cos \phi = \epsilon' \sin \delta = \epsilon' \tan \delta, \text{ since } \delta \text{ is usually very small.} \quad (1)$$

From the known values of dielectric constant power factor, $\tan \delta$ (both of which may be determined over a Schering bridge or a capacity bridge), the dielectric loss may be computed.

Now for a condenser having dielectric loss, the current in phase with the applied voltage may be expressed as

$$I_r = I \sin \delta = I \tan \delta, \text{ since } \delta \text{ is small.} \quad \dots (2)$$

And the expression for current through a condenser C when an alternating voltage V is impressed at its terminals is

$$I = \omega CV \quad \dots (3)$$

Therefore substituting in (2) for I, we have

$$I_r = \omega CV \tan \delta \quad \dots (4)$$

But $\tan \delta = \epsilon''/\epsilon'$ from (1) and substituting this value of $\tan \delta$ in (4) we can further write

$$I_r = \omega CV \frac{\epsilon''}{\epsilon'} = 2\pi f CV \frac{\epsilon''}{\epsilon'} \quad (5)$$

Again for a parallel plate condenser the capacity C of a condenser is given by

$$C = \frac{A\epsilon'}{4\pi d \times 9 \times 10^{11}} \quad \text{farads} \quad (6)$$

where A, d and ϵ' are the effective area, the thickness and the dielectric constant respectively of the insulating material of the condenser. Substituting this value of C in (5), we have

$$I_r = 2\pi f \cdot \frac{AV\epsilon'}{4\pi d \times 9 \times 10^{11}} \cdot \frac{\epsilon''}{\epsilon'} = \frac{fAV\epsilon''}{d \times 18 \times 10^{11}} \quad (7)$$

If however K_t is the total specific conductivity of the dielectric of the condenser comprising both the d.c. conductivity K_0 and the a.c. conductivity K, this may be written as

$$K_t = K_0 + K \quad \dots (8)$$

And the current I_r may therefore be represented as

$$I_r = \frac{AVK_t}{d} \quad (9)$$

Hence from (7) and (9), we obtain the relation

$$\epsilon''f = 18 \times 10^{11} K_t \quad \dots (10)$$

The total specific conductivity in this expression yields the value of total dielectric loss on computation. Pure a.c. dielectric loss may, however, be ascertained by taking the a.c. conductivity value K instead of K_t in the above expression. Hence the expression for pure a.c. dielectric loss is

$$\epsilon'' = \frac{18 \times 10^{11} \times K}{f} \quad \dots (11)$$

EXPERIMENTAL

Apparatus.—For the lower frequencies a Schering bridge was used for the determination of dielectric constant and power factor and for the higher frequencies a radio-frequency bridge was employed. The details of the bridges, detectors and the sources of current supply used in this investigation have been previously reported (Bhattacharya, 1944).

Electrodes.—The vertical type parallel plate gold condenser, described previously, was employed for soft lac resin and shellac wax, but for hard lac resin (α -lac) tin foil electrodes backed by hollow metal electrodes for the circulation of oil from a thermostat for controlling temperature could only be used. These have also been described earlier.

Materials.—Soft lac resin was obtained by Soxhlet extraction with diethyl ether from a sample of Kusmi shellac. This resin was then dissolved in ethyl acetate and boiled with decolourising charcoal to remove any colouring matter. After this treatment the soft resin was again boiled with petroleum ether under a reflux and the resin was vigorously stirred from time to time with a glass rod. After a few renewal of the petroleum ether, the soft resin was almost free from any wax, and this soft lac was heated at about 100°C in a vacuum-oven till it was free from any adherent solvent.

Hard lac resin was prepared from a sample of Kusmi lac by Soxhlet extraction with ether. Lac was ground to a fine powder, mixed with quartz sand and repeatedly extracted first with diethyl ether and then with petroleum ether in Soxhlet apparatus for the removal of soft lac resin and shellac wax. Finally the resin was dissolved in alcohol, filtered free from sand, precipitated again from a large volume of distilled water and then drawn into fibre on softening from the boiling water. These fibres were dried in air, powdered in a mortar and then finally dried in a vacuum-oven at 40°C .

Shellac wax was obtained by purifying Angelo Bros.' commercial shellac wax. The commercial wax was dissolved in benzene, boiled with decolourising charcoal under a reflux for 3 hours and then filtered. The wax recovered from the solution, after freeing it from the adherent solvent, was used for the experiments.

Method of procedure.—Soft lac resin and shellac wax could be melted at a higher temperature without any difficulty and so the vertical parallel plate condenser was used for their measurements. Detailed procedure regarding precautions to be taken to avoid adherent air bubbles, etc., has been given in the earlier paper. Shellac wax has a large contraction on solidification and so the molten wax was slowly allowed to solidify from the bottom in order that void formation may be avoided.

A few $4''$ discs were moulded out of hard lac resin using a very small quantity of stearic acid as mould lubricant. Higher pressure was necessary to mould hard lac than is generally

necessary for whole lac. The technique was the same as described previously (Bhattacharya, 1942). After about 80°C the discs began to soften and further readings could only be obtained with difficulty up to 90°C. But unlike whole lac hard lac could not be melted to such a degree of fluidity that the parallel plate condenser could be dipped in that molten mass. It was, therefore, not possible to obtain for hard lac readings at temperatures higher than 90°C.

CALCULATIONS

The formulæ used for the calculation of air capacitance of the test condenser, the correction for edge-capacitance of the condenser, etc., have been given in the previous paper.

RESULTS

(a) Soft lac resin

TABLE I

Dielectric constant—temperature data at different frequencies

Frequency in Kc/s	Dielectric constant ϵ' at the temperature of (°C)									
	10°	20°	30°	40°	50°	60°	70°	80°	90°	100°
500	3.35	3.52	3.74	3.99	4.24	4.60	4.99	5.33	5.55	5.71
100	3.46	3.68	3.94	4.24	4.56	5.10	5.56	5.86	6.00	6.06
50	3.50	3.75	4.06	4.38	4.76	5.36	5.82	6.08	6.13	6.14
25	3.56	3.80	4.14	4.50	4.92	5.60	6.06	6.28	6.28	6.22
10	3.60	3.90	4.26	4.68	5.20	5.96	6.28	6.38	6.36	6.30
5	3.66	3.95	4.36	4.82	5.44	6.12	6.53	6.44	6.40	6.34
3	3.70	4.01	4.46	4.99	5.61	6.27	6.48	6.51	6.46	6.40
2	3.76	4.08	4.55	5.11	5.88	6.43	6.60	6.62	6.57	6.50
1	3.84	4.19	4.70	5.34	6.11	6.70	6.72	6.66	6.60	6.53
0.5	3.95	4.33	4.92	5.73	6.59	6.90	6.88	6.79	6.66	6.54
0.05	4.20	4.87	5.80	6.55	6.90	7.02	7.00	6.87	—	—

TABLE II

Measured power factor data at different temperatures and frequencies

Frequency in Kc/s	Power factor (uncorrected for D.C. conductivity) at the temperature of (°C)									
	10°	20°	30°	40°	50°	60°	70°	80°	90°	100°
500	.0304	.0405	.0499	.0564	.0666	.0802	.0864	.0920	.0785	.0674
100	.0303	.0387	.0483	.0603	.0716	.0821	.0873	.0736	.0565	.0428
50	.0308	.0389	.0485	.0633	.0752	.0842	.0829	.0668	.0509	.0337
25	.0287	.0389	.0516	.0654	.0796	.0894	.0708	.0530	.0369	.0333
10	.0260	.0391	.0535	.0691	.0833	.0805	.0592	.0421	.0360	.0396
5	.0230	.0384	.0548	.0719	.0862	.0673	.0499	.0354	.0352	.0558
3	.0227	.0391	.0563	.0752	.0830	.0589	.0427	.0344	.0426	.0814
2	.0236	.0384	.0583	.0806	.0757	.0544	.0394	.0374	.0532	.1420
1	.0181	.0361	.0601	.0870	.0662	.0427	.0316	.0502	.0850	—
0.5	.0176	.0370	.0672	.0823	.0581	.0373	.0431	.0742	—	—
0.05	.0042	.0601	.0802	.0568	.0500	—	—	—	—	—

TABLE III

Total A.C. conductivity data at different temperatures and frequencies

Frequency in Kc/s	Calculated ($K, \times 10^8$) values from measured power factor at ($^{\circ}\text{C}$)									
	10°	20°	30°	40°	50°	60°	70°	80°	90°	100°
500	2.831	3.959	5.186	6.250	7.841	10.25	12.39	13.62	12.12	10.69
100	0.582	0.791	1.056	1.421	1.813	2.326	2.697	2.396	1.884	1.442
50	0.299	0.405	0.546	0.771	0.995	1.254	1.307	1.127	0.867	0.575
25	0.142	0.206	0.296	0.400	0.544	0.695	0.596	0.515	0.323	0.288
10	0.052	0.085	0.127	0.180	0.241	0.267	0.206	0.149	0.127	0.139
5	0.023	0.042	0.066	0.096	0.130	0.114	0.088	0.063	0.062	0.098
3	0.014	0.026	0.042	0.063	0.078	0.062	0.046	0.037	0.046	0.087
2	0.009	0.017	0.029	0.046	0.049	0.039	0.029	0.028	0.039	0.102
1	0.004	0.008	0.016	0.026	0.022	0.016	0.012	0.019	0.031	0.067
0.5	0.002	0.004	0.009	0.013	0.011	0.007	0.008	0.014	—	—
0.05	—	0.001	0.002	0.001	—	—	—	—	—	—

TABLE IV

Resistivity or conductivity—temperature data

Temperature		$1/T \times 10^3$	Resistivity $\rho_0 \times 10^{12}$	D.C. Conductivity $K_0 \times 10^{12}$	$\log \rho_0$
$t^{\circ}\text{C}$	$T^{\circ}\text{K}$				
20°	293	3.413	121	0.008	14.08
30°	303	3.300	25.0	0.040	13.40
40°	313	3.195	3.60	0.278	12.56
50°	323	3.096	0.57	1.750	11.76
60°	333	3.003	0.08	12.50	10.90
70°	343	2.915	0.022	45.40	10.34
80°	353	2.833	0.005	200.0	9.70
90°	363	2.755	0.002	500.0	9.30

TABLE V

Dielectric loss—temperature data at different frequencies

Frequency in Kc/s	Dielectric loss ϵ'' (Corrected for D.C. conductivity) at the temperature of ($^{\circ}\text{C}$)								
	10°	20°	30°	40°	50°	60°	70°	80°	90°
500	.1019	.1425	.1866	.2250	.2823	.3692	.4300	.4901	.4320
100	.1047	.1423	.1901	.2558	.3265	.4180	.4845	.4260	.3302
50	.1076	.1457	.1966	.2774	.3581	.4500	.4800	.4001	.2901
25	.1023	.1480	.2134	.2943	.3918	.4990	.4264	.3200	.1965
10	.0936	.1527	.2250	.3231	.4331	.4769	.3610	.2361	.1500
5	.0841	.1515	.2389	.3465	.4687	.4068	.3040	.1620	.0450
3	.0838	.1568	.2511	.3763	.4660	.3600	.2460	.1160	—
2	.0850	.1564	.2653	.4125	.4436	.3370	.2200	—	—
1	.0694	.1509	.2823	.4645	.3996	.2590	.1280	—	—
0.5	.0695	.1602	.3308	.4700	.3743	.2139	—	—	—
0.05	.0176	.2922	.4600	.3668	.2620	—	—	—	—

TABLE VI
Corrected Power factor—temperature data at different frequencies

Frequency in Kc/s		Power factor, $\tan \delta$ (corrected for D.C. conductivity) at the temperature of ($^{\circ}\text{C}$)							
		20°	30°	40°	50°	60°	70°	80°	90°
500	.0304	.0405	.0499	.0564	.0666	.0802	.0863	.0910	.0778
100	.0302	.0386	.0483	.0603	.0716	.0820	.0871	.0727	.0550
50	.0307	.0388	.0485	.0633	.0752	.0841	.0828	.0658	.0473
25	.0287	.0389	.0515	.0654	.0796	.0890	.0703	.0510	.0413
10	.0260	.0391	.0535	.0691	.0833	.0800	.0575	.0370	.0235
5	.0230	.0383	.0548	.0719	.0862	.0664	.0476	.0251	.007
3	.0226	.0390	.0563	.0752	.0830	.0575	.0379	.0178	
2	.0236	.0380	.0583	.0806	.0757	.0523	.0333	—	
1	.0181	.0361	.0601	.0870	.0600	.0387	.0190	—	
0.5	.0176	.0370	.0670	.0820	.0565	.0310	.0200	—	
0.05	.0042	.0601	.0800	.0560	.0380	—	—	—	

(b) Hard Lac Resin

TABLE VII
Dielectric constant—temperature data at different frequencies

Frequency in Kc/s	Dielectric constant ϵ' at the temperature of ($^{\circ}\text{C}$)						
	30°	40°	50°	60°	70°	80°	90°
500	3.54	3.64	3.93	4.22	4.52	5.00	5.42
100	3.65	3.74	4.03	4.36	4.74	5.32	5.97
50	3.69	3.77	4.08	4.42	4.80	5.55	6.18
25	3.72	3.80	4.10	4.44	5.00	5.76	6.38
10	3.76	3.82	4.15	4.54	5.12	5.84	6.60
5	3.77	3.85	4.18	4.60	5.29	6.01	6.90
3	3.80	3.87	4.23	4.66	5.41	6.21	7.10
2	3.82	3.90	4.30	4.78	5.53	6.35	7.24
1	3.85	3.96	4.33	4.95	5.76	6.60	7.37
.05	3.90	4.09	4.54	5.25	5.37	7.57	8.13

TABLE VIII
Measured power factor data at different temperatures and frequencies

Frequency in Kc/s	Power factor (uncorrected) at the temperature of ($^{\circ}\text{C}$)						
	30°	40°	50°	60°	70°	80°	90°
500	.0327	.0279	.0307	.0350	.0418	.0554	.0664
100	.0237	.0194	.0221	.0289	.0448	.0611	.0756
50	.0187	.0157	.0188	.0253	.0446	.0717	.0773
25	.0149	.0141	.0188	.0265	.0462	.0907	.0806
10	.0126	.0128	.0153	.0295	.0569	.0783	.0831
5	.0105	.0107	.0135	.0278	.0612	.0818	.0786
3	.0084	.0064	.0118	.0234	.0659	.0868	.0713
2	.0085	.0036	.0072	.0211	.0676	.0900	.0672
1	.0072	.0012	.0023	.0183	.0694	.0823	.0562
0.05	.0051	.0010	.0032	.0285	.0818	.0612	.0200

TABLE IX

Dielectric loss—temperature data at different frequencies

Frequency in Kc/s	Dielectric loss ϵ'' (corrected) at the temperature of ($^{\circ}\text{C}$)						
	30°	40°	50°	60°	70°	80°	90°
500	0.1156	0.1015	0.1206	0.1479	0.1888	0.2726	0.3582
100	0.0867	0.0724	0.0888	0.1262	0.2125	0.3253	0.4482
50	0.0688	0.0591	0.0769	0.1119	0.2145	0.3972	0.4753
25	0.0553	0.0535	0.0773	0.1179	0.2309	0.5170	0.5081
10	0.0472	0.0488	0.0635	0.1338	0.2914	0.4573	0.5484
5	0.0394	0.0414	0.0565	0.1277	0.3240	0.5032	0.5347
3	0.0321	0.0249	0.0498	0.1091	0.3565	0.5463	0.5012
2	0.0324	0.0141	0.0309	0.1009	0.3736	0.5556	0.4753
1	0.0275	0.0048	0.0097	0.1908	0.3995	0.5400	0.4103
0.05	0.0203	0.0041	0.0141	0.1502	0.5243	0.4512	0.1532

(c) *Lac-Wax*

TABLE X

Dielectric constant—temperature data at different frequencies

Frequency in Kc/s	Dielectric constant ϵ' at the temperature of ($^{\circ}\text{C}$)									
	10°	20°	30°	40°	50°	60°	70°	80°	90°	100°
500	2.60	2.61	2.60	2.61	2.62	2.63	2.68	2.69	2.67	2.63
100	2.62	2.62	2.62	2.64	2.65	2.66	2.70	2.70	2.67	2.63
10	2.69	2.68	2.69	2.68	2.59	2.69	2.76	2.72	2.68	2.63
1	2.77	2.78	2.77	2.75	2.76	2.76	2.79	2.74	2.68	2.63

TABLE XI

Measured power factor data at different temperatures and frequencies

Frequency in Kc/s	Power factor (uncorrected) at the temperature of ($^{\circ}\text{C}$)									
	10°	20°	30°	40°	50°	60°	70°	80°	90°	100°
500	.0082	.0110	.0142	.0123	.0107	.0104	.0042	.0034	.0001	.0010
100	.0100	.0098	.0118	.0137	.0145	.0106	.0076	.0068	.0004	.0008
10	.0120	.0110	.0135	.0127	.0085	.0068	.0078	.0034	.0016	.0035
1	.0013	.0012	.0013	.0009	.0009	.0003	—	—	—	—

DISCUSSION

We shall analyse the dielectric data collected for the three constituents of lac and discuss their implications separately. In a previous paper (Bhattacharya, 1944) the dielectric behaviour of whole lac has been fully discussed and in this paper reference to that earlier communication will be frequently made in order to avoid repetition of the conclusions drawn previously. Of

the three constituents the most complete study could be made of the soft lac resin owing to the comparative ease with which this resin could be handled at high temperatures without the apprehension of its being heat-hardened unlike whole lac or hard lac. Shellac wax was even better in this respect but it would be seen that it behaves almost like a non-polar wax and so a complete analysis of its dielectric data is not necessary. Practical difficulties, as stated in the previous section, stood in the way of recording dielectric data of hard lac resin at temperatures higher than 90°C .

Soft lac resin.—The power factor—temperature curves have been shown in figures 1 and 2.

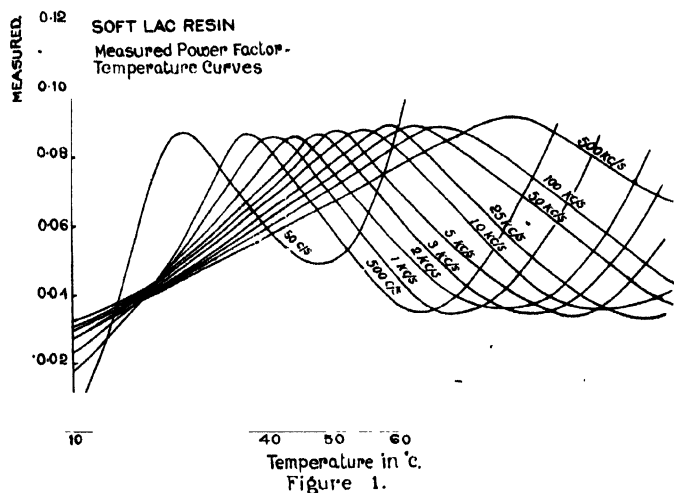
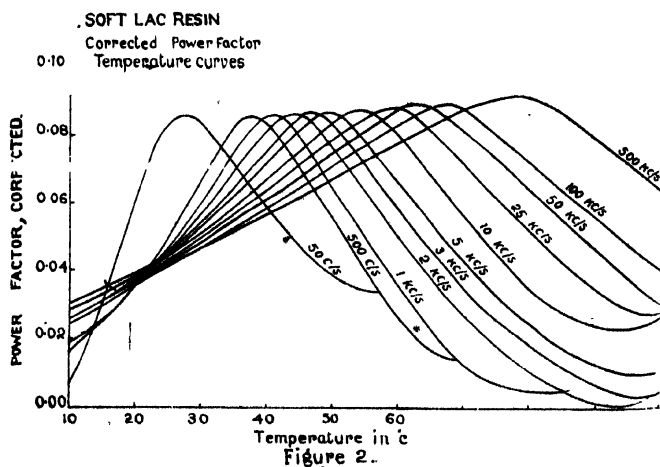


Figure 1 shows the variation of power factor of soft lac with temperature as measured, i.e., without any correction for the d.c. conductivity of the material whilst figure 2 shows the pure a.c. power factor—i.e., after correcting for the d.c. conductivity—plotted against temperature. The nature of these curves is similar to those obtained for whole lac and in general for polar liquids. Each curve rises gradually to its maximum

height and then falls again. The maximum point is indicated by a temperature which is characteristic of a frequency.

Unlike curves for whole lac however the maximum value of power factor practically remains the same for all frequencies and is about 0.085—0.090. For whole lac the maximum value was 0.105 at 50 cycles/second and with increasing frequency it gradually fell to 0.0805 at 100 Kc/s. At 50 c/s the maximum power factor of soft resin takes place at so low a temperature as 27.5°C , whereas at 500 Kc/s this



occurs at 79°C . The value of power factor at 22°C for practically all frequencies above 500 c/s is about 0.04 and at both higher or lower temperatures it varies with frequency.

The dielectric constant—temperature curves and the dielectric loss—temperature curves have been shown in figures 3 and 4. They are typical polar resin curves. Each curve in figure 3 is characterised by a sudden rise in dielectric constant and afterwards by a tendency

towards a flat maximum followed by a slow decrease in the flat maximum value. For whole lac the drooping portion of such curves could not be obtained since it occurred at higher temperatures than 110°C and there was the apprehension of considerable heat hardening in the resin at such temperatures. For soft lac, however, there was no such difficulty and a complete curve could be obtained. The maximum value of dielectric constant for any frequency is lower for soft resin than for whole lac as may be seen from the curves. Thus ϵ_m' for soft lac at 50 c/s is 7.0, for 500 c/s it is 6.9 and for 1, 3, 5, 10, 50 and 100 Kc/s the respective values are 6.75, 6.50, 6.44, 6.38, 6.15 and 6.10, whereas for whole lac the respective values are higher even at 110°C .

The dielectric loss curves are also similar to those of whole lac. The maximum loss ϵ_m'' , however, is less and is less than 0.5 for all frequencies. The general nature of these curves is also similar to those of lac except that no definite decreasing tendency in the ϵ_m'' value with rising frequency can be noticed.

Now as in the case of lac we can just get an idea of the relaxation time of the soft lac molecule from the relation

$$\epsilon_m'' = \frac{\epsilon_0' - \epsilon_{\infty}'}{2}$$

where

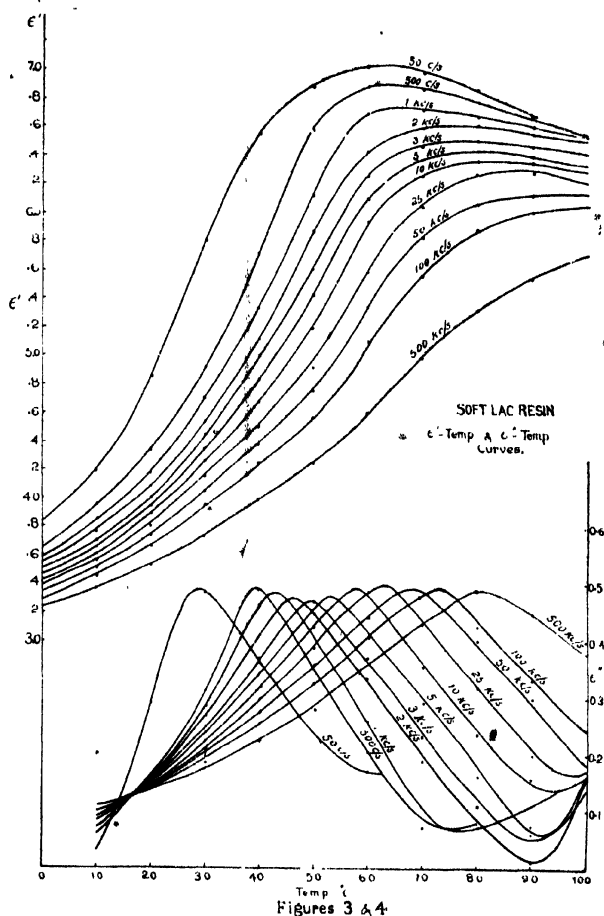
ϵ_m'' = the maximum value of dielectric loss,

ϵ_0' = the static dielectric constant,

and

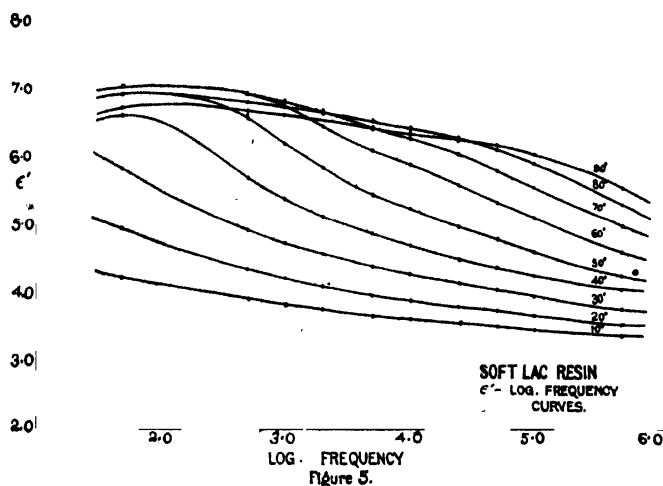
ϵ_{∞}' = the low temperature value of dielectric constant.

Adopting the estimated value 7.5 for ϵ_0' and 3.5 for ϵ_{∞}' at 60°C (from figure 5) we see that the maximum loss value should have been 2.0 according to the simple Debye theory, but actual ϵ_m'' obtained is only 0.5 which is only a quarter of the calculated value. Hence, although the soft resin molecule has a comparatively lower molecular weight, a distributed range of relaxation times is suggested for this smaller molecule too. It has been already mentioned



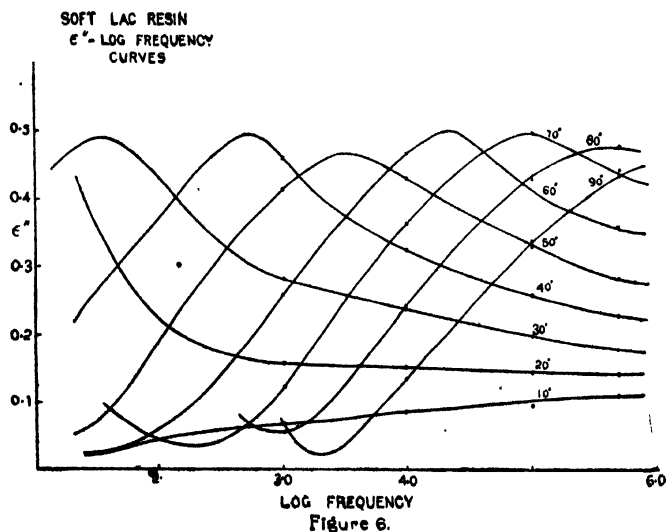
how the effect of a distributed range of relaxation time in a molecule can be shown from

theoretical grounds (Yager, 1936) to diminish the ϵ_m'' values and also to widen the dispersion band. In order to show the spread of the dispersion band in this case, figures 5 and 6 have been included. From figure 6 it may be seen, that the band spreads over a very wide range, viz., for at least 5 or 6 decades. From both these considerations, viz., the diminished ϵ_m'' value as well as the widespread dispersion range, a distributed range of relaxation time of the soft



resin molecule suggests itself. If ϵ''/ϵ_m'' values are plotted against f/f_m , which may be easily be computed from the ϵ'' - $\log f$ graph, more bluntness or flatness of the curve than the Debye graph shows the effect of distributed relaxation time in the molecule. A comparative study of the degree of such an effect in different molecules may be made by the plot of such curves in a single graph, where more blunt curves will indicate greater effect of distributed relaxation time and the coincidence with the Debye curve will naturally show absence of distribution, i.e., a single relaxation time.

Fig. 7 shows such a graph for soft lac resin and the existence of a distributed range of relaxation time in the molecule may be seen from the bluntness of the curve. A comparison with the whole lac curve can also be made from this graph for which curve (B) has been included. This is for Kusmi lac resin taken from the previous paper (Bhattacharya, 1944). It is observed that the bluntness of the soft lac curve (curve A) is slightly less than the Kusmi whole lac curve (curve B). This is just what may be expected since the soft lac molecule being smaller in size than the whole lac molecule should follow more closely the ideal Debye curve meant only for small polar molecule with a single relaxation time.



A method of finding out the distribution coefficient of relaxation times of a polar molecule has very recently been given by Fuoss and Kirkwood (1941). They observe that for polar resins the loss factor ϵ'' can be represented by the approximate equation

$$\epsilon'' = A \operatorname{sech} \alpha x$$

where A is a constant, characteristic of the resin and derivable from dielectric constant data, α is the parameter which measures the width of the distribution and x is the natural logarithm of the ratio of the frequency at maximum absorption to the frequency at which ϵ'' is measured. They

have also given a method whereby α , the distribution parameter of relaxation times of a polar system can be calculated from the observed loss factor—frequency curves. By following their method of calculation a value of 0.40 was obtained for α , the distribution parameter of soft lac. It may be remembered that α gave a value of 0.35 for Kusmi lac, and that distribution coefficient of relaxation times may be compared favourably with the distribution parameter of a resin system containing 80% polyvinyl chloride and 20% diphenyl (Fuoss and Kirkwood, *loc. cit.*). Soft lac resin has a still higher value of distribution parameter and in order to get an idea of this distribution by comparison with a polyvinyl chloride—diphenyl system we can only observe that a much higher percentage of the plasticiser will be required to yield a similar resin.

Now in order to get an idea of the dimensions of the rotating unit, which contributes to the dielectric loss, we can use the relation

$$\tau = \frac{4\pi\eta a^2}{kT}$$

where

τ = relaxation time of the rotator,

η = coefficient of viscosity,

a = radius of the rotator,

k = Boltzman constant,

and

T = Temperature on Absolute scale.

τ can be calculated by means of the equation

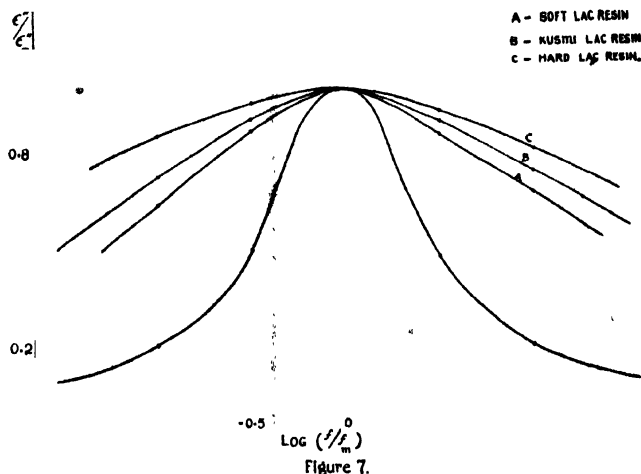


Figure 7.

at the point where maximum dielectric loss takes place for any frequency in the loss factor—temperature ($\epsilon''-t$) graph ϵ' and ϵ_0' are the values of dielectric constant at infinite and

zero frequencies respectively i.e., dielectric constant at very high frequencies or low temperatures and that at very low frequencies or the static value of the dielectric constant respectively. These values may be estimated from $\epsilon' - \log f$ graph and can be used in the calculation of relaxation time τ .

But the viscosity of soft lac resin at different temperatures was not known. In order to collect viscosity data of soft lac, therefore, a set of Lee's modified Ostwald viscometer usually meant for measurement on tar (Lee, 1934) was employed. The results have been shown in Table VII, it may be observed that these data can be represented by the usual logarithmic

$$\text{formula } \log \eta = A + \frac{B}{T} = A + \frac{Q}{RT}$$

TABLE XII
Viscosity—temperature data

Temperature		$T/1 \times 10^3$	Viscosity in poise η	$\log \eta$
$t^\circ\text{C}$	$T^\circ\text{K}$			
55°	328	3.049	25,200	4.40
60°	333	3.003	10,100	4.00
70°	343	2.915	2,000	3.30
80°	353	2.833	503	2.70
90°	363	2.755	134	2.13

The graphical representation has been shown by the top line of figure 8. It was not possible to carry out the measurement of viscosity at any temperature below 55°C, as the viscosity seemed to be too high to be measured even with Lee's viscometer of the largest capillary diameter (6 mm.). From this graph, however, viscosity at any temperature within the range of measurement can be obtained.

Now the temperature of maximum loss at any frequency (Fig. 4) which falls within the above range of temperature may be taken and τ calculated from the relation

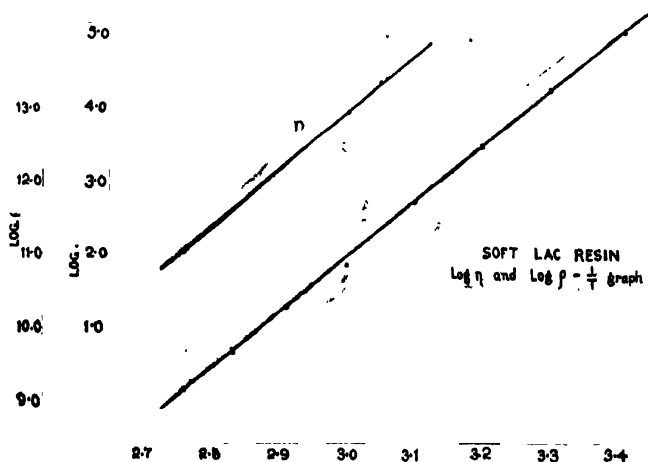


Figure 8.

The viscosity, corresponding to this maximum loss temperature, determined from the viscosity—temperature graph, may now be used in the equation

$$\tau = \frac{4\pi\eta a^3}{kT}$$

and thus the average radius of the rotating unit obtained. Table XIII shows the results of such calculations, from which it may be seen that, as in the case of whole lac, soft lac also yields practically the same value of radius for its rotator, viz., about 1.50×10^{-8} cm. The conclusions arrived at previously have thus been strengthened by an independent set of measurements on soft lac and may, therefore, be repeated here. In the alternating current field the molecules of neither whole lac nor soft lac can rotate as a whole but the most probable polar group, viz., the hydroxyl group takes part in the rotation. It is really very interesting that, on calculation from data obtained at different frequencies, practically the same value of radius has been obtained and that coincides with the radius of the most probably polar group in the molecule of either whole lac or soft lac. The only argument that can be placed against this calculation is the uncertainty regarding the inner friction coefficient of soft lac for which the macroscopic viscosity determined experimentally has been taken as equal. It has already been stated that the results of experiments with various polar liquids have shown that at least for liquids the macroscopic viscosity and the inner friction are the same, and from our present knowledge regarding the physico-chemical behaviour of thermoplastic resins we are inclined to include them in the category of liquids.

TABLE XIII

Calculated relaxation time and radius of the rotator

Loss max. temperature t ^m	Relaxation time τ	Frequency f	Viscosity η	Radius of the rotator a
63°	4.00×10^{-6}	25 Kc/s	5×10^3	1.43×10^{-8} cm
69°	2.04×10^{-6}	50 Kc/s	2.4×10^3	1.47×10^{-8} cm
74°	1.02×10^{-6}	100 Kc/s	1.2×10^3	1.49×10^{-8} cm
83°	2.08×10^{-7}	500 Kc/s	2.63×10^2	1.45×10^{-8} cm

The relation $\tau = \frac{4\pi\eta a^3}{kT}$ is based upon Stoke's law which is generally applicable to liquids.

But we can test from experimental data whether the inner frictional torque is proportional to macroscopic viscosity or not. To do this let us first of all assume that it is so. In that case we can write.

$$\tau = \xi / 2KT = C \eta / T$$

or, $T\tau = C \eta$

or, $\log T\tau = C' + \log \eta$

Substituting for $\log \tau$, the above relation can further be written as

$$\log T\tau = C' + \frac{Q}{RT}, \quad [\text{since } \log \eta = A + \frac{Q}{RT}]$$

where Q = molar activation energy and R = molar gas constant

If the above assumption is true, a straight line graph is expected when $\log T\tau$ is plotted against $1/T$.

An actual plot for frequencies of 50 c/s, 1 Kc/s and 10 Kc/s shows that straight lines are obtained (Fig. 9). The relaxation time τ was calculated from the relation.

$$\omega\epsilon'' = \frac{\epsilon' + 2}{\epsilon_0' + 2} \epsilon_m'' \pm \sqrt{\epsilon_m''^2 - \epsilon''^2}$$

Thus we see that the macroscopic viscosity is at least proportional to inner friction, if not equal.

TABLE XIV

Log $T\tau$ and $1/T$ data

Frequency f	Temperature		Relaxation time τ	$T\tau$	$1/T \times 10^3$	$\log T\tau$
	$t^\circ\text{C}$	$T^\circ\text{K}$				
50 Kc/s	20°	293	67.0×10^{-4}	1.9630	3.413	0.2930
	30°	303	13.7×10^{-4}	0.4151	3.300	0.3819
	40°	313	63.7×10^{-5}	0.1993	3.195	0.7004
	50°	323	19.1×10^{-5}	0.0617	3.096	1.2098
	60°	333	62.1×10^{-5}	0.1820	3.413	0.7400
1 Kc/s	20°	293	31.4×10^{-6}	0.0951	3.300	1.0217
	30°	303	13.7×10^{-6}	0.0428	3.195	1.3678
	40°	313	47.8×10^{-6}	0.0154	3.096	1.8114
	50°	323	26.9×10^{-6}	0.0895	3.003	2.0478
	60°	293	62.1×10^{-6}	0.0182	3.413	1.7400
10 Kc/s	20°	293	41.2×10^{-6}	0.0125	3.300	1.9037
	30°	303	26.0×10^{-6}	0.0081	3.195	2.0895
	40°	313	17.0×10^{-6}	0.0055	3.096	2.2604
	50°	323	83.0×10^{-7}	0.0022	3.003	2.5585
	60°	333				

Another checking of this may be made from the d.c. conductance data. The d.c. con-

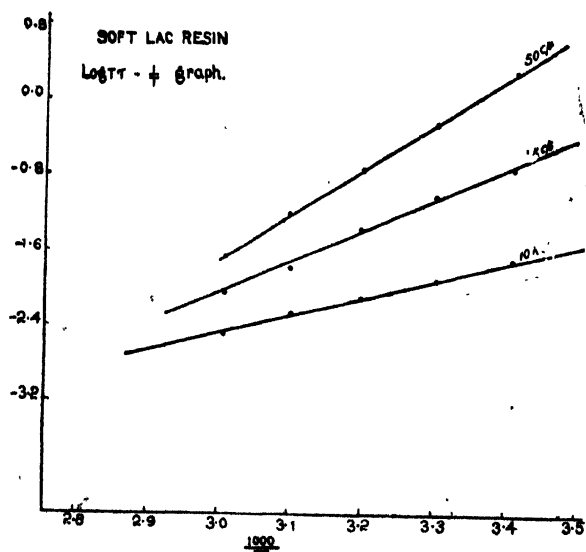


Figure 9.

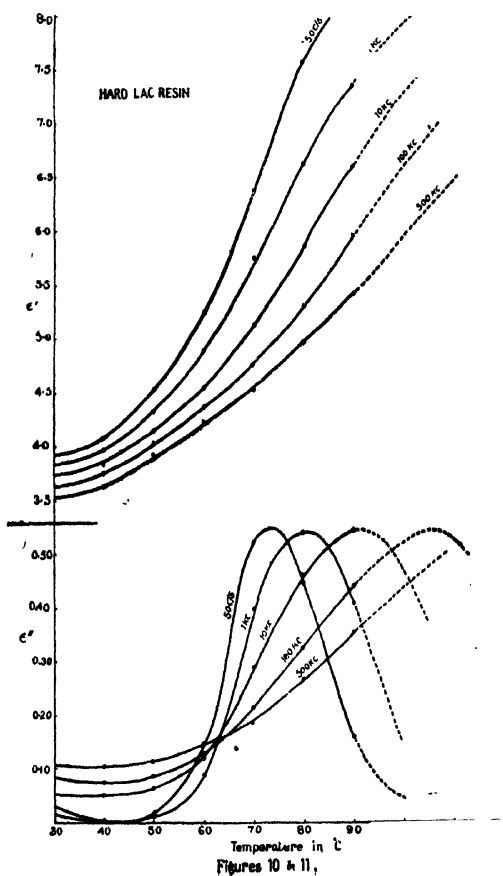
ductance of an insulating material is believed to be due to the mobility of its free ions. As the mobility is directly proportional to fluidity or inversely to viscosity at any temperature, an idea can be had as to how the inner friction varies with temperature from the d.c. conductance-temperature relation of the material. The bottom line of figure 8 shows that the logarithm of d.c. conductance K_0 of soft lac gives a straight line plot with $1/T$ throughout the whole range of investigation. And this straight line has

practically the same slope with x -axis as the viscosity line, or in other words both of them have the same Q value. Thus we see from this angle of view too that the macroscopic viscosity and the inner friction vary exactly similarly with temperature.

Calculating from the slope of these lines with $1/T$ axis, we find that the molar activation energy Q yields a value of 33.8 K-cal from d.c. conductivity data. Thus both these values are practically the same. Similarly the molar activation energy can be calculated from the $\log Tr-1/T$ graphs of figure 9. The value of Q will be different frequencies here, as is evident from the inclination of each line with the $1/T$ axis. The value of Q will be less and less with increasing frequency as is seen from the graph. In fact Q for 10 Kc/s is 8.0 K-calorie, for 1 Kc/s is 14.6 K-cal and for 50 c/s is 21.3 K-cal on calculation from the slope of these lines. Thus we see that the value of Q for still lower frequencies than 50 c/s will be greater than 21.3 K-cal and the value of about 34.0 K-cal obtained from the d.c. conductivity data is more or less in agreement with the value 33.0 K-cal obtained from the a.c. data by extrapolation to zero frequency.

If we compare these Q values with those of Kusmi lac calculated under similar conditions we find that the activation energy at 50 c/s is practically the same for both Kusmi lac and soft lac *viz.*, approximately 21.0 K-cal. But with the increase of frequency soft lac requires comparatively less energy than whole lac. Thus at 1 Kc/s soft lac requires about 15.0 K-cal whereas whole lac approximately 20.0 K-cal and at 10 Kc/s the value of Q for soft lac is only 8.0 K-cal whilst for whole lac it is 15.0 K-cal.

The dielectric constant of soft lac even at 0°C is pretty high compared with the square of its refractive index at that temperature. The value of refractive index at 20°C is 1.4976 and computing from the temperature coefficient of refractive index (Bhattacharya, 1940) the value at 0°C may be estimated to be approximately 1.505. Hence we should expect that the dielectric constant of soft lac will be less and less at temperatures below zero till it approximates to the square of its refractive index at that temperature. This will happen when the dielectric constant will have the approximate value of 2.3, and assuming the linear variation at such low temperatures this may be expected to take place at -40°C or so.



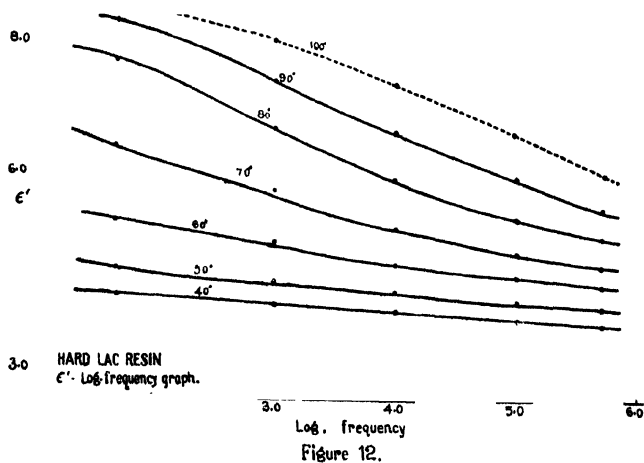
Figures 10 & 11.

Hard Lac Resin.—Measurements on hard lac discs could only be carried up to 80°C and with difficulty up to 90°C. Thereafter the discs began to get deformed due to softening. The results have, however, been shown in figures 10 and 11. For the sake of clearness in drawing curves at 50 c/s, 1 Kc/s, 10 Kc/s, 100 Kc/s and 500 Kc/s only have been drawn. They are just like Kusmi lac curves so far as could be judged from their nature and some of them have been extrapolated freely in order to study their nature at higher temperatures. The extrapolated part of each curve has been shown in broken line.

The first difference that may be noticed in these dielectric loss curves from the Kusmi lac ones is their similarity in the maximum height. The value of ϵ_m'' , therefore, does not increase with decreasing frequency. Soft lac also showed more or less constant value of loss peak for all frequencies. If we take whole lac as a solid solution of pure lac in soft lac, the phenomenon of having increasing ϵ_m'' with decreasing frequency remains apparently unexplained. A further study of this abnormal behaviour of lac is being made and the result will be reported in another paper.

The loss peak of hard resin at 50 c/s takes place at 74°C whilst at 1 Kc/s, 10 Kc/s and 100 Kc/s the maximum loss probably takes place at 81°C, 91°C and 106°C respectively. The last two values are obtained by extrapolation and so may not be accurate. Comparing with soft lac and whole lac it appears that for any frequency the loss curve of hard lac takes up the extreme right position on the same temperature axis, that of whole lac the middle position and the soft lac curve the left position. The softening points of these resins are also in this order and if whole lac is looked upon as hard lac plasticised with soft lac each loss curve of hard lac will shift leftward, the amount of shift depending upon the soft resin content of lac. Such a behaviour has been observed by others (Davies, Miller and Busse, 1941; Fuoss, 1941) while experimenting with plasticised synthetic resins. The role of plasticiser is to shift any loss curve towards the left as a result probably of diminishing inner viscosity.

The ϵ' —frequency and ϵ'' —frequency curves have been included in figures 12 and 13.



From the loss curves it will appear that for hard lac the dispersion band is wider at any temperature than whole lac. The ϵ''/ϵ_m'' plot against f/f_m has been included in figure 7 along with soft lac. The 80°C data have been used for this purpose. Here also it may be seen that the curve for hard lac is more blunt than the Kusmi lac curve. Owing to the difficulty of measurement the viscosity data of hard lac could not be obtained and so the size of the hard lac

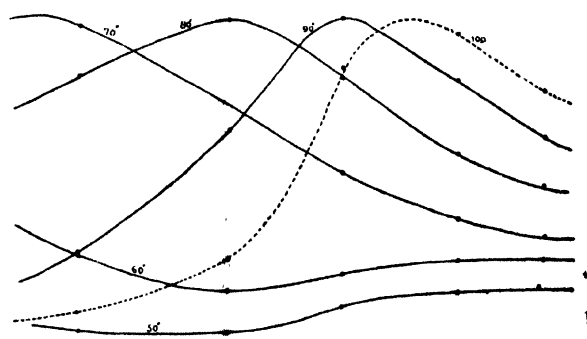
rotating unit remains undetermined. But the distribution coefficient of relaxation times of the hard lac rotating unit could be determined according to the method of Fuoss

and Kirkwood and the value obtained for the distribution parameter was only 0.26. Thus we see that gives a value of 0.40, 0.35 and 0.26 for soft lac, whole lac and hard lac respectively showing thereby that of the three soft lac conforms most to the ideal Debye curve.

We have seen that loss curves of Kusmi lac begin to rise abruptly between 35°C and 40°C; for hard lac this happens after 50°C. For soft lac, however, such a point is difficult to obtain and if it exists at all this must be at a temperature below the experimental range, *i.e.*, below 10°C. The refractive index experiments also showed the existence of such a transition temperature for hard lac at 50°C or so (Bhattacharya, 1940). There it was observed that the temperature coefficient of refractive index of hard lac above 50°C was about three times that below it. But for soft lac no such temperature could be noticed and the temperature coefficient was uniform throughout the experimental range of temperature, *i.e.*, between 20°C and 90°C.

Lac-wax.—From the nature of dielectric constant-temperature graph (Fig. 14) it appears at first sight that lac-wax behaves almost as a non-polar substance. This lac-wax, it must be remembered, was purified from the commercial lac-wax, *i.e.*, it was only the alcohol soluble wax which is of course the main constituent comprising about 85% of the total. Tschirch and Schaefer (1926), investigated into the nature of this wax and they considered that it consisted of wax ester which on saponification gave an alcohol, probably $C_{26}H_{52}O$, and an acid $C_{26}H_{50}O_2$. On the evidence of crystal spacings, however, Chibnall and his

HARD LAC RESIN
C²-log frequency graphs.



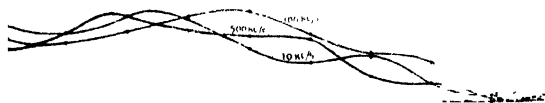
Log frequency
Figure 13.

C²75



CHIFFLAC WAX
Temp. and loss
graphs

C² 0.015



Figures 14 & 15

co-workers (1934), are of the opinion that alcohol-soluble lac-wax is simply a mixture of primary alcohols of even number carbon atoms from C_{26} to C_{34} .

Alcohols are of course polar substances the molecules of which have an average moment of 1.68 Debye units but their dielectric constants decrease with the increase of carbon atoms

in the molecule. Thus dielectric constants of methyl and ethyl alcohol at 20°C are 31.2 and 25.8 whilst those of heptyl and octyl alcohols are 4.2 and 3.4 respectively. This may easily be explained if we consider that although the electric moment of the individual molecule of an alcohol remains practically the same the number of molecules per unit volume decreases with the lengthening of the carbon chain. Hence the dielectric constant is lowered. Baker and Smyth (1938), have recently studied the dielectric constant as well as the anomalous dispersion of cetyl alcohol, $C_{16}H_{33}OH$. They find that although the dielectric constant at 50 Kc/s near about 20°C is only 2.23 there is definite evidence of anomalous dispersion taking place just below the melting point of the alcohol, the dielectric constant at the melting point being about 4.30. We find from this that the variation of dielectric constant for the anomalous dispersion range is small and it may be expected that with a further increase of carbon chain this change of dielectric constant will be still smaller.

For lac-wax we find that a sudden discontinuity arises in the dielectric constant—temperature curve near about 60°C for practically all the frequencies used and above 80°C there is a tendency for all the curves to mix up. At 100°C or so the dielectric constant is practically independent of frequency. But at temperature below 60°C the dielectric constant is not independent of frequency but almost independent of temperature. The melting point of the wax was 83°C and the softening point 67°C, when determined by the mercury surface method (Rangaswami & Sen, 1942). From the temperature dependence of dielectric constant it appears, therefore, that the inner softening of the wax starts somewhat earlier than the temperature indicated by the softening point as determined by the mercury surface method. It should also be seen that even in the solid state of the wax there is some freedom of movement of the polar group—some form of dipole orientation—although general rotational freedom is not possible. This is clear from the frequency dependence of dielectric constant at low temperatures as well as from the inequality of these values from the square of the optical refractive index (about 2.2). The study of dielectric constant of many other solids has also indicated such a possibility. In the case of lac wax of course some explanation for the high value of dielectric constant just below the melting point of the wax is possible, *e.g.*, it being a physical mixture the presence of some components in the liquid phase just below the melting point of the wax is possible especially when a sharp melting point, as is generally obtained for pure organic compounds, is wanting here. But such an explanation is untenable at still lower temperatures, for all the components of this wax are primary alcohols containing no less than 26 carbon atoms and their individual melting points must be high. At ordinary temperatures all of them are expected to be solids and therefore the possibility of some amount of dipole orientation even at such a state should be entertained.

It is difficult to draw any useful conclusion from the power factor—temperature curves of lac-wax (figure 15). But we find that the power factor is extremely low at high temperatures when the wax is completely in the liquid phase. We thus see that all the molecules present in the wax can freely orient with the applied a.c. field after melting. This is possible because although their average molecular weight is about 450, being only primary alcohols they have simple structure. Their inner friction, therefore, is low and the resistance to orientation small. Hence the energy absorbed is small. The undulating nature of the curve at any frequency is probably the result of several peaks of which two are distinctly discernible.

It may now be noticed that lac-wax has no undesirable dielectric property which some people ascribe to it (Rangaswami and Sen, *loc. cit.*) noticing probably the widespread use of wax-

free shellac in some electrical industries. The use of de-waxed shellac has spread mainly for good adhesion and less water absorption of the varnish film and not for any undesirable dielectric property of lac wax. In fact the dielectric properties of lac wax are even better than those of either pure lac resin or soft lac regarding loss at slightly high temperatures. But its adhesion properties are poor since it is only a waxy material and not a resin and the water absorption of the de-waxed lac film has been found to be less than that of the whole lac film. Moreover the wax-free shellac film gives a more attractive appearance owing to its clearness and transparency although it suffers from some mechanical defects especially elasticity. Baking improves some of its mechanical properties and on comparing the properties of film produced from whole lac and wax-free lac one investigator (Rangaswami, 1933) is of the opinion that "a wax-free film or one with a low percentage of wax is preferable whenever baking is practicable as, for example, in the electrical industry." These are the reasons why wax-free lac is used in the electrical industry and not for any inferior dielectric property of lac wax.

ACKNOWLEDGMENT

The author is grateful to Dr. H. K. Sen, Director of this Institute, for his kind interest in this work.

PHYSICAL AND PHYSICO-CHEMICAL LABORATORIES,
INDIAN LAC RESEARCH INSTITUTE,
NAMKUM, RANCHI.

REFERENCES

- Baker, W. O. and Smyth, C. P., 1938, *J. Amer. Chem. Soc.*, **60**, 1229.
 Bhattacharya, G. N., 1940, *Ind. J. Phys.*, **14**, 237;
 „ „ 1942, „ „ **16**, 261;
 „ „ 1944, „ „ **18**, 1,
 Chibnail, A. C., Piper, S. H., Pollard, A., Williams, E. F., and Sahai, P. N., 1934,
Biochem. J., **28**, 2189
 Davies, J. M., Miller, R. F. and Busse, W. F., 1941, *J. Amer. Chem. Soc.*, **63**, 361.
 Fuoss, R. M., 1941, *J. Amer. Chem. Soc.*, **63**, 378.
 Fuoss, R. M. and Kirkwood, J. G., 1941, *J. Amer. Chem. Soc.*, **63**, 385.
 Lee, A. R., 1934, *J. Soc. Chem. Ind. (Trans.)*, **53**, 69T
 Rangaswami, M., 1933, *I. L. R. I Res. Note No. 8*, 2.
 Rangaswami, M. and Sen, H. K., 1942, *A Handbook of shellac analysis. (Ind. Lac Res. Institute)*, 25.
 Tschirch, A. and Shaefer, H. H., 1926, *Pharm. Acta Helvetiae*, **1**, 9 (A. C. Abstr. **20**, 2390)
 Yager, W. A., 1936, *Physics*, **7**, 434.

THE DIELECTRIC PROPERTIES OF DIFFERENT MIXTURES OF HARD AND SOFT LAC RESIN

By G. N. BHATTACHARYA

ABSTRACT. The dielectric properties of mixtures of hard lac and soft lac have been measured over a wide range of frequency and temperature and the results analysed in the light of those obtained previous for whole lac as well as its constituents. The anomalous dielectric loss behaviour of whole lac compared to those of its constituents has been traced to the presence of a small amount of moisture which lac retains even on ordinary desiccation. It has been shown that this moisture is in the combined state and cannot be in the free state. The nature of this moisture, whether extraneous or not, has been fully discussed.

INTRODUCTION

In two previous papers of this series (Bhattacharya, 1944) it has been reported that both lac resin and its two chief constituents behave as typical polar resins in the a.c. field. But there is a slight difference in the behaviour of whole lac from that of either soft or hard lac regarding dielectric loss. In the case of whole lac the maximum value of dielectric loss slowly increases with the decrease of frequency whereas for either soft or hard lac this effect is not distinctly visible. In the case of these constituents ϵ_m'' the maximum value of loss is more or less constant throughout the range of frequency investigated. According to our present knowledge lac, as, such is simply a mixture of three main constituent bodies, viz., (1) hard lac, pure lac or α -lac (2) soft lac and (3) lac wax. Of these three constituents the last one does not usually comprise more than 5% of the total lac and its loss has also been observed to be very small. The other two constituents are, therefore, mainly responsible for the loss of whole lac. Now the maximum value of dielectric loss at the lower frequencies for both hard and soft lac lies near about 0.5 whilst ϵ_m'' for whole lac is definitely more than this figure and is approximately 0.7 at 50 c/sec. It is difficult to explain this increased loss if it is supposed that lac is a solid solution of hard lac in soft lac. In order to see whether a mixture of dry hard and soft lac in the proportion in which they are present in whole lac also exhibits similar behaviour regarding loss, this investigation was undertaken. The plan was to take a few mixtures of desiccated hard lac and soft lac in different proportions, determine their dielectric properties and see if the results follow any general rule regarding dielectric loss and temperature shift for compositions containing different proportion of constituents. For it has already been observed that the presence of soft resin in lac is responsible for diminishing the internal viscosity of hard lac and so shifts the dielectric loss curve towards the low temperature side. In other words soft resin acts as a plasticiser for hard lac and whole lac is only a plasticised hard lac with soft lac so far as dielectric properties are concerned. Other workers (Fuoss, 1941; Davies, Miller and Busse, 1941) have also studied the effect of plasticiser content on some synthetic resins and found that an increase of plasticiser results in the decrease of internal viscosity of the resin and this is manifested by a shift towards the low temperature side of the loss curve.

T H E O R E T I C A L

We know that the complex dielectric constant ϵ of a substance is usually expressed as

$$\epsilon = \epsilon' - i\epsilon''$$

where ϵ' = the real or ordinary dielectric constant, and ϵ'' = the imaginary part or the loss factor; and that $\epsilon'' = \epsilon' \tan \delta$, δ being the complementary phase angle or the loss angle. Thus both ϵ' and ϵ'' can be determined over any capacity bridge, which usually gives the value of capacity of a condenser and its power factor, $\tan \delta$.

But the expression for current in phase with the applied voltage is

$$I_r = I \tan \delta = \omega CV \tan \delta = 2\pi f CV \epsilon'' = \frac{fAV\epsilon''}{d \times 18 \times 10^{11}}$$

Since $C = \frac{A\epsilon'}{4\pi d \times 9 \times 10^{11}}$ farads for a parallel plate condenser

And if K , is the total conductance of this condenser

$$I_r = \frac{AV.Kt}{d}$$

Hence from the last two equations, we have

$$\epsilon'' = \frac{18 \times 10^{11} \times Kt}{f}$$

A part of this loss will be due to d.c. conductivity of the material if that is appreciable and its measure will be

$$\epsilon''_{k_0} = \frac{10^{11} \times 18 \times K_0}{f}$$

Hence pure a.c. loss is given by $\epsilon'' = \frac{18 \times 10^{11} \times (Kt - K_0)}{f} = \frac{18 \times 10^{11} \times K}{f}$

E X P E R I M E N T A L

Apparatus.—A Schering bridge was used for the determination of dielectric constant and power factor at lower frequencies and a General Radio radio-frequency bridge which is a modified form of Schering bridge was employed at higher frequencies. These bridges were the same as had been used on previous occasions.

Electrodes.—The vertical type parallel plate gold condenser which has already been described was utilised for different mixtures of soft and hard lac. The mixtures were taken in such proportions that they could be easily melted and the gold condenser put in that molten mass.

Materials.—The samples of soft and hard lac used for these experiments were the same as had been used for the determination of their dielectric properties. The details of the method of purification of these lac constituents have been reported in a previous paper (Bhattacharya, *loc. cit.*)

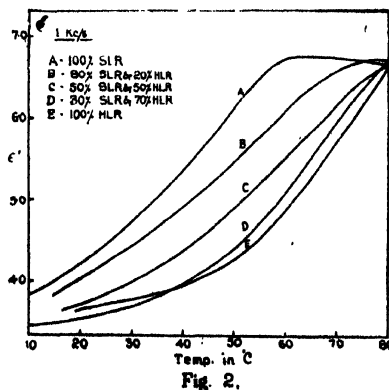
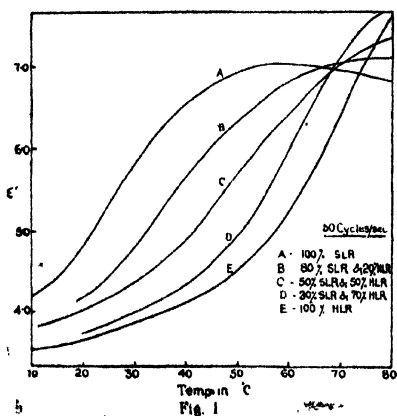
Method of procedure.—The required quantities of the two lac constituents were weighed separately according to the proportion taken and then they were mixed up intimately using the following method. This procedure was found most suitable after many attempts to mix them thoroughly and intimately were made. Soft lac was first taken in a basin and melted

TABLE II (contd.)

Frequency	Temp. °C	100% S. L. R.	80% S. L. R. 20% H. L. R.	50% S. L. R. 50% H. L. R.	30% S. L. R. 70% H. L. R.	100% H. L. R.
1 Kc/s	30°	0.282	0.122	0.046	0.024	0.028
	40°	0.465	0.241	0.109	0.043	0.005
	50°	0.400	0.411	0.232	0.100	0.100
	60°	0.259	0.463	0.408	0.231	0.091
	70°	0.128	0.252	0.486	0.490	0.400
	80°	—	0.098	0.281	0.482	0.540
	90°	—	—	0.099	0.263	0.410

DISCUSSION

The results have been shown in Tables I and II in which data for soft resin and pure lac resin have been taken from the previous paper of this series. Figures 1, 2, 3 and 4 show the dielectric constant-temperature relationship for these resin mixtures as well as soft resin and pure resin at 50 c/s, 1 Kc/s, 10 Kc/s and 100 Kc/s respectively. Figures 5 and 6 show their dielectric loss-temperature variation at 50 c/s and 1 Kc/s. All these curves belong to a group in which gradual transition from one to the other may be made by simply increasing or decreasing one or the other component. Thus from Figs 1, 2, 3, 4, 5 and 6 curve A representing 100% soft resin and curve E representing 100% pure resin there may be seen three curves B, C and D whose nature gradually changes from that of A to E. Figure 7 shows the variation of dielectric loss with the composition of the mixture of soft and hard lac resins at constant temperatures. The nature of these curves, it may be seen from the above figure, is similar to a dielectric loss temperature curve at constant frequency when a definite composition is taken. But there is a distinct difference which may be noted. At lower temperatures, such as 30°C or 40°C, these loss curves rise sharply to a peak and then fall again to low values. As the temperature gradually rises these peaks become more and more blunt



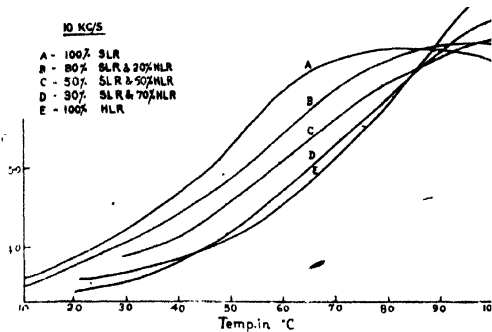


Fig.3

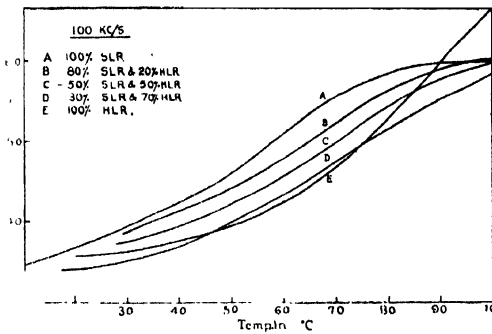


Fig.4.

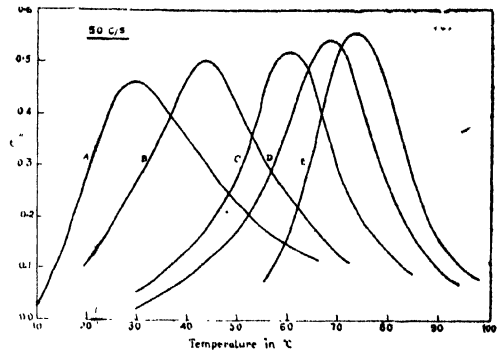


Fig.5.

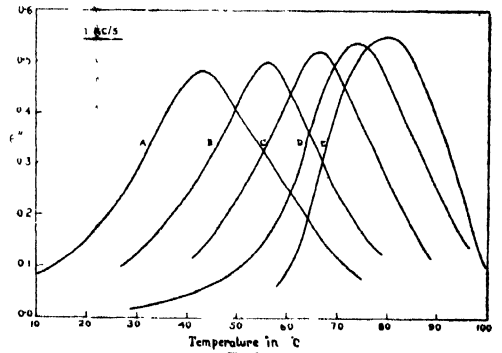


Fig.6.

till at about 70°C the peak becomes very blunt. The physical meaning of this bluntness is that near about such temperature the loss is insensitive to soft resin content of the mixture up to about (Fig. 7) 25-30%. In electrical machines usually a temprature rise of 40°C is permitted above the room temperature. In tropical countries, such as India, this means that the

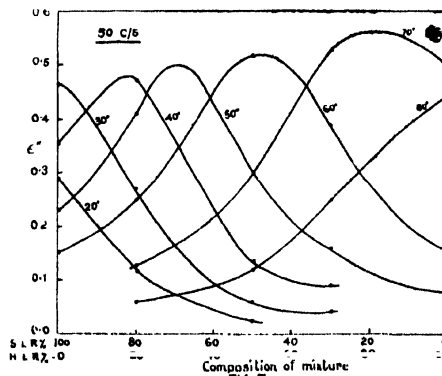


Fig.7.

machines may attain a temperature of 70°C. In such a case practically no advantage will be obtained by using pure lac resin instead of whole lac so far as loss is concerned. But if the temperature attained in the machine is only 60°C or slightly less definite advantage may be obtained by such use. If the temperature, however, falls below 50°C very little advantage may be gained since the value of loss becomes very low in both the cases.

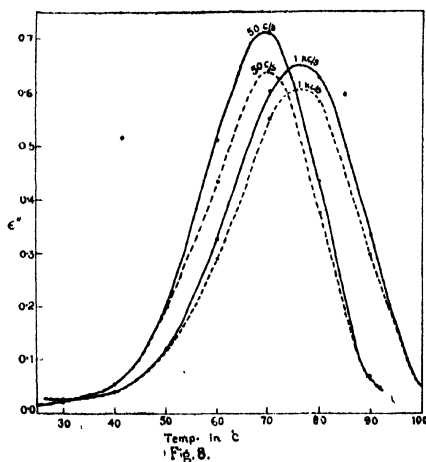
TABLE III

Comparative dielectric constant and dielectric loss data of whole lac and a mixture of hard lac and soft lac of similar composition

Frequency	Temp. °C	Whole lac (Kusmi)	Resin mixture	Difference	Whole lac (Kusmi)	Resin Mixture	Difference
50 c/s.	30°	3'91	3'96	-0'05	'029	'022	-0'002
	40°	4'28	4'30	-0'02	'051	'076	-0'025
	50°	4'95	4'90	0'05	'200	'180	0'020
	60°	6'00	6'00	0'00	'511	'371	0'140
	70°	7'12	7'10	0'02	'710	'535	0'178
	80°	7'85	7'80	0'05	'435	'261	0'174
1 Kc/s	30°	3'69	3'68	0'01	'026	'024	0'002
	40°	3'92	3'90	0'02	'039	'043	-0'004
	50°	4'36	4'34	0'02	'119	'100	0'019
	60°	5'08	5'06	0'02	'324	'231	0'093
	70°	5'96	5'95	0'01	'606	490	0'116
	80°	6'72	6'70	-0'02	'629	'482	0'147
	90°	7'36	7'35	0'01	'329	263	0'066
10 Kc/s	30°	3'57	3'57	0'00	'044	'041	0'003
	40°	3'75	3'76	-0'01	'049	'045	0'004
	50°	4'18	4'16	0'02	'098	'101	-0'003
	60°	4'65	4'60	0'05	'203	'200	0'003
	70°	5'22	5'20	0'02	'383	'376	0'007
	80°	5'80	5'80	0'00	'512	'502	0'010
	90°	6.46	6'43	0'03	'537	'523	0'014
100 Kc/s	30°	3'48	3'46	0'02	'086	'084	0'002
	40°	3'67	3'66	0'01	'089	'088	0'001
	50°	4'00	4'01	-0'01	'112	'110	0'002
	60°	4'37	4'36	0'01	'157	'158	-0'001
	70°	4'76	4'77	-0'01	'256	'254	0'002
	80°	5'04	5'04	0'00	'357	'352	0'005
	90°	5'42	5'41	0'01	'443	'440	0'003

We shall now compare the curve D in Fig. 5 representing a mixture of 70% hard lac resin and 30% soft lac resin with that of Kusmi lac reported earlier. Table III shows these data for dielectric constant ϵ' as well as loss factor ϵ'' . It may be seen that dielectric constant data at practically all frequencies agree quite well, but ϵ'' data differ, the difference in general diminishing with increasing frequency. Thus the difference between ϵ'' values of Kusmi lac and the corresponding values of resin mixture at any temperature for 100 Kc/s is practically negligible, for 10 Kc/s very slight, whereas for 1 Kc/s it is appreciable and for 50 c/s quite large. We have already pointed out that the maximum value of dielectric loss of pure lac resin for practically all frequencies is near about 0.55 and of soft resin 0.50, the temperature at which such maximum loss takes place depending upon frequency. For any composition of these constituent mixtures ϵ_m'' should lie within these limits provided no association takes place. In fact different compositions of mixture of these resins show that there is no abnormality present in their behaviour from that of their constituents, i.e., no association of any sort is taking place between their molecules.

The unexpected high value of ϵ_m'' of whole lac especially at lower frequencies seems at first sight very peculiar and even one may be tempted to doubt the proposition that lac is a simple mixture of soft and hard lac. But we have arrived at the above proposition from different angles of view (Bhattacharya, 1943) and the anomaly which exists in the behaviour of lac may be explained if it is supposed that a third substance is present in lac. This has actually been found to be moisture. In fact vacuum desiccation at an elevated temperature of 40°-45°C for 5-6 hours has been found to diminish this maximum loss considerably though not completely. It must be stated here that it is comparatively easier to free lac constituents from moisture than lac itself. This is probably due to the fact that pure lac resin becomes very crisp and porous during its preparation from lac and when in fine powder form it readily gives out its absorbed or adsorbed moisture, while soft resin itself does neither take up moisture so readily nor retain it so tenaciously. In lac, however, moisture, which is probably held by pure resin, is prevented from escaping easily by soft resin which serves as a coating. The difference in loss behaviour of the same sample of Kusmi lac after ordinary desiccation over calcium chloride overnight and after vacuum desiccation at 40°-45°C for about 6 hours has been shown



in figure 8 and the data included in Table IV. This clearly shows that the anomalous higher loss may be reduced by prolonged and efficient desiccation.

TABLE IV

Dielectric loss of whole lac (Kusmi) before and after vacuum desiccation at 40°-45°C. for 6 hours.

Frequency.	Temp. °C	After overnight desiccation over CaCl_2 .	After vacuum desiccation at 40°-45°C.	Frequency.	After overnight desiccation over CaCl_2 .	After vacuum desiccation at 40°-45°C.
50 c/s.	30°	'020	'022	1 Kc/s.	026	'024
	40°	'051	'050		039	'040
	50°	'200	'192		'119	'114
	60°	'511	'430		'324	'293
	70°	'710	'642		'606	'551
	80°	'435	'371		'629	'582
	90°	—	'070		'329	'296

It is not known how moisture is retained by lac. But it must be said that it is not present in the free state. In that case it would have contributed towards the increase of dielectric constant and not loss factor. For, at frequencies at which measurements were made water molecule should freely orient with the alternating field and should not show any anomalous dispersion at all. Hence its dielectric constant should have been high but loss negligible. It is seen however that such is not the case. The difference of dielectric constant values of Kusmi lac and the resin mixture is very small and of loss factor appreciable. Thus it can be explained only when this moisture is in a combined state. It is difficult to say how this moisture can be in the combined state and if absorbed or adsorbed moisture can behave in this fashion, but Langmuir and others (Adam, 1930_a) have shown that adsorbed gases are sometimes held by metal surfaces so tenaciously that it is difficult to distinguish between such an adsorbed state and a combined state. It is also known how extremely difficult it is to free a glass surface of its adsorbed gases including water vapour. Even prolonged heating near about the softening point of glass under high vacuum has been found to be ineffective in completely removing all adsorbed gases (Adam, 1930_b). It is, therefore, supposed that the phenomenon may not be confined to the surface only but probably the gases are absorbed some distance into the material. Langmuir (1918) has also found out that the amount of water vapour adsorbed by mica corresponds to two molecules thick, one layer of which probably forms part of the mica lattice structure. Thus we see that water vapour or more generally gases, adsorbed or absorbed by certain materials may be held so tenaciously that they behave as if in a combined state with those materials. It is, therefore, not unnatural to see that the absorbed water vapour in lac behaves in this fashion.

We can also look at the picture from another angle. This is to suppose that the moisture eliminated from lac at the elevated temperature of 40°-45°C under vacuum is actually not extraneous but results from slow condensation-polymerisation of lac. In such a case we shall have to take it for granted that during its preparation and desiccation under vacuum pure lac resin also gets considerably polymerised and hence its loss-maximum ϵ_m'' , that we generally obtain by measurement on such a sample, is not the actual ϵ_m'' that we

could have expected had the sample not polymerised at all, but is a reduced figure owing to the elimination of some water. In such a case ϵ_m'' for all the resin mixtures, whose components are not polymerised, would have been higher and probably the value of ϵ_m'' of lac would have fitted in that series. The loss-temperature curve of Kusmi lac at any frequency could then reasonably belong to a group whose other members are obtained from mixtures of unpolymerised lac constituents at that frequency.

The latter explanation, though may seem at first sight unfamiliar, is not improbable or unreasonable, since lac is known to polymerise even at room temperature on ageing. It is probable, therefore, that lac polymerises much rapidly under vacuum at slightly higher temperatures. If we are prepared to accept this we shall have no hesitation in accepting also that pure lac resin under similar conditions will polymerise much more quickly. The usual method of drying lac or pure lac resin in a vacuum-oven at 40°C, therefore, may result in partial polymerisation. In the lac-trade of course this polymerisation or ageing is only tested by practical methods such as insolubility in cold or hot alcohol (Rangaswami and Sen, 1942), but there may be stages of this polymerisation in the early ones of which lac may be quite soluble even in cold alcohol. The cold alcohol solubility is, therefore, only a crude test of polymerisation and this is quite good from the consumers' point of view. But it is quite insensitive to the degree of polymerisation to which we are referring here, especially at the initial stages. Very recently such partially polymerised lac has been isolated from aged lac at this Institute (Sen, 1944) using mixed solvents and their molecular weight determination shows that they are higher than that of fresh lac. These partially polymerised lac are all soluble in cold alcohol. This fact, therefore, strengthens the latter explanation that pure lac resin usually gets partially polymerised during its preparation and drying and so the ϵ_m'' values obtained by measurement on such a sample are lower than what we should have obtained had the sample not polymerised at all.

It may, therefore, be concluded that moisture, whatever its nature may be, whether extraneous or not, is responsible for contributing to slightly higher loss to lac when compared to its constituents especially at lower frequencies. And this moisture is not present in the free state in lac but must be in the combined state. If it is extraneous moisture, we must explain this character by saying that the absorbed moisture forms part of the resin molecule by some sort of association. If, however, this moisture is not extraneous, it is expelled by a process of condensation—polymerisation of lac during vacuum desiccation.

ACKNOWLEDGMENT

The author expresses his indebtedness to Dr. H. K. Sen, Director of this Institute, for his kind interest in this work.

PHYSICAL AND PHYSICO-CHEMICAL LABORATORIES,
INDIAN LAC RESEARCH INSTITUTE,
NAMKUM, RANCHI.

REFERENCES

- Adam, N. K., 1930. *The Physics and Chemistry of Surfaces* (Oxford), (a) 260, (b) 258.
Bhattacharya, G. N., 1943, *Ind. J. Phys.* 17, 153; 1944, *Ind. J. Phys.*, 18, 1.
Davies, J. M., Miller, R. F., and Busse, W. F., 1941, *J. Amer. Chem. Soc.*, 63, 361.
Floss, R. M., 1941, *J. Amer. Chem. Soc.*, 63, 378.
Langmuir, I., 1918, *J. Amer. Chem. Soc.*, 40, 1361.
Rangaswami, M., and Sen, H. K., 1942, *A Handbook of Shellac Analysis*, (Ind. Lac. Res. Inst.) 12, 22.
Sen, H. K., 1944, *Proc. Ind. Sci. Cong.*, part III., 66.

THE DIELECTRIC PROPERTIES OF MODIFIED LAC

By G. N. BHATTACHARYA

ABSTRACT The measurement of the dielectric properties of two important modified lac compositions, *viz.*, the shellac-urea-formaldehyde resin and the shellac-melamine-formaldehyde resin, have been made over a wide range of temperature and frequency. The result shows that these modified lacs retain the thermoplastic character of lac to a large extent and, therefore, cannot be truly thermosetting. The chemical reaction of these modified lacs have been discussed and it has been suggested that in order to obtain a truly thermosetting resin from lac the long-chain groups of shellac molecule should first be broken to smaller complexes with strongly reactive polar groups so that three dimensional cross-linking may yield the desired result.

INTRODUCTION

A new type of resin is gradually taking its place among the two already existing types *viz.*, natural and synthetic resins. This type of resin has been called 'semi-synthetic' or 'quasi-synthetic' and is usually obtained by modifying a natural resin by means of chemicals so that improved properties towards certain directions are obtained. To this class may be mentioned ester gum and chlorinated rubber. Shellac, although one of the finest and oldest known natural resin, has of late been similarly modified in order to suit itself to the bakelite moulding technique, and to improve upon its heat and water resistance. Amongst these shellac modified with formaldehyde and urea (Venugopalan and Sen, 1939) and with formaldehyde and melamine (Sankaranarayanan and Sen, 1940) have been found to have the best properties so far. These resins have been found to have sufficient thermosetting characteristics so that articles may be moulded and ejected at the same temperature and that has been as high as 140°C-150°C. These, therefore, have sufficient thermo-hardening properties for most practical purposes but are not perfectly thermosetting in the sense that rejected moulded articles of these resins may be recrushed and re-used for further moulding—a fact which has turned to be a decided advantage for the moulding industry. But this fact seems to show that polymerisation of urea or melamine shellac-formal under the usual conditions of manufacture does not progress to such an extent that it can be said to be a perfectly thermosetting resin owing to the development of macro-molecules through cross-linking. Nevertheless, these resins are not truly thermo-plastic since their flow properties are poor compared to most chain polymer-resins and they gradually harden after each moulding operation. According to Sen (1941), these resins are the borderland products between a thermoplastic and a thermo-hardening one. It may be concluded, therefore, that these modified shellac resins are either thermo-hardening resins with insufficiently developed cross-linkages or mixtures which harden at different rates under same conditions. There is apparently no simple way of knowing the nature and extent of changes brought about by the temperature and pressure of moulding except by the Marten's oven test, *i.e.*, by the determination of the softening point of the moulded test bar. The dielectric properties of such resins are expected to be of some help in elucidating the inner mechanism of changes and to some extent the degree of polymerisation. The object of this paper is to report the results of such a study on modified lac resins, which are assuming more and more important positions in the moulding industry.

THEORETICAL

The complex dielectric constant ϵ of a substance is expressed as

$$\epsilon = \epsilon' - i\epsilon''$$

where ϵ' = the real part or the ordinary dielectric constant,
and ϵ'' = the imaginary part or the loss factor.

This loss factor ϵ'' is related to the ordinary dielectric constant ϵ' through a factor, $\tan \delta$, which is called power factor, δ being the loss angle; thus

$$\epsilon'' = \epsilon' \tan \delta$$

The current in phase with the applied voltage

$$I_r = I. \tan \delta = \omega CV. \tan \delta = 2\pi f CV. \frac{\epsilon''}{\epsilon'}$$

But for a parallel plate condenser of area A and thickness d

$$C = \frac{A\epsilon'}{4\pi d \times 10^{11}} \text{ farads}$$

Therefore

$$I_r = \frac{fAV\epsilon''}{d \times 18 \times 10^{11}}$$

Now if K_t is the total conductance of this condenser

$$I_r = \frac{AVK_t}{d}$$

Equating r.h.s. of these two equations, we have $\epsilon'' = \frac{18 \times 10^{11} \times K_t}{f}$ This is the expression for total loss factor and this includes loss due to d.c. conductance of the material, the measure of which is given similarly by substituting K_o instead of K_t ,

i.e.,

$$\epsilon k_o'' = \frac{18 \times 10^{11} (K_o)}{f}$$

Hence pure a.c. loss is given by

$$\begin{aligned} \epsilon'' &= \frac{18 \times 10^{11} (K_t - K_o)}{f} \\ &= \frac{18 \times 10^{11} \times K}{f} \end{aligned}$$

EXPERIMENTAL

Apparatus.—As reported earlier (Bhattacharya, 1944) a Cambridge Schering bridge and a General Radio radio-frequency bridge were employed at lower and higher frequencies respectively for the determination of dielectric constant and power factor. The power source was a General Radio modulated oscillator type 684-A for high frequencies and a beat frequency oscillator for low frequencies. For 50 c/s a sine-wave alternator was used.

Electrodes.—Tin foil electrodes were used backed by hollow metal electrodes through which oil from a thermostat could be passed by means of a circulation pump. The test specimens were moulded discs of about 4 inch diameter.

Materials.—The materials were all unfilled modified lac resin. The main two composition, *viz.*, shellac-urea-formaldehyde resin and shellac-melamine-formaldehyde resin, were employed for this study. Other compositions such as shellac-casein (Venugopalan and Sen, 1940a) shellac-coal tar (Venugopalan and Sen, 1940b), shellac-vegetable protein, etc. were not employed since they present a more complicated picture for the study of their structure than the first two and also because they have comparatively less importance in the trade up till now.

Method of procedure.—A few test-discs were moulded out of the compositions using the bakelite moulding technique. Tin foil electrodes were pressed on both the surfaces of a disc using a small quantity of petroleum jelly as adhesive. Hollow metal electrodes were placed on these foil electrodes and oil from a thermostat was circulated through these hollow electrodes in order to keep the disc at any desired temperature. Capacity measurements were made on the bridges when the temperature equilibrium was established. The d.c. conductivity was measured on the same assembly using d.c. voltage and a high sensitivity galvanometer.

CALCULATION

The air capacitance of the test condenser formed by tin foil electrodes was calculated according to Kirchhoff's formula for parallel discs, *viz.*

$$C = \frac{R^2}{4D} + \frac{R}{4\pi} \left[\log_e \frac{16\pi R(Dt)}{D^2} \frac{t}{D} \log_e \frac{Dt}{t} - \right]$$

where R = the radius of electrodes in cms.,
 t = the thickness of electrodes in cms.,
 D = the distance between electrodes in cms.,
 and C = capacity of condenser in cms.

The correction for edge capacitance, leads, etc. has been dealt with in a previous paper (Bhattacharya, 1944).

RESULTS

(a) Shellac-urea-formaldehyde resin

TABLE I

Dielectric constant-temperature data at different frequencies.

Frequency in Kc/s.	Dielectric constant ϵ' at the temperature of ($^{\circ}\text{C}$)							
	30°	40°	50°	60°	70°	80°	90°	100°
500	4.81	5.07	5.40	5.69	5.95	6.18	6.19	6.26
100	4.95	5.24	5.62	5.97	6.25	6.63	6.63	6.63
50	5.07	5.38	5.71	6.11	6.47	6.80	6.90	6.87
10	5.14	5.47	5.95	6.47	6.99	7.46	7.46	7.10
1.0	5.38	5.76	6.42	7.18	7.99	9.03	9.41	8.85
0.05	5.40	5.92	6.86	8.34	9.96	—	—	—

TABLE II

Measured power factor data at various temperatures and frequencies.

Frequency in Kc/s.	Measured power factor at the temperature of (°C)							
	30°	40°	50°	60°	70°	80°	90°	100°
500	.0319	.0336	.0358	.0415	.0493	.0574	.0612	.0656
100	.0184	.0291	.0335	.0420	.0589	.0668	.0721	.0747
50	.0235	.0292	.0378	.0506	.0566	.0744	.0754	.0911
10	.0136	.0290	.0434	.0600	.0787	.0950	.1088	.1050
1.0	.0321	.0412	.0545	.0666	.0931	.1137	.1870	—
0.05	.0240	.0440	.0900	.1800	—	—	—	—

TABLE III

Corrected dielectric loss—temperature data

Frequency in Kc/s.	Dielectric loss ϵ'' at the temperature of (°C)							
	30°	40°	50°	60°	70°	80°	90°	100°
500	.153	.170	.193	.236	.293	.354	.374	.378
100	.091	.153	.188	.250	.373	.438	.462	.457
50	.119	.157	.216	.309	.363	.496	.487	.423
10	.071	.159	.257	.385	.536	.659	.647	.394
1.0	.173	.237	.345	.450	.603	.526	.104	—
0.05	.120	.255	.532	.910	—	—	—	—

(b) Shellac-melamine-formaldehyde resin

TABLE IV

Dielectric constant-temperature data at different frequencies.

Frequency in Kc/s.	Dielectric constant at the temperature of (°C)							
	30°	40°	50°	60°	70°	80°	90°	100°
500	4.78	5.10	5.37	5.79	6.11	6.34	6.16	5.96
100	5.00	5.32	5.67	6.14	6.56	6.81	6.61	6.31
50	5.10	5.40	5.79	6.31	6.78	7.05	6.86	6.53
10	5.22	5.62	6.09	6.61	7.20	7.45	7.48	7.00
1.0	5.57	5.99	6.86	7.60	8.69	9.40	9.50	9.00
0.05	5.61	6.31	7.85	9.59	11.21	—	—	—

TABLE V

Measured power factor data at different temperatures and frequencies.

Frequency in Kc/s.	Power factor (uncorrected) at the temperature of (°C)							
	30°	40°	50°	60°	70°	80°	90°	100°
500	.0424	.0453	.0477	.0514	.0589	.0643	.0645	.0624
100	.0343	.0365	.0453	.0530	.0641	.0700	.0688	.0705
50	.0304	.0308	.0496	.0601	.0645	.0671	.0731	.0804
10	.0331	.0392	.0502	.0671	.0841	.1040	.1280	.2020
1.0	.0459	.0608	.0783	.0964	.1260	—	—	—
0.05	.0380	.0980	.2100	—	—	—	—	—

TABLE VI

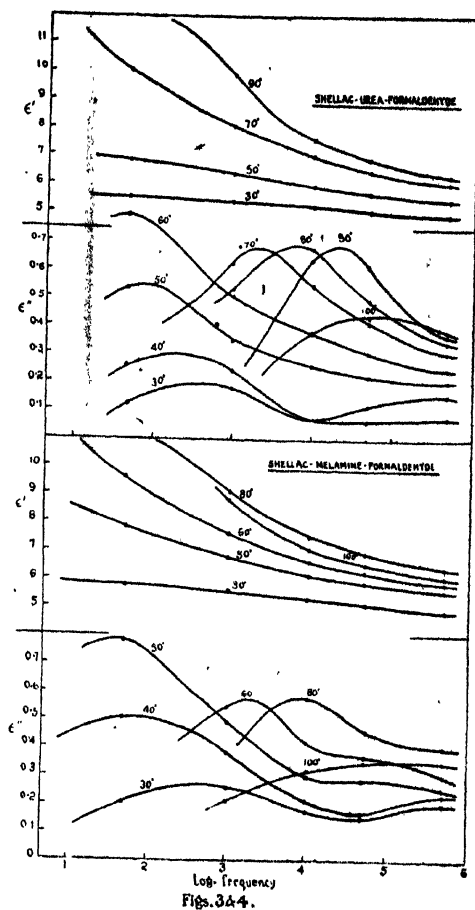
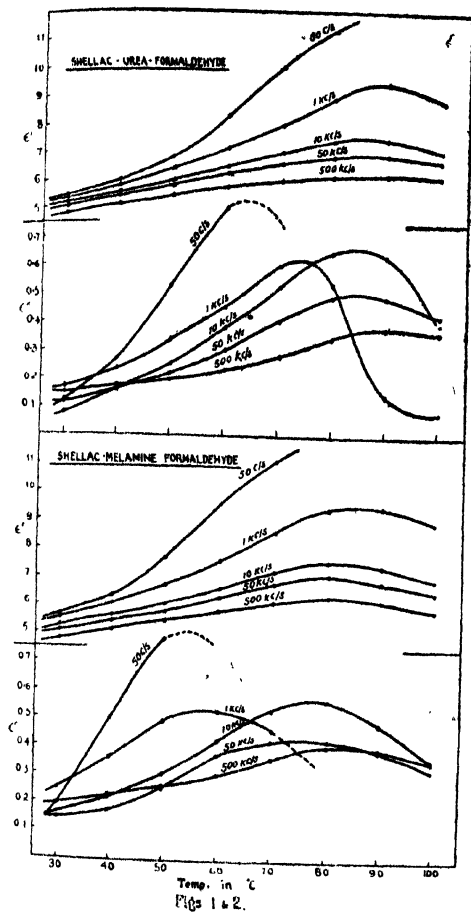
Corrected dielectric loss—temperature data

Frequency in Kc/s.	Dielectric loss at the temperature of (°C)							
	30°	40°	50°	60°	70°	80°	90°	100°
500	.203	.231	.256	.298	.359	.403	.388	.352
100	.171	.194	.256	.323	.413	.456	.408	.342
50	.155	.166	.257	.375	.423	.433	.407	.320
10	.173	.220	.301	.422	.531	.569	.489	.360
1.0	.255	.359	.493	.520	.458	—	—	—
0.05	.200	.510	.780	—	—	—	—	—

DISCUSSION

The dielectric constant-temperature curves of figures 1 & 2 should be observed carefully. Fig. 1 shows curves for shellac-urea-formaldehyde in respect of ϵ' and ϵ'' whilst Fig. 2 for shellac melamine-formaldehyde. It may be seen that the maximum value of dielectric constant for any frequency decreases as the frequency increases. In fact the maximum value of ϵ' , which is attained between the temperature range of 80°C to 90°C for practically all the frequencies, is near about 6 at 500 Kc/s and more than double this figure at 50 c/s. This suggests that shellac molecule with the interposition of formaldehyde and urea or melamine has increased so much in size that it becomes less and less probable for it to orient in response to the increasing frequency of the alternating field owing to its large time of relaxation. If it is considered, however, that the whole molecule does not take part in the rotation, the explanation may be that the polar groups, responsible for loss in lac, are bound up in such a way with cross-linking forces under this reaction that their freedom of movement is very much restricted. With the decrease of frequency of the applied field more and more molecules of polar groups can contribute towards the increase of the dielectric constant by aligning themselves as far as possible along the field. From this we also see that cross-linking has not developed in this reaction to such an extent that orientation of individual molecule or rotation of polar groups becomes altogether impossible. In fact these resins are not truly thermo-setting and, although diminished to a great extent,

they have still retained their thermoplastic character. This will be more evident if we scrutinise the loss factor—temperature curves of both of them. It will be seen that up to 10 Kc/s the



maxima of loss curves appear in the order in which they are expected for a thermoplastic resin. After 10 Kc/s, the value of the maximum gradually diminishes and its position also shifts but slightly. The picture that can be drawn at once to explain such a behaviour is the same as has been depicted above. The rotating unit is large or more possibly bound up with cross-linkages to a large extent and is not free to take up positions in response to the applied field. The internal viscosity has also increased to a great extent since the material does not melt but softens very slightly at high temperatures, the softening being manifested by the loss of its elasticity only. But still its thermoplastic character is not altogether destroyed and this is clearly manifested by its dielectric properties. Measurements at 50 c/s could not be pursued over the Schering bridge above 50°C or 60°C since the sensitivity of the bridge decreased immensely with the increase of power factor of the material. But the readings were sufficient to reveal the character of the curves.

The frequency-dielectric constant or loss factor (Figs. 3 & 4) curves also bring out the same conclusions. If we examine loss-frequency curves of shellac-urea-formaldehyde we

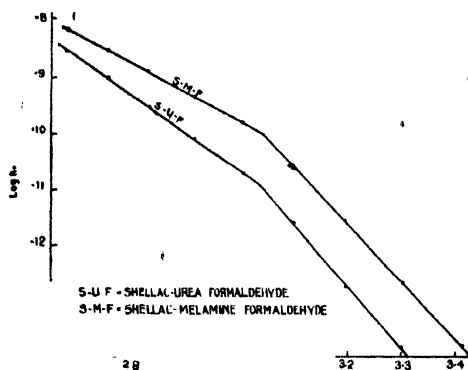


Fig. 5.

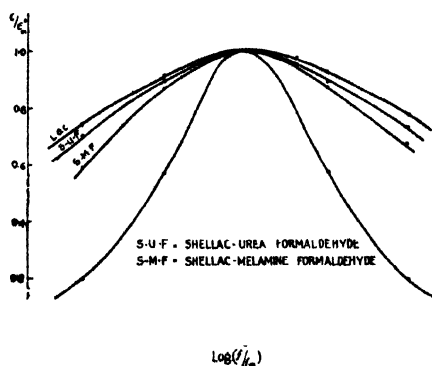


Fig. 6

shall find that after 60°C the character of a polar thermoplastic resin is noticeable although there is no outward melting of the resin or even softening. At temperatures lower than 60°C the three dimensional forces are more prominent and as a result the loss-maximum decreases gradually with the fall of temperature without any appreciable shift of position. In the case of shellac-melamine-formaldehyde resin also the same behaviour is noticeable but probably the inner change of state starts a bit earlier—the magnitude of which may not be more than a few degrees only.

In order to throw more light on the question of inner change of state the indirect method of d.c. conductance measurement gave some important information, since it was not possible to apply the direct method of measuring plasticity or viscosity at different temperatures. It may be seen that two straight lines are obtained if log d.c. conductance values are plotted against the reciprocal of absolute temperature for any of these modified lac resins (Fig. 5) and they meet at a point which corresponds to near about 55°C. It must be understood, however, that actually this point may not be so sharp but probably the change of state takes place over a small range of temperature between 50°C and 60°C. In the case of whole lac a similar behaviour was noticed (Bhattacharya, 1944) and a break was observed in the $\log K_0 - 1/T$ line at about 60°C, with the difference that there the inclination of the line with $1/T$ axis was less after 60°C whereas it is more here. The activation energies calculated from these slopes are naturally very different, showing that some fundamental change has taken place in the molecule. In fact the activation energy of shellac-urea-formaldehyde at temperatures higher than 60°C is 30.4 K-cal and lower than 50°C is 50.1 K-cal whilst the same for shellac-melamine-formaldehyde are 23.6 K-cal and 46.0 K-cal respectively. This difference is not much and from these considerations it can be said that the nature of reaction in both shellac-urea-formaldehyde and shellac-melamine-formaldehyde is the same. But there is very little coincidence between the log-conductance— $1/T$ line of whole lac and of these modified lacs except that the break occurs at about the same place. It may be that near about this temperature some inner change of state due to weakening of inter-molecular forces occurs and this peculiarity of lac is retained even when lac is modified with formaldehyde and urea or melamine since the main structure of lac is not destroyed by such reactions.

TABLE VII

D.C. conductance—temperature data of shellac-urea-formaldehyde

Temperature		$1/T \times 10^3$	D. C. conductance K_0	log K_0
$t^\circ\text{C}$	$T^\circ\text{K}$			
30°	303	3.300	1.50×10^{-14}	-13.824
40°	313	3.196	1.62×10^{-13}	-12.790
50°	323	3.096	1.38×10^{-12}	-11.623
60°	333	3.003	1.55×10^{-11}	-10.810
70°	343	2.915	7.81×10^{-11}	-10.107
80°	353	2.833	4.77×10^{-10}	-9.558
90°	363	0.755	9.20×10^{-10}	-9.036
100°	373	2.681	1.15×10^{-9}	-8.668

TABLE VIII

D.C. conductance-temperature data of shellac-melamine-formaldehyde

Temperature		$1/T \times 10^3$	D.C. conductance K_0	Log K_0
$t^\circ\text{C}$	$T^\circ\text{K}$			
25°	298	0.356	5.16×10^{-14}	-13.288
30°	303	3.300	1.85×10^{-13}	-12.733
40°	313	3.195	3.00×10^{-13}	-11.513
50°	323	3.096	2.45×10^{-11}	-10.611
60°	333	3.003	1.18×10^{-10}	-9.928
70°	343	2.915	4.13×10^{-10}	-9.384
80°	353	2.833	1.14×10^{-9}	-8.943
90°	363	2.755	2.60×10^{-9}	-8.585
100°	373	2.681	5.71×10^{-9}	-8.244

According to Sen (1941), a shellac formal is formed by the interaction of shellac with formaldehyde and this formal is more plastic than lac itself. It has also got the property of slower polymerisability under heat. The mechanism of action of urea on this formal has been expressed by him to be of a condensation type with the elimination of water. The introduction of formal grouping has increased the reactivity of the rather inert lac molecule. The mechanism of reaction of melamine with shellac formal is also similar and is brought about through the amino-groups, as in the case of urea. But the plot of e''/e''_m against f/f_m reveals some interesting and unexpected facts. The higher softening points and thermosetting properties of these modified lacs would at first sight suggest that these resins would have very wide distribution range of relaxation times of the molecule. But actual plot in Fig. 6 shows that the shellac-melamine-formaldehyde resin has a lower distribution range than the corresponding urea resin and that both of them have lower range of distribution of relaxation times than lac itself. This is rather surprising but not improbable if it is considered that the introduction of aldehyde, amino and other polar groups in place of a few hydroxyls has, in fact, concentrated the distribution instead of dispersing it. The whole molecule does not evidently rotate but these different polar groups contribute towards the dielectric loss. The distribution naturally depends upon their individual relaxation time and their freedom of rotation which again is

dependent upon their position in the molecule. We have already seen (Bhattacharya, *loc. cit.*), that the hydroxyl groups are the main rotating units in the case of whole lac; evidently their position on the body of the molecule and hence their freedom to rotate determines the distribution. It is probable, therefore, that by introducing formal grouping and then amino groups through urea or melamine the effect of distribution becomes less since they are all concentrated near a few fixed spots and so their chances to act collectively as a single unit are more. It should be remembered that the execution of complete rotation by the polar body is not necessary for dielectric polarisation but movement from one position to another by turning through a small angle is usually sufficient. It is difficult to depict the true picture of the rotating polar units in these semi-synthetic resins, since the structure of the main body, *viz.* lac resin, is not yet known and the knowledge regarding this is far from satisfactory at the present moment. All that we can say with definiteness now is that the lac molecule contains five hydroxyl groups and that aleuritic acid, 9, 10, 16 trihydroxypalmitic acid, must be one of its main constituents, since it can be obtained in good yield on hydrolysis of lac by strong caustic alkali. This acid is an open chain fatty acid of simple structure, containing 16 carbon atoms like palmitic acid with the addition of three hydroxyls at the positions indicated above. There is sufficient evidence to show that urea (Bhattacharya, 1940) or melamine (Sankaranarayanan and Sen, 1944) reacts at the carboxyl of lac and not at the free hydroxyls, but when shellac formal is formed by the interaction of formaldehyde it reacts at the formal grouping and not at the carboxyl (Sen, 1941). If only the aleuritic acid part of the structure of lac is considered it can be said that the formal and amino groups are on the side chain and hence are in a position to execute vibrations better than if they had been on the main chain. This fact probably explains the more thermoplastic character of lac formal also.

One thing, however, is very clear from this dielectric study, *viz.*, the thermoplastic character of lac, which is usually believed to be due to its having long chain groups in the molecular structure (Houwink, 1934), is not destroyed in these so called thermo-hardening reactions. This is to be expected since most of these reactions take place only at free carboxyls at the end of the chain-structure. In order to make, therefore, a truly thermo-setting resin from shellac the long molecule should first be broken up into simpler complexes so that cross-linking may yield a really hardened product.

ACKNOWLEDGMENT

The author wishes to record his deep sense of gratitude to Dr. H. K. Sen, Director of this Institute, for his kind interest in this work.

PHYSICAL AND PHYSICO-CHEMICAL LABORATORIES,
INDIAN LAC RESEARCH INSTITUTE, NAMKUM, RANCHI.

REFERENCES

- Bhattacharya, G. N., 1940, *Ind. Lac. Res. Inst. Bull.* 42.
 " " 1944, *Ind. J. Phys.*, 18, 1.
 Houwink, R., 1934, *Aktid. Vetage* 187.
 Sankaranarayanan, Y. and Sen, H. K., 1940, *Ind Lac. Res. Inst.* Note 22.
 " " " " " 1944, " " " " 21.
 Sen, H. K., 1941, *J. Ind. Chem. Soc.* 18, 47.
 Venugopalan M., and Sen, H. K., 1939, *British Plastics*, 10, 626.
 " " " " " 1940(a), *Ind. Lac. Res. Inst.* Note 21.
 " " " " " 1940(b), " " " " 23.

SOUND ABSORPTION CHARACTERISTICS OF INDIAN MATERIALS—PART I

By S. CHATTERJEE

AND

N. DUTT

(Received for publication, 8th May, 1944)

ABSTRACT. A proper understanding of the acoustical properties of materials is becoming increasingly important because of the wide variety of important applications in which they are finding use. A simple and useful method is presented for the investigation on the acoustic properties of some of the materials available in India. The effect of various angles of incidence for different audio frequencies (64 c.p.s.—8192 c.p.s.) on the absorption coefficients of the materials have been studied. The paper also outlines the method giving description of the equipment and measurements on the characteristics of the chamber and the source of sound employed for the purpose.

INTRODUCTION

Since a long time the reverberation has been found to be the most important acoustical defect of a room and as early as 1835 Reid suggested that this defect is minimised if the surrounding space could be more absorbent, that is by making the surfaces of the wall rough and irregular.

Roger Smith in his 'Acoustics of Public Buildings' remarked, 'In empty houses a great reverberation is perceptible which diminishes as the floors are covered with carpets and the rooms filled with furniture.'

Johnstone Stoney (1885) tested a room having its walls papered over a lining of canvas which was stretched in front of a framework fixed on the wall and from his experiment he inferred that public rooms could be freed from effects of echo by lining the walls and ceiling in such a manner.

So it was clearly realised about a century ago that one of the best remedies for removing the acoustical defect of a room is to introduce a sufficient area of a sound absorbing material.

The problem of measuring sound absorption coefficients of different materials and utilising these data in the acoustical treatment of rooms is getting more important, since any design of recording or broadcasting studio presupposes a knowledge of the acoustical quality of the chamber, in other words a knowledge of the absorption coefficients of the materials to be used in the interior finish of the chamber.

THEORETICAL WORK ON SOUND ABSORPTION

The relation between the absorption coefficient of a material and its porosity was first deduced by Lord Rayleigh (1883). He dealt with the case of sound

incident normally on a flat surface perforated by a great number of similar channels perpendicular to the face. The channels were supposed to be cylindrical and that expansion and rarefaction of air within these channels took place isothermally. The depth of the pores was assumed to be small compared to the wavelength of sound, but sufficiently large relative to the diameter of the pores and the portion of the sound energy entering the pores to be completely dissipated. His expression for the absorption coefficient (a) is

$$a = \frac{4M}{2M^2 + 2M + 1} \quad (1)$$

where,

$$M = \frac{2(1+g)\sqrt{\nu\gamma}}{r\sqrt{w}}$$

and g = ratio of unperforated to perforated areas of porous surface.

ν = kinematic viscosity of the gas.

γ = ratio of the specific heats of the gas.

r = radius of the pores.

$w = 2\pi \times$ frequency.

In a later paper Rayleigh (1920) dealt with the case of sound waves incident at any angle on a porous wall and found that the amplitude of the reflected waves depends on the angle of incidence, the amplitude of the reflected beam (B) and the angle of incidence θ being given by the relation

$$\frac{B-1}{B+1} = \frac{\sigma}{\sigma + \sigma'} \cdot \frac{1}{\cos \theta} \cdot \frac{K' \tan K'l}{iK} \quad \dots (2)$$

where, σ = area of the perforated surface.

σ' = area of the unperforated surface.

$$K' = K^2 - \frac{iwh}{v^2}$$

$$K = 2\pi/\lambda$$

$$w = 2\pi f$$

h = Rayleigh's dissipation factor.

v = Velocity of sound in air.

l = Depth of the pores.

Assuming the energy of the incident wave to be unity the absorption coefficient is given by

$$a = 1 - B^2$$

This formula does not give a direct relation between the absorption coefficient for any angle of incidence and the porosity of the sample and the frequency of the sound wave incident on the surface.

The theoretical aspect of the present investigation, therefore, led us to use the Rayleigh equations and deduce a more general formula. From eq. (2)

$$B = \frac{(1+g)\cos\theta - x}{(1+g)\cos\theta + x} \quad \text{where,} \quad x = -\frac{K' \tan K'l}{iK} \quad \text{and} \quad g = \frac{\sigma'}{\sigma}$$

Therefore

$$a_{\theta} = 1 - B^2 = 1 - \left\{ \frac{(1+g)\cos\theta - x}{(1+g)\cos\theta + x} \right\}^2 = \frac{4(1+g)\cos\theta x}{\{(1+g)\cos\theta + x\}^2}.$$

Replacing the value of x by

$$x = \frac{(2M^2 + 1) \pm \sqrt{4M^4 + 1}}{2M/(1+g)}$$

the final equation becomes

$$a_{\theta} = \frac{8M\{(2M^2 + 1) \pm \sqrt{4M^4 + 1}\} \cos\theta}{\{(2M^2 + 2M \cos\theta + 1) \pm \sqrt{4M^4 + 1}\}^2} \quad \dots (3)$$

This reduces to the expression for normal incidence as found by Rayleigh by putting $\theta = 0^\circ$

$$a_0 = \frac{4M}{2M^2 + 2M + 1}^*$$

For calculating theoretically the absorption coefficient of a given material it will be, therefore, necessary to ascertain the value of M and correlate the value with different inclination for different values of absorption.

PREVIOUS METHODS OF MEASUREMENT

Reverberation Method.—Sabine (1895) first started experimental investigation on absorption coefficients of different materials. His method consisted of finding, by means of a stop-watch, the reverberation periods first of a chamber without and then with the test sample and calculating the absorption coefficient from the difference of the two periods of reverberation. The ear was used as a detecting instrument and the threshold of hearing was fixed as the point of reference. His method has been subsequently modified by Wentz and Bedell (1930) and Olson and Kreuser (1930) and further by the U. S. Bureau of Standards (1930) in which the electro-acoustic devices have been used for producing and detecting the sound.

The reverberation method gives a more practical value of absorption coefficient as here the test sample is subjected to sound waves incident upon it in random manners from all directions, just as in practical field of application. But small samples cannot be tested by this method as in this case it is necessary that the area covered by the test sample should be comparable to the area of the room, so that there may be a measurable difference between the two time periods. Moreover large test rooms are required so that there may be a uniform mixing of sound energy throughout the room.

Stationary Wave Method.—The stationary wave method of measuring the absorption coefficient of small samples was suggested by Tuma (1902) and subsequently modified by Weisbach (1910), later on by Taylor (1913) and Paris (1927). In this method a long metal tube, with walls thick enough to prevent them vibrating appreciably, is provided with a source of sound at one end

and closed at the other end by the test specimen. Sound waves from the generator travel down the pipe and is incident normally upon the sample where a portion of it (depending on the absorption coefficient of the sample) is reflected back to the other end of the tube giving rise to a stationary wave system. Pressure amplitude varies continuously along the pipe passing through a series of maxima and minima, and the absorption coefficient of the test sample is given by

$$a = \frac{A}{2 + \frac{A}{N} + \frac{N}{A}}$$

where, N and A are equal to maximum and minimum amplitudes respectively.

This method yields values of absorption coefficients of small samples at normal incidence only. Heyl, Chrisler and Snyder (1930), working at the U. S. Bureau of Standards, modified the stationary wave apparatus for investigation on the absorption coefficient of sound at oblique incidences but their method yielded abnormal results contrary to those obtained from theoretical considerations. Paris (1930) discussed about the drawbacks of their apparatus and the unsuitability of determining the absorption coefficients at oblique incidences by the stationary wave method.

Watson's Method.—Watson (1922) devised a method by which the absorption coefficient is calculated from a direct measurement of sound waves transmitted and reflected by the test sample. Sound emanating from the source, an organ pipe placed at the focus of a paraboloidal reflector, undergoes reflexion and transmission from the test sample clamped over an aperture between two adjacent rooms and then passes to the measuring instrument, a Rayleigh Disc with suitable resonators. This method has been adopted by the National Physical Laboratory (1927) with the modification that electrical equipments have been used in the method of producing and measuring sound.

This method has the advantage that by varying the angle of incidence of the sound waves upon the test sample, the absorption coefficients for different angles of incidence can be studied and samples of any size can be tested simply by making the beam of sound large enough to cover the whole surface.

Kuhl and Meyer (1932) adopted this method to measure the relation of absorption to angle of incidence but they carried out the experiment in the open air on the flat roof of their Institute.

PRESENT METHOD OF MEASUREMENT

The present method of measurement is a modification of the Watson's method and consists in measuring the absorption coefficient of the test sample at various angles of incidence over the audio frequency band. It involves the measurement of the amplitude of the sound wave reflected first from a complete reflector and then from the test sample and the diminution of the sound energy in the second case is due to absorption of sound energy by the sample. If B_1 and B_2 be the amplitudes of the beam reflected from the complete reflector and

the test sample respectively and since sound energy is proportional to the square of the amplitude, the absorption coefficient α is then given by

$$\alpha = \frac{B_1^2 - B_2^2}{B_1^2}$$

The complete reflector used is a $\frac{1}{4}$ " thick metal plate backed by a 2" thick wooden board. The investigation has been conducted in an especially constructed sound chamber and the relative amplitudes in the two cases have been measured by means of electrical devices.

Sound Chamber.—The sound chamber is planned and constructed in such a way as to attain a low time of reverberation and high insulation from external noises. It is a rectangular room 20 feet by 15 feet by 10 feet proportional to the dimensions recommended by the American Standards and situated inside another big room having thick brick walls and concrete floor and ceiling. The chamber is divided into two portions by means of a thick partition wall, the source of sound is placed in one of them while measurements are carried out in another. There is a window 2' \times 2' in the partition wall for holding the test sample. All exposed surfaces inside the rooms are heavily lagged with sound absorbing materials to suppress reflexions from the surfaces and minimise interference phenomena. The walls have been treated with a layer of acoustic celotex followed by 4 inches of air gap and then 4 inches thick mattresses of cocoanut fibres. The ceiling is treated with acoustic celotex and 6 inches cotton wool padding. The floor

is covered with a thick lining of fibrous mattresses. The inside acoustical treatment of the room has also helped to reduce the intensity of sound in the region outside the main beam. Fig. 1 shows the plan view of the room. The reverberation time of the room was found to be very low.

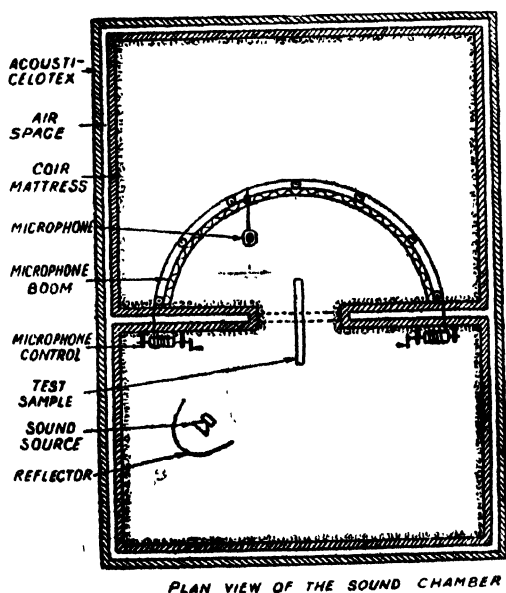


FIG. 1

Source of Sound.—The source of sound is a dynamic type loudspeaker fed from a high grade beat-frequency oscillator, the output of which can be varied by means of a calibrated attenuator. The quality of the tone produced by the source has been checked by receiving the sound through a velocity micro-

phone in conjunction with a high grade resistance-coupled amplifier and examining the wave form of the output on a cathode ray oscillograph.

The source of sound is placed at the focus of a paraboloidal reflector to obtain a parallel beam of sound directed towards any particular direction. Measurements of the intensity of sound on the central axis of the beam at a distance of 3 feet from the source and also at points off-axis show that the incident beam is moderately uniform over a width of about 2 feet and drops down beyond that to a marked degree. The result for one frequency is shown in Fig. 2.

While carrying on preliminary investigation, the result was found to vary depending on the distance between the test sample and the source of sound and it was due to the formation of stationary wave-pattern inside the chamber. In order to minimise this effect the pattern has been made to shift continuously from one position to another by varying the frequency of the source through a narrow band, that is by warbling the tone. This is accomplished by means of a small variable air-condenser rotated by a constant speed motor and placed externally in parallel with the main tuning condenser of the beat-frequency oscillator. The band width of warbling was kept under experimental control

FIG. 2

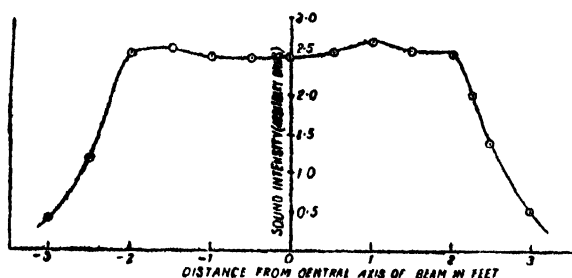


FIG. 3

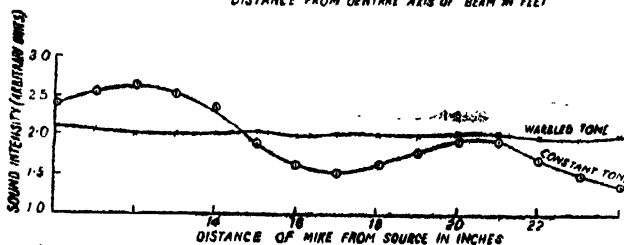
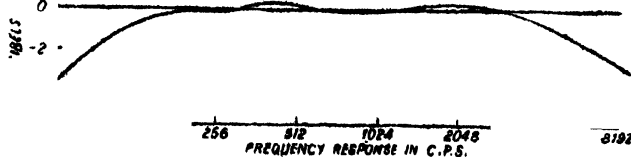


FIG. 4



as the variation of capacity of the rotating condenser could be adjusted by means of a cam arrangement. The segment of rotation was such that the frequency shifts were about 8 times per second. The band width has been chosen so that they were approximately 10% of the middle frequency band. The formation of stationary wave pattern and the effect of the warbled tone on its suppression are shown in the Fig. 3.

A milliammeter was connected in series with the input to the loud speaker so that the energy input to it at a given frequency could be kept constant during a set of observations.

MEASUREMENT OF AMPLITUDE OF SOUND WAVE

The amplitude of the sound wave is measured by means of a velocity microphone connected to a high-gain amplifier, the output of which was indicated by a valve-voltmeter. The overall characteristic of the microphone and the amplifier combined is shown in Fig. 4. The position of the microphone inside the chamber was controlled from outside by swinging it on a boom by means of a remote control arrangement as shown in Fig 1. Fig. 5 shows a schematic diagram of the complete equipment.

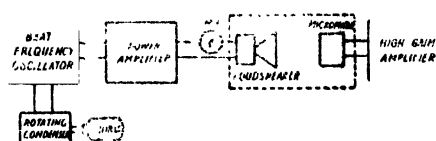


FIG. 5

EXPERIMENTAL RESULTS

The materials tested are : (1) Indian white cotton, (2) Silk cotton, (3) Coconut fibres and (4) Jute fibres. Test samples have been first of all prepared from these materials.

White cotton and Silk cotton have been loosely packed inside thin cotton fabric bags and made into a thickness of 2 inches.

Coconut fibres are woven into 2 inches thick mattress with the fibres arranged in such a manner so that they lie side by side and their tips form the surface of the sample.

Jute fibres are cut into pieces 2 inches long and they are fixed side by side by means of wire nettings, the tips of the fibres forming the surface of the sample.

The values of the absorption coefficients of the four samples at different audio frequencies and for various angles of incidence are given in Table I to IV.

TABLE I

Indian White Cotton

		Sound Absorption Coefficients for frequencies in cycles per sec.							
Angle of Incidence		64	128	256	512	1024	2048	4096	8192
15°	.10	.17	.33	.46	.57	.48	.45	.42	
30°	.14	.20	.34	.48	.58	.49	.46	.44	
45°	.19	.225	.40	.50	.62	.51	.49	.465	
60°	.225	.30	.43	.58	.68	.60	.51	.50	
75°	.23	.31	.425	.58	.66	.59	.495	.49	

TABLE II
Silk Cotton

Angle of Incidence	Sound Absorption Coefficients for frequencies in cycles per sec.							
	64	128	256	512	1024	2048	4096	8192
15°	.22	.25	.35	.51	.60	.57	.48	.415
30°	.24	.265	.365	.52	.625	.60	.50	.42
45°	.25	.30	.40	.55	.64	.62	.53	.435
60°	.30	.34	.44	.60	.70	.63	.55	.52
75°	.33	.40	.43	.61	.68	.59	.54	.50

TABLE III
Cocoanut Fibres

Angle of Incidence	Sound Absorption Coefficients for frequencies in cycles per sec.							
	64	128	256	512	1024	2048	4096	8192
15°	.225	.25	.34	.52	.68	.72	.54	.48
30°	.24	.26	.345	.535	.69	.775	.56	.50
45°	.25	.29	.37	.575	.71	.78	.60	.53
60°	.28	.32	.395	.64	.75	.80	.635	.575
75°	.32	.33	.43	.67	.76	.79	.65	.57

TABLE IV
Jute Fibres

Angle of Incidence	Sound Absorption Coefficients for frequencies in cycles per sec.							
	64	128	256	512	1024	2048	4096	8192
15°	.295	.47	.70	.81	.72	.61	.55	.48
30°	.31	.485	.72	.83	.735	.655	.58	.52
45°	.34	.52	.75	.865	.78	.685	.61	.575
60°	.38	.54	.80	.89	.81	.72	.67	.62
75°	.40	.62	.83	.91	.81	.73	.69	.63

CONCLUSION

From tables I to IV it is found that absorption coefficients of all the samples tested vary with the angle of incidence as well as with the frequency.

The value of the absorption coefficients gradually increases with the angle of incidence and attains maximum value at about 60° in some cases and in some cases it goes on increasing up till 75° up to which measurements have been taken.

It is in agreement with the results deduced from the equation based upon the theory of Rayleigh. It also confirms the results derived by Paris from the conception of "Acoustical Admittance."

As regards variation of absorption coefficient with frequency it is seen that White cotton and Silk cotton attain maximum values at 1000 c.p.s., Coconut fibres at 2000 c.p.s. and Jute fibres at 500 c.p.s.

The value of the absorption coefficients as calculated theoretically from the dimensions of the pores and porosity of the sample and relation between the theoretical and measured values will be dealt in the subsequent paper (Part II.)

ACKNOWLEDGMENT

The whole of the work has been conducted in the Kanodia Electrical Communication Engineering Laboratories, Department of Applied Physics, University of Calcutta. The authors desire to express their grateful thanks to Prof. P. N. Ghosh, Head of the Department of Applied Physics for his kind interest and guidance throughout the course of the work. The authors also acknowledge with thanks the valuable suggestions given by Mr. S. P. Chakravarti in designing and constructing the sound chamber. They also wish to acknowledge their indebtedness to Dr. W. G. Macmillan of the Indian Jute Mills' Association for supplying different samples of jute.

APPLIED PHYSICS LABORATORY,
UNIVERSITY OF CALCUTTA

REFERENCES

- Heyl, Chrisler and Snyder (1930), *U. S. Bureau of Standards, Journal of Research*, **4**, 289.
 Johnstone Stoney (1885), *Roy. Dub. Soc. Proc.*, **4**, 53.
 Kuhl and Meyer (1932), *Nature*, **130**, 580.
 National Physical Laboratory (1927), *Phil. Mag.*, **3**, 177.
 Olson and Kreuser (1930), *Jour. Acou. Soc. America*, **2**, 78.
 Paris (1927), *Phys. Soc. Proc.*, **39**, 269.
 Paris (1927), *Proc. Roy. Soc.*, **115**, 407.
 Paris (1930), *Nature*, **126**, 9.
 Rayleigh (1883), *Phil. Mag.*, **16**.
 Rayleigh (1920), *Phil. Mag.*, **39**, 225.
 Reid (1835), *British Association Report*, p. 13.
 Sabine (1895), *Collected Papers on Acoustics*.
 Taylor (1913), *Phys. Rev.*, **2**, 270.
 Tuma (1902) *Wien, Ber.*, **111**, 402.
 U. S. Bureau of Standards (1930), *Journal of Research*, **6**, 957.
 Watson (1922), *Bull. Univ. of Illinois, Eng. Expt. St.*, N. 127.
 Weisbach (1910), *Ann. d. Phys.*, **33**, 763.
 Wentz and Bedell (1930), *Jour. Acou. Soc. America*, **1**, 422.

THE DISTORTION OF PLANE X-WAVE AND ITS EFFECT ON ELASTIC SCATTERING IN COULOMB FIELD

BY K. C. KAR

(Received for publication, 20th April, 1944)

ABSTRACT. A new method is discussed for finding the effect of distortion of the incident χ -wave. It is shown that to a first approximation the distortion has no effect on the intensity of elastic scattering and the wavestatistical value of the critical approach.

In the wavestatistical theory of elastic scattering already discussed by the writer (Kar, 1937), it is assumed that the incident electron wave is plane. The wave equation for it is

$$\Delta\chi + k^2\chi = 0; \quad k = \frac{2\pi mv}{h} \quad \dots (1)$$

On coming within the potential field the wave equation is modified and becomes

$$\Delta\chi + k^2\left(1 - \frac{V}{E}\right)\chi = 0 \quad \dots (2)$$

At small distance from the scattering centre the potential V becomes appreciable and has the effect of perturbing the wave-function thereby causing scattering. However, at large distance V is small but not negligible as in eq. (1). Its effect is to bring about slight distortion of the plane wave. The distorted plane wave then encounters the large potential field at close distance and is scattered.

The method adopted in the present paper for finding out the distortion is somewhat different from that of Temple (1928) and others.

The well known solution of (1) is

$$\chi = R(r)P_l^m(\cos\theta)e^{im\phi} \quad \dots (3)$$

where R satisfies the differential equation

$$\frac{d^2R}{dr^2} + \frac{2}{r} \frac{dR}{dr} + k^2R - \frac{l(l+1)}{r^2}R = 0 \quad \dots (3.1)$$

On putting $\rho = kr$ and $R = \rho^{\frac{1}{2}}R_1$, we have from (3.1) after simple transformations

$$\frac{d^2R_1}{d\rho^2} + \frac{1}{\rho} \frac{dR_1}{d\rho} + \left\{1 - \frac{(l+\frac{1}{2})^2}{\rho^2}\right\}R_1 = 0 \quad \dots (3.2)$$

which is the well known Bessel's equation whose solution is

$$R_1 = A_l J_{l+\frac{1}{2}}(kr) \quad \dots (3.3)$$

Thus the solution of the wave equation (1) may be taken in the general form

$$\chi = \frac{1}{\sqrt{k\tau}} \sum_{l,m} A_{l,m} J_{l+\frac{1}{2}}(k\tau) P_l^m(\cos\theta) e^{im\phi} \quad \dots (4)$$

where each term of the series is a solution of (1). If, however, it is supposed that the incident electron wave is plane and is proceeding along x -axis, the solution of (1) is obviously

$$\chi = A e^{ikx} \quad \dots (4.1)$$

As in this case the wave-function χ has axial symmetry about the x -axis, we cannot take the solution in the general form (4) but have to assume $m=0$. Thus (4) becomes

$$\chi = \frac{1}{\sqrt{k\tau}} \sum_l A_l J_{l+\frac{1}{2}}(k\tau) P_l(\cos\theta) \quad (4.2)$$

It may be easily seen on expanding e^{ikx} after Rayleigh (*vide* Theory of Sound, Vol. II) that the solutions (4.1) and (4.2) are identical.

Now, in the above treatment we have neglected the Coulomb potential at large distance and obtained the wave-function for a plane wave. If, however, the potential is taken into account, the wave is modified. And we have for the R-equation from (2), taking $V = + (Ze^2/\tau)$,

$$\frac{d^2 R}{d\tau^2} + \frac{2}{\tau} \frac{dR}{d\tau} + k^2 R - \frac{l(l+1)}{\tau^2} R - \frac{2a'kZ}{\tau} R = 0 \quad (5)$$

where $a' = \frac{2\pi e^2}{h\nu}$. On putting $\rho = k\tau$ and $R = \rho^{-\frac{1}{2}} R_1$ as before, we have from (5)

$$\frac{d^2 R_1}{d\rho^2} + \frac{1}{\rho} \frac{dR_1}{d\rho} + \left\{ 1 - \frac{(l+\frac{1}{2})^2}{\rho^2} \right\} R_1 - \frac{2a'Z}{\rho} R_1 = 0 \quad (5.1)$$

Let us make the substitutions

$$R_1 = (\rho - \rho_x) e^{ia'Z} \quad R_2, \rho = k\tau, \rho_x = kx$$

Hence on differentiating we get

$$\begin{aligned} \frac{dR_1}{d\rho} &= (\rho - \rho_x) e^{ia'Z} \left[\frac{dR_2}{d\rho} - \frac{ia'Z}{\rho} R_2 \right] \\ \frac{d^2 R_1}{d\rho^2} &= (\rho - \rho_x) e^{ia'Z} \left[\frac{d^2 R_2}{d\rho^2} - \frac{2ia'Z}{\rho_x} \frac{dR_2}{d\rho} + \frac{ia'Z}{\rho_x^2} \rho R_2 - \frac{ia'Z}{\rho_x} \left(\frac{dR_2}{d\rho} - \frac{ia'Z}{\rho_x} R_2 \right) \right] \end{aligned}$$

So we have from (5.1)

$$\begin{aligned} \frac{d^2 R_2}{d\rho^2} + \frac{1}{\rho} \frac{dR_2}{d\rho} + R_2 \left\{ 1 - \frac{(l+\frac{1}{2})^2 + a'^2 Z^2 \frac{\rho^2}{\rho_x^2}}{\rho^2} \right\} - 2a'Z \left(\frac{1}{\rho_x} \frac{dR_2}{d\rho} + \frac{R_2}{\rho_x} \right) \\ + \frac{ia'Z}{\rho \rho_x} \left(\frac{\rho^2}{\rho_x^2} - 1 \right) R_2 = 0 \quad \dots (5.2) \end{aligned}$$

At large distance $\rho \rightarrow \rho$ and so (5.2) may be written in the form

$$\frac{d^2 R_2}{d\rho^2} + \frac{1}{\rho} \frac{dR_2}{d\rho} + R_2 \left\{ 1 - \frac{(l + \frac{1}{2})^2 + a'^2 Z^2}{\rho^2} \right\} - \frac{2a'Z}{\rho} \left(i \frac{dR_2}{d\rho} + R_2 \right) = 0 \quad (5.3)$$

It may be easily seen that if $a'Z$ is neglected, there would be no distortion and (5.3) would reduce to (3.2). Thus it follows that the distortion is negligible for high speed incident particles and also for scattering by light atoms.

The following method may be adopted to solve the differential eq. (5.3). For small distortion the last term of eq. (5.3) is quite small. So we neglect it at first and get the solution in Bessel Function as in (3.2). We have evidently

$$\left. \begin{aligned} R_2 &= A_s J_{s+\frac{1}{2}}(\rho) \\ (s+\frac{1}{2})^2 &= (l+\frac{1}{2})^2 + a'^2 Z^2 \end{aligned} \right\} \quad \dots (5.4)$$

On using the well known asymptotic value

$$\sqrt{\frac{n}{2\rho}} J_{s+\frac{1}{2}}(\rho) \sim i^{-s} \frac{e^{i\rho}}{\rho}$$

it may be easily seen that

$$i \frac{dR_2}{d\rho} = -R_2 \quad \dots (6)$$

for large value of ρ . Consequently, to this order of approximation, the last term in (5.3) vanishes. Thus (5.4) may be taken as an asymptotic solution of (5.3). Again, as $a'^2 Z^2$ is a small quantity of the second order we may neglect it and take $s=l$ in (5.4) and so the asymptotic value of the wave-function for the distorted incident wave becomes

$$\chi = \frac{1}{\sqrt{k}} \sum_l A_l J_{l+\frac{1}{2}}(kr) e^{ia \log k(r-\lambda)} P_l(\cos\theta) \quad \dots (7)$$

On summing the series in the usual way we have for the alternative form

$$\chi = A e^{ikx + ia \log k(r-\lambda)} \quad \dots (7.2)$$

in agreement with Temple's formula, his unimportant constant factors being supposed to be included in the unknown constant A .

Let us next find the effect of the above distortion on the first order scattering function. The well known differential equation determining the scattering function without distortion, is

$$\Delta(\lambda_1 \chi_1) + k^2 \lambda_1 \chi_1 = \frac{8\pi^2 m}{h^2} V \chi_0 \quad \dots (7.2)$$

where χ_0 is the undistorted incident wave-function. If, now, we take account of the effect of distortion, (7.2) should be

$$\Delta(\lambda_1 \chi_1) + k^2 \left(1 - \frac{V}{E} \right) \lambda_1 \chi_1 = \frac{8\pi^2 m}{h^2} V \chi \quad \dots (7.3)$$

where x is given by (7.1).

On solving (7.3) we have

$$\lambda_1 \chi_1 = -\frac{A}{4\pi} \frac{8\pi^2 m}{h^2} \int V(r_1) e^{ikx_1 + ia \log k(r_1 - x_1)} \cdot e^{-ikr_1 - ia \log k(r_1 - x_1)} \\ \times e^{ikr_2 + ia \log k(r_2 - x_2)} \cdot \frac{d\tau}{r_{12}} \dots (7.4)$$

$$= -\frac{2\pi mA}{h^2} e^{ia \log k(r_2 - x_2)} \int V e^{ikx_1} \frac{e^{ikr_{12}}}{r_{12}} d\tau \dots (7.5)$$

On integrating in the usual manner as before, we get for the scattering function

$$\lambda_1 \chi_1 = -\frac{A}{2mv^2} \text{cosec}^2 \frac{1}{2} \theta \cdot \frac{e^{ikr_1 + ia \log k(r_1 - x)}}{r} \dots F(r_0) \dots (8)$$

where

$$F(r_0) = k' \int_{r_0}^{\infty} \sin k'r V(r) r dr \dots (8.1)$$

It is the same as the formula of Temple when the wave statistical connection for critical approach is neglected. On evaluating $F(r_0)$ for the coulomb repulsive force, we have for the relative intensity of scattering

$$I = \left(\frac{Ze^2}{2mv^2} \right)^2 \text{cosec}^4 \frac{1}{2} \theta \cos^2 k' r_0 \dots (8.2)$$

being the same as the formula derived before by Kar (1937) without considering the effect of distortion. Thus, it follows that the distortion of the incident wave has no effect on the relative intensity of scattering. The critical approach r_0 is also unaffected and is the same as that given by Kar (1937), viz.,

$$r_0 = \rho \cdot \frac{Ze^2}{mv^2} (\text{cosec}^2 \frac{1}{2} \theta + 1); \quad \rho = 1.35 \dots (8.3)$$

In the above treatment I have not considered the effect of relativity. It is, however, obvious that by taking into account the distortion, one would find no change in the relativistic expressions for the intensity of scattering and the critical approach. It may be easily checked if necessary.

PHYSICAL LABORATORY
PRESIDENCY COLLEGE,
CALCUTTA

REFERENCES

- Kar, K. C., 1937, *Phil. Mag.*, **24**, 971.
Kar, K. C., Ghosh, M., and Mukherjee, K. K., 1937, *Phil. Mag.*, **24**, 964.
Temple, 1928, *Proc. Roy. Soc. A.*, **121**, 672.

THE CRYSTAL STRUCTURES OF METALLIC FLUOBERYLLATES, DOUBLE FLUOBERYLLATES AND SULPHATO-FLUOBERYLLATES

By P. L. MUKHERJEE

(Received for publication, 13th May, 1944)

(Plates IIa and IIb)

ABSTRACT. Crystals of the fluoberyllates of Rubidium, thallium, potassium and ammonium have been studied goniometrically and by X-rays. It has been found that these crystals are isomorphous among themselves as well as with the crystals of the sulphates of the corresponding metals, both as regards crystal class and axial lengths. The space group of the crystals of the potassium compound has been determined and found to be identical with that of potassium sulphate. Crystals of the double fluoberyllates (a) $\text{Zn}(\text{NH}_4)_2(\text{BeF}_4)_2, 6\text{H}_2\text{O}$ (b) $\text{Co}(\text{NH}_4)_2(\text{BeF}_4)_2, 6\text{H}_2\text{O}$ and (c) $\text{Ni}(\text{NH}_4)_2(\text{BeF}_4)_2, 6\text{H}_2\text{O}$ and also of the substance $\text{NiK}_2\text{BeF}_4, \text{SO}_4, 6\text{H}_2\text{O}$ are isomorphous among themselves as well with the sulphates. The axial lengths of $\text{Ni}(\text{NH}_4)_2(\text{BeF}_4)_2, 6\text{H}_2\text{O}$ have been measured and found identical with those of corresponding double sulphate.

INTRODUCTION

Works of Sarkar and Roy (1929) on the Fluoberyllates furnished quite a new example of a homologous radical in BeF_4 of the radical SO_4 . They actually observed that many simple and complex salts (including alums) of these two ions are perfectly isomorphous—their respective solubilities and molecular volumes are also very close, and even the organic salts of the corresponding acids are physically and chemically similar. They further found the crystals of a fluoberyllate to grow uniformly well in a saturated solution of the corresponding sulphate.

It is a well-established fact in crystallography, which has been corroborated by X-ray evidence, that chemically and physically isomorphous selenates and sulphates are also isomorphous crystallographically and structurally [Koch Holm and Schonfeld (1926)]. In the light of this result the author was led to investigate whether the chemical analogy of the fluoberyllates and sulphates as discovered by Sarkar and Roy can be pushed further so as to establish a real crystallographic and structural isomorphism among these substances too.

Three types of fluoberyllates taken up for investigation were :—

(1) Simple fluoberyllates—

(a) Rb_2BeF_4 ; (b) Tl_2BeF_4 ; (c) K_2BeF_4 ; (d) $(\text{NH}_4)_2\text{BeF}_4$.

(2) Double fluoberyllates—

(a) $\text{Zn}(\text{NH}_4)_2(\text{BeF}_4)_2, 6\text{H}_2\text{O}$;

(b) $\text{Co}(\text{NH}_4)_2(\text{BeF}_4)_2, 6\text{H}_2\text{O}$;

(c) $\text{Ni}(\text{NH}_4)_2(\text{BeF}_4)_2, 6\text{H}_2\text{O}$.

(3) Sulphato fluoberyllates—

(a) $\text{Zn}(\text{NH}_4)_2\text{BeF}_4 \cdot \text{SO}_4, 6\text{H}_2\text{O}$;

(b) $\text{NiK}_2\text{BeF}_4 \cdot \text{SO}_4, 6\text{H}_2\text{O}$.

GONIOMETRIC MEASUREMENTS

Goniometric measurements of the crystals of these salts were carried out by means of a Fuess two-circle goniometer.

(1) Simple Fluoberyllates—

(a) Rubidium fluoberyllate Rb_2BeF_4 .

Class.—Orthorhombic bi-pyramidal.

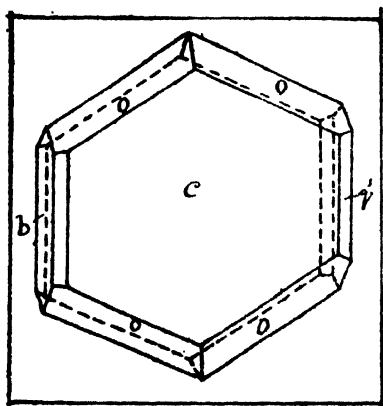
Preparation.—The salt was prepared by double decomposition of $(\text{NH}_4)_2\text{BeF}_6$ and RbNO_2 . Crystals are easily obtainable from saturated aqueous solution of the salt at ordinary temperatures. These crystals possess a very high tendency to get twinned.

Habit.—The substance forms transparent crystals with a large growth in the directions of 'a' and 'b' axes. They occur as thin plates of c (001) faces bounded by the faces b (010), k (021), o (111) and occasionally q (011). (Fig. 1).

Specific gravity = 3.243.

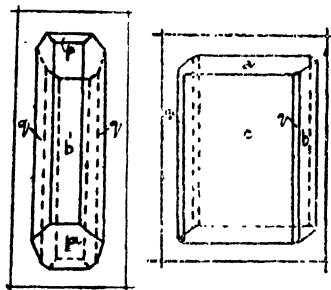
Axial ratios of Rb_2BeF_4 $a:b:c = 0.5766:1:0.7560$.

Axial ratios of Rb_2SO_4 $a:b:c = 0.5723:1:0.7485$.



Rb_2BeF_4

FIG. 1



Tl_2BeF_4

FIG. 2(a)

FIG. 2(b)

—	—	Observed	Calculated	Corresponding sulphate
001	021	56°34'	56°31'	56°15'
010	021	33°37'	33°30'	33°45'
001	111	56°21'	56°31'	56°26'
021	111	49°10'	49°19'	49°22'
010	111	65°26'	65°22'	—
111	111	49°1'	49°8'	48°54'
011	111	46°10'	46°17'	—

(b) Thallium fluoberyllate Tl_2BeF_4 .*Class*.—Orthorhombic bipyramidal.*Preparation*.—The substance was prepared by double decomposition of thallium nitrate and ammonium fluoberyllate.

The crystals were easily obtained as slightly transparent needles from saturated solution of the substance in water at ordinary temperatures. These crystals possess a very great tendency to become twinned though the faces of each component of a twinned crystal are generally quite perfect.

Habit.—The crystals are mostly very narrow elongated needles consisting of faces b (010), c (001) and limited by a top face a (100); when these needles are a bit thicker, the faces q (011) also appear [Fig. 2(a)]. Needles are also seen with a single top face m (110) or n (130) instead of a (100). Elongated thin plates of faces c (001) bounded by b (010) and a (100) are also found to occur occasionally. [Fig. 2(b)].

Specific gravity = 6.650.

Axial ratios of Tl_2BeF_4 $a:b:c = 0.5638:1:0.7368$.Axial ratios of Tl_2SO_4 $a:b:c = 0.5555:1:0.7328$.

—	—	Observed	Calculated	Corresponding sulphate
010	130	$30^\circ 31'$	$30^\circ 36'$	$30^\circ 58'$
010	011	$53^\circ 37'$	$53^\circ 37'$	$53^\circ 46'$
010	110	$60^\circ 38'$	$60^\circ 35'$	$60^\circ 57'$

(c) Potassium fluoberyllate K_2BeF_4 .*Class*.—Orthorhombic bipyramidal.

Preparation.—The salt was prepared by digesting beryllium carbonate in a solution of potassium bifluoride. The substance being very much less soluble in water comes down immediately. After purification by recrystallisation single crystals are finally obtained from a saturated aqueous solution.

Habit.—Crystalline habits of the substance are (1) very short prism with faces (010), (001) with an additional face (021) and with end faces (111), (110). Fig. 3(a).

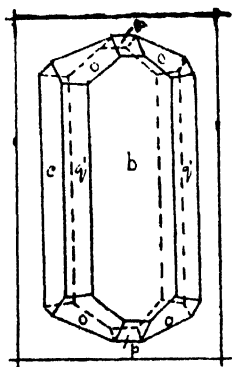


FIG. 3(a)

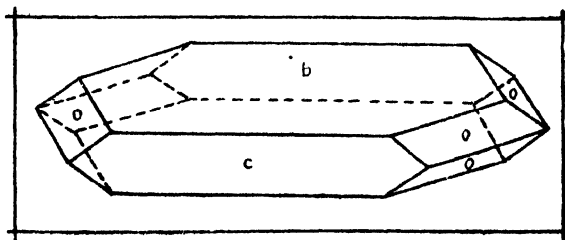


FIG. 3(b)

(2) Thick plates (010) bounded by the faces (001) and (111) (the most common type). Fig. 3(b).

(3) Thin plates (100) bounded by faces (111) occurring very rarely. Fig. 3(c).

(4) Needles with faces (010), (001), (021) limited by faces (111). Fig. 3(d).

Specific gravity = 2.649.

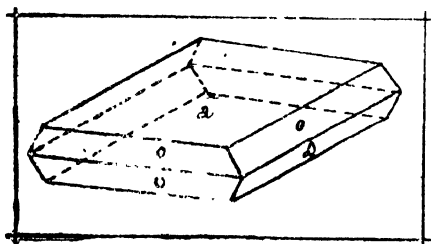


FIG. 3(c)

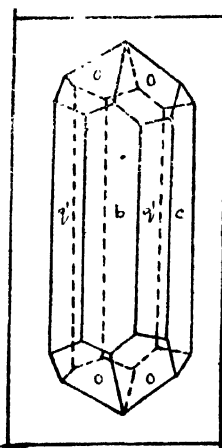


FIG. 3(d)

This crystal has been goniometrically studied by Marignac. His data has been confirmed by our measurements. The data for this substance given below are Marignac's data quoted from Groth's *Chemische Krist.* Vol. I, p. 342.

Axial ratios of K_2BeF_4 $a:b:c = 0.5708:1:0.7395$.

Axial ratios of K_2SO_4 $a:b:c = 0.5727:1:0.7418$.

—	—	Observed	Calculated	Corresponding sulphate
110	$\bar{1}\bar{1}0$	59°26'	59°26'	—
111	111	48°40'	48°38'	48°46'
111	$\bar{1}\bar{1}\bar{1}$	88°20	87°39'	—
112	112	34°50'	34°20'	—
112	$\bar{1}\bar{1}2$	62°10'	62°31'	—
001	021	56°0'	55°56'	56°1'
001	111	56°10'	56°10'	—
021	111	49°10'	49°14'	49°12
021	112	45°48'	46°1'	—

(d) Ammonium fluoberyllate $(\text{NH}_4)_2\text{BeF}_4$.

Class.—Orthorhombic bipyramidal.

Preparation.—The substance was obtained by decomposing beryllium carbonate with ammonium bifluoride.

Crystallisation.—It is very difficult to get suitable single crystals. The aqueous solution becomes highly supersaturated and then suddenly gives out a crop of transparent crystals which are abnormally twinned.

Habit.—The crystal forms long needles of faces (001), (010), (011) limited either by one pair of (100) faces or two pairs of (110) faces of which one is much larger than the other. The (001) face is always much broader than the (010) face and this broadening often becomes so prominent as to give rise to thin narrow plate-like types.

Specific gravity = 1.683.

The crystal has also been studied by Marignac whose measurements have been confirmed by us. The data given below are from Groth's *Chemische Krist.* Vol. I p. 342.

Axial ratios of $(\text{NH}_4)_2\text{BeF}_4$ $a : b : c = 0.5655 : 1 : 0.7367$.

Axial ratios of $(\text{NH}_4)_2\text{SO}_4$ $a : b : c = 0.5635 : 1 : 0.7319$ $(\text{NH}_4)_2\text{BeF}_4$.

—	—	Observed	Calculated	Corresponding sulphate
010	110	60°30'	60°22'	60°41'
111	111	48°16'	48°28'	
001	021	55°50'	55°50'	55°40'
001	111	56°5'	56°8'	
111	011	46°12'	46°12'	
111	021	49°13'	49°16'	
110	021	66°2'	65°51'	

(2) Double Fluoberyllates—

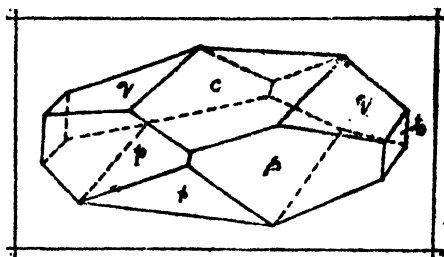
(a) Zinc Ammonium Fluoberyllate



Class.—Monoclinic prismatic.

Preparation.—Zinc fluoberyllate is prepared by double decomposition of zinc chloride and thallium fluoberyllate and zinc fluoberyllate mixed with requisite amount of $(\text{NH}_4)_2\text{BeF}_4$. Crystallisation of this substance is difficult. Aqueous solution becomes highly supersaturated forming a syrupy liquid. The solution, however, gives very beautiful colourless transparent crystals when crystallisation is induced by throwing a crystal of zinc ammonium sulphate.

Habit.—These crystals commonly occur as large thick plates of faces $c(001)$, $q(011)$, $s(201)$ and $o(111)$ which are not so prominent [Fig. 4]. The prismatic type is also met with frequently.



$\text{Am}_2\text{Zn}(\text{BeF}_4)_2, 6\text{H}_2\text{O}$

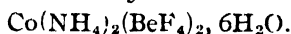
FIG. 4

Specific gravity = 1.859.

Axial ratios $a : b : c = 0.7387 : 1 : 0.4909$; $\beta = 106^\circ 34'$.

—	—	Observed	Calculated	Corresponding sulphate
110	110	$70^\circ 33'$	$70^\circ 36'$	$70^\circ 26'$
110	010	$54^\circ 41'$	$54^\circ 42'$	$54^\circ 47'$
110	011	$62^\circ 50'$	$62^\circ 52'$	$62^\circ 27'$
110	011	$88^\circ 0'$	$88^\circ 0'$	$88^\circ 0'$
110	201	$53^\circ 1'$	$53^\circ 3'$	$52^\circ 34'$
110	111	$88^\circ 13'$	$88^\circ 3'$	$87^\circ 36'$
110	001	$76^\circ 33'$	$76^\circ 33'$	$76^\circ 17'$
001	201	$64^\circ 1'$	$64^\circ 1'$	$64^\circ 56'$
001	011	$25^\circ 11'$	$25^\circ 12'$	$25^\circ 33'$
001	111	$44^\circ 14'$	$44^\circ 13'$	$45^\circ 5'$

(b) Cobalt Ammonium Fluoberyllate



Class.—Monoclinic prismatic.

Preparation.—The method of preparation was very similar to that followed by Sarkar and Roy. Good pink-coloured transparent crystals were easily obtained from its aqueous solution.

Habit.—Thick prisms of faces (110) and (010) limited by the top faces (001), (011), (201) and (111) are generally seen [Fig. 5(a)]. It must be noted that the faces (201) and (111) are very much diminished in size. Another type consists of plate-like prisms of faces (110), (001), (201) and (011) [Fig. 5(b)].

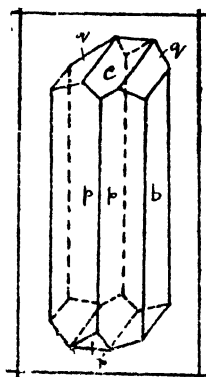


FIG. 5(a)

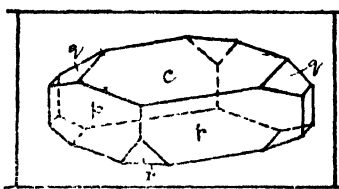
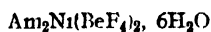


FIG. 5(b)



Specific gravity = 1.821.

Axial ratios of $\text{Co}(\text{NH}_4)_2(\text{BeF}_4)_2, 6\text{H}_2\text{O}$:

$$a : b : c = 0.7405 : 1 : 0.4852 ; \beta = 106^\circ 46'$$

Axial ratios of $\text{Co}(\text{NH}_4)_2(\text{SO}_4)_2, 6\text{H}_2\text{O}$:

$$a : b : c = 0.7392 : 1 : 0.4985 ; \beta = 106^\circ 56'$$

—	—	Observed	Calculated	Corresponding sulphate
110	$\bar{1}\bar{1}0$	70° 35'	70° 40'	70° 32'
010	110	54° 44'	54° 40'	54° 44'
110	001	76° 23'	76° 24'	76° 15'
111	111	38° 16'	38° 8'	38° 40'
111	011	26° 30'	26° 26'	26° 51'
011	001	24° 54'	24° 35'	25° 30'

(c) Nickel Ammonium Fluoberyllate



Class.—Monoclinic prismatic.

Preparation.—The substance was prepared by Sarkar and Ray's method. Bluish-green transparent crystals are obtained from aqueous solution. Faces often become distorted.

Habit.—Similar to cobalt ammonium fluoberyllate, only difference being that (111) faces also appear in this case. Elongated needle-like prisms [Fig. 5(a)] as well as short thick prisms [Fig. 5(b)] are equally prevalent. The forms usually occurring in these crystals are (110), (011), (201), (111), (001), (111) and (010).

Specific gravity = 1.843.

Axial ratios of $\text{Ni}(\text{NH}_4)_2(\text{BeF}_4)_2, 6\text{H}_2\text{O}$:

$$a : b : c = 0.7373 : 1 : 0.4914; \quad \beta = 106^\circ 40'.$$

Axial ratios of $\text{Ni}(\text{NH}_4)_2(\text{SO}_4)_2, 6\text{H}_2\text{O}$:

$$a : b : c = 0.7370 : 1 : 0.5032; \quad \beta = 107^\circ 4'.$$

—	—	Observed	Calculated	Corresponding sulphate
110	$\bar{1}\bar{1}0$	70° 30'	70° 28'	70° 20'
110	011	62° 42'	62° 46'	62° 14'
$\bar{1}\bar{1}0$	011	88° 2'	88° 3'	88° 6'
110	201	52° 51'	52° 58'	52° 24'
011	001	25° 12'	25° 13'	25° 41'
201	001	64° 18'	64° 12'	65° 21'
110	001	76° 27'	76° 27'	—
010	110	54° 44'	54° 46'	54° 50'
110	111	58° 58'	59° 6'	58° 29'
111	$\bar{1}\bar{1}0$	87° 56'	88° 3'	87° 56'
001	$\bar{1}\bar{1}1$	44° 33'	44° 28'	45° 24'
011	$\bar{1}\bar{1}1$	34° 46'	34° 39'	35° 20'
001	111	33° 46'	33° 41'	—

(3) Sulphato-Fluoberyllates—

(a) Zinc Ammonium Sulphate-Fluoberyllate



Class.—Monoclinic Prismatic.

Preparation.—The substance was prepared by Sarkar and Ray's method. It easily crystallises from its aqueous solution at ordinary temperatures as small transparent colourless crystals.

Habit.—The crystals are more or less prismatic, the prisms being of faces (110) [Fig. 6(a)]. In the latter case the (001) faces and one of the (010) faces often become strongly developed thus deviating from the prismatic habit [Fig. 6(b)]. Occasionally the prism faces remain shorter where the top faces (001) become larger still, so as to give the crystal a thick plate-like nature [Fig. 6(c)]. The most common forms are (110), (001), (011), (010), (201) and (111).

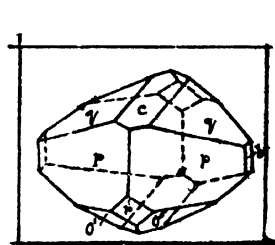


FIG. 6(a)

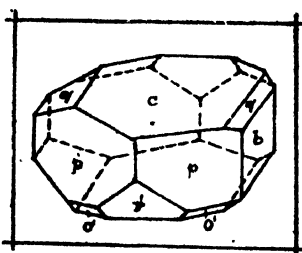


FIG. 6(b)

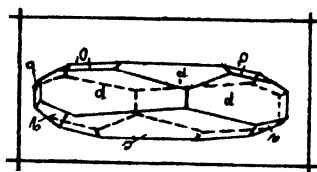
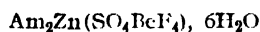


FIG. 6(c)



Specific gravity = 1.843.

Axial ratios $a : b : c = 0.7382 : 1 : 0.4942; \beta = 106^\circ 43'$

—	—	Observed	Calculated
110	110	$70^\circ 32'$	$70^\circ 32'$
010	110	$54^\circ 44'$	$54^\circ 44'$
110	001	$76^\circ 26'$	$76^\circ 15'$
110	011	$62^\circ 39'$	$62^\circ 40'$
110	201	$52^\circ 55'$	$52^\circ 45'$
110	111	$88^\circ 5'$	$88^\circ 3'$
111	001	$44^\circ 34'$	$44^\circ 39'$
111	111	$49^\circ 15'$	$49^\circ 20'$
201	001	$64^\circ 18'$	$64^\circ 24'$
011	001	$25^\circ 11'$	$25^\circ 20'$
110	011	$88^\circ 3'$	$88^\circ 0'$

(b) Nickel Potassium Sulphato Fluoberyllate



Class.—Monoclinic prismatic.

Preparation.—Same as in the case of zinc-ammonium sulphato-fluoberyllate. Bluish green crystals were easily obtained from its saturated solution in water at ordinary temperatures. The faces of these well-formed crystals have got a marked tendency to become distorted.

Habit.—Prisms of faces (110) with additional faces (010) limited by top face ($20\bar{1}$), (001), (011) are very common [Fig. 7(a)]. In some cases only two of the prism faces become highly developed (others remaining reduced) and the crystal assumes a plate-like appearance [Fig. 7(b)]. Occasionally the faces (001) and ($20\bar{1}$) become peculiarly magnified while the faces (010) and (011) are completely suppressed. Plates of faces (001) bounded by faces (110), ($20\bar{1}$) and (011) are also met with [Fig. 7(c)]

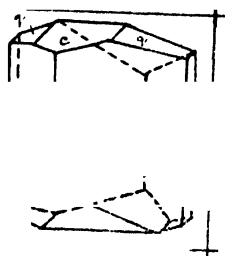


FIG. 7(a)

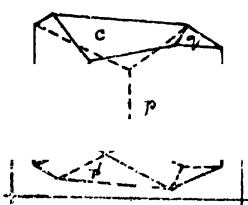


FIG. 7(b)

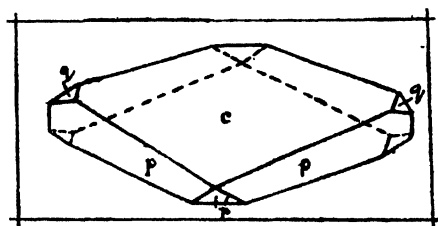
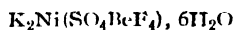


FIG. 7(c)



Specific gravity = 1.856

Axial ratios $a : b : c = 0.7405 : 1 : 0.5077$; $\beta = 104^\circ 44'$

—	—	Observed	Calculated
010	110	$54^\circ 22'$	$54^\circ 24'$
110	001	$78^\circ 4'$	$78^\circ 4'$
110	011	$63^\circ 52'$	$63^\circ 46'$
110	011	$86^\circ 1'$	$85^\circ 56'$
110	$20\bar{1}$	$52^\circ 15'$	$52^\circ 4'$
$20\bar{1}$	001	$63^\circ 39'$	$63^\circ 51'$
011	001	$26^\circ 9'$	$26^\circ 9'$

X-RAY MEASUREMENTS

Rotation pictures were taken about the three crystallographic axes with copper $K\alpha$ radiation and a cylindrical camera to determine the cell dimensions of potassium fluoberyllate, rubidium fluoberyllate, thallium fluoberyllate, ammonium fluoberyllate and nickel ammonium fluoberyllate.

Structures of Metallic-, Double- and Sulphato-fluoberyllates 157

The dimensions of the unit cells of the different fluoberyllates are given below in Angstrom units :—

Metallic Radical.	Fluoberyllates			Sulphates		
	a	b	c	a	b	c
Potassium ...	5.63	9.83	7.29	5.73	10.00	7.42
Rubidium ...	5.85	10.13	7.66	5.94	10.39	7.78
Thallium ...	5.87	10.43	7.68			
Ammonium ...	{ 5.89	10.39	7.49	5.95	10.56	7.72
	{ (5.8	10.2	7.5)	from Hultgren (1934)		
Nickel Ammonium ...	{ 9.04	12.31	6.04	8.98	12.22	6.10
	$\beta = 106^\circ 40'$			$\beta = 107^\circ 4'$		

The above axial lengths and the monoclinic angles together with the values of the specific gravities gave the following numbers of molecules per unit cell in the different cases.

Substance.	No. of molecules per unit cell.
K_2BeF_4	4
Rb_2BeF_4	4
Tl_2BeF_4	4
$(NH_4)_2BeF_4$...
$Ni(NH_4)(BeF_4)_2, 6H_2O$...

Oscillation photographs were taken about the 'b' and the 'c' axes at intervals of 10 for the correct indexing of the planes. The indices of the spots appearing on the photographs were deciphered by Bernal's method (1927). The following results were obtained with potassium fluoberyllate and nickel ammonium fluoberyllate.

Potassium Fluoberyllate

- (1) (h k o) reflections are absent when h + k is odd.
- (2) (h o l) reflections are absent when l is odd.

This leads to the space group D_{2h}^{16} Pmcn.

Nickel Ammonium Fluoberyllate

- (1) Reflections from (h o l) planes are absent when h is odd.
- (2) (o k o) reflections are absent if k is odd.

These halvings correspond to the space group C_{2h}^5 P₂₁/a.

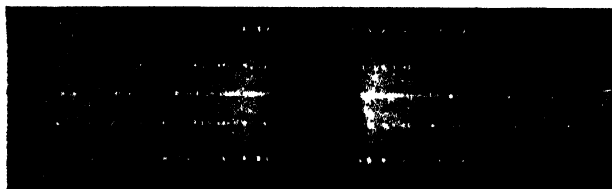
The experimental part of this investigation was carried out at the Physical Laboratory of the Dacca University. The author expresses his thanks to Prof. S. N. Bose for suggesting the problem and providing facilities for the work and to Prof. K. Banerjee for guidance and discussions throughout the progress of the work and to Mr. R. K. Sen for some calculations.

INDIAN ASSOCIATION FOR THE
CULTIVATION OF SCIENCE,
CALCUTTA.

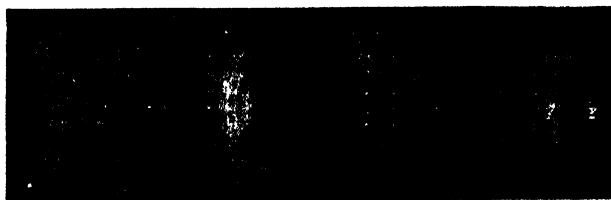
REFERENCES

- Bernal, J. D. (1927), *Proc. Roy. Soc.*, **113A**, 117.
Hulthgen, R. (1934), *Zeits. f. Krist.*, **88A**, 233.
Koch-Holm, E., and Schonfeldt, N. (1927), *Wiss. Veroff. Siemens Konz.*, **6**, 177.
Sarkar, P. B., and Ray, N. (1929), *J. Ind. Chem. Soc.*, **6**, 987.

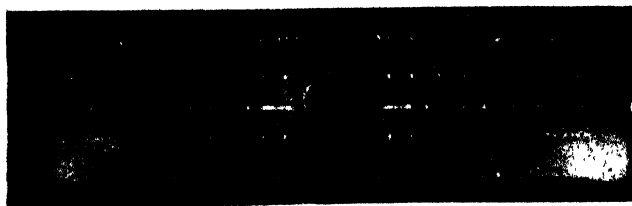
A



Rotation Photograph of Rubidium Fluoberyllate
about a—axis

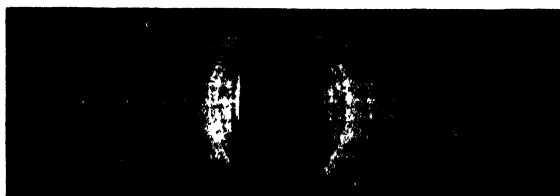


Rotation Photograph of Thallium Fluoberyllate
about b—axis.

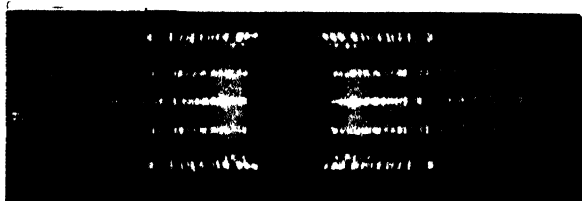


Rotation Photograph of Potassium Fluoberyllate
about a—axis.

D



Rotation Photograph of Potassium Fluoberyllate
about b--axis



Rotation Photograph of Ammonium Fluoberyllate
about a--axis.



Rotation Photograph of Ammonium Fluoberyllate
about b--axis.

THE DIELECTRIC PROPERTIES OF DAMMAR AND MASTIC RESINS

By G. N. BHATTACHARYA*

ABSTRACT. The paper contains the results of measurement of dielectric properties of two natural resins, dammar and mastic, over a wide range of temperature and frequency. The results show typical polar characteristics. The measurement of viscosity of mastic resin within the range $90^{\circ} - 120^{\circ}\text{C}$ and of dammar resin within the range $120^{\circ} - 150^{\circ}\text{C}$ shows that they follow the logarithmic relation of a liquid with temperature. The d.c. conductance measurement for both these resins also shows that the same law holds good within the range of measurement, *viz.*, $60^{\circ} - 150^{\circ}\text{C}$, with a discontinuity in the slope of the line obtained by plotting $\log K_0$ against $1/T$ at 80°C for mastic and at 113°C for dammar. A distributed range of relaxation times in the molecules of both these resins has been established and the distribution coefficient calculated. The average radius of the rotating unit in the a.c. field has been calculated for each of these resins and the result shows that their polar units are bigger than those of lac. The average radius of the mastic rotating unit is 4.5 A.U. whereas that of dammar is only 2.7 A.U. The activation energy of both these resins has been calculated above and below the transformation point.

INTRODUCTION

In a previous paper (Bhattacharya, 1944*a*) on the dielectric properties of lac it has been observed that anomalous dispersion takes place near about its melting point and that the resin acts like a polar liquid when placed in an alternating current field. But the whole molecule being large and complex does not take part in the rotation, the hydroxyl groups only acting as rotators. In a subsequent paper (Bhattacharya, 1944*b*) it has been reported that lac constituents also behave in a more or less similar fashion and the rotating unit of soft lac resin in the alternating electric field is also the hydroxyl group. Hartshorn and co-workers (1940) also arrived at a similar conclusion working with some synthetic thermoplastic resins. It is therefore of interest to study a few other thermoplastic resins regarding their dielectric properties and to calculate therefrom the dimensions of the rotating unit.

Dammar and mastic are two important natural resins, which give very clear spirit varnishes largely used on account of their lustre and paleness as paper varnishes for the protection of pictures. Dammar is also used as a binder for moulded electrical insulation. These are thermoplastic resins and they have been selected here for the study of their dielectric properties chiefly owing to their comparatively low melting points among the important natural resins. Fossil resins, such as copals, although important from the standpoint of utility, were not selected for such a study as measurement of their dielectric properties would have involved practical difficulties owing to their high melting points. This study therefore is a part of a general scheme for the study of electrical properties of natural resins of which lac probably occupies the most important position.

THEORETICAL

The dielectric properties of a substance may be expressed as

$$\epsilon = \epsilon' - i\epsilon''$$

* Fellow of the Indian Physical Society.

where $\epsilon =$ the complex dielectric constant,
 $\epsilon' =$ the ordinary dielectric constant, specific inductive capacity or permittivity,
 and $\epsilon'' =$ the dielectric loss factor.

The dielectric loss factor ϵ'' is related to the dielectric constant ϵ' through a factor, called power factor and expressed as $\tan \delta$, where δ is the loss angle. That is,

$$\epsilon'' = \epsilon' \tan \delta.$$

The current in phase with the applied voltage of a circuit may be expressed in terms of vectors as

$$\begin{aligned} I_r &= I \tan \delta \\ &= \omega CV \tan \delta, \text{ for a circuit containing a condenser } C \\ &= 2\pi f CV \frac{\epsilon''}{\epsilon'} \end{aligned}$$

But for a parallel plate condenser of area A and thickness d the value of C is given by

$$C = \frac{A\epsilon'}{4\pi d \times 9 \times 10^{11}} \text{ farads.}$$

Therefore substituting this value of C

$$I_r = \frac{fA}{18 \times 10^{11} \times d} \epsilon''$$

Now if K_t is the total conductance of the condenser this current can also be expressed as

$$I_r = \frac{A_s V K_t}{d}$$

From the r.h.s. of these equations we therefore have

$$\epsilon'' = \frac{18 \times 10^{11} \times K_t}{f}$$

This relation gives the value of total loss including that due to d.c. conductance of the dielectric of the condenser, the measure of which may similarly be written by substituting K_0 instead of K_t

$$\text{i.e., } \epsilon''_{k_0} = \frac{18 \times 10^{11} \times K_0}{f}$$

Hence pure a.c. loss is expressed by

$$\epsilon'' = \frac{18 \times 10^{11} (K_t - K_0)}{f} = \frac{18 \times 10^{11} \times K}{f}$$

EXPERIMENTAL

Apparatus.—The bridge method was employed for the measurement of capacity and power factor. For lower frequencies a Schering bridge, and for higher frequencies a General Radio—radio frequency bridge, type 516-C, were

used. For the latter ratio-arms and transformers were changed as advised by the manufacturers for different frequencies. Two oscillators, a beat frequency oscillator for audio-frequency currents and a General Radio modulated oscillator, type 684-A, for higher frequencies, were made use of. A wide-band amplifier in conjunction with a pair of high sensitivity headphones served as detector. The cell was the vertical type parallel plate gold condenser described earlier (Bhattacharya, 1944a). D.C. conductance measurements were made on the same assembly with D.C. voltage and a high sensitivity d'Arsonval galvanometer and a universal shunt. Viscosity measurements were made with a set of Lee's tar viscometers (Lee, 1934).

Materials.—The samples of dammar and mastic resins were supplied by Napier Paint Works Ltd., Calcutta. They were of ordinary commercial quality, but before use both of them were melted and filtered through two folds of muslin cloth to get rid of any dirt and woody matter, if present. The scum that floated on the surface of the molten resin was carefully removed and the clear liquid on the bottom taken for these experiments. The constants for these samples are as follows :

	Acid value.	Softening range (Mercury surface method.)	Melting range (Mercury surface method.)
Mastic	57.8	70-72°C	78-85°C
Dammar	39.5	100-104°C	112-117°C

METHOD OF PROCEDURE

The molten resins were poured into the experimental cell which had been kept heated in a circulating air-oven and the vertical plate condenser put into it. The precautions necessary to avoid air-bubbles adhering to the surface of the condenser plates as well as to avoid cracking of the experimental cell has already been dealt with in a previous paper (Bhattacharya, 1944c). The constancy of the capacity after several melting and stirring of the resin showed proper filling of the condenser. Capacity measurements were made by the substitution method on the radio-frequency bridge. D.C. conductance and viscosity measurements were made by the usual method.

CALCULATIONS

The standardisation of the experimental condenser was done by using pure and dry benzene, taking its dielectric constant at 25°C to be 2.2725. The 'Zero-capacity,' *i.e.*, the capacity for leads, etc., is given by

$$C_0 = \frac{C_{A\epsilon_B} - C_B}{\epsilon_B - 1}$$

where C_A = the capacity of the experimental condenser with air,
 C_B = the capacity of the same with benzene,
 and ϵ_B = the dielectric constant of benzene.

The dielectric constant of the resin ϵ was obtained from the relation

$$\epsilon = \frac{C_R - C_0}{C_A - C_0}$$

where C_R = the capacity of the resin filled condenser.

The power factor and the dielectric loss factor were calculated from the bridge readings as reported earlier (Bhattacharya, 1944a).

RESULTS

TABLE I

Dielectric constant-temperature data at different frequencies

Resin	Temp. °C	Dielectric constant ϵ' at the frequency of				
		500 Kc/s.	100 Kc/s.	50 Kc/s.	10 Kc/s.	1 Kc/s.
Mastic	20	2.79	2.82	2.83	2.85	2.88
	30	2.82	2.84	2.86	2.88	2.91
	40	2.85	2.88	2.90	2.92	2.96
	50	2.90	2.94	2.96	2.98	3.04
	60	2.95	3.00	3.02	3.05	3.14
	70	3.03	3.10	3.12	3.18	3.33
	80	3.12	3.20	3.23	3.34	3.62
	90	3.20	3.32	3.39	3.58	4.12
	100	3.32	3.54	3.65	4.02	4.72
	110	3.50	3.83	4.02	4.50	5.08
	120	3.72	4.18	4.38	4.84	5.19
	130	3.96	4.44	4.64	4.92	5.10
	140	4.18	4.58	4.72	4.88	5.02
	150	4.36	4.64	4.72	4.82	4.96
Danmar	20	2.66	2.68	2.69	2.70	2.71
	30	2.66	2.68	2.69	2.70	2.71
	40	2.67	2.69	2.70	2.71	2.72
	50	2.68	2.70	2.70	2.72	2.72
	60	2.69	2.71	2.72	2.73	2.74
	70	2.71	2.73	2.74	2.74	2.76
	80	2.73	2.76	2.76	2.78	2.80
	90	2.76	2.78	2.79	2.81	2.86
	100	2.78	2.82	2.83	2.89	3.01
	110	2.83	2.88	2.91	3.00	3.25
	120	2.90	3.00	3.09	3.30	3.74
	130	2.99	3.17	3.28	3.58	3.97
	140	3.06	3.30	3.48	3.78	4.02
	150	3.20	3.52	3.66	3.85	3.97

TABLE II

Measured power factor data at various temperatures and frequencies

Resin	Temp. °C	Power factor at the frequency of				
		500 Kc/s.	100 Kc s.	50 Kc/s.	10 Kc/s.	1 Kc/s.
Mastic	20	.0088	.0084	.0076	.0072	.0063
	30	.0097	.0089	.0085	.0077	.0064
	40	.0121	.0100	.0093	.0078	.0074
	50	.0150	.0117	.0116	.0094	.0095
	60	.0171	.0141	.0138	.0134	.0148
	70	.0209	.0190	.0206	.0220	.0293
	80	.0251	.0267	.0271	.0367	.0568
	90	.0352	.0407	.0426	.0641	.0841
	100	.0495	.0619	.0802	.0947	.1830
	110	.0714	.0914	.0947	.1031	.0574
	120	.0935	.1037	.1031	.0760	.0310
	130	.1057	.0976	.0896	.0448	.0256
	140	.1050	.0734	.0593	.0307	.0363
	150	.0890	.0510	.0371	.0242	.0779
Dammar	20	.0084	.0051	.0042	.0038	very low
	30	.0084	.0052	.0047	.0038	"
	40	.0088	.0051	.0045	.0038	"
	50	.0088	.0050	.0041	.0038	.0021
	60	.0089	.0050	.0041	.0039	.0022
	70	.0094	.0053	.0045	.0039	.0022
	80	.0103	.0061	.0054	.0061	.0062
	90	.0117	.0078	.0070	.0088	.0135
	100	.0140	.0117	.0120	.0182	.0359
	110	.0178	.0186	.0224	.0358	.0561
	120	.0287	.0396	.0485	.0674	.0622
	130	.0432	.0627	.0669	.0787	.0449
	140	.0577	.0717	.0650	.0653	.0252
	150	.0754	.0763	.0690	.0399	.0125

TABLE III

Corrected dielectric loss data at different temperatures and frequencies

Resin	Temp. °C.	Dielectric loss ϵ'' at the frequency of				
		500 Kc/s.	100 Kc s.	50 Kc/s.	10 Kc/s.	1 Kc/s.
Mastic	20	.0244	.0237	.0214	.0204	.0182
	30	.0275	.0254	.0244	.0221	.0186
	40	.0344	.0287	.0271	.0228	.0220
	50	.0436	.0343	.0344	.0279	.0290
	60	.0506	.0424	.0415	.0410	.0464
	70	.0634	.0588	.0642	.0699	.0975
	80	.0792	.0855	.0876	.1226	.2057
	90	.1126	.1350	.1444	.2295	.3463
	100	.1644	.2192	.2929	.3805	.3907
	110	.2500	.3500	.3805	.4637	.2881
	120	.3476	.4332	.4516	.3663	.1460
	130	.4185	.4327	.4144	.2136	.0621
	140	.4386	.3344	.2769	.1345	.0308
	150	.3873	.2326	.1667	.0758	—

TABLE III (contd.)

Resin	Temp. °C.	Dielectric loss ϵ'' at the frequency of				
		500 Kc/s.	100 Kc/s.	50 Kc/s.	10 Kc/s.	1 Kc/s.
Dammar	20	.0222	.0135	.0113	.0103	very low
	30	.0223	.0140	.0125	.0103	"
	40	.0235	.0136	.0120	.0104	"
	50	.0237	.0135	.0111	.0105	.0058
	60	.0239	.0136	.0113	.0105	.0059
	70	.0254	.0145	.0124	.0106	.0060
	80	.0281	.0167	.0150	.0170	.0172
	90	.0323	.0217	.0196	.0248	.0385
	100	.0389	.0330	.0340	.0525	.1081
	110	.0503	.0537	.0652	.1074	.1823
	120	.0832	.1187	.1499	.2223	.2323
	130	.1292	.1988	.2196	.2975	.1778
	140	.1764	.2367	.2472	.2467	.1004
	150	.2412	.2684	.2524	.1544	.0473

TABLE IV

D.C. conductance data at different temperatures

Resin	Temperature		1000/T	D.C. conductance K_0	Log K_0
	t°C	T°K			
Mastic	60	333	3.003	very low	—
	70	343	2.915	8.84×10^{-15}	-14.05
	75	348	2.874	1.30×10^{-14}	-13.88
	80	353	2.833	2.53×10^{-14}	-13.60
	90	363	2.755	1.19×10^{-13}	-12.93
	100	373	2.681	5.44×10^{-13}	-12.26
	110	383	2.611	1.99×10^{-12}	-11.70
	120	393	2.545	8.20×10^{-12}	-11.09
	130	403	2.481	3.81×10^{-11}	-10.42
	140	413	2.421	8.40×10^{-11}	-10.08
	150	423	2.364	2.27×10^{-10}	-9.64
Dammar	70	343	2.915	very low	—
	80	353	2.833	8.84×10^{-15}	-14.05
	90	363	2.755	1.39×10^{-14}	-13.86
	100	373	2.681	2.00×10^{-14}	-13.70
	110	383	2.611	3.00×10^{-14}	-13.52
	120	393	2.545	6.10×10^{-14}	-13.21
	130	403	2.481	2.20×10^{-13}	-12.66
	140	413	2.421	6.00×10^{-13}	-12.22
	150	423	2.364	1.35×10^{-12}	-11.87

DISCUSSIONS

The power factor—temperature curves (Figs. 1 and 2) of both these resins indicate that they behave as typical polar liquids. The dielectric constant and the dielectric loss-temperature curves (Figs. 3 and 4) also show the same characteristics. Both these resins therefore furnish very good examples of a typical polar resin. At temperatures below its softening range dammar resin has a very low value of power factor and it gives practically a horizontal straight line graph

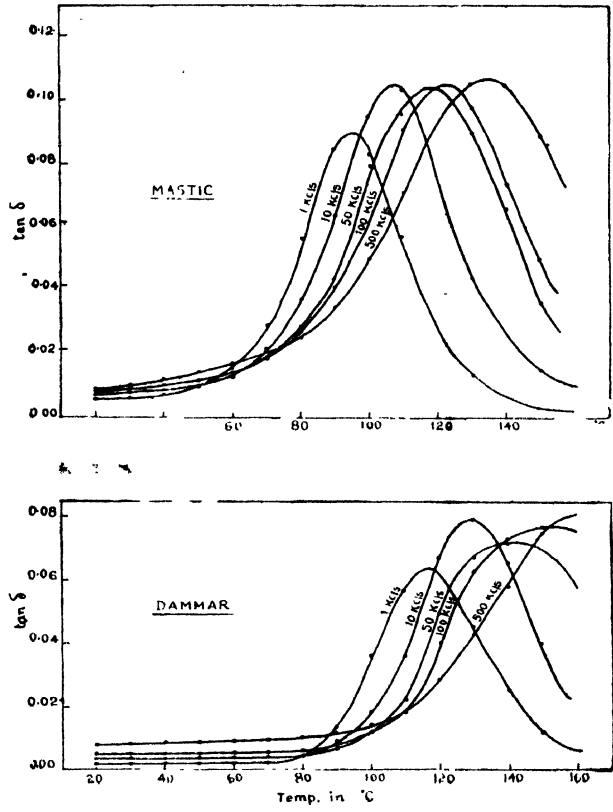


Fig. 2.

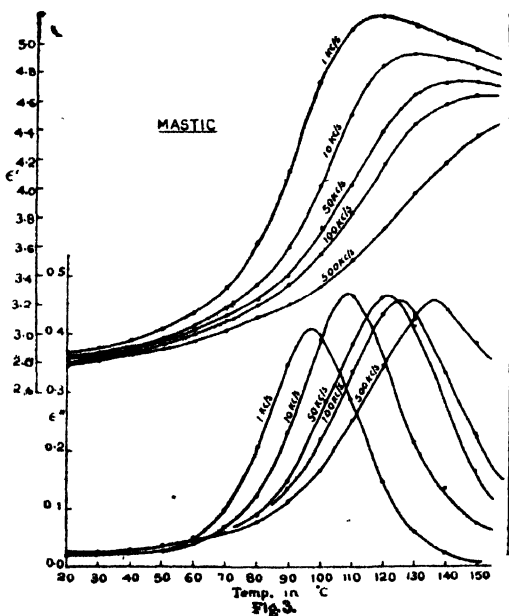


Fig. 3.

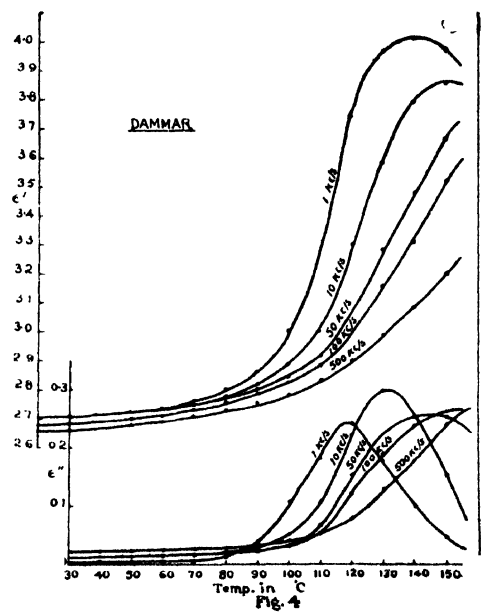


Fig. 4.

with the temperature axis. From the softening point power factor curves begin to rise, the slope of the curves depending on the frequency. For both these resins the temperature range 20°C to 150°C has been used and the frequency range extends from 1 Kc/s to 500 Kc/s. The temperature range was sufficient to bring out the characteristic nature of the curves and it was considered unnecessary to go beyond the higher limit of this range owing to the rapidly increasing d.c. conductance of these resins at high temperatures. The peak of any dielectric loss curve of these resins appears at a temperature at which there is maximum variation of dielectric constant at that frequency. This is in conformity with Debye's theory of polar molecules. The anomalous dispersion for these resins has been shown in figures 5 and 6. There is nothing special to comment on these curves except probably that they provide us with a beautiful and typical set of polar resin curves. Unlike lac which begins to harden at high

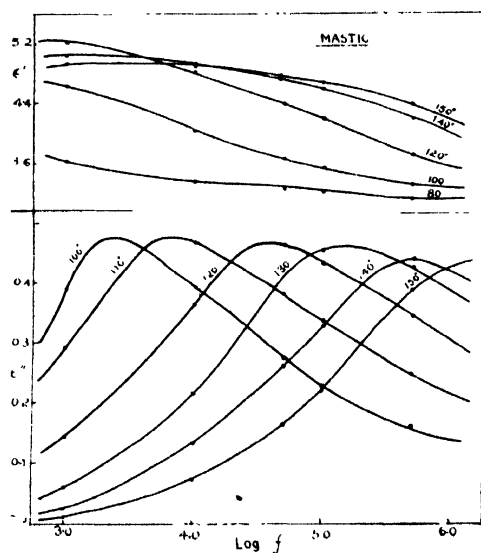


Fig. 5.

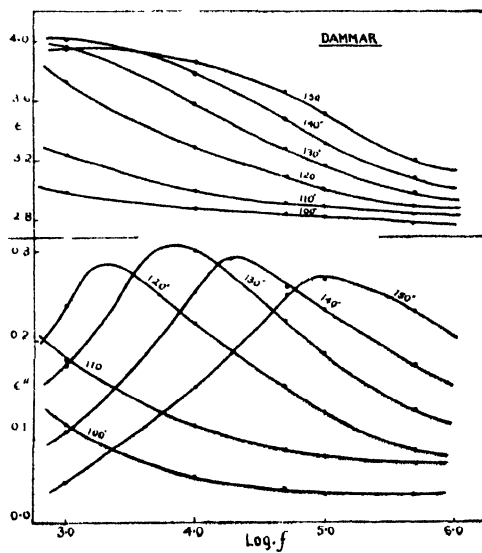


Fig. 6.

temperatures these resins belong to the non-hardening class and that is why it has been possible to obtain such accurate data at various temperatures and frequencies.

Now it should be observed that mastic resin has a higher value of power factor maximum (Fig. 1) at any frequency than the peak of the corresponding dammar resin curve (Fig. 2). Obviously the loss maxima of mastic at different frequencies are also higher (Figs. 3 and 4). For example, the power factor maximum of mastic has a value of about 0.11 for practically all frequencies but 1 Kc/s in which case it is 0.09 only, whereas the corresponding figures for dammar resin are 0.08 and 0.06 approximately. Similarly the figures for loss-maximum of mastic are 0.45 and 0.40 at frequencies other than 1 Kc/s and at 1 Kc/s respectively, whilst the same for dammar resin give 0.30 and 0.25 respectively. The first thing that strikes one for an explanation of this is the lower acid value of dammar compared with mastic resin. According to Glimman (1896) the important constituents of dammar resin consist of an acid

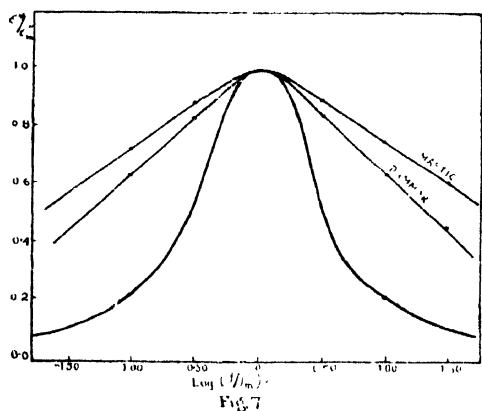
which is called dammarolic acid, $C_{54}H_{77}O_3 (COOH)_2$, and two other resins called α -dammar resin, $C_{11}H_{17}O$ and β -dammar resin, $C_{31}H_{52}O$. The acid is present to the extent of 23% only. In the case of mastic resin the chief constituents are also acids and resins. Tschirch and Reutter (1904) found a Chios mastic sample to contain five acids, *viz.*, α - and β -masticic acids, $C_{23}H_{36}O_4$, masticolic acid, $C_{23}H_{36}O_4$, and α - and β -masticonic acids, $C_{32}H_{48}O_4$, and two resins, *viz.*, α -mastico-resin, $C_{36}H_{66}O_4$, and β -mastico-resin. The acids were 42.5% of the total resin. The resins are unclassifiable, inert, oxygenated organic compounds of which very little is known at present. If these are left out from our consideration for the present, we may see that the number of carboxyls per unit volume are more in mastic resin than in dammar, although dammarolic acid is a dicarboxylic acid. This may perhaps explain the lower maximum of dielectric constant curves or loss curves of dammar resin.

It has already (Bhattacharya, 1944a) been stated that the maximum value of dielectric loss of a pure polar liquid can be represented by

$$\epsilon''_M = \epsilon'_0 - \epsilon'_\infty$$

where ϵ''_M = the maximum value of loss, ϵ'_0 = the static dielectric constant, and ϵ'_∞ = the value of dielectric constant at very high frequencies.

In the case of lac as well as soft lac resin it has been noticed that the actual



loss-maximum falls far short of the theoretical value demanded by the above equation. From this as well as the wide range of anomalous dispersion obtained experimentally for these materials the natural conclusion is that this is the effect of distributed relaxation time in the molecules of these substances. Similar effects of distribution in the relaxation time have been observed in the case of a few synthetic thermoplastic

resins such as, phenol-formaldehyde, cresol-formaldehyde, polyvinyl chloride, polyvinyl chloroacetate, polychlorostyrene, etc. (Fuoss, 1941; Hartshorn, *et al*, 1940). If we examine the loss-maximum values of dammar and mastic resins in the light of the above relation, we shall find that here also they fall far short of the calculated value and in fact the actual loss-maximum of either of them is only about one-third of the theoretical value. The spread of the anomalous dispersion for these resins can be seen from figures 5 and 6. We have reasons to conclude from all these, just as in the case of lac and soft lac resin, that the rotating units have a distributed range of relaxation times. A rough estimate of this distribution may be had, as we have seen previously, from a comparison of the flatness of curves obtained by plotting ϵ''/ϵ''_M against

f/f_m . Figure 7 shows these curves along with the Debye curve for pure polar liquids. It will be seen that the effect of distribution in the relaxation times of rotating units of both these resins is clearly visible from this figure by the bluntness of these curves in comparison to the Debye curve. This distribution however is wider in the case of mastic resin than dammar,—a fact brought out by more flatness of the mastic curve than the dammar one. Actual calculation according to the method of Fuoss and Kirkwood (1941) for the determination of distribution coefficient of relaxation times gives a value of 0.49 for mastic and 0.54 for dammar. It may be recalled that lac gives a value of 0.35 whilst soft lac resin 0.40 and hard lac resin 0.26 for this distribution co-efficient. This means that the distribution of relaxation time around the most probable value is more concentrated for these resins than for the constituents of lac resin. Or, in other words, dammar and mastic resins conform better to the theoretical Debye curve than lac or its constituents.

We can now proceed to calculate the dimensions of the rotating unit for these resins as in previous cases. Making use of the relation $\tau = \xi/2kT$ and Stoke's law $\xi = 8\pi\eta a^3$, we can write as usual

$$\tau = \frac{4\pi\eta a^3}{kT}$$

where τ = relaxation time, ξ = frictional torque, k = Boltzmann constant, T = absolute temperature, η = coefficient of viscosity, and a = radius of the rotator.
 a may be calculated by means of the equation

$$\omega\tau = \frac{e^{\infty} + 2}{e^{\infty} + 1}$$

TABLE V
Viscosity data at different temperatures

Resin	Temperature		1000/T	Viscosity in poise	Log η
	t°C	T°K			
Mastic	90	363	2.755	14670	4.166
	95	368	1.717	5940	3.774
	100	373	2.681	2305	3.362
	110	383	2.611	495	2.694
	120	393	2.545	130	2.114
Dammar	120	393	2.545	24290	4.386
	130	403	2.481	3716	3.570
	140	413	2.421	755	2.878
	150	423	2.364	196	2.292

at the point where the dielectric loss is maximum of any curve showing the variation of loss with temperature at constant frequency. But unless the viscosity coefficient at that temperature is known, the average radius of the rotating units cannot be found out. In order to collect viscosity data of these resins at various temperatures Lee's tar viscometers were employed. Measurements were

made by the usual mercury pressure as detailed in the original paper of Lee (1934). The results give a straight line plot with the reciprocal absolute temperature. This has been shown in figure 9. Measurements could not be pursued below 90°C for mastic and 120°C for dammar, as the viscosity attained a very high value, but there are reasons to believe from the d.c. conductance $-1/T$ graphs (Fig. 8) that a change of state takes place somewhat below these tempera-

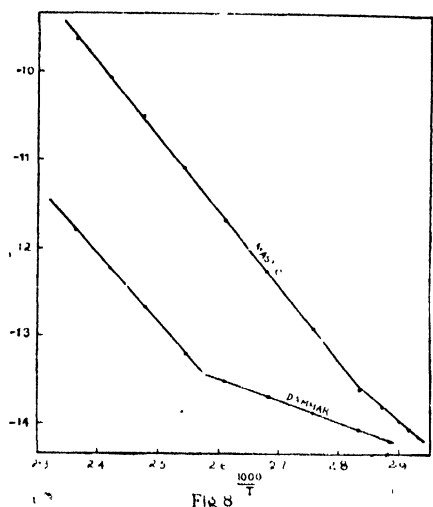


Fig 8

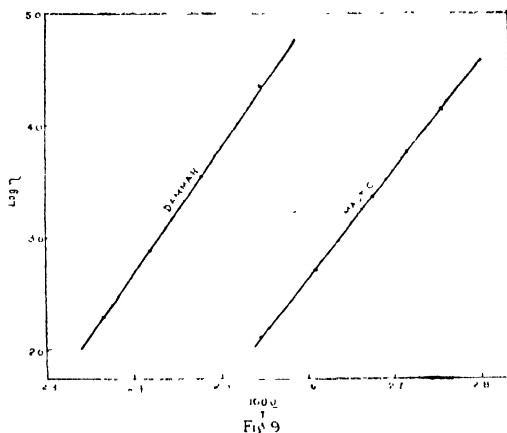


Fig 9

tures. Dammar shows a sharp break in the line near about 113°C in the graph (actually this may not be so sharp as shown and may extend over a few degrees). Similarly mastic has a linear graph till about 80°C when it changes its slope. Readings at lower temperatures than 70°C could not be taken owing to the very low conductivity of the material, but the lower two points clearly show the change of direction of the lower line. Thus the temperature 113°C for dammar or 80°C for mastic may be called 'transformation points' according to Berger (1934). There may however be a 'transformation interval' (Tammann, 1933) near-about these temperatures, but the range definitely is small in such a case as for example in selenium glass. The activation energy Q calculated from the slope of the d.c. conductance $-1/T$ straight line graph of mastic resin gives a value of 39.0 K-cal and 27.7 K-cal above and below 80°C respectively. From the viscosity $-1/T$ graph of the same resin a value of 42.1 K-cal is obtained. This is more or less in agreement with the value 39.0 K-cal obtained from d.c. conductance data above 80°C. But dammar shows slight difference in this respect. The value of Q obtained from d.c. conductance data is 37.0 K-cal whilst from viscosity data it is 46.7 K-cal, thus showing some difference. No comment on this difference can be made here, but we shall make use of the viscosity data obtained experimentally for our calculations of the dimensions of rotating units. High accuracy in the viscosity data is not necessary for this purpose since cube root of viscosity comes in the calculation of the radius of the rotator. The results of such calculations have been included in Table VI. It will be seen that the average radius of the rotator of mastic is about

TABLE VI

Calculated relaxation time and radius of the rotator

Resin	Frequency f	Loss-max temp. t_m	Relaxation time τ	Viscosity in poise η	Radius a
Mastic	1 Kc/s	97°	0.96×10^{-4} sec	4217	4.5×10^{-8} cm.
	10 Kc/s	110°	0.96×10^{-6} "	495	4.3×10^{-8} cm.
	50 Kc/s	122°	1.92×10^{-6} "	89	4.5×10^{-8} cm.
Dammar	1 Kc/s	119°	1.16×10^{-4} sec	25420	2.7×10^{-8} cm.
	10 Kc/s	132°	1.15×10^{-6} "	2985	2.6×10^{-8} cm.
	50 Kc/s	144°	2.32×10^{-6} "	501	2.8×10^{-8} cm.

4.5×10^{-8} cm., whereas dammar has a comparatively smaller rotating unit whose average radius is only 2.7×10^{-8} cm. Actual shape of these rotators may not be spherical, but this figure indicates the radius of the imaginary sphere which has the same volume as the average rotating unit. The constituents of these resins are all organic compounds having large molecules and their dimensions are expected to be bigger than 4.5 \AA or 2.7 \AA . The natural conclusion is that the whole molecule does not take part in the rotation, as we have already seen in the case of lac or lac constituents, but only some polar groups take part in the rotation. The position of these polar groups in the molecule determines their freedom to rotate and hence the extent to which they can contribute towards the polarisation. We see however that these rotators are much bigger in size than those of lac or its constituents.

The relaxation times of rotators of these resins are comparatively high both on account of their bigger size as well as greater inner friction at any particular temperature when compared with lac. For example, dammar rotating unit has an average relaxation time of 1.1×10^{-4} second at 120°C whereas at the same temperature mastic rotator has the value of 2.0×10^{-6} second and lac 1.5×10^{-8} second. The higher inner friction is generally the result of inter-molecular forces. If this factor can be reduced to a negligible figure, as for example in very dilute solutions of such a resin in a non-polar solvent, the relaxation time will give an idea of the size of rotating units from another side. An attempt will be made therefore to make such a study of very dilute solutions of some of these resins, and the result will be reported in another communication.

ACKNOWLEDGMENT

The author is indebted to Dr. H. K. Sen, Director of this Institute, for his kind interest in this work.

REFERENCES

- Berger, E., 1934, *Z. Tech. Physik.*, **15**, 443
Bhattacharya, G. N., 1944, (a) *Ind. J. Phys.*, **18**, 1; (b) *ibid.*, **18**, 97; (c) *ibid.*, **18**, 116.
Fuoss, R. M., 1941, *J. Amer. Chem. Soc.*, **63**, 369.
Fuoss, R. M., and Kirkwood, J. G., 1941, *J. Amer. Chem. Soc.*, **63**, 385.
Glimmann, G., 1896, *Archiv. Pharm.*, **234**, 584.
Hartshorn, L., Megson, N. J. and Rushton, E., 1940, *J. Soc. Chem. Ind.*, **59**, 129T.
Lee, A. R., 1934, *J. Soc. Chem. Ind.*, **53**, 69T.
Tammann, G., 1933, *Der Glaszustand*, 40.
Tschirch, A., and Reutter, L., 1904, *Archiv. Pharm.*, **242**, 104.

NON-COULOMB CENTRAL FIELD FOR POTASSIUM ATOM

By JATINDER NATH NANDA

ABSTRACT. The potential field for KII is obtained. Out of the four methods described it is shown that for calculation of line intensities or term values of the atomic spectrum, empirical field obtained from Prokofjew method is the best. For heavy atoms a simple method based on Fermi statistical field is given, where the field for the neutral atom is altered due to the removal of the optical electron.

To calculate line intensities, etc., of potassium atom from the Schrodinger equation, a potential function known at every point is required. Hartree's (1934), self-consistent field is available, but apart from the huge labour involved in such computation, Hartree (1927-28) has pointed out that the self-consistent field can be used best only when charge distribution is required explicitly, *e.g.*, in X-Ray scattering work. For calculation of line intensities some other empirical potential field is to be used. In the elucidation of atomic spectra the field required is the one acting on the outermost optical electron due to the rest of the atom, *i.e.*, the ion.* Fermi and Thomas have given a field for a heavy neutral atom from statistical considerations. The field due to the ion can be deduced from that of the neutral atom as will be shown below.

Fermi (1928), and Condon and Shortly (1935), have shown that for a fairly continuous charge distribution due to electrons in a heavy atom (Z), potential field V is obtained from :

$$\nabla^2 V = 4\pi e \cdot \frac{8\pi}{3h^3} (2mc)V^{\frac{3}{2}}.$$

Put

$$V = \frac{Ze}{r} \chi(r), \text{ and } r = xb,$$

where

$$b = \frac{1}{2} \left(\frac{3\pi}{4} \right)^{\frac{2}{3}} \frac{a}{Z^{\frac{1}{3}}}$$

and a is the Bohr radius, and other constants are obvious.

The equation reduces to

$$x^{\frac{1}{2}} \frac{d^2 \chi}{dx^2} = \chi^{\frac{3}{2}}$$

which has been solved mechanically, by Bush and Caldwell (1931), for neutral atoms, *i.e.*, under the boundary conditions $\chi=1$ and 0, at $\rho=0$ and ∞ respectively. From tables given by them, Z (effective) $= \chi Z$ can be calculated for any neutral atom (Z). To get the field for the ion, the method employed by Fermi (1928), was to get the statistical field for the neutral atom of atomic number ($Z-1$), and to impose upon it the field due to an additional proton at the centre.

* Strictly speaking the field required in any calculation will be the one obtained after a disturbance has been imposed upon the true ion field by the optical electron. Field II and III out of the four are most appropriate in this respect.

Thus for ion of atom Z , the Z_{eff} at distance r is give by $(Z-1)\chi(r) + 1$. But this added proton sensibly closes up the distribution of the electrons. Best way appears to be to subtract the contribution of the outermost negative electron from the Z_{eff} of neutral atom. Any departure of the field obtained in this way from the true ionic field, as given by Baker (1930), will in fact represent to a close approximation the disturbance of that field by the optical electron for any particular calculation. This electron subtraction method is explained below with potassium as an example.

From the statistical calculation of Fermi the number of electrons per c.c., in a field given by $Z_{\text{eff}} = \chi Z$ in heavy neutral atom, is

$$n = \frac{8\pi}{3h^3} \left(2mc \frac{\chi Z c}{r} \right)^{\frac{3}{2}}$$

Number of electrons in a shell of thickness dr of radius r is

$$4\pi r^2 \frac{8\pi}{3h^3} (2mc^2 \chi Z / r)^{\frac{3}{2}} dr.$$

Putting $r = \rho a$, we have number of electrons in a shell extending from ρ_1 to ρ_2 as

$$\int_{\rho_1}^{\rho_2} (2mc^2 \chi Z / \rho a)^{\frac{3}{2}} (8\pi / 3h^3) 4\pi \rho^2 a^3 d\rho$$

which integral reduces to Z if limits are from 0 to ∞ , as it should. Substituting for the constants the integral becomes

$$1.195 \int_{\rho_1}^{\rho_2} (\chi Z)^{\frac{3}{2}} \rho^{\frac{1}{2}} d\rho.$$

Now, by drawing a graph between $(\chi Z)^{\frac{3}{2}} \rho^{\frac{1}{2}}$ and ρ , one can find the region which contains the outermost electron. Thus, from the relation

$$1.195 \int_{\rho_{\text{ion}}}^{\rho_{\infty}} (\chi Z)^{\frac{3}{2}} \rho^{\frac{1}{2}} d\rho = 1$$

and integrating graphically (at very large ρ asymptotic $\chi Z = c^k \rho$ can be used) the radius ρ_{ion} can be determined. For potassium atom $\rho_{\text{ion}} = 3.78$, removal of this negative charge means that we must add to the previous χZ the magnitude of its effect. Knowing that potential inside a charged spherical shell of radius R and charge Q is equal to Q/R , we have for all points at $\rho < \rho_{\text{ion}}$, contribution towards potential as

$$\int_{\rho_{\text{ion}}}^{\rho=\infty} \frac{dc}{\rho a} = \frac{1.195c}{a} \int_{\rho_{\text{ion}}}^{\rho_{\infty}} \frac{(\chi Z)^{\frac{3}{2}} \rho^{\frac{1}{2}}}{\rho} d\rho$$

and since $V(\rho) = \frac{e}{\rho a} \cdot Z_{\text{eff}}$, contribution towards Z_{eff} for all points at $\rho < \rho_{\text{ion}}$ is,

$$1.195 \rho \int_{\rho_{\text{ion}}}^{\rho_{\infty}} \frac{(\chi Z)^{\frac{3}{2}}}{\rho^{\frac{1}{2}}} d\rho = \frac{\rho}{\rho a}$$

From graphical integration, $\rho_a = 5.424$ for potassium atom. For points at $\rho > \rho_{\text{ion}}$, contribution towards Z_{eff} is made of two parts, (i) due to charge lying

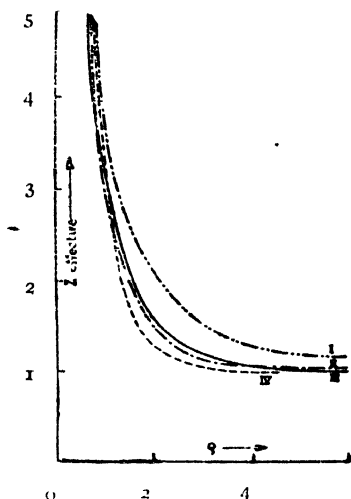
beyond ρ , and (ii) due to charge lying between ρ_{ion} and ρ which can be supposed to be placed at the centre. These are therefore

$$\rho \times 1.195 \int_{\rho}^{\rho_{\infty}} (\chi Z)^{\frac{3}{2}} \frac{1}{\rho^{\frac{1}{2}}} d\rho, \text{ and } 1.195 \int_{\rho_{\text{ion}}}^{\rho} (\chi Z)^{\frac{3}{2}} \rho^{\frac{1}{2}} d\rho$$

Thus the required field is given by

$$\text{For } \rho < \rho_{\text{ion}}; \quad Z_{\text{eff}} = \chi Z + \frac{\rho}{\rho_a}.$$

$$\text{For } \rho > \rho_{\text{ion}}; \quad Z_{\text{eff}} = \chi Z + 1.195 \rho \int_{\rho}^{\rho_{\infty}} (\chi Z)^{\frac{3}{2}} \frac{1}{\rho^{\frac{1}{2}}} d\rho + 1.195 \int_{\rho_{\text{ion}}}^{\rho} (\chi Z)^{\frac{3}{2}} \rho^{\frac{1}{2}} d\rho.$$



- I. Statistical Proton addition
- II. Statistical Electron Subtraction.
- III. Empirical Prokofjew method.
- IV. Hartree Self-consistent method.

The results are given in the accompanying graph and Table II.

The statistical method being applicable only to heavy atoms, another method using experimentally observed term values of the neutral atom has been given by Sugiura (1927), and Prokofjew (1929) based upon simple Bohr-Sommerfeld theory. A useful form of the quantum condition obtained by Kramers is

$$n - k = \frac{\sqrt{2}}{\pi} \int_{\rho_{\min}}^{\rho_{\max}} \sqrt{-\frac{1}{2} \frac{v}{R} \rho^2 - \frac{1}{2} k^2 + Q(\rho)} \frac{d\rho}{\rho}$$

where

$$Q = \rho Z_{\text{eff}}, \quad \text{and} \quad \rho =$$

ρ_{\max} and ρ_{\min} are the boundaries of the N_k orbit and are in fact the limits in which the integral has a sense. ρ_{\max} and ρ_{\min} are the roots of the expression under the square root when equated to zero. Sugiura and Prokofjew calculated the field function Q for sodium atom employing the Brillouin-Kramers approximation, viz., that of replacing k by $k - \frac{1}{2}$. Prokofjew following an algebraic method got different expressions for Q in different regions. For each term the integration was carried out portion by portion in the region where it was valid, ρ_{\max} and ρ_{\min} being the higher root and the lower root respectively of corresponding equations. The algebraic method of Prokofjew is more sensitive and gives the results in a more useful form than the graphical method of Sugiura.

Hartree (*loc. cit.*) has shown that as far as we can picture an orbit corresponding to a given solution of the wave equation its angular momentum is defined by $\sqrt{l(l+1)}$ in place of k . Thus the quantum condition becomes

$$n - \sqrt{l(l+1)} = \frac{\sqrt{2}}{\pi} \int_{\rho_{\min}}^{\rho_{\max}} \sqrt{-\frac{1}{2} \frac{v}{R} \rho^2 - \frac{1}{2} l(l+1) + Q} \frac{d\rho}{\rho} \quad \dots (1)$$

As an example the field Q for potassium has been obtained below. Table I gives v/R against various N_K values. Orbits marked * were actually used in the evaluation of the field in the order shown :

TABLE I

N_K	v/R	N_K	v/R	N_K	v/R	N_K	v/R
4.* ₁	265.6	43	.06933	63	.03015	83	.01666
2 ₁	—	44	.06277	64	.02786	1.* ₈₄	.01563
5.* ₂₂	21.73	51	.1274	71	.04313	91	.02149
3 ₁	—	52	.09385	72	.03505	92	.01882
6.* ₃₂	1.254	53	.04393	73	.02193	93	.01306
3.* ₃₃	1.230	54	.04014	74	.02045	101	.01633
4 ₁	.319	61	.06883	81	.02952	102	.01455
4 ₂	.2005	62	.05471	82	.02533	2.* ₁₀₃	.01053

Field Q is given below against ρ . As this field is based upon actual experimental results, it is the factual field and requires no extra corrections :

Orbit used.	ρ	Q
1	∞ to 6.31	ρ
2	6.31 to 1.90	0.068 $\rho^2 + .1418 \rho + 2.708$
3	1.90 to 1.106	0.1595 $\rho^2 - .2078 \rho + 3.0406$
6	1.106 to .5111	0.6059 $\rho^2 - 1.1942 \rho + 3.586$
6	.5111 to .4412	-10.0 $\rho^2 + 9.647 \rho + .806$
5	.4412 to .1053	-12.1 $\rho^2 + 11.593 \rho + .3951$
4	.1053 to 0.0	-47.7 $\rho^2 + 19.00 \rho$

Test for such work is to see if equation I is satisfied for any term not already used in the evaluation of Q . Taking the term 10₂ we have L.H.S.=8.59 and computed R.H.S.=8.60, the integral having a sense from $\rho=.0624$ to $\rho=136.46$, i.e., using up all the seven expressions which shows that method has not gone wrong anywhere.

The soft X-ray levels 2₁ and 3₁ which have not been experimentally determined are foretold by this field to be 26.41 and 2.72 respectively. Hartree's corresponding values are 26.68 and 3.084. Bearing in mind that the polarization corrections to be applied to Hartree values are negative, these results appear to be correct.

CONCLUSION

For calculation of line intensities, etc., empirical fields based upon experimental observation are best. The empirical method given by Prokofjew followed here for potassium is better than those given by Sugiura and others. For heavy atoms this field can be easily obtained by the electron subtraction method from

Fermi-Thomas statistical field for neutral atoms. Z_{eff} for potassium is tabulated against ρ in Table II from different methods.

TABLE II

ρ	$Z_{\text{effective}}$			
	I. Proton addition.	II. Electron subtraction	III. Prokofjew.	IV. Self-consistent
0.0	19.0	19.0	19.0	19.0
0.02	18.1	17.9	18.046	17.576
0.04	17.2	16.9	17.092	16.346
0.06	16.4	16.2	16.138	15.316
0.08	15.5	15.0	15.184	14.433
0.1	14.5	14.0	14.230	13.652
0.2	11.2	11.0	11.039	10.564
0.3	9.2	8.8	9.190	8.444
0.4	7.8	7.3	7.651	7.054
0.5	6.7	6.2	6.259	6.094
0.6	5.8	5.3	5.147	5.353
0.7	5.2	4.5	4.353	4.722
0.8	4.7	4.0	3.773	4.162
0.9	4.2	3.5	3.326	3.660
1.0	3.9	3.1	2.998	3.218
1.2	3.3	2.6	2.517	2.504
1.4	2.8	2.2	2.188	1.997
1.6	2.5	1.9	1.947	1.650
1.8	2.3	1.7	1.769	1.420
2.0	2.1	1.5	1.628	1.270
3.0	1.5	1.13	1.248	1.028
4.0	1.3	1.07	1.091	1.002
5.0	1.2	1.05	1.023	1.000
6.0	1.15	1.04	1.001	"
7.0	1.10	1.03	1.000	"
8.0	1.05	1.02	"	"
9.0	1.02	1.01	"	"
10.0	1.02	1.0	"	"

In the end, I wish to thank Dr. P. K. Kichlu, of the Government College, Lahore, for constant encouragement afforded to me and for his valuable suggestions. My thanks are also due to Professor D. S. Kothari of the Delhi University for looking over the manuscript and to Dr. A. M. Mian of the Punjab University for help in solving definite integrals connected with Prokofjew field.

PHYSICS LABORATORY,
GOVERNMENT COLLEGE,
LAHORE.

REFERENCES

- Baker, 1930, *Phys. Rev.*, **36**, 630.
 Bush and Caldwell, 1931, *Phys. Rev.*, **38**, 1808.
 Condon and Shortly, 1935, *Theory of Atomic Spectra*, p. 336.
 Fermi, 1928, *Zett. f. Phys.*, **48**, 73.
 " 1928, " " " **49**, 550.
 Hartree, 1927-28, *Proc. Camb. Phil. Soc.*, **24**, 111.
 " 1934, *Proc. Roy. Soc.*, **143**, 506.
 Prokofjew, 1929, *Zett. f. Phys.*, **58**, 255.
 Sugiura, 1927, *Phil. Mag.*, **4**, 495.

PIEZO-ELECTRIC CONSTANTS OF CRYSTALS— GROUP-THEORETICAL TREATMENT

BY BISHAMBHAR DAYAL SAKSENA

ABSTRACT. The number of piezo-electric moduli and the relations between them have been obtained by using group-theoretical method. The results are in agreement with those given by Voigt.

INTRODUCTION

Some crystals develop an electric moment when they are subjected to mechanical stress. Such crystals are said to be piezo-electric. The components of stress t_{ik} or of strain r_{kz} are related to the components of electric moment p_i by relations of the type

$$p_i = q_{kzi} t_{kz} \text{ and } p_i = c_{kzi} r_{kz}$$

q_{kzi} and c_{kzi} are called piezo-electric moduli and piezo-electric constants respectively. There are 18 such constants and their number reduces to one for crystals of the cubic class and some crystals of the tetragonal and hexagonal classes. The relations for all the crystallographic point-groups were investigated by Voigt and a summary of this work in English is given by Wooster (1938). The derivation of these relations as usually given is rather complicated and it is therefore proposed to give here an easy method, based on the theory of groups, for obtaining the number of piezo-electric constants and their relations for all classes of crystal symmetry.

METHOD

The components of stress and of strain are second order tensors and therefore q_{kzi} and c_{kzi} are third order tensors. Second order tensors are given by nine coefficients which reduce to six in symmetric tensors on account of the relation $c_{rs} = c_{sr}$. The components of stress (also of strain) are given by six components $t_{xx}, t_{yy}, t_{zz}, t_{xy} = t_{yx}, t_{yz} = t_{zy}, t_{xz} = t_{zx}$. Under an operation $R\phi$ consisting of a rotation through ϕ or a rotation reflection through ϕ , these coefficients transform as products of cartesian co-ordinates. The following relations show the transformation of cartesian co-ordinates and tensor components by a rotation about an axis of symmetry (z axis).

$$\left. \begin{aligned} x &\rightarrow x \cos \phi + y \sin \phi; & y &\rightarrow -x \sin \phi + y \cos \phi; \text{ and } \\ z &\rightarrow \pm z \text{ (negative sign refers to rotation reflection)} \end{aligned} \right\} \dots \quad (1)$$

$$R(t_{xx}) \rightarrow t_{xx} \cos^2 \phi + t_{yy} \sin^2 \phi + 2t_{xy} \sin \phi \cos \phi$$

$$R(t_{yy}) \rightarrow t_{xx} \sin^2 \phi + t_{yy} \cos^2 \phi - 2t_{xy} \sin \phi \cos \phi$$

$$R(t_{zz}) \rightarrow t_{zz}$$

$$R(t_{xy}) \rightarrow -t_{xz} \cos \phi \sin \phi + t_{yz} \cos \phi \sin \phi + t_{xy} (\cos^2 \phi - \sin^2 \phi) \left. \vphantom{\begin{aligned} R(t_{xx}) \\ R(t_{yy}) \\ R(t_{zz}) \end{aligned}} \right\}$$

$$R(t_{yz}) \rightarrow \pm t_{yz} \cos \phi \mp t_{xz} \sin \phi \left. \vphantom{\begin{aligned} R(t_{xx}) \\ R(t_{yy}) \\ R(t_{zz}) \end{aligned}} \right\} \text{the lower sign refers to}$$

$$R(t_{xz}) \rightarrow \pm t_{yz} \sin \phi \pm t_{xz} \cos \phi \left. \vphantom{\begin{aligned} R(t_{xx}) \\ R(t_{yy}) \\ R(t_{zz}) \end{aligned}} \right\} \text{rotation-reflection.}$$

The piezo-electric moduli q_{kzi} (or the constants c_{kzi}) which connect the components of stress tensor (or the strain tensor) with the components of the electric

moment vector will be 18 in number and may be written as

$$\begin{array}{cccccccc}
 q_{xxx} & q_{yyx} & q_{zzx} & q_{yxx} & q_{xzx} & q_{xyx} & \text{or} & q_{11} & q_{21} & q_{31} & q_{41} & q_{51} & q_{61} \\
 q_{xxy} & q_{yyy} & q_{zzy} & q_{yyz} & q_{xzy} & q_{xyy} & & q_{12} & q_{22} & q_{32} & q_{42} & q_{52} & q_{62} \\
 q_{xxz} & q_{yyz} & q_{zzz} & q_{yzz} & q_{xzz} & q_{xyz} & & q_{13} & q_{23} & q_{33} & q_{43} & q_{53} & q_{63}
 \end{array}$$

if we write as

xx	yy	zz	yz	xz	xy	x
1	2	3	4	5	6	1
						3

The transformation matrix for various q_{lzt} can be easily written down with the help of the transformations (2) and (1)

$$\begin{aligned}
 R(q_{xxx}) &\rightarrow q_{xxx} \cos^3 \phi + q_{yyx} \cos \phi \sin^2 \phi + 2q_{xxy} \sin \phi \cos^2 \phi \\
 &\quad + q_{xxz} \cos^2 \phi \sin \phi + q_{yyz} \sin^3 \phi + 2q_{xyz} \sin^2 \phi \cos \phi \\
 R(q_{yyx}) &\rightarrow q_{xxy} \cos \phi \sin^2 \phi + q_{yyx} \cos^3 \phi - 2q_{xzy} \sin \phi \cos^2 \phi \\
 &\quad + q_{xxy} \sin^3 \phi + q_{yyz} \cos^2 \phi \sin \phi - 2q_{xyz} \sin^2 \phi \cos \phi \\
 R(q_{xxy}) &\rightarrow -q_{xxy} \sin \phi \cos^2 \phi + q_{yyx} [\sin \phi \cos^2 \phi + q_{xyx} \cos 2\phi \cos \phi \\
 &\quad - q_{xxy} \sin^2 \phi \cos \phi + q_{yyz} \sin^2 \phi \cos \phi + q_{xyz} \cos 2\phi \sin \phi \\
 R(q_{xzy}) &\rightarrow -q_{xzy} \sin \phi \cos^2 \phi - q_{yyz} \sin^3 \phi - 2q_{xyx} \sin^2 \phi \cos \phi \\
 &\quad + q_{xzy} \cos^3 \phi + q_{yyz} \sin^2 \phi \cos \phi + q_{xyz} 2 \cos^2 \phi \sin \phi \\
 R(q_{yyz}) &\rightarrow -q_{xzy} \sin^3 \phi - q_{yyz} \cos^2 \phi \sin \phi + 2q_{xyx} \sin^2 \phi \cos \phi \\
 &\quad + q_{xzy} \cos \phi \sin^2 \phi + q_{yyz} \cos^3 \phi - q_{xyz} 2 \sin \phi \cos^2 \phi \\
 R(q_{xzz}) &\rightarrow q_{xxx} \sin^2 \phi \cos \phi - q_{yyz} \sin^2 \phi \cos \phi - q_{xxy} \cos 2\phi \sin \phi \\
 &\quad - q_{xxy} \sin \phi \cos^2 \phi + q_{yyz} \sin \phi \cos^2 \phi + q_{xyz} \cos 2\phi \cos \phi
 \end{aligned} \tag{3a}$$

$$\begin{aligned}
 R(q_{yyx}) &= \pm q_{yyx} \cos^2 \phi \pm q_{yyz} \cos \phi \sin \phi \mp q_{xzx} \sin \phi \cos \phi \mp q_{xzy} \sin^2 \phi \\
 R(q_{xyx}) &= \mp q_{xyx} \cos \phi \sin \phi \pm q_{xzy} \cos^2 \phi \pm q_{xzx} \sin^2 \phi \mp q_{xzy} \sin \phi \cos \phi \\
 R(q_{xzx}) &= \pm q_{xzy} \cos \phi \sin \phi \pm q_{xyx} \sin^2 \phi \pm q_{xzx} \cos^2 \phi \pm q_{xzy} \sin \phi \cos \phi \\
 R(q_{xzy}) &= \mp q_{xzy} \sin^2 \phi \pm q_{xyx} \sin \phi \cos \phi \mp q_{xzx} \sin \phi \cos \phi \pm q_{xzy} \cos^2 \phi
 \end{aligned} \tag{3b}$$

$$\begin{aligned}
 R(q_{xzx}) &= \pm q_{xzx} \cos^2 \phi \pm q_{yyz} \sin^2 \phi \pm q_{xyx} 2 \sin \phi \cos \phi \\
 R(q_{yyz}) &= \pm q_{xzx} \sin^2 \phi \pm q_{yyz} \cos^2 \phi \mp q_{xyx} 2 \sin \phi \cos \phi \\
 R(q_{xyz}) &\rightarrow \mp q_{xzx} \sin \phi \cos \phi \pm q_{yyz} \sin \phi \cos \phi \pm q_{xyx} \cos 2\phi
 \end{aligned} \tag{3c}$$

$$\begin{aligned}
 R(q_{yyx}) &\rightarrow q_{yyx} \cos \phi - q_{xzx} \sin \phi \} \\
 R(q_{xzx}) &\rightarrow q_{yyx} \sin \phi + q_{xzx} \cos \phi \} \quad \dots \tag{3d}
 \end{aligned}$$

$$R(q_{xxx}) \rightarrow \pm q_{xxx} \quad \dots \tag{3e}$$

$$\begin{aligned}
 R(q_{xxx}) &\rightarrow q_{xxx} \cos \phi + q_{xxy} \sin \phi \} \\
 R(q_{xxy}) &\rightarrow -q_{xxx} \sin \phi + q_{xxy} \cos \phi \} \quad \dots \tag{3f}
 \end{aligned}$$

The character of the transformation matrix in (3) is given by $8 \cos^3 \phi \pm 8 \cos^2 \phi + 2 \cos \phi$ (+ or - sign to be taken according as the operation is a pure rotation or rotation-reflection).

The linear substitutions in (3) constitute a reducible representation of group G. The 18 mutually orthogonal and independent linear combinations in (3) can be divided into six sets (3a), (3b), (3c), (3d), (3e), (3f)—the members in each set transform among themselves for every operation of the group G. These will form the basis of a new and completely reducible representation of the group G and the character $R\phi$ in this representation is the same as before as the two are equivalent. The number of times n_i , a particular irreducible representation, repeats itself in the representation Γ of the new variables is given by (Wigner,

1931; Bhagavantam) $n_i = \frac{1}{N} \sum_j h_j \chi_i(R) \chi'_j(R)$ where $\chi_i(R)$ is the character of the irreducible representation, $\chi'_j(R)$ the character of Γ' which is the same as that of the transformation matrix (3), h_j the number of elements in the j^{th} class of the point-group and N the order of the group. Since we want to know the number of combinations that remain invariant for all operations of group G we find n_i corresponding to the totally symmetric irreducible representation. Hence

$$\chi_i(R) = 1 \text{ and } n_i = \frac{1}{N} \sum_j h_j \chi'_j(R) \quad \dots (4)$$

where $\chi'_j(R) = 8 \cos^3 \phi \pm 8 \cos^2 \phi + 2 \cos \phi$, (the lower negative sign to be taken for rotation-reflection axes). This result gives the number of piezo-electric moduli for any given point-group as these moduli remain invariant for all operations of the group.

For the totally symmetric irreducible representation $R(q_{xy}) = q_{xy}$, and so we get 18 equations from (3a), (3b), etc., which enable us to find the relations between the various piezo-electric moduli. This gives yet another method of finding the number of piezo-electric moduli for any point-group. The vanishing piezo-coefficients for various symmetry operations are given below.

(1) z -axis as the axis of two-fold symmetry.

$$q_{xxz} = q_{xzy} = q_{yyz} = q_{yyx} = q_{zzx} = q_{zxy} = q_{yzz} = q_{yxx} = q_{zyx} = q_{zyy} = 0$$

These relations can be obtained from (3) by putting $\phi = \pi$ or directly. A symmetry about z -axis implies that for every point x, y, z there is another $-x, -y, z$. As the tensor components transform as products of cartesian co-ordinates $R(q_{xxz}) \rightarrow -q_{xxz}$, but as $R(q_{zzx}) \rightarrow q_{zzx}$, for the totally symmetric representation $q_{xxz} = -q_{xxz} = 0$.

(2) x -axis as the axis of two-fold symmetry

$$q_{xxy} = q_{xxz} = q_{yyy} = q_{yyx} = q_{xzy} = q_{xzx} = q_{yyz} = q_{yyx} = q_{zyx} = q_{zyy} = 0$$

(3) y -axis as the axis of two-fold symmetry

$$q_{xxz} = q_{xxz} = q_{yyz} = q_{yyx} = q_{xzy} = q_{xzx} = q_{yyz} = q_{yyx} = q_{zyx} = q_{zyy} = 0$$

(4) σ_z (plane perpendicular to z -axis) as plane of symmetry. A reflection in a plane is equivalent to a rotation reflection of 360° . Also the symmetry signifies that for every point x, y, z there is a point $x, y, -z$. Therefore by putting $\phi = 2\pi$ in (3) or directly as above

$$q_{xxz} = q_{yyz} = q_{zzx} = q_{yxx} = q_{yzy} = q_{zxx} = q_{zyx} = q_{zyy} = 0$$

(5) σ_y (plane perpendicular to y -axis) as plane of symmetry

$$q_{xxy} = q_{yyy} = q_{xzy} = q_{yxx} = q_{yzz} = q_{xzy} = q_{yxx} = q_{yzz} = 0$$

(6) σ_x as plane of symmetry

$$q_{xxz} = q_{yyz} = q_{xxz} = q_{yyz} = q_{xzy} = q_{yxx} = q_{yzy} = q_{xzy} = 0$$

(7) z -axis as the four-fold axis of rotation (C_4) and of rotation reflection (S_4)

Substituting $\phi = \pi/2$ in (3) we get from (3a)

$$q_{xxy} = q_{yyx}, q_{xxz} = q_{yyz}, q_{xzy} = q_{yxx}$$

$$q_{xxy} = -q_{yyx}, q_{xxz} = -q_{yyz}, q_{xzy} = -q_{yxx}$$

$\therefore q_{xxy} = q_{yyx} = 0, q_{xxz} = q_{yyz} = 0, q_{xzy} = q_{yxx} = 0$. Also from (3b) and (3f)

$q_{yyz} = q_{xxz} = 0, q_{xxz} = q_{yyz} = 0$. From (3b) and (3c),

$$q_{yxx} = \mp q_{xxy}, q_{yzy} = \pm q_{xxz}, q_{yyz} = \pm q_{xxz}, q_{zyx} = \mp q_{xxy}, q_{zzx} = \pm q_{xxz}$$

TABLE I

System	Point group	Symmetry elements	No. of piezo-electric coeff.	Non-vanishing piezo-electric coefficients and their inter-relations
Tri-clinic Mono-clinic	C_1	E	18	All coefficients
	C_2	E, i	0	
	C_2	E, σ_v	10	
Ortho-rhombic	C_2	E, C_2	8	$q_{11}, q_{12}, q_{21}, q_{22}, q_{31}, q_{32},$ $q_{43}, q_{53}, q_{61}, q_{62}$
	C_{2h}	E, C_2, i, σ_v	0	$q_{13}, q_{23}, q_{33}, q_{42}, q_{51},$ q_{52}, q_{63}
	C_{2v}	$E, C_2, \sigma_v, \sigma_v'$	5	$q_{13}, q_{23}, q_{33}, q_{42}, q_{51}$
	D_2	E, C_2, C_2', C_2''	3	q_{41}, q_{52}, q_{63}
	D_{2h}	$E, C_2, C_2', C_2'', i, \sigma_v, \sigma_v', \sigma_v''$	0	
Tetragonal	C_4	$E, 2 C_4, C_2$	4	$q_{13} - q_{23}, q_{33}, q_{41} = -q_{52},$ $q_{42} = q_{51}$
	S_4	$E, 2S_4, C_2$	4	$q_{13} = -q_{23}, q_{41} = q_{52},$ $q_{42} = -q_{51}, q_{63}$
	C_{4h}	$E, 2C_4, C_2, i, 2S_4, \sigma_v$	0	
	C_{4v}	$E, 2C_4, C_2, 2\sigma_v, 2\sigma_v' (\sigma_v, \sigma_v')$	3	$q_{13} = q_{23}, q_{33}, q_{42} = q_{51}$
	D_{2d}	$E, C_2, C_2', C_2'', \sigma_v, 2S_4, \sigma_v'$	2	$q_{13} = -q_{23}, q_{42} = -q_{51}$
Hexagonal	D_4	$E, 2C_4, C_2, 2C_2', 2C_2'' (C_2', C_2'')$	1	$q_{41} = -q_{52}$
	D_{4h}	$E, 2C_4, C_2, 2C_2', 2C_2'', i, 2S_4, \sigma_v, 2\sigma_v', 2\sigma_v''$	0	
	C_3	$E, 2C_3$	6	$q_{11} = -q_{21} = -q_{62},$ $q_{22} = -q_{12} = -q_{61}, q_{13} = q_{23},$ $q_{33}, q_{41} = -q_{52}, q_{42} = q_{51}$
	S_6	$E, 2C_3, i, 2S_6$	0	
	C_{3v}	$E, 2C_3, 3\sigma_v (\sigma_v \text{ or } \sigma_v')$	4	$q_{22} = -q_{12} = -q_{61}, q_{33},$ $q_{13} = q_{23}, q_{11} = q_{51} \text{ for } \sigma_v;$ $q_{11} = -q_{21} = -q_{62}, q_{33},$ $q_{13} = q_{23}, q_{42} = q_{51} \text{ for } \sigma_v'$
	D_3	$E, 2C_3, 3C_2 (C_2' \text{ or } C_2'')$	2	$q_{11} = -q_{21} = -q_{62},$ $q_{41} = -q_{52} \text{ for } C_2', q_{22} = -q_{12}$ $= -q_{61}, q_{41} = -q_{52} \text{ for } C_2''$
	D_{3d}	$E, 2C_3, 3C_2, i, 2S_6, 3\sigma_v$	0	
	C_{3h}	$E, 2C_3, \sigma_h, 2S_6$	2	$q_{11} = -q_{21} = -q_{62},$ $q_{22} = -q_{12} = -q_{61}$
	C_6	$E, 2C_6, 2C_3, C_2$	4	$q_{13} = q_{23}; q_{33}, q_{41} = -q_{52},$ $q_{42} = q_{51}$
	C_{6h}	$E, 2C_6, 2C_3, C_2, i, 2S_6, 2C_3, \sigma_h, 3\sigma_v$	0	
	D_{3h}	$E, 2C_3, 3C_2, \sigma_h, 2S_6, 3\sigma_v [3\sigma_v']$	1	$q_{11} = -q_{21} = -q_{62} \text{ for } C_2'$ and $q_{22} = -q_{12} = -q_{61}$ for C_2''
	C_{6v}	$E, 2C_6, 2C_3, C_2, 3\sigma_v, 3\sigma_v'$	3	$q_{13} - q_{23}, q_{33}, q_{42} = q_{51}$
	D_6	$E, 2C_6, 2C_3, C_2, 3C_2, 3C_2', 3C_2'', 2S_6, \sigma_h, 3\sigma_v, 3\sigma_v'$	1	$q_{41} = -q_{52}$
Cubic	D_{6h}	$E, 2C_6, 2C_3, C_2, 3C_2, 3C_2', i, 2S_6, 2S_6, \sigma_h, 3\sigma_v, 3\sigma_v'$	0	
	T	$E, 3C_2 (C_2', C_2'', C_2'''), 8C_3$	1	$q_{41} = q_{52} = q_{63}$
	T_h	$E, 3C_2, 8C_3, i, 3\sigma, 8S_6$	0	
	T_d	$E, 3C_2, 8C_3, 6\sigma, 6S_4$	1	$q_{41} = q_{52} = q_{63}$
	O	$E, 8C_3, 3C_2, 6C_2, 6C_4$	0	
	O_h	$E, 8C_3, 3C_2, 6C_2, 6C_4, i, 8S_6, 3\sigma, 6\sigma, 6S_4$	0	

the upper sign refers to pure rotation and the lower to rotation reflection. Thus for the C_4 axis $q_{xyx} = 0$, but not for S_4 axis.

(8) z -axis an axis of more than two-fold symmetry ($C\phi$). From (3a) we have

$$\begin{aligned} q_{xxz} + q_{yyz} &= \cos \phi (q_{xxz} + q_{yyz}) + \sin \phi (q_{xxy} + q_{yyx}) \\ q_{xxy} + q_{yyx} &= -\sin \phi (q_{xxz} + q_{yyz}) + \cos \phi (q_{xxy} + q_{yyx}) \\ q_{xxz} + q_{yyz} &= \cos \phi (q_{xxz} + q_{yyz}) + \sin \phi (q_{xxy} + q_{yyx}) \\ q_{xxy} + q_{yyx} &= -\sin \phi (q_{xxz} + q_{yyz}) + \cos \phi (q_{xxy} + q_{yyx}) \\ \therefore q_{xxz} + q_{yyz} &= 0, q_{xxy} + q_{yyx} = 0; q_{xxz} + q_{yyz} = 0, q_{xxy} + q_{yyx} = 0 \\ \text{or } q_{xxz} &= -q_{yyz}, q_{xxy} = -q_{yyx}; q_{yyz} = -q_{xxz}, q_{xxy} = -q_{yyx} \end{aligned}$$

from (3d) and (3f) $q_{xxz} = q_{yyz} = 0; q_{xxy} = q_{yyx} = 0$

from (3c)

$$\begin{aligned} q_{xxz} - q_{yyz} &= \cos 2\phi (q_{xxz} - q_{yyz}) + 2q_{xxy} \sin 2\phi \\ 2q_{xxy} &= -\sin 2\phi (q_{xxz} - q_{yyz}) + 2q_{xxz} \cos 2\phi \\ \therefore q_{xxz} - q_{yyz} &= 0; q_{xxy} = 0 \end{aligned}$$

from (3b)

$$\begin{aligned} q_{yyz} + q_{xxz} &= \cos 2\phi (q_{yyz} + q_{xxz}) + \sin 2\phi (q_{yyz} - q_{xxz}) \\ q_{yyz} - q_{xxz} &= -\sin 2\phi (q_{yyz} + q_{xxz}) + \cos 2\phi (q_{yyz} - q_{xxz}) \\ \therefore q_{yyz} + q_{xxz} &= 0, q_{yyz} - q_{xxz} = 0 \end{aligned}$$

RESULTS

We are thus led to Table I for various point-groups. The second column gives the point-group (Schonfleiss notation), the third column the symmetry elements, the fourth the number of piezo-coefficients with the help of formula (4), and the last the relation between the coefficients or the non-vanishing coefficients with the help of the relations (1 to 8) found above.

It is seen that the piezo-electric effect does not exist in crystals having a centre of symmetry, and in cubic crystals belonging to point-group O having no centre of symmetry. The results in every case agree with those given in Wooster's book.

REFERENCES

- Bhagavantam, Light scattering and the Raman effect, appendix
 Voigt, *Lehrbuch der kristall Physik*, p. 829.
 Wooster, 1938, *Crystal Physics*, p. 190
 Wigner, 1931, *Gott Nach.*

THE BAND SPECTRUM OF BISMUTH MONOXIDE, (BiO)

By A. K. SEN GUPTA*

INTRODUCTION

Our knowledge about the spectra of the diatomic oxide molecules of Group V(b) elements has been, much extended during the recent years with the lone exception of the BiO molecule. The latest investigation of the spectrum of this molecule seems to be that of Ghosh (1933) who observed a large number of bands in a flaming arc fed with metallic bismuth or bismuth chloride, lying within the region $\lambda 4300$ to $\lambda 6700$ and arranged them into four singlet systems. Ghosh followed Mecke and Guillery (1927) in attributing these bands to the diatomic bismuth oxide molecule, BiO, though previous to that Saper (1931) had attributed some of these bands, specially those lying in the shorter wave-length part of the spectrum, to the diatomic chloride, BiCl, as their emitter. Saper's analysis was confirmed first by Morgan (1936) and finally by Roy (1942) who made an extensive investigation of the BiCl band spectrum both in emission and in absorption. The bands in the higher wave-length part of the spectrum observed by Ghosh were completely absent in the absorption plates taken by Roy. Though these bands were developed in the emission spectrum of a flaming arc fed with bismuth trichloride in the lower electrode, they could not be incorporated in the BiCl band systems analysed by Roy. Furthermore the chloride isotope effect observable in all the strong BiCl bands was not discernible in the case of these bands. They show moreover, even under the moderate dispersion of a Hilger E. 1 spectrograph, a resolution of the structure lines at the tail parts of the strong bands which is hardly to be expected in the case of bands emitted by such a heavy emitter as BiCl. These considerations lead one to infer that they might be due to the diatomic oxide emitter, BiO.

In analogy with the other oxide molecules of this group (Group Vb), the ground stage of BiO is expected to be a $^2\Pi$ state and the band systems associated with this state must therefore be double systems. Ghosh analysed them however into singlet systems. Moreover the constants of the ground state evaluated by him are, as has been pointed out by Rochester (1936), smaller than what one should expect for BiO. It was therefore thought desirable to undertake a fresh investigation of the BiO spectrum in order to arrive at a correct vibrational analysis for the evaluation of the molecular constants. This is all the more desirable in view of the fact that a proper correlation of the band systems and constants associated with diatomic oxide molecules of group V(b) elements remains incomplete for want of reliable data for BiO.

EXPERIMENTAL

For light source the flame of an arc between bismuth and carbon electrodes as previously used by Ghosh, was employed. Plates for measurements were

* Fellow of the Indian Physical Society.

obtained by photographing the bands with a Hilger E52 glass spectrograph as also in the first order of a 6 ft. concave grating on a Paschen mounting. Ilford fine-grained plates were used to obtain the best definition of the band heads. Neon and iron arc lines were photographed for comparison.

Measurements of band heads were carried out with a Gaertner precision comparator (M101) in the usual way. Several sets of measurements were taken. The readings are expected to be correct within 0.1 Å.

VIBRATIONAL ANALYSIS

The bands discussed in the present communication are all degraded to the red and lie in the region $\lambda 5550$ to $\lambda 6720$. All the bands are apparently single-headed and show no existence of double heads even in the spectrograms taken in the first order of a 6 ft. concave grating. From experimental evidence, the emitter of these bands is expected to be the normal diatomic bismuth oxide molecule and we should expect the band systems to arise from transitions between doublet electronic states as in the case of homologous molecules, NO, PO, AsO and SbO. Hence it was first attempted to arrange the bands into two sub-systems. A few trials proved the futility of these attempts and all the bands observed were arranged in a single system, which gave vibrational constants of the right order of magnitude. It seems therefore probable that these bands form only a sub-system of a doublet system, the other sub-system being either on the shorter or on the longer wave length side of these bands. We shall discuss this point more thoroughly in a latter section.

TABLE I

λ in air Å	ν in vacuo in cm^{-1}	(ν' , ν'') Assign- ment.	λ in air Å	ν in vacuo in cm^{-1}	(ν' , ν'') Assign- ment.
5563.9	17968	(6,0)	6217.6	16079	(2,0)
5638.5	17730	(7,1)	6299.3	15870	(3,1)
5712.0	17502	(5,0)	6380.0	15670	(4,2)
5786.1	17278	(6,1)	6411.7	15592	(1,0)
5867.9	17037	(4,0)	6495.8	15390	(2,1)
5943.5	16820	(5,1)	6583.0	15186	(3,2)
6022.3	16600	(6,2)	6621.5	15098	(0,0)
6036.9	16560	(3,0)	6710.3	14898	(1,1)
6116.7	16344	(4,1)			

Table I gives the wave lengths in air of all the measured heads, their wave-numbers in vacuo as also the ν' , ν'' -values assigned to each band. Using the wave-number data of the heads, the following equation has been derived in the usual way

$$\nu_h = 15194.5 + \{500.0(\nu' + \frac{1}{2}) - 3.10(\nu' + \frac{1}{2})^2\} - \{702.1(\nu'' + \frac{1}{2}) - 5.20(\nu'' + \frac{1}{2})^2\}$$

The arrangement of the bands referred to above shows that the ν' progression (with $\nu''=0$) bands are fairly strongly developed while of the ν'' progression (with $\nu'=0$) bands, only the first member is present. No trace of the other bands of

this progression was obtained even on our heavily exposed plates. This may be due to the insensitivity of the plates in the region in which these bands are expected to occur. It is found that although the first members of the sequences are fairly strong the sequences themselves are comparatively short. This of course is to be expected from the magnitudes of the vibrational constants which lead one to expect the maximum intensity distribution curve to be a rather wide condon parabola. In the bands under investigation the above seems to be exactly the case, with one limb of the parabola apparently absent.

DISCUSSION

In a recent communication dealing with a new ultra-violet band system of antimony monoxide (SbO), the author (Sen Gupta, 1943) has dealt in some detail with the characteristics of band systems emitted by diatomic oxide molecules of group V(b) elements. There it was shown that the γ -system which is the most prominent and intense amongst the band systems of NO and PO becomes weaker with increasing molecular weight of the emitter. In fact in the case of the SbO molecule, the analogue to the γ -system is so weakly developed that it seems probable as suggested in the above paper, that this band system may not at all be observable in the case of the next higher molecule namely, BiO . As the γ -bands are due to a $^2\Sigma \rightarrow ^2\Pi$ transition, their presence would have been indicated by the presence of doubly double-headed bands, which in the case of systems with large doublet separations as expected in the case of BiO , would look like simple double-headed bands. A thorough search of the spectrum emitted by the BiO molecule, has failed, however, to indicate the presence of any such bands. It seems certain, therefore, that the analogue of the γ -band is really too weak to be observed in the case of the BiO molecule at least with methods of excitation and experimental technique which were employed to excite these bands in the case of the other members of the group.

It is now of interest to see whether the BiO bands under investigation have any analogue in the spectra of the other homologous monoxide of group V(b) elements. As mentioned earlier, each of the diatomic oxide molecules shows $^2\Pi$ ground state whose separation increases with the increasing weight of emitting molecule, and all the observed band systems of these molecules arise from transitions to this $^2\Pi$ ground state from one or more upper states, which may be either $^2\Sigma$, $^2\Pi$ or $^2\Delta$. As $^2\Sigma \rightarrow ^2\Pi$ or $^2\Delta \rightarrow ^2\Pi$ transitions would give rise to double-headed bands, their absence shows that the bands under consideration arise from a transition to the $^2\Pi$ ground state from an upper $^2\Pi$ state. Further it has been mentioned earlier in this paper that these bands could not be arranged into two sub-systems associated with the normal transitions $^2\Pi_{3/2} \rightarrow ^2\Pi_{1/2}$ and $^2\Pi_{1/2} \rightarrow ^2\Pi_{3/2}$. One is therefore led to conclude that these bands constitute only a sub-system of a system arising out of a $^2\Pi \rightarrow ^2\Pi$ transition.

It is of interest to discuss the whereabouts of the missing sub-system and the causes of its non-appearance. It is now well-known that the doublet inter-

vals in the $^2\Pi$ ground states of NO, PO. AsO and SbO are 121 cm.^{-1} , 224 cm.^{-1} , 1026 cm.^{-1} and 2272 cm.^{-1} respectively. A separation larger than 2272 cm.^{-1} is therefore expected in the case of BiO. It is now well known that the molecules NS and PO which have the same number of electrons have practically identical doublet separations in their $^2\Pi$ ground levels. The diatomic molecule, with the largest number of electrons, known to have a $^2\Pi$ ground state, appears to be SnCl (Jevons, 1932) having a separation of 2360 cm.^{-1} with 67 electrons, and the largest observed separation in a $^2\Pi$ state is found in the case of HgH molecule, which with 81 electrons, has a $^2\Pi$ state (not a ground state) with a separation of 3684 cm.^{-1} . Hence for BiO with 91 electrons the separation of the $^2\Pi$ ground state may be expected to lie between 4000 cm.^{-1} to 4500 cm.^{-1} . Now the probable position of the other sub-system could be predicted with some degree of certainty only if the doublet separations of both the states involving in the transition be known. Though we have some idea of the magnitude of the separation in the $^2\Pi$ ground state, it is impossible to form any idea as regards the magnitude of the separation of the upper $^2\Pi$ state. Under the circumstances, the best that we can do is to indicate the region in which the sub-system in question might have occurred assuming a doublet separation in $^2\Pi$ upper state, negligible in comparison with that of the lower $^2\Pi$ state. Assuming the missing sub-system to be the shorter wavelength component, its (o,o) band would occur near 5200\AA , while if it be the higher wave-length component, the (o,o) band should occur near 9000\AA .

Considering the first alternative, though comparatively strong BiCl bands are present in that region, it is probable that the presence of at least some of the strong bands would have been indicated. But no such bands, not included in the BiCl band spectrum were present in that region, indicating thereby that the missing sub-system is in all probabilities, the higher wave length component of the band system in question. This view further explains the absence of the sub-system on our plates inasmuch as the sensitised plates employed in the investigation are not at all sensitive in the region near 9000\AA . It might be useful to search for these bands in the above region with properly sensitized plates, but unfortunately this could not be done owing to such plates or the necessary dyes being not available at the present time.

In this connection, it may not be out of place to mention here, that in the literature there are some cases of heavy diatomic molecules, where only one sub-system of a doublet system has been found, the other being absent. The present bands may also be an addition to the above list, which question can only be finally settled after the search for these bands in the expected region has been carefully carried out.

between maximum and minimum gram molecular susceptibility in the horizontal plane ; then

$$\Delta\chi = \frac{\alpha_c - \pi/4 - \sigma}{90 \cos 2\sigma} \cdot \frac{C}{H^2} \cdot \frac{M}{m}.$$

where m is the mass of the crystal, H is the strength of the magnetic field, M is the molecular weight, c is the torsional constant of the fibre, and $\pi/4 + \sigma$ is put for ϕ . For the experiment c and H are so adjusted that α_c is more than 2π so that σ is negligible and hence

$$\Delta\chi = \frac{\alpha_c - \pi/4}{90} \cdot \frac{C}{H^2} \cdot \frac{M}{m}.$$

The principal susceptibilities in any one convenient direction is measured by the balancing method of Krishnan and Banerjee (1933). The method consists in suspending the crystal by a fine quartz fibre in a nonhomogeneous magnetic field, in a liquid bath whose volume susceptibility can be varied as desired. The crystal is allowed to take up its equilibrium orientation and the volume susceptibility of the bath is so adjusted that there is no lateral displacement of the crystal, when the magnet is excited. Evidently the volume susceptibility of the crystal along the direction of the field is equal to the volume susceptibility of the liquid. The balancing liquid is then compared with a standard solution by the well known Guoy method.

RESULTS

The results of measurements are collected in Tables I and II. The principal gram molecular susceptibilities along a , b and c crystallographic axes are represented by χ_a , χ_b and χ_c . $\Delta\chi$ is the magnetic anisotropy in the horizontal plane of suspension. $\bar{\mu}$ is the effective mean Bohr magneton number and is given by $2.84 \sqrt{\chi'}$; χ' is the gram molecular mean susceptibility corrected for diamagnetism. Diamagnetism for K and O_4 was taken to be -29×10^{-6} ; since $KMnO_4$ is feebly paramagnetic it is necessary to consider the diamagnetism of Mn^{++} also, which was calculated by the method of Slater as modified by Angus (1932) to be equal to -15×10^{-6} .

TABLE I

The unit adopted for χ 's is 10^{-6} of a C.G.S. electromagnetic unit,

Crystal.	Crystallographic data.	Mode of suspension	Orientation in the field.	$ \Delta\chi $	Magnetic anisotropy.
KMnO ₄	Orthorhombic V_h^{16}				
	$a = 9.1 \text{ \AA}$	'a' axis vert	'c' axis along the field	.08	
	$b = 5.69 \text{ \AA}$	'b' axis vert	'a' " " " "	1.07	$\chi_a - \chi_c = 1.07$
	$c = 7.4 \text{ \AA}$	'c' axis vert	'a' " " " "	1.14	$\chi_a - \chi_b = 1.14$
	$z = 4$				Cal. $\Delta\chi = 1.15$

TABLE II

The susceptibilities are expressed in the usual unit, *viz.*, 10^{-6} of a C.G.S. e.m.u.

Crystal.	Direction along which susceptibility was measured.	Temp.	Density of the crystal	Vol. susceptibility	Corresponding gm. mol. susceptibility.	Mean susceptibility at 30°C.	μ^2
No. I	Along 'a' axis	30°C	2.673	0.431	25.4	24.7	0.17
" II	" " "	34°C	2.550	0.401	25.1	24.4	0.17

CRYSTAL STRUCTURE AND MAGNETIC ANISOTROPY OF KMnO_4

Krishnan and the present writer (1938) have shown that anisotropy of paramagnetic crystals arises from certain paramagnetic units. Those units are constituted as follows. Each paramagnetic ion in the crystal is under the influence of the electric field of its neighbours. The magnitude and assymetry of this field is determined by the positions of the atoms immediately surrounding the paramagnetic ion. If this field is assymmetric the crystal will exhibit magnetic anisotropy. In general there will be more than one such group in the unit cell of the crystal. So the crystal anisotropy is determined by the anisotropy of these units and their orientation relative to one another.

In KMnO_4 crystal (MnO_4) group is the paramagnetic unit. From the fine structure study of KMnO_4 crystals by Mooney (1931) it appears that in (MnO_4) group the four oxygens are disposed more or less symmetrically about the manganese atom, being situated at the corners of a tetrahedron with manganese at the centre. One oxygen atom (O_I) is at a distance of 1.68 Å and two other oxygenes (O_{II}) are at distances 1.58 Å, and another (O_{III}) at a distance of 1.52 Å from the manganese atom. The direction of $\text{Mn}-\text{O}_I$ is almost along the normal to the plane containing the three other oxygens. The electric intensity will therefore be greater for directions parallel to this plane than for directions normal to it. There are four such groups of tetrahedra in the unit cell of the crystal. The direction $\text{Mn}-\text{O}_I$ lies along the (010) plane. So out of the four molecules in the unit cell there will be pairs, each pair having the $\text{Mn}-\text{O}_I$ directions parallel to one another. Let us represent these directions for the two pairs by Z_1 and Z_2 . Z_1 and Z_2 are inclined to each other at an angle $2\psi = 140^\circ$ and Z_1 axis makes angles $15^\circ.3$, 90° and $74^\circ.7$ with a , b and c crystallographic axes respectively. Let the susceptibility along Z_1 or Z_2 be represented by K_{11} and for directions normal to it by K_1 (K_1 will be normal to the plane containing Z_1 and Z_2). K_{11} will be greater than K_1 since the distance along $\text{Mn}-\text{O}_I$ is greater and consequently the electric field smaller than the other $\text{Mn}-\text{O}$ directions. Two of the principal susceptibilities of the crystal χ_c and χ_a along 'c' and 'a' axes will be the bisectors of the obtuse and acute angle between Z_1 and Z_2 while χ_b , the susceptibility along 'b' axis will be normal to the plane containing Z_1 and Z_2 .

Consequently χ_b will be the smallest of the susceptibilities while χ_a will be greater than χ_c . The angle ψ does not differ much from a right angle so that χ_a and χ_c will be almost equal. In other words the crystal will be magnetically uniaxial, a result which is not obvious since the crystal is rhombic. Referring to table I we find that $\chi_a > \chi_c > \chi_b$ and χ_a is almost equal to χ_c .

From the structure as proposed by X-ray method we have then,

$$\chi_a = K_{11} \sin^2 \psi + K_1 \cos^2 \psi$$

$$\chi_b = K_1$$

$$\chi_c = K_{11} \cos^2 \psi + K_1 \sin^2 \psi$$

$$\frac{\chi_a + \chi_b + \chi_c}{3} = \frac{K_{11} + 2K_1}{3}$$

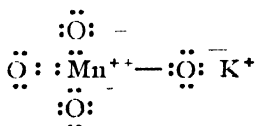
and

$$\tan \psi = \sqrt{(\chi_a - \chi_b) / (\chi_c - \chi_b)}.$$

Substituting for $(\chi_a - \chi_b)$ and $(\chi_c - \chi_b)$ from table I, ψ comes out to be equal to $75^\circ.1$ which agrees well with the X-ray value $74^\circ.7$. Using X-ray value of ψ , $K_{11} - K_1$ equal 1.23×10^{-6} . So that the anisotropy of the paramagnetic unit is 4.9%.

FERBILIE PARAMAGNETISM OF KMnO_4

X-ray study reveals that all the four oxygens in KMnO_4 are not in the same footing. $\text{M}-\text{O}_{\text{III}}$ distance being the shortest, O_{III} will form a double bond; $\text{Mn}-\text{O}_{\text{I}}$ distance, being largest O_{I} will form polar bond while the two oxygens (O_{II}) having intermediate distance will form semipolar bond. The electronic structure well representative of the given $\text{M}-\text{O}$ distances will be



Mn^{3+} ion has 4 electrons outside the closed shells. Of the different configurations that might resonate in the $(\text{MnO}_4)^-$ ion, the above configuration will apparently be the most predominant. The crystalline field involved is assumed to be strong so as to destroy Russel-Saunders coupling between the moments of different electrons in the ion.

Van Vleck (1935) has shown that in the case of certain complex salts, notably ferro and ferricyanides, the interatomic forces, if sufficiently large, will disrupt the Russel-Saunders coupling and make the deepest state have a smaller spin than that given by the Hund rule, whatever type of atomic bonding be adopted. As the $(\text{MnO}_4)^-$ ion contains an even number of electrons there will be no spin free and hence it will contribute nothing to paramagnetism. The only contribution to paramagnetism will therefore be from the high frequency elements, i.e., from the fluctuations of the orbital moment which can occur when there is more than one centre of force.

The author wishes to express his thanks to Prof. K. Banerjee, D.Sc., F.N.I., F.I.A.S., for his interest in the work and Mr. R. Sen, M.Sc., for his valuable discussions.

INDIAN ASSOCIATION FOR THE CULTIVATION OF SCIENCE
210, BOW BAZAR STREET, CALCUTTA.

R E F E R E N C E S

- Angus, W. R. (1932), *Proc. Roy. Soc. A* **136**, 569.
Gorter, C. J. (1932), *Phys. Rev.*, **42**, 437.
Krishnan, K. S. and Banerjee, S. (1933), *Phil. Trans.*, **231**, 265
Banerjee, S. *Phil. Trans.* **284**, 265.
Krishnan, K. S. and Mookherji, A. (1938), *Phys. Rev.*, **54**, 534.
Van Vleck, J. H. (1932), **Theory of Electric and Magnetic Susceptibility**.
Van Vleck, J. H. (1933), *Jour. Chem. Phys.*, **3**, 807.

THE DIELECTRIC DISPERSION OF A FEW NATURAL RESINS IN NON-POLAR SOLVENTS

By G. N. BHATTACHARYA*

ABSTRACT. The dielectric dispersion of a few natural resins in non-polar solvents has been studied. The resins include pure lac resin, soft lac resin, dammar and mastic. The critical frequency and the relaxation time of these resins have been calculated and the results confirm the comparative values of the dimensions of their rotating polar units obtained previously.

INTRODUCTION

In a previous paper (Bhattacharya, 1944 *a*) it was pointed out that dilute solutions of natural resins in non-polar solvents might yield interesting results regarding dielectric properties since the molecules of these resins would be free to move about uninfluenced by intermolecular forces. The study of anomalous dispersion of such solutions may also provide means of determining the size of ultimate particles of these resins on a comparative basis. It has already been observed (Bhattacharya, 1944 *a, b, c*) that such a dielectric study of a resin as such has helped to obtain fruitful and interesting results in some cases. On account of the polar nature of most of the natural resins as well as their large and complex molecules the dielectric dispersion method of study of their solutions in non-polar solvents is expected to be of material help in elucidating the inner structure of these macroscopic molecules.

The present study concerns only three natural resins in non-polar solvents, viz., dammar and mastic in benzene and lac in dioxane. Lac as such has not been used but its two main constituents, pure lac resin (reinharz or α -lac) and soft lac resin, have been used separately in dioxane solutions for reasons already stated (Bhattacharya, 1943). We have arrived at some conclusions regarding the particle size of these resins from their behaviour in the alternating electric field. The study of their solutions now provides means of testing those results from another point of view, since inner friction of these resins is greatly reduced in these solutions.

THEORETICAL

Williams and Oncley (1931) have extended Debye's dipole theory to the binary system in which a non-polar solvent is used as regards the variation of dielectric constant and dielectric loss with frequency. They have shown that Debye's original equations (1929) for polar liquids under the influence of high frequencies may be applied to such binary systems. Thus they obtain the following equations,

$$\epsilon'_{12} = \epsilon_{12}^{\infty} + \frac{\epsilon_{12}^0 - \epsilon_{12}^{\infty}}{1 + x^2} \quad \dots \quad (1)$$

* Fellow of the Indian Physical Society.

$$\epsilon''_{12} = (\epsilon_{12}^0 - \epsilon_{12}^\infty) \frac{1}{1 + \lambda^2} \quad (2)$$

where

$$\lambda = \frac{\epsilon_{12}^0}{\epsilon_{12}^\infty + 2} \cdot \frac{2}{\omega\tau} = \frac{\epsilon_{12}^0 + 2}{\epsilon_{12}^\infty + 2} \cdot \frac{2\pi f}{\omega}$$

ϵ'_{12} = dielectric constant of solution at frequency f ,

ϵ''_{12} = dielectric loss of solution at frequency f ,

ϵ_{12}^∞ = dielectric constant of solution at very high frequencies,

ϵ_{12}^0 = dielectric constant of solution at low frequencies,

and

τ = relaxation time of solute.

The ϵ_{12}^∞ value is usually obtained from refractive index measurement from the relation

$$\epsilon_{12}^\infty = n_{12}^2$$

The dielectric loss attains the maximum value at a frequency f_c which is called the critical frequency and is given by the relation

$$2\pi f_c \tau = 1 \quad \dots (3)$$

Thus from (1), (2) and (3) the relaxation time τ and the critical frequency f_c of the solute particles may be calculated when ϵ'_{12} , ϵ_{12}^∞ and ϵ_{12}^0 are known.

EXPERIMENTAL

Apparatus.—The substitution bridge method was used for the measurement of capacity. The frequency range employed was from 1 Kc/s to 2 Mc/s. The bridge was the high frequency type 516-C of General Radio Co. The detector was a pair of high-sensitivity headphones used in conjunction with a high-gain wide-band amplifier designed by Dr. H. Rakshit, of the University College of Science and Technology, Calcutta. The oscillator was the General Radio-modulated oscillator type 684-A. The condenser could be set to an accuracy of better than 0.05 $\mu\mu$ F.

The experimental cell was constructed of pyrex glass according to the design of Sayce and Briscoe (1925). The silvering was done according to the directions given by Sugden (1933). This cell could be placed inside a big thermo-flask. The temperature of water in this flask could be maintained constant to $25^\circ \pm 0.05^\circ\text{C}$ and thus it served as a good thermostat. The thermo-flask water was earthed. Screened cables were used for connecting the bridge with the oscillator and the amplifier.

MATERIALS

Benzene.—The method of purification of the sample of benzene used has already been described (Bhattacharya, 1942). Its constants agreed well with the standard data and are as follows:—

$$\text{F.P.} = 5.5^\circ\text{C}, n^{26} = 1.4985, d^{25} = 0.8738, \epsilon^{25} = 2.2725$$

Dioxane.—The sample used was American produce bottled by A. Boake Roberts & Co., Ltd., of England. This was purified according to the method described earlier in another paper (Bhattacharya, 1942). The constants of this sample are as follows:—

$$\text{I.P.} = 11.6^{\circ}\text{C}, n^{25} = 1.4198, d^{25} = 1.0282, e^{25} = 2.2024.$$

Dammar.—The sample of dammar was obtained from Napier Paint Works, Ltd., Calcutta, and was very pale yellow in colour. It was melted and filtered through two folds of muslin cloth in order to free it from dirt and woody matter which might have been present. It was remelted and the scum that formed on the top was removed. The clear liquid at the bottom was allowed to solidify. This resin, when cold, was powdered to pass through a 80 mesh sieve and desiccated under vacuum. Its constants are:

Acid value 39.5, softening range 100° - 104°C , melting range 112° - 117°C .

Mastic.—The mastic resin was also obtained from Napier Paint Works, Ltd., Calcutta, and was in the form of rounded pale yellow granules. It was subjected to the same method of purification as dammar resin. The constants of this are as follows:

Acid value 58.5, softening range 70° - 72°C , melting range 78 - 85°C .

Pure lac resin.—The sample used was the same as had previously been utilised for the determination of its electric moment. The method of purification was fully described in that earlier paper (Bhattacharya, 1943).

Soft lac resin.—This was also the same sample which previously had been used for the measurement of its dipole moment. For details of the method of purification, etc., the previous paper (Bhattacharya, 1943) may be referred to.

METHOD OF PROCEDURE

All solutions were made by weight in glass-stoppered Erlenmeyer flasks. When a resin was completely dissolved in the solvent, the solution was quickly filtered through a Jena fritted glass filter No. 11G2 under reduced pressure and closed volume. This solution was then put into the experimental cell. The measurement of capacity was done only when the cell attained the temperature of the thermostat. The power-factor knob of the bridge was adjusted from time to time in order to obtain the best condition of silence in the headphones due to conductivity of solutions.

CALCULATION

The apparatus was calibrated with pure and dry benzene taking its dielectric constant as 2.2725 at 25°C. The 'Zero-capacity' of the cell was obtained very carefully from the relation

$$C_0 = \frac{C_A \epsilon_B - C}{\epsilon_B - 1}$$

where C_0 = Zero capacity of the cell,
 C_A = air capacity of the same,
 C_B = capacity of the cell filled with benzene,
 and ϵ_B = dielectric constant of benzene.

For any resin solution the dielectric constant was then determined from the relation

$$\epsilon'_{12} = \frac{C_A - C_0}{C_A - C_0}$$

RESULTS

The results obtained have been shown in Tables I and II.

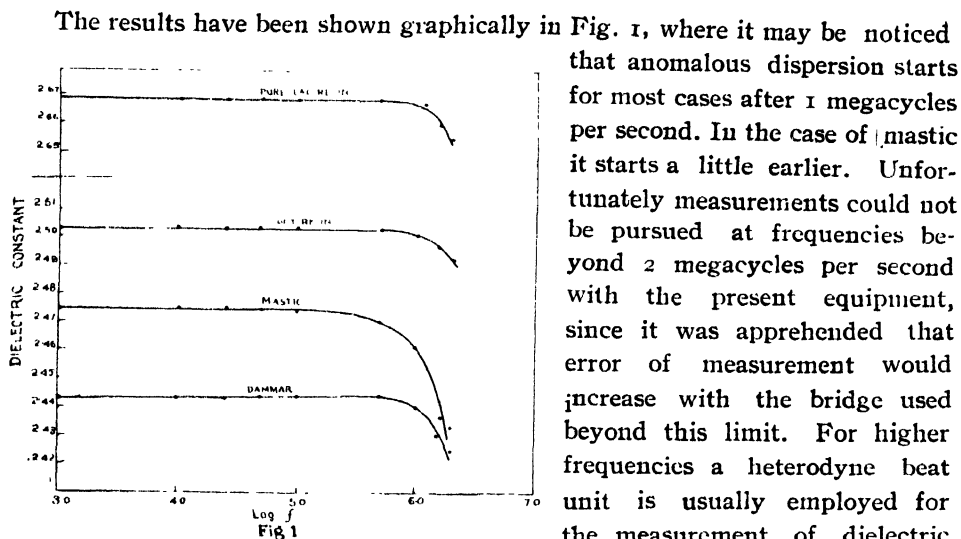
TABLE I
Dielectric constant data

<i>f</i>	Dammar in benzene (0.45% soln.)	Mastic in benzene (8.15% soln.)	Pure lac in dioxane (5.98% soln.)	Soft lac in dioxane (0.28% soln.)
1.0 Kc/s	2.443	2.475	2.669	2.503
10 Kc/s	2.443	2.475	2.669	2.503
25 Kc/s	2.442	2.475	2.669	2.503
50 Kc/s	2.443	2.473	2.669	2.503
100 Kc/s	2.443	2.473	2.668	2.503
500 Kc/s	2.443	2.470	2.669	2.502
1.0 Mc/s	2.440	2.461	2.668	2.500
1.5 Mc/s	2.430	2.436	2.659	2.466
2.0 Mc/s	2.425	2.433	2.651	2.492

TABLE II

Solution	n_{12}	ϵ_{12}^0	ϵ'	τ	f_c
Pure lac	1.4236	2.027	2.654	1.062×10^{-8} sec.	15.0 Mc/s
Soft lac	1.4270	2.036	2.492	1.108×10^{-8} sec.	14.4 Mc/s
Dammar	1.5006	2.252	2.425	2.458×10^{-8} sec.	6.5 Mc/s
Mastic	1.5002	2.251	2.433	3.634×10^{-8} sec.	4.4 Mc/s

DISCUSSION



The results have been shown graphically in Fig. 1, where it may be noticed that anomalous dispersion starts for most cases after 1 megacycles per second. In the case of mastic it starts a little earlier. Unfortunately measurements could not be pursued at frequencies beyond 2 megacycles per second with the present equipment, since it was apprehended that error of measurement would increase with the bridge used beyond this limit. For higher frequencies a heterodyne beat unit is usually employed for the measurement of dielectric

constant but such an apparatus could not be built owing to the difficulty of obtaining supplies of necessary equipment due to the international situation. The experimental results obtained with the present equipment, however, are interesting and useful for the calculation of relaxation times of solutes and their critical frequency. Dammar and mastic resins were dissolved in benzene but the constituents of lac resin, being insoluble in hydrocarbon solvents, were dissolved in dioxane in which they are soluble and which is also a non-polar solvent. No variation of dielectric constant of either benzene or dioxane could be noticed over the range of frequency used in this investigation. Very dilute solutions were not employed owing to the difficulty of measuring very small changes in the dielectric constant values, but since these resins are comparatively high-molecular-weight bodies the molar concentrations of the resins in the solutions used for these experiments were not high. It was also noticed that indices of refraction of very dilute solutions differed little from those of their respective solvents. This is another reason why more concentrated solutions were used.

Refractive index measurements were made with a Zeiss-Abbe refractometer. The instrument was tested for the correctness and reproducibility of its readings with distilled water, carbon disulphide, benzene and dioxane. The results of measurement on resin solutions have been included in Table II along with the calculated values of relaxation times and critical frequencies. These were calculated using dielectric constant values at 2 megacycles per second for ϵ'_{12} in each case. The respective curves in figure 1 are in agreement with the critical frequency obtained for each resin.

It may be observed from Table II that the relaxation times of pure lac resin and soft lac resin rotating units are practically the same, giving thereby almost the same critical frequency for both. If we consider these solutions dilute for all

practical purposes *i.e.*, if the resin molecules are considered to be free from any interaction among themselves, their inner friction will be negligible. Hence we can have an idea of the comparative particle size of these from the values of their relaxation times. From this, therefore, it may be seen that the ultimate rotating particles of pure lac resin and soft lac resin are practically equal in size. Dammar rotators are bigger in size than lac particles, whilst mastic resin has a still bigger rotating unit. This finding is in conformity with our previous results where we have seen that the radii of rotators of pure lac, soft lac, dammar, and mastic are 1.5 \AA , 1.5 \AA , 2.7 \AA and 4.4 \AA respectively. Too much stress cannot of course be laid on the absolute value of any relaxation time obtained experimentally from measurement on dilute solutions of these resins since it may be considered that the change in dielectric constant is only a second order effect and so the calculated value will have considerable accumulated errors. But as the accuracy of dielectric constant measurement is fairly high here (the accuracy ordinarily available for such measurements is very high now-a-days), their comparative values may safely be accepted. Gross, Ott and Arnold (1939) have similarly made use of this procedure in order to obtain the relaxation times of some methacrylate resins. The results obtained here are interesting and in agreement with the portions of curves obtained experimentally and showing anomalous dispersion (figure 1). Unfortunately the complete curves could not be obtained at present for reasons already stated. These results indicate, however, that we were on the right track in our previous calculations of particle size from dielectric loss and viscosity data.

REFERENCES

- Bhattacharva, G. N., 1942, *Ind Jour. Phys.*, **16**, 369.
 „ „ 1943, „ **17**, 153.
 „ „ 1944 (a) „ **18**, 1.
 „ „ (b) „ **18**, 97.
 „ „ (c) „ **18**, 116.
 Bye, P., 1929, *Polar molecules* (Chem. Cat. Co.), 94.
 Gross, G.W., Ott, H.C., Arnold, O.M., 1939, *Trans. Electrochem. Soc.*, **74**, 193.
 Savce, L.A., and Briscoe, H.V.A., 1925, *J.C S.*, **127**, 315.
 Sugden, S., 1933, *J C S.*, 768.
 Williams, J. W., and Onclv, J. L., 1931, *J Rheol*, **2**, 271.

EXPERIMENTAL ARRANGEMENTS

Measurements were made in the visible range using photographic method, (Corter, 1933) partly to get higher accuracy and partly to study the effect over the whole visible range closely. Another main difficulty in using visual method of measurement was that with a tungsten or mercury arc as source it presented difficulty in sorting out the corresponding wavelengths and there occurred a general illumination over the whole field even when the beam of light from each source was passed through proper light filters. Light from the arc source flickers, which also presented difficulty in correct measurements.

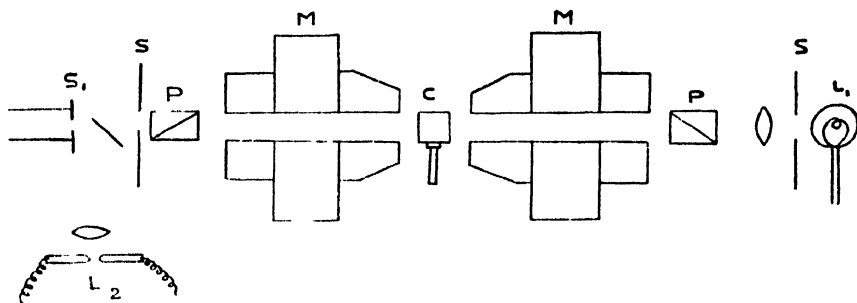


FIG. 1

M, M Electro-magnet, L₁ - Pointolite lamp, C cell, P, P Polariser and Analyser, S, S-stops, S₁ - slit of spectrograph, L₂ - Cu-arc.

The figure 1 illustrates roughly the arrangements of the apparatus used. The apparatus consisted of an electro-magnet with bored pole-pieces separated by a distance which could be adjusted. A beam of light from a pointolite lamp of 500 c.p. was passed through a half-shade polariser before entering the magnet and through the half-shade analyser (Belingham-Stanley) provided with a circular scale graduated up to the minutes. Finally the beam of light was received by a fuess-quartz spectrograph. Several stops were employed to make the beam of light limited and great care was taken to get rid of stray-light. The geometrical path of the beam was made well-defined with precision.

The magnetic field in between the pole-pieces was carefully explored by a search coil of length 4 cms. and diameter as that of the cell and the glass cell of length 3.63 cms. was properly placed in the gap. To avoid the disturbance due to multiple reflection the end plates of the cell were slightly inclined to each other. For the end plates of the cell ordinary very thin watch glass were employed, the rotation of which was negligible. A current of 8 amps., from a battery of storage cells, was passed through the electro-magnet, provided with a suitable cooling arrangement. Care was also taken to make the current steady during the time it was passed.

The line of separation of the half-shade was made luminous and was focussed on the slit of the spectrograph dividing into two parts. The spectrum appeared to consist of one upper and one lower half corresponding to two halves of the field. In the absence of the magnetic field the intensity of illumination in two

lives of the continuous spectrum was matched visually by rotating the analyser, and to obtain the exact null position the analyser was rotated through $1'$ more or less and a series of photographs were taken. With the help of the micro-photometric analysis of the photograph very accurate adjustment could be made.

When the field was kept on and the analyser given a rotation, two maxima or minima appeared in the spectrum, one in each half, the intensity distribution in which were displaced with respect to each other. In between the two maxima or minima position the spectra were equally intense. The rotation given to the analyser corresponds to this wavelength. On the spectrum a few lines from a Cu-arc were allowed to fall. The photographs were subjected to micro-photometric analysis and the wavelength corresponding to the given rotation was observed by intra-polation of the comparison-spectra of known wavelengths. In this way the analyser was given a series of regular rotations with an interval of $15'$, and each plate was micro-photographed when the wavelengths corresponding to different rotations were known. In this way the entire range of the spectrum was studied. The photographic plate used for the purpose was Ilford Panchromatic (Rapid). On each plate were recorded the image corresponding to 12 to 14 settings of the analyser. The exposure times in minutes were varied according to the nature and concentration of the solutions and the wavelengths in question.

Specific magnetic rotation was calculated from the formula, $V = \Sigma [V_m]$, gm, where Σ is summation over the different types of substances present, $V =$ observed Verdet's constant, $V_m =$ specific rotation, gm = number of gms. per c.c. of the solution. In presence of HCl, specific rotation was calculated from the formula

$$V = V_w \times \omega + [V]_{\text{HCl}} \cdot \omega_{\text{HCl}} + [V]_x \cdot \omega_x$$

where

$\omega =$ amount of water per c.c. of the solution.

$\omega_{\text{HCl}} =$ number of gms. of HCl per c.c. of the solution.

$[V]_{\text{HCl}} = \text{specific rotation of HCl} = \frac{\text{Molecular rotation of HCl}}{\text{Molecular wt. of HCl}}$

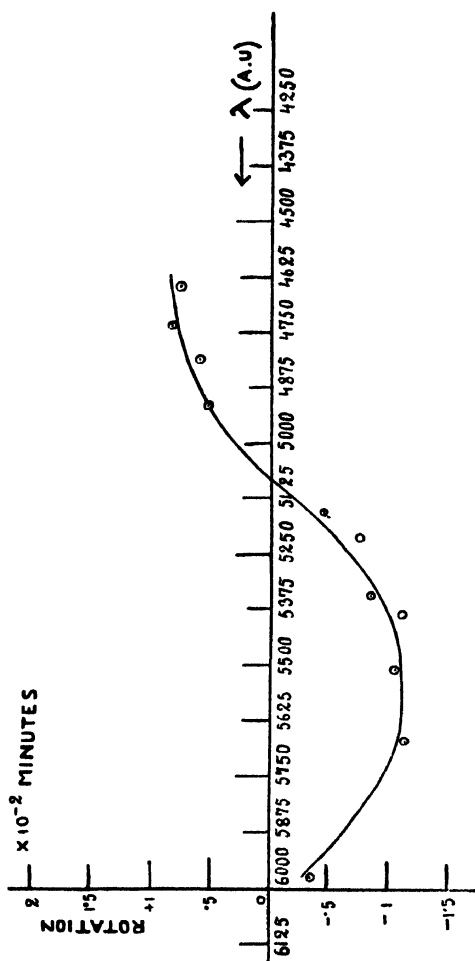
Molecular rotation of HCl was observed from the graph drawn from (wavelength—molecular rotation) data of Handbuch der Expt. Physik

EXPERIMENTAL RESULTS

Ni^{++} (NiCl_2 in water and HCl solution)—Magnetic rotation of NiCl_2 was studied from 6000Å to 4625Å. Curve I shows the nature of variations. From 6000Å to 5050Å rotation is less than that of water and on the short wavelength side of 5030Å it is positive. The selective absorption wavelengths of Ni^{++} are at 6870Å and 4070Å according to Houston (1910). Diamagnetic positive character of rotation of Ni^{++} is observed on the low frequency side of the two absorption regions, which is due to the contribution of two B or C terms of the same sign in Serber's formula. In between the two absorption regions the rotation is zero near 5050Å.

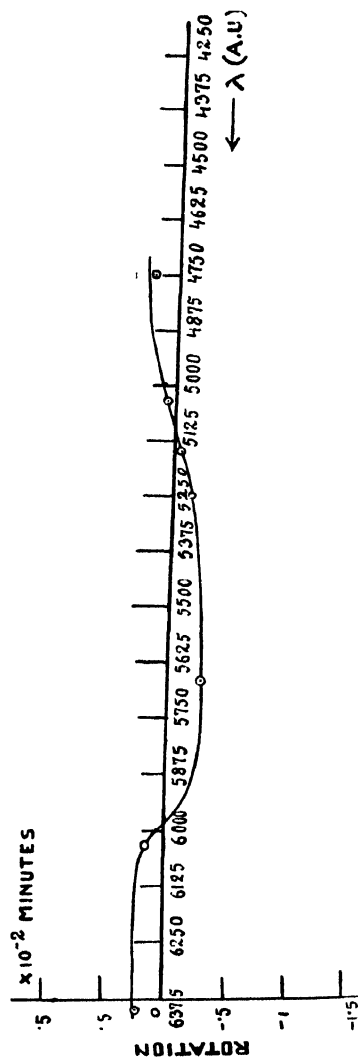
As observed by Datta and Deb (*loc. cit*) the absorption of NiCl_2 in HCl

solution is at 4370\AA and there are also a large number of absorption bands after 6000\AA . Like NiCl_2 in water it gives a rotation—dispersion curve of the same nature, positive on the longer wavelength side of the absorption region.



CURVE I

Rotation of NiCl_2 in water (corrected for water) 1 c.c. contains .01663 gms. of NiCl_2 and .0048 gms. of Ni.

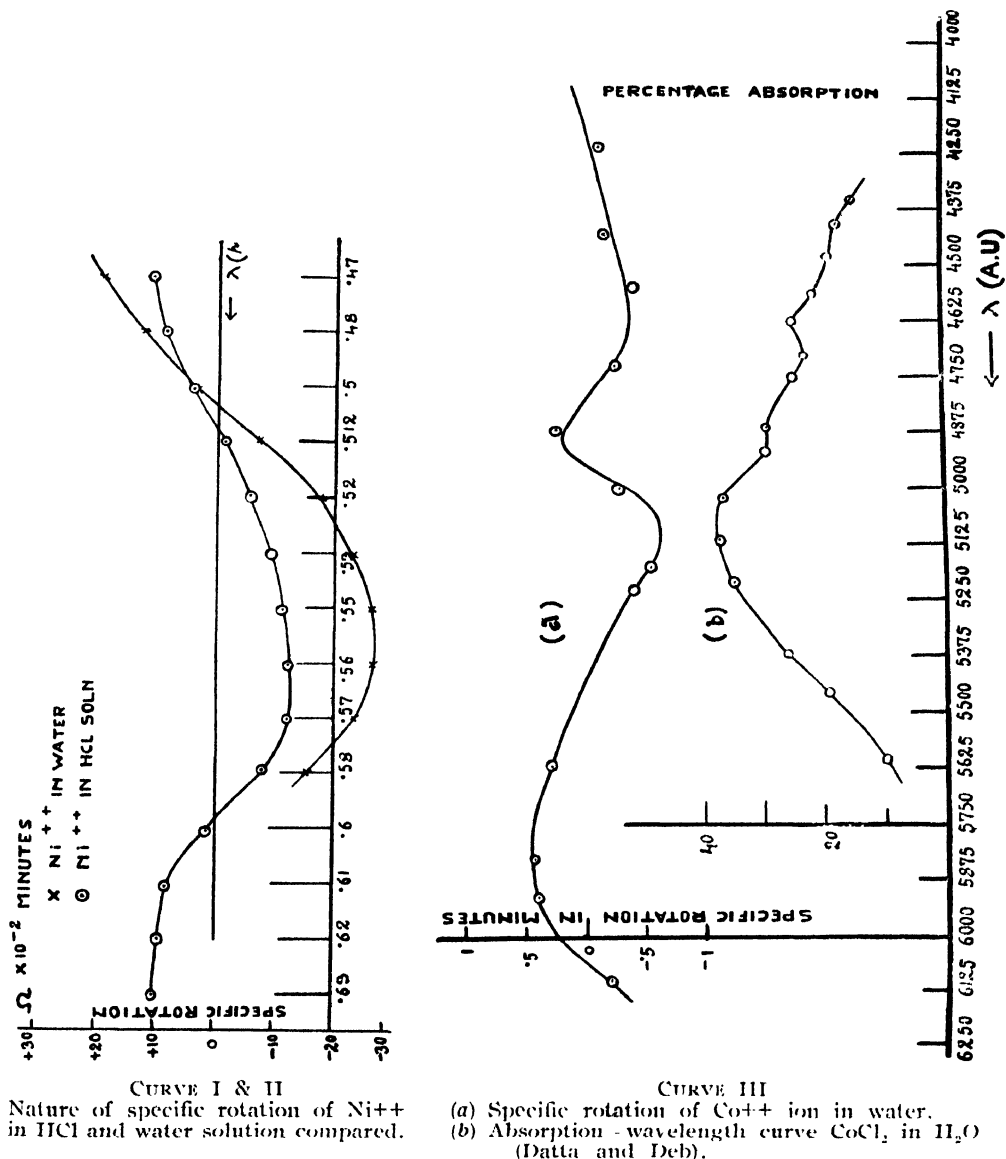


CURVE II

Rotation of NiCl_2 in HCl (corrected for water and HCl) 1 c.c. contains .00626 gms. of NiCl_2 , .0177 gms. of HCl and .0028 gms. of Ni.

Here the rotation is smaller than that of NiCl_2 in water. Another interesting fact is observed, that Curve II (NiCl_2 in HCl) attains zero value at 5075\AA and the Curve I (NiCl_2 in water) attains zero value at 5030\AA . As NiCl_2 in HCl solution has greater percentage of absorption than that of the same in water, the curve of NiCl_2 in HCl is as a whole shifted to the low frequency side (Datta and Deb).

$\text{Co}^{++}(\text{CoCl}_2 \text{ in water and HCl solution})$ —According to Roberts (1930) and his fellow-workers, rotation of Co^{++} is negative from 5780Å to 2482Å. It has been studied that the trend and behaviour of the rotation of CoCl_2 shows dispersion near the absorption band at 5100Å. The general trend of the curve is negative from 5312Å to 4202Å. Datta and Deb studied absorption spectra of

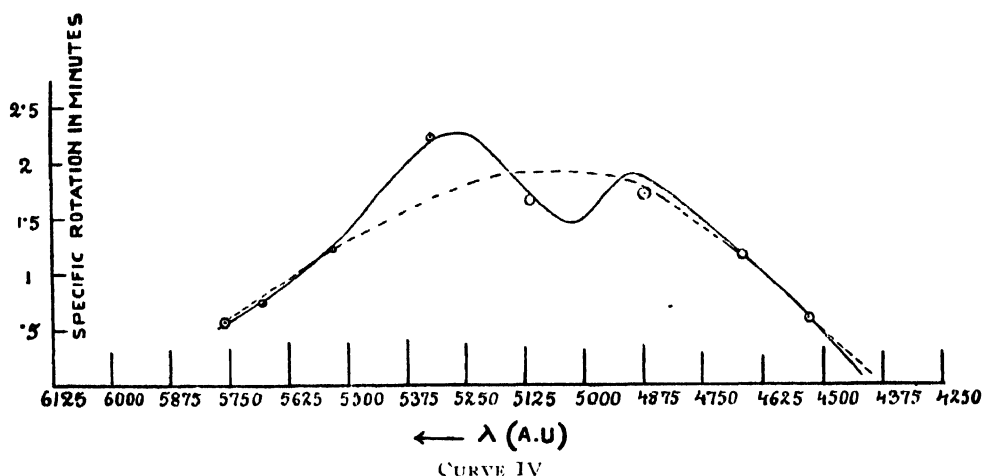


CoCl_2 in water and in HCl solution and found the absorption maxima in the former case to be at 5150Å and there are also some comparatively weak absorptions at 4862Å and 4620Å. The Curve III shows dispersion near these absorption regions emphasising the existence of these bands. In between the two

absorptions at 4862Å and 4620Å the curve is of para-magnetic nature due to B-type contribution.

Owing to experimental difficulty magnetic rotation of CoCl_2 in HCl solution could not be taken near its maximum absorption at 6840Å. The rotation is strongly positive and dispersive near 5150Å, 4862Å and 4620Å, the absorption region of CoCl_2 in water (Curve IV). This interesting fact observed suggests that though the absorptions are not observed at those places in the case of CoCl_2 in HCl yet the variation of magnetic rotation occurs there.

Ti^{+++} (TiCl_3 in HCl solution)—In Curve V, rotations of TiCl_3 are shown. From (Bose and Datta, 1933) measurement of absorption of Curve V of Ti^{+++} maximum absorptions are at 6125Å and 5200Å.



Rotation of Co^{++} in HCl (corrected for HCl and water. 1 c.c. contains 0.00119 gms. of CoCl_2 , 0.18 gms. HCl and 0.00086 of Co.

The general tendency of the curve is from positive to negative, being zero at 5200Å—quite usual as observed in NiCl_2 etc. But the nature of the curve at 5580Å suggests that this behaviour is due to the effect of two absorptions at 5300Å and 6125Å.

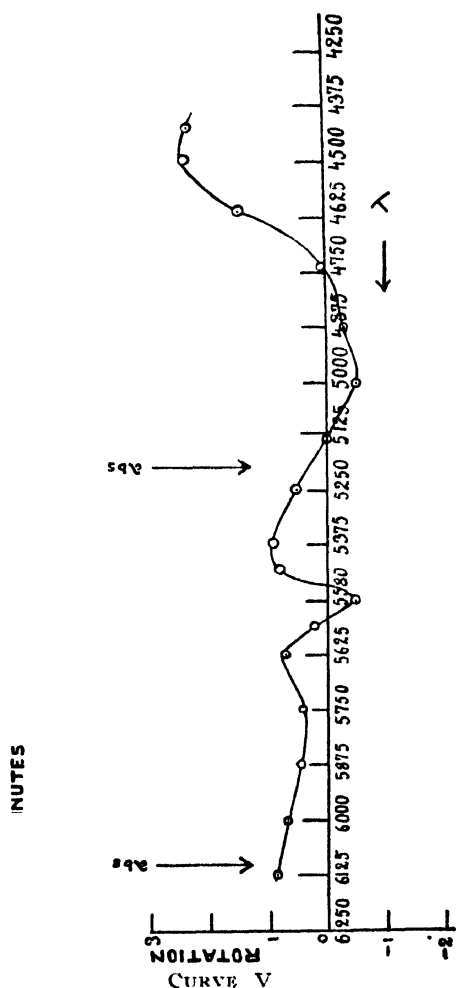
Again near 4875Å it shows a similar effect slightly. This behaviour might be attributed to the absorptions at 5200Å and at near ultra-violet region due to chlorinē.

$\text{V}(\text{ClO}_4)_2$ —In Curve VI, specific rotation due to vanadium is studied in $\text{V}(\text{ClO}_4)_2$ solution. Near 5600Å and 5400Å the curve shows dispersion. Again at 4200Å the sharp variation of rotation value is observed.

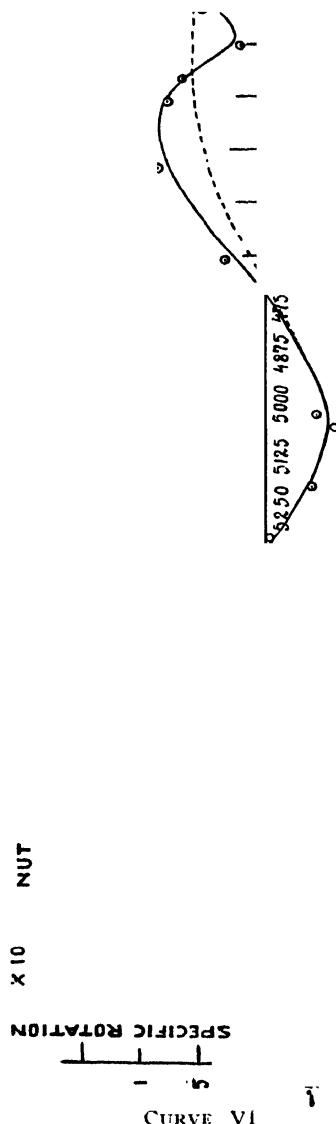
According to Kato, VCl_2 dissociates into $(\text{V})^{+++} 2\text{Cl}^{--}$, the absorptions bands will be due to $(\text{V})^{++}$ which is at 7400°Å. The magnetic rotation changes sign at several places which are absorption regions of V^{+++} and V^{++} .

In most cases of paramagnetic ions it is observed that between two maximum absorptions the nature of the curve is undulating; and between

weak absorptions there are marked variations in the rotation value. If we attribute, these variation in rotation—dispersion curve, to the absorptions, then taking differences of the Verdet's constant values in actual curve from the



Rotation of titanium in TiCl_3 (corrected for HCl , H_2O and TiCl_4). Concentration .006215 gm/cc. Density 1.0106.



Specification for vanadium V $(\text{ClO}_4)_3$ (corrected for water). 1 c.c. contains .00145 gms. of C and V $(\text{ClO}_4)_3$.00758 gms.

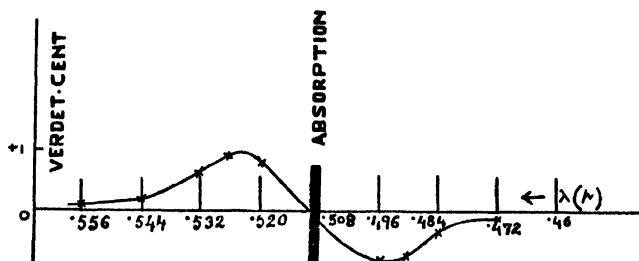
theoretical dotted curve, a curve is obtained which is a typical para-magnetic curve near the absorption region. (Curve VII)

Thus qualitatively it is a clue to investigate the existence of the fine-structure of absorption band of the paramagnetic ions in solution.

DISCUSSIONS

In order to explain the number and frequency of broad absorption bands observed in the absorption spectra of solutions of paramagnetic ions, Bose and Mukherji, (1938) proposed a theory that the paramagnetic ions, when dissolved in liquid containing dipole water molecules, form complexes with these molecules. The dipole molecules are polarised due to the electric field of the central ion and in turn produce a field acting on the ion which is proportional to the charge on the ion. In this electric field the ground level of the ion is split-up into a number of equidistant levels; the number of such levels is $L + 1$, L being the orbital quantum number of the ground term. That is an electric quantum number e_L is supposed to be associated, where $e_L = 0, 1, 2, \dots, L$. The absorption spectra is due to transition from the lowest of these levels to the higher ones, so that, in general, L absorption bands are to be expected, whose frequency is given by the empirical formula, $\Delta\nu = \frac{Ne [\Delta e_L]}{E} K_0$ where

Ne = ionic charge, Δe_L = change in electric quantum number, E = the dipole moment of the molecule associated with the central ion, K_0 = a constant. It was noticed that absorptions bands for these ions, which have F and D terms, show a doublet structure having frequency difference of about 2000 cm^{-1} and 750 cm^{-1} respectively. Thus the frequency difference is independent of ionic charge, purely depends upon the L -quantum number of the ion. This fact must be due to the further splitting up of ground terms of the ions in the induced electric field of the associated molecules. The existence of such a field of lower order of symmetry was reasonably drawn from the idea of the field of trigonal symmetry in the case of paramagnetic alums as developed by Van Vleck (1932). Van Vleck (1939), in order to explain the magnetic



CURVE VII

A paramagnetic rotation curve.

behaviour of vanadium, titanium and chrome alums, proposes an additional crystalline field of trigonal symmetry to exist. From the scheme developed by Van Vleck it was concluded that the effect of the trigonal field on the ion

of the type X^{+++} , $6H_2O$ [$X = Ti, V, Cr$] is to show a doublet structure of frequency difference ranging from 1450—2000 cm^{-1} in the case of ions with O -term and 460—860 cm^{-1} in the case of ions with F -term. This agreement in the value of frequency difference of the doublet structure in the absorption band of ions with F and D terms both in alums and solutions suggests a trigonal field to exist, superimposed on the cubic field of the paramagnetic ions in solutions. In the case of paramagnetic hydrated crystals this perturbation field of trigonal symmetry was supposed to exist on the assumptions that the non-cubic part of the field exerted on the central paramagnetic ion is due to (a) the direct action of the distant atoms other than six water molecules, which are disturbed in trigonal symmetry, (b) indirect action of the distant atoms which disturbs the normal octahedral arrangement of the associated water molecules, (c) the fact that the most stable arrangement of the polyatomic molecule is unsymmetrical to lift any orbital degeneracy which may be present in central ion: that is, it is supposed that the cluster X^{+++} , $6H_2O$ is embedded in a trigonal field of force.

Now these causes of the origin of the trigonal field in case of alums (hydrated) are also present in paramagnetic ions in solution. In solutions each ion forms a cluster of six co-ordinated water molecules and similarly each anion is associated with a cluster of water molecules. Between these anionic and cationic clusters there are unassociated water molecules. These unattached water molecules experience polarising force from these groups. These intermediate water molecules and the directed positions of the anions with respect to cations, satisfy the origin of respective perturbing forces of a trigonal symmetry.

The following Table gives the absorption bands for various ions having D and F terms—

Ions	Configura- tion	Ground term	Selective λ (A.U.)	Absorp- tion ()	Centre of gravity cm^{-1}	Transi- tions	$K' \wedge^p$ $N \wedge^p \epsilon_L$	Observer
Ti^{+++}	$3d^1$	$^2D_{5/2}$	6100 5200	16,389 } 19,225 }	17,807	0-2	2968	Bose & Datta
V^{++}	$3d^1$	$^2D_{3/2}$	7400			0-2	3377	
Co^{+++}	$3d^6$	5D_4	6120 4000	16,335 25,000	16,389 23,803	0-2	2731	Topp. Kato
V^{+++}	$3d^2$	3F_2	6100 4200	16,389 23,803		0-3	2645	
Co^{++}	$3d^7$	$^4F_{7/2}$	12500 7700	8,000 12,982	12,620	3-1	3245	Kato Dreisch
			5150	19,413		3-0	3235	
$NiCo^{++}$	$3d^8$	3F_4	12100 6870	8,262 14,552	12,620	0-1	4131	Houston Houston
			4050	24,684		0-3	4114	
V^{++}	$3d^3$	$^4F_{3/2}$	8200 } 7660 { 5600 } 5400 }	12,192 } 13,051 } 17,852 } 18,513 }	18,180	0-2	3155	Kato
						0-3	3055	

In cases where the specific rotations of the ions have been observed near the absorption regions, dispersion or assymmetric behaviours have been marked

emphasising the existence of the absorptions bands both weak and strong, origin of which is just explained.

The nature of sharp dispersion of Ti^{+++} near the absorption region shows the doublet structure of the absorption band. From Van Vleck's theory of the Stark splitting of D and F terms of different ions, splitting of D term of Ti^{+++} should be inverted (Bethe, 1939). But both from absorption and specific rotation measurements it shows doublet structure, giving sufficient evidence that splitting is upright.

As already mentioned specific rotation of Co^{++} in $CoCl_2$ solution shows a behaviour at $515\text{ m}\mu$ exactly similar to Ti^{+++} near its absorption region, indicating a doublet structure of the band. Van Vleck's theory predicts the upper F level of Co^{++} to be inverted, hence no structure and Ni^{++} upright—hence doublet. Datta and Deb experimentally observed the absorption of Co^{++} and Ni^{++} and obtained for the highest absorption of Co^{++} and Ni^{++} to be respectively doublet (505 and $525\text{ m}\mu$) and no structure ($410\text{ m}\mu$). Van Vleck's theory proposes that in a cubic field the upper level of Co^{++} will be non-degenerate and of Ni^{++} ion will be triply degenerate contrary to the observation.

In conclusion I wish to express my grateful thanks to Prof. D. M. Bose for his kind suggestions and guidance during the progress of the work. My thanks are due to Prof. M. N. Saha for providing all laboratory facilities to carry on the experimental work. My thanks are also due to Dr. D. P. Roy Chaudhury for his valuable help during the experiments and calculations.

PALIT LABORATORY OF PHYSICS,
UNIVERSITY COLLEGE OF SCIENCE,
92, UPPER CIRCULAR ROAD,
CALCUTTA.

REFERENCES

- Bethe, H., 1939, *Ann. der. Phys.*, **3**, 133.
 Bose D. M. and Datta, S., 1933, *Zits. f. Phys.*, **28**, p. 376.
 Bose, D. M. and Mukherji, P. C., 1939, *Ind. Jour. Phys.*, **13**, 219.
 Bose, D. M. and Mukherji, P. C., 1938, *Phil. Mag.*, Ser. 7, Vol. 26.
 Datta, S. and Deb, M., 1935, *Phil. Mag.*, Ser. 7, Vol. XX.
 Gorter, C. J., 1933, *Phys. Zeits.*, **34**, 238.
 Houston, 1910, *Proc. Roy. Soc. Edin.*, **31**, 538.
 Roberts, R. W. and Adams, S. F., 1939, *Phil. Mag.* **7**, Vol. 28
 Serber, R., 1932, *Phys. Rev.*, **41**, 489.
 Van Vleck, J. H., 1932, *Phys. Rev.*, **41**, 208.
 Van Vleck, J. H., 1939, *Jour. Chem. Phys.*, **7**, 61.

ENERGY IN LIQUID STATE

By M. F. SOONAWALA

ABSTRACT. Potential energy is calculated for water between 30°C and 365°C, assuming the surface of the liquid to be a potential barrier for the passage of a molecule from the liquid to the vapour state. The changes in the free energy and the internal energy and the rate of variation of the former with temperature are calculated for the same range of temperature. Similar values are suggested for other liquids but at their critical temperatures only.

This paper is a continuation of a previous one by the author (Soonawala, 1936). Reviewing that paper in brief, the probability of transition of a molecule from the liquid to the vapour state was calculated assuming the surface to be a potential barrier. As the potentials of the liquid, the surface, and the vapour were there selected, it amounted to taking $W = U_0$ and $W = U_2$ in Eqn(2) of the original paper to be the kinetic energy of the molecule, and $W = U_1$ to be equal to the kinetic energy less $2mL$, where m is the mass of the molecule and L the latent heat of transition (Frenkel). This was in accordance with Laplace's theory of capillarity, which assumes $2L$ to be the work necessary to remove a unit mass of the liquid and scatter it as gas at the temperature of transition so that the molecules are so widely separated that no interaction exists between them. If n is the number of molecules per c.c. in the liquid, the number per c.c. in the vapour would be given by nF , where F is the calculated probability of passage of a liquid molecule across the barrier into the vapour state. Thus, F would be the ratio of the densities of the saturated vapour and its liquid, provided the molecules in the vapour state are so widely separated that there is no interaction between them. This would hold for low vapour densities such as are obtained at the lower temperatures. If $b/2$ is the potential energy per unit mass of the liquid, the probability F was found to be of the form $A.I. \exp(-kmb)$, where A is a function of the mass of the molecule and the temperature, k is the Boltzmann constant, and I an integral depending upon k , m , and b . (Eqns. (8), (12) and (13) of the original paper). It was found that F so calculated did not agree with the ratio of the densities when b was assumed to be equal to $4L$, as required by Laplace's theory of capillarity. Thus, at the critical temperature, $L=0$, and $b=0$, and $F=0.5 \times 10^{-8}$, while the ratio of the densities must necessarily be equal to one. This led to the conclusion that b was not equal to zero but had a value, β , such that F became equal to one. This reduces to multiplying $A.I. \exp(-kmb)$ by a factor, $\exp(km\beta)$. This gives the potential energy of the liquid at the critical temperature as β_2 . This is taken as a clue that a similar procedure is necessary for bringing the values of F in line with those of r , the ratio of the densities of the saturated vapour and its liquid at other temperatures also by multiplying or dividing, as the case may be, by a factor, $\exp(km\beta)$. Thus, as seen from

equations (13) and (22) of the previous paper, β becomes an addition to be, and the potential energy of the liquid becomes equal to $\frac{1}{2}(b + \beta)$. These calculations are here carried out for the temperatures 30° , 70° , 100° , 180° , and the critical temperature, 365°C , and the results are summarized in Table I. The first and second rows give the latent heat per gram in calories and ergs, respectively. The values of F are shown in the third row, and those of r in the fourth row, β is calculated in the sixth row from the relation $\exp. (km\beta) = r/F$, or F/r , according as r is greater or less than F . This gives

$$A.I. \exp. (-km(b + \beta)) = r;$$

from which

$$\beta = 1/km. \ln A/r + 1/km. \ln I - b.$$

If b is changed by an amount c to $b + c$, β changes to $\beta + c'$, so that

$$\beta + c' = 1/km. \ln A/r + 1/km. \ln I' - b - c,$$

where I' corresponds to $b + c$. This gives

$$c' = -c + 1/km. \ln I'/I.$$

As I depends principally upon km and to a lesser extent upon b , we find c and $-c'$ almost equal in value. Thus, $b + \beta$ adjust itself to a constant value inspite of any errors in the assumed value of b . The fifth row shows the values of b taken to be equal to $4Q$, and the calculated values of β are included in the sixth row. The sign assigned to β is with reference to b taken positive.* The seventh row shows values of $\frac{1}{2}(b + \beta)$, which is the potential energy per unit mass of the liquid. This is seen to increase steadily with temperature, as it should when referred to a ground state where the molecules are bound together as firmly as possible. The increase with temperature is due to the loosening of the bond which holds the molecules together under a force of attraction. Thus, $\frac{1}{2}(b + \beta)$ measures the work done per unit mass in loosening the bonds between the molecules from a state of firm compression to the mean molecular distance proper at the temperature concerned, transporting the molecules in the unit mass across the surface of the liquid, and scattering them as free gas at that temperature. This will, therefore, correspond to the change in the free energy, Π , between the states of firm compression of the molecules and their infinite separation as a gas. We can also calculate the corresponding change in the internal energy, E . This will be given by $dQ - p.dv$, where dQ is change in the heat content of the system, and $p.dv$ measures the work of external expansion. In the first stage of the transition, when the molecular bonds are loosened in the liquid, there is no heat absorption nor any work of expansion against external pressure, all the work being done against the large internal pressure. An amount of heat, equal to the latent heat, is absorbed during the second stage of passage from the liquid to the vapour state, and an amount of external work, equal to $p(v_2 - v_1)$, is also performed, p being the pressure during the transition

* All values of β and ϕ given in Table II of the original paper have to be multiplied by a factor of 5.30, as, due to an oversight, the factor 0.4343 was used instead of 2.303 in transforming from hyperbolic to ordinary logarithms.

and v_1 and v_2 the specific volumes of the liquid and the vapour, respectively. We expect the Thomson equation, $H = E + T \cdot dH/dT$ to hold. The values of $H - E$, or, $H - Q + p(v_2 - v_1)$ are given in the ninth row, and those of the quotient of this quantity and the absolute temperature in the tenth row, which thus shows the values of dH/dT . The figures indicate a slow increase of dH/dT with temperature. On the other hand Fig. 1, illustrates the variation of H with temperature as given by the data of the seventh row. The value for the critical temperature is not included, as, due the increase in density, we cannot treat the state as one of infinite separation of the molecules. The figure shows a value of dH/dT equal to 7.3×10^7 ergs per degree centigrade between 30°C and 180°C , which agrees well with the figures in the tenth row, ranging from 6.5×10^7 to 7.7×10^7 . This completes the treatment for water of the calculations of variations of the internal energy, free energy and its rate of change with temperature between 30°C and the critical temperature, 365°C .

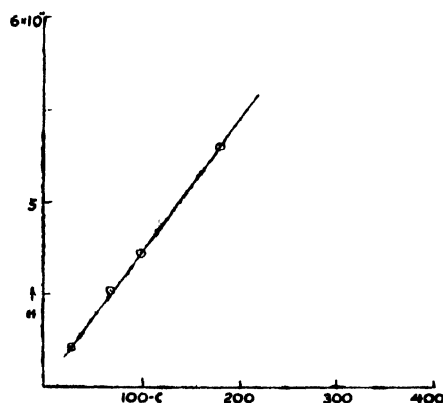


Fig. 1

It is not possible to carry out similar calculations for other liquids as the relevant data about the densities of the liquids and their vapours are lacking. Making certain comparisons between the behaviour of the integral I for water and several such liquids, the values of β were calculated for a number of liquids at the critical temperatures, as shown in Table II of the original paper. $\beta/2T$ would give the approximate values of dH/dT , but only at the critical temperature in each case; and then also the limitations mentioned above have to be borne in mind.

TABLE I

	30°C	70°C	100°C	180°C	365°C	
I	580.3	557.9	539.0	482.2	0	
$Q - LJ$	2.426	2.332	2.253	2.015	9.0×10^{10}	calcs.
F	2.75×10^{-10}	8.0×10^{-10}	2.05×10^{-10}	3.00	9.5×10^8	ergs.
b	2.64×10^{-10}	1.98×10^{-10}	6.32×10^{-11}	5.9×10^{-11}	1	
β	9.70	9.33	9.01	8.06	$0. \times 10^{10}$	ergs.
β	1.26×10^{10}	2.84×10^9	4.01×10^9	2.56×10^{10}	$+1.21 \times 10^{11}$	ergs.
$H - \frac{1}{2}(b + \beta)$	4.22	4.52	4.71	5.32	6.01×10^{10}	ergs.
$p(v_2 - v_1)$	1.61	1.61	1.71	1.91	$0. \times 10^9$	ergs.
$H - E$	1.96	2.35	2.63	3.50	6.01×10^{10}	ergs.
$\frac{H - E}{T}$	6.5	6.9	7.0	7.7	9.44×10^7	

MAHARAJA'S COLLEGE,
JAIPUR (RAJPUTANA).

REFERENCES

- Frenkel, 'Wave Mechanics, Elementary Theory', p. 114.
Soonawala, M. P., 1936, *Ind. Jour. Phys.*, **10**, 5, 353.

NOTE ON THE COWLING MODEL OF A CONVECTIVE-RADIATIVE STAR*

By

N. R. SEN AND U. R. BURMAN

ABSTRACT. The question how far the simple Cowling model of a star of the convective-radiative type conforms to Bethe's law of energy generation, is examined from different points of view, and it is also indicated how an agreement of the Cowling model with Bethe's law may be best achieved.

Since the appearance of Bethe's law of energy generation (1939) in stellar interiors, it has become clear that energy is generated in the main sequence stars within a small core around the centre. Attention has been directed to the construction of stellar models with an energy generating core in convective equilibrium, surrounded by a radiative envelope. Cowling (1935) constructed a stellar model of this nature; it is a point source model with a central convective core, surrounded by an envelope in which the transfer of energy is entirely by radiation. The effect of radiation pressure being assumed to be negligible, the core is an Emden polytrope of index $n=3/2$. The principal characteristics of the model are the following:—

(i) the core occupies 16.9 p.c. of the total radius and encloses 14.5 p.c. of the total mass;

(ii) the radiative temperature gradient in the envelope is given by

$$\frac{d\theta}{d\xi} = -Q \frac{\sigma^2 \theta^{6.5}}{\xi^2}$$

with $Q = \frac{\kappa_0 L}{16\pi a c} \frac{\beta}{\rho_c^{7.5}} = 0.1968$ (a numerical constant); (1)

$$\alpha = \left(\frac{5k}{8\pi\mu GH} \frac{T_c}{\rho_c} \right)^{1.2},$$

L = total luminosity, κ_0 = constant in Kramers' opacity formula $\kappa = \kappa_0 \rho / T^{3.5}$, which is assumed to hold here; ξ , σ and θ are respectively central distance, density and temperature in suitable units.

(iii) the mass, radius, central temperature and the central density are connected by the following formulae—

$$T_c = 0.9 \frac{\mu H}{k} \frac{GM}{R}, \quad (2)$$

$$\rho_c = \frac{\xi_1^3}{4\pi\psi_1} \frac{M}{R^3},$$

where $\xi_1 = 7.027$, denotes the boundary of the configuration, and

$$\psi_1 = \left(-\xi^2 \frac{d\theta}{d\xi} \right)_{\xi=\xi_1} = 3.1237.$$

This simple model is of considerable importance in view of Bethe's law of energy generation, which demands a stellar model to be of the convective-

* A short note on the subject has been published in *Nature*, 153, 166, 1944.

radiative type. It would be useful to examine how far this model is able to predict any of the 3 observed quantities L , M and R of a star, and to compare the luminosity furnished by this model with that calculated from Bethe's formula. We give here some calculations from three different points of view.

We first note that there are 7 parameters occurring in the above equations, viz., L , M , R , κ_0 , T_c , ρ_c and μ which are of course not all independent. κ_0 is connected with the H_2 -content X , and hence with the mean molecular weight μ by the relations

$$\kappa_0 = 3.9 \times 10^{21} (1 - X^2) \frac{1}{t}, \quad \mu = \frac{2}{1 + 3X} \quad (3)$$

(He-content being assumed negligible), where t denotes the average guillotine factor. The value of t will be an uncertainty in our calculations. A limiting value $t=2$, as taken by Chandrasekhar in his theory of stellar envelopes, will be rather low for our purpose since the averaging should extend over the entire radiative envelope. Near the interface where the temperature is quite high, the guillotine factor has certainly a much higher value. In our calculations we have therefore used two values of t , (i) $t=2$ (an extreme case) and (ii) t —some higher value appropriate to the temperature and density conditions.

Case 1. We take the observed values of L , M , R of a star, and obtain from equations (1), (2) T_c , ρ_c , μ and hence by (3) X . For instance, for the

(i) *Sun* ($L = L_\odot$, $M = M_\odot$, $R = R_\odot$), we obtain, taking $t=2$,

$$T_c = 2.4 \times 10^6 \text{ degrees, } \rho_c = 52.3 \text{ gm/cm}^3, \mu = 1.175, X \approx 0.22.$$

For the higher value of t , we take $t=5$ as suggested by Strömberg. The corresponding values are:

$$T_c = 2.1 \times 10^6 \text{ degrees, } \rho_c = 52.3 \text{ gm/cm}^3, \mu = 1.028, X \approx 0.31.$$

(ii) η -Cassiopeiae A ($L = 0.83 L_\odot$, $M = 0.72 M_\odot$, $R = 0.83 R_\odot$) $t=2$ gives

$$T_c = 26.1 \times 10^6 \text{ degrees, } \rho_c = 65.8 \text{ gm/cm}^3, \mu = 1.443, X \approx 0.13, \quad t=5 \text{ gives}$$

$$T_c = 23.1 \times 10^6 \text{ degrees, } \rho_c = 65.8 \text{ gm/cm}^3, \mu = 1.273, X \approx 0.19.$$

Evidently $t=5$ gives more acceptable results in these two cases. From Chandrasekhar's theory of stellar envelopes it is known that the influence of radiation pressure in η -Cassiopeiae A is small, and so comparison with the Cowling model is justified. These calculated central values in themselves not improbable, will however lead to a serious discrepancy. If the stellar equations are integrated from the centre outwards with these central conditions, and the luminosity (required to determine the change to radiative gradient) calculated by Bethe's formula, we arrive at an all-convective model in each case, there being no radiative envelope. This can be verified by calculations; a theoretical proof (for the general case) and other connected results will be given in a different communication.

Case 2. Here we prescribe M , R and μ . Then equations (2) give T_c , ρ_c and hence (1) gives L which we call L_c . On the other hand the luminosity may be calculated by Bethe's formula, using the above values of T_c , ρ_c and the results of integration; this value we denote by L_B . A comparison of these two values of L will give us an idea regarding the compatibility of the Cowling

model with Bethe's law of energy generation. For instance, for the Su_8 (with $\mu=1$, $N=0.35$, $t=2$) we obtain on the above basis

$$\begin{aligned} T_c &= 20.8 \times 10^6 \text{ degrees,} & \rho_c &= 52.3 \text{ gm/cm}^3. \\ L_G &= 1.2 \times 10^{33} \text{ ergs/sec.,} & L_B &= 6.9 \times 10^{33} \text{ ergs/sec.} \end{aligned}$$

For $t=5$ the only modified value is $L_G = 3.0 \times 10^{33}$ ergs/sec.

The discrepancy in the value of L arising out of the use of Bethe's formula in the Cowling model is by a factor between 2 and 6 (for t varying from 5 to 2) which may be regarded as fairly satisfactory. But here also the discrepancy is high enough to yield an all-convective model, if integrated from inside as stated in case 1.

Case 3. Here we assign μ and then choose T_c , ρ_c in such a manner that L_G calculated from (1) is identical with L_B calculated from Bethe's formula and both equal to say, the solar luminosity. Then equations (2) will give the values of M and R which may be compared with the observed solar values. We briefly give the method of this calculation.

The equation for the luminosity-determination is

$$L(r) = \int_0^r 4\pi\rho r^2 \epsilon dr$$

where $\epsilon = \epsilon_0 \rho T^{2.3} e^{-B/T^{1/3}}$ (Bethe's formula),

ϵ_0 is a constant depending on the composition, and $B = 56 \times (2 \times 10^7)^{1/3}$.

Introducing the variables ξ , σ and θ defined by $r = \alpha\xi$, $\rho = \rho_c \sigma$ and $T = T_c \theta$,

where $\alpha = \left(5k/8\pi\mu GH \frac{T_c}{\rho_c} \right)^{1/2}$

and using the polytropic relation $\sigma = \theta^{3/2}$ ($n=3/2$), we obtain after some calculations

$$L(\xi) = A \rho_c^{1/2} I(\xi, T_c) \quad (4)$$

where

$$A = 4\pi\epsilon_0 \left(\frac{5k}{8\pi\mu GH} \right)^{3/2} T_c^{5/6}$$

and

$$I(\xi, T_c) = \int_0^\xi \theta^{7/3} e^{-b/\theta^{1/3} \xi^2} d\xi \quad (b = B/T_c^{1/3}).$$

For a given T_c , the constant A and the integral $I(\xi, T_c)$ can be evaluated and hence $L(\xi)$ determined as a function of ρ_c only. Also the luminosity can be calculated from (1) and expressed in the form

$$L = Q \frac{16\pi ac}{3\kappa_0} \left(\frac{5k}{8\pi\mu GH} \right)^{1/2} \frac{T_c^{8/3}}{\rho_c^{5/2}} = B/\rho_c^{5/2} \quad (5)$$

where

$$B = Q \frac{16\pi ac}{3\kappa_0} \left(\frac{5k}{8\pi\mu GH} \right)^{1/2} T_c^8.$$

Hence for the agreement between the two values of L given by (4) and (5) we must have at the interface $\xi = \xi_i$ of the convective core

$$\begin{aligned} A \rho_c^{1/2} I(\xi_i, T_c) &= B/\rho_c^{5/2} \\ \rho_c^3 &= B/AI(\xi_i, T_c). \end{aligned} \quad (6)$$

or

This equation determines ρ_c when T_c is assigned. By a little trial T_c , ρ_c

may be so adjusted that the calculated luminosity becomes identical with the luminosity of the given star.

Taking $\mu=1$, $X=0.35$, for the Sun, and $t=2$, we find by a little trial that $T_c=20.5 \times 10^6$ degrees, $\rho_c=31.6$ gm/cm³, satisfy the above conditions, and yield the solar luminosity $L=3.8 \times 10^{33}$ ergs/sec. The corresponding mass and radius, calculated from (2) come out to be $M=2.5 \times 10^{33}$ gm, $R=8.8 \times 10^{10}$ cm. For $t=5$ the results are further improved, and we obtain $M=2.1 \times 10^{33}$ gm, $R=7.6 \times 10^{10}$ cm, the corresponding values of T_c and ρ_c being 20.3×10^6 degrees and 43 gm/cm³ respectively. The very close agreement in respect of mass and radius for $t=5$ is indeed remarkable. It may be noted that the convective-radiative character of the model is not disturbed by these central conditions (as happened in Cases 1 and 2). If we perform the same calculations in the case of the η -Cassiopeiae A, taking $\mu=1$, $X=0.35$ and $t=5$, we obtain

$$T_c=20.0 \times 10^6 \text{ degrees, } \rho_c=46.4 \text{ gm/cm}^3, M=1.9 \times 10^{33} \text{ gm}$$

$$R=7.2 \times 10^{10} \text{ cm, } L_c=L_B=3.0 \times 10^{33} \text{ ergs/sec.}$$

In this case the agreement is not as good as in the case of the Sun. We have of course assumed the same H₂-concentration as for the Sun; a slightly higher H₂-concentration for η -Cassiopeiae A will very much improve the results, while a lower concentration will make the discrepancy worse. It appears possible to so choose the hydrogen concentration that a close agreement between the observed and calculated values (by the Cowling model) may be achieved.

From these calculations it appears that the agreement of the Cowling model with Bethe's formula for the Sun will be the best and very satisfactory, if the central conditions are so chosen that with a plausible value of the average guillotine factor, the calculated and observed luminosities become identical. It appears possible that for the main sequence stars of small masses, by an adjustment of the H₂-content near about $X \sim 0.35$, a close agreement between calculated and observed stellar parameters may be obtained in many cases. One may thus form an estimate of the H₂-content in these stars on the basis of the Cowling model and Bethe's energy generation formula. It is also permissible to suggest, that a main sequence stellar model with approximately the solar mass, and of the convective-radiative type in agreement with Bethe's energy generation formula, should have a central temperature of the order of twenty million degrees as suggested by the standard model, but the central density should be very much lower than that of the standard model, if the idea of an H₂-content of about $X \sim 0.35$ is to be retained.

DEPARTMENT OF APPLIED MATHEMATICS,
UNIVERSITY OF CALCUTTA.

REFERENCES

Bethe, H. A., 1939, Energy production in stars, *Phys. Rev.*, **55**, 434.

Cowling, T. G., 1935, The stability of gaseous stars, *M. N.*, **96**, 57.

For an illuminating account of the Cowling model, see also Chandrasekhar's "Introduction to the study of Stellar Structure", p. 351.

HUMID HYSTERESIS OF MAHAJAN'S OPTICAL HYGROMETER AND OTHERS

By L. D. MAHAJAN

ABSTRACT. In this paper, humid hysteresis of Mahajan's optical hygrometer and some other types of hygrometers have been studied. The coercive time, residual humidity and humid hysteresis loop of hygrometers have also been explained.

It is observed that on traversing the path of a cycle of observations, the return path is different from the direct path, on increasing and decreasing the relative humidity respectively. This cycle of observations do not take the same path when repeated again. Its period is also reduced when it is repeated for some time without a break.

Almost all hygrometers exhibit the phenomena of humid hysteresis, coercive time, and residual humidity. The coercive time and residual humidity of a hygrometer are not of constant values, but they vary with the type of hygrometer depending on its construction, nature of its hygroscopic substance, rate of flow of air through it, and its immediate past history. The area enclosed by a loop of humid hysteresis decreases if such cycles are repeated for some times without a break.

In the previous papers the author has dealt with the construction and theory of working of Mahajan's (Mahajan, 1941) optical hygrometer. The time lag and humid fatigue of various types of hygrometers have also been studied. Now in this paper the author has attempted the study of humid hysteresis which is a phenomenon very commonly exhibited by various types of hygrometers, such as, Mahajan's optical hygrometer, hair hygrometer, paper hygrometer, humatograph etc. Their coercive times and residual humidities have been determined and discussed in detail. The method used and the results obtained are given below in brief.

APPARATUS

The apparatus used for the study of hysteresis of hygrometers, their coercive times and residual humidities is the same which was used by the author for measurement of time lag and humid fatigue of hygrometers and the same has been described in his previous paper on the said subject.

HUMID HYSTERESIS

The observations of variations of humidity as indicated by the optical hygrometer with respect to time were recorded in rapid succession without any break in cycles by exchanging the surrounding medium from moist to dry

and vice-versa. A few sets of such cycles of observations are given below in Table I.

TABLE I
Mahajan's Optical Hygrometer

No. of set.	Cycle	Humidity-reading of surrounding medium.	Observation of humidity reading.	Time taken in minutes.	Remarks
1.	2.	3.	4.	5.	6.
I set.	I cycle (direct)	98.5 cm.	90.0	0	Time lag 22 min.
			93.0	3	
			95.0	10	
			95.3	13	
			97.0	17	
			98.3	22	
	(reverse)	91.0 cm.	98.3	0	Time lag 39 min.
			96.0	2	
			95.0	7	
			93.6	15	
			93.3	22	
			92.5	25	
			91.9	30	
			91.5	34	
			91.4	39	
II set.	I cycle (direct)	96.0 cm.	92.3 cm.	0 min.	Time lag 22 min.
			94.7	3	
			95.3	8	
			95.5	16	
			96.0	22	
	(reverse)	92.0 cm.	96.0 cm.	0 min.	Time lag 45 min.
			95.8	1	
			95.6	3	
			95.3	10	
			94.3	15	
			93.7	20	
			93.4	25	
			93.0	37	
			92.9	45	
	II cycle (direct)	100.0 cm.	92.7 cm.	0 min.	Time lag 17 min.
			95.8	3	
			96.0	5	
			96.6	10	
			100.0	17	
	(reverse)	92.0 cm.	100.0 cm.	0 min.	Time lag 38 min.
			99.0	6	
			97.8	10	
			96.5	15	
			95.3	19	
			94.0	23	
			92.5	32	
			92.3	38	
III set.	I cycle (direct)	88.0 cm.	81.5 cm.	0 min.	Time lag 18 min.
			86.3	3	
			86.5	5	
			87.7	11	
			88.0	18	
			88.0	23	

TABLE I—(contd.)

No. of set.	Cycle	Humidity-reading of surrounding medium.	Observation of humidity reading.	Time taken in minutes.	Remarks
	2	3.	4.	5	6.
	(reverse)	82.0 cm.	87.3 cm. 87.0 86.0 85.3 85.0 84.4 83.7 83.2 82.8 82.8	0 min. 1 2 7 11 13 21 27 34 39	Time lag 34 min
	II cycle (direct)	86.5 cm	81.5 cm. 84.3 85.6 86.2 86.2	0 min. 4 9 11 14	Time lag 11 min
	(reverse)	82.0 cm	86.2 cm. 85.0 83.8 83.3 82.9 82.6 82.4 82.3 82.3	0 min. 2 6 9 14 18 21 23 25	Time lag 23 min

DISCUSSION OF RESULTS

The observations given in Table I set III have been plotted in curves given in figure 1, wherein the abscissa represents time in minutes and the ordinate readings actually recorded on on the Mahajan's optical hygrometer. They are the typical curves and of interesting nature.

In figure 1 the point *a* is the starting point. When a current of moist air is pushed inside the chamber its relative humidity increases rapidly with time in the beginning but this speed of rise of humidity slackens on regularly with time as is apparent from the curve *abcd*. If further observations are recorded the readings do not show any increase, as the steady state has arrived and the curve represents the path *dc*, which is a horizontal line. The maximum time taken by the hygrometer to reach the steady state is *t*₁.

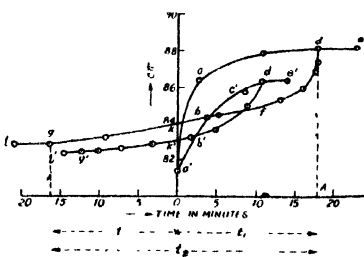


FIG. 1

Now the dry air is pushed into the chamber and the readings of relative humidity on the instrument are again observed at known intervals. These observations are represented by the part of the curve *dfbkg*. Here, the time has been counted in the reverse order from the point *d*—the starting point of

the last steady state de . The direction for measurement of time is shown by an arrow in the figure. In this case A is the initial point and t_2 the maximum time taken by the hygrometer to reach the steady state gl . This portion of the curve $dfbkg$ also shows that the relative humidity decreases very rapidly in the beginning but slowly later on, till a steady state gl —is reached. Thus the rate of change of humidity in the variable state varies with time in logarithmic relation as stated in the previous paper (Mahajan 1940), for it depends on adsorption of moisture or desorption of moisture by the soil or any other absorbant used in the hygrometer.

The portion of the curve $dfbkg$ representing the return path is different from the former curve $abcd$. Thus the observations in the two cases differ. It further shows that the hygrometer reaches the steady state gl after time t_2 ($t_1 + t$) which is greater than the former time t_1 . This return curve (ii) cuts the ordinate passing through o at k . Thus the additional time taken to reach the steady state is $(t_2 + t_1) - t$ minutes which has always some positive value in almost all hygrometers.

Now on repeating the same cycle of observations, it is observed that the observations do not traverse the old path of the former cycle but adopt a new one $abcdfk$ which is different from the former one $abcd/g$. This time the hygrometer reaches the steady state de and gl in comparatively shorter times. The additional time $(t_2 - t_1) - t$ is also less. Moreover, the area enclosed by the second loop is much smaller than that of the first one. This area becomes minimum when such cycles of observations are repeated a number of times without a break for the hygroscopic substance gets acclimated to the variable conditions. But the shape of such loops remain almost the same which indicates that the nature of behaviour of these cycles is the same. The possible causes for traversing different paths of cycles are that firstly the hygroscopic substance in the hygrometer has its rates of adsorption of moisture and desorption of moisture slightly different and secondly the instrument has some time lag. It is, therefore, desirable that such a substance should be selected which has its powers of adsorption and desorption of moisture equal and these powers have linear relation with time. If these conditions are fulfilled no loop will be formed but the same path will be traversed on repeating the cycles.

Residual Humidity.—From the figure it is further evident that the value of humidity as represented by a hygrometer on its return cycle is not the initial one when the reversed time period AO is equal to the direct time period OA . The relative humidity on the reverse path is slightly higher than the initial humidity by ak which is the residual humidity of hygrometer. The value of this residual humidity is different in different hygrometers depending on their construction, nature of the substance used in them, rate of flow of air through them and their immediate past history. The values of residual humidity of some of the hygrometers are given in Table II below.

Coercive Time.—The extra time required to allow the hygrometer to come

to its initial humidity is $(t_2 - t_1) = t$ as is indicated in figure 1. This is coercive time of a hygrometer. It varies with the construction of a hygrometer, nature of the substance used in it, rate of flow of air through it and its immediate past history. The values of coercive time of some of the hygrometers have been studied and are given below in Table II.

TABLE II

No. of set.	No. of Cycle.	Kind of hygrometer.	Residual humidity	Coercive time.
I set.	I cycle	Mahajan's optical-hygrometer	0.7 cm.	23 min.
	II cycle		0.4 cm.	21 min.
II set.	I cycle		1.3 cm.	16 min.
	II cycle		0.8 cm.	12 min.
Mean.			0.8 cm.	18 min.
I set.	I cycle	Hair-hygrometer	6% H	8 min.
	II cycle		5% H	6 min.
II set.	I cycle		8% H	10 min.
	II cycle		6% H	8 min.
Mean.			6% H	8 min.
I set.	I cycle	Paper-hygrometer	9% H	25 min.
	II cycle		6% H	21 min.
II set.	I cycle		10% H	27 min.
	II cycle		6% H	22 min.
Mean.			8% H	24 min.

Humid Fatigue.—The observations recorded in Table II indicate that the values of coercive time and residual humidity do not remain constant but decrease when such cycles of observations are repeated in rapid succession without a break. The details of this effect has already been dealt with by the author (Mahajan, 1944) in one of his previous papers on the subject.

Humid Hysteresis.—The effects produced by humidity of the surrounding medium tend to persist *i.e.*, tend to lag behind the cause. The reading of humidity given by a hygrometer is always slightly greater than what the humidity actually is when the relative humidity of the surrounding medium is diminishing, and it is always slightly less when relative humidity of the surrounding medium is increasing. Thus it always requires an additional time to bring relative humidity to the initial value or the actual value of the surrounding medium. This phenomenon of hygrometers is humid hysteresis (to lag behind). Hysteresis in this case is the lagging of relative humidity, as indicated by a hygrometer, behind the relative humidity of the surrounding medium which produces it.

Humid Hysteresis Loop.—The loop formed by the cycle of observations of humidity with respect to time is the hysteresis loop of humidity.

CONCLUSIONS

The results obtained from the above investigations are interesting and some of the important ones are given below :

1. The return path of a cycle of observations (when humidity is decreasing is different from the direct path of the same cycle (when humidity is increasing).
2. The cycles of observations do not traverse the same path when repeated again. The period of cycle is reduced when they are repeated for a number of times without a break.
3. Almost all hygrometers exhibit hysteresis of humidity.
4. Almost all hygrometers have their coercive time and residual humidity.
5. The residual humidity and coercive time are not constant but they vary with the type of hygrometer depending on its construction, its hygroscopic substance, rate of flow of air through it and its immediate past history.
6. The area enclosed by a loop of humid hysteresis decreases if such cycles are repeated for some time without a break.

Further work is in progress and will be published in due course of time.

ACKNOWLEDGMENTS

The author takes this opportunity to thank His Highness' Government, Patiala, for providing facilities to carry out this work in the Physics Research Laboratory, Mahendra College, Patiala. Besides, he is also grateful to Sir C. V. Raman, M.A., Ph.D., D.Sc., F. Inst.P., F.R.S., Nobel Laureate, for suggesting this problem for investigations.

PHYSICS RESEARCH LABORATORY,
MAHENDRA COLLEGE, PATIALA.

REFERENCES

- Mahajan, L. D., 1941, *Current Science*, **9**, 2, 100.
" " 1941, *Ind. Jour. Phys.*, **15**, 425.
" " 1944, *Current Science*, **13**, 73.
" " 1940, *Ind. Jour. Phys.*, **14**, 441.

THE SCATTERING OF FAST β -PARTICLES BY ELECTRONS

By K. C. KAR

AND

MRS. C. BASU

ABSTRACT. In Sec. A a general relativistic treatment is given of the problem of collision of two particles of unequal masses, one being initially at rest, and general expressions connecting energies, momenta, angles of deflection,etc., in C- and L- systems are derived. In Sec. B the relativistic wave statistical formula for the intensity of electron-electron scattering is derived. It is shown to be in decidedly better agreement than Möller's with the experiment of Champion. In Sec. C a general relativistic theory of scattering for unequal masses has been developed.

In the present paper we propose to develop the relativistic wave-statistical theory of scattering of fast β -particles by electrons (*vide* Sec. B) and also of a particle of mass m_1 by a second particle of mass m_2 , under coulomb field (*vide* Sec. C). Before going into the problem of scattering it appears useful to give (*vide* Sec. A) a systematic theory of relativistic collision of two particles of unequal masses and the relations between the centre of gravity (C-) and laboratory (L-) systems. As far as we are aware, a systematic treatment of these problems has not been given before. Only a few results which were found useful have been derived so far (Champion 1932, Bethe 1932 and Wolfe 1931).

Sec. A: Theory of relativistic collision

Suppose that the C-system for two colliding particles moves with velocity u and that the second particle of rest mass m_{02} is initially at rest. It is thus evident that the relative velocity between C- and L- systems is u . Therefore using the well-known relativistic addition theorem of velocities and denoting the C-system by 'star' we have the following rigorous relations between energies and momenta in C- and L-systems, the first particle being supposed to move along x -axis before collision.

Before Collision

First particle

$$p_{1x}^* = \gamma^* \left(p_{1x} - \frac{u}{c^2} E_1 \right)$$

$$p_{1y}^* = p_{1y} = 0$$

$$p_{1z}^* = p_{1z} = 0$$

$$E_1^* = \gamma^* (E_1 - u p_{1x})$$

$$E_1 = m_{01} \gamma c^2$$

$$p_{1x} = m_{01} \gamma v = m_{01} c \sqrt{\gamma^2 - 1}$$

Second particle

$$p_{2x}^* = \gamma^* \left(p_{2x} - \frac{u}{c^2} E_2 \right)$$

$$p_{2y}^* = p_{2y} = 0$$

$$p_{2z}^* = p_{2z} = 0$$

$$E_2^* = \gamma^* (E_2 - u p_{2x})$$

$$E_2 = m_{02} c^2$$

$$p_{2x} = 0$$

Or, the reciprocal relations, viz.,

$$p_{1x} = \gamma^* \left(p_{1x}^* + \frac{u}{c^2} E_{1x}^* \right), \text{ etc.,}$$

Or, the reciprocal relations

$$p_{2x} = \gamma^* \left(p_{2x}^* + \frac{u}{c^2} E_{2x}^* \right), \text{ etc.,}$$

where $\gamma^* = \frac{1}{\sqrt{1 - \frac{u^2}{c^2}}}$ u the velocity of the first particle before collision and

$\gamma = \frac{1}{\sqrt{1 - \frac{v^2}{c^2}}}$ If we suppose that the scattering takes place in xz -plane, we have

for the corresponding relations after collision denoted by dash

After Collision

First particle

$$p_{1x}^{*'} = \gamma^* \left(p_{1x}' - \frac{u}{c^2} E_{1x}' \right)$$

$$p_{1y}^{*'} = p_{1y}' = 0$$

$$p_{1z}^{*'} = p_{1z}' \neq 0$$

$$E_{1x}^{*'} = \gamma^* (E_{1x}' - u p_{1x}')$$

Or, the reciprocal relations

$$p_{1x}' = \gamma^* \left(p_{1x}^{*'} + \frac{u}{c^2} E_{1x}^{*'} \right), \text{ etc.,}$$

Second particle

$$p_{2x}^{*'} = \gamma^* \left(p_{2x}' - \frac{u}{c^2} E_{2x}' \right)$$

$$p_{2y}^{*'} = p_{2y}' = 0$$

$$p_{2z}^{*'} = p_{2z}' \neq 0$$

$$E_{2x}^{*'} = \gamma^* (E_{2x}' - u p_{2x}')$$

Or, the reciprocal relations

$$p_{2x}' = \gamma^* \left(p_{2x}^{*'} + \frac{u}{c^2} E_{2x}^{*'} \right), \text{ etc.,}$$

Let $\gamma_1' = \frac{1}{\sqrt{1 - \frac{v_1'^2}{c^2}}}$ and $\gamma_2' = \frac{1}{\sqrt{1 - \frac{v_2'^2}{c^2}}}$ where v_1' and v_2' are the velocities of first and second particles after collision, in L-system.

In our general treatment we shall always consider three special cases, viz., (I) $m_{01} = m_{02}$ (relativistic) which has been discussed by Möller (1932), (II) $m_{02} \gg m_{01}$ and (III) $m_{01} \neq m_{02}$ (non-relativistic) which has been discussed before by Kar (1941).

Now, from the condition of conservation of momentum in C-system we have

$$p_{1x}^{*'} + p_{2x}^{*'} = 0. \quad \dots (1)$$

On substituting the values of the momenta from the relativistic equations given before we get the general relation

$$u = \frac{\gamma \frac{m_{01}}{m_{01}}}{\gamma + \frac{m_{02}}{m_{01}}} \quad \dots (1.1)$$

and hence

$$\gamma^* = \frac{1 + \gamma \frac{m_{01}}{m_{02}}}{\sqrt{1 + 2 \frac{m_{01}}{m_{02}} + \left(\frac{m_{01}}{m_{02}} \right)^2}} \quad \dots (1.2)$$

Case I :— $m_{01} = m_{02}$ (relativistic)

$$u = \frac{\gamma}{\gamma + 1} v \quad \dots (1'3)$$

$$\gamma^* = \sqrt{\frac{\gamma + 1}{2}}$$

Neglecting the effect of relativity i.e., taking $\gamma = 1$, we have $u = \frac{1}{2}v$ and $\gamma^* = 1$.

Case II :— $m_{02} \gg m_{01}$. In this case we have

$$u = 0 \quad \dots (1'4)$$

$$\gamma^* = 1$$

Case III :— $m_{01} \neq m_{02}$ (non-relativistic). In this case $\gamma = 1$ and so

$$\left. \begin{aligned} u &= \frac{m_{01}}{m_{01} + m_{02}} v \\ \gamma^* &= 1 \end{aligned} \right\} \quad \dots (1'5)$$

Relations between the angles of Scattering of the Colliding particles in C- and L-systems

Let θ_1, θ_1^* and θ_2, θ_2^* be respectively the angles of scattering of the first (colliding) and second particles in L- and C- systems. Now, from the principles of conservation of energy and momentum we have (in L- system)

$$m_{01}\gamma_1' + m_{02}\gamma_2' = m_{01}\gamma + m_{02} \text{ (energy)} \quad \dots (2)$$

$$p_2'^2 = p_1'^2 + p_1'^2 - 2p_1p_1'\cos\theta_1; \quad p_{1x} = p_1 \text{ (momentum)} \quad \dots (2'1)$$

and

$$p_1'^2 = p_1'^2 + p_2'^2 - 2p_1p_2'\cos\theta_2 \text{ (momentum)} \quad \dots (2'2)$$

Eqs. (2'1) and (2'2) may be transformed to

$$\gamma_2'^2 - 1 = \left(\frac{m_{01}}{m_{02}}\right)^2 (\gamma^2 + \gamma_1'^2 - 2) - 2\left(\frac{m_{01}}{m_{02}}\right)^2 \sqrt{(\gamma^2 - 1)(\gamma_1'^2 - 1)} \cos\theta_1 \quad \dots (2'3)$$

and

$$\gamma_1'^2 - 1 = \gamma^2 - 1 + \left(\frac{m_{02}}{m_{01}}\right)^2 (\gamma_2'^2 - 1) - 2\left(\frac{m_{02}}{m_{01}}\right) \sqrt{(\gamma^2 - 1)(\gamma_2'^2 - 1)} \cos\theta_2 \dots (2'4)$$

On eliminating γ_2' from (2) and (2'3) and then solving the quadratic equation in γ_1' we get

$$\gamma_1' = \frac{-\left(1 + \frac{m_{02}}{m_{01}}\gamma\right)\left(\gamma + \frac{m_{02}}{m_{01}}\right) \pm (\gamma^2 - 1)\cos\theta_1 \sqrt{\cos^2\theta - 1 + \{m_{02}^2/m_{01}^2\}}}{(\gamma^2 - 1)\cos^2\theta_1 - \left(\gamma + \frac{m_{02}}{m_{01}}\right)^2} \quad \dots (2'5)$$

Similarly on eliminating γ_1' from (2) and (2'4) and then solving the quadratic equation in γ_2' we get

$$\gamma_2' = \frac{\left(\gamma + \frac{m_{02}}{m_{01}}\right)^2 + (\gamma^2 - 1)\cos^2\theta_2}{\left(\gamma + \frac{m_{02}}{m_{01}}\right) - (\gamma^2 - 1)\cos^2\theta_2} \quad \dots (2'6)$$

Case I :— $m_{01} = m_{02}$ (relativistic). We have from (2'5) and (2'6)

$$\left. \begin{aligned} \gamma_1' &= \frac{1 + \gamma + (\gamma - 1)\cos^2\theta_1}{1 + \gamma - (\gamma - 1)\cos^2\theta_1} \\ \gamma_2' &= \frac{1 + \gamma + (\gamma - 1)\cos^2\theta_2}{1 + \gamma - (\gamma - 1)\cos^2\theta_2} \end{aligned} \right\} \quad \dots (2'7)$$

Case II :— $m_{02} \gg m_{01}$. We have from (2'5) and (2'6)

$$\left. \begin{aligned} \gamma_1' &= \gamma \\ \gamma_2' &= 1 \end{aligned} \right\} \quad \dots (2'8)$$

Case III :— $m_{01} \neq m_{02}$ (non-relativistic). We have from (2'5) and (2'6)

$$\left. \begin{aligned} \gamma_1' &= 1 \\ \gamma_2' &= 1 \end{aligned} \right\} \quad \dots (2'9)$$

Now, on using the relativistic relations between momenta in C- and L-systems and remembering that $p_{1x}^{*'} = p_1^{*'}\cos\theta_1^*$, $p_{1z}^{*'} = p_1^{*'}\sin\theta_1^*$, $p_{1x}' = p_1'\cos\theta_1$, $p_{1z}' = p_1'\sin\theta_1$ and similarly for the second particle, we have

$$\left. \begin{aligned} \cot\theta_1^* &= \gamma^* \left(\cot\theta_1 - \frac{u}{c} \operatorname{cosec}\theta_1 \cdot \frac{\gamma_1'}{\sqrt{\gamma_1'^2 - 1}} \right) \\ \cot\theta_2^* &= \gamma^* \left(\cot\theta_2 - \frac{u}{c} \operatorname{cosec}\theta_2 \cdot \frac{\gamma_2'}{\sqrt{\gamma_2'^2 - 1}} \right) \end{aligned} \right\} \quad \dots (3)$$

These are general relations which may be transformed into simpler forms for the three special cases, by substituting the corresponding values of γ_1' and γ_2' obtained before. However, the second equation of (3) may be reduced to the following form without any simplifying assumption. On substituting the general value of u from (1'1) and that of $\frac{\gamma_2'}{\sqrt{\gamma_2'^2 - 1}}$ from (2'6) we have after easy transformation

$$\cot\theta_2^* = \gamma^* \left(\cot\theta_2 - \frac{1}{2} \frac{u^2}{c^2} \cot\theta_2 \right). \quad \dots (3'1)$$

After easy trigonometric transformations we have

$$\sin\theta_2^* = \gamma^* \cdot \frac{\sin 2\theta_2}{\cos^2\theta_2 + \gamma^* \sin^2\theta_2} \quad \dots (3'2)$$

$$\theta_2^* = \frac{\cos^2 \theta_2 - \gamma^{*2} \sin^2 \theta_2}{\cos^2 \theta_2 + \gamma^{*2} \sin^2 \theta_2} \quad \dots \quad (3.3)$$

$$\sin \theta_2^* d\theta_2^* = \sin 2\theta_2 d\theta_2 \frac{2\gamma^{*2}}{(\cos^2 \theta_2 + \gamma^{*2} \sin^2 \theta_2)^2} \quad \dots \quad (3.4)$$

These relations have been obtained by Möller (*l.c.*) for the special case $m_{01} = m_{02}$. But it is evident that Eqs. (3.1)–(3.4) are perfectly general for the second particle.

Case I :— $m_{01} = m_{02}$ (relativistic). On substituting the value of γ_1' from (2.7) in (3) we get for the first particle

$$\cot \theta_1^* = \gamma^* (\cot 2\theta_1 - \frac{1}{2}(u^2/c^2) \cot \theta_1) \quad \dots \quad (3.5)$$

and so after trigonometric transformations

$$\sin \theta_1^* = \gamma^* \frac{\sin 2\theta_1}{\cos^2 \theta_1 + \gamma^{*2} \sin^2 \theta_1} \left\{ \begin{array}{l} \dots \quad (3.6) \\ \text{etc., etc.} \end{array} \right.$$

as obtained by Möller. The corresponding relations for the second particle are perfectly general and are already given in (3.2)–(3.4).

For non-relativistic case $\gamma^* = 1$ and from (3.6) $\theta_1^* = 2\theta_1$ and similarly $\theta_2^* = 2\theta_2$.

Case II :— $m_{02} \gg m_{01}$. Using the conditions (1.4) for this case we have at once from (3)

$$\theta_1^* = \theta_1, \quad \dots \quad (3.7)$$

which also follows from the fact that in this case C- and L- systems are identical. Now, because for the second particle $\gamma_2' = 1$ (*vide* (2.8)), the second equation of (3) cannot be used in this case. We get from any of Eqs. (3.1)–(3.3)

$$\theta_2^* = 2\theta_2. \quad \dots \quad (3.8)$$

It should be noted that in this case the second particle is at rest. So θ_2^*, θ_2 represent the direction in which the momentum is imparted to the second particle by the first.

Case III :— $m_{01} \neq m_{02}$ (non-relativistic). Because in this case from (2.9) we find $\gamma_1' = 1$ to a first approximation, we have to take the second approximation value to evaluate

$$\frac{\gamma_1'}{\sqrt{\gamma_1'^2 - 1}}$$

in (3). We have then

$$\gamma_1' + 1 = 2 \text{ to a first approx.}$$

$$\gamma_1' - 1 = \frac{1}{2} (v^2/c^2) \frac{\{\cos \theta_1 \mp \sqrt{\cos^2 \theta_1 - 1 + (m_{02}^2/m_{01}^2)}\}^2}{[1 + (m_{02}/m_{01})]^2}$$

to a second approx. from (2.5)

Hence, we have

$$\frac{\gamma_1'}{\sqrt{\gamma_1'^2 - 1}} = (c/v) \cdot \frac{1 + (m_{02}/m_{01})}{\cos \theta_1 \mp \sqrt{\cos^2 \theta_1 - 1 + (m_{02}^2/m_{01}^2)}} \quad \dots (3.9)$$

and so from (3)

$$\cot \theta_1^* = \cot \theta_1 - \frac{\operatorname{cosec} \theta_1}{\cos \theta_1 \mp \sqrt{\cos^2 \theta_1 - 1 + (m_{02}^2/m_{01}^2)}}, \quad \dots (3.10)$$

or, after trigonometric transformations

$$\sin \theta_1^* = \sin \theta_1 \cdot (m_{01}/m_{02}) \{ \cos \theta_1 \mp \sqrt{\cos^2 \theta_1 - 1 + (m_{02}^2/m_{01}^2)} \} \quad \dots (3.11)$$

$$\cos \theta_1^* = (m_{01}/m_{02}) \{ -\sin^2 \theta_1 \mp \cos \theta_1 \sqrt{\cos^2 \theta_1 - 1 + (m_{02}^2/m_{01}^2)} \} \quad \dots (3.12)$$

Therefore, we have

$$\theta_1^* = \theta_1 + \sin^{-1} [(m_{01}/m_{02}) \sin \theta_1], \quad (3.13)$$

which is the formula derived by Kar (1941). For the second particle we get immediately from (3.1)–(3.3)

$$\theta_2^* = 2\theta_2 \quad \dots (3.14)$$

the same as (3.8) of case II. For $m_{01} = m_{02}$, (3.13) gives $\theta_1^* = 2\theta_1$ while for $m_{02} \gg m_{01}$, $\theta_1^* = \theta_1$.

We shall next find the angle between the paths traced by the scattered and scattering particles after collision in C- and L-systems. This will be useful in the theory of scattering to be discussed in Sec. B.

From conservation of momentum in C-system (*vide* Eq. (1)) we have

$$\left. \begin{aligned} p_{1x}^* + p_{2x}^* &= 0 \\ p_{1z}^* + p_{2z}^* &= 0 \end{aligned} \right\} \quad \dots (4)$$

From (4) we get

$$\tan \theta_2^* = \tan \theta_1^* \quad \dots (4.1)$$

Or, we have

$$\theta_2^* = \theta_1^* + 180^\circ \quad \dots (4.2)$$

which is evidently a general relation. So we need not consider the three special cases. The relation between θ_1 and θ_2 may be easily obtained by solving the triangle of momentum in L-system. We have

$$\frac{p_1}{\sin(\theta_1 + \theta_2)} = \frac{p_1'}{\sin \theta_2} = \frac{p_2'}{\sin \theta_1} \quad \dots (4.3)$$

Because $p_1 = m_{01}c\sqrt{\gamma^2 - 1}$, etc., we have from (4.3)

$$\sin \theta_1 \cot \theta_2 + \cos \theta_1 = \sqrt{\frac{\gamma^2 - 1}{\gamma_1'^2 - 1}} \quad \dots (4.4)$$

in which the general value of γ_1' should be taken from (2.5).

Case I :— $m_{01} = m_{02}$ (relativistic). On substituting the value of γ_1' from (2.7) in (4.4) we get

$$\sqrt{\frac{\gamma^2 - 1}{\gamma_1'^2 - 1}} = \frac{1 + \gamma - (\gamma - 1) \cos^2 \theta_1}{2 \cos \theta_1}$$

Hence from (4.4) we have

$$\cot \theta_2 = \frac{\gamma + 1}{2} \tan \theta_1 \quad \dots (4.5)$$

For non-relativistic case $\gamma \rightarrow 1$, so that

$$\theta_1 + \theta_2 = 90^\circ \quad \dots (4.6)$$

Case II :— $m_{02} \gg m_{01}$. In this case γ_1' is given in (2.8), so that the right hand side of (4.4) becomes unity. Hence after easy trigonometric transformations we have

$$\theta_2 + (\theta_1/2) = 90^\circ \quad \dots (4.7)$$

This also follows from the geometry. It should be of course noted here that the second particle is at rest, so that θ_2 gives the direction of the momentum imparted to it.

Case III :— $m_{01} \neq m_{02}$ (non-relativistic). In this case $\gamma = 1$, $\gamma_1' = 1$ to first approximation. So to evaluate the right hand side of (4.4) we have to use the second approximation values of γ_1' (*vide* (3.9)) and γ . We have

$$\sqrt{\frac{\gamma^2 - 1}{\gamma_1'^2 - 1}} = \frac{1 + (m_{02}/m_{01})}{\cos \theta_1 + \sqrt{\cos^2 \theta_1 - 1 + (m_{02}^2/m_{01}^2)}} \quad \dots (4.8)$$

the negative sign in (3.9) being rejected as it gives zero value for the momentum in the case $m_{01} = m_{02}$. On combining (4.4) and (4.8) and after easy trigonometric transformations, we have

$$\cot (\theta_1 + \theta_2) = \frac{(m_{02}/m_{01}) \cot \theta_1 - \operatorname{cosec} \theta_1 \sqrt{\cos^2 \theta_1 - 1 + (m_{02}^2/m_{01}^2)}}{1 + (m_{02}/m_{01})} \quad \dots (4.9)$$

giving (i) $\theta_1 + \theta_2 = 90^\circ$ for $m_{01} = m_0$ and (ii) $\theta_2 + \theta_1/2 = 90^\circ$ for $m_{02} \gg m_{01}$, as obtained before in (4.6) and (4.7)

The energies of Colliding particles in C- and L-systems

From the relativistic equations given before, we find for the energies of the first and second particles in C-system before collision,

$$\begin{aligned} E_1^* &= m_{01} \gamma^* (c^2 - uv) \\ E_2^* &= m_{02} \gamma^* c^2 \end{aligned} \quad (5)$$

Using the general value of u given in (1.1), we have from (5), for the total energy in C-system

$$E^* = E_1^* + E_2^* = m_{01} \gamma^* c^2 \frac{1 + 2\gamma(m_{02}/m_{01}) + (m_{02}/m_{01})^2}{\gamma + (m_{02}/m_{01})} \quad (5.1)$$

Case I :— $m_{01} = m_{01} = m_0$ (relativistic). From the value of u' given in (1.3) it may be easily shown that

$$\gamma(1 - uv/c^2) \sim 1$$

to second approximation. Thus from (5)

$$E_1^* = E_2^* = m_0 \gamma^* c^2 \quad \dots (5.2)$$

also from (5.1)

$$E^* = 2m_0 \gamma^* c^2 \quad \dots (5.3)$$

Hence for the non-relativistic case $E^* = 2E_1^* = 2E_2^* = \frac{1}{2}m_0 v^2$.

Case II :— $m_{02} \gg m_{01}$. From (1.4) and (5) we have

$$\begin{aligned} E_1^* &= m_{01} \gamma c^2 \\ E_2^* &= m_{02} c^2 \end{aligned} \quad (5.4)$$

The total energy may be obtained from (5.1) by taking values up to second approximation or from (5.4) by addition. For the non-relativistic case, we have from (5.4)

$$\begin{aligned} E_1^* &= \frac{1}{2} m_{01} v^2 \\ E_2^* &= 0 \end{aligned} \quad \dots (5.5)$$

Case III :— $m_{01} \neq m_{02}$ (non-relativistic). From (1.5) and (5) we have

$$\begin{aligned} E_1^* &= \frac{1}{2} m_{02} / (m_{01} + m_{02}) \cdot \mu v^2 \\ E_2^* &= \frac{1}{2} m_{01} / (m_{01} + m_{02}) \cdot \mu v^2 \end{aligned} \quad \dots (5.6)$$

where $\mu = m_{01} m_{02} / (m_{01} + m_{02})$. The total energy may be obtained from (5.6) or by subtracting the total rest energy, i.e., $(m_{01} + m_{02})c^2$ from (5.1) and we have

$$E^* = E_1^* + E_2^* = \frac{1}{2} \mu v^2 \quad \dots (5.7)$$

Next we proceed to find the energies in C- and L-systems after collision. We have for the general values of energy in L-system

$$\begin{aligned} E_1' &= m_{01} \gamma_1' c^2 \\ E_2' &= m_{02} \gamma_2' c^2 \end{aligned} \quad \dots (6)$$

where γ_1' and γ_2' are given in (2.5) and (2.6). The total energy may be obtained by adding the energies given in (6) and substituting the values of γ_1' , γ_2' . This is a laborious method. We may, however, get it directly from the principle of conservation of energy

$$E_1' + E_2' = E_1 + E_2 = m_{01} c^2 \left(\gamma + \frac{m_{02}}{m_{01}} \right). \quad \dots (6.1)$$

The energy of the second particle may also be expressed in the form

$$E_2' = m_{02}c^2 \cdot \frac{p^2 \cos^2 \theta_2 + m_{01}^2 c^2 \left(\gamma + \frac{m_{02}}{m_{01}} \right)^2}{m_{01}^2 c^2 \left(\gamma + \frac{m_{02}}{m_{01}} \right)^2 - p^2 \cos^2 \theta_2}, \quad \dots (6.2)$$

where $p = m_{01}c \sqrt{\gamma^2 - 1}$ (momentum).

Case I.— $m_{01} = m_{02}$ (relativistic). The values of E_1' , E_2' may be obtained from (6) by substituting the values of γ_1' , γ_2' from (2.7). It may be easily shown that in this case the colliding particle loses energy. Thus the scattering is *inelastic*. It should be noted that the values of E_1' , E_2' may also be obtained directly from the reciprocal relativistic equations, when E_1^* , E_2^* , p_1^* , p_2^* are known. We have

$$\left. \begin{aligned} E_1' &= m_0 c^2 [\gamma^{*2} + (\gamma^{*2} - 1) \cos \theta_1^*] \\ E_2' &= m_2 c^2 [\gamma^{*2} - (\gamma^{*2} - 1) \cos \theta_2^*] \end{aligned} \right\} \quad \dots (6.3)$$

Case II.— $m_{02} \gg m_{01}$. We have from (6) and (2.8)

$$\left. \begin{aligned} E_1' &= m_{01} \gamma c^2 \\ E_2' &= m_{02} c^2 \end{aligned} \right\} \quad \dots (6.4)$$

Thus the energies of the particles are same as before collision and so the scattering is *elastic*.

Case III.— $m_{01} \neq m_{02}$ (non-relativistic). The energy of the first particle is in this case

$$E_1' = m_{01} c^2 (\gamma_1' - 1) \quad \dots (6.5)$$

On substituting the value of γ_1' from (2.7) and after simplification, we get

$$E_1' = \frac{1}{2} m_{01} v^2 \cdot \frac{\left\{ \cos \theta_1 \mp \sqrt{\cos^2 \theta_1 - 1 + \frac{m_{02}^2}{m_{01}^2}} \right\}}{1 + \frac{m_{02}}{m_{01}}} \quad \dots (6.6)$$

where the minus sign should be rejected as it gives zero energy for $m_{01} = m_{02}$. For the special case $m_{01} = m_{02}$ we have from (6.6)

$$E_1' = \frac{1}{2} m_0 v^2 \cos^2 \theta_1 \quad \dots (6.7)$$

and consequently the loss of energy is

$$\Delta E_1' = \frac{1}{2} m_0 v^2 \sin^2 \theta_1. \quad \dots (6.8)$$

The physical significance of the results in (6.7) and (6.8) may be easily understood. For the second particle we have

$$E_2' = m_{02} c^2 (\gamma_2' - 1). \quad \dots (6.9)$$

This may be taken as the non-relativistic energy or the *relativistic gain* of energy of the second particle. Eq. (6.9) may be easily reduced to [vide (6.2)]

$$E_2' = 2m_{02}c^2 \cdot \frac{p^2 \cos^2 \theta_2}{(m_{01}c\gamma + m_{02}c)^2 - p^2 \cos^2 \theta_2} \quad \dots \quad (6.10)$$

$$\begin{aligned} \text{(Or, because } \gamma &= \frac{(p^2 + m_{01}^2 c^2)^{\frac{1}{2}}}{m_{01}c}, \\ &= 2m_{02}c^2 \cdot \frac{p^2 \cos^2 \theta_2}{[m_{02}c + (p^2 + m_{01}^2 c^2)^{\frac{1}{2}}]^2 - p^2 \cos^2 \theta_2} \quad \dots \quad (6.11) \end{aligned}$$

It is evident from (6.11) that the energy transferred is maximum for $\theta_2 = 0$ i.e., for head on collision. Eq. (6.11) has been given by Rossi and Greisen (1941). Now, because $p < m_{01}c$, (6.10) may be further simplified and we have

$$E_2' = 2m_{02} \cdot \frac{p^2 \cos^2 \theta_2}{(m_{01} + m_{02})^2} = 2m_{02}v^2 \cdot \frac{\cos^2 \theta_2}{\{1 + (m_{02}/m_{01})\}^2} \quad \dots \quad (6.12)$$

For the case $m_{01} = m_{02} = m_0$, (6.12) gives

$$E_2' = \frac{1}{2}m_0 v^2 \cos^2 \theta_2 \quad \dots \quad (6.13)$$

which is easily found to be in agreement with the conclusions arrived at in (6.7) and (6.8) when it is remembered that in the non-relativistic case $\theta_1 + \theta_2 = 90^\circ$. It is thus evident that the maximum angle of scattering for $m_{01} = m_{02}$ is 90° . For the case $m_{02} \gg m_{01}$ we get from (6.12) $E_2' = 0$, as it should be since the second particle is at rest [vide (6.4)].

From the relativistic equations after collision, we find for the energies in C-system

$$\begin{aligned} E_1^* &= \gamma^* (E_1' - u \cos \theta_1 p_1') = m_{01} \gamma^* c^2 \left\{ \gamma_1' - \frac{\sqrt{(\gamma^{*2} - 1)(\gamma_1'^2 - 1)}}{\gamma^*} \right\} \\ E_2^* &= \gamma^* (E_2' - u \cos \theta_2 p_2') = m_{02} \gamma^* c^2 \left\{ \gamma_2' - \frac{\sqrt{(\gamma^{*2} - 1)(\gamma_2'^2 - 1)}}{\gamma^*} \right\} \quad \dots \quad (7) \end{aligned}$$

The total energy after collision may be obtained by adding the two equations in (7). However, it need not be determined, as from the conservation of energy in C-system

$$E_1^* + E_2^* = E_1^* + E_2^* = E^*, \quad \dots \quad (7.1)$$

which is already given in (5.1).

Case I.— $m_{01} = m_{02} = m_0$ (relativistic). We have from (7), (1.3) and (2.7)

$$E_1^* = E_2^* = m_2 \gamma^* c^2, \quad \dots \quad (7.2)$$

as obtained by Möller. Thus the energy of any particle in C-system remains unchanged by collision (vide (5.2)). Or, the collision is elastic in C-system.

Case II.— $m_{02} \gg m_{01}$. We have from (7), (1.5) and (2.9)

$$E_1^* = E_1^* = E_1' = E_1 \quad \dots \quad (7.3)$$

C -system being identical with the L -system in this case.

Case III.— $m_{01} \neq m_{02}$ (non-relativistic). On subtracting $m_{01}c^2$, $m_{02}c^2$ from the two equations in (7) we get after easy transformation

$$\left. \begin{aligned} E_1^{*'} &= E_1^* \\ E_2^{*'} &= E_2^* \end{aligned} \right\} \quad \dots (7.4)$$

where E_1^* , E_2^* are given in (5.6).

Momenta of Colliding particles in C - and L -systems

From the relativistic equations given before, we get the momenta of the first and second particles in C -system before collision (since $p_{1x}^* = p_1^*$, $p_{2x}^* = p_2^*$)

$$p_1^* = -p_2^* = m_{02}\gamma^*u \quad \dots (8)$$

Case I.— $m_{01} = m_{02} = m_0$ (relativistic). We get at once from (8)

$$p_1^* = -p_2^* = m_0\gamma^*u \quad \dots (8.1)$$

Case II.— $m_{02} \gg m_{01}$. Because, when $m_{02} \rightarrow \infty$, $u \rightarrow 0$, the momenta given by (8) is indeterminate. From physical consideration we get it to be m_1v , the initial momenta of the colliding particle.

Case III.— $m_{01} \neq m_{02}$ (non-relativistic). From (8) and (1.5) we have

$$p_1^* = -p_2^* = \mu v \quad \dots (8.2)$$

Next, we proceed to find the momenta after collision in C - and L -systems. We have for the general values of momenta in L -system

$$\left. \begin{aligned} p_1' &= m_{01}c\sqrt{\gamma_1'^2 - 1} \\ p_2' &= m_{02}c\sqrt{\gamma_2'^2 - 1} \end{aligned} \right\} \quad \dots (9)$$

Case I.— $m_{01} = m_{02} = m_0$ (relativistic). On substituting the values of γ_1' , γ_2' from (2.7) we have from (9)

$$\left. \begin{aligned} p_1' &= 2p \cdot \frac{\cos \theta_1}{1 + \gamma - (\gamma - 1)\cos^2 \theta_1} \\ p_2' &= 2p \cdot \frac{\cos \theta_2}{1 + \gamma - (\gamma - 1)\cos^2 \theta_2} \end{aligned} \right\} \quad (9.1)$$

For the non-relativistic case $\gamma \rightarrow 1$ and so $p_1' = p \cos \theta_1$, $p_2' = p \cos \theta_2$. It should be noted that corresponding to (6.3) one may get the values of p_1' , p_2' by using the reciprocal relativistic equations, when $p_1^{*'}$, $p_2^{*'}$, $E_1^{*'}$, $E_2^{*'}$ are known.

Case II.— $m_{02} \gg m_{01}$. From (9) and (2.8) we have

$$p_1' = p,$$

since the collision is elastic. Because from (2.8) $\gamma_2' \rightarrow 1$ we have to take in this case second order values in (9) and we have

$$p_2' = 2p \cos \theta_2 \quad (9.3)$$

which is apparent if the geometry is considered.

Case III.— $m_{01} \neq m_{02}$ (non-relativistic). In this case we have to take second order values and we get from (9)

$$\left. \begin{aligned} p_1' &= p \cdot \frac{\cos \theta_1 + \sqrt{\cos^2 \theta_1 - 1 + (m_{02}^2/m_{01}^2)}}{1 + (m_{02}/m_{01})} \\ p_2' &= \frac{m_{02}}{m_{01} + m_{02}} \cdot 2p \cos \theta_2 \end{aligned} \right\} \dots \quad (9.4)$$

If we take $m_{02} \gg m_{01}$ we have from (9.4) $p_1' = p$, $p_2' = 2p \cos \theta_2$ as in (9.2) and (9.3). If, again, we take $m_{01} = m_{02}$ we have $p_1' = p \cos \theta_1$, $p_2' = p \cos \theta_2$ as in case I.

From the relativistic equations after collision, the momenta in C-system for the three cases may be easily obtained.

Case I :— $m_{01} = m_{02} = m_0$ (relativistic). From the relativistic equations and Eqs. (9.1), (2.7), (3.3) and (3.6) we get

$$\left. \begin{aligned} p_{1x}^{*'} &= m_0 \gamma^* u \cos \theta_1^* \\ p_{2x}^{*'} &= -m_0 \gamma^* u \cos \theta_2^* \end{aligned} \right\} \dots \quad (10)$$

and hence

$$p_1^{*'} = -p_2^{*'} = m_0 \gamma^* u \dots \quad (10.1)$$

as obtained by Möller.

Case II :— $m_{02} \gg m_{01}$. From the relativistic equations and Eq. (6.4) we have

$$\left. \begin{aligned} p_{1x}^{*'} &= p_{1x}' - m_{01}u \\ p_{2x}^{*'} &= p_{2x}' - m_{02}u \end{aligned} \right\} \dots \quad (10.2)$$

Or, we have (*vide* (1.1), (1.4), (9.2) and (9.3))

$$\left. \begin{aligned} p_1^{*'} &= p_1' = p \\ p_2^{*'} &= -p \end{aligned} \right\} \dots \quad (10.3)$$

the sign being determined from the condition of conservation of momentum, *viz.*, $p_1^{*'} + p_2^{*'} = 0$.

Case III :— $m_{01} \neq m_{02}$ (non-relativistic). Because $E_1' = m_{01}c^2 + E_1'$ (non-relativistic) and similarly for E_2' , we get (10.2) in this case also, from the relativistic equations already given neglecting the effect of relativity. Thus on substituting the value of u from (1.5) and those of p_{1x}' , p_{2x}' from (9.4) we get from (10.2)

$$\left. \begin{aligned} p_{1x}^{*'} &= \frac{p}{1 + \{m_{02}/m_{01}\}} \left\{ \cos^2 \theta_1 + \cos \theta_1 \sqrt{\cos^2 \theta_1 - 1 + \{m_{02}^2/m_{01}^2\}} - 1 \right\} \\ p_{2x}^{*'} &= -\frac{m_{02}}{m_{01} + m_{02}} p (2 \cos^2 \theta_2 - 1) \end{aligned} \right\} \quad (10.4)$$

The values of $p_{1x}^{*'}$ and $p_{2x}^{*'}$ may be easily obtained from (9.4) and the relativistic equations. Therefore we get

$$p_{1x}^{*'} = \frac{p}{1 + \{m_{02}/m_{01}\}} \left\{ (\cos \theta_1 + \sqrt{\cos^2 \theta_1 - 1 + \{m_{02}^2/m_{01}^2\}})^2 - 2 \cos \theta_1 (\cos \theta_1 + \sqrt{\cos^2 \theta_1 - 1 + \{m_{02}^2/m_{01}^2\}}) + 1 \right\}^{\frac{1}{2}} \quad \dots (10.5)$$

$$\text{and} \quad p_{2x}^{*'} = -\frac{m_{02}}{m_{01} + m_{02}} p = -\mu v \quad \dots (10.6)$$

Two special cases may now be considered. (a) If $m_{01} = m_{02} = m_0$ we have from (10.5) and (10.6)

$$p_{1x}^{*'} = -p_{2x}^{*'} = \frac{1}{2} p \quad \dots (10.7)$$

which also follows from (10.1) if the correction for relativity is neglected.

(b) If $m_{02} \gg m_{01}$ we have from (10.5) and (10.6)

$$p_{1x}^{*'} = -p_{2x}^{*'} = p \quad \dots (10.8)$$

being the same as (10.3).

Section B. Theory of relativistic Scattering (equal masses)

We are now in a position to discuss the theory of relativistic scattering of a particle by a second particle of the same mass being initially at rest. We shall take the interacting potential to be Coulombian.

Taking $m_{01} = m_{02} = m_0$, we have for the total energy of the particles in L-system

$$E = m_0 c^2 (\gamma + 1). \quad \dots (11)$$

This total energy as it appears to the observer in C-system is

$$E = m_0 \gamma^* c^2 (\gamma + 1). \quad \dots (11.1)$$

It should be noted that it is different from the total energy in C-system, which is from (5.3)

$$E^* = 2m_0 \gamma^* c^2. \quad \dots (11.2)$$

Now, if E_t is the total energy, as it appears to the observer in C-system, at the centre of gravity, we have

$$E_t = \frac{1}{2} (E - E^*) = \frac{1}{2} m_0 \gamma^* c^2 (\gamma - 1). \quad \dots (11.3)$$

On the other hand, because the total mass at *c.g.* for the observer in C-system is $m_0\gamma^*(\gamma+1)$, we have also

$$E_1 = \frac{1}{2}m_0\gamma^*(\gamma+1)u^2, \quad \dots (11.4)$$

where u is the velocity of C-system being equal to $c\sqrt{\frac{\gamma-1}{\gamma+1}}$ (*vide* (1.3)). On substituting this value of u in (11.4) we get the same result as in (11.3).

Now, to the observer in C-system the relativistic χ -equations for the two particles are

$$\left. \begin{aligned} \Delta_1\chi_1 + \frac{4\pi^2}{h^2c^2}\{(E_1 - V)^2 - E_0^2\}\chi_1 &= 0 \\ \Delta_2\chi_2 + \frac{4\pi^2}{h^2c^2}\{(E_2 - V)^2 - E_0^2\}\chi_2 &= 0 \end{aligned} \right\} \quad \dots (12)$$

$$\text{where } \Delta_1 = \frac{d^2}{dx_1^2} + \frac{d^2}{dy_1^2} + \frac{d^2}{dz_1^2}, \Delta_2 = \frac{d^2}{dx_2^2} + \frac{d^2}{dy_2^2} + \frac{d^2}{dz_2^2}, E_1 = m_0\gamma\gamma^*c^2,$$

$$E_2 = E_0 = m_0\gamma^*c^2.$$

In the relativistic theory of scattering we neglect V^2 -term within $\{ \}$ -bracket, to a first approximation. And so (12) may be written in the form

$$\left. \begin{aligned} \Delta_1\chi_1 + \frac{4\pi^2}{h^2c^2}E_1\left(E_1 - \frac{E_0^2}{E_1} - 2V\right)\chi_1 &= 0 \\ \Delta_2\chi_2 + \frac{4\pi^2}{h^2c^2}E_2\left(E_2 - \frac{E_0^2}{E_2} - 2V\right)\chi_2 &= 0 \end{aligned} \right\} \quad \dots (12.1)$$

On substituting for E_1, E_2 we have

$$\left. \begin{aligned} \frac{h^2}{4\pi^2m_0\gamma\gamma^*} \cdot \Delta_1\chi_1 + \left(E_1 - \frac{E_0^2}{E_1} - 2V\right)\chi_1 &= 0 \\ \frac{h^2}{4\pi^2m_0\gamma^*} \cdot \Delta_2\chi_2 + \left(E_2 - \frac{E_0^2}{E_2} - 2V\right)\chi_2 &= 0 \end{aligned} \right\} \quad \dots (12.2)$$

Because the total wave function $\Psi = \chi_1\chi_2$, where χ_1, χ_2 are functions of x_1, x_2 respectively, (12.2) takes the form

$$\frac{h^2}{4\pi^2m_0\gamma\gamma^*} \Delta_1\Psi + \frac{h^2}{4\pi^2m_0\gamma^*} \Delta_2\Psi + \left(E - \frac{E_0^2}{E_1} - \frac{E_0^2}{E_2} - 2V\right)\Psi = 0 \quad \dots (12.3)$$

where $E = E_1 + E_2$. Or, after substituting the values of E ...etc.,

$$\frac{h^2}{4\pi^2m_0\gamma\gamma^*} \Delta_1\Psi + \frac{h^2}{4\pi^2m_0\gamma^*} \Delta_2\Psi + \left(m_0c^2\gamma^* \cdot \frac{\gamma^2-1}{\gamma} - 2V\right)\Psi = 0 \quad \dots (12.4)$$

Let us take Ψ , the joint wave statistical probability for both the particles, as the product

$$\Psi = \psi\chi \quad \dots (12.5)$$

where ψ is a function of (ξ, η, ζ) the coordinates of the centre of gravity and χ is a function of x, y, z , in which

$$\begin{aligned}x &= x_1 - x_2, \quad m_0 \gamma^* (\gamma + 1) \xi = m_0 \gamma^* \gamma x_1 + m_0 \gamma^* x_2 \\y &= y_1 - y_2, \quad m_0 \gamma^* (\gamma + 1) \eta = m_0 \gamma^* \gamma y_1 + m_0 \gamma^* y_2\end{aligned}$$

Thus, we have

$$\begin{aligned}\frac{\partial}{\partial x_1} &= \frac{\partial}{\partial x} + \frac{\gamma}{\gamma + 1} \frac{\partial}{\partial \xi}, \quad \frac{\partial}{\partial x_2} = -\frac{\partial}{\partial x} + \frac{1}{\gamma + 1} \frac{\partial}{\partial \xi} \\ \frac{\partial^2}{\partial x_1^2} &= \frac{\partial^2}{\partial x^2} + \left(\frac{\gamma}{\gamma + 1} \right)^2 \frac{\partial^2}{\partial \xi^2} + 2 \frac{\gamma}{\gamma + 1} \frac{\partial^2}{\partial x \partial \xi} \\ \frac{\partial^2}{\partial x_2^2} &= \frac{\partial^2}{\partial x^2} + \frac{1}{(\gamma + 1)^2} \frac{\partial^2}{\partial \xi^2} - 2 \frac{1}{\gamma + 1} \frac{\partial^2}{\partial x \partial \xi}\end{aligned}$$

Hence in terms of the new variables x, ξ the wave equation (12.4) transforms into

$$\frac{h^2 (\gamma + 1)}{4\pi^2 m_0 \gamma \gamma^*} \Delta_x \chi \cdot \psi + \frac{h^2}{4\pi^2 m_0 \gamma^* (\gamma + 1)} \Delta_\xi \psi \cdot \chi + \left(m_0 c^2 \gamma^* \frac{\gamma^2 - 1}{\gamma} - 2V \right) \chi \psi = 0 \dots (12.6)$$

$$\text{where } \Delta_x = \frac{\partial^2}{\partial x^2} + \frac{\partial^2}{\partial y^2} + \frac{\partial^2}{\partial z^2} \text{ and } \Delta_\xi = \frac{\partial^2}{\partial \xi^2} + \frac{\partial^2}{\partial \eta^2} + \frac{\partial^2}{\partial \zeta^2}.$$

On dividing the above equation by $\chi \psi$ the variables are completely separated. Since V the interaction potential, depends on the mutual distance, it should be taken with χ . Thus we have for ψ and χ equations

$$\left. \begin{aligned} \Delta_\xi \psi + \frac{4\pi^2 m_0 \gamma^* (\gamma + 1)}{h^2} \lambda \psi &= 0 \\ \Delta_x \chi + \frac{4\pi^2 m_0 \gamma \gamma^*}{h^2 (\gamma + 1)} \left(m_0 c^2 \gamma^* \frac{\gamma^2 - 1}{\gamma} - \lambda - 2V \right) \chi &= 0 \end{aligned} \right\} \dots (12.7)$$

where λ is a constant. From elementary principles of wave-statistics, it follows that the frequency and velocity of ψ -waves are

$$\nu = \frac{2E_\psi}{h} = \frac{m_0 \gamma^* c^2 (\gamma - 1)}{h} \text{ from (11.3)}$$

and

$$v \equiv u = c \sqrt{\frac{\gamma - 1}{\gamma + 1}}$$

and that the ψ -equation should be

$$\Delta_\xi \psi + \frac{4\pi^2 \nu^2}{v^2} \psi = 0 \dots (12.8)$$

Or, on substituting for ν and v

$$\Delta_\xi \psi + \frac{4\pi^2 m_0^2 \gamma^* c^2 (\gamma^2 - 1)}{h^2} \psi = 0 \dots (12.9)$$

On comparing (12.7) and (12.9) we get

$$\lambda = m_0 \gamma^* c^2 (\gamma - 1), \dots (13).$$

Hence from (12.7)

$$\Delta_x \chi + \frac{4\pi^2 m_0 \gamma \gamma^*}{h^2 (\gamma + 1)} \left(m_0 c^2 \gamma^* \frac{1}{\gamma} - 2V \right) \chi = 0 \quad \dots (13.1)$$

which gives the wave function within the potential field. Outside the potential it becomes

$$\Delta_x \chi_0 + k^2 \chi_0 = 0; \quad k^2 = \frac{4\pi^2}{h^2} \cdot \frac{m_0^2 \gamma^* c^2 (\gamma - 1)}{\gamma + 1} \quad \dots (13.2)$$

On proceeding in the usual manner we have for the differential equation of the first order scattering function

$$\Delta_x (\lambda_1 \chi_1) + k^2 (\lambda_1 \chi_1) = \frac{8\pi^2}{h^2} \cdot \frac{m_0 \gamma \gamma^*}{\gamma + 1} V \chi_0 \quad (13.3)$$

On solving it in the usual way (Kar and others, 1937) we have for the scattering function

$$\lambda_1 \chi_1 = - \frac{\gamma}{2m_0 c^2 (\gamma - 1) \gamma^*} \operatorname{cosec}^2 \frac{1}{2} \theta^* \frac{1}{\sqrt{v}} \cdot \frac{e^{i k r}}{r} F(r_0) \quad (13.4)$$

where for Coulomb repulsive force $F(r_0) = e^2 \cos k' r_0$, $k' = 2k \sin \frac{1}{2} \theta^*$, k being given in (13.2).

Because in the present case the two colliding particles are indistinguishable we have to consider the effect of exchange. In so doing we shall not introduce new symbols but shall only use 'dash' and 'double dash' for notations which are functions of θ^* . In these new notations we have for the scattering functions before and after exchange (*vide* (4.2))

$$\left. \begin{aligned} \lambda_1 \chi_1' &= - \frac{e^2 \gamma}{2m_0 c^2 (\gamma - 1) \gamma^*} \operatorname{cosec}^2 \frac{1}{2} \theta^* \frac{1}{\sqrt{v}} \cdot \frac{e^{i k' r}}{r} \cos k' r_0' \\ \lambda_1 \chi_1'' &= - \frac{e^2 \gamma}{2m_0 c^2 (\gamma - 1) \gamma^*} \sec^2 \frac{1}{2} \theta^* \frac{1}{\sqrt{v}} \cdot \frac{e^{i k'' r}}{r} \cos k'' r_0'' \end{aligned} \right\} \quad \dots (13.5)$$

where

$$\left. \begin{aligned} k' &= 2k \sin \frac{1}{2} \theta^* \\ k'' &= 2k \cos \frac{1}{2} \theta^* \end{aligned} \right\} \quad \dots (13.6)$$

and r_0' , r_0'' the critical approaches before and after exchange are given by

$$\left. \begin{aligned} r_0' &= 2.7 \times \frac{c^2}{2m_0 v^2} \sqrt{\frac{2(\gamma + 1)}{\gamma^2}} (\operatorname{cosec} \frac{1}{2} \theta^* + 1) \\ r_0'' &= 2.7 \times \frac{c^2}{2m_0 v^2} \sqrt{\frac{2(\gamma + 1)}{\gamma^2}} (\sec \frac{1}{2} \theta^* + 1) \end{aligned} \right\} \quad (13.7)$$

On considering the effects of spin and exchange in the usual way (Kar, 1942) we get for the total relative intensity of scattering after substituting for γ^* from (1.3)

$$\begin{aligned} I &= 2\pi \left(\frac{e^2}{2m_0 v^2} \right)^2 \cdot \frac{2(\gamma + 1)}{\gamma^2} \left[\operatorname{cosec}^4 \frac{1}{2} \theta^* \cos^2 k' r_0' + \sec^4 \frac{1}{2} \theta^* \cos^2 k'' r_0'' \right. \\ &\quad \left. - \operatorname{cosec}^2 \frac{1}{2} \theta^* \sec^2 \frac{1}{2} \theta^* \cos k' r_0' \cos k'' r_0'' \right] \sin \theta^* d\theta^* \quad \dots (13.8) \end{aligned}$$

After simple trigonometric transformations it may be written in the form

$$I = 8\pi \left(\frac{e^2}{2m_0 v^2} \right)^2 \cdot \frac{2(\gamma + 1)}{\gamma^2} f(\theta^*, r_0', r_0'') \sin \theta^* d\theta^* \quad \dots (13.9)$$

where

$$f(\theta^*, r_0', r_0'') = \frac{2(\cos^2 k' r_0' + \cos^2 k'' r_0'')}{\sin^4 \theta^*} - \frac{\cos^2 k' r_0' + \cos^2 k'' r_0'' + \cos k' r_0' \cos k'' r_0''}{\sin^2 \theta^*} + \frac{2 \cot \theta^*}{\sin^3 \theta^*} (\cos^2 k' r_0' - \cos^2 k'' r_0'') \dots (13.10)$$

Neglecting the wave statistical correction for the critical approach, we have from (13.10)

$$f(\theta^*) = \frac{4}{\sin^4 \theta^*} - \frac{3}{\sin^2 \theta^*} \quad \dots (13.11)$$

which is Möller's formula without his spin correction term. Thus our formula (13.9) for the relative intensity of scattering takes into account the wave statistical correction for the critical approach but is free, to this order of accuracy, from the effect of spin-orbit interaction. It becomes in the laboratory coordinates

$$I = 64\pi \left(\frac{e^2}{2m_0 v^2} \right)^2 \cdot \left(\frac{\gamma + 1}{\gamma} \right)^2 \cdot \frac{f(\theta^*) \sin \theta d\theta}{(1 + \cos^2 \theta + \gamma \sin^2 \theta)^2} \quad \dots (14)$$

Now, in order to verify (14) with the help of the observations of Champion (1932) in Wilson chamber, it would be necessary to write it in the following form. If l be the total track length and N_0 the number of scattering centres per unit volume, we have for N_θ the number of scattered β -particles observed at an angle between θ and $\theta + d\theta$ in laboratory coordinates

$$N_\theta = 64\pi \left(\frac{e^2}{2m_0 v^2} \cdot \frac{\gamma + 1}{\gamma} \right)^2 \cdot \frac{N_0 l f(\theta^*) \sin 2\theta d\theta}{(1 + \cos^2 \theta + \gamma \sin^2 \theta)^2} \quad \dots (14.1)$$

As l in Champion's experiments denotes the total track length for the whole range of β -ray spectrum used and as the number of β particles incident at different velocities is different we are to multiply (14.1) by yet another factor n_β denoting the fraction of β -particles incident with velocities lying within the range of velocities $c\beta$ and $c(\beta + d\beta)$. Thus we have finally

$$N_\theta = 64\pi N_0 n_\beta \left(\frac{e^2}{2m_0 v^2} \cdot \frac{\gamma + 1}{\gamma} \right)^2 \cdot \frac{f(\theta^*) \sin 2\theta d\theta}{(1 + \cos^2 \theta + \gamma \sin^2 \theta)^2} \quad \dots (14.2)$$

giving the number scattered for given velocity of incidence of the β -particles and for the angular range θ and $\theta + d\theta$ in laboratory coordinates.

In the following table are compared the theoretical values from different formulae with the experimental values of Champion (1932). In the second column are given the observations of Champion for different angular ranges. In the third, fourth and fifth columns respectively are given the theoretical values from our formula (14.2) and the formulae of Möller and Mott. The theoretical values in the last two columns are taken from Champion's paper (1932). The

TABLE I

Angle θ	Observed	From formula (14.2)	Möller	Mott
10°—20°	214	215	230	650
23°—30°	26	26.7	30	105
30°—max	10	9.7	13	28
Total	250	251.4	273	783

theoretical values from (14.2) for different angular ranges have been calculated by integrating (14.2) by the graphical method. Unfortunately, however, in Champion's paper cited above the value of N_0 is not given. Accordingly, we had to go through the laborious process of finding it by graphically integrating Möller's formula over the different angular ranges and then equating the values thus obtained with the Möller's values given by Champion. The values of n_β for different velocities of incidence has been taken from Champion's previous paper (1932). It should be noted that a formula which takes account of exchange should be minimum at 45°. Of course, due to the effect of relativity the angle is slightly deviated. Thus, for example, when in the Table, the scattering is considered between 10°-20° it is evidently the total including those between the angular range 80°-90°. And so the maximum angle means 45° approximately.

It is evident from the above table that the formula derived by us is in remarkably good agreement with the experimental values. Möller's value is throughout higher than the experimental. The difference between our value and that of Möller is mainly due to his additional spin term, although it is slightly affected by our taking the critical approach. It should be noted that the correction for the critical approach is very small in the present case because of the high velocity of incidence and also because the Coulomb field is small, z being unity. Lastly, it may be mentioned that Mott's value is extremely high because his formula is applicable only for low velocity of incidence where the relativistic effect is negligible.

Section C. Theory of relativistic Scattering (unequal masses)

As, in the present case, the particles are distinguishable one should not consider the effect of exchange. Again, as the matter for discussion in this section may be looked upon as an easy generalisation of our treatment in Sec. B, we shall try to be as brief as possible.

It is evident that for unequal masses (12.3) should take the form

$$\frac{h^2}{4\pi^2 m_{01} \gamma^*} \Delta_1 \Psi + \frac{h^2}{4\pi^2 m_{02} \gamma^*} \Delta_2 \Psi + \left(E - \frac{E_{01}^2}{E_1} - \frac{E_{02}^2}{E_2} - 2V \right) \Psi = 0 \quad \dots (15)$$

On substituting the values of E , E_1 , ... etc., we get from (15)

$$\frac{h^2}{4\pi^2 m_{01} \gamma \gamma^*} \Delta_1 \Psi + \frac{h^2}{4\pi^2 m_{02} \gamma^*} \Delta_2 \Psi + \left(m_{01} \gamma^* c^2 \cdot \frac{\gamma^2 - 1}{\gamma} - 2V \right) \Psi = 0 \quad \dots (15.1)$$

On changing variables as in Sec. B to (x, y, z) and (ξ, η, ζ) where, however,

$$x = x_1 - x_2, \dots \text{etc.}$$

but $\gamma^*(m_{01}\gamma + m_{02})\xi = \gamma^* \gamma m_{01} x_1 + \gamma^* m_{02} x_2, \dots \text{etc.},$

we get corresponding to (12.7)

$$\left. \begin{aligned} \Delta_\xi \psi + \frac{4\pi^2 m_{01} \gamma^* \lambda}{h^2} \left(\gamma + \frac{m_{02}}{m_{01}} \right) \psi &= 0 \\ \Delta_x \chi + \frac{4\pi^2 \gamma \gamma^*}{h^2} \cdot \frac{m_{02}}{\gamma + m_{02}/m_{01}} \left(m_{01} \gamma^* c^2 \cdot \frac{\gamma^2 - 1}{\gamma} - \lambda - 2V \right) \chi &= 0 \end{aligned} \right\} \dots (15.2)$$

Now, the velocity of ψ -wave is

$$v \equiv u = c \cdot \frac{\sqrt{\gamma^2 - 1}}{\gamma + m_{02}/m_{01}} \quad (\text{vide (1.1)}) \quad \dots (15.3)$$

Again, the kinetic energy at the centre of gravity, as it appears to the observer in C -system, is

$$E_t = \frac{1}{2} \gamma^* (m_{01} \gamma + m_{02}) u^2 = \frac{1}{2} m_{01} c^2 \gamma^* (\gamma^2 - 1) \left/ \left(\gamma + \frac{m_{02}}{m_{01}} \right) \right. \quad \dots (15.4)$$

Hence, the frequency of ψ -wave is

$$\nu = \frac{2E_t}{h} = \frac{m_{01} c^2 \gamma^* (\gamma^2 - 1)}{h \left[\gamma + (m_{02}/m_{01}) \right]} \quad \dots (15.5)$$

Thus corresponding to (12.9), we have

$$\Delta_\xi \psi + \frac{4\pi^2 m_{01}^2 \gamma^* c^2 (\gamma^2 - 1)}{h^2} \psi = 0. \quad \dots (15.6)$$

On comparing (15.2) and (15.6) we get

$$\lambda = \frac{m_{01} \gamma^* c^2 (\gamma^2 - 1)}{\gamma + (m_{02}/m_{01})} \quad \dots (15.7)$$

On substituting the above value of λ in (15.2) we have

$$\Delta \chi + \frac{4\pi^2 \gamma \gamma^*}{h^2} \cdot \frac{m_{02}}{\gamma + m_{02}/m_{01}} \left(\frac{m_{02} \gamma^* c^2 (\gamma^2 - 1)}{\gamma (\gamma + m_{02}/m_{01})} - 2V \right) \chi = 0, \quad \dots (15.8)$$

giving the wave function within the potential field. Outside the potential field (15.8) becomes

$$\Delta \chi_0 + k^2 \chi_0 = 0; \quad k^2 = \frac{4\pi^2}{h^2} \cdot \frac{m_{02}^2 \gamma^* c^2 (\gamma^2 - 1)}{[\gamma + (m_{02}/m_{01})]^2} \quad \dots (15.9)$$

Thus proceeding in the usual manner we have for the first order scattering function

$$\lambda_1 \chi_1 = - \frac{\gamma [\gamma + (m_{02}/m_{01})]}{2m_{02} c^2 (\gamma^2 - 1) \gamma^*} \operatorname{cosec}^2 \frac{1}{2} \theta^* \frac{1}{\sqrt{v}} \cdot \frac{e^{ikr}}{r} F(\tau_0), \quad \dots (15.10)$$

with thick yoke ends (Y_1, Y_2). The coils were wound with enamelled copper wire on thin ebonite reels through which rods could be easily inserted and then clamped to the yokes. Two terminals (T_1 & T_2) at the middle of the yoke plates served to carry electrical currents through the iron.

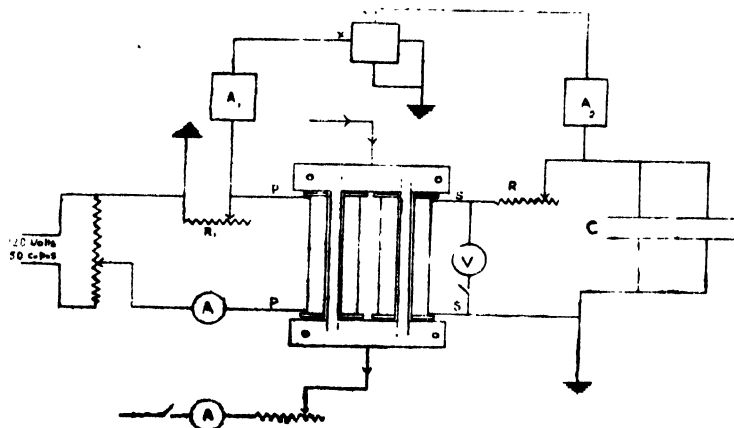


FIG. 1

An adjustable alternating current (50 c.p.s.) from the mains traverses the

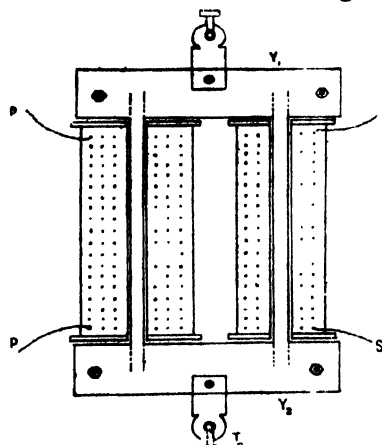


FIG. 2

primary coil and the magnetising field (H), in iron, is proportional to this current. The voltage built up by this primary current in a series resistance (R_1), (Fig. 1), is applied after suitable amplification (A_1) to the X plates of a cathode ray oscilloscope giving a horizontal traverse of the beam. The voltage developed across the terminals of the secondary is proportional to the rate of change of the magnetic flux, and it is therefore necessary to integrate this voltage, in order to get a vertical deflection proportional to (B). Also this secondary voltage is $\pi/2$ out of phase with the primary.

The necessary phase shift and integration

is obtained through a circuit consisting of a suitable condenser along with a

series resistance $\left(R \geq \frac{1}{c\omega}\right)$ connected to the secondary coil.

The voltage across the condenser is $q/c = \int i/c \, dt$. If the reactance of c is made quite small compared with R , then $i = V/R$ and therefore the voltage across the condenser is $\int V/cR \, dt$, as voltage is proportional to dN/dt the above expression is proportional to flux N and thus to induction B . One terminal of the condenser is connected through an amplifier (A_2) to the Y plates giving vertical deflection.

RESULTS

Plate IV (*a*, *b*, *c*) shows the hysteresis loops and the modified contracted ones when direct current of 10, 15 and 20 amps. were sent through. The current traversing each of the core rods would however be half of the above value.

In this series of our experiments the camera was always placed at the same distance from the oscilloscope screen and the amplifier controls were kept in the same position so that both the electrical and optical adjustments were unchanged throughout. The curves, therefore, although they do not give the actual values of the hysteresis loss, etc., provide comparative results from which suitable conclusions can be made.

In a previous investigation by Sarna and others (1943), one of us had used a transformer with a core made of iron strips and with a sectional area of 1 sq. inch. Upon sending a comparatively smaller direct current of 5 amps. no modification of the loop was observable. In the present work using cylindrical rods, 4 mm. diameter, much larger current densities are obtained and also the current distribution is uniform.

The contraction produced in the loop on the passage of currents through the core is instantaneous so that one would infer that it is not a heat effect, also as is seen from the photographs, the modified loop is equally clear as the first one; if however, the changes were due to the heating, a much broadened trace corresponding to the changes of temperatures would be expected. However, in order to prevent any heating of the specimen, we passed the currents for short intervals of time waiting sufficiently between such intervals. Recently Perkins and Doolittle (1941), while examining the effect of longitudinal electric current on the residual magnetism of a permalloy and Norway iron cylindrical rods found that if the rod is initially magnetised beyond a certain minimum value, the passage of the electric currents tends to increase the residual magnetism, instead of decreasing it. They are of the opinion that two effects are produced, one of which operates with striking rapidity tending to increase the residual magnetism, while the second one, which is slower in its action decreases the residual magnetism. The increase in residual magnetism as observed by Perkins and Doolittle or the decrease as observed by us by oscilloscope method may in general be considered as due to the magnetic field of the traversing current through the test rod or by some effect of the current itself on the elementary magnets (as Perkins and Doolittle have supposed) or due to both these causes. Although Ewing has indicated that flowing current will produce an effect similar to mechanical shock or vibration to the material, yet in order to be able to differentiate between the relative effects of electrical current itself and its accompanying magnetic field on the contraction of the hysteresis loop, we modified our experiment by sending the current not through the rod, but through an insulated copper wire running through a bore along the axis of the rod. For this purpose the rods were bored, and inserted in the end plates in the same way as shown in Fig. 2, the bore of the rods being continued through the plates in order to lead the copper wire outside. Now when current is sent through the wire, it produces a circular magnetic field in the iron rod and there is no flow of electrons

tion curve corresponding to the maximum value of $H_0 \sin \omega t$ (i.e., the magnetising field varies between H_0 and $-H_0$) used in the experiment, there will be a corresponding value of the induction B proportional to which, will be the maximum vertical deflection of the electron beam. Thus in a complete cycle we shall get a normal hysteresis curve. However, when an electric current is sent through the specimen rod, then, as shown in Fig. 3, O_5 is the direction in which the magnetisation of the material takes place, instead of OA in the absence of the field OB , O_5 making an angle $\tan^{-1}(OB/OA) \equiv \theta$ with the axis (θ varies from zero at the axis to θ at the surface of the rod). If we represent the magnitude of O_5 as H_r , i.e., the resultant field, and if B' is the induction corresponding to H_r , then in this case, the vertical deflection will be proportional to

$$B' \cos \theta = B' \frac{H_0 \sin \omega t}{H_r} \equiv B' \frac{H_0}{H_r} \quad (\text{corresponding to point P}) \quad (i)$$

(For simplification we have supposed the circular field to be constant throughout the material. However, for the actual case the circular field is zero at the axis and maximum at the surface of the rod. Thus, if we take this into account H_r will vary in direction and magnitude as we proceed from the axis to the periphery and the case will be a bit complicated, the character of the phenomenon, however, remains unaltered.)

If μ is the permeability of the material for the magnetising field H_0 and μ' for H_r , then the expression (i) can be written as

$$\mu' H_r \frac{H_0}{H_r} = \mu' H_0 \quad B' = \mu' H_r$$

Thus whereas the vertical deflection in the first case is proportional to μH_0 , in the second case it is proportional to $\mu' H_0$. Hence the change in induction is

$$\delta B = B' - B = (\mu' - \mu) H_0. \quad \dots (ii)$$

As is clear from the Plate (a, b, c) the maximum value of $H_0 \sin \omega t$ ($\equiv H_0$) corresponds to a point P (Fig. 4), lying on the portion of the magnetisation curve, where the permeability is decreasing, i.e., μ' will be less than μ and hence δB is negative which indicates a decrease in B , as we have observed. The exact value of δB can be determined only, provided we know the magnetisation curve, and the value of the permeability of the material for different fields. However, we have measured the relative values of δB from the photographs which come out to be 12.6, 9.1, 5.9% for the currents of 10, 7.5, 5 amps. We have also measured the areas with a planimeter, of the original and the contracted loops. The values are given below :

Current density	Original area	Contracted area	Contraction produced
5 amps.	4.43 sq. cms.	4.01 sq. cms.	.42 sq. cms.
7.5 "	4.37 "	3.68 "	.69 "
10 "	4.43 "	3.51 "	.92 "

The area of the hysteresis loop progressively decreases with the increasing current density.

In order to explain the increase in residual magnetism [observed by Perkins

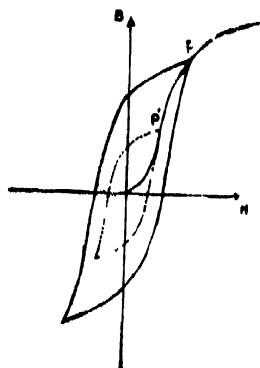


FIG. 4

and Doolittle we consider the hysteresis curve to be traced with the maximum value of $H_0 \sin \omega t$ corresponding to a point P' (Fig. 4) on the portion of the magnetisation curve where the permeability is increasing. Then evidently $\mu' > \mu$ and consequently δB is positive, thus indicating an increase in residual magnetism.

If we consider a point P'' (Fig. 4) on the saturation portion of the magnetisation curve then as the variations in the permeability become very small then for the value of OB of the present order (a few Gauss) μ' does not differ from μ appreciably, and therefore δB will be practically zero, a point which remains to be tested.

SUMMARY

Using Kreiselsheimer's circuit, we have studied the effect of electric current (D.C.) on the hysteresis curve of a specimen of iron. An explanation for the decrease observed by us and the increase observed by Perkins and Doolittle is given on the basis of the variations in the permeability of the material. The qualitative nature of the phenomena is explained.

ACKNOWLEDGMENTS

Our gratitude is due to Professor K. S. Krishnan, F.R.S., for his kindly interest and suggestions about this work. We are deeply indebted to Professor J. B. Seth, I.E.S., for his sympathetic attitude and for the facilities provided.

PHYSICS LABORATORY,
GOVERNMENT COLLEGE,
LAHORE.

REFERENCES

- Ewing, *Magnetic Induction in Iron*, pp. 318.
- Kreiselsheimer, K., 1942, *J. Sci. Inst.*, **19**, 107.
- Perkins and Doolittle, 1941, *Phys. Rev.*, **60**, 811.
- Reyner, *Cathode Ray Oscillographs*.
- Sarna, Kalia and Jai Dial, 1943, *Current Science*, **12**, 251.

MAGNETIC STUDIES ON MOLYBDENITE

BY AJIT KUMAR DUTTA

ABSTRACT. A method for determining the principal magnetic susceptibility in a particular direction of the crystal where the balancing method is not suitable has been developed. The magnetic anisotropy and the principal susceptibilities of molybdenite have been measured. The anisotropy is discussed with the known structure of the crystal.

INTRODUCTION

According to the modern theories of semiconductors (Wilson, 1931, 1932, 1939) the appreciable electrical conductivity exhibited by these crystals at ordinary temperatures is due either to electrons in a nearly empty energy band, or to "holes" in a band nearly filled with electrons. These electrons are furnished by impurity centres in the crystal whence they are thermally excited into the lowest empty band of allowed levels, where these are free to move through the lattice. While the mobile "holes" are likewise created in a nearly full band by electrons being raised from that band to the vacant energy levels which may be present in the impurity atoms, these impurities being due to the stoichiometric excess of one of the constituent elements in the crystal over the other. The former class of semi-conductors are known as "excess conductors," and the latter as "defect conductors." Experimentally this classification is generally effected by the measurement of the Hall Coefficient,—"excess conductors" having negative and "defect conductors" having positive Hall Coefficients. Molybdenite has been found to have a negative Hall effect which means that the current in it is mainly carried by electrons. If, however, the distribution of these electrons deviates from a spherical one, modern ideas of diamagnetism suggest the presence of a directed diamagnetic effect towards the normal to the plane of motion of these few conduction electrons. The only magnetic measurement on molybdenite that has been reported, is by Tjabbes (1932), that too being with powders of molybdenite, thereby supplying no clue to our above conjecture.

From the above considerations it is evident that the study of the magnetic properties of single crystals of molybdenite will be of considerable interest. The present paper gives an account of these measurements made at room temperatures. The measurement of the magnetic properties of molybdenite at temperatures other than the room temperature, both high and low, the Hall effect and other important allied properties are in progress and will be published in due course.

MEASUREMENT OF THE MAGNETIC ANISOTROPY OF MOLYBDENITE

The magnetic anisotropy was measured by the torsional method adopted by Krishnan and his collaborators (1935). The crystal is suspended with its

basal plane vertical in a uniform magnetic field at the end of a fine calibrated quartz-fibre, the other end of which is attached to a graduated torsion head. The crystal tends to bring its basal plane to parallelism with the field, showing that the specific susceptibility of the crystal along directions in the basal plane, say χ_1 , is greater (algebraically) than that along the vertical axis, χ_n . The torsion head is suitably rotated, so that in the natural setting position of the crystal, when the field is on, the torsion of the fibre is zero. The torsion head is then slowly rotated until the equilibrium is just unstable; this is the position of maximum couple. If this angle is denoted by α , the difference in maximum and minimum susceptibilities in the horizontal plane of suspension is given by (Banerjee and Bhattacharyya, 1928)

$$C(\alpha - \psi) = \frac{Im}{2M} \cdot H^2(\chi_1 - \chi_n) \sin 2\psi \quad \dots (1)$$

where ψ is the angle of rotation of the crystal, C is the torsional constant of the fibre, M and m are the molecular weight and mass of the crystal respectively and H is the field strength. The strength of the magnetic field and the dimension of the fibre are so adjusted that the angle through which the torsion head is rotated to bring the crystal from the initial position corresponding to zero torsion to that corresponding to the maximum couple, always attains a value more than 360 degrees so that the approximate formula

$$\chi_1 - \chi_n = \frac{(2\alpha - \pi/2)MC}{mH^2} \quad \dots (2)$$

holds true. By rotating the torsion head in both clockwise and anticlockwise directions, α can be accurately determined and therefore $\chi_1 - \chi_n$.

Since the crystal is a naturally occurring one and in view of the uncertainty regarding the impurities present in the crystal obtained from different sources, the measurements were repeated with a number of specially chosen single crystals. The values of $\chi_1 - \chi_n$ obtained in these measurements were found to be slightly different for different crystals as will be seen in Table I.

MEASUREMENT OF THE PRINCIPAL SUSCEPTIBILITIES

After completing the measurement of $\chi_1 - \chi_n$, if we can determine the absolute value of either χ_1 or χ_n , both of them will be known. Since χ_1 is numerically smaller than χ_n , it is desirable to choose χ_1 for this measurement.

On trial the balancing method of Krishnan (*loc. cit.*) for measuring the absolute susceptibility has been found to be unsuitable in the determination of χ_1 . This is due to the fact that the volume susceptibility of molybdenite in that direction is greater than that of any of the solutions ordinarily used. So the method has been modified as follows.

The crystal is attached with its basal plane vertical to one end of a stout glass rod of suitable length, the other end being attached to the middle of a fine silver wire stretched horizontally between a graduated torsion head and a metal chuck. By rotating the torsion head small lateral displacements can be imparted.

to the crystal. The whole arrangement is so placed that the crystal is about 4 to 5 mm away from the vertical sides of the flat polepieces and so in a non-homogeneous magnetic field, the gradient being in the horizontal direction. The attachment of the molybdenite crystal to the end of the glass rod is effected in such a way that its basal plane is always parallel to the direction of the uniform part of the field. To be sufficiently ensured that the horizontal gradient of the field is only effective in laterally displacing the crystal, the silver wire

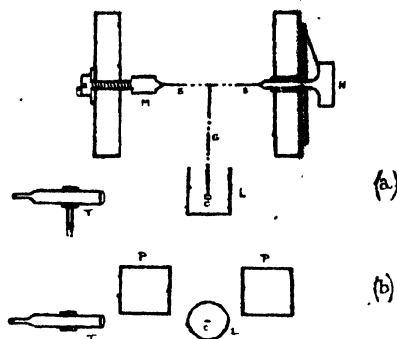


FIG. 1

(a) Vertical Section	(b) Horizontal Section
M—Metal chuck	SS—Silver wire
H—Torsion head	G—Glass rod
L—Liquid bath	T—Telemicroscope
PP—Pole pieces	C—Crystal.

is always kept sufficiently stretched. The entire arrangement is suitably encased to prevent it from dust and wind. Fig. 1 represents diagrammatically the different parts of the arrangement.

For measuring the susceptibility, the crystal is kept suspended in a liquid of known volume susceptibility, say K_1 , and viewed through a telemicroscope, one of whose scale marks is made coincident with an edge of the crystal. When the field is switched on the crystal moves laterally along the gradient in a direction away from the field. The torsion head is then slowly rotated until the crystal returns to its original position. Let θ_1 be the angle through which the torsion head has been rotated. If K_c be the volume susceptibility of the crystal, the force displacing it away from the field is given by

$$\frac{1}{2}AHx \frac{dHx}{dx} (K_c - K_1)$$

where A is the cross-section of the crystal and H is the field strength, the horizontal direction being taken to be the x -direction. This force has been balanced by the torsion of the silver wire. Therefore

$$\frac{1}{2}AHx \frac{dHx}{dx} (K_c - K_1) = R\theta_1 \quad (3)$$

where R is the torsional constant of the wire. The liquid is then replaced by another liquid having a different volume susceptibility, say K_2 , and the whole procedure is repeated. If θ_2 be the corresponding angle through which the torsion head has been rotated, then

$$\frac{1}{2}AHx \frac{dHx}{dx} (K_c - K_2) = R\theta_2.$$

The gradient remains the same in both the cases, the crystal being brought to the same position every time; so from (3) and (4) we have

$$\frac{K_c - K_1}{K_c - K_2} = \frac{\theta_1}{\theta_2} \quad \dots (5)$$

and hence K_c can be easily calculated. The density of the crystal being known, the mass susceptibility is easily determined. In our case this corresponds to χ_1 .

In our actual experiment the liquids used were conductivity water and a standard Nickel chloride solution. Measurements were repeated with a number of crystals obtained from different samples. The values of susceptibilities were found to differ slightly from crystal to crystal as will be seen from Table I.

RESULTS

The experimental results are given in Table I, where measurements on crystals from five different samples of molybdenite are shown. Here χ_{11} represents the susceptibility along the hexagonal axis and χ_1 that at right angles to the axis, while $\bar{\chi}$ represents the mean, susceptibility, i.e., $\bar{\chi} = (2\chi_1 + \chi_{11}/3)$, and the corresponding volume susceptibility being denoted by K . All the above quantities are expressed in E. M. C. G. S. units. The data in the table refers to measurements taken near about 30°C .

TABLE I

Crystal	$(\chi_1 - \chi_{11})$ $\times 10^{-6}$ per gm. mol.	Volume susceptibility $K \times 10^{-6}$	Density	Corresponding $\chi_1 \times 10^{-6}$ per gm. mol.	Mean $(\chi_1 - \chi_{11})$ $\times 10^{-6}$ per gm. mol.	Mean $\chi_1 \times 10^{-6}$ per gm. mol.	Mean susceptibility $\bar{\chi} = \frac{2\chi_1 + \chi_{11}}{3}$ per gm. mol.
1	42.4	-1.243	4.804	-41.4			
2	42.5	-1.360	4.782	-45.5			
3	41.3	-1.435	4.854	-47.3	42.8	-44.3	-58.6
4	44.4	-1.293	4.926	-42.0			
5	43.3	-1.404	4.949	-45.4			

DISCUSSIONS

Molybdenite crystal belongs to the hexagonal system and has a perfect basal cleavage. It occurs in nature in the form of thin flakes parallel to the basal plane. Its structure has been determined by Pauling and Dickinson (1923) and Hassel (1924). They found that the X-ray diffraction photographs agreed with a typical hexagonal layer lattice. Each sulphur atom is equidistant from three molybdenum atoms, and each molybdenum atom is surrounded by six equidistant sulphur atoms at the corners of a trigonal prism of altitude 3.17\AA and edge 3.15\AA . The atoms in the crystal are so situated that all the trigonal prismatic units are oriented parallel to one another, the hexagonal axis being perpendicular to the triangular faces of the prism. Each layer of the crystal consists of three planes,—one of molybdenum atoms surrounded on either side by a plane of an equal number of sulphur atoms; two layers of sulphur atoms are contiguous. The distance from the molybdenum atom to the nearest sulphur atoms has been calculated to be 2.41\AA , which is exactly equal to the sum of the radii of molybdenum and sulphur atoms, *i.e.*, 1.36\AA and 1.05\AA respectively and the interatomic distances in the planes of a layer being 3.15\AA . But the distance between two such parallel layers is 3.66\AA . This great distance between the layers is undoubtedly connected with the excellent basal cleavage of molybdenite.

The structure of molybdenite having a trigonal prismatic configuration, arrived at by the X-ray methods has been puzzling various workers due to a belief prevalent formerly that the Mo—S bond should be ionic in character, in which case the octahedral arrangement would be more stable. Moreover the large number of its octahedral complexes containing electron pair bonds would also suggest an octahedral electron pair bond structure. But it has been found by Hultgren (1932) from a wave mechanical treatment, that in this case six equivalent bonds of strength 2.983 (considerably higher than that of octahedral bond eigenfunctions) directed towards the corners of a trigonal prism can be formed. The theoretical ratio of altitude to base of the prism should be unity while that obtained experimentally is 1.007, confirming the trigonal prismatic orientation.

From the above structural considerations of the crystal it is evident that the atoms in it are held together by different types of bindings. The three planes, one of molybdenum having two sulphur planes on either side of it are bound into a compact layer of the crystal by forces that are undoubtedly of the type that arises out of covalency (as evidenced from the above discussions) and form a gigantic two dimensional molecule. These molecules are then held together largely, presumably by Van der Waal's forces. But on looking into the interatomic distances in the different planes of the layers, it is very difficult to ascertain the exact type of binding between them. Goldschmidt (1929) on the discussions of the structures of metallic disulphides observed that the appearance of layer lattices seems to depend upon whether the metal is able to

ionise with four electrons and thereby split the molecule S_2 . Therefore, metals with high valency and large radii may give rise to layer lattices, while pyrites type of lattices are restricted to metals with low valencies and small radii. Thus from his considerations it is clear that the bindings between the atoms in the planes composing the layers, may be thought to be of partially ionic in character. Certain properties of molybdenite such as electrical conductivity (different in different directions), metallic lustre, resistance to mechanical and thermal treatment photo-conductivity and etc. also suggest that the presence of binding of a slightly metallic type in the planes does not seem to be quite improbable.

One consequence of such a type of binding in the planes, will be an amount of enhanced diamagnetism in a direction perpendicular to the planes. That is exactly what has been observed in our case. Whereas the susceptibility along directions in the basal plane is -44.3×10^{-6} per gm. mol., that along the hexagonal axis is about -87.1×10^{-6} per gm. mol., i.e., the anisotropy is about 72 per cent.

From the considerations of Hultgren and others (*loc. cit.*), it is found that strong d-s-p bonds are formed between Mo and S. Therefore, strong crystalline electric fields arising out of this covalency is sufficient to quench the orbital magnetic moments. Kimball (1940) has shown that in MoS_2 having trigonal prismatic orientation, d^4sp bonds are formed with Mo. Again Mo being quadrivalent in molybdenite (Pauling, 1939) two electrons are left which can be accommodated in the one 4d orbital left after bond formation. According to Pauli's principle, the spins of the electrons in that orbital, being antiparallel, balance one another. Thus no paramagnetic effect is possible from the spin or orbital moments. However, there might be a contribution of the orbital moment's high frequency elements, in which case the susceptibility, according to Van Vleck (1932), is given by

$$\chi = -\frac{Le^2}{6mc^2} \sum r^2 + \frac{3}{2} \sum \frac{|m^0(n';n)|^2}{h\nu(n';n)} \text{ per gm. mol.} \quad \dots (6)$$

where $m^0(n';n)$ is an element of the electronic angular momentum matrix corresponding to transition frequency $\nu(n';n)$. The material is diamagnetic or paramagnetic depending upon whether the first or second term of (6) is greater. After deducting the diamagnetic contribution of sulphur as determined by Nilakantan (1936) molybdenum is found to be diamagnetic. If, however, we take into account the diamagnetic contribution from the molybdenum atom, which has been calculated according to the method of Slater (1930) as modified by Angus (1932), molybdenum is found to be still diamagnetic which contradicts the suggestion put forward by Roychowdhury and Sengupta (1936) that molybdenum will be paramagnetic in MoS_2 after correcting for the diamagnetism of molybdenum atom. Thus our experimental finding is quite in agreement with the above theoretical discussions, the high frequency paramagnetism being practically evanescent in this case.

In conclusion, the author wishes to express his best thanks to Prof. K. Banerjee, D.Sc., F.N.I., F.I.A.S., for his keen interest in the work and to Mr. A. Mookherji, M.Sc., for helpful discussions.

INDIAN ASSOCIATION FOR THE CULTIVATION OF SCIENCE
210, BOWBAZAR STREET, CALCUTTA.

REFERENCES

- Angus, W. R., 1932, *Proc. Roy. Soc.*, **A**, **136**, 569
 Banerjee, K. and Bhattacharyya, J., 1938, *Zeits. f. Krist.*, **100**, 420.
 Goldschmidt, V. M., 1929, *Trans. Farad. Soc.*, **25**, 278.
 Hassel, O., 1924, *Zeits. f. Krist.*, **61**, 92
 Hultgren, R., 1932, *Phys. Rev.*, **40**, 891.
 Kimball, G. E., 1940, *Jour. Chem. Phys.*, **8**, 188.
 Krishnan, K. S. and Banerjee, S., 1935, *Phil. Trans.*, **A**, **234**, 265.
 Nilakantan, P., 1936, *Proc. Ind. Acad. Sci.*, **A**, **4**, 419.
 Pauling, L. and Dickinson, R. G., 1923, *Jour. Am. Chem. Soc.*, **45**, 1466.
 Raychowdhury, D. P. and Sengupta, P. N., 1936, *Ind. Jour. Phys.*, **10**, 253.
 Slater, J. C., 1930, *Phys. Rev.*, **36**, 57.
 Tjabbes, B. Th., 1932, *Proc. Roy. Acad. Amstdam*, **38**, 693.
 Van Vleck, J. H., 1932, *The Theory of Electric and Magnetic Susceptibilities*, 275.
 Wilson, A. H., 1931, *Proc. Roy. Soc.*, **A**, **133**, 458.
 „ „ 1932, *Proc. Roy. Soc.*, **A**, **134**, 277.
 „ „ 1939, *Semiconductors and Metals*.

ON THE RADIUM CONTENT OF A NEW MINERAL FROM RAJPUTANA

By B. D. NAG CHAUDHURI*

ABSTRACT. The quantity of uranium and thorium present in the mineral has been determined by estimating the β -activity and the absorption in aluminium. The percentage of uranium by weight is 60% and that of thorium is 0.7%. The radium content of the mineral has been estimated and compared to the various radium ores from which radium is at present extracted. The feasibility of the present ore as a source of radium is discussed.

The quantitative estimation of uranium and thorium in a mineral can be made very conveniently from the radioactivity of the samples. For samples containing a very small amount of uranium and thorium, that is, less than a tenth of one per cent of the radioactive elements a method of estimating the radioactive content has been developed by Finney and Evans (1935), by counting the number of α -particles emitted by the sample and measuring their ranges. The method, however, ceases to be useful when the samples are very much stronger. The β -activity of the samples can then provide a quick and useful method of estimating uranium and thorium. The method developed in this laboratory, yields quick and accurate results as has been confirmed in three ways. The method consists mainly of an analysis of the absorption curve of the β -rays in aluminium and will be discussed in another paper. The results have been confirmed by (1) a chemical analysis of the sample, (2) the verification of the analysis by the method of Finney and Evans and (3) taking a known mixture of uranium and thorium and analysing by the β -absorption methods and the method of Finney and Evans. The results are summarised below. The β -ray ionisation chamber used for these measurements is filled with dry air at room temperature with a thin air-tight aluminium window.

Mineral	Method Used	Uranium	Thorium
Thorianite	Finney and Evans	$20.0 \pm 1.3\%$	$61.9 \pm 2\%$
Same	Nag and others (1924)		
Same	β -absorption	$21.1 \pm 1.1\%$	$60.5 \pm 1.8\%$
Mixture of 80%-urani- um and 10%-thorium	Chemical analysis	$21 \pm 1\%$	$61.0 \pm 1.1\%$
	Finney	$78.5 \pm 2\%$	$10.2 \pm 0.4\%$
	and Evans β -absorp- tion	$79.8 \pm 1.3\%$	$9.9 \pm 0.3\%$

The present sample was an orange yellow mineral of altered appearance from Rajputana with a very high specific activity. Most of the activity was due to uranium which was present in the form of oxides and the sample may be described as an uranium ochre. One hundred milligrams of the mineral was taken from the sample which was first crushed to an uniformly fine powder to ensure an average sampling. The hundred milligrams were spread out in an aluminium disc to a uniform circle of five cms. diameter and used for the β -ray absorption measurements. The amounts of uranium and thorium contained in the mineral are given in percentages of the total weight of the mineral.

* Fellow of the Indian Physical Society.

Uranium	...	$60.1 \pm 1.2\%$
Thorium	...	$0.7 \pm 0.05\%$

This is a very high value of uranium content for any mineral and the high specific activity of the mineral compares favourably with the present uranium minerals used in the extraction of radium. The uranium content of the minerals most commonly in use for the extraction of radium are tabulated below :

Mineral	Locality	Uranium		Thorium	Remarks
		Max	Min.		
Pitchblende (Report, 1905-38)	Colorado	68%	38%	Negligible	In use
Pitchblende (Keevil, 1938; Nier, 1941)	Joachimstal	60%	—	Negligible	Earliest source of radium
Pitchblende	Katanga (Congo)	73%	23%	Negligible	Largest source
Uraninite	Huron Claim	52%	—	10%	Canadian
Uraninite	Parry Sound	69%	51%	3%	„ richest ore
Uraninite	Wilberforce	54%	—	12%	Canadian

All these uranium minerals are mined or have been mined for radium and it may be noted that the uranium ochre under discussion compares favourably with the minerals listed, provided, of course, that the mineral occurs in large enough deposits to be mined economically. The actual amounts of radium available from these minerals may also be compared. The uranium ochre will yield 234 milligrams of radium per ton of the ore, whereas the Canadian ore from Parry Sound yields about 266 milligrams per ton of the ore. The highest yield possible is 285 milligrams per ton of ore, a figure that has not been reached by any available ore. The radium ores of Belgian Congo have been mined profitably even when the yield was as low as 130 mgms. per ton. The present ore thus stands comparison favourably when one remembers that the Canadian ore is flown from inaccessible regions and the Belgian ore has to be carried from inaccessible regions to the coast and thence to Belgium for extraction.

It is a pleasure to thank Prof. Saha and Dr. P. B. Sarkar for interesting discussions about the mineral. Thanks are also due to Mr. A. K. Mousûf for insetting the apparatus and taking readings.

CYCLOTRON LABORATORY,
UNIVERSITY COLLEGE OF SCIENCE,
CALCUTTA.

REFERENCES

- Evans, 1941, *Jour. App. Phys.*, **12**, 297.
 Finney and Evans, 1935, *Phys. Rev.*, **48**, 563
 Keevil, 1938, *Economic Geology*, **33**, 685.
 Nag, Das & Das Gupta, 1944, *Proc. Nat. Inst.*, **10**, 167..
 Nier, 1941, *Phys. Rev.*, **60**, 112.
 Report, 1935-38, Committee on Determination of Geological Time of the National Research Council, U.S.A.

RECTIFICATION IN DISCHARGE TUBES*

By K. R. CHAUDHARI

ABSTRACT. A detailed study of rectification phenomena in air following the earlier work of Chiplonkar is given. The effect in hydrogen and CO is also discussed.

Recently Mr. Chiplonkar (1939) has made some quantitative investigations of the well-known phenomenon of rectification in discharge tubes. His work was mainly confined to the study of the precise role of the electrodes, their relative sizes and the inter-electrode distance in determining the rectification effect. This paper is an extension of Mr. Chiplonkar's work and deals with a detailed study of rectification phenomena in air. The effect in hydrogen and CO has also been partly studied.

E X P E R I M E N T A L

The discharge tube had an internal diameter of 3.8 cm. and was provided with a cup-like cylindrical anode of aluminium (diameter 1.6 cm. and height 2 cm.), the latter being fitted within a side tube. The cathode was made of an aluminium cylinder 9 mm. thick and with a diameter of 3 cm., and the distance between the anode and the cathode was 16 cm. A hole of 1 mm. diameter was bored coaxially at the centre and it was mounted coaxially by a brass rod of 3 mm. thickness. The brass rod was used only to facilitate the electrical connections. The window of the discharge tube was at a distance of 16 cm. from the cathode and the length of the tube from the window to the conical end was 42 cm. Thus the general form of the tube was similar to that suggested by Thomson (1933).

The electrical circuit employed was the same as that used by Chiplonkar (*loc. cit.*). In order to prevent the ascent of mercury vapour from the diffusion pumps and other measuring instruments liquid air traps were employed except in the case of CO, in the investigation of which traps of freezing mixture of ice and CaCl_2 were used. The total current passing through the discharge tube was measured by an A.C. Weston milliammeter of the rectifier type, the rectified part of the current being measured by a D.C. Crompton milliammeter connected in series with the first. The current was measured every time immediately after starting the discharge. The ratio of the rectified to the total current is designated here as the rectification ratio and denoted by the symbol ρ . The heating of the tube due to discharge was avoided, as far as possible, by interrupting the discharge for a suitable length of time, between two successive observations. Evacuation of the tube was obtained by means of a set of mercury diffusion pumps of the Waren type backed by a Cenco Hyvac oil pump.

The results for air, hydrogen and CO are shown graphically in Figure 1, where the values of the rectification ratio ρ are plotted against the corresponding values of pressure p . Different sets of observations were taken and the values of the rectification ratio obtained always gave the same type of curve.

* Communicated by Dr. D. V. Gogate.

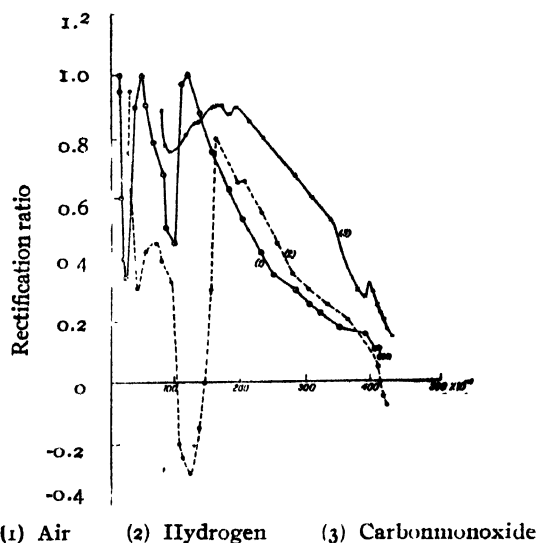


FIG. 1

It can be easily seen from the graphs that the rectification ratio ρ is always positive in the case of air and H_2 , while in the case of CO the value of ρ becomes negative at a pressure of 110×10^{-4} cm. of Hg.

It may be noted here that Chiplonkar (*loc. cit.*) has recorded negative values of ρ in the case of air, nitrogen and oxygen at low pressures (about 50×10^{-4} cm. of Hg.). At these low pressures the fourth type of discharge begins and as Thomson remarks, the phenomena under these conditions become very complicated. In general the nature of the discharge is always different with different tubes. The heating of the tubes and the electrification of its walls modify the discharge considerably. The high speed cathode rays ionise the gas and cause changes in the current in the discharge tube.

Again radiation is emitted from some parts of the discharge and especially from the negative glow, which, falling on the metal of the cathode, would by photo-electric effect cause it to emit electrons. There are also several sources of ionisation besides these, *e.g.*, the impact of positive ions against the cathode, moving electrons in dark space, etc.

All these factors contribute to the variations in the rectified current which may lead either to positive or negative values of ρ depending upon the nature of the gas, nature of the electrodes and so on.

In Table I are given the values of the first maxima and minima of the rectification ratio ρ against the corresponding pressures p for different gases. If we look to the densities of these gases, it becomes at once apparent that the first maxima-minima values of ρ appear at higher pressures for gases of lower densities, *e.g.*, the first maximum value of ρ for hydrogen appears at a pressure of 180×10^{-4} cm. of Hg., while those for CO and air appear at 160×10^{-4} cm. of Hg. and 125×10^{-4} cm. of Hg. respectively. This conclusion is supported by the experimental data given by Chiplonkar (*loc. cit.*) also.

It may be mentioned here that the hydrogen curve (Fig. 1) has got subsidiary maxima-minima in the beginning at pressures 398×10^{-4} cm. of Hg. and 391×10^{-4} cm. of Hg. respectively and they are marked with asterisks.

TABLE I

No.	Gas	Density of gas gm. per litre	First Maxima		First Minima		Authors
			Pressure X, 10^{-4} cm. of Hg.	ρ	Pressure X 10^{-4} cm. of Hg.	ρ	
1	air	1.29	160	0.88	100	0.10	Chiplonkar (1939).
2	oxygen	1.43	125	0.85	80	0.00	"
3	nitrogen	1.25	180	0.90	100	0.20	"
4	air	1.29	125	1.00	95	0.40	Author
5	CO	1.25	160	0.80	110	0.30	"
6	H ₂	0.09	180	0.83	170	0.75	"
7	"	"	398*	0.30*	391*	0.25*	"

VARIATION OF RECTIFICATION WITH TIME

It was found that the rectified current always fell down rapidly within the first half minute and then after an interval of 5 to 15 minutes it became steady. During the study of this phenomenon in the case of air, it was particularly observed that there was a very marked fluctuation around the maxima and minima values of ρ (Fig. 1). Therefore the points around these values were chosen as the most suitable ones for the study of variation of the rectified current, with time. Figure 2 gives a few typical curves showing the fall of the rectified part of the current with the time for which the discharge was passed.

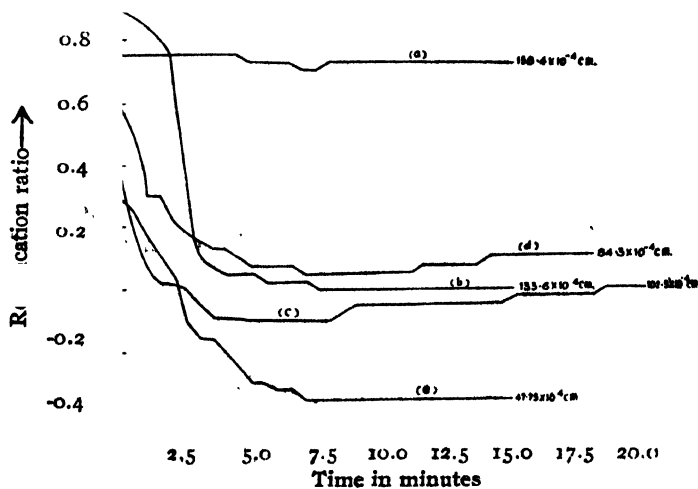
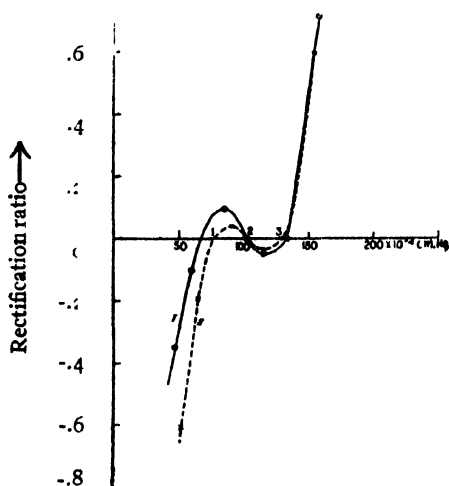


FIG. 2

The uppermost curve 'a' clearly shows that at a pressure of 158×10^{-4} cm. of Hg. the variation in the rectified current is comparatively very small and the rectification ratio ρ becomes steady at a value of 0.72. At this high value of pressure, the fluctuation is always very small but at low pressures the rectified current goes on falling continuously for about 5 minutes and then becomes fairly steady at a very low value of ρ (see curves b, c, d, e—Fig. 2).

It may also be interesting to study the variation of the steady value of ρ with pressure p . Figure 3 is a plot of the steady values of ρ (taken from Fig. 2), against the corresponding values of pressure p .



I. Experimental. II Theoretical.

FIG. 3

The form of experimental curve (Fig. 3) suggests that it can be represented by an equation of the type—

$$y = (x-1)(x-2)(x-3)$$

where y denotes the value of ρ and x that of p . In Figure 3, side by side with the experimental curve is also given the theoretical curve satisfying the above equation. The point corresponding to $x=2$ represents a pressure 102×10^{-4} cm. of Hg. The part of the experimental curve on the right hand side of this point very nearly coincides with the theoretical curve. The other part on the left hand side of the point $x=2$ (Fig. 3) shows an increasing divergence from the theoretical curve.

This divergence can be explained if we consider the heating of the tube due to the continuous discharge. The heating causes a rise of pressure in the discharge tube and consequently the actual pressure existing in the discharge tube for any value of ρ is higher than that indicated on the pressure gauge. Thus the value of ρ obtained experimentally for the different values of pressure as recorded on the pressure gauge really corresponds to higher pressures actually existing in the

heated discharge tube. This naturally places the ρ values on the experimental curve above those on the theoretical ones for the corresponding pressures.

EFFECT OF CARBON MONOXIDE ON ELECTRODES

While working with CO, it was observed that the curves obtained for different sets showed wide differences, especially when the interval between the sets was sufficiently long (about a fortnight), observations were therefore repeated with air but here also a wide departure from the original curve (Fig. 1) was noticed. This definitely indicates that the electrodes were polluted by CO. This is in agreement with Oliphant's (Thomson—*loc. cit.*) observations.

SUMMARY

This paper gives a detailed account of some quantitative measurements of the rectification in air in the discharge tubes. The variation of the rectification ratio ρ with pressure in H_2 and CO has also been studied. It is found that the first maxima-minima values of ρ appear at higher pressures for gases of lower densities. While studying the variation of rectification with time, it is observed that the rectified current falls down rapidly at first and then becomes steady at a very low value of ρ .

When steady values of ρ are plotted against the corresponding pressures, a curve is obtained which can be represented by an equation of the form—

$$y = (x - 1)(x - 2)(x - 3).$$

Lastly the effect of CO on the electrodes is discussed.

ACKNOWLEDGMENTS

I wish to express my gratitude to Dr. R. K. Asundi and to Dr. D. V. Gogate for their valuable help and discussion. My sincere thanks are also due to Dr. S. S. Joshi for giving me every sort of facility for work in his laboratory, and to Mr. V. T. Chiplonkar for the use of the apparatus.

PHYSICS DEPARTMENT,
BARODA COLLEGE,
BARODA.

REFERENCES

- Chiplonkar, 1939, *Proc. Ind. Acad. Sci.*, **10**, 381.
Thomson, 1933, *Conduction of Electricity Through Gases*, Vol. 2 (Ed. 3), p. 320.

ON THE INFLUENCE OF MAGNETIC FIELD ON THE ABSORPTION SPECTRA OF LIQUIDS

By A. K. BANERJEA

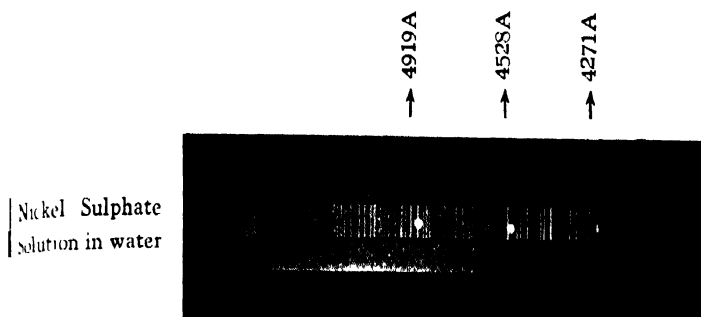
(Plate IV)

ABSTRACT. The width of the absorption band and the intensity of the transmitted light through an absorption cell containing solutions of crystals of $\text{NiSO}_4 \cdot 7\text{H}_2\text{O}$, $\text{CoSO}_4 \cdot 6\text{H}_2\text{O}$, $\text{FeCl}_3 \cdot 7\text{H}_2\text{O}$, MnCl_2 and pure liquids like benzene, xylene, etc., has been found to change under the influence of moderately strong magnetic fields. In the case of solutions of para-magnetic crystals, it was observed that the intensity of the transmitted light was less with field than without field. In the case of dia-magnetic liquids the intensity of the transmitted light was greater with field than without it. The magnetic field was of the order 13 kilo gauss.

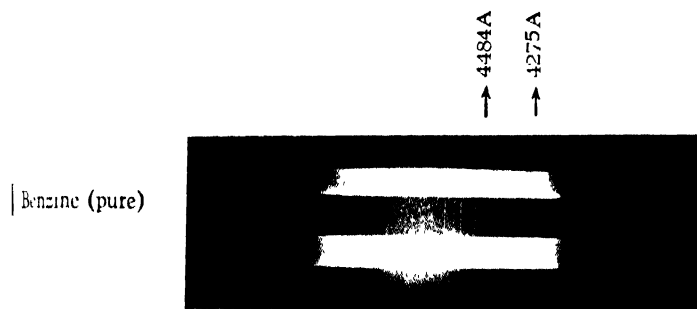
During the study of the absorption spectra of para-magnetic solutions it was found that there were both a general diminution in the intensity of the spectra and a shift of the absorption edge as a result of application of the magnetic field. That the observed effect is undoubtedly a result of the influence of the magnetic field and not the spurious result of (i) any variation of the intensity of the source of light, (ii) temperature variations in the absorbing liquid, or (iii) any difference in the times of exposure, will be amply clear from the account of the experimental work which follows below. This conclusion is further confirmed by the observations on dia-magnetic liquids, of which the absorption spectra suffer an opposite change under the influence of a magnetic field.

The para-magnetic solution experimented upon consisted in the first instance of semi-normal ($N/2$) solutions of pure crystals of $\text{NiSO}_4 \cdot 7\text{H}_2\text{O}$, $\text{CoSO}_4 \cdot 6\text{H}_2\text{O}$, $\text{FeCl}_3 \cdot 7\text{H}_2\text{O}$ and MnCl_2 . The absorption-cell was a glass tube of diameter 1.40 cm. and 3.10 cm. long, closed at both ends by flat glass pieces cemented to it. This cell had a small hole at the top through which the liquid could be poured in and which was then closed with a small rubber stopper to provide against any loss by evaporation. The source of white light consisted of a frosted 220V, 100W, A. C. lamp having a sliding resistance and an accurate ammeter (Hartmann Braun, reading 0.05 amps per division) in series to check the constancy of the current through the lamp. The white light from the lamp passed through the absorption-cell and was focussed on the slit of a constant-deviation spectrograph in which the spectrum was photographed, the cell was placed between the pole-pieces of a large and powerful Du Bois electro-magnet having a diameter of 9.5 cms. and a separation of 2.0 cms. The cell was thus in a fairly uniform field. The magnetic field was at right angles to the direction of transmission of light. The spectrograph was provided with a Hartmann slit, so that three spectra could be photographed on the same plate one above the other, the one above being without the magnetic field, the second one in the magnetic field and the lowest one with the field off again, the time of exposure in the three cases being exactly the same.

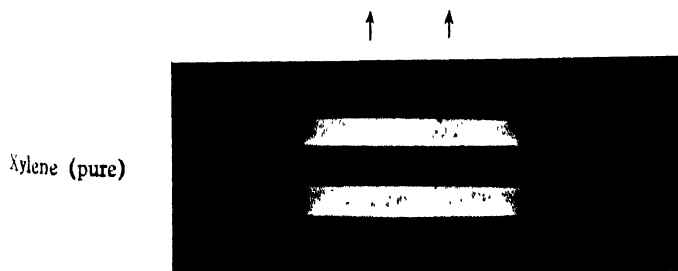
(i) To test for the constancy of the source of light, the transmitted light was focussed on a photo-voltaic cell and the photo-voltaic current was observed to



- Absorption spectra in Magnetic field
- Iron comparison spectra.
- Absorption spectra without Magnetic field.



- Absorption spectra without field
- Copper comparison spectra
- Absorption spectra in Magnetic field



- Absorption spectra without field
- Copper comparison spectra
- Absorption spectra in Magnetic field

remain constant within $\frac{1}{2}\%$ over a period of 50 mins., the times of exposure, however, ranged from 10 mins. to 20 mins. only.

(ii) To study the influence of the time of exposure on the width of the absorption band, absorption-spectra were obtained by exposing the plates for periods ranging from 10 mins to an hour and no appreciable change in the width and character of the absorption edges was observed.

(iii) To test for the influence of temperature, the spectra were obtained when the solution was at room temperature 28.8°C . and again when it was heated through 7°C . No remarkable changes were observed. The temperature of the solution during the period of observation could not have varied by more than 0.5°C (as revealed by a thermo-couple immersed in the solution).

Plate III is a typical absorption spectra of a semi-normal solution of nickel sulphate, $7\text{H}_2\text{O}$ in distilled water at 28.8°C . The one below is without magnetic field (*i.e.*, in zero field); the central one is the iron comparison spectra and the uppermost spectrum is the absorption spectrum of the same solution under a uniform magnetic field of about 13000 gauss. Fig. 1 is a record of the intensity-distribution in the spectra as obtained by a non-recording Hilger microphotometer. Curve (a) of Fig. 1 gives the distribution when the field is on,

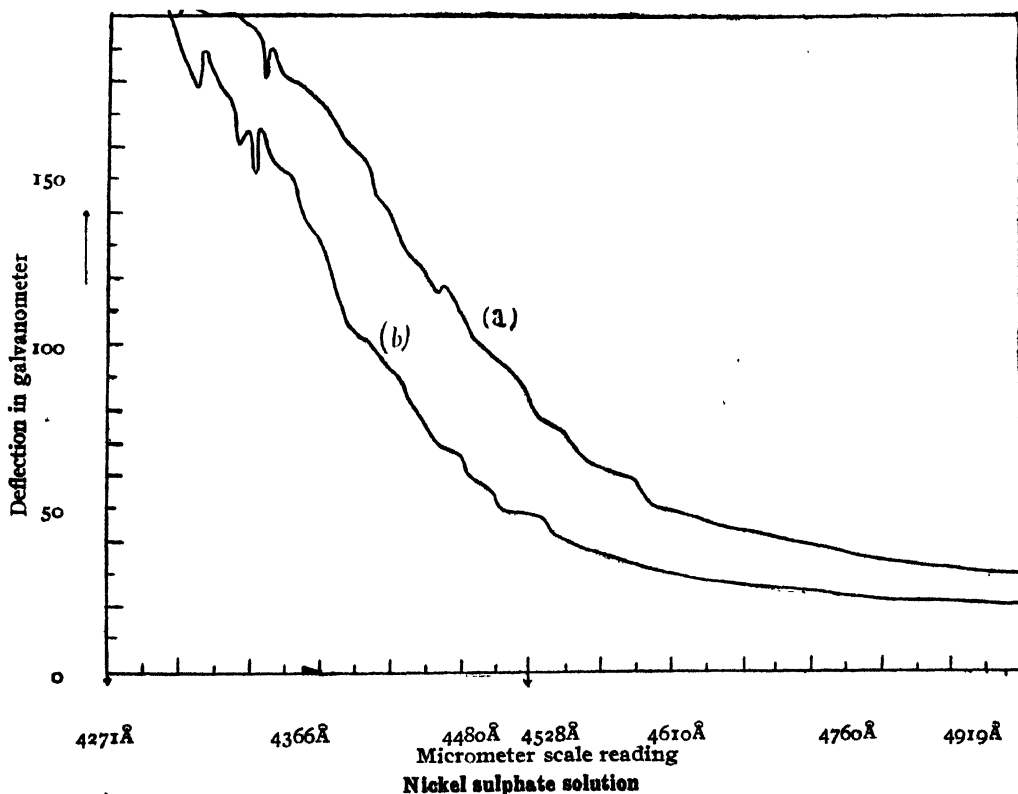


FIG. 1

and curve (b) when the field is off. It can be seen that the solution gives an absorption band whose long-wavelength edge roughly corresponds to 4325\AA at about 28.5°C . A uniform field of 13000 gauss applied at right angles to the beam transmitted by the solution, pushes the long-wavelength edge of the band to the long wave side by about 58°\AA . It has been found that the change in the intensity of the absorption spectra varies with the strength of the applied magnetic field up to a certain extent, only above which it is fairly independent of the strength of the field. This indicates the existence of a saturation phenomenon. Further work is necessary to confirm this view. For a given magnetic field the change of intensity is not the same for all wavelengths. (Curves 'a' and 'b' of Fig. 1 and the table below will show this.)

TABLE I

Deflection of galvanometer

Micrometer scale reading	When light passed through absorption spectra without any field	When light passed through absorption spectra in magnetic field
2mm	189	202
4mm	160	196
5mm	151	180
6mm	129	172
8mm	191	136
10mm	64	109
11mm	53	94
13mm	40	71
15mm	32	56
18mm	26	42
20mm	23	38
23mm	21	32
25mm	20	30

The change of the intensity of the absorption-band on the application of the magnetic field has been calculated by noting the change in the galvanometer deflections when light passed through the absorption spectra without and with magnetic field. In the particular case of nickel sulphate solution the ordinates at any reading of the micrometer scale corresponding to the two cases,—with and without magnetic field—have been read out, and the change in the intensity of the absorption-band has been calculated (see Fig. 1).

It may be observed that the change in the intensity of the band is maximum at about 4528\AA . (This has been found for NiSO_4 solution.)

Similar results have been obtained with $\text{CoSO}_4 \cdot 6\text{H}_2\text{O}$, $\text{FeCl}_3 \cdot 7\text{H}_2\text{O}$, etc.

In order to ascertain how far the solvent, *i.e.*, water in these cases, was responsible for the observed changes, the experiments were repeated with only distilled water in the absorption-cell. Up to a magnetic field of 13000 gauss, no appreciable change in the intensity of the spectra of the transmitted light through the cell was observed, there being no absorption band in the glass region.

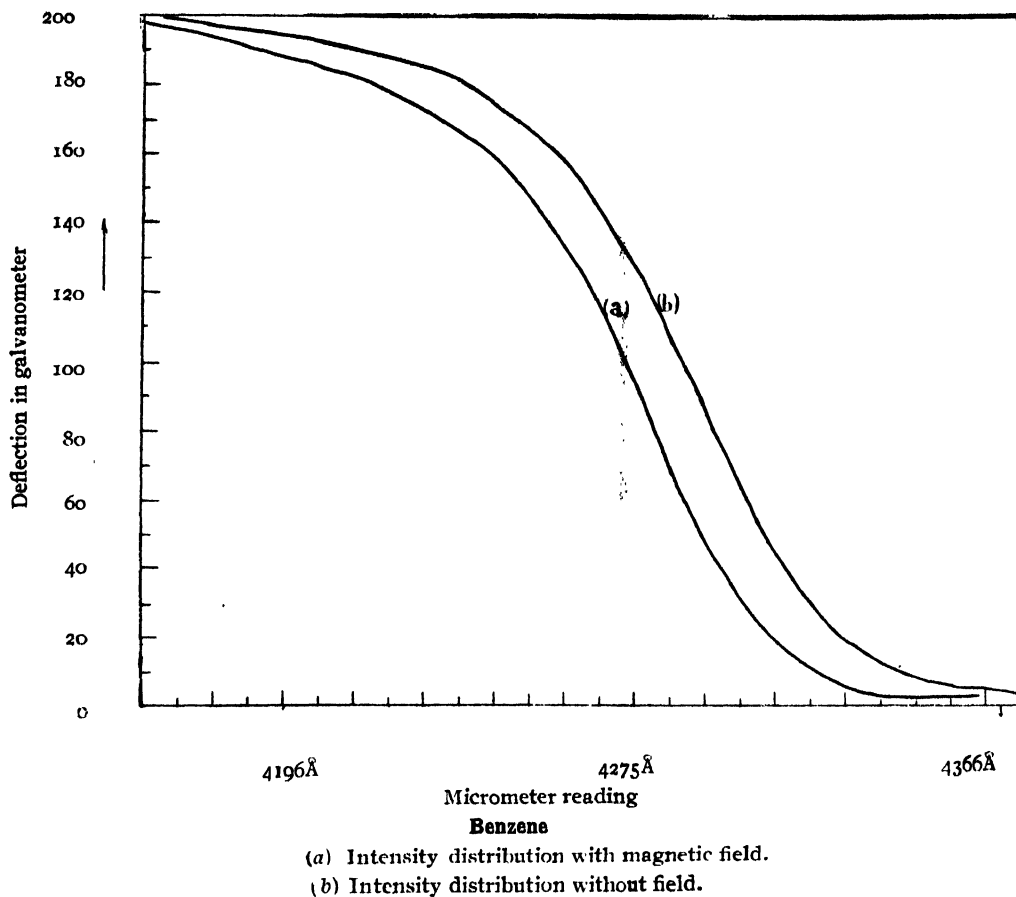


FIG. 2

It has been remarked that the dia-magnetic liquids like benzene, xylene, etc., show a similar effect but in the opposite sense. (For benzene see Fig. 2 and for xylene see Fig. 3.)

It has been observed that the application of the magnetic field shifts the absorption edge to the shorter wavelength side of the spectrum and produces a general increase in the intensity of the light transmitted through the cell.

Further work on a number of pure liquids like CS_2 , CCl_4 , aniline is in progress.

The effect discussed above appears analogous to the effect observed by Muller and others (1942), who have found that a magnetic field changes the intensity of the light transmitted through clear transparent colloidal suspensions of magnetite, rouge and other substances. It is hazardous at this stage to attempt a full theoretical explanation of the effects observed until more experimental data are made available. But there can be no doubt that the effect observed is a statistical effect. Under the influence of the magnetic field the para- or dia-molecules tend to attain a preferred orientation which is opposed by thermal

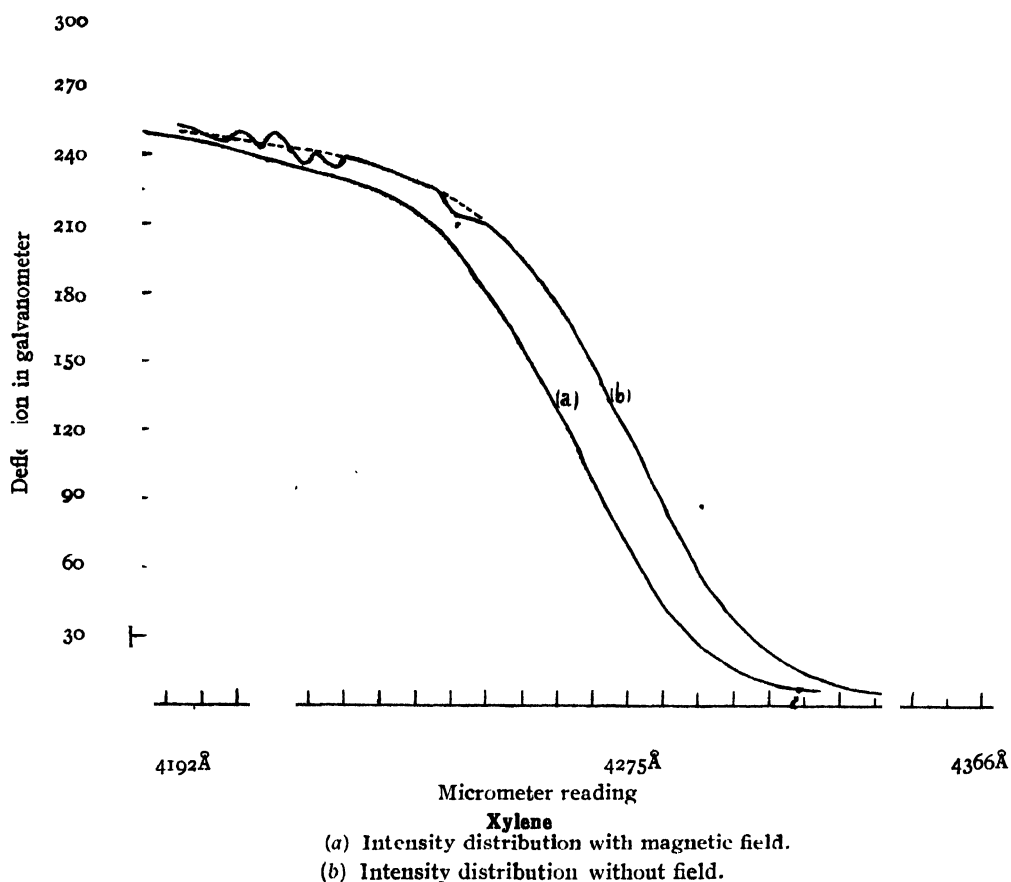


FIG. 3

agitation until a balance is obtained. That this preferred orientation affects the transmission of light in one sense in the case of para-magnetic molecules and in the opposite sense in the case of dia-magnetic molecules indicates a certain space-asymmetry in the shape of the molecules or molecular groups. It may not be far from the truth to suppose that the variation of the resolved part of the cross-section of the oriented molecules or the molecular groups, perpendicular to the direction of transmission of the rays may be responsible for the changes in the intensity of the transmitted beam.

My thanks are due to Professor S. P. Prasad and Professor M. N. Verma for their able guidance and to the Government of Bihar for the award of a Research scholarship. My thanks are also due to Principal K. Prasad for his keen interest in the work.

PHYSICS LABORATORY,
SCIENCE COLLEGE,
PATNA.

REFERENCE

Muller, 1942, *Phys. Rev.*, 61, 631.

DISINTEGRATION OF BORON BY SLOW NEUTRONS

BY S. D. CHATTERJEE

(Plate V)

ABSTRACT. The disintegration of boron by slow neutrons has been investigated using an ionisation chamber filled with boron trichloride in conjunction with a linear amplifier and loop oscillograph.

The various factors which can affect the size of oscillograph deflections and thereby introduce a distortion in the shape of the distribution curve have been discussed.

The experimental evidence points to a reaction energy of about 2.5 eMV. It appears that the transition to the ground state of ${}_3\text{Li}^7$ is forbidden, and that the reaction leads to an excitation state in the ${}_3\text{Li}^7$ nucleus, with different angular momentum for which the transition is allowed.

INTRODUCTION

The nuclear transformation of Boron by slow neutrons has been the subject of several investigations. With slow neutrons, three different particle-disintegration processes are energetically possible. These are :

- $$\begin{aligned} (1) \quad & {}_5\text{B}^{10}(n, \alpha){}_3\text{Li}^7 \\ (2) \quad & {}_5\text{B}^{10}(n, p){}_4\text{Be}^{10} \\ \text{and } (3) \quad & {}_5\text{B}^{10}(n, 2\alpha){}_1\text{H}^3 \end{aligned}$$

From the known mass-data occurring on both sides, we get $Q = 2.98$ eMV and $Q = 0.41$ eMV respectively for the first two reactions. The third involves a double process and takes place only with fast neutrons. For the investigation with particle emission, one can proceed in two different ways: Firstly, one can measure, in a cloud chamber, the sum of the ranges $R_\alpha + R_{\text{Li}}$, from the photographs of the tracks and ascertain the energy-balance from the range-energy relation of α -particles, given by Bethe (1937), or secondly, one can directly estimate the energy release $E_\alpha + E_{\text{Li}}$ with an ionisation chamber and proportional amplifier or Hoffmann electrometer. The energy of incident slow neutrons may be taken to be zero and therefore, in the present case, the energy release is identical with the energy balance. The energy-balance of the reaction, computed from cloud chamber studies have yielded Q -values from 2.15 to 2.66 eMV. These are too low compared to $Q = 2.98$ eMV obtained from mass-data. This discrepancy cannot be accounted for as being due to experimental errors. It leads one to suspect that the rather infrequent emission of α -particle in which the final nucleus ${}_3\text{Li}^7$ is formed in the ground state has probably been missed in the cloud chamber, the tracks recorded being those in which ${}_3\text{Li}^7$ is formed in one of its excited states. Consequently, the kinetic energy of the outgoing α -particle is less than its maximum value by the excitation energy of the ${}_3\text{Li}^7$ nucleus above the ground state. The proton-emission process has also been missed in the cloud chamber studies. If it so happens that the range of the α -particle from the first reaction and that of the proton from second reaction are accidentally almost equal, there will be serious confusion between α -tracks and proton tracks in the cloud

chamber photographs. The Q -values of the two reactions being widely different, the cloud chamber data will give misleading result.

In order to study the boron disintegration process more accurately, Maurer and Fisk (1939) adopted the second method, *viz.*, the ionisation chamber and proportional amplifier method. This method offers some obvious advantages: (1) It gives immediately the energy-balance and so makes the use of the rather inaccurate range-energy curve superfluous. (2) In the comparatively small time a large number of boron disintegrations can be observed and an energy distribution curve of the emitted particles is obtained with sufficiently low statistical error, and (3) the Q -values of α -emission and proton-emission processes being widely different, they can be easily distinguished. A careful analysis of the distribution curve led these authors to the conclusion that in the disintegration of boron by slow neutrons, both α -particles and protons are emitted, according to the reactions: ${}_5\text{B}^{10}(n, \alpha){}_3\text{Li}^7$ and ${}_5\text{B}^{10}(n, p){}_4\text{Be}^{10}$ respectively. The protons emitted in the (n, p) process do not show any discrete group-structure. The α -particles due to (n, α) process, on the other hand, show four definite groups of particles. The first of these corresponds to the formation of ${}_3\text{Li}^7$ in the ground state, while the others correspond to the three excited states ${}_3\text{Li}^7$ at 200, 410 and 640 eKV.

The accuracy of the above results is questioned by Wilson (1941). He carries out the same experiment by identical method, but does not confirm the results of Maurer and Fisk. He finds evidence for only two disintegration energies. The greater energy corresponds to the formation of ${}_3\text{Li}^7$ nucleus in the ground state and is of the value 2.99 eMV., while the smaller energy, which is released in about 93-94% of the disintegrations, is 2.57 eMV. No evidence for the (n, p) process is available. Wilson gives a detailed analysis of the factors affecting the shape of the distribution curve, and suggests that the multiple peaks in the distribution curve of Maurer and Fisk is due to distortion in their amplifier, coupled with statistical variations.

Wilson's analysis containing factors governing the form of the distribution curve obtained by this method, is of far-reaching consequence. The main considerations for such an analysis are discussed below.

FACTORS AFFECTING THE SHAPE OF THE DISTRIBUTION CURVE

(a) Influence of the time constants of circuits on the wave-form of pulses

If a number of pairs of ions of charge q is formed between the electrodes of an ionisation chamber of capacity C and there is a steady potential difference between the plates, the potential of the collecting plate will rise approximately linearly with time,

$$\begin{aligned} V_t &= V_0(1 - e^{-t/\tau_c}) \\ &= V_0 t / \tau_c \text{ (approx.) for } t < \tau_c \end{aligned}$$

where V_0 (maximum potential change) $= q/C$ and τ_c collecting time of the ions.

The function of the electrometer tube extends over two periods—a charging period, corresponding to the time of collection of the ions and a period of discharge necessary for the leakage. The amplitude of the pulses and their duration are determined by the time constant of the circuit assembly of the collecting electrode and the grid, which is equal to $R_0 C_0$ where R_0 is the resistance of the whole circuit and C_0 the capacity with respect to earth. As stated by Ortner and Stetter (1929), the potential of the grid of the electrometer tube attains a value

$$V = R_0 \cdot q / \tau_c \cdot (1 - e^{-t/R_0 C_0}) \quad \text{for } 0 < t \leq \tau_c$$

while the recovery to the equilibrium potential of the grid is affected according to the equation

$$V = R_0 \cdot q / \tau_c \cdot (1 - e^{-\tau_c/R_0 C_0}) \cdot e^{-(t-\tau_c)/R_0 C_0} \quad (\text{for } t > \tau_c).$$

The time constant $K = 1/R_0 C_0$ thus appears to be the parameter which determines the amplitude and at the same time the duration of the pulse. The time taken to reach a maximum is that taken by the slowest ion to reach the plates. The exponential decay, depending upon K , is usually a matter of a few seconds; so it is sufficient to consider V as a constant while considering the decay of the grid voltages of the succeeding valves of the amplifier. Such an impulse is fed to the input of the first valve of the linear amplifier. The input (first) coupling circuit consists of a grid resistance R_1 in series with a grid condenser C_1 . The voltage across them is V and the voltage V_{g1} across the resistance is applied to the grid of the succeeding valve. During the initial charging up period V_{g1} will increase simultaneously with V which is the varying potential on the anode of the electrometer tube. It may be shown that during the initial rise of the grid potential, V_{g1} rises according to the law

$$V_{g1} = V_0 \cdot \tau_c / \tau_e \cdot (1 - e^{-t/\tau_e})$$

where

$$\tau_e = R_1 C_1.$$

When V reaches its maximum value V_0 at time $t = \tau_c$, V_{g1} also attains its maximum value

$$\begin{aligned} V_{g1} (\text{max.}) &= V_0 \cdot \tau_e / \tau_c \cdot (1 - e^{-\tau_c/\tau_e}) \\ &= V_0 (\text{approx.}) \text{ because } \tau_c / \tau_e \ll 1. \end{aligned}$$

The grid potential of the succeeding valves also reach their maximum values simultaneously. In considering the subsequent behaviour of V_{g1} it is sufficient to consider V as a constant.

Thus V_{g1} decays exponentially according to the law

$$V_{g1} = V_0 e^{-t/\tau_e}.$$

In considering the form of the impulse at later stages of amplification it will be sufficient to treat it as rising instantaneously to a certain value and then decaying according to the law given below.

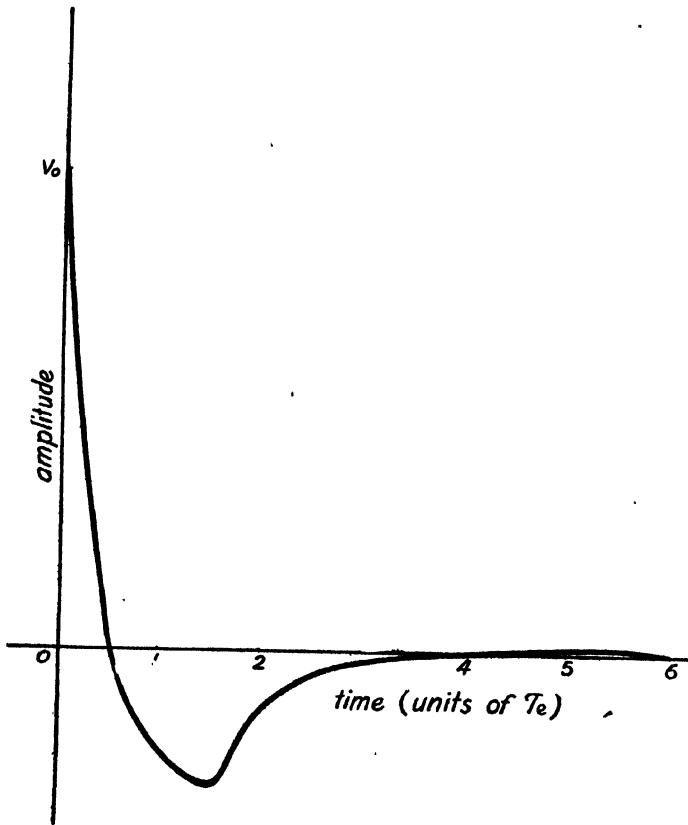
After passing through the second coupling circuit

$$V_{g2} = V_{g1} (\text{max.}) (1 - t/\tau_e) e^{-t/\tau_e}.$$

After passing through the third coupling circuit

$$V_{g_3} = V_{g_3}(\max) \left(1 - \frac{t}{\tau_c} + \frac{1}{2} \frac{t^2}{\tau_c^2} \right) e^{-t/\tau_c}.$$

The anode current of the third valve (power valve) of the linear amplifier which actuates the oscillograph, undergoes a corresponding variation. The form of the impulse is depicted in Fig. 1. If a second pulse arrives before the original



Form of impulse after passing through three similar coupling stages

FIG. 1

one dies out, evidently the recorded size of the second pulse is different from its ideal value. This causes a broadening of the distribution curve at the skirts. A slow counting rate, depending upon the time constant of the circuit must therefore be used.

(b) *Collecting time*

It has been shown in the previous section that as the ions formed inside the ionisation chamber are all collected, the grid of the electrometer tube attains a value

$$\begin{aligned} V_0 &= R_0 q / \tau_c \cdot (1 - e^{-\tau_c / R_0 C_0}) \\ &= q / C_0 \quad \text{when } \tau_c \ll R_0 C_0. \end{aligned}$$

where C_0 is the capacity of the electrodes and associated circuits, and then very slowly decays exponentially to zero. Such an impulse will be distorted on passing through the intervalve couplings of the linear amplifier. We have seen that passing through the first coupling circuit,

$$V_{g1} = V_0 \tau_c / \tau_e (1 - e^{-\tau_c / \tau_e}),$$

i.e., the maximum will be reduced to a fraction $(1 - e^{-\tau_c / \tau_e}) \cdot \tau_c / \tau_e$, of its ideal value.

For short collecting times $\tau_c \ll \tau_e$

$$V_{g1} = V_0 (1 - \frac{1}{2} \tau_c / \tau_e),$$

i.e., the fractional reduction in voltage is $\frac{1}{2} \tau_c / \tau_e$; the effects of successive stages are additive, so that for n similar coupling stages the reduction of voltage is $n \tau_c / 2 \tau_e$. When disintegrations take place in a gas, τ_c will vary according to the place where the disintegration occurs, and so also with the size of kick on the oscillograph. The form of the distribution curve will consequently be broad at the peak. This broadening is greatest for long collecting times.

If therefore we wish to have a spread of less than 10% in the peak,

$$\frac{n \tau_c}{2 \tau_e} < \frac{1}{10}, \text{ or, } \tau_c < \frac{2 \tau_e}{10n} < \frac{\tau_e}{15}$$

for an amplifier as ours, consisting of three similar coupling stages. Thus, it is essential that the collecting time of the ions must be much smaller than the time-constant of the coupling circuits.

(c) Geometry

If disintegrations take place in the gas of an ionisation chamber, then a number of disintegration particles will strike the electrode or pass out of the effective collecting volume, and the full number of ions will not be collected. Wilson has shown that for a parallel infinite pair of plates and for an isotropic disintegration, the distribution of the lengths of the paths is represented by a back-ground of uniform height upon which is superimposed a peak of the same shape as the original but reduced in size. If the separation of the plates is d , and the length of the path of the disintegration particles is l_0 , then the fraction of the total which is in the back-ground is $l_0 / 2d$ ($l_0 \leq d$). Since the shape of the peak is unaltered, it is unnecessary to use a very large separation of the plates to avoid 'edge' effects, although it is an advantage to have the diameter of the plates large compared with their separation.

From the above considerations it is obvious that the conditions for obtaining a sharp peak in the distribution curve are:

- (a) Short collecting time
- (b) An amplifier with coupling circuits of long time constant
- (c) Slow counting rate.

EXPERIMENTAL ARRANGEMENT

Schematically, the experimental arrangement consists of :

- (1) an ionisation chamber which collects the ions formed by the passage of the incident particle
- (2) an electrometer tube which receives the charges collected and transmits them in the form of a voltage impulse
- (3) a linear amplifier
- (4) an oscillograph for recording the final impulse.

(1) IONISATION CHAMBER

The two essential parts of an ionisation chamber are the collecting electrode and the high voltage electrode, between which pervades the gaseous space in which the ions are formed by virtue of collision with the incident particle. In order to have a highly sensitive chamber, its capacity is made as small as possible, the variation of charge being proportional to the inverse of capacity. It is therefore advantageous to increase the depth of the chamber with electrodes of a given form inasmuch as the length of the path of the incident particle is increased and so also the number of ions produced. For this reason there is a tendency to increase the interior volume. This is, however, not always convenient. If the gas pressure is p and the separation of the plates is d , then the collecting time is proportional to pd^2 for a given collecting voltage. The edge effect is inversely proportional to pd . If we are limited, as in this case, by the total available voltage to be applied to the H. T. electrode of the ionisation chamber, then the small chamber at high pressure has the advantage over a large one at low pressures. Besides, when one works in the presence of γ rays, the number of secondary electrons produced is greater the greater the volume. This phenomenon is manifested as an increase in the back-ground hiss, thus reducing the relative sensitivity of the measurements. It is also difficult to screen a big chamber from electrical interference, as one point only is effectively earthed.

Maurer and Fisk used an ionisation chamber 30 cms. diameter and 30 cms. deep. The effective volume was enclosed between two H. T. plates 20 cms. diameter, the separation between them being also about 20 cms. The collecting electrode was situated midway between the H. T. electrodes and surrounded by an earthed guard-ring, so that the electric field between them was essentially homogeneous. A stabilised H. T. of about 8000 volts was put on the H. T. electrodes of the ionisation chamber. The chamber was filled with boron trichloride at varying pressures from 70 to 210 mm. It may be incidentally pointed out that the collecting time at the higher pressure is not lower than $1/100$ sec. A weak source was kept inside an angular space situated above one of the H. T. electrodes. A narrow hole, in front of the source restricted the number of α -particles to about six per minute. A thin mica foil was also placed in front of the source so that the emerging α -rays have an energy of about the same order as the boron disintegration α -rays.

The chamber used by Wilson had plates 8 cm. diameter separated by 9 mm. and was filled with boron trichloride to a pressure of 53 cms. at 20°C. The calibration was done by means of α particles from a source of thorium active deposit, when the ionisation chamber was filled with air.

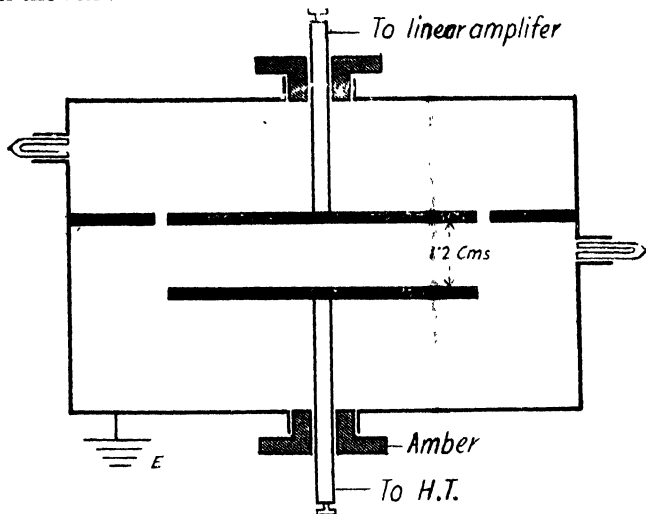


FIG. 2(a)

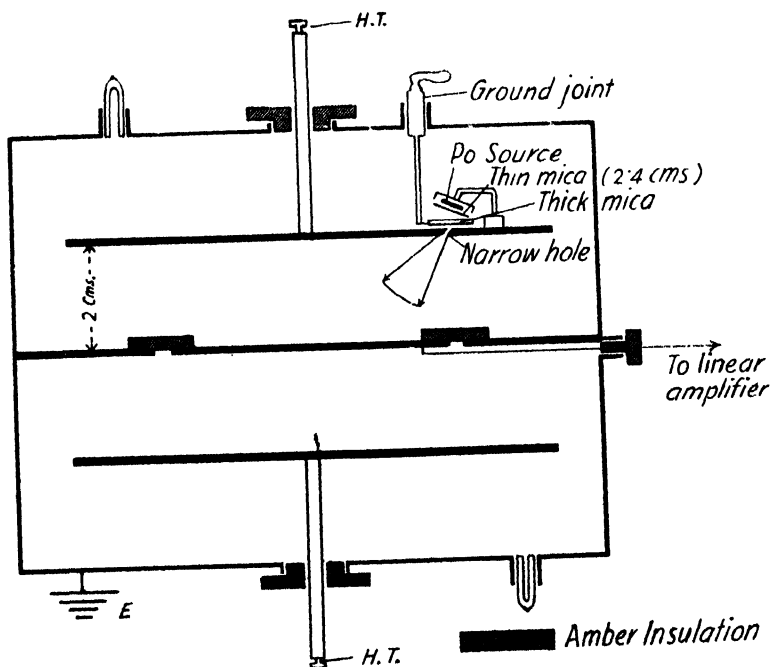


FIG. 2(b)

The chamber used mostly in the present experiment was essentially similar to that of Wilson. It consisted of a parallel plate condenser, the plates having

diameter of 8 cms. and separation 1.2 cms. They were housed in a cylindrical brass chamber which had "earth" potential. The leads to the plates passed through amber plugs. One of the plates was given +1800 volts, coming from a neon stabiliser. The chamber was filled with boron trichloride to a pressure of 57 cms. at 25°C. When the chamber had been filled with air, the amplifier was calibrated by means of freshly deposited Po α -rays. A second ionisation chamber, closely resembling that of Maurer and Fisk, but much reduced in size, was also used for subsidiary experiments. An essential difference in this arrangement was that the Po source was covered by a thick mica vane which completely cut off the α -rays from entering the effective volume of the chamber. By the manipulation of a ground joint from outside, the mica vane could be removed from the path of the beam when calibration was necessary. The schematic diagrams of both the chambers are given in Figs. 2(a) and 2(b).

The neutron source consisted of a glass tube containing 65 mc (Ra-Be) placed inside a lead house of 10 cms. thickness. The latter was covered on all sides by paraffin bricks of 5 cms. thickness. The source was kept at a sufficient distance from the chamber so that the maximum counting rate was about 30 per minute. The ionisation chamber was also surrounded by 5 cms. of paraffin wax. A weak (Po-Be) source was also occasionally used.

(2) FIRST STAGE : ELECTROMETER TUBE

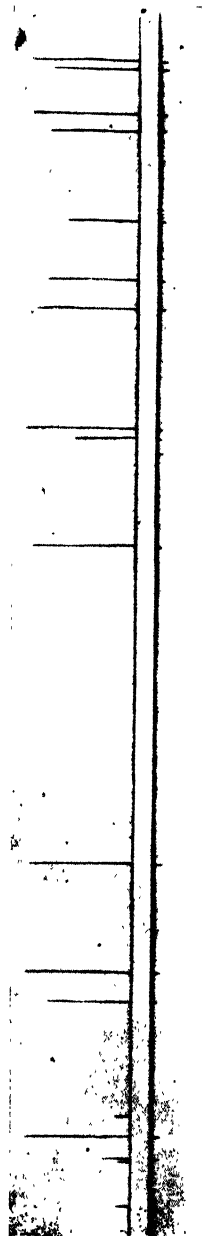
The electrometer tube was a triode, whose highly insulated grid was directly connected to the collector electrode of the ionisation chamber; it transformed the impulses produced by the passage of α -particles across the chamber into plate current variations. In order to avoid the Johnson (1927) fluctuations in leak resistances, a floating grid was used. It was biased by itself and attained an equilibrium potential determined by the space charge of the electrometer tube. The leakage of the charges arriving at the grid was assured by the electron current itself. The tube was mounted vertically along the axis of an air-tight brass chamber, always in presence of desiccating substances. Mechanically it was supported on the shield itself by means of a very flexible rubber suspension which eliminated shocks and vibrations and also protected the valve from light.

A high positive voltage was used on the H.T. electrode of the ionisation chamber, enabling the accumulation of positive ions on the collecting electrode. This ensures a much more rapid discharge of the grid than when a negative voltage is applied, *i.e.*, when the voltage is of the same sign as the space charge of the electrons.

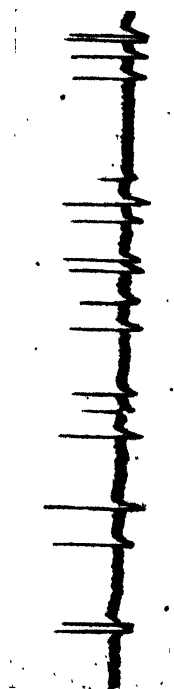
(3) SECOND STAGE : AMPLIFIER

The role of the amplifier is to amplify each pulse linearly. Using valves of very high amplification factor, one can now-a-days obtain with a set of three pentodes an amplification equal to or greater than what could be obtained previously with five or six valves; the fluctuations incumbent upon them have,

Registration of Boron—disintegration Pulses



Recording by Loop oscillograph



Recording by Cathode-ray oscilloscope

therefore, been considerably reduced. The role of amplification fell on the first two valves while the last, a power pentode, produced output pulses of sufficiently strong current to move an oscillograph.

The plate of the electrometer tube was $r-c$ coupled to the grid of the first amplifying tube. As the method was generally used for high-speed recording of α -particles, high resolving power was necessary. Hence artificial distortion was deliberately applied for sharpening the pulses by making the time constant of the first coupling stage of the amplifier small. Wynn-Williams and Ward (1931) made the time-constant even much less with a view to amplifying only the start of the discharge and to make pulses very sharp. If it so happens, as in the case of Maurer and Fisk, that the time constant of the first coupling stage be smaller than the collecting time of the ions, the shape of the distribution curve will evidently be distorted as pointed out by Wilson. In the present experiment, the three coupling circuits had time-constants of $1/20$ second each. The shielding of the elements of the amplifiers and its connection to earth together with perfect decoupling of all voltage supplies were essential precautions taken in setting up the apparatus and obtaining stable operation and a very reduced background hiss due to Shot effect. The resistances were all wire-wound and condensers were of mica.

Tests of the linear response of the amplifier and constancy of amplification were frequently made by applying a small variable alternating voltage to the ionisation chamber and measuring the corresponding amplitude of the oscillations reproduced by the oscillograph. If the amplification is proportional, the amplitude-voltage curve is a straight line. Further test was made by plotting the Bragg curve, with shallow ionisation chamber, for α -particles of known range and specific ionisation such as those emitted by Po electrochemically deposited on a silver foil, and comparing it with a standard curve.

(4) RECORDING APPARATUS

In selecting this two essential qualities need be considered: its resolving power and sensitivity. It should have sufficiently low period, less than the power of resolution of the amplifier, so that pulses which have been separately handled in the amplifier may not be superposed or confused with one another. In practice, frequencies of the order of 1000 to 5000 are enough.

Two types of oscillograph were made and experimented with. The moving armature type was a modification of Wynn-Williams recorder. Owing to a large number of turns in the coil, it had an appreciable inductance and so caused the anode current rise exponentially with the characteristic time-constant. By using a pentode of high impedance and high mutual conductance for the output stage, this lag was appreciably reduced. The performance of the loop oscillograph was, however, very satisfactory. It consisted of a loop of ribbon running over grooves in two ivory bridges and held in tension by an ivory pulley. It carried a tiny mirror $1\frac{1}{2}$ mm. \times $\frac{1}{2}$ mm. and was situated in a

strong magnetic field. Its frequency of response was over 5000. The oscillograph was critically damped in oil. The pulses were registered on a slowly moving cine-film. A record of the pulses is shown in Plate V(a).

Preliminary adjustments were made by visual observations with a cathode ray oscillograph. The pulses, were usually so fast that it was difficult to get their trace on the running film. Using a higher time-constant in the last coupling stage, the pulses, though slightly distorted, were easily photographed. A record of the Cathode ray oscillograph pulses is shown in Plate V(b). The recording camera was specially designed for running perforated cine-films at constant speed over a widely variable range.

RESULTS

A systematic study of the shape of the distribution curve was made under different experimental conditions imposed by changing (a) the collecting time of ions, (b) the time-constant of coupling circuits and (c) the counting rate. The distribution curve obtained under best conditions is shown in Fig. 3. The single

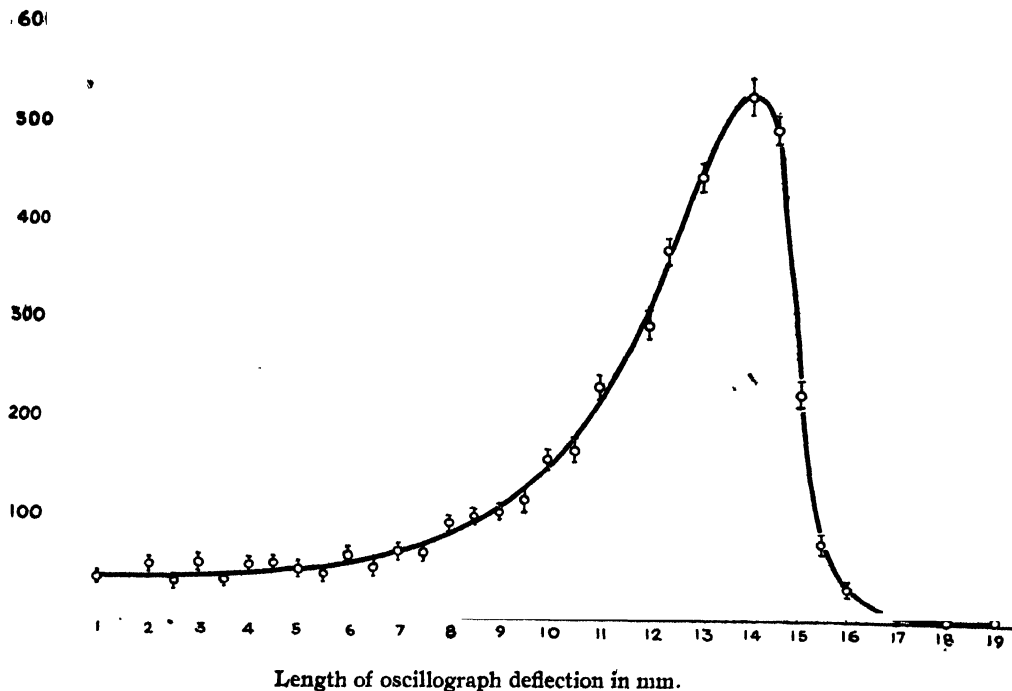


FIG. 3

peak must clearly correspond to the reaction commonly observed. The energy-release is approximately 2.5 eMV. Using the ionisation chamber 2(b) this energy release could be conveniently compared with the pulses due to α -particles. It was found, however, that the chamber used to get contaminated within a few

days and emitted short pulses even in absence of the neutron source.* The idea of putting the calibrating source within the chamber was therefore abandoned and the distribution curve shown in Fig. 3 was obtained with chamber 2(a), which, incidentally, had negligible back-ground effect.

It will be seen that the second peak obtained by Wilson, corresponding to an energy release of 2.99 eMV and whose magnitude is about 6-7% of the disintegrations, has been missed in our case. Although there are oscillograph kicks representing the corresponding energy release, there is little evidence of a peak in that area in our distribution curve.

Fig. 4 shows the distribution curve under different experimental conditions. It was obtained when the Ra-Be source was kept near the ionisation chamber and therefore a much higher counting rate was employed. The curve is broadened in spite of the fact that a time-constant of 1/500 sec. was employed for the first coupling stage.

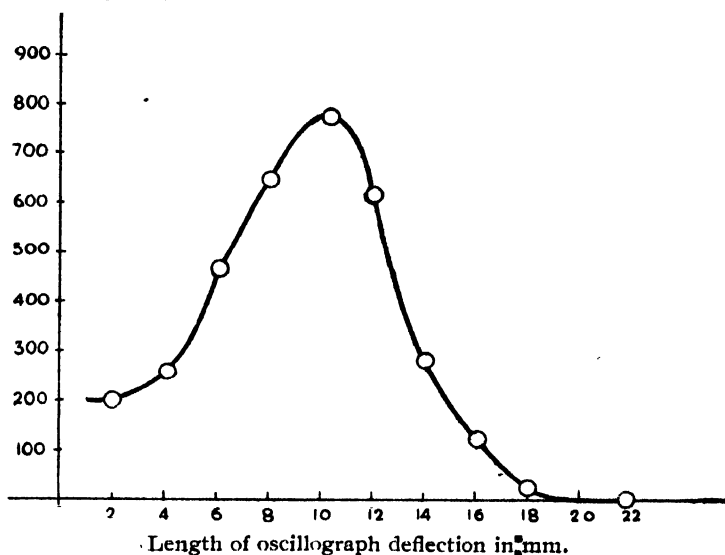


FIG. 4

DISCUSSION OF RESULTS

The experimental evidence points to a reaction energy of about 2.5 eMV. The energy calculated from mass-values gives $Q=2.99$ eMV. A possible explanation is that the transition to the ground state of ${}_3\text{Li}'$ is forbidden and that the reaction leads to an excitation state in the ${}_3\text{Li}'$ nucleus, with different angular momentum, for which the transition is allowed. The following piece of experimental evidence lends support to the above interpretation :

(1) The non-capture excitation of ${}_3\text{Li}'$ by α -particles in the reaction

* It is not unlikely that the occurrence of numerous short pulses in Maurer and Fisk's arrangement, ascribed to protons, may be traced to be due to the constant presence of the calibrating source of Po within the ionisation chamber.

${}_3\text{Li}^7(\alpha, \alpha+\gamma){}_3\text{Li}^7$ results in γ radiation of about 0.4–0.6 eMV indicating such a level.

(2) Rumbaugh and Hafstad (1936) obtained two proton groups from the reaction ${}_3\text{Li}^6(\alpha, \gamma){}_3\text{Li}^7$. The long range group probably corresponded to the formation of ${}_3\text{Li}^7$ in the ground state, while the short range group indicated an excitation level in ${}_3\text{Li}^7$ at about 0.44 eMV. The corresponding γ -ray of energy about 0.40 eMV was detected by Williams, Shepherd and Haxby (1937).

(3) According to Roberts, Heydenburg and Locher (1938) and also Maier-Leibnitz (1938) the radioactive ${}_4\text{Be}^7$ is accompanied by a γ -radiation of energy 0.425 eMV when it is being transformed into ${}_3\text{Li}^7$ by the process of β -ray decay. It is suggested that the γ -ray energy arises from a transition between the two levels in the resultant ${}_3\text{Li}^7$ (e.g., Livingstone and Bethe (1937), Rumbaugh, Roberts and Hafstad (1938)).

(4) The ${}_3\text{Li}^7$ nuclei formed in the excited state in the reaction ${}_5\text{B}^{10}(n, \alpha){}_3\text{Li}^7$ will go to the ground state by the emission of a γ -ray. Fleischmann (1935) and also Kikuchi, Aoki, Husimi (1936) indicated the presence of a γ -ray. Wilson has, however, definitely proved its existence by using a boron-lined proportional counter in coincidence with an adjacent γ -ray counter. The neutron source and both counters were embedded in blocks of paraffin wax. The resolving time of the coincidence circuit was rather less than 2×10^{-6} sec. so that no coincidence between the γ -rays and neutrons emitted by the source could be recorded owing to the fact that the neutrons take a time of about 10^{-5} second to slow down to thermal velocities. The coincidences observed were therefore due to γ -rays associated in time with the α -rays from the boron disintegration. The absorption coefficient of the radiation was measured by measuring the coincidence rates when different thicknesses of lead were placed between the two counters. The energy of the observed radiation was about 0.5 eMV.

The author expresses his grateful thanks to Prof. D. M. Bose, Director, Bose Research Institute, for his kind and helpful interest in this work. His thanks are also due to Mr. S. K. Chatterjee and Dr. H. Rakshit for unflinching support.

BOSE RESEARCH INSTITUTE,
93, UPPER CIRCULAR ROAD,
CALCUTTA.

REFERENCES

- Bethe and Livingstone, 1937, *Rev. Mod. Phys.*, **9**, 266
 Fleischmann, 1935, *Zeit. f. Phys.*, **97**, 242.
 Johnson, 1927, *Phys. Rev.*, **29**, 367.
 Kikuchi, Aoki and Husimi, 1936, *Nature*, **137**, 745.
 Livingstone and Bethe, 1937, *Rev. Mod. Physics*, **9**, 325
 Maier-Leibnitz, 1938, *Naturwissenschaften*, **25**, 614.
 Maurer and Fisk, 1939, *Zeit. f. Phys.*, **112**, 436
 Ortner and Stetter, 1929, *Zeit. f. Phys.*, **54**, 449.
 Roberts, Heydenburg and Locher, 1938, *Phys. Rev.*, **53**, 1016.
 Rumbaugh and Hafstad, 1936, *Phys. Rev.*, **50**, 681.
 Rumbaugh, Roberts and Hafstad, 1938, *Phys. Rev.*, **54**, 655.
 Williams, Shepherd and Haxby, 1937, *Phys. Rev.*, **52**, 390.
 Wilson, 1941, *Proc. Roy. Soc. (A)*, **177**, 382.
 Wynn-Williams and Ward, 1931, *Proc. Roy. Soc. (A)*, **131**, 391.

A NEW BAND SYSTEM OF THE HgBr MOLECULE.

BY K. R. RAO AND G. V. S. RAMACHANDRA RAO

(Plate VI)

ABSTRACT. A new band system of the HgBr molecule is obtained in the ultra-violet between $\lambda 2470$ and $\lambda 2430$, consisting of about 20 bands, which are headless and diffuse. The three sequences $\Delta v = 0$ and ± 1 are identified. The bands are represented by the formula

$$\begin{aligned} \nu = & 40720 + [166(v' + \tfrac{1}{2}) - 1.1(v' + \tfrac{1}{2})^2] \\ & - [183(v'' + \tfrac{1}{2}) - 2.0(v'' + \tfrac{1}{2})^2] \end{aligned}$$

The system is considered as due to a transition from a higher $^2\Sigma$ state to the lower ground state $^2\Sigma$, determined previously by Wieland.

INTRODUCTION

It is well-known that the diatomic halides of the elements of Group II-a of the Periodic Table give rise to band systems ascribed to transitions from a higher $^2\Pi$ or $^2\Sigma$ to a lower $^2\Sigma$ state. That the ground state is a $^2\Sigma$ has been established from experiments on the absorption of a few of the halides. Our knowledge of the similar molecules of the Group II-b elements is still far from complete. Reporting the analysis of the HgI bands, an attempt has been made by Howell (1943) to systematise and interpret the band spectra of the diatomic halides of Zn, Cd and Hg. In the light of Howell's observations, a reinvestigation of the spectra of HgCl, HgBr and HgI has been undertaken by the authors, in continuation of the work carried out by Sastry (1941 and 1942) in this laboratory.

The results obtained by us in the case of HgCl (reported briefly in *Current Science* in press) show that there are two distinct band systems of this molecule in the ultra-violet, due to transitions from two different $^2\Pi$ states to a common lower $^2\Sigma$ state, which is considered to be the ground state of the molecule, on the analogy of the other related molecules. One of the systems (lying between $\lambda 2900$ and $\lambda 2700$), was analysed partially by Cornell (1938) and more completely by Sastry (1941). The separation is about 90 cm^{-1} . The other system, also due to $^2\Pi - ^2\Sigma$, has the electronic width as large as 3890 , leading to widely separated components $^2\Pi_{3/2} - ^2\Sigma$ and $^2\Pi_{1/2} - ^2\Sigma$, the former being the one designated as Class I by Wieland (1929). The latter has been established by the authors in the region $\lambda 2900 - \lambda 2700$. A full discussion of these would be presented in another paper.

HgBr BANDS

In the case of HgBr as well, two band systems are known in the ultra-violet, as investigated by Wieland and by Sastry; the correlation between the two does not appear to be satisfactory. The interval between the (0, 0) bands of these two systems is 4014 cm^{-1} and agrees well with what might correspond to the electronic doublet width, expected for this molecule on the basis of

Howell's suggestion. But the constants obtained for the two systems indicate no common level.

Table I shows a comparison of the vibrational constants for the ground states of HgF and HgCl (in cms^{-1}).

TABLE I.

Molecule	ω''	$x''\omega''$
HgI ¹	490.8	4.05
HgCl	293.4	1.82
HgBr	W186.25 S372.3	W0.975 S3.8

For HgBr the upper values marked W are those derived by Wieland and the lower by Sastry, for the two different systems. The upper value is in conformity with that expected to be the normal state of HgBr. The lower value, if it proves to be real, must correspond to a $^2\Sigma$ state, different from the ground state of this molecule.

A reinvestigation of the HgBr bands, to bring them, if possible, into conformity with the HgCl bands mentioned above, is considered desirable. With this aim, the spectrum has been photographed again under different temperature and pressure conditions, using the same source as that employed by Sastry previously. Particular attention is paid to examine the variations, if any, in the intensity distribution among the bands leading to the possibility of splitting the less refrangible system into two different systems. While this work is still in progress, it has been noticed that a third band system is emitted by the HgBr molecule in the ultra-violet region, which was just mentioned by Sastry. The purpose of the present paper is to present details of these new bands. They occur between λ_{2470} and λ_{2430} , under the same conditions as the two previously known ultra-violet systems of HgBr. They are absent in discharges through vapours of various other salts, such as HgCl, HgI, HgO, HgS, etc.

Plate VI is a reproduction of the bands. They are headless and somewhat diffuse. Twenty-two of these could be measured on the high dispersion plates taken with Hilger E. 1 Quartz Littrow Spectrograph (2.5 Å per mm.).

Three well separated sequences, $\Delta v = 0$ and ± 1 , ascribed to a single system, have been identified, the sequence degradation of the bands being towards the less refrangible side. Table II gives the wave-lengths, intensities and wave-numbers of the bands and the last column shows the classification. The wave-numbers are given only to the nearest integer, as no greater accuracy can be obtained, on account of the nature of the bands, although the dispersion of the spectrograph is high.

In any single sequence, the band head intensity rises to a maximum and then falls off. Table III gives the intensity distribution arranged in the usual diagonal array. The intensities are visual estimates.

TABLE II
HgBr Bands

Wave-length	(Int.)	Wave-number	Classification (v' , v'')
2469.5	(0)	40481	(6, 7)
2468.8	(2)	40493	(5, 6)
2468.3	(0)	40501	(4, 5)
2467.8	(2)	40509	(3, 4)
2467.3	(4)	40518	(2, 3)
2466.9	(1)	40525	(1, 2)
2466.4	(2)	40533	(0, 1)
2459.5	(1)	40646	(5, 5)
2458.5	(2)	40663	(4, 4)
2457.8	(3)	40675	(3, 3)
2457.0	(4)	40687	(2, 2)
2456.7	(2)	40693	(1, 1)
2455.6	(2)	40711	(0, 0)
2452.4	(2)	40764	(8, 7)
2451.2	(2)	40784	(7, 6)
2450.3	(2)	40799	(6, 5)
2448.8	(3)	40824	(5, 4)
2448.1	(4)	40835	(4, 3)
2447.5	(3)	40846	(3, 2)
2446.5	(1)	40862	(2, 1)
2445.9	(0)	40873	(1, 0)
2437.7	(2)	41010	(4, 2)

TABLE III
Intensity Distribution

v' v''	0	1	2	3	4	5	6	7
0	2	2
1	0	2	1
2	...	1	4	4
3	3	3	2
4	2	4	2	0
5	3	1	2	...
6	2	...	0
7	2	...
8	2

The (0, 0) band is not the most intense in the system, the parabola being displaced and analogous to what is obtained in the Si N. bands (Jevons' Report, p. 66). An alternative analysis would be to consider the most intense band in each sequence as the first Q head in the sequence and regarding the fainter bands as the component P heads. This would give ω'' a value of about 172 cm^{-1} , differing much and probably beyond observational error from Wieland's value $\omega'' = 186.25$ for the ground $^2\Sigma$ state of the HgBr molecule shown in Table I. With the classification adopted here, $\omega'' = 183$. This agreement is regarded also as lending support to the assignment of the bands to the HgBr molecule.

Further confirmation from isotope shifts could not be obtained as the shifts are small and the band heads are diffuse.

The following formula has been calculated which represents the wave-numbers of the band heads approximately.

$$\begin{aligned} \nu = & 40720 + [166(v' + \frac{1}{2}) - 1.1(v' + \frac{1}{2})^2] \\ & - [183(v'' + \frac{1}{2}) - 2.0(v'' + \frac{1}{2})^2] \end{aligned}$$

The system probably arises from the transition ${}^2\Sigma - {}^2\Sigma$, the lower one being the normal state of the molecule.

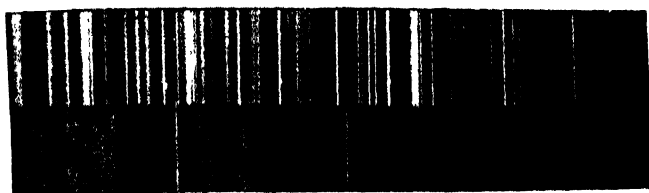
ANDHRA UNIVERSITY,
GUNTUR.

REFERENCES

- Cornell (1938), *Phys. Rev.*, **54**, 341.
 Howell (1943), *Proc. Roy. Soc.*, **A**, **182**, 95.
 Sastry (1941), *Proc. Nat. Inst. Sci. Ind.*, **7**, 351 and 359.
 „ (1942), „ „ „ „ „ **8**, 289.
 Wieland (1929), *Helv. Phys. Acta.*, **2**, 46 and 77.
 „ (1932), *Zeit. f. Phys.*, **77**, 157.

λ 2470

λ 2430



$\Delta\nu$ $\begin{array}{c} | \\ \text{Hg}_2 \\ -1 \end{array}$

$\begin{array}{cc} | & | \\ 0 & +1 \end{array}$

Band Spectrum of HgBr.

Fig. A

ON THE VARIATION IN THE EXPERIMENTALLY DETERMINED VALUES OF THE MESON MASS

By D. M. BOSE *

AND

Miss BIBHA CHOUDHURI

(Received for Publication, September 9, 1944)

ABSTRACT. In this paper all reliable data on meson mass determinations have been collected together. The assumptions underlying the different experimental methods as well as their reliability have been discussed. It is found that large variations in the meson mass values occur, both when different experimental methods are used as well as when the same method is used by different observers. It is made probable that apart from the large errors of measurements associated with the present methods of meson mass determinations, the variation in mass values depend also in some way not representable by the relativity formula on the velocity of the meson particle. Possible causes of such variations are discussed.

1. INTRODUCTION

In a previous paper by one of us, (Choudhuri 1944), (referred to as Paper I), a method is described of measuring the mass of cosmic ray particles which produce single ionisation tracks on photographic plates exposed under air to cosmic rays at Sandakphu (elevation 12,000 ft.). The results of measurements made on two plates exposed at different times to cosmic radiation is given in Table I.

Plates I and II were Ilford new halftone plates, taken from two different batches ordered from England at intervals of one year, and sent to Sandakphu on two different occasions between which one year intervened. Plate I recorded a larger number of ionization tracks than Plate II; in the latter very few tracks were found in which the mean grain spacing between silver grains deposited along them lay between 5 and 6μ . In spite of the differences in the sensitiveness of the two plates, the average mass of the penetrating particles had very similar values and varied in a similar way with the energy. Such agreement between the mass values as function of the mean energy of the particles, appeared to us to preclude the possibility of the mass variation being due to statistical errors. Starting from low energy particles, it will be noticed that the average mass diminishes with increasing energy of the particles to a minimum, and then again it increases.

It is well-known that wide variations in the experimentally determined meson mass values have been obtained by competent observers, using different experimental methods. Even the same experimental method used by different investigators have led on different occasions to widely differing mass values. Such variations, in the results obtained by one and the same observer may be due partly to experimental difficulties, and in the results of different investigators using the same technique, to the different methods of interpreting their experimental observations. One good example of such differences in interpretation is the different empirical methods used by Williams and Wilson (1939), and by Corson and Brode (1938) of deducing the velocity βc of the ionising particles as function of the relative ionization density D along their tracks (see section 3 A).

* Fellow of the Indian Physical Society.

But even making allowances for the occurrence of large experimental errors, the mass values obtained are so widely different that it has led competent investigators like Anderson and Neddermeyer (1939) to the statement "it has become increasingly likely that a complete interpretation of the experimental data is not found in the single assumption of an unstable particle with a single charge and a unique mass of the order of 200 electron mass".

Another characteristic constant of the meson, *viz.*, its proper life time τ_0 , also shows large variations in experimentally determined values. Weisz (1941) has recalculated the rest life time of cosmic ray mesons obtained by different observers, on the basis of the same rest mass. The values of the rest time thus recalculated still disagree amongst themselves and they are shown by Weisz to be function of the mean path-length of the decaying meson employed in the different experiments. Weisz says "when instead of the existence of only one possible value of the rest mass, for which we have no experimental evidence, a distribution of rest mass is assumed, the described phenomena can be accounted for, regardless of what form the mass distribution may have". The assumption made by Weisz is 'that at each energy there is a distribution of rest mass amongst the mesons'. Bernadini (*et al* 1941) conclude their recent short communication "Differential measurement of meson life time at different elevations" with the remark "we wish to call attention to our results that $(\mu c^2)/\tau$ increases with increased altitude and *average meson energy*." Since $(\mu c^2)/\tau = (\mu c^2)/\tau_0 \sqrt{1-\beta^2}$ this quantity should diminish with increasing β , *i.e.*, if the interpretation of their experimental results by these investigators is valid, then it would imply that the rest mass of the meson increases with its energy in a manner not accountable by the theory of relativity.

With such variety of results and of their interpretations, on the existence and possible cause of the variation in the rest mass of the meson, it seemed worthwhile to examine the existing experimental data on meson mass measurement and to find out whether any correlation can be found between the kinetic energies of the meson particles and their rest mass values.

The experimental data discussed in this paper are taken from

- (i) a collection of results of twenty-four mass determinations of Wheeler and Ladenburg (1941).
- (ii) additional four mass determinations recently published by Nielson and Powell (1943).
- (iii) five mass determinations contained in Paper I.

2. THEORY

The methods which have so far been employed for determining the mass of the penetrating cosmic ray particles are based upon observations on the tracks of such particles in Wilson cloud chamber. Only in the method developed by us have observations been made on tracks of such particles in photographic emulsion. The principal characteristics of such ionising particles are its charge Ze , mass μ and velocity v . Under certain special circumstances, *e.g.*, during close

collisions of such high energy particles with atomic nuclei, the other characteristic constants of the particles, *viz.*, its spin and magnetic moment become effective. Further during close collisions interaction of non-electrical nature can occur. For our present purpose the knowledge of the first three constants are sufficient. It is an observed fact that, barring some results of Schopper (1939) on tracks of cosmic ray particles in photographic emulsions, all the cosmic ray particle tracks with β near unity, have approximately the same ionization density, from which the conclusion is drawn that these cosmic ray particles carry the same charge e . Using this assumption it is necessary to make two independent observations for the determination of the mass of the penetrating particles. For all Wilson chamber observations, one such determination is the curvature of the tracks of the particles in magnetic fields : the latter is given by the equation

$$pc = He\rho, \text{ where } p = \frac{\mu\beta c}{\sqrt{1-\beta^2}} \quad \dots (1)$$

The other measurement is usually based upon the loss of energy suffered by the penetrating particles in the media traversed by them. The specific charge on these particles is such, that radiation loss of energy is negligible.

The ionization of such singly charged particles is given by the equation

$$\frac{dI}{dx} = \frac{2\pi NZe^4}{mc^2\beta^2} \left[\log \frac{mc^2\beta^2 W_m}{(1-\beta^2)I^2 Z^2} + (1-\beta^2) \right] \quad \dots (2)$$

Where W_m is the maximum energy transferred by collision from the moving particle of mass μ and velocity βc to an electron, and I is the average excitation potential of the atoms traversed by the particle. The calculations of the energy loss is rather complicated when we come to the relativistic region. Ladenburg and Wheeler (1941) have shown that the expression for the energy loss takes a

$$\text{simple form} \quad \frac{dE}{dx} = \frac{A}{\beta^2} \left[\ln K + \ln \frac{\beta^2}{1-\beta^2} + (1-\beta^2) \right] \quad \dots (3)$$

when the following approximations are made. (a) The mass μ of the primary particle is large compared to the electron mass, (b) its energy is small compared to

$$\left(\frac{\mu}{m} \right) \mu c^2,$$

(c) it is moving faster than the bound electrons in the stopping atoms, and (d) its capture and loss of electron can be neglected and its nuclear charge is not very large. It will be seen that the mass and the energy of the penetrating particles used for mass determinations lie in such regions that these criteria are generally satisfied ; only in the case of the passage of heavy particles in photographic emulsions, it was shown by one of us (Choudhuri, 1942) that the conditions (c) & (d) are not satisfied,

3. METHODS

We shall now discuss the different experimental methods.

Method A. Ionization loss and curvature—The largest number of mass determinations has been made from measurements of the curvature of penetrating

particle tracks in a magnetic field, together with a count of the average number of ions per cm length of the track. The function on the right hand side of (3) varies as $1/\beta^2$ for $\beta < 0.9$ and has a minimum value for $\beta = 0.97$ and then increases with increasing β . The ionization corresponding to this minimum value is denoted by I_0 . For such measurements only particles are selected for which $\beta < 0.97$. We define a quantity $D = I/I_0$ as the relative specific ionization, and the experimental technique consists in deducing the value of β from measurements of D .

For this purpose two methods have been used

(a) Wilson and Williams (1939) have counted the number of distinct groups of droplets per cm length in sharply defined Wilson chamber tracks of low energy electrons. Each group correspond to one primary ion pair. They represent the number of ions produced by the empirical formula $I = I_0\beta^{-1.4}$. According to Corson and Brode (1938) the theoretical expression (3) can well be represented in the interval $0.2 < \beta < 0.9$ by a similar expression $I = I_0\beta^{-1.8}$. The mass values determined by the empirical curve are larger than those obtained from the theoretical curve.

(b) In the method used by Corson and Brode (1938) the expansion of the chamber is delayed, to enable the oppositely charged ions produced along the track of the ionizing particle to separate under the influence of an applied electric field. The measurements then made do not give the primary ionization, but the probable ionization, *i.e.*, the primary ionization plus the ionization produced by secondaries of energy lower than a certain critical energy. The minimum probable ionization was found to be 50 ions per cm track in air, O_2 and N_2 at N.T.P. Corson and Brode have constructed a nomograph, from which knowing the value of $H\rho$ and D the value of μ can be obtained.

In Table II A are collected all the data on the meson mass determinations using the above method. In view of the large discrepancy in the values obtained by different observers, and the different methods used by them to correlate D with β we have grouped separately the results of the measurements of (i) William and Pickup, (ii) Nielson and Powell, and (iii) also a number of isolated measurements by other investigators. In each group the data are arranged in order of increasing kinetic energies of the particles. The kinetic energies of these particles given in column I are calculated from their momenta, on the assumption that the mesotron mass is $200 m_0$.

Method B. Curvature and Range—This is a convenient method as it does not involve measurement of specific ionisation loss and is therefore independent of any special assumptions underlying the ionisation loss formula. Since the loss of energy per cm of track of all particles carrying the same charge, depend only on their velocities we can write the range $R = k \cdot m \cdot f(v)$; and for all

particles starting with the same initial velocity $\frac{R_1}{R_2} = \frac{m_1}{m_2}$. If we take the

second particle a proton, we can, by putting a reasonable value for m_1 , find the value R_2 the range of a proton particle starting with the same initial velocity.

βc . The value of βc for a proton with a given range can be obtained from the empirical curves given by Livingston and Bethe (1937). The correct value $m_1 = \mu$ will be such as to satisfy the equation $\frac{\mu \beta c}{\sqrt{1-\beta^2}} = H\rho$; where $H\rho$ is obtained experimentally. Corson and Brode (*loc. cit.*) consider this to be the most accurate method of measuring mass, provided all the data are given with the same degree of precision. But as Ladenburg and Wheeler (1941) point out, the drawback of the method is that as the particle slows down it is subject to increasing amount of scattering which it is difficult to make allowances for. Thus it is found that the largest amount of discrepancy occur amongst the mass determinations by this method. The results are given in Section B of Table II. The results obtained by Maier Leibnitz and some obtained by Anderson and Neddermeyer have been omitted as being widely outside the probable range of values of the meson mass, which we take to vary between $150 m_0 - 300 m_0$.

Method C. Curvature and Momentum loss—The change of momentum suffered by a fast particle after traversing a heavy metal plate of known thickness can be used for accurate measurement of mass in the non-relativistic region according to Ladenburg and Wheeler. The change of momentum suffered after traversal through a thickness Δx of the given plate is $\Delta p = \frac{He}{c} \cdot \Delta \rho$ from which

we have the relation $\frac{\Delta E}{\Delta x} = c\beta \frac{\Delta p}{\Delta x}$. This value can be introduced in equation

(2) or (3) to get the value of β . The resolving power of the method is poor for $H\rho \gg 4 \times 10^5$ gauss cm. The mass determinations according to this method are given in section C of Table II. Nishina originally determined the meson mass using Bloch's form of the energy loss formula and found the value of μ to be between $180-260 m_0$. Later on using Bhabha's formula for relativistic loss, he found the value of μ to be $(180 \pm 20) m_0$. The energy of his particle is $\sim 10^8$ eV and falls within the non-relativistic range, hence there appears to be no justification for his using the relativistic energy loss formula.

Method D. Curvature and electron collision—The recoiling electron receives such a large amount of energy from the colliding primary particle, that it can produce an ionization track of at least a centimeter length. The energy or momentum of the recoiling electron can be determined either from its range or curvature in the magnetic field.

Method E. Photographic plate method—Here the mean ionisation along a long meson track and its curvature due to multiple scattering are determined. The average number of silver grains deposited per unit length of the cosmic ray particles is assumed to be proportional to the initial kinetic energy of the particle. Further it is assumed that both the meson and the proton carry one unit of charge, so that when these two particles start with the same velocity, the mean grain number deposited along their tracks will be the same. The mean kinetic energy of a number of cosmic ray particles which have the same

mean grain number can be deduced from the mean curvature of their tracks in the photographic emulsion due to multiple scattering. In this method the ratio of the mass of the unknown particle to that of the proton is determined from the ratio of the kinetic energies of these two particles which have the same mean grain spacing along their respective tracks in a given photographic emulsion (Table I).

4. DISCUSSIONS.

It will be noticed that in spite of large variations in the values of the meson mass obtained, (i) by using different experimental methods and (ii) by different investigators using the same method, that certain general trend in the variation of the meson mass with the kinetic energy of the particles appear. For example it is found that for higher velocities the meson mass, as determined by the different methods, appear to increase with the particle energy, in a way not representable by the relativity formula. Further it also appears, from a consideration of the results obtained by the methods A and E, and they contain the largest number of measurements, that starting with the low velocity particles, the measured values of the meson mass diminish initially with the particle energy to a minimum value, which appear to lie in the region of 6 to $10 \times 10^6 eV$ in the case of Wilson chamber meson tracks, and of $1.0 \times 10^6 eV$ in the case of meson tracks in photographic emulsion. That this variation is dependent on the particle energy is shown by the measurements made on photographic tracks. Each mass measurement is based upon summation taken over track lengths varying from 10 to 33 in number. This is contrary to the assumption made by Weisz (1941) "that at each energy there is a distribution of rest mass." We shall next discuss the possible explanations which can be put forward to explain such observed variations in the meson mass.

(a) The energy loss equation is correct, but the assumptions underlying the deduction of formula (3) are not satisfied, *viz.*, (i) the energy of the particle is small compared to $\mu c^2 \left(\frac{\mu}{m_0} \right)$ which for mesons is $\sim 10^{10} eV$ and (ii) the particle velocity is large compared to those of the bound electrons of the atoms traversed by the particle. The first condition is satisfied by all the penetrating particles used in the mass determinations, and so also the second condition.

It was shown by one of us (Choudhuri, 1942) that the second condition was not satisfied in the case of α -particles of energy between 5 to $10 \times 10^6 eV$. It was observed that the ratio of track lengths of α -particles of a given energy in photographic emulsion/air, came to 7×10^{-4} against a theoretically expected value of 5×10^{-4} . This was explained by us as being due to the presence of heavy atoms like Ag, Br, etc., in the photographic emulsion, in respect of some of whose inner bound electrons condition (ii) is not satisfied by the particles.

(b) The theoretical ionisation loss formula does not correctly represent experimental facts. Against this it may be pointed out that the methods B and E

do not make use of the ionisation loss formula. In both use is made of the empirically determined relation between the range and energy of protons in air and in photographic emulsions.

TABLE I

Plate	m. g. s. in μ	No. of Tracks	Mean energy	Mass in units of m_0
E. I	6-5	12	$2.7 \times 10^6 \text{eV}$	221
...	5-4	22	$1.05 \times 10^6 \text{eV}$	160
...	4-3	33	$0.6 \times 10^6 \text{eV}$	263
II	5-4	10	$1.1 \times 10^6 \text{eV}$	180
...	4-3	15	$0.68 \times 10^6 \text{eV}$	257

TABLE II

No.	Energy	Mass	Method	Reference
A (i)	$5.6 \times 10^6 \text{eV}$	220 ± 50	Curvature and ionisation	William & Pickup, Nature 141, 684 (1938).
	$5.8 \times 10^6 \text{eV}$	160 ± 30	"	ditto
	9.2×10^6	190 ± 60	"	"
(ii)	$5 \times 10^6 \text{eV}$	225 ± 20	"	Neilson & Powell, Phys. Rev. 63, 384 (1943)
	5.6×10^6	240 ± 15	"	ditto
	1.15×10^7	155 ± 30	"	ditto
	2.3×10^7	230 ± 20	"	"
(iii)	$4 \times 10^6 \text{eV}$	160	...	Stret & Stevenson, Phys. Rev. 53, 1003 (calculated by Corson & Brode) (1937)
	$4.5 \times 10^6 \text{eV}$	180 ± 25	...	Starr & Brode, Phys. Rev. 53, 3 (1938)
	$1.03 \times 10^7 \text{eV}$	250	...	Corson & Brode, Phys. Rev. 53, 215 (1938)
	$1.6 \times 10^7 \text{eV}$	200	...	Ehrenfest, Jr. C. R. Paris, 206, 428 (1938).
B	$.68 \times 10^6 \text{eV}$	170 ± 8	Curvature and Range	Nishina, Takeuchi, Phys. Rev. 55, 585 (1939) (Considered doubtful)
	$1.3 \times 10^6 \text{eV}$	< 200	"	Brode & Starr, Phys. Rev. 53, 3, (1938)
	$1.3 \times 10^6 \text{eV}$	~ 350	"	Anderson & Neddermeyer, Phys. Rev. 50, 26 (1936)
	$1.3 \times 10^7 \text{eV}$	220 ± 35	"	Anderson & Neddermeyer, Phys. Rev. 54, 88 (1938)
C	$9 \times 10^6 \text{eV}$	170 ± 20	Change in curv. due to passing through lead plate.	Wilson, Proc. Roy. Soc. 172, 521 (1939)
	$1.6 \times 10^6 \text{eV}$	250 ± 50		Wilson ditto
	$1.8 \times 10^6 \text{eV}$	$180 \sim 260$		
		180 ± 20 (recalculated)	"	Nishina, Phys. Rev. 55, 585 (1939)
D	$4.5 \times 10^6 \text{eV}$	180 ± 25	Curvature and collision with electron	Hugles, Phys. Rev. 60, 414 (1941).
	$4.3 \times 10^7 \text{eV}$	240 ± 20		Leprince, Ringuet, Phys. Rev. 59, 460 (1941).

(c) The charge on the meson does not remain constant—there has been a certain amount of speculation as to the existence of neutral meson (neutretto). According to the recent theory of Hamilton, Heitler and Peng (1943), the existence of neutretto is assumed. The cross section for the transformation of a neutretto into a charged meson is taken to $\sim e^{-6}$, where ϵ is its energy. Thus at comparatively low energies of the order of $10^6 - 10^7$ eV, there is some probability of a charged meson losing and recovering its charge by nuclear collisions, depending in some way on its velocity. If that happens the average charge on a low energy meson will be less than unity, and be some function of its velocity.

(d) The meson mass is not a constant, but is a function of its kinetic energy. This assumption will also support the interpretation given by Bernadini et al (1941) of their observations on the values of meson life time at different elevations.

The above discussion on the possibility of the meson mass being dependent in some unknown way on its velocity is of an exploratory nature only; its purpose is to draw attention to the desirability of undertaking further accurate investigations on mass determination of cosmic ray penetrating particles with different methods and using particles of widely varying kinetic energies. With these additional results it will be possible to find out whether such a variation of mass exists, and if so how the variation depends upon the kinetic energy of the meson particles.

BOSE RESEARCH INSTITUTE,
CALCUTTA.

REFERENCES

- Anderson & Neddermeyer (1939) *Rev. Mod. Phys.*, **11**, 195.
 Bernadini, G. D et al. (1941) *Phys. Rev.*, **60**, 910.
 Choudhuri Bibha (1942) *Trans. Bose Inst.*, **15**, 910.
 „ „ (1944) *Ind. Jour. Phys.*, **18**, 57.
 Corson & Brode (1938) *Phys. Rev.* **53**, 773.
 Hamilton, Heitler, Peng (1943) *ibid.*, **64**, 78.
 Ladenburg, Wheeler (1941) *ibid.*, **60**, 754.
 Livingston, Bethe (1937) *Rev. Mod. Phys.*, **9**, 268.
 Nielson Powell (1943) *Phys. Rev.*, **63**, 384.
 Schopper and Schopper (1939) *Phys. Zeit.*, **40**, 22.
 Weisz, P., (1941) *Phys. Rev.*, **59**, 845.
 Wilson, Williams, R. J., (1939) *Proc Roy. Soc. Lond. A.*, **172**, 194.

TIME LAG AND HUMID FATIGUE OF HYGROMETERS

(MAHAJAN'S OPTICAL HYGROMETER AND OTHERS)

By L. D. MAHAJAN *

(Received for publication, 23rd August, 1941)

ABSTRACT.—By experiments it is found that the best substance for use in the pans of the optical hygrometer is a mixture of about 1% calcium chloride, 9% plaster of Paris and 90% small pieces of hair.

Some improvements have been made in the construction of the optical hygrometer, such as, hard glass agate grooves are fitted into thick heads of the screws, which are fitted into the slotted supports.

The methods adopted for determination of time lag and humid fatigue are described.

It is found that the optical hygrometer behaves like other kinds of hygrometers. Its time lag is about 16 minutes which is smaller than that of the other types of hygrometers. Time lag of all hygrometers depends on their construction, rate of circulation of air in them and their immediate past history.

The rate of change of humidity decreases rapidly with time in the logarithmic relation and the major change takes place in the first few minutes.

INTRODUCTION

In previous papers (Mahajan, 1941a) the author explained the construction, theory and working of the optical hygrometer in detail. Since then, further work has been conducted on its time lag. Time lag of a few other kinds of hygrometers have also been studied and compared with that of this hygrometer. The hygroscopic substance used in the instrument has also been improved. The method used for determination of its time lag and the results obtained therein are given below in detail.

SELECTION OF HYGROSCOPIC SUBSTANCES

In the last paper (Mahajan, 1941b) a short account has already been given regarding the selection of suitable hygroscopic substances for the instrument. But further study of many other substances and mixtures reveals that the mixture of 1% calcium chloride, 9% plaster of Paris and 90% small pieces of animal hair forms the best substance for this instrument, as it has high power of absorption of moisture from the moist air and desorption of moisture to the dry air, and these rates of absorption and desorption are fairly equal.

IMPROVEMENT IN CONSTRUCTION

The construction of this instrument has also been improved. The perforated base of the instrument has been slightly enlarged in size and a groove has been made all round it. The rectangular glass cover just fits into this groove. The revolving rod of brass has been substituted by a fine rod of best steel, which is

* Fellow of the Indian Physical Society.

thicker in the middle and very thin at the ends. In place of ordinary screws the thick screws are fitted in the slotted supports (only the tops of the supports are slotted) with their thick heads inwards. Hard glass agate grooves are fitted into the thick heads of the screws and the thin ends of the revolving rod are fitted in them. The details of its construction are clearly shown in figure 1.

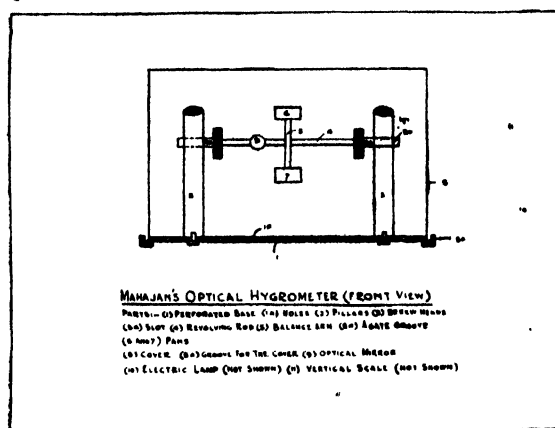


FIG. 1

THE METHOD

The method used for the study of time lag and humid fatigue is the same as that devised by the author for the study of adsorption of moisture from the moist air by the soils and is described in the paper (Mahajan, 1940), on the subject. The instrument was placed inside a rectangular glass vessel which was connected by means of two rubber tubes, with two bottles, each of one litre capacity, one containing water and the other strong sulphuric acid. A current of air was passed through either vessel by means of pressure pump, according to the requirements. When the humidity was to be decreased inside the glass chamber, a current of air through the sulphuric acid vessel was sent to the glass chamber and when the humidity was to be increased a current of air through the water vessel was pushed into it. Thus by regulating rates of flow or quantity of dry and wet currents of air, any humidity could be arranged inside the chamber.

The optical hygrometer was placed inside a glass chamber and humidity of air inside it was varied. The time period was recorded for attaining a constant reading at various humidities.

In the same way, humidity of air inside a chamber was varied and readings on the vertical scale of the optical hygrometer were recorded after regular intervals of time.

The instrument was placed under a glass cover on a separate wooden support fixed in the wall in order to avoid even the slightest disturbances to it by any means. It was placed at some distance from the walls as they are good absorbent of moisture from the air. The distance between the instrument and the vertical scale was kept about two metres so as to make it very sensitive.

TABLE I(a)

Serial No.	Kind of hygrometer.	Initial reading on the vertical scale in cms	Reading on the vertical scale in cms.	Time taken in minutes from the start.	Time-lag in minutes.	REMARKS
1	Optical hygrometer.	87.3	87.3 87.7 92.6 93.0 93.5 93.5 93.5	0 1 5 10 15 20 30	15	1. Variable humidity chamber used. 2. Decrease of humidity.
2	"	98.0	98.0 96.0 94.0 91.3 90.5 90.5 90.5	0 5 10 15 20 25 30	20	Decrease of humidity.
3	"	90.0	90.0 91.3 93.3 94.2 94.5 94.5	0 2 8 15 20 25	20	Increase of humidity.
4	"	80.0	80.0 81.0 86.6 87.1 87.2 87.2	0 1 5 10 15 20	15	"
5	"	90.0	90.0 86.0 83.0 82.0 81.0 80.0 80.0 80.0	0 5 10 15 20 25 30 35	20	Decrease of humidity.
6	"	95.6	95.6 97.5 98.0 98.7 99.0 99.0	0 3 5 8 13 21	13	1. Increase of humidity. 2. Current of moist air passed in for the first three minutes
7	"	85.3	85.3 86.2 89.8 90.8 90.8	0 3 8 15 19	15	"
8	"	86.5	86.5 88.8 89.5 90.5 90.6 90.6	0 4 5 8 11 13	11	"

Mean time lag 16 minutes

Besides this apparatus, two dessicators, one containing strong sulphuric acid and the other water, were also used for arranging 0% and 100% humidity chambers. The optical hygrometer was placed in them and the effects of extreme limits of humidity on the instrument were also studied. Similarly time lag of a few other kinds of hygrometers were also studied by the above method.

THE OBSERVATIONS

The optical hygrometer was kept inside a chamber of any known humidity and the time lag was observed for the decrease as well as increase of humidity. Similarly, similar observations were recorded for some other kinds of hygrometers. A few sets of observations are given below in Table I (b, c, d and e).

TABLE I(b)

Number of sets. 1	Kind of hygrometer. 2	Initial humidity. 3	Final humidity. 4	Time taken in minutes. 5	Time lag in minutes. 6	REMARKS. 7
1	Hair-hygrometer.	61%	61% 76 89 80 81 81	0 5 12 17 22 34	22	Increase of humidity.
2	"	79%	79% 62 52 51 50 50	0 2 5 9 15 26	15	Decrease of humidity.
3	"	50%	50% 70 74 75 75	0 4 10 15 20	15	Increase of humidity.
4	"	75%	75% 68 65 63 61 60 60	0 3 6 10 15 20 25	20	Decrease of humidity.
5	"	90%	90% 88 86 82 80 80	0 5 10 15 20 25	20	"

Mean time lag 19 minutes.

DISCUSSION OF RESULTS

Time lag.—The study of observations recorded in Table I (a, b, c, d and e) clearly shows that every hygrometer needs a period for which it should be exposed to a surrounding medium in order to reach a steady state and to indicate the correct reading. This period is the time lag of the hygrometer. It is different for different hygrometers. It is approximately 16 minutes for the optical hygrometer, 19 minutes for the hair hygrometer, 35 minutes for the paper hygrometer, 50 minutes for the humatograph and 18 minutes for the wet and dry bulb hygrometer. Thus the time lag for the optical, the hair, and the wet and dry bulb hygrometers are almost the same. The range of variations of time lag is 11 to 20 minutes for the optical hygrometer, 15 to 22 minutes for the hair hygrometer

TABLE I(c)

Number of sets. 1	Kind of hygrometer 2	Initial humidity 3	Final humidity. 4	Time taken in minutes. 5	Time lag in minutes. 6	REMARKS. 7
1	Paper hygrometer	60%	60% 72 74 75 75.6 76 76	0 5 14 20 30 35 45	35	Increase of humidity.
2	"	50%	50% 50 71 76 78 79 79 79	0 5 13 20 25 30 35 40	30	"
3	"	79%	79% 75 71 67 64 62 59 58 57 57	0 5 10 15 20 25 30 35 40 45 50	40	Decrease of humidity.
4	"	76%	76% 72 69 67 66 65 64.5 64 64	0 5 10 15 20 25 30 35 40	35	"

Mean time lag 35 minutes.

TABLE I(d)

Number of sets. 1	Kind of hygrometer. 2	Initial humidity. 3	Final humidity. 4	Time taken in minutes. 5	Time lag in minutes. 6	REMARKS. 7
1	Humatograph (containing hair)	54%	54% 61 74 78 83 88 92 94 95 97 98 98 98	0 5 12 15 20 26 31 35 40 45 50 55 60	50	Increase of humidity.
2	"	80%	80% 75 73 69 66 62 61 61 61	0 5 10 15 20 33 50 55 60	50	Decrease of humidity.

Mean time lag 50 minutes.

TABLE I(e)

Number of sets 1	Kind of hygrometer. 2	Initial humidity. 3	Final humidity. 4	Time taken in minutes. 5	Time lag in minutes. 6	REMARKS. 7
1	Wet and dry bulb hygrometer.	100%	100% 84 83.5 83 82 82	0 3 5 10 15 20	15	1. Wet cloth used to start with. 2. Decrease of humidity.
2	"	40%	40% 54 59 64 67 67	0 5 10 15 20 25	20	1. Dry cloth used to start with. 2. Increase of humidity.
3	"	64%	64% 69 72 75 77 77	0 5 10 16 20 25	20	1. Wet cloth used to start with. 2. Increase of humidity.

Mean time lag 18 minutes.

15 to 20 minutes for the wet and dry bulb hygrometer, 35 to 40 minutes for the paper hygrometer and 50 to 55 minutes for the humatograph. Therefore it seems better that these instruments are exposed to the surrounding medium for their respective maximum time lag periods and a steady reading be taken.

This period of time lag also depends upon the flow of current of air in the hygrometer. It is long when there is no current of air passing through it or when there is very slow current of air passing through it. But it decreases rapidly with the increase of speed of current of fresh air through it. The observations recorded in the case of the optical hygrometer in Table 1a show that the mean time lag when the current of air is not passing inside the chamber is 17 minutes (mean of the first five observations), and the mean time lag when the current of moist air is passed for three minutes in this chamber is 13 minutes (mean of the last three observations). Thus the time lag decreases very effectively when the regular current of air is passed through the hygrometer. It is why the time lag of humatograph which is also a kind of hair hygrometer enclosed inside a big cover, has a very long time lag (say, 50 minutes in this case), while an open type of hair hygrometer has about 19 minutes time lag.

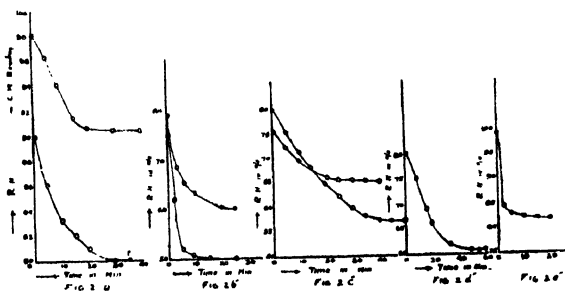


FIG. 2

In figure 2, some curves have been drawn showing the relation between time and humidity (when it is increasing) during the unsteady state, *i.e.*, before the reading becomes steady, as well as between time and humidity when it is decreasing. The curves *a*, *b*, *c*, *d*, and *e* in figure 2, represent the speed of increase of the humidity in the optical hygrometer, hair-hygrometer, paper hygrometer, humatograph, and the wet and dry bulb hygrometer respectively and the curves *a'*, *b'*, *c'*, *d'*, and *e'* in the same figure represent the speed of decrease of humidity in the same said hygrometers respectively. These curves indicate very high speed of variations in the beginning but much slow later on. The speed of variation goes on decreasing very rapidly with time. After the time lag, the curves give a horizontal line and the reading becomes steady. All these curves are similar in shape. The curves for the increase of humidity and the decrease of humidity are roughly complimentary.

HUMID FATIGUE

By the method given above, the observations of the time lags of the various types of hygrometers were recorded while treating them with currents of moist

and dry air alternately without any break in the cycle. Such cycles of observations were repeated again and again on each hygrometer. Time lags of some of the hygrometers for each cycle are given below in Table II.

TABLE II

Kind of hygrometer. 1	No. of set of obser- vation. 2	I cycle		II cycle		REMARKS 7
		Increase of humidity. 3	Decrease of humidity. 4	Increase of humidity. 5	Decrease of humidity. 6	
Mahajan's Optical hygrometer.	1st set	22 min.	37 min.	21 min.	34 min.	All sets taken on different days and times.
	2nd „	20 „	38 „	15 „	30 „	
	3rd „	18 „	34 „	11 „	23 „	
	Mean	20 „	36 „	16 „	29 „	
Hair hygrometer	1st set	20 „	40 „	17 „	29 „	„
	2nd „	17 „	39 „	16 „	27 „	
	3rd „	18 „	38 „	15 „	25 „	
	Mean	18 „	39 „	16 „	27 „	
Paper hygrometer	1st set	35 „	45 „	22 „	32 „	„
	2nd „	29 „	43 „	25 „	29 „	
	3rd „	34 „	48 „	21 „	35 „	
	Mean	33 „	45 „	23 „	32 „	
Wet and dry bulb hygrometer.	1st set	20 „	42 „	18 „	39 „	„
	2nd „	18 „	38 „	18 „	37 „	
	3rd „	16 „	36 „	15 „	35 „	
	Mean	18 „	39 „	17 „	37 „	

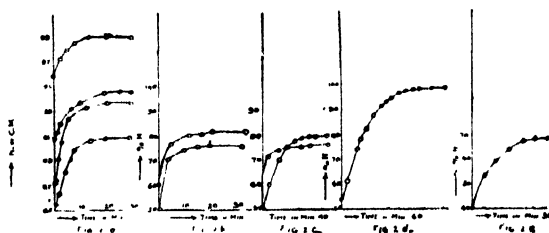


FIG. 3

In the above table, column 3 gives time lag when hygrometer is treated with a current of moist air, and column 4 represents time lag when it is merely exposed to dry air of the room. Time lag is longer in the latter case as the circulation of air was not as rapid as in the former case.

Then just after this first cycle, the second cycle of action is repeated in the same way, and its observations are recorded in columns 5 and 6. The data

clearly indicates that the time lags in the second cycle are less than the corresponding time lags in the first cycle. For example, the time lag to start with in the case of optical hygrometer is about 20 minutes but immediately after when exposed to dry air it takes 36 minutes to come to the steady state. Again when this cycle is repeated, the time lags are 16 and 29 minutes respectively.

This shows that the time lag of hygrometer which has been treated a number of times with rapid changes of humidity by currents of moist and dry air alternately comes to rest and gives a constant value in a shorter time than otherwise. Therefore time lag of hygrometer is not a constant factor depending merely on kind of hygrometer and speed of circulation of air in it but also depends upon the immediate past history of hygrometer.

The time lags of other types of hygrometers under similar conditions were also studied and are given in the same table. The results indicate that the effect of immediate past history is found in other types of hygrometers as well. This phenomenon may be called *the humid fatigue of hygrometers*.

The effect of humid fatigue is large in the paper hygrometer and almost negligible in wet and dry bulb hygrometer.

CONCLUSION

The results obtained from the above investigations are encouraging and interesting. Some of the important results are given below :—

1. The optical hygrometer behaves like the other kinds of hygrometers, such as, paper hygrometer and hair hygrometer.
2. Its sensitiveness increases when agate edges or grooves are used in thick heads of screws.
3. It is more sensitive than the other types of hygrometers and minor changes in humidity of the surrounding medium can easily be detected with it.
4. Its time lag is about 16 minutes and is much smaller than the time lag of other hygrometers.
5. The time lag of all types of hygrometers depends on (i) their type, (ii) rate of circulation of air in them and (iii) their immediate past history.
6. The rate of change of humidity in the optical hygrometer decreases rapidly with time in the logarithmic relation. The major change takes place in the first few minutes.

ACKNOWLEDGEMENTS

The author takes this opportunity to thank His Highness' Government, Patiala, for providing facilities to carry out this work in the Physics Research Laboratory, Mahendra College, Patiala. Besides, he is also grateful to Sir C. V. Raman, Kt., M.A., Ph.D., D.Sc., F.Inst.P., F.R.S, Nobel Laureate, for having suggested this problem for investigations and his keen interest in the work.

REFERENCES

- Mahajan, L. D., 1941a, *Curr. Sci.*, **9**, 2, 100.
Mahajan, L. D., 1941b, *Ind. Jour. Phys.*, **15**, 425
Mahajan, L. D., 1941, *Proceedings of the Indian Science Congress, Benares*,
Abstracts 33.
Mahajan, L. D., 1942, *Proceedings of the Indian Science Congress, Baroda*,
Abstracts 36.
Mahajan, L. D., 1943, *Proceedings of the Indian Science Congress, Calcutta*,
Abstracts 12.
Mahajan, L. D., 1941, *Proc. Nat. Acad. Sci.*, Feb.
Mahajan, L. D., 1941, *Ind. Jour. Phys.* **15**, 425.
Mahajan, L. D., 1940, *Ind. Jour. Phys.* **14**, 441.

PROTON-PROTON SCATTERING AT LOW VELOCITY

By K. C. KAR AND S. N. MITRA

ABSTRACT. It is shown that Kar's formula for proton-proton scattering explains the angular variation of 'departure from Mott's formula' as observed by Ragan and others for low velocities, if it is assumed that the short range Yukawa force is due to the formation of mesons having mass 152 e.u. and short range charge $\frac{1}{2}$ or other submultiple of its mass. The mass thus determined is different from the mass 110 e.u. obtained previously by applying Kar's formula to high velocity proton-proton scattering.

Recently one of us (Kar, 1942) derived a formula for proton-proton scattering assuming the short range interaction potential to be of Yukawa type $V = -(A/r)e^{-\alpha r}$. The formula was found to be in very good agreement with the observations of Heydenburg, Hafstad and Tuve (1939) at high velocity of incidence. The values of α and A in Yukawa potential for which there is agreement with the above experiment give for the mass of meson $m = 110$ e.u. (approx.) and for the short range meson charge $\sqrt{A} = 6e$ (approx.). These identical values of mass and charge of mesotron have more recently been obtained by Kar and Roy (1943) by applying the above Kar's formula (modified for the absence of Coulomb repulsive force) to neutron-proton scattering at high velocity of incidence. Again, Kar and Roy (1943) have shown that the binding energy of deuteron may be correctly determined by their self-consistent method, if it is assumed that the energy is due to a meson field of mass 110 e.u.

Thus, it follows from Kar's theory of scattering that whenever a proton, due to its high velocity, comes very near a neutron or a second proton, a short range field is developed due to the temporary creation of mesons, of mass 110 e.u., within neutron and proton. It has been pointed out before on several occasions that the mesons are only temporarily created; for otherwise there would have been some cases for which the short range meson field is found to be repulsive. Actually, however, we find the meson field to be always attractive, although positive and negative mesons are found in nature.

Now, in the different experiments referred to above, on neutron-proton and proton-proton scattering, the absolute values of the intensity of scattering are never given. Only the ratio of the observed intensity to the Mott's value for Coulomb interaction is given for different scattering angles. This ratio is evidently considered as a measure of the departure from Coulomb scattering given by Mott's formula. It is found experimentally that the observed value of the departure as defined above becomes maximum at 45° for proton-proton scattering at incident velocities 867 k.e.v., 776 k.e.v. and 670 k.e.v. The departure decreases with the angle of scattering and attains a value nearly $\frac{1}{5}$ for very small angle. These characteristic changes with the angle for different incident velocities are completely explained by Kar's theory of scattering cited above.

Recently, however, Ragan, Kanne and Taschek (1941) have studied proton-proton scattering at low velocity of incidence. They find that, for incident velocities between 200 k.e.v. and 300 k.e.v., the departure attains a minimum

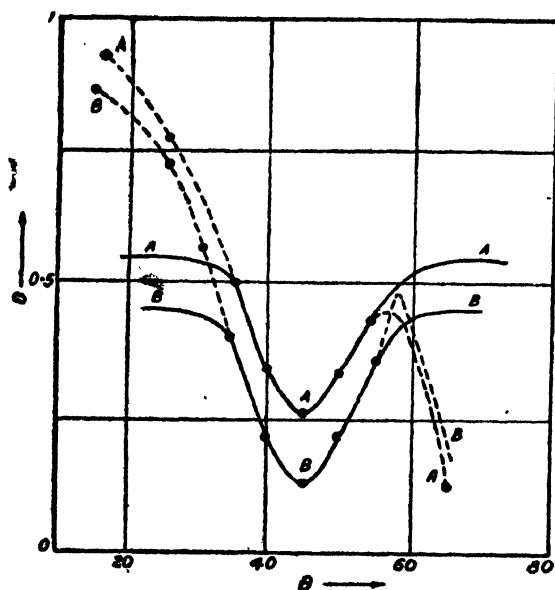


FIG. 1

Curve A—Incident Velocity 249.5 k.e.v.

Curve B— " " 298.3 k.e.v.

value at 45° , instead of a maximum as before. It is evident from Fig. 1 that the departure rises symmetrically on either side of 45° . For smaller angles the rise continues up to very small angle, whereas for larger angles the rise is followed by a decrease in the departure (D) at about 57° , which appears to continue up to 90° . Thus the experimental D- θ curve, which is drawn dotted in Fig. 1, is not symmetrical about 45° . This asymmetry, it appears, is due to multiple scattering at small angles. And, at low velocity of incidence, the Wenzel angle, giving the limit of multiple scattering, may be as large as 35° as in Fig. 1.

At first sight the observations of Ragan and others (1941) appear to be anomalous and to go against the theory of scattering given by Kar (1942). However, on close examination we find that Kar's theory, which is perfectly rigorous, is also applicable to low velocity proton-proton scattering. The fitting values of the parameters A and α in Yukawa potential are, however, different in this case. It is found that for meson mass $m=152$ e.u. and short range meson charge $\sqrt{A} = \frac{1}{2} \times 152 e$, there is very good agreement for the angular range between 35° and 55° , for incident velocity 249.5 k.e.v., while for incident velocity 298.3 k.e.v., there is very good agreement for the above angular range for meson mass $m=152$ e.u. and short range meson charge $\sqrt{A} = \frac{1}{2} \times 152 e$.

It is significant that the short range meson charges are submultiples of the same meson mass in both the cases. Further, for higher incident velocity the fraction rapidly decreases. This suggests that there must be some interesting relation between the meson mass and its short range charge. Ragan and others (*loc. cit.*) have not studied the angular variations for other incident velocities. Consequently it is not possible for us to find out if the meson of mass $m=152$ e.u. have other submultiple values for its short range charge. Fortunately, however, Ragan, Kanne and Taschek have given the values of the departure at 45° for a number of incident velocities. We find that for incident

velocities 275.3 k.e.v. and 321.4 k.e.v. the values of the departure at 45° are correctly given by Kar's formula if we take the meson mass $m=152$ e.u. but short range charges $\frac{1}{3} \times 152$ e.u. and $\frac{1}{3} \times 152$ e.u. respectively. In the following table, the theoretical values thus obtained are compared with the experimental values given by Ragan and others.

TABLE I

Incident Proton energy	Angle of Scattering	I/I (Mott) (Expt.)	I/I (Mott.) (Theoretical)	m	\sqrt{A}/e
176.5 k.e.v.	45°	0.544
200.2 "	"	0.448
225.9 "	"	0.353
249.5 "	"	0.256	0.2565	152	$\frac{1}{3} \times 152$
275.3 "	"	0.177	0.178	"	$\frac{1}{3} \times 152$
298.3 "	"	0.118	0.1154	"	$\frac{1}{3} \times 152$
321.4 "	"	0.0703	0.0819	"	$\frac{1}{3} \times 152$

It follows from the above table that up to proton energy 321.4 k.e.v., the mass of meson formed due to the virtual fission of proton is 152 e.u., while its short range charge is as low as 30 e.u. So it is quite likely that at higher incident energy, the charge may be still lower and may be so low as 6 e.u. obtained theoretically for incident energies between 670 k.e.v. and 867 k.e.v. It is, however, significant that for such high incident energies, the mass of meson obtained theoretically is 110 e.u. while for lower energies the mass is greater, being 152 e.u. Without commenting on the law of fission of proton, it may be said that the mesons formed within a neutron or a proton have variable mass and charge. And it is highly probable that this formation of bound mesons of variable mass is intimately connected with the widely varying masses of free mesons yet determined by different experimenters.

In conclusion, we may remark that the downward bend in the $D-\theta$ curve at 57° degrees may be explained if it is assumed that, within the protons, mesons of different mass and charge are formed at this distance. The mass and charge are such that $D-\theta$ curve has a maximum at 45° . Thus the curve between 57° and 90° may be considered as a portion of the above curve having maximum at 45° . Investigations in this direction are still in progress.

PHYSICAL LABORATORY, PRESIDENCY COLLEGE
AND
PHYSICAL LABORATORY, VIDYASAGAR COLLEGE,
CALCUTTA.

REFERENCES

- Heydenburg, N. P., Hafstad, L. R. and Tuve, M. A., 1939, *Phys. Rev.*, **56**, 1078.
 Kar, K. C., 1942, *Ind. Jour. Phys.*, **16**, 187.
 Kar, K. C. and Roy, R. R., 1943, *Ind. Jour. Phys.*, **17**, 316 and 321.
 Ragan, G. L., Kanne, W. R. and Taschek, R. F., 1941, *Phys. Rev.*, **60**, 628.

RUPTURE OF WATER DROPS OVER LIQUID SURFACES

By B. K. SAHAY*

ABSTRACT. The critical height to produce rupture of water drops of different sizes over oils and their mixtures have been observed. A linear relation is found to exist between the critical height and the reciprocal of the mass of the drop, for a given liquid. The variation of the critical height for a particular size of the drop with different liquids of different viscosities, shows a distinct minima in each case of the experimental curves. The surface tension, interfacial surface tension, and density of the oils have also been measured, which may throw light on the true mechanism of the rupture of water drops.

INTRODUCTION

When water drops are allowed to fall on certain liquids whose densities are less than that of water and which are not miscible with it, it has been found (Singh and Sinha, 1944) that either the drops sink as a whole or rupture into two distinct droplets permanently. There is a certain critical height such that when the drops fall through a height less than this critical value they sink as a whole but as soon as the height exceeds this critical value, they rupture into two or more distinct droplets.

EXPERIMENTAL

The experimental arrangement to produce the water drops of different sizes was as follows :—A glass jar was filled with water having a side-hole near the bottom. Capillary tubes of different sizes were taken and joined to the side hole of the glass jar by means of a rubber tubing, having a pinch cock to regulate a steady formation of the water drops. The glass jar was raised to a certain level to produce the hydrostatic pressure for forcing out the water from the end of the capillary tube. This hydrostatic pressure was kept constant throughout by an adjustment of the water level in the jar. The velocity of impact of the water drop on the liquid surface to produce its rupture is given by $v = \sqrt{2gh}$, if it starts initially from rest, where g is the acceleration due to gravity and h is the critical height. This condition can be rigidly obtained if the capillary tube through which the water drops fall is kept in a horizontal position. For the sake of experimental facility, the capillary tube was kept in a vertical position, but here also the initial velocity is approximately zero as the drop remains sticking at its tip before falling under gravity.

There was considerable difficulty in selecting the liquids which are lighter than water, not miscible with it and at the same time their viscosities and other properties are changing in regular order. The only alternative was to take a

* Fellow of the Indian Physical Society.

mixture of two liquids in which one is highly viscous and not the other has got a low coefficient of viscosity and the two mix completely without any chemical reaction. A mixture of turpentine oil and castor oil satisfied these criterions to a considerable extent and hence their mixtures of different proportion by volume were taken.

There was considerable difficulty in ascertaining the critical height for turpentine oil. Fluctuating results were obtained on different occasions. The probable reason for this is that penene $C_{10}H_{16}$, which is the chief constituent of turpentine oil absorbs oxygen from air with the formation of H_2O_2 and production of resin etc. The constitution of penene is based largely upon that of pinole, $C_{10}H_{16}O$ a product obtained by the elimination of water from soberol, $C_{10}H_{16}(OH)_2$ which is formed when penene is left exposed to sunlight in contact with air and water. The constitution of turpentine oil was changing daily and the critical height was fluctuating on different days.

The mixture of turpentine oil and castor oil in various proportions were not transparent at first. After the passage of a number of water drops and exposure to air, the mixtures became clear and the rupture of water drops was visible with ease. As all the liquids contained turpentine oil in a definite proportion, the readings of the critical heights were taken rapidly and they were kept in corked bottles after separating the water from the liquids which settled below them.

The experimental liquid was kept in a beaker which was raised or lowered by means of a screw arrangement. The height was measured from the centre of the drop at the end of the capillary tube to the surface of the liquid in the beaker. At first when the liquid surface was quite near the end of the capillary tube, the drops sink as a whole. With increase in height a very tiny droplet is occasionally seen either along with the parent drop or sometimes separated from it which soon disappears instead of becoming more distinct as the height is further increased. Hence heights at which this happened was discarded. With further increase in height, the tiny droplet again reappears which increases in size as the height is increased. This was the critical height and was measured carefully. After further increase of the height, the satellite droplet coalesces with the parent one and then ruptures into two or more distinct droplets as the height is still further increased. It seems that there are more than one critical height and further work on them is still in progress. Here the observation was only confined with the first critical height, to break the drop permanently into two or more droplets.

The density of the liquid mixtures was determined by means of asp. gr. bottle. The surface tension was measured by means of the capillary ascent method while the interfacial surface tension was measured by the drop weight method (Guye and Perrot 1901). In order to find the coefficient of viscosity of the liquids, the time of flow of a certain volume of the liquid as well as that of the same volume of water was noted. Knowing the coefficient of viscosity of water at that temperature, the coefficients of the other liquids were calculated out.

Table 1 gives the first critical height of the water drops of different masses, for the various mixtures. Table 2 gives the values of density, coefficient of viscosity, surface tension and interfacial surface tension of the various liquids used. The market castor oil was taken and hence much reliance cannot be put on the absolute values of these measurements. Only the relative values may be emphasised which mark the qualitative features of the experimentally obtained graphs.

TABLE 1

Capillary tube no	Wt. of water drop m in gm.	$\frac{1}{m}$	Critical height in cms.						
			Liq. 1	Liq. 2	Liq. 3	Liq. 4	Liq. 5	Liq. 6	Liq. 7
1	0107 gm.	93.46 gm.	9.0	8.4	3.9	3.2	3.1	5.4	10.0
2	0160 „	62.5 „	6.4	6.0	3.1	2.7	2.5	4.2	7.2
3	0271 „	36.9 „	4.2	3.9	2.5	2.2	2.0	3.0	5.1
4	0364 „	27.47 „	3.4	3.2	2.2	2.0	1.8	2.6	4.3
5	0494 „	22.43 „	3.0	2.8	2.0	1.8	1.7	2.4	4.0
6	0831 „	12.03 „	2.1	2.0	1.8	1.7	1.5	1.9	3.1
7	1116 „	8.96 „	1.9	1.8	1.7	1.6	1.4	1.8	2.7

TABLE 2

Liq. No.	Comp. by volume		Density in gm./cc.	Coefficient of viscosity in c. g. s. units at 28°C	Surface tension in dynes/cm	Interfacial S. T. in dynes/cm.
1	50% C. O.	50% T. O.	.92	.1942	7.88	20.94
2	40% „	60% „	.91	.1738	5.75	19.82
3	30% „	70% „	.89	.0562	5.51	19.31
4	20% „	80% „	.88	.0324	5.48	18.14
5	10% „	90% „	.87	.0182	5.33	17.46
6	0% „	100% „	.85	.0105	5.18	20.66
7	Kerosene oil		.77	.0082	4.20	22.84

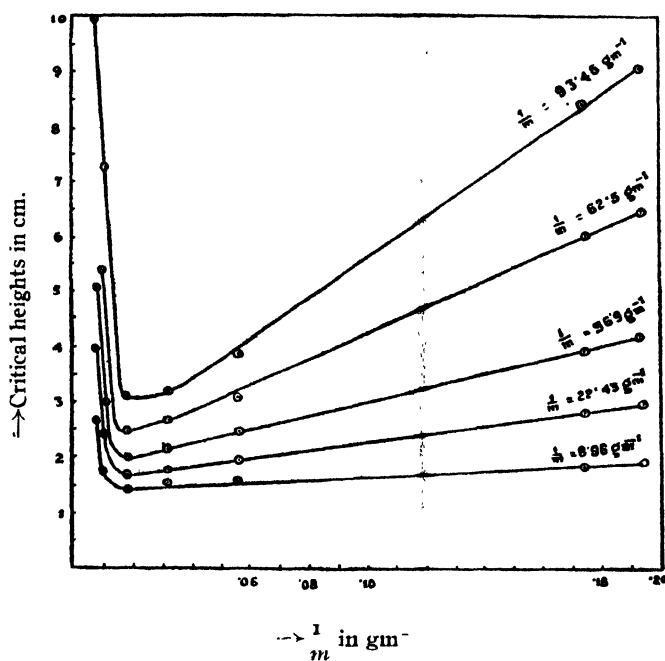


FIG. 1

DISCUSSION OF RESULTS

A plot of h the critical height in cm. against $1/m$ where m denotes the mass of each drop in gms. gives a straight line characteristic of the liquid used as shown in Fig. 1. The equations of the straight lines are $h = 1/m \tan e + c$ where $\tan e$ is the inclination and c is the intercept on the y -axes. Therefore $mh - mc = \tan e$ or $mgh - mgc = g \tan e \times a$ a constant quantity for a particular st. line, where g is the acceleration due to gravity. The dimension of c is that of height and hence the left hand side denotes the difference of two energy terms. The first energy term is the kinetic energy generated at the expense of the potential energy which tends to produce the rupture of the water drop while the second term represents a constant energy for a particular drop. Probably it may be due to the adhesive forces of surface tension, the symmetry of the drop and the other properties of the liquid which oppose the rupture of the water drop. It may be noted that there is a tendency of convergence of all the straight lines of the various mixtures except that of kerosene oil whose intercept on the y -axes is of a different length. It may also be noted that the slope of the straight lines goes on diminishing as the coefficient of viscosity becomes less, but after a certain value of the coefficient it begins to increase instead of decreasing with further decrease in the coefficient of viscosity.

A plot of h the critical height in cms. against μ the coefficient of viscosity of the various liquids for a particular value of the mass of the drop is shown in

Fig. 2. Only five curves for five masses of water drops have been plotted here

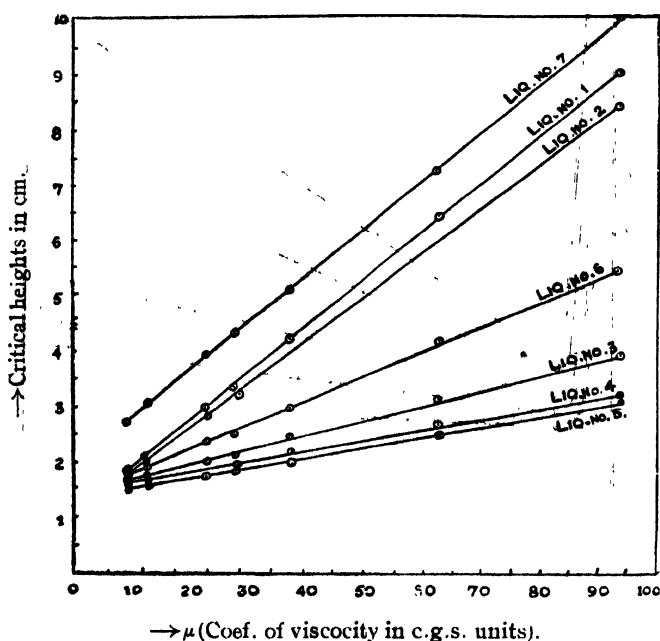


FIG. 2

for fear of too much congestion. The critical height at first decreases, takes a stationary value and then increases all of a sudden as the value of the coefficient of viscosity gradually decreases. The particular value of the coefficient of viscosity of which the curves takes a sharp bend and the value of the critical height becomes stationary, is nearly the same in all the curves of different masses of the water drop.

With the present data, it is not safe to suggest anything about the actual mechanism of the rupture of the water drop and whether there is more than one such type of mechanism. Further work on the second and third critical height is still in progress which may help in the understanding of the hydrodynamics of the drop.

ACKNOWLEDGMENTS

The author is highly indebted to Dr. B. N. Singh for suggesting the problem and to Rev. Dr. C. P. Saldanha, S. J., for giving all facilities for the work.

ST. XAVIER'S COLLEGE, RANCHI.

REFERENCES

- Guay and Perrot, 1901, *Arch. Sci. Phys. et Nat.*, 11, 225.
Singh and Sinha, 1944, *Curr. Sci.*, 13, 157.

MOBILITY OF ATMOSPHERIC VORTICES

By S. N. SEN, H. R. PURI AND S. MAZUMDAR

ABSTRACT. A rectilinear vortex, as an entity, has no tendency to be mobile in an unlimited mass of fluid. A single vortex in an atmospheric street would remain stationary but for the velocities caused by the other vortices in the street and also those caused by external forces as obtain in the directive field (Sen, 1943).

While discussing the mobility of vortices, it is necessary to visualise separately the groupings of the vortices according to sign and the dynamical state of the medium in which they move. The chief topic of this note is the travel of a tropical cyclone, although incidental references have been made to the travel of an anticyclone in Indian latitudes. As regards the thermodynamical state, it may be mentioned that recent observations of temperature over India suggest that the regions of double vortices are characterised by feeble horizontal gradients of potential temperature. A graphical method of forecasting the path of a tropical cyclone has been developed.

In treatises on aerodynamics, it is customary to idealise the vortices in a street into point or rectilinear vortices. The vertical core-cylinders, as depicted in the annexed diagram (normal vortex streets for December on maps of India and adjoining countries shown at two levels, 'generative' and 'directive,' in perspective), are lines of concentrated vorticity or rectilinear vortices (Lamb, 1930), with small circular section. For practical purposes, the circular cross-section may be taken to represent a solid rotation in the presence of neutral air U_0 (irrotational and stagnant) so that the rectilinear vortices in the street behave as truly solid rotating cylinders with circulation round them.

The wind gradient, inside the two walls (Glauert, 1926) of dilatation and compression (outflow and inflow in a wake) increases, remains constant or decreases towards the neutral point, according as the angle between the walls is greater than, equal to or less than, a right angle. The isopleths of wind speed aloft in the daily charts confirm this theoretical requirement.

A street migrates downstream by the shedding of alternate (Bairstow, 1939, Goldstein, 1938) positive and negative vortices from the two ends of the *equivalent bluff obstacle*. In fact, the passage of a train of alternate cyclones and anticyclones, as obtains in the surface isobars of high latitudes, is strongly reminiscent of an atmospheric street migrating. In the Indian region, however, a chain of migrating "sources" and "sinks" is not in evidence in the surface isobaric charts. Nevertheless, the atmospheric streets aloft, drawn from upper winds, reveal vortices migrating at intervals.

Single Vortex.—A single vortex is shed at the end of a dilatation axis, often accompanied by weather. It is observed that a point vortex shed outside a cyclic field, is transported away in the sinuous streamlines of the directive field.

Vortex Pair.—Two rectilinear vortices of equal strength and opposite signs, when they are close together in a medium of U_0 , constitute a *vortex pair*. If one vortex in a pair becomes alternately weaker and stronger than the other, the system may be called a *degenerate pair*. If the vortices in a pair are small, a doublet may form by their coming close (Ramsay, 1935) together. A pair may appear in the same street as between two converging streets from the same direction, having a phase difference of about 180° . A vortex pair has no cyclic field.

Examples of vortex pairs are common in the transition months, when streets from the same direction usually predominate. For instance, on the morning of the 15th June, 1944, the positive core-cylinder of a vortex pair was over Kathiawar and the negative core-cylinder was over West Rajputana, and they extended at least to the 6 km level. Ice accretion was reported between Surat and Jamnagar at about 3-4 km level and the horizontal gradient of potential temperature was feeble around the pair. This picture is consistent with the characteristic stream-line pattern associated with a pair. In the daily charts, isobars drawn at 1 mb interval may often reveal a pair. In a medium of irrotational air U_0 , the vortices will move in parallel directions. The track of a degenerate pair is sinuous.

Vortex Twin.—It has already been asserted elsewhere that a "locking" or "belting" of opposite streets takes place in a medium of U_0 , the neutral air. The belting process is somewhat as follows.

Let two rectilinear vortices of the same sign (say two electric charges of the same sign, as an analogy), find themselves in a medium of neutral air. In the case of cyclogenesis, this often occurs in the seasonal trough when U_4 is stationary and in the north U_2 or U_3 is migrating according to season. The charts suggest that the vortex twin in U_0 begins to revolve round a centre on the line joining the two vortices and gives rise to a *belt* in the neutral air. The twin vortices may be considered to be secluded inside the belt. As a matter of fact, two contiguous core-cylinders of the same sign, belonging to two opposite streets and having a phase difference of 180° , belted together, may be called a *twin*. Two cyclonic core-cylinders form a *positive twin* and two anticyclonic ones a *negative twin*.

The Neutral Cylinder.—It should be noted that two (vortex) sources or two sinks, rotating like a "dumb-bell" in U_0 are not strictly equal in the daily charts. In these cases the contour of the belt is nearly oval. In three dimensions, the rotating neutral air belt may be called the *neutral cylinder*. Briefly speaking, the isopleths of wind speed in a cyclic field, drawn in the direction of line of motion in the field, show that the belt is, for all practical purposes, a "a forced vortex" and looks like an "expanded vortex" in the charts. When the point vortices generating the belt are themselves very close together, the belt tends to become circular.

In actual practice, the neutral cylinder is to be regarded as a solid cylinder, the circulation round which is represented by the inner periphery of the *mantle* or

the simple vortex. A neutral cylinder and the mantle thus constitute the Rankine "Combined Vortex" (Ramsay, *loc cit.*). The centre of rotation of the dumb-bell is therefore the centre of a solid rotation or the "no wind" centre and the solid rotation portion moves faster than its mantle.

Coloval.—If one of the undisturbed streams diffuses after preliminary belting of a twin (positive or negative) a "disc" (Sen and Ganesan, 1940) (a neutral cylinder in three dimensions) is left. This is a partly diffused belt. If both the undisturbed streams weaken after belting, a diffused belt or a "coloval" is left. A coloval is thus a diffused solid-rotation.

By the time the neutral air U_0 is destroyed by the diffusion of vorticity, the coloval may be fractured initiating col-activity. In other words, the process simply means that the hitherto secluded rectilinear vortices of the twin may now respond individually to the fluctuations in the respective undisturbed streams. The expression "col-activity" may be further generalised to mean the weather produced by rectilinear vortices of the same sign coming close together in any manner and then retreating from each other.

Cyclone Track in Generative Shell.—The proper perspective of anticyclonogenesis and cyclonogenesis can be obtained only when the magnitude of free convection along moist adiabates, and free subsidence along dry adiabates (a Carnot's cycle when horizontal motions of air at the surface and aloft are considered to be isothermal), in an extensive generative field is known. Meanwhile, a restricted view regarding the sequence of events in the cyclonogenesis field, finally leading to the translation of a cyclone, will be briefly stated.

The sequence of events, as set out below, may differ somewhat in an individual cyclone, according to season. Moreover, the field B, in which the cyclone forms, may quickly come to the convergent state and therefore some of the stages noted below may not be in evidence in a particular case without frequent charts.

Let the westerly undisturbed stream or the monsoon U_4 be diffused in the beginning with U_0 in the seasonal trough or the base a warm anticyclone.

It may be recalled that an important sign of cyclogenesis in the surface isobaric chart is the steepening of the horizontal pressure gradient to the south of the seasonal trough. This corresponds to the diffused westerly street reviving, *i.e.*, the monsoon winds U_4 strengthening, along the inflow axis a_2n_2 in the annexed diagram. The vortex at a_2 finds itself in U_0 , which is drawn through convergent channel along n_3a_2 .

The easterly street U_3 moves into position. The rectilinear vortices at b_2 and a_2 (a twin) in U_0 form a "dumb-bell" which usually has two unequal heads (vortices of different strengths) and a neutral cylinder is formed.

In the initial stage, the angle $a_2n_2b_2$ is obtuse. The wind gradient, therefore, increases as the neutral point n_2 is approached. Consequently, the neutral cylinder is pushed towards n_2 . The portion a_2b_1 of the track (Fig. 1 of the annexed diagram) is traversed.

The "undisturbed stream" of the easterly street (U_3) strengthens. The cyclic field, $n_3a_2n_2b_2$, hitherto diffused, now becomes pronounced and stable with the neutral cylinder inside.

Some vorticity is shed by the nose of the coloval (initially pointing towards b_2) into the triangle $b_2n_2a_2$. Strong vortex layers are shed at the ends of the dilatation axis as the mantle begins to grow with the advent of the humidity wave. The wind gradient to the western side of the neutral cylinder thus increases with time.

The angle $b_2n_2a_2$ becomes a right angle and then acute and the wind gradient in the triangle $a_2n_2b_2$ decreases. A thrust on the cylinder is now directed from an easterly to a westerly direction. The portion of the track, t_1A_2 (Fig. 1) is thus traversed at right angles to the axis of U_4 . If the angle $b_2n_2a_2$ is obtuse, the cyclone is likely to travel faster than usual.

By the time the neutral cylinder moves some distance towards n_2 , determined by wind gradient, the journey is over so far as the travel of a tropical cyclone is concerned. The westward track may be almost as long as the wave length of the participating streets. If conditions continue favourable, a cyclone travelling further westwards should diffuse and then re-intensify in the next cyclic field $n_4a_3n_3b_3$.

Recurving Cyclones.—A cyclone "recurves" when it passes from U_e to U_w of the "general circulation." The herring-bone line in the diagram represents the track of a recurving cyclone. It is observed from the charts that on the eve of recurvature the equatorial U_3 diffuses (a cyclone may initially form between U_3 and U_4 in any season) and the cyclic field $n_2b_2n_3a_2$ opens out to form the pseudo-cyclic field $n_7c_2n_3a_2n_2c_1$ so that the cyclone begins to move to the new neutral point n_7 . The portion A_2B_2 of the track is thus traversed. Fig. I shows the familiar S-track of cyclones which, as observations show, is independent of the diameter of the neutral cylinder.

Directive Field.—This is the "constant density" layer. The preceding paragraphs explain the trend of motion of a cyclone owing to forces arising in the generative field. The streamlines in directive field above the cyclone past the contour of the core-cylinders, however, indicate the direction of the external force. The streamlines in the directive field are to be regarded as representing the "translation" of a twin in a uniformly rotating fluid in the generative shell.

The annexed diagram depicts the average streamlines for December. The streamlines on individual occasions are similar. It is a curious fact that a cyclonic twin should move anticyclonically in a cyclonic cyclic field in case the directive drive so dictates. Every streamline in the directive field is a potential cyclone track and available records of tracks of cyclones in the Bay of Bengal and the Arabian Sea and those of the western disturbances in the north are in agreement with this view. As the annexed diagram shows, some of the streamlines are cyclonically while others are anti-cyclonically curved. In actual forecasting, the streamlines at the 6 km. level have been used with satisfactory results.

TRANSLATION OF A WINTER CYCLONE (DECEMBER)

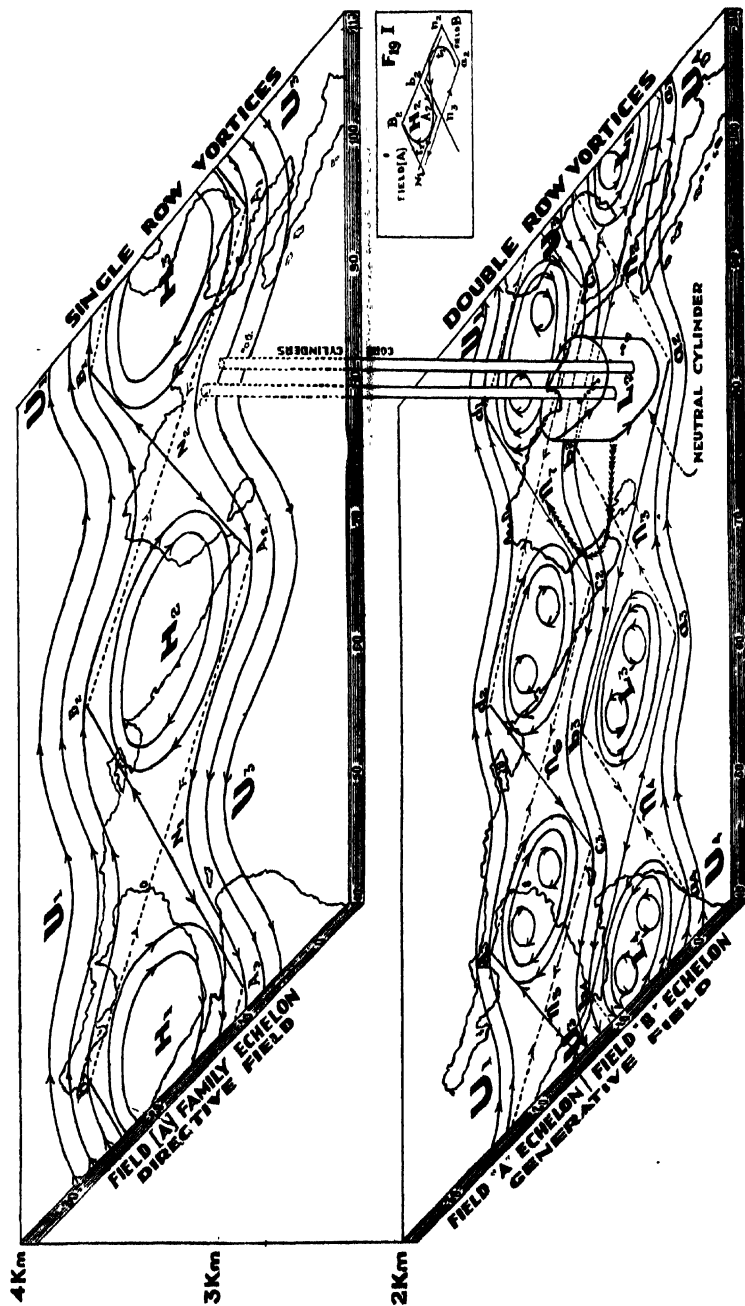


FIG. I

It may be recalled in this connection that a street of single row vortices (Bairstow, *loc. cit.*) is unstable and this is an important feature of the directive field. As a matter of fact, horizontal gradient of potential temperature aloft are found to be weak in the neighbourhood of the vortices. The twin may change "drive" from cyclonic to anticyclonic and vice versa owing to the streamlines in the directive field becoming unsteady.

If anticyclogenesis develops (*i.e.* spiral descent of air) in the directive shell in one part (*e.g.* H_2 of the directive field) and a cyclone (or spiral ascent of air) is below the field in another part (*e.g.* L_2 of the generative field), the streamlines in the directive field become unsteady. The anticyclonic ceiling of the cyclone in the directive field is thus lowered. The sloping ceiling $N_1B_2N_2A_2$ extend southwards sufficiently to bar the way of the cyclone advancing westwards. The daily charts show that the directive cyclic field $B_2N_2A_2N_1$ or H_2 often extends southwards in the post-monsoon months. It may be recalled that the isentropes appreciably slope down from north to south in this season. The cyclone then halts for a time at the anticyclonic wall (dilatation) and then recurves at comparatively low latitudes (about lat. $15^\circ N$ on the average in pre-monsoon and post-monsoon months).

It may be observed that the generative and directive fields are "parallel walls" at right angles to the axis of the neutral cylinder. In case the mantle and the neutral cylinder begin to rotate uniformly and sufficiently fast without relative motion, the cyclone would move with the same velocity as obtains in the appropriate streamlines above the two core-cylinders in the directive field. It may be assumed that there is no difference in density between the neutral cylinder and its mantle in any level.

The variation of horizontal velocity of the equatorial along the z axis is small and the average normal velocity in the xy plane of the directive field is roughly of the order of 400 km. per day. A tropical cyclone, therefore, may move as one entity with this average velocity.

Vorticity.—The question of uniform translation of a cyclone (or anticyclone) by the directive field arises only when mass can be "annihilated" in the region of vorticity inside the generative cyclic field so that the mantle may appear mostly outside the cyclic field. The wet phase of the humidity wave fulfills the requirements and its volume and intensity apparently determines the extent of the mantle.

The vorticity accumulates at the four corners of the cyclic field, outside the belt. In the wet phase of a humidity wave, this region of vorticity gives rise to a simple vortex or mantle round the belt, which in due course begins to contract. The mantle thus consists of transitional air masses.

In case there is a marked relative motion between the mantle and the neutral cylinder, a vortex layer will arise at the Rankine joint which in daily charts is a region of heavy rainsqualls. This is an important feature of the tropical cyclones.

Humidity Wave.—It is interesting to observe that high pressure centres of the warm anti-cyclonic chain along latitude 15° lie between two air masses, the equatorial U_3 and the tropical U_1 . The negative twin in each anticyclone, *e.g.*

H_1 , H_2 or H_3 is known to produce the strongest "humidity wave" in three dimensions when both the undisturbed streams strengthen. Layers from these sources enter cyclogenesis field.

A brief "life history" of the generative field, cyclonic and anticyclonic, in the shape of changes of surface vapour pressure or minimum temperature (in the absence of rain and katabatic flow) in 120 hrs. usually provides the background of a three dimensional picture of the humidity wave. The "current changes" of these elements in 24 hrs. are helpful in interpreting the "life history."

Vortex pairs simulating cyclones.—A recurving cyclone, as a rule, weakens rapidly. While approaching the dilatation axis of the directive field, one of the core-cylinders may be in a streamline of anticyclonic curvature and the other in a streamline of cyclonic curvature. The vortices in the twin may thus separate from each other. Moreover the dilatation axis of the field [A] (square brackets indicating directive functions) is divergent and of anticyclonic vorticity. A change of drive, therefore, is usually responsible for the weakening of a cyclone. A diffusion of U_3 or U_4 etc. may also contribute to the rapid weakening of a recurving cyclone while passing to U_w . Moreover, a cyclone may also lose its free convection threshold for moist air in U_1 while recurving into U_w .

Let a positive twin in the positive cyclic field $n_3a_2n_2b_2$, for example, and a negative twin in the negative cyclic field $n_6d_2n_7c_2$ be simultaneously translated. It may so happen that the positive twin may meet the negative twin on c_2n_7 and pair off, in case the cyclic field is weakening. The two pairs may then travel in opposite directions.

As regards examples of pairing off of twins in the daily charts, it may be recalled that very often weather is unsettled in the north and southwest Bay of Bengal simultaneously, shortly after the passage of a cyclone, giving the wrong impression of a quick and fresh cyclonic formations. Numerous examples of this phenomenon are to be found in the October charts.

CENTRAL METEOROLOGICAL OFFICE,
KARACHI.

REFERENCES

- Baird, L., 1939, *Applied Aerodynamics*, p. 290
 Glauert, H., 1926, *Airfoil and Airscrew Theory*, p. 56.
 Goldstein, S., 1938, *Modern Developments in Fluid Dynamics*, p. 557.
 Lamb, H., 1930, *Hydrodynamics*, p. 202.
 Ramsay, A. S., 1935, *A Treatise on Hydromechanics*, Pt. II, London, p. 244.
 Sen, S. N., 1943, *Science and Culture*, Vol. IX, 90.
 Sen, S. N., & Ganesan V., 1940, *Science and Culture*, Vol. X, August.

INVESTIGATIONS ON THE SPECTRUM OF BROMINE

PART II—STRUCTURE OF Br II

By R. RAMANADHAM AND K. R. RAO*

ABSTRACT. The analysis of the spectrum of Br. II, reported by Bloch and Lacroute has been confirmed by a close examination of the individual lines forming the various triplet groups. With the aid of some of the known terms, the fundamental triplet giving the ground term $4p^3p$ has been identified in the vacuum grating region. The analysis is extended to include new terms, chiefly of the $5d$ configuration, based on the 3D state of the ion. Altogether about hundred lines have been newly classified, thirty of which are lying below $\lambda 1100$.

INTRODUCTION

In Part I of these investigations (Rao and Krishnamurty, 1937) the structure of the spectrum of doubly ionised Bromine (Br III) was described and the energy values of some of the doublet and quartet terms of the spectrum were determined. This part is devoted to the elucidation of the structure of the singly ionised atom (Br II), which is as yet not known completely.

The previously published work on the analysis of Br II comprises mainly of two different investigations, one by S. C. Deb (1930) and the other by Bloch and Lacroute (1931 and 1934). The conclusions arrived at by Deb are found to be entirely erroneous and will not be considered here. Bloch and Lacroute (1931) were the first to locate the prominent quintuplet groups in the visible region. In later work (1934) they reported the identification of 45 terms of Br. II based on the 4S and 3D states of Br III. Some of these identifications were confirmed by a study of the Zeeman effect of 26 lines of Br II. Still, many of the characteristic terms of Br II, which are to be predicted on Hund's theory and shown in Table I, have remained unidentified, the most important of these being the ground terms 3P , 1D , 1S , of the deepest $4p$ configuration.

TABLE I

Predicted terms of Br II

Electron configuration	Terms					
	Limit $4S$		3D			3P
$4s^24p^4$	4S	3P	1D			1S
$4s^24p^3 5s$	4S	3S	3D	1D		3P
$4s^24p^3 5p$	5P	3P	3F	3D	3P	$^3D^3P^3S$
			1F	1D	1P	$^1D^1P^1S$
$4s^24p^2 4d$	5D	3D	3G	3F	3D	$^3F^3D^3P$
			1G	1F	1D	$^1F^1D^1P$
$4s^24p^2 5d$	5D	3D	3G	3F	3D	$^3F^3D^3P$
			1G	1F	1D	$^1F^1D^1P$
$4s^24p^2 6s$	5S	3S	3D	1D		3P
						1P

In the present paper an extension of the analysis is made and terms of the 4p and 5d (2D) configurations are determined.

The main experimental work forming the basis of this investigation was already described in Part I. In addition, an examination is made of the feeble spark spectra between graphite poles containing various bromides and discharges through the vapours of bromides excited by a small induction coil, with a view mainly to identifying the groups of lines which have similar behaviour and appearance—under different conditions of excitation. These observations helped in allocating lines to the same multiplet, *e.g.* ($^3D \rightarrow ^3F$) or ($^3F \rightarrow ^3G$) etc. without depending merely on the equality of wave number intervals which sometimes might be accidental.

ANALYSIS

A close scrutiny of the plates, in the manner described above, has enabled the authors first of all to confirm the identification of $5s\ ^3S$, 3S and $5p\ ^3P$, 3P and the group of terms of the 5p configuration based on 2D state of the ion, made previously by Bloch and Lacroute. With the help of these terms and the combinations which they are expected to form in the vacuum grating region, the terms $4p\ ^1P\ ^1D$ and $5s\ ^3P\ ^1P$ have been detected. The chief triplet $4p\ ^3P$ - $5s\ ^3S$ is identified, leading to further classifications which are shown in Table 2a. The $5s\ ^1D$ term determined by Bloch and Lacroute as 65657.1 has been altered to 61179.5, the intensities of the combinations supporting the alteration.

All the 5p terms shown in Table 2 are due to Bloch and Lacroute with the exception of $5p\ ^3F_4$ which is newly determined. The 5D terms identified by Bloch and Lacroute are here assigned to the 5d instead of to the 4d state, as the latter are expected to be deeper than the $4d\ ^3D$ term and of the same order of magnitude as the $5s\ (^4S)$ terms. A comparison of the relative values of 4d and 5s terms in Se I., Br II and Kr III indicates that a crossing of the curves takes place at the third stage in Kr III. The combinations between $5d\ ^5D$ and the 5p terms shown in Table 2(a) and due to Bloch and Lacroute. They have expressed a doubt as to the correctness of the components 5D_0 and 5D_1 . The level 5D_0 depends on the assignments of the single line 25540.8. The behaviour and appearance of the lines are not inconsistent with Lacroute's classification which is here adopted. The 5d 3D assignments are due to the authors. Table 2(b) contains multiplets involving the 5d (2D) terms. Only four of these are due to Bloch and Lacroute. The rest are new. The 6s (2D) terms are also shown in the same table but their identification is incomplete and perhaps uncertain. The level 3D_1 gives nine combination lines of which three are otherwise classified.

In addition to the terms shown in Table 2 Bloch and Lacroute have also mentioned the following terms:—77679.6, 75311.6—65657.1 and 37909.0. The first two of these give combination lines with some of the 5p terms and also with $4p\ ^3P_2$. As the reality of these is not yet definitely confirmed they are omitted from the table. The two remaining levels are considered unreal as combinations with these occur elsewhere.

TABLE 2 (a)—Multiplets in Br II

$4p^4$	$(^4S)^3P_0$ 17027.9	$3P_1$ 17038.0	$3P_2$ 17411.9	$(^2D)^3D_2$ 16271.0	$5p(^4S)3P_1$ 59436.2	$5P_2$ 59300.9	$5P_3$ 58042.8	$3P_0$ 56284.7	$3P_1$ 56557.5	$3P_2$ 56351.4
$5s(^4S)^3S_2$ 80191.5 3S_1 75642.6	94628(5)	90788(1) 95329(20)	93918(9) 98470(20)		20755.3(10) 16226.3(1)	20806.6(10) 16341.7(3)	21248.7(10)	19358.0(8)	23034.0(3) 19085.1(10)	23840.0(6) 19290.9(10)
$5s(^3D)^3D_1$ 64690.8 3D_2 64436.5 3D_3 63740.8 $1D_2$ 61179.5		106294(3) 108802(4)	109683(5) 110377(10) 112933(2)	98284(0) 111530(10)						
$5s(^3P)^3P_0$ 52965.0 3P_1 52561.0 3P_2 51490.0 $1P_1$ 57333.0	117714(2) 112933(2)	118015(1) 118417(0) 110488(3)	121556(1) 122627(5) 116797(7)	105377(20)						
$4d(^4S)^3D_1$ 61723.1 3D_2 62388.5 3D_3 61658.5	108559(5)	109259(4) 108394(6)	111528(10) 112457(20)		21111.6(6)	20976.1(7) 22789.8(2)	20618.1(7)		18233.2(0) 20046.6(5)	18027.0(1) 19840.7(6)
$6s(^4S)^3S_2$ 38324.7 3S_1 36511.0			137607(2)							
$5d(^4S)^3D_0$ 33893.5 3D_1 33896.3 3D_2 33012.0 3D_3 33824.5 3D_4 33826.9 3D_5 34668.8		137374(2)	140512(6)		25540.8(6) 25539.6(10) 25824.4(6)	25404.8(5) 25668.9(8) 25476.4(8)	25330.7(3) 25118.4(5) 25116.1(10)		22662.4(0) 22945.5(2)	22455.3(1) 22739.5(5)
$3D_1$ 33995.5 3D_2 34661.5	135617(3)	136587(2)	140125(1) 139266(0)		24767.4(4) 25441.0(6)	25305.4(7) 24439.3(2)	24947.2(3) 24081.3(3)	21616.2(0)	21888.4(1) 22562.1(4)	22356.0(5) 21490.2(6)
$6s(^3D)$ 3D_1 22660.7 $a = 35992.0$		134992(4)			36775.2(1)	36640.0(1)	36282.9(1)	20290.5(4)	20565.7(3)	33691.6(5) 20359.8(2)

TABLE 2(b)—Multiplets in Br. II

$sp(^2D)$	$3F_2$	$3F_3$	$3F_4$	$3D_1$	$3D_2$	$3D_3$	$3P_0$	$3P_1$	$3P_2$	$1F_3$	$1D_2$	$1P_1$
5s ^(4S) 75642.6	32133.9(0)		42373.3	45442.7	44153.1	43465.1	40544.4	40517.9	40840.9	42430.3	37511.3	
5s ^(2D) 3D ₁ 64600.8	21181.6(7)											
3D ₂ 64436.5		21626.1(8)		19248.0(6)	20537.6(4)	20917.3(8)	24146.6(6)	24173.1(6)	23595.6(6)	22006.1(10)	21395.6(4)	
3D ₃ 63740.8		20930.4(5)	21367.5(10)	18993.7(4)	20283.3(8)	20275.6(9)		23918.8(8)	22869.9(20)	21310.4(11)	21141.2(6)	
1D ₂ 61179.5	17670.4(11)	18369.3(3)		15736.4(8)	17026.4(2)			20661.7(2)	20338.7(0)	18749.3(10)	17884.3(7)	
4d ^(4S) 3D ₁ 61723.1	18213.9(6)			16280.4(4)			21178.9(8)	21205.3(2)	21747.7(4)	20158.2(2)	18428.1(7)	
3D ₂ 62588.5	19079.4(0)			17145.6(6)	18435.6(8)	19123.6(3)		22070.8(6)	20817.4(6)		25077.3(5)	
3D ₃ 61658.5	18149.1(1)		19285.2(4)	17145.6(6)	17505.3(5)	18193.1(6)					24146.6(6)	
5d ^(2D) 3G ₃ 18002.9	25506.2(7)	24808.0(2)										
3G ₄ 17966.7		24843.6(6)	24406.4(2)									
3G ₅ 17843.4			24529.9(5)									
3F ₂ 18527.4	24981.4(2)			26915.3(7)	25625.6(6)	24938.3(5)				23902.7(1)		24767.4(4)
3F ₃ 18082.7			24290.2(4)		26070.3(7)	25382.4(4)				24347.7(1)		
3F ₄ 17434.6			24938.3(5)			26030.5(4)				24995.3(3)		
3D ₁ 22761.2	20747.9(3)			22681.6(4)	21391.8(2)		17783.1(2)	17900.8(2)				
3D ₂ 22616.7	20892.3(0)	20193.5(3)		22826.0(3)	21536.3(6)	20848.2(4)						
3D ₃ 21738.4	21770.7(0)	21071.9(3)	20634.7(5)	21071.9(3)	22414.6(2)	21726.6(6)			19102.4(5)			24533.5(0)
3P ₀ 14861.1												
3P ₁ 16485.3	27023.8(1)	30581.6(0)		30581.6(0)	27668.0(3)			25566.8(3)	24354.9(2)			
3F ₃ 15884.7		28956.7(1)		28956.7(1)	28269.1(3)			24031.7(5)	24956.6(3)			
3S ₁ 16393.1												21626.1(8)
1G ₄ 19134.4												
1F ₃ 13231.3		23676.6(2)								23295.9(7)		
1D ₂ 21286.7				24156.1(2)	22866.4(3)			24124.1(0)	24447.8(2)	29198.8(7)	24280.0(5)	
1P ₁ 20030.3		21523.6(2)							27609.4(2)	21143.6(5)	16224.7(6)	22008.5(5)
6s ^(2D) 3D ₁ 22660.7	20848.2(4)			22782.8(2)	21493.0(3)		17884.3(7)					23464.9(5)
3D ₂ 18094.0			24280.0(5)			25371.1(2)						
1D ₂ 19117.5						24347.7(1)			22746.9(5)	23312.3(2)	18393.8(6)	20634.7(5)

In Tables 2 the wave numbers are from the measurements of Bloch and Lacroute for all lines except those in the vacuum region. The latter and the intensities for all the lines are from our plates. A few lines occur at more than one place in the scheme. The term values are also shown in the same tables, all the new terms identified in the present work being calculated relative to those established by Bloch and Lacroute.

A brief consideration of the term intervals may be of importance, as it gives an idea of the degree of approach of the Br II spectrum to the (*jj*) type of coupling. The deepest term $4p^2\ ^3P$ is completely inverted and the interval ratio between its components, 4.4:1, is far from the theoretical value derived from the simple (*LS*) coupling. The variation of these intervals and of their ratio in SI and SeI like spectra shown in Table 2, supports the correctness of the identification.

TABLE 3
(3P_2 — 3P_0) intervals

	Ratio			Ratio		
SI	572	1.74	CHII	994	1.58	A III
Se I	2534	1.51	BrII	3838	1.39	Kr III
						1574
						5313

The values of Br II are also in agreement with the limits as determined approximately by Kiess and de Bruin (1930) from the series of terms in Br I.

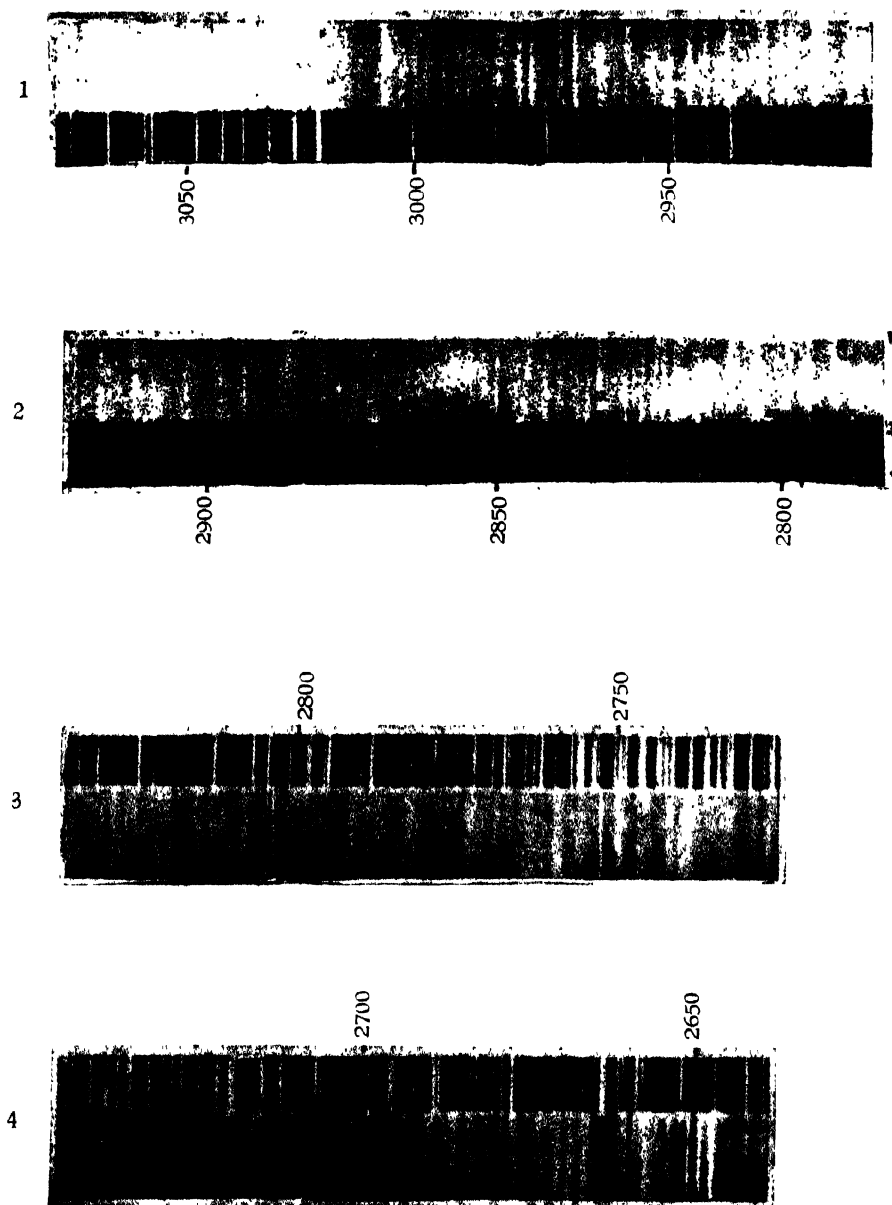
The terms in Br II as shown in Table I converge to the limits 4S , 2D and 2P of Br III. The values of these limiting terms obtained by the authors (Ramanadham and Rao, 1944) are $^4S_{1\frac{1}{2}} - ^2D_{1\frac{1}{2}} = 15042$ and $^2D_{2\frac{1}{2}} - ^2P_{\frac{1}{2}} = 10613$ units. It is seen that the average differences between the following sets of terms,

$$\begin{aligned}
 &5s\ (^4S)\ ^5S, \ ^3S - 5s\ (^2D)\ ^3D\ ^1D. \\
 &5d\ (^4S)\ ^5D\ ^3D - 5d\ (^2D)\ ^1^3G\ \text{to}\ ^1^3S \\
 &5p\ (^4S)\ ^5P\ ^3P - 5p\ (^2D)\ ^1^3F\ \text{to}\ ^1^3P
 \end{aligned}$$

are approximately 14400, 16000, and 15570 respectively. These are of the same order of magnitude as the difference $^4S - ^2D$ of Bromine III. An accurate determination of the limits is not possible unless a long Rydberg series of terms is identified. The sources used in the present experimental work are not favourable for the production of such higher members. For this purpose an attempt is being made to study the hollow cathode spectrum of bromine and to extend the identification further to detect the terms based on the 3P state of the ion. These will be dealt with in a later communication.

REFERENCES

- Bloch, L. E. and Lacroute, 1934, *Compt Rend*, **199**, 41.
Bloch, L. E. and Lacroute, 1931, *Compt Rend*, **197**, 233.
Deb, 1930, *Proc. Roy. Soc. (Lond.) A*, 127.
Kiess and de Bruin, 1930, *Bur. Stand. Jour. Res.*, **4**, 667.
Lacroute, 1935, *Annales de. Phys.*, **3**, 3.
Rao Krishnamurty, 1939, *Proc. Roy. Soc. (Lond.) A*, **161**, 3
Ramanadham and Rao, 1944, *Curr. Sc.*, **18**, 72.



HgI Bands and Fe arc comparison
1 and 2 System C, 3 and 4 System D.

ULTRA-VIOLET BAND SYSTEMS OF THE MERCURY IODIDE MOLECULE.—PART I

By K. R. RAO,* M. G. SASTRY AND V. G. KRISHNAMURTI

(Plate VII)

ABSTRACT. The ultra-violet bands of the mercury iodide, excited in a discharge tube, are photographed with a Hilger large quartz Littrow spectrograph. The systems C and D lying in the regions $\lambda_{3100}-\lambda_{2800}$ and $\lambda_{2800}-\lambda_{2650}$ are measured. The wavelengths of the C system are compared with those published by Wieland, the data obtained in the system D being entirely new. Analysis of the two systems have led to the following vibrational constants—

	ν_e	ω'	$x'\omega'$	ω''	$x''\omega''$
System C :	32730.9	235.6	2.16	125.9	1.07
System D :	36269.2	178.0	1.14	125.7	1.10

*They are in agreement with the values determined approximately by Wieland from the study of fluorescence of HgI. The origin of the D system is, however, different from that suggested by Wieland. With the classification obtained in the present work, the systems could be attributed to the two components of a $\Pi^2\Sigma-\Sigma$ electronic transition with a ${}^2\Pi$ interval of 3538 cm^{-1} which is shown to be in conformity with the corresponding intervals obtained for the other mercury halides, HgI[†] and HgCl.

INTRODUCTORY

The mercury iodide molecule has an extensive band spectrum in the ultra-violet. Wieland (1929) investigated these bands with a grating having a dispersion of 10Å. per mm. in the first order and quartz spectrographs of nearly the same dispersion at λ_{2500} . The systems reported by him are shown in Table 1, together with those observed by later investigators, Prilheshejewa (1932) and Sastry (1942)

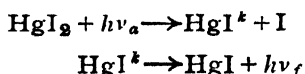
TABLE 1

Author	Region	Previous designation	Present designation
Wieland	4500—3400	Class III	B
... ..	3100—2800	„ II	C
.....	2800—2650 ?	„ I	D
.....	2700 ? 2530	E
Sastry	2560—2530	Class A	F
Prilheshejewa	2240—2168	G
.....	2160—2114	H

In his earlier work Wieland *loc. cit.* investigated these bands in emission but the wavelength data were given only for the system C. Although no analysis

*Fellow of the Indian Physical Society.

was presented, certain regularities were indicated among the bands of this system and the bands themselves were ascribed to the triatomic molecule HgI_2 . In later work, studying the absorption and fluorescence of the vapour of mercury iodide, Wieland (1932) ascribed these bands to the diatomic molecule. By optical excitation of the vapour by sparks from different metals and using suitable filters, fluorescence spectra were obtained which were associated with the equations



where the difference $(h\nu_a - h\nu_f) \geq$ the dissociation energy of $\text{HgI}_2 \longrightarrow \text{HgI} + \text{I}$. The fluorescent systems were measured and from a study of their structure, the following approximate formulæ were suggested,

$$\text{System C: } \nu = 32784 + [233.3\nu' - 2.25\nu'^2] - [124.0\nu'' - 1.0\nu''^2]$$

$$\text{System D: } \nu = 36130 + [175\nu' - 1.20\nu'^2]$$

For system B no analysis was given but the occurrence of the wave number intervals 120 and 180 was mentioned, which is suggestive of the probable electronic transition involved in their emission.

One of the writers (Sastry, 1942) published the wavelength data of the system E obtained in emission with a Hilger E_1 quartz Littrow spectrograph and in addition obtained a new system between $\lambda\lambda 2530-2560$ (designated by him as class A but hereafter will be referred to as system F in conformity with the designation of the other systems). The system E was found by him to consist of two components α_1 and β_1 having a common final state and an electronic width of about 766 cm^{-1} . The system F was attributed by him to a transition $^2\Pi - ^2\Sigma$ showing four component heads and an electronic separation of 126 wave number units. As was mentioned by Sastry, the analysis does not show any level in common with the other bands of HgI . In view of this, a reinvestigation seemed desirable to systematise the analysis and interpretation of all the known bands of mercury iodide and to examine if they can be correlated with the band systems of the other mercury halides.

As a first step, the systems C and D are considered in this paper, a preliminary report of which appeared in *Current Science* (in press). Both the systems are newly photographed and measured, as no wavelength data appear to have been published at all for system D and system C was obtained by Wieland with a comparatively lower dispersion instrument.

EXPERIMENTAL

The bands were excited in a pyrex discharge tube about 10 cms by 1.5 cms diameter, containing mercury iodide in a small side bulb which could be heated if necessary. The excitation was either by a quarter-kilo watt transformer giving about 15000 volt or by a small 8 inch induction coil. Continuous evacuation by a Cenco-Hyvac pump was necessary. The discharge was bright violet and could be maintained easily for hours with just occasional heating

of the mercury iodide container. Two Hilger quartz spectrographs were used for photographing the spectrum, the measurements being made by the larger one of the Littrow type with a dispersion of 3.8Å per mm. at $\lambda 2800$. The measurements, made by a Hilger measuring micrometer, are the average of three independent settings. Iron arc lines were used as standards for determining the wavelengths.

The spectrum is shown in plate VII.

In both systems the bands on the long wavelength side have somewhat sharper edges, getting diffuse as they occur towards shorter wave lengths. At the extreme ultra-violet end, they are very crowded, exhibit no edges at all and are diffuse and mostly unresolved. In measuring the plates the micrometer settings were made against the edges of the bands where they are sharp and against the central maximum where they are diffuse. About 130 bands are measured in system D. Table 2 gives the wavelengths and wave numbers of the heads, the intensities being the usual visual estimates.

ANALYSIS

The fourth column in the Table 2 gives the assignment of the vibrational quantum numbers, as determined in the present work. About 90 bands are classified. A few of the bands are assigned twice. One difficulty met with, in working out the analysis, is the ambiguity in the possible assignment of the bands lying particularly in the extremely crowded region below about $\lambda 2700$. This makes the classifications in this part of the spectrum somewhat uncertain. There is need for photographing this region with a much higher dispersion in order to clear the ambiguities. The following formula is calculated to represent the band heads :

$$\nu = 36269.2 + [178.0(v' + \frac{1}{2}) - 1.14(v' + \frac{1}{2})^2] - [125.70(v'' + \frac{1}{2}) - 1.10(v'' + \frac{1}{2})^2]$$

For about 70 bands the "obs-calc" values are less than 3 units. The larger discrepancies in the remaining bands are believed to be due to the uncertainties in the measurement and the ambiguities in the classification referred to above.

The constants ω' and ω'' agree well with those obtained approximately by Wieland (1932) from the fluorescent system but it will be seen that the system origin is shifted towards the violet by about 160 cms^{-1} . Many of the stronger bands in emission are thereby brought into the scheme of classification. This shift is also supported by the view advanced by Howell (1943) and discussed in a later paragraph of this paper.

The intensities of the bands are shown in the usual diagonal matrix in Table 3 which contains also the values of ΔG in the upper and lower states.

The band spectra of several iodides show an intensity distribution corresponding to an open parabola. Such a definite characteristic is not seen in the present bands. The (0, 0) band is no doubt not the most intense and the stronger bands occur in the two progressions $v'=0$ and $v''=0$. There is however, an asymmetrical development of the sequences, those giving rise to bands on the

lower frequency side of the origin being very poorly developed while on the violet side long sequences are obtained for $\Delta\nu = +3$ to $+7$.

TABLE 2 Hg I bands. (System D)

Wavelength	Int	Wave number	Classification (ν', ν'')	Obs-cal.
2808.88	3	35590.0	0,6	2.3
08 47	3	596.2
00 40	2	698.2	0,5	-0.6
00.22	2	701.0
2798.22	2	726.5	2,8	8.4
95.31	2	763.7	1,6	0.7
93.05	1	792.7
91.29	5	815.1	0,4	0.6
86.66	3	874.7	1,5	-0.8
83.81	1	911.4	5,11	-2.3
82.16	5	932.7	0,3	1.3
80.21	2	957.9	4,9	5.6
77.13	3	997.8	3,7	0.4
74.97	2	36025.8
73.05	5	050.7	0,2	0.2
72.42	3	058.9	4,8	-0.7
69.51	2	096.9
65.80	2	145.2
64.50	3	162.2	2,4	-1.5
63.77	3	171.8	0,1	0
59.64	2	226.0	1,2	0.8
57.17	2	258.6
55.60	2	279.0	2,3	-1.6
			4,6	2.4
2754.37	2	36295.3	0,0	0
51.16	1	337.8	3,4	2.9
50.46	4	346.8	1,1	-0.7
47.33	3	388.2	4,5	-1.9
45.67	2	410.2
44.29	2	428.5
43.20	...	442.7	5,6	-0.5
42.66	2	450.2	3,3	-1.6
41.17	5	469.9	1,0	-1.1
38.66	3	503.4	4,4	-0.4
37.46	2	519.4	2,1	-1.6
36.49	2	532.4
34.93	2	553.1	5,5	-2.6
33.69	2	569.8	3,2	-1.1
30.47	3	613.0
28.24	5	642.9	2,0	-1.6
26.42	4	667.3	5,4	-3.1
24.33	2	695.4
21.93	2	727.8
21.12	2	738.7	4,2	-1.1
16.90	3	795.8
15.64	5	812.9	3,0	-2.8
14.67	4	826.0	8,7	6.9
12.18	3	859.8	4,1	-1.3
11.20	3	873.1	9,8	4.6
10.38	3	884.3	7,5	2.2
09.78	3	892.4
08.98	1	903.3	5,2	3.1
08.59	2	908.7
07.58	2	922.4	10,9	4.6
06.96	3	930.8	8,6	1.4
05.51	4	950.6	6,3	-1.0
03.27	5	981.2	9,7	4.6
2702.18	3	36996.2	7,4	-0.6
00.01	3	37025.9	5,1	-1.8
			10,8	2.2

TABLE 2 (contd.)

Wavelength	Int.	Wave number	Classification (ν', ν'')	Obs.-cal.
2697.91	2	054.8	8,5	13.8
96.93	2	068.2	6,2	-2.5
96.65	2	072.0	11,9	1.3
95.80	2	083.8
95.51	1	087.8	9,6	0.9
94.34	2	103.8
93.74	2	112.1	7,3	-1.6
92.72	3	126.2
92.24	3	132.8	10,7	1.0
91.27	2	146.2	5,0	-5.0
91.00	3	149.9
90.19	2	161.1	8,4	4.5
89.81	2	166.3	13,11	1.7
88.87	2	179.3	11,8	2.7
88.07	2	190.4	6,1	-0.6
87.64	3	196.3
87.37	4	200.9	9,5	1.5
86.73	3	208.9	14,12	-2.5
86.07	2	218.1	12,9	-3.3
85.07	3	232.0	7,2	-0.8
84.35	2	242.0
83.93	2	247.7
83.21	2	257.7	15,13	-0.4
82.62	3	266.0	13,10	-1.1
81.69	2	278.9	8,3	5.4
81.21	2	285.6	11,7	0.9
80.73	2	292.2
79.22	2	313.3	14,11	2.6
			9,4	-0.8
78.63	3	321.4
78.27	3	326.4	12,8	-0.9
2677.29	3	37340.1
76.81	3	346.8
76.33	2	353.5	10,5 } 15,12 }	-1.1 } -1.7 }
75.26	4	368.4
74.95	3	372.8
74.16	1	383.8
73.52	3	392.8	8,2 } 11,6 }	0.2 } 2.2 }
72.72	2	403.9	16,13	4.3
71.72	2	418.0	14,10	4.8
71.42	3	422.2
71.00	3	428.1
70.53	2	434.6	9,3 } 12,7 }	3.6 } -0.6 }
70.03	1	441.6	17,14	-2.4
69.57	2	448.1
69.24	3	452.7	15,11	-1.8
68.58	2	462.0	10,4	-7.3
67.80	1	472.9	13,8	-2.8
67.23	2	480.9	7,0	3.5
66.52	2	491.0	16,12	-5.7
65.81	2	500.9	11,5	-6.6
64.82	3	514.8	14,9 } 8,1 }	-1.1 } 1.4 }
63.64	4	531.5
63.19	0	537.8	12,6	-7.4
62.48	4	547.8	9,2	-2.3
61.30	5	564.4	15,10	-2.6
60.76	4	572.1
60.07	3	581.8

TABLE 2 (contd.)

Wavelength	Int.	Wave number	Classification (ν', ν'')	Obs.-cal.
59.36	3	591.8	16,11	-4.2
58.78	2	600.1
58.12	2	609.4
57.66	2	615.9	11,4	-6.3
57.56	3	617.3	14,8	-4.5
56.68	2	629.8	17,12	-6.2
2654.84	2	37655.9	12,5	-2.3
54.57	0	662.5	15,9	2.8
54.00	1	667.8
53.10	3	680.5
52.83	2	684.4	13,6	-9.7
51.46	2	703.9	16,10	5.4
50.93	2	711.4
50.07	0	723.6	14,7	-6.3
49.59	0	730.4	17,11	-4.9
48.48	0	746.4	11,3	7.3
47.42	2	761.4	15,8	-4.2

TABLE 3

Intensity distribution in Hg I bands (System D)

$\begin{matrix} \nearrow \nu'' \\ \searrow \nu' \end{matrix}$	0	1	2	3	4	5	6	7	8	9	10	11	12	13	14	$\Delta G' (v+\frac{1}{2})$
0	2	3	5	5	5	2	3									175.0
1	5	4	2			3	2									172.8
2	5	2		2					2							172.3
3	5		2	2	1											167.6
4	5	3	2		3	3	2		3	2						164.7
5	2	3	1		4	2	1					1				165.5
6		2	2													162.8
7	2		3		3	3										165.8
8		3		2	2	2	3	4								153.5
9			4	2	2	4	1	5	3							153.3
10			2	3	2	2	2	3	3	2						151.8
11				0	2	2	2	3	2	2						148.4
12					2		0	2	3	2						147.7
13							2	3	1	4	3	2				144.0
14								0	3	3	3	2	3			144.7
15									2	0	5	3	2	2		140.6
16											2	3	2	2		138.7
17												0	2		1	
$\Delta G'' (v+\frac{1}{2})$	123.2	121.6	116.3	120.3	112.6	112.6	105.6	107.5	104.2	99.1	107.1	101.3	91.5			

The values of ΔG shown in this table cannot be considered as very satisfactory, the irregularities are very probably due to the diffuseness of the bands and consequent uncertainties in the determination of their wave lengths.

Tables 4 and 5 give the measurements, classification and the intensity distribution among the bands of system C. About 86 bands have been obtained, some of them being new. The ΔG values of the lower state of this system accord

fairly closely with the corresponding values shown in Table 3 for system D. That these two systems have a common final state is indicated by the following formula calculated for system C

$$\nu = 32730.9 + [235.6(\nu' + \frac{1}{2}) - 2.16(\nu' + \frac{1}{2})^2] \\ - [125.9(\nu'' + \frac{1}{2}) - 1.07(\nu'' + \frac{1}{2})^2]$$

TABLE 4
Mercury iodide bands (system C)

Wave-number (Wieland)	Int	Wave-number (Authors)	Int	Classification	Obs-cal.
32536.2	4	32540.3	5	0,2	0.9
650.0	4	650.3	3	2,5	4.7
		652.3	5	1,3	2.1
660.0	5	661.1	4	0,1	0
761.3	4	763.1	4	2,4	2.3
770.9	3	772.1	4	1,2	2.4
782.8	5	784.9	4	0,0	0
870.1	4	872.8	5	2,3	-5.4
		891.6	4	1,1	2.3
974.7	1	976.6	3	4,6	1.1
		988.1	3		
997.0	2	999.6	4	2,2	1.9
33014.4	3	33017.2	5	1,0	2.0
		021.5	5		
		33085.3	1	4,5	-1.3
		097.2	1		
33102.4	1	103.4	3	3,3	0.6
118.0	1	120.0	3	2,1	0.6
188.7	1	190.9	1	5,6	7.4
199.7	2	204.8	1	4,4	3.0
		222.3	2	3,2	2.0
242.8	4	243.3	5	2,0	0.1
		293.1	2	5,5	-3.5
319.8	1	319.9	3	4,3	0.7
341.4	5	342.2	5	3,1	0.2
		358.3	2		
		390.1	2	6,6	-7.1
414.3	2	416.1	4	5,4	4.3
437.3	3	438.6	4	4,2	-2.1
464.8	3	466.5	4		
		479.4	1		
		494.5	1	7,7	4.9
506.8	3	510.2	3	6,5	-0.1
		520.6	3		
531.0	2	530.6	2	5,3	1.4
558.5	4	559.1	5	4,1	-1.8
589.0	1	589.0	5	8,8	5.2
		631.0	2	6,4	5.5
650.6	4	649.2	4	5,2	0.5
		652.5	4		
680.1	1			4,0 ?	2.6 }
711.3	1	739.8	4	8,7 }	-3.8 }
739.2	2	739.8	3	6,3	-3.0
771.7	3	771.2	3	5,1	0.8
803.1	2	803.1	2	8,6	-0.5
		810.5	2		
827.1	1	831.5	2	7,4	2.6
858.6	3	859.4	3	6,2	-3.0
862.0	3				

TABLE 4 (contd.)

Wave-number (Wieland)	Int.	Wave number (Authors)	Int.	Classification	Obs-cal.
33891.9	1	33892.7	3	5,0 }	-1.5 }
...	9.7 }	3.4 }
...	...	909.6	2	8,5	-7.1
944.2	2	946.1	4	7,3	-0.2
949.4	2	950.6	3	11,10	1.3
977.7	1	978.2	3	6,1	-5.9
982.9	2
34028.0	3	34030.7	4	8,4	-1.2
061.6	1	065.0	2	7,2	-0.8
...	...	084.1	2	10,7	2.3
110.4	1	110.7	5	6,0 }	2.8 }
...	9,5 }	-2.7 }
143.6	3	144.6	4	8,3	-2.7
186.8	1	181.9	2	7,1	0.4
223.1	3
226.0	4	226.2	4	9,4	-2.4
...	...	263.3	3	8,2	-5.5
304.1	3	300.8	4	10,5	-5.1
337.2	2	338.9	3	11,6 }	1.6 }
...	9,3 }	-7.1 }
381.4	2	382.5	3	8,1	-8.0
408.6	0
415.1	1	417.0	3
...	...	423.2	2	10,4	2.1
451.3	0
457.8	2	460.3	3	9,2 }	-5.2 }
...	12,7 }	6.6 }
489.9	2	492.7	2	11,5	-1.3
512.6	1	512.1	3
534.6	0	538.9	3	10,3	-0.4
566.2	0	567.8	3	12,6	3.0
...	...	593.6	2	14,9	0.4
611.1	0	614.1	4	11,4	4.9
642.9	2	640.8	3	13,7	7.7
676.5	0	677.6	3	12,5	-0.8
715.1	2	716.8	3
...	...	726.0	2	16,11	2.2
34750.7	2	34753.1	2	13,6	9.0
...	...	764.8	1	15,9	1.2
786.9	0	789.0	3	12,4	0.4
...	...	806.6	4	14,7	-2.1
821.5	2	821.0	3	16,10	-5.2
860.3	0	868.3	0	15,8	-2.5
890.8	1
893.8	2
931.6	2	928.9	3	16,9	-1.8
964.6	0	965.0	0
35000.1	0	35005.0	0
...	...	35040.6	2	16,8	3.2

Isotope Effect.—As iodine has no isotopes, the band spectra of iodides are particularly suitable for the study of the isotopes of the combining atom—Hg in this case. The known isotopes of Hg and their percentage abundance are given below (Seaborg, 1944).

196, 198, 199, 200, 201, 202, 204

0.15, 10.1, 17.0, 23.3, 13.2, 29.6, 6.7

TABLE 5
Intensity Distribution (System C)

ν'/ν''	0	1	2	3	4	5	6	7	8	9	10	11	ΔG ($\nu + \frac{1}{2}$)
0	4	4	5										231.5
1	5	4	4	5									225.6
2	4	3	4	5	4	3							224.4
3	4	5	2	3	3	5							216.9
4	3	5	4	3	1	1							210.2
5	5	3	4	2	4	2							209.3
6		3	3	3	2	3							204.0
7		2	2	4	2			1					198.2
8		3	3	4	4	2		4	5				198.4
9			3	3	4	5		3					193.1
10				3	3	4		2					197.0
11					4	2							176.5
12					3	3		3					182.9
13								3					165.8
14								4					171.2
15									0	2			168.2
16									2	3	3	2	
$\Delta G''$ ($\nu + \frac{1}{2}$)	125.8	119.8	120.2	114.1	117.3	111.5	110.2	99.8	108.2	107.9	95.0		

The separation of the isotopic heads of a given band (ν' , ν'') is given by

$$\nu' - \nu = (P - 1) [(\nu - \nu_e) - \chi' \omega' (\nu' + \frac{1}{2})^2 + \chi'' \omega'' (\nu'' + \frac{1}{2})^2]$$

Where ν' refers to the less abundant molecule. The isotopic separation is calculated from this formula for the two isotopes 198 and 202. The maximum separation is about 5 to 6 units and is certainly measurable for the bands remote from the origin. Examination of the spectrum failed to reveal any faint heads which could unmistakably be assigned as such. They must have been marked by the considerable overlapping arising from the unresolved rotational structure and the proximity of bands due to different vibrational transitions. The diffuseness of the bands justifies this assumption.

INTERPRETATION

The ultra violet emission spectra of mercury fluoride was analysed by Howell (1943) into two systems which were interpreted as the two components of a $^2\Pi - ^2\Sigma$ transition with the $^2\Pi$ interval $\Delta\nu$ being 3940 cm^{-1} . By a comparison of this separation with the over all width of the 3P state of the Hg atom, Howell showed that the molecular constant $A (= \Delta\nu)$ for a Π electron giving rise to a $^2\Pi$ state in HgF is of the same order as the coupling constant $a (= 2265)$ for the 6p electron giving the $6s 6p^3P$ state of the Hg atom. This approximate equality together with the important observation by Carnell that all the ultra violet band spectra of the halides of Zn, Cd and Hg studied by him occur near the resonance lines of the metal atom led Howell to put forward the view that the transition involved in the emission

of the band systems of these halides is atomic in nature. The doublet splitting of the $^2\Pi$ state should then be nearly the same in all the halide bands of any particular metal atom Zn, Cd or Hg, the influence of the halogen atom being negligible. This feature was shown by Howell to hold in the various halide bands for which data were available. Examining the HgI band systems C and D in the light of this view, it would appear that these systems might form the two components $^2\Pi-^2\Sigma$ transition, the interval $^2\Pi_{3/2}-^2\Pi_{1/2}$ being equal to 3538 cm^{-1} . In Table 6, the separations between the (0,0) bands of what are believed to be such analogous components in the halides bands of Zn, Cd and Hg are collected. The data are mostly tentatively suggested by Howell (*loc. cit.*). The value for Hg Cl is confirmed recently by one of the authors (Rao, 1944), and that for HgI is from the present work.

TABLE 6

	Hg	Zn	Cd
F	3934	1179	370
Cl	3889	1115	383.5
Br	—	—	408
I	3510	—	—
Atomic coupling constant	4265	1140	386

There is a definite decrease in the value of the molecular constant from the lightest Hg F to the heaviest Hg I molecule, indicating an increasing departure from the atomic coupling constant 4265 cm^{-1} , a feature which should be expected as the influence of the halogen atom, cannot be altogether neglected. Accurate data on the other spectra are also needed before further light can be thrown on this question. Experiments in this direction are in progress in this laboratory.

ANDHRA UNIVERSITY,
GUNTUR

REFERENCES

- Howell, 1943, *Proc. Roy. Soc. (Lond.) A*, **182**, 95.
 Pritheshejewa, 1932, *Phys. Z. Sowjet.* **1**, 189.
 Rao K. R., 1944, *Curr. Sci.* **23**, 279.
 Sastry, 1942, *Proc. Nat. Inst. Sci. India*, **8**, 289.
 Seaberg, 1944, *Rev. Mod. Phys.*, **16**, 1.
 Wieland, 1929, *Helv. Phys. Acta*, **2**, 46 and 77.
 Wieland, 1932, *Zetts. f. Phys.*, **76**, 801

ON THE CATHODE DARK-SPACE OF A GLOW DISCHARGE IN GASES AT LOW PRESSURES

By R. M. CHAUDHURI* AND S. H. ZUBERI

ABSTRACT. Experiments have been performed with a movable anode in a discharge tube. It is observed that the tube voltage and current show no variation as the anode is brought closer to the cathode till the former cuts out a certain length of the negative glow. If the anode is pushed further the current decreases while the voltage to maintain a smaller current rises continuously. The drop in the current is linear with the displacement of the anode till it reaches a point near the edge of the cathode dark-space.

It is concluded from the experimental curves that there is always a supply of the positive ions to the cathode dark-space from the negative glow which is not consistent with Thomsons' assumptions.

INTRODUCTION

Experiments of Aston (1911), of Gunther-Schulze (1923, 1924), and of Geddes (1926) show that the cathode dark-space is a very active region of a glow discharge in a gas at low pressures. In a normal discharge, according to Thomsons (1933), the positive ions which strike the surface of the cathode and maintain the discharge by liberating the secondary electrons therefrom are wholly produced in the cathode dark-space itself and very few of them drift into it from the negative glow. They, moreover, consider it probable that on account of their high density in the dark-space, some of them flow back from the dark-space, into the negative glow by diffusion against the electric field. In an abnormal discharge the ionisation in the dark-space is much less intense than in the normal case and it is likely that a part of the supply of positive ions to the cathode dark-space is from the negative glow. Loeb (1939) assumes that there is always a rush of the positive ions from the negative glow to the cathode dark-space. There is, however, no direct experimental evidence in favour of these assumptions or against them.

Aston (1907) in determining the width of the dark-space uses an optical method and believes that its boundary can thus be marked accurately within a fraction of a millimeter. Gunther-Schulze has determined the length of the dark-space electrically by gradually pushing the anode plate towards a similar cathode. The distance between the two parallel electrodes when the voltage required to maintain the discharge abruptly rises is taken to be the length of the dark-space. In Thomson's experiments (1931) on the intermittence of a discharge, with two parallel plane electrodes the applied voltage is kept constant and the changes in the discharge current are recorded as the two electrodes are brought closer together. The discharge current is found to remain unaltered

* Fellow of the Indian Physical Society.

as long as the anode is away from the boundary of the dark-space but it becomes unstable as it approaches the boundary and dies out as the anode enters the dark-space. Very few data are, however, available which give the variations of the discharge current as the applied discharge voltage is changed with the anode at varying distances from the cathode. Such experiments are likely to yield information if positive ions flow at all from the negative glow into the cathode dark-space and would therefore prove of importance in the theory of a glow discharge. The present work is devoted to these investigations.

THE APPARATUS

The apparatus is given in Fig. (1).

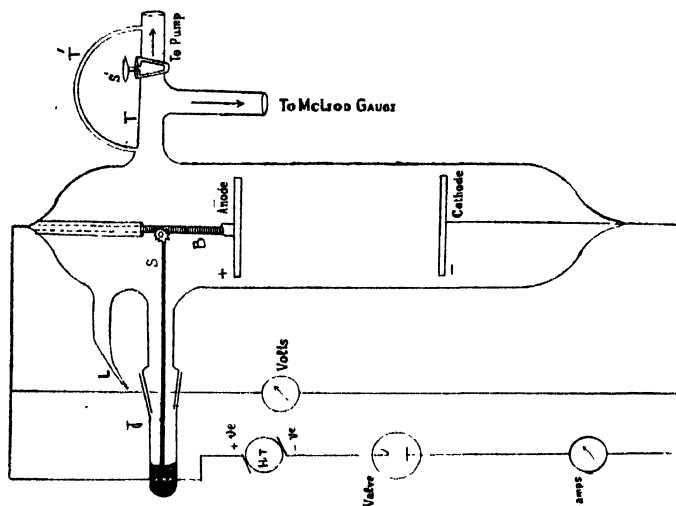


FIG. 1

The discharge passed in a cylindrical pyrex glass tube 5 cms in diameter and 15 cms. long. The anode and cathode were two plane parallel circular brass discs, each 4 cms. in diameter and 5 mms. thick. The anode was screwed at its centre to the end of a long grooved solid brass rod, B, about 8 mms. in diameter, which could move up and down in a hollow brass tube, waxed with the main body of the discharge tube. A second brass rod, S, of about the same thickness as B, carried a wheel at one end with its teeth closely fitting into the grooves of the first rod and was firmly held with wax in a side ground glass joint J. The anode was lowered or raised by rotating the joint J and thus the rod, S. The distance between the electrodes could be adjusted at will with this arrangement within a fraction of a mm. without disturbing the pressure inside the apparatus during the experiments.

The apparatus was exhausted with a single stage Gaede's all steel mercury diffusion pump backed by a Cenco Hyvac pump through the side tube T. The gas entered the discharge tube through a fine glass capillary leak, L, from a large

glass reservoir and its pressure in the discharge was adjusted by regulating the pressure in the reservoir and was read with a McLeod gauge.

The voltage for the discharge was obtained from a D. C. motor generator set and was read with an electrostatic voltmeter. The current in the discharge tube was stabilised by putting a diode valve in series with it and was measured with a moving coil milliammeter.

EXPERIMENTAL PROCEDURE AND THE RESULTS

The apparatus was first made air-tight and before starting the experiments the whole system, including the gas reservoir, was highly evacuated with the tap, S', open. The reservoir was washed for about half an hour at a low pressure of the gas under experiment and was then filled with it at a suitable pressure, read by a mercury manometer. The tap, S', was then closed and the gas allowed to flow from the reservoir to the discharge tube through the leak L, while the pumps worked continuously. The gas from the discharge tube streamed through the capillary T' to the pumping system for over an hour which removed from the experimental tube the foreign vapours and impurities occluded from the glass walls, metal parts and the wax joints and let it settle down to a steady pressure before any observations were taken. A wide range of working pressure, which remained constant for a sufficiently long time for recording several sets of observations together could be maintained in the discharge with this arrangement.

The discharge was started with the distance between the electrodes always much greater than the width of the cathode dark-space, usually it was 9-10 cms. The anode was then gradually pushed towards the cathode and the tube voltage and the current which this maintained in the discharge were recorded step by step.

The experiments were performed in air and oxygen only. Air was drawn from the atmosphere and oxygen was taken from a commercial cylinder.

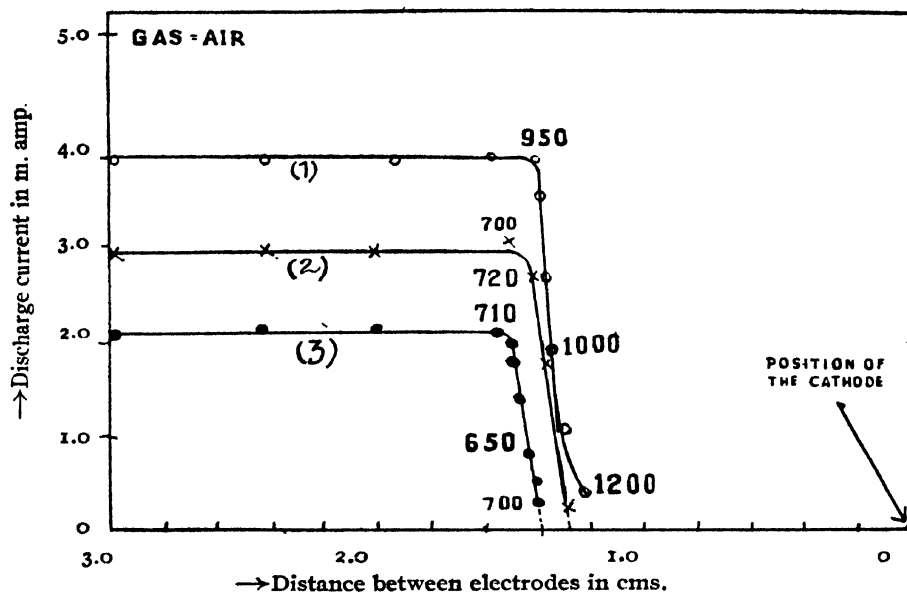
A large number of curves connecting the discharge current and the distance between the electrodes were taken under different conditions of the discharge. In air the observations were taken over a pressure range 0.030-0.142 mm., voltage range 350-1500 volts and current range 1.2-4.0 m. amps; corresponding values for oxygen are 0.122-0.165 mm., 400-550 volts and 1.8-3.2 m. amps.

Typical results in air are given in Figs. 2-4. Curves in Fig. 2 were obtained at a constant pressure while those in Figs. 3 are for initial constant voltages. The results obtained at the lowest pressure used are given in curve (1) of Fig. 4.

The results at a constant pressure and at an initial constant voltage in oxygen are represented by the curves in Figs. 5 and 6 respectively.

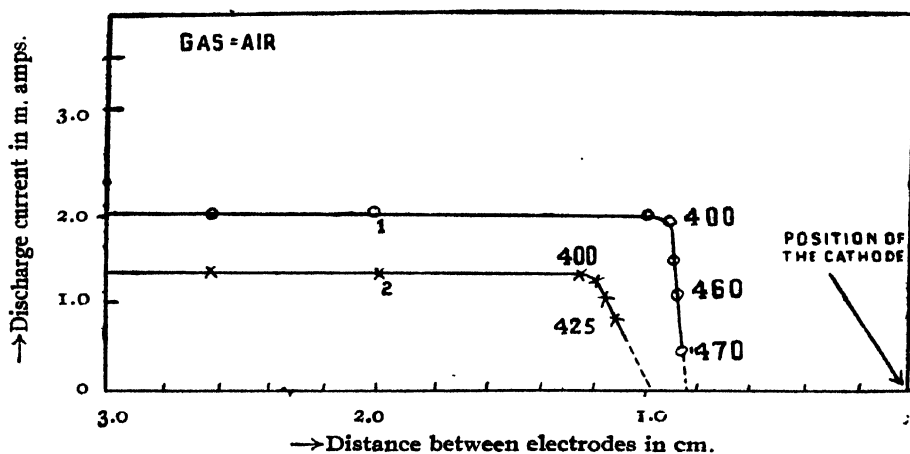
It is evident from all the curves that the discharge current and voltage remain constant till the anode reaches a point in the negative glow near the boundary of the cathode dark-space. The position of the anode where the voltage and current begin to change lies in the negative glow a few mms,

Discharge pressure = 0.0539 mm.



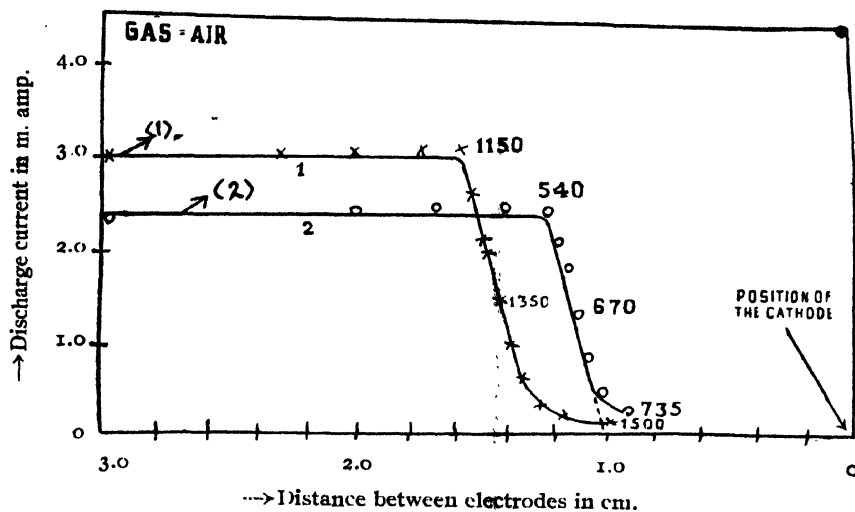
Curve (1) Dark-space (measured) = 1.225 cm.
 " (from curve) = 1.230 "
 (2) " (measured) = 1.225 "
 " (from curve) = 1.260 "
 (3) " (measured) = 1.315 "
 " (from curve) = 1.360 "

FIG. 2



Curve (1) Discharge pressure = 0.1324 mm.
 Dark-space (observed) = 0.835 cm.
 " (from curve) = 0.840 "
 (2) Discharge pressure = 0.1016 mm.
 Dark-space (observed) = 0.100 cm.
 " (from curve) = 0.100 "

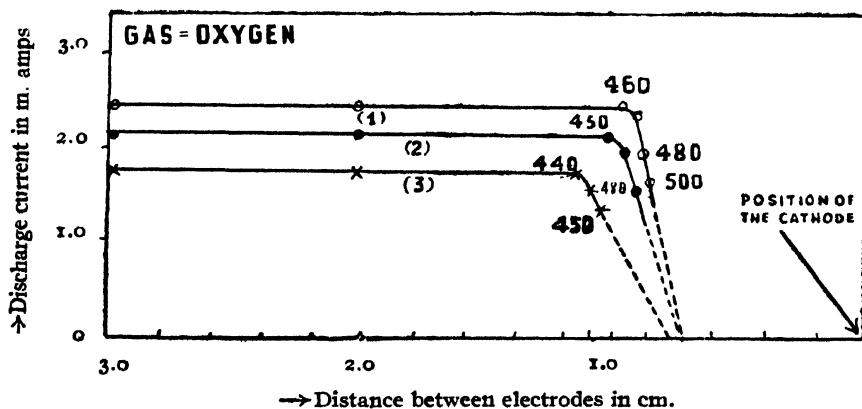
FIG. 3



Curve (1) Discharge pressure = 0.0308 mm.
Dark-space (from curve) = 1.30 cm.

(2) Discharge pressure = 0.0791 mm.
Dark-space (observed) = 1.02 cm.
" (from curve) = $\begin{cases} 1.030 \\ 1.040 \end{cases}$

FIG. 4

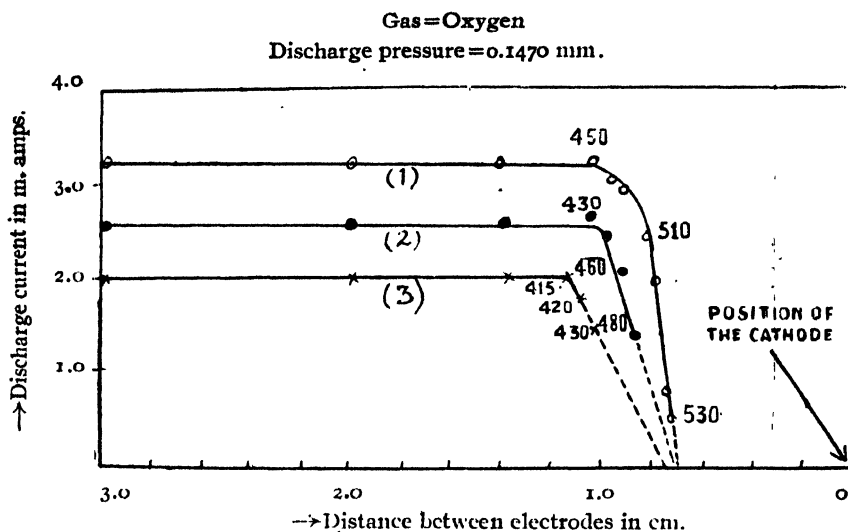


Curve (1) Dark-space (measured) = 0.700 cm.
" (from curve) = 0.700 "

(2) " (measured) = 0.725 "
" (from curve) = 0.715 "

(3) " (measured) = 0.760 "
" (from curve) = 0.770 "

FIG. 5



Curve (1)	Dark-space (measured)	= 0.670 cm.
	" (from curve)	= 0.675 "
(2)	" (measured)	= 0.700 "
	" (from curve)	= 0.705 "
(3)	" (measured)	= 0.725 "
	" (from curve)	= 0.750 "

FIG. 6

away from the edge of the cathode dark-space. The distance between the cathode dark-space boundary and this point is found to be a function of discharge pressure and voltage. As the anode is moved forward towards the cathode beyond this point the discharge current falls regularly and the voltage required to maintain it rises above its previous value. This drop in the discharge current in almost all cases is linear with the displacement of the anode till the latter reaches near the edge of the dark-space.

It is interesting to observe that if the straight falling part of any curve is produced out to the distant axis the point of intersection of the two lies away from the cathode equal to the width of the cathode dark-space.

The dark-space in these experiments was measured by a visual method using a cathetometer and always keeping the distance between the two electrodes much larger than its length. These values and those obtained from the curves are given in the figures above.

The voltage required to maintain the discharge at different positions of the anode is given along the curves at each step in all cases.

DISCUSSION OF RESULTS.

Aston (1911) has found that the electric field in the cathode dark-space of a glow discharge varies linearly with the distance from the edge of the negative glow to the surface of the cathode. This would be consistent with the assumption

that the ionisation in the dark-space is uniform throughout its length. Thomson and Thomson (1933) have shown that the number of positive ions produced by an electron in the cathode dark-space is large enough to liberate one such particle from the cathode by their impact on it and do not think it necessary to assume that the positive ions flow into dark-space from any other section of the discharge or that any agency other than the positive ions is required to cause the secondary electronic emission from the cathode in a self-sustaining discharge. In other words if a single secondary electron is liberated from the cathode metal by the action of a positive ion on it, then according to Thomson and Thomson all these positive particles are produced in the cathode dark-space itself due to ionisation by that electron across this space. The process of the production of ions and electrons in the dark-space is thus regenerative. There is, however, a different view held by Ryde (1923) and by Compton and Morse (1927) regarding the mechanism of the flow of current across this region of the discharge.

According to Ryde the supply of positive ions to the dark-space is mainly from the negative glow which acts as an emitter and the cathode as a collector, of the positive ions. Besides, the current to the cathode obeys the Langmuir's space-charge law which is true for the electronic emission from a hot metal in a high vacuum. Compton and Morse hold that this will be particularly so when the discharge is abnormal.

Following Thomson and Thomson we also believe that the ionisation in the dark-space is mainly produced by the cathode rays and that the positive ions are the chief agency which liberate the secondary electrons from the cathode. Our experimental results, however, are not consistent with their assumption that the positive ions flowing to the cathode come from the dark-space alone. The discharge current and the voltage would not suffer any change as the distance between the two electrodes is diminished as long as there is constant supply of the positive ions to the cathode. This is how the horizontal part of any curve is accounted for. The downward bend in the curves as the distance between the two electrodes is reduced to less than a critical value is, we believe, due to a partial cut off in the supply of the positive ions to the dark-space. In this case fewer ions reach the cathode and the secondary electron emission from it is correspondingly small. This, as well as the fact that now these electrons traverse a shorter path, cause a decrease in the discharge current. The linear fall in the current with the displacement of the anode is, probably, due to a uniform distribution of the positive ions in the region between the edge of the dark-space and the point where the bend in the curve occurs. The minimum voltage required to maintain the discharge when the anode lies in this region is always greater, the current is smaller for closer distances between the electrodes. The rise in the discharge voltage, which results in the increase of the average energy of the positive ions compensates for the decrease in the length of the electron path over which ionisation now occurs. To explain further suppose that when the discharge voltage and current are v and i respectively, n positive ions flow to the cathode and liberate therefrom i , secondary

electrons. If by displacing the anode through a distance x the number of the positive ions reaching the cathode is cut down to $n/2$ the secondary emission would fall to $i_s/2$ if the average energy of the ions (i.e. the discharge voltage) remains unaltered. Now these secondaries would ionise over a distance which is shorter by x and consequently the discharge current would fall to less than $i/2$. If however, the energy of these $n/2$ ions (i.e. the discharge voltage) increases to a suitable value they may produce secondary electrons greater than $i_s/2$ which, though travel a smaller path, may cause a current $i/2$ to flow in the discharge.

We have come to the following conclusions from these experiments :—

1. The positive ions reaching the cathode do not all come from the dark-space but a considerable number of them flow into the dark-space from the negative glow under all conditions of the discharge studied.
2. The discharge current is carried across the common boundary of the dark-space and the negative glow both by the cathode rays and the positive ions travelling in opposite directions.
3. The length of the negative glow which acts as a source of the positive ions to the dark-space depends upon the discharge voltage and pressure.

Experiments at still lower pressure and higher voltages are in progress.

It is a great pleasure to record our thanks to Lt. Col. Dr. Sir Zia Uddin Ahmad, Vice-Chancellor, for grant of funds to the Research Laboratory and the encouragement given to carry out the work. Our thanks are also due to Professor M. L. Oliphant, F.R.S., of the University of Birmingham, for his interest throughout in the work done in this Laboratory.

MUSLIM UNIVERSITY.
ALIGARE.

REFERENCES

- Aston, F. W. (1907), *Proc. Roy. Soc. A*, **79**, 80.
 Aston, F. W. (1911), *Proc. Roy. Soc. A*, **84**, 526.
 Compton and Morse (1927), *Phys. Rev.*, **30**, 305.
 Geddes, A. E. M. (1925), *Proc. Roy. Soc., Edin.*, **46**, 2.
 Gunther-Schulze (1923), *Zeits. f. Physik*, **20**, 1. 1.
 Gunther-Schulze (1924) *Zeits. f. Physik*, **23**, 5. 334.
 Loeb, L. B. (1939), "Fundamental Processes of Electrical discharge in gases."
 Ryde (1923), *Phil. Mag.* **14**, 1149.
 Thomson, J. J. and Thomson, G. P. (1933), "Conduction of Electricity through gases"
 3rd Edition, Vol. 2, pp. 316-322.
 Thomson J. J. (1931), *Phil. Mag.* **16**, 728.

ACOUSTICAL IMPEDANCE OF FOG

By R. N. GHOSH

ABSTRACT. The acoustical impedance of porous bodies has been related to their porosity, and flow resistance, and it is possible to evaluate it when their physical properties are known. In the present note the acoustical impedance of air containing water particles in suspension has been calculated in a straight forward manner directly from the hydrodynamical laws. The resulting formula is practically similar to that for solids.

Sewell (1910) calculated the amount of energy scattered by water particles ; he found that the fraction of energy scattered is very small. The present author has utilised some of his results, specially the formula which determines amplitude of vibration of the water particles with respect to the vibrating air particles.

The hydrodynamical resistance to oscillatory air flow against smooth water particles is given by (Lamb, 1930)

$$R = n \frac{4\pi}{3} \rho_0 a^3 \left[\frac{1}{2} + \frac{9}{4a} \sqrt{\frac{2\nu}{\sigma}} \right] \frac{dU}{dt} + n 3\pi \rho_0 a^3 \sigma \left[\frac{1}{a} \sqrt{\frac{2\nu}{\sigma}} + \frac{1}{a^2} \frac{2\nu}{\sigma} \right] U.$$

where a = radius of solid particles, ρ_0 = density of air, $\sigma = 2\pi$ (frequency), ν = kinematic viscosity, n = number of particles per c.c.

In evaluating the resistance due to a large number of particles, the diffraction of sound by the neighbouring particles has been neglected. If $U \propto e^{j\sigma t}$ then $R = R_0 + jX$ where

$$\left. \begin{aligned} R_0 &= 6\pi \rho_0 a \nu n \left(1 + a \sqrt{\frac{\sigma}{2\nu}} \right) \\ X &= \frac{4\pi}{3} \rho_0 a^3 n \sigma \left(\frac{1}{2} + \frac{9}{4a} \sqrt{\frac{2\nu}{\sigma}} \right) \end{aligned} \right\} \dots (1)$$

When the air flow is not oscillatory, X is zero, and we have

$$R'_0 = 6\pi a n \eta$$

which is Stokes' law. The following table gives the values of R_0/ρ_0 and X/ρ_0 for different frequencies

$$R_0 = 6\nu \rho_0 a n (1 + f), \quad f = a \sqrt{\pi N / 132}$$

$$a = 10^{-3} \text{ cm.}; \quad n = 10^6, \quad \nu = 132$$

$$f = 4.84 \times 10^{-3} \sqrt{N}$$

$$N = \text{frequency.}$$

TABLE I

N	f	R_0/ρ_0	X_0/ρ_0
128	.054	2.48×10^3	1.28×10^3
256	.075	2.53×10^3	1.94×10^3
512	.105	2.66×10^3	2.60×10^3
1024	.140	2.76×10^3	3.80×10^3
2048	.196	2.90×10^3	5.55×10^3

It will be noticed that R_0 is much larger than X_0 ; and that f affects R_0 at very high frequencies only. Consequently if we replace R_0 by the flow resistance R'_0 much error will not be produced in the case of small particles of the order of 10^{-3} cm. When the particles increase in size, f becomes appreciable, and the flow resistance R'_0 will be much smaller than R_0 .

Equation of continuity.—Since there are n particles per unit volume, they occupy a volume β and, therefore, the volume available is, $(1-\beta)$,

where

$$\beta = \frac{4}{3} \pi a^3 n$$

Considering the flow of air through planes perpendicular to the x axis at x and $x+\Delta x$ we obtain

$$-\frac{dp}{dx} u \Delta x = \frac{d\rho}{dt} (1-\beta) \Delta x \quad \dots (2)$$

since the water particles are not compressible, u being the particle velocity of air. Writing $P = (1-\beta)$ and designating it as porosity we re-write the above equation as

$$-\frac{du}{dx} = -\frac{P}{\rho_0} \frac{d\rho}{dt}$$

If we assume the gas law $P_1 \rho^{-\gamma} = \text{constant}$, γ being the ratio of specific heats, then

$$p = \frac{\gamma P_0}{\rho_0} \Delta \rho$$

p = excess pressure, P_0, ρ_0 normal pressure and density.

In the present case if the suspensions are supposed to take part in the heat reactions, then the resulting value of γ_3 is given by

$$\Gamma = \frac{PC_p + \lambda(1-P)}{PC_v + \lambda(1-P)} \quad \dots (3)$$

where λ is the specific heat of the suspension, which in the present case is unity. When these modifications are introduced the equation (2) becomes

$$\frac{du}{dx} = -\frac{P}{\Gamma \rho_0} \frac{dp}{dt} = -\frac{Pj\sigma}{\rho_0 \Gamma} p \quad \dots (4)$$

where $p \propto e^{j\sigma t}$.

While the equation of motion is

$$-\frac{dp}{dx}\Delta x = \rho_0\Delta x \frac{du_1}{dt} + \rho'\Delta x \frac{du_2}{dt} + (R_0 + jx)(u_1 - u_2) \quad \dots (5)$$

where $\rho' = \frac{4}{3}\pi a^3 \rho_1$, ρ_1 = density of water particles, u_1 particle velocity for air, and u_2 the same for the suspensions. The first term represents the difference of pressure between the points x and $x + \Delta x$ in the positive direction of x axis. In the right hand side $\frac{du_1}{dt}$ represents the acceleration of air particles, $\frac{du_2}{dt}$ the same for water particles of mass $\rho'\Delta x$ in volume Δx . The third term represents the resistance due to water particles, $(u_1 - u_2)$ being the relative velocity of air with respect to water particles. Sewell (*loc. cit.*) has shown that

$$u_2/u_1 = (1 - jq)L^2 \quad \dots (6)$$

$$q = \frac{2}{9} \frac{a^2 \sigma}{\nu} \frac{\rho_1}{\rho_0}; \quad L = \frac{1}{(1 + q^2)^{\frac{1}{2}}},$$

ρ_1 = density of water particles. Hence

$$-\frac{dp}{dx} = u_1 j \sigma \left\{ \rho_0 + \rho' L^2 + \frac{X(1 - L^2) + R_0 q L^2}{\sigma} \right\} + u_1 \{ R_0(1 - L^2) - X q L^2 \} \quad (7)$$

$$-\frac{dp}{dx} = R_1 u_1 + j \sigma \rho_2 u_1 \quad \dots (8)$$

$$R_1 = \{ R_0(1 - L^2) - X q L^2 \}; \quad \rho_2 = \rho_0 + \rho' L^2 + \frac{X(1 - L^2) + R_0 q L^2}{\sigma}$$

With the help of (4) we get

$$\begin{aligned} \frac{d^2 p}{dx^2} &= \frac{P p}{C_2^2 \rho_2} (j \sigma R_1 - \sigma^2 \rho_2), \quad C_2^2 = \Gamma P_0 / \rho_2 \\ \text{i.e., } \frac{d^2 p}{dx^2} &= \frac{j^2 Q^2 \sigma^2 P}{C_2^2} p \quad \dots (9) \end{aligned}$$

where

$$Q = (1 - j R_1 / \sigma \rho_2)^{\frac{1}{2}}$$

Therefore

$$p = A e^{-\frac{j \sigma Q \sqrt{P}}{C_2} x} e^{j \sigma t}$$

Since

$$\frac{du}{dx} = -\frac{P}{C_2^2 \rho_2} \frac{dp}{dt} = -\frac{P j \sigma}{C_2^2 \rho_2} p$$

$$Z_2 = \frac{p}{u} = \frac{C_2 \rho_2}{\sqrt{P}} Q = \frac{C_2 \rho_2}{\sqrt{P}} \left(1 - \frac{j R_1}{\sigma \rho_2} \right)^{\frac{1}{2}} \dots \dots$$

and

$$\frac{Z_2}{Z_0} = \left(\frac{\Gamma \rho_2}{\gamma \rho_0} \right)^{\frac{1}{2}} \frac{1}{\sqrt{P}} \left(1 - \frac{j R_1}{\sigma \rho_2} \right)^{\frac{1}{2}} \quad \dots (10)$$

where $Z_0 = C_0 \rho_0$.

TABLE 2

$$a = 10^{-3} \text{ c.m.}, \quad n = 10^6, \quad \nu = .132, \quad f_1 = 4.84 \times 10^{-3} \sqrt{N}.$$

N	f_1	q	q^2	L	L^2	$\frac{1}{2} + \frac{9}{4a} \sqrt{\frac{2\nu}{\sigma}}$
128	.054	1.02	1.04	.66	.43	41.0
256	.075	2.05	4.10	.45	.20	30.0
512	.105	4.10	16.20	.24	.06	21.0
1024	.140	8.20	64.4	.12	.014	15.0
2048	.196	16.40	269.0	.06	.0036	11.0

Let
$$\chi = \frac{4}{3} \pi \rho_0 \sigma a^3 n \left(\frac{1}{2} + \frac{9}{4a} \sqrt{\frac{2\nu}{\sigma}} \right)$$

$$\rho_2 / \rho_0 = 1 + \frac{4}{3} \pi a^3 n \frac{\rho_1}{\rho_0} L^2 + \frac{\chi(1-L^2)}{\sigma \rho_0} + \frac{R_0 q L^2}{\sigma \rho_0}$$

or
$$\rho_2 / \rho_0 = 1 + \alpha + (\beta + \delta) / \sigma$$

where
$$d = \frac{4}{3} \pi a^3 n \frac{\rho_1}{\rho_0} L^2; \quad \beta = \chi(1-L^2) / \rho_0$$

$$\delta = R_0 q L^2 / \rho_0.$$

TABLE 3

N	R_0 / ρ_0	χ / ρ_0	d	β	δ	$(\beta + \delta) / \sigma$	ρ_2 / ρ_0
128	2.48×10^3	1.28×10^2	1.33	$.73 \times 10^2$	1.11×10^3	1.50	3.83
256	2.53 "	1.94 "	.62	1.47 "	1.06 "	.80	2.42
512	2.66 "	2.60 "	.186	2.44 "	.66 "	.26	1.50
1024	2.76 "	3.8 "	.045	3.70 "	.31 "	.11	1.15
2048	2.90 "	5.55 "	.011	5.6 "	.20 "	.063	1.07

TABLE 4

N	$(1 - \rho_2 / \gamma \rho_0)^{\frac{1}{2}}$	R_1 / ρ_0	$R_1 / \sigma \rho_2$	Q	Z_2 / Z_0	Reflection coeff.
128	1.67	1.36×10^3	.46	$1.02 - j.23$	$1.7 - j.38$	24%
256	1.35	2.00 "	.54	$1.04 - j.27$	$1.32 - j.34$	14%
512	.98	2.44 "	.53	$1.04 - j.28$	$1.02 - j.26$	6.7%
1024	.90	2.66 "	.43	$1.02 - j.28$	$0.92 - j.19$	4.2%
2048	.79	2.87 "	.22	$1.05 - j.11$	$0.81 - j.088$	4.0%

TABLE 5

$$a = 10^{-4} \text{ cm.}; \quad n = 10^9$$

N	f_1	q	L	$\frac{1}{2} + \frac{9}{4a} \sqrt{\frac{2\nu}{\sigma}}$	χ/ρ_0	R_0/ρ_0	ρ_2/ρ_0	$\left(\frac{\rho_2}{\gamma\rho_0}\right)^{\frac{1}{2}}$	$R_1/\sigma\rho_2$
128	.0054	.0012	1	410	1.25×10^3	2.38×10^5	7.2	2.3	-2.3×10^{-3}
256	.0075	.0205	1	300	1.84	2.384	5.6	2.0	-4.31×10^{-3}
512	.0105	.0410	1	210	2.58	2.40	4.85	1.85	-7.00×10^{-3}
1024	.0104	.0820	1	150	3.65	2.41	4.48	1.78	-1.06×10^{-2}
2048	.0196	.164	1	110	5.34	2.42	4.43	1.76	-1.6×10^{-2}

TABLE 6

N	Ω	Z_2/Z_0	Reflection coefficient
128	$1+j \ 2.3 \times 10^{-3}$	$2.3(1+j2.3 \times 10^{-3})$	40%
256	$1+j \ 4.30 \ ,$	$2.0(1+j4.3 \ ,)$	33%
512	$1+j \ 7.00 \ ,$	$1.85(1+j7.00 \ ,)$	30%
1024	$1+j10.6 \ ,$	$1.78(1+j10.6 \ ,)$	28%
2048	$1+j16.0 \ ,$	$1.76(1+j16.0 \ ,)$	27%

Tables (2) to (4) give the values of the relevant quantities in the case of water particles of radius 10^{-3} cm. which represents the size of fog particles, while tables (5) and (6) do the same for finer drops. It will be noticed that the amplitude of vibration of the former kind in relation to that of air particles, represented by L, is appreciable at low frequencies but it drops down at high frequencies. While much finer particles 10^{-4} cm. radius, have practically the same amplitude as that of air particles throughout the given range of frequencies. It will further be observed from equation (10) that R_1 contributes to the reactance of the particle-air medium in Z_2 . For particles of 10^{-3} cm. radius R_1 has a positive value and the reactance is negative. While for finer particles 10^{-4} cm. radius, R_1 is negative and the added reactance is positive. This indicates that in the case of fine particles they contribute mostly towards inertia of the medium, while their resistance to compression predominates in the case of particles of 10^{-3} cm. radius.

The effective value of the acoustical resistance of the medium is greatly altered. For particles of 10^{-3} cm. radius it varies from 1.7 to 0.81 times that of air at different frequencies. In the case of finer particles the resistance varies from 2.3 to 1.76 times that of air in the same range of frequencies. The reflection coefficient varies from 24% to 4%, while in the case of finer particles the variation ranges from 40% to 27% over the same range of frequencies.

It will also be noted that on account of the smaller available volume for compression and the inertia, the velocity of sound in air containing suspensions, is greatly altered. The effective part taken by the various factors can be easily estimated from equation (9). Most important part is taken by the porosity P , the altered Γ and the effective density. The formula relating to Γ supposes that the suspensions remain at rest, while they actually oscillate, hence it does not represent the correct value of Γ . It will actually be less than that given by (3), because by their motion work of compression will raise the temperature more than that for stationary particles.

It has been pointed out in the early part of the paper that the *flow resistance* R' can be substituted for the actual resistance due to oscillatory air current at low frequencies to a first approximation. At high frequency this approximation fails.

The present paper has given a picture of the phenomenon that takes place in the case of a gaseous medium containing suspensions; it is now possible to extend these results to the case of porous bodies, and the author proposes to do so in a subsequent paper.

DEPARTMENT OF PHYSICS,
ALLAHABAD UNIVERSITY.

REFERENCES

- Lamb, 1930, *Hydrodynamics*, 605.
Sewell, 1910, *Phil. Trans.*, **210**, 239.

ON THE STUDY OF ABSORPTION AND FLUORESCENCE SPECTRA OF SOME AROMATIC HYDROCARBONS IN SOLUTION

By S. C. GANGULY

ABSTRACT. Effects of the variations of wave-lengths of the exciting radiation on the fluorescence of some aromatic hydrocarbons have been studied. It has been found in all cases that the long wave-length limit of the exciting radiation is the longest wave-length of the absorption band of the material.

INTRODUCTION

There is up to the present time no satisfactory theory for fluorescence in solutions. According to Perrin (1918) emission of fluorescence by organic substances was due to flashes of exploded molecules. But the experimental results of Wood (1922) and Pringsheim (1922) were not capable of explanation by Perrin's hypothesis. Pringsheim suggests that molecules being excited by absorption of light energy may revert into the normal state with the emission of fluorescence. Hence fluorescence is defined as the reverse of light absorption, where absorbed light energy is re-emitted without causing any change in the structure of the absorbing system. Thus fluorescence and absorption are inter-related phenomena. If so, it is quite natural for one to ask—how are they related? Is there for each absorption band a corresponding fluorescence band or are all the fluorescence bands chained into one? Is it possible to isolate any fluorescence band from the remaining? What is the long wave-length limit of the exciting radiation for each substance? Is there any change of intensity of fluorescent light as we pass from one absorption band to another through non-absorbing interval? In order to understand the true mechanism of fluorescence and to find out the relation between absorption and fluorescence, particularly the influence of frequency of incident radiation the present work was undertaken and the paper describes the result so far obtained. Simple aromatic hydrocarbons are taken because they dissolve in organic liquids as neutral molecules.

They yield the same fluorescence bands in vapour, in solution and in the pure crystal, except for the small shifts of the bands, depending on the neighbours of the fluorescing molecules. The absorption as well as fluorescence spectra of some aromatic compounds have been studied by a number of workers particularly by Seshan (1936), Pringsheim (1939) and Sambursky and Wolfshn (I, 1940 ; II, 1942).

For studying fluorescence, usually ultra-violet radiations from a mercury arc are used for exciting light waves and fluorescence is observed by ordinary complimentary filters method. By this method we cannot study the properties

of an individual band and we do not get any information mentioned above. As the Hg arc emits only a few lines in its spectrum, only a few definite wave-lengths can be obtained from it, and so a continuous variation of wave-length is not possible. To avoid that difficulty we have used monochromatic light isolated by means of a slit from the spectrum of white light as our source.

EXPERIMENTS

The source of light is a coiled-coil gas filled lamp. Light is condensed by a condenser on to the slit of the spectrograph which is focussed properly. The spectrum is received on a screen with a movable slit. From the spectrum with the help of the movable slit, we take out any monochromatic beam as exciting radiation. The solution under examination is taken in a cell. The incident and the fluorescent rays are again condensed on the slit of another spectrograph. Time of exposure was the same all through. As the intensity of the incident beam depends on the current, through the lamp, it was carefully kept constant.

RESULTS

Anthracene, Naphthacene, Phenanthrene and Perylene were dissolved in alcohol and the solution was taken in a cell. By moving the slit radiations of different wave-lengths were allowed to be incident on the solution. Thus we pass from one wave absorption band to the other through non-absorbing interval. The results are summarised below :

(1) The positions and the number of fluorescence bands remain unchanged with the change of exciting radiation.

(2) The longest absorption band of each substance is its longest critical wave for exciting fluorescence. Light-wave longer than the longest absorption band of the substance cannot excite fluorescence.

(3) As the exciting radiation is changed from one absorption band to another through non-absorbing interval, the total intensity of fluorescence bands is also changed. Absorption band wave as incident radiation produces the maximum intensity of fluorescence.

Results are tabulated below :—

TABLE I

	Absorption bands in A	Fluorescence bands in A	Critical Exciting radiation in A
Anthracene	3750, 3550, 3380 & 3220	4500, 4240, 4000 & 3790.	3750
Perylene	4250, 4000, 3790 & 3590	5000, 4700 & 4480	4250
Naphthacene	4680, 4380 & 4140	5460, 5080 & 4750	4680
Phenanthrene	3750, 3690, 3550 & 3460	4490, 4250, 4030 & 3850	3750

TABLE II

Solute	Solvent	Refractive Index	Longest absorption wave-length in A. U.	Critical exciting wave-length in A.U.
Naphthacene	acetone	1.359	4660	4660
	alcohol	1.362	4670	4670
	CCl ₄	1.465	4780	4780
	Solid solution in Anthracene.		4910	4910

In Table I are given the longer limit of wave-length for excitation of these substances in alcoholic solutions and also the positions of fluorescence and absorption spectra.

Table II gives the positions of the longer wave-length limit of absorption and of excitation of fluorescence of Naphthacene. This substance was studied in detail in solution. The absorption and fluorescence spectra of this substance were studied in different solvents and also the different critical exciting wave-lengths for them were determined.

In concluding, the author would like to take the opportunity of thanking Prof. K. S. Krishnan for suggesting the problem and Prof. K. Bancrjee for his interest and advice during the progress of work.

INDIAN ASSOCIATION FOR THE
CULTIVATION OF SCIENCE.

REFERENCES

- Perrin, J. (1918), *Ann. de Phys.*, **10**, 133.
 Pringsheim, P. (1922), *Zell. f. Phys.*, **10**, 176.
 Pringsheim, P. (1939), *Trans. Faraday Soc.*, **35**, 18.
 Sambursky, S. and Wolfsohn, G I (1940), *Trans. Faraday Soc.*, **36**, 427.
 Sambursky, S. and Wolfsohn, G II (1942) *Phys. Rev.*, **62**, 357.
 Seshan, P. K. (1936), *Proc. Ind. Acad. Sc.*, **A**, **3**, 148.
 Wood, R. W. (1922). *Phil Mag.*, **43**, 757.